NILE
RIVER BASIN

Nile Basin Adaptation to Water Stress
Comprehensive Assessment of Flood & Drought Prone Areas

UNEP

SWEDEN

NILE BASIN INITIATIVE
Initiative du Bassin du Nil

Acknowledgments

Table of Contents

Table of Contents

Figures

Table of Contents

Table of Contents

Executive summary

Background

The Nile basin is one of the most critical and perhaps most important shared water basins in Africa. The Nile is a crucial resource for the economy of eastern and north-eastern Africa as agriculture, energy production and livelihoods in general, all depend strongly on the river flow. There are a number of challenges facing policy-makers, decision-makers and water managers to achieve the sustainable and integrated management of this resource.

The area surrounding Lake Victoria in Kenya and Uganda, the Ethiopian highlands surrounding the Blue Nile and the banks of the Nile in Egypt are all in the Nile Basin and considered the three highest population concentrations in Africa (UNEP, 2010). Four of the Nile basin countries have population growth rates in the top 10 globally, 9 are above the mean growth rate of Africa and all are above the global average (UNESA 2010; UNEP 2010). As the population in the Nile basin continues to grow, the pressure on this resource will increase water stress in all sectors (Bates et al., 2008; Boko et al., 2007). In addition to the rising levels of water scarcity and

high population growth, the region faces watershed degradation and loss of environmental services. Any future changes in the water quantity and quality and their distribution in space and time will have important impacts on the local and basin-wide economies and environment and on the sustainability of the water resources.

The climate in the region is marked by significant inter-annual and inter-decadal variability, which has important implications for the management of water resources in the Nile (Conway, 2005). In addition, the water resources are critically sensitive to climate change (Conway et al., 2007). It is expected that future climate change may exacerbate the level of water stress across the basin and it is therefore important to assess and manage the potential effects of such changes.

Managing and developing the water resources within the basin must not only address different water uses, but also the trade-off between developments upstream and water use downstream between countries. This requires a regional approach to both water management and climate adaption.

To address these many and various challenges,

managers and decision-makers require tools and information at all levels, from local to national to regional, to support their decisions. The key goal of this work is to support their efforts and inform their decision-making by providing tools and information concerning climate change at the regional level.

This report is a contribution to the UNEP project "Adapting to climate change induced water stress in the Nile River Basin". It summarises the technical developments and assessments carried out under Work package WP1.1 "Comprehensive Assessments of Flood and Drought Prone Areas" by DHI and the UK Met Office in collaboration with the Nile Basin Initiative (NBI). The project was launched in March 2010 as a partnership between UNEP and the Nile Basin Initiative (NBI), sponsored by SIDA. The overall project goal is to build the resilience of ecosystems and economies that are most vulnerable to climate change induced water stress in the Nile Basin countries[1] through building key adaptive capacity and piloting adaptation in "hotspots" with technical, policy and financial interventions.

WP1: Comprehensive Assessments is divided into 3 parts with the following objectives (lead organisations in square brackets):
WP1.1: Undertake assessments identifying flood and drought prone areas; including appropriate hydrological modelling, develop criteria for identification of "hot-spots"; Downscaling of global models [DHI].
WP1.2: Development of an assessment framework to involve the themes, tools, criteria and indicators for selecting hotspots and linked to scenario development [UNEP-DEWA].
WP1.3: Undertake stock-taking of existing activities related to climate change adaptation in the basin, key players (research, policy etc.) and existing projects at regional, national and local level [UNEP-DEPI - CCAU].

The focus of "WP1.1 Comprehensive Assessments of Flood and Drought Prone Areas" has been to develop projections of climate change and water demand in order to assess projected changes in water stress, related both to too much and too little water. These assessments provide information that

can be used to support decision-making for climate adaptation at the regional scale, i.e. at the scale of the Nile Basin rather than the national or local scale. These assessments and regional hydrological model developed can be used in the future to support and inform water resources management under a changing climate as well as the evaluation of alternative climate change adaptation measures at the regional level.

Methodology

The overall approach has been to develop and apply a *regional scale operational framework* for assessing climate change. This framework consists of combining regional scale climate modelling with distributed hydrological modelling to both assess the impacts of climate change on the water resources and provide the capability to evaluate adaptation measures at the regional scale. This was motivated by the clear perception that such tools to assess climate adaptation at the regional scale are missing. This is particularly critical for transboundary rivers, where the downstream impacts of national water resources management need to be considered. The implementation of adaptation measures, depending on the type of interventions, may need to treat the basin as a whole and a regional modelling framework is required to evaluate alternatives to avoid regrettable outcomes.

One of the characteristics of the Nile Basin is that the flows within the river constitute the most important component of water resources. To simulate flows and water levels at the regional scale for water resource management, climate change assessment, and climate adaptation scenarios, a distributed hydrological model has been developed for the entire Nile.

For this study a set of regional climate model (RCM) simulations have been performed for the Nile River Basin using the most recent generation of the UK Met Office GCM-based perturbed physics ensembles (PPE) for two projection horizons, the near future, 2020-2049, and the far future, 2070-2099. The projections for 2020-2049 are particularly relevant for regional water resource planning as this corresponds to typical planning and implementation horizons for major infrastructure projects. The projections for 2070-2099 are more uncertain but indicate whether any trends found in the near future continue into the far future.

The RCM projections used here were developed from a subset of five of the most recent Hadley Centre perturbed physics GCM simulation ensembles for the

A1B SRES scenario using dynamical downscaling. This subset was selected using a recently developed systematic methodology (McSweeney et al., 2012) to capture the range of outcomes produced by the full 17 member ensemble, while excluding those unable to represent the African climate realistically. This is an important step towards quantification of uncertainties, which is fundamental to decision-making, but often overlooked. This study is a pioneering application of the PPE approach outside of Europe. Although the methodology adopted has been designed to explicitly account for uncertainties in model projections it is emphasized that it does not account for the full range of uncertainty.

The original concept of this particular work package was concerned with the identification of local "hot spots" with significant projected water resource, climate or other impacts. While such locations are easily identified for some types of impact assessments e.g. population growth or pollution studies, climate change impacts and associated adaption measures are more appropriately investigated in a larger geographical perspective, e.g. "hot spot regions" located within distinct types of natural environments in the Nile. In this study the impacts of climate change and water demand scenarios are therefore examined not only across the entire basin at the regional scale but more detailed assessments have been made in selected "hot spot regions":

- The Equatorial Lakes basin
- The Ethiopian Highlands (Blue Nile and Atbara basins)
- The Egypt and Sudan water demand region.

While some assessment of climate change impacts on another important "hot spot region", the Sudd, has been carried out here, it must be treated as preliminary given the complex hydrology of the swamps, multiple flow paths and scarcity of data.

Outcomes & benefits

This study has contributed to an enhanced understanding of climate vulnerability in the Nile in relation to water stress (high and low flows) and the provision of vulnerability indicators.

Two workshops have been conducted by DHI/UK Met Office for NBI staff to provide in-depth knowledge about:

- Regional scale climate modelling using the PRECIS model (by Met Office Hadley Centre).

- Regional hydrological modelling using the MIKE BASIN/HYDRO model (by DHI).
- Presentation of the methodology, key findings and perspectives for combined climate change and water resources modelling.

More specifically, the project has provided a number of important findings in relation to:
- State-of-the-art regional climate modelling results, including provision of change factors within the Nile Basin, made available to all NBI countries for application at the regional or national level.
- Improved understanding of the key climatic processes and the predictive ability of regional versus global climate models.
- Regional hydrological modelling results made available to all NBI countries.

As a result of the project the following modelling tools have been established:
- A regional scale hydrological tool suitable for modelling the impact of climate change, development scenarios, and climate adaptation measures at the regional scale in both high and low flow regimes (floods and water scarcity).
- A regional water resource tool that can be used as boundary conditions and starting point for more detailed local modelling of both water resources and climate for investigating national and local adaptation measures for floods and droughts.

This study has used the same hydrological modelling tools (DHI MIKE series), which are currently being used in the region, and for which NBI already has many licenses. It is therefore compatible with other Nile Basin projects, particularly the NBI Decision Support System (DSS) currently being developed by DHI for the basin.

Key results

Comparison of the RCM results with observations show that this ensemble appears to correctly capture the annual cycle of temperature, both for Africa as a whole and for the sub-regions.

The projections of precipitation from climate models are generally less reliable and exhibit less consistency and greater variability than the temperature projections. For example, although

global models agree on drying over Africa for the 20th century, there is no robust agreement in their predictions of 21st century rainfall (Giannini et al. 2008). Within the Nile Basin several previous studies indicate that there are large uncertainties in both the direction and magnitude of climate changes (e.g. IPCC 2007; Boko et al 2007; Elshamy et al. 2008; Beyene et al., 2010).

Nevertheless, the fact that the climate models can replicate key features of the current climate provides some degree of confidence in the ability of the models to represent future climate. The RCM ensemble appears to slightly over-estimate precipitation, but captures the annual cycle for most of the regions. Most importantly, the RCM ensemble shows a significant improvement over the traditional GCM ensemble in many parts of Africa.

Regional changes in temperature

Although not directly related to the water balance and water resources over the basin, all the RCM projections show consistent increases in temperature both for the near future (2020-2049) and the far future (2070-2099).

The near future scenario shows increases of approximately 1.5 °C, though with significant spatial and temporal variation, which is consistent with previous studies (IPCC, 2007b; Butts et al. 2011). It shows maximum increases over Egypt and the northern part of Sudan during the hottest months.

The far future scenario shows even larger increases, in the range of 4-6 °C, during the summer months. While these changes are quite large they are consistent with results from the IPCC 4th assessment, which show increases of 3.5 °C or more during the summer season.

Temperature rises may both reduce the productivity of major crops and increase crop water requirements (Eid et al. 2006). The projected large increases in temperature will certainly increase water demand in major population centres both for food production and domestic water supply.

Regional changes in precipitation & water resources

Even though the climate projections for precipitation over the Nile are highly uncertain, it is nevertheless possible to extract useful information for decision-making.

Climate "consensus" maps developed over the region were found to be a useful means to address the uncertainty in climate projections for precipitation. Even though the different RCM projections show significant differences in both the direction and magnitude of changes in precipitation, these "consensus" maps highlight regions within the Nile Basin where the regional climate models provide consistent (at least 4 out of 5 agree on the direction) projections and conversely identify areas where the regional models do not agree on the direction of change.

The regional changes in flows provide the most directly relevant impact information, primarily because the flows represent the major part of the water resource for much of the Nile basin. In addition, the flows integrate the effect of changes in both precipitation and potential evapotranspiration over larger areas. So even if the climate signals are 'noisy' and uncertain, the change in flows may show a much clearer signal.

White Nile

The RCM projections over much of the White Nile, particularly for the Equatorial Lakes, also including the Sudd, show a significant decrease in precipitation for the near future projections (2020-2049). Significant decreases in precipitation over the Lake Victoria Basin from April-November are projected. It should be noted that the RCM in the "short" rainy season (October, November and December) seems to over-estimate the projections, exhibiting a strong positive bias directly over the lake. These changes in precipitation are directly reflected in the projected Nile river flow at Malakal in South Sudan, which integrates the contributions from all parts of the White Nile basin including the Equatorial Lakes basin to the south, the Bahr El-Ghazal basin to the west[2], the Sobat to the east and the Bahr-Jebel basin including the Sudd. The near future scenarios (Figure 1) show consistent reductions in flows over the year with some variation in the magnitude of these reductions amongst the RCM ensemble members. The 2020-2049 near future period corresponds to the typical planning horizon for many infrastructure projects, and any planned adaptation measures must respond to a potential reduction in flow in the White Nile area. Such measures must be robust to take into account the degree of uncertainty in the flow projections. The reduction in rainfall may have important impacts for rain-fed agriculture, but these

[2]The contributions from the Bahr El Ghazal basin to the Nile flows are considered negligible, not included in the regional hydrological model
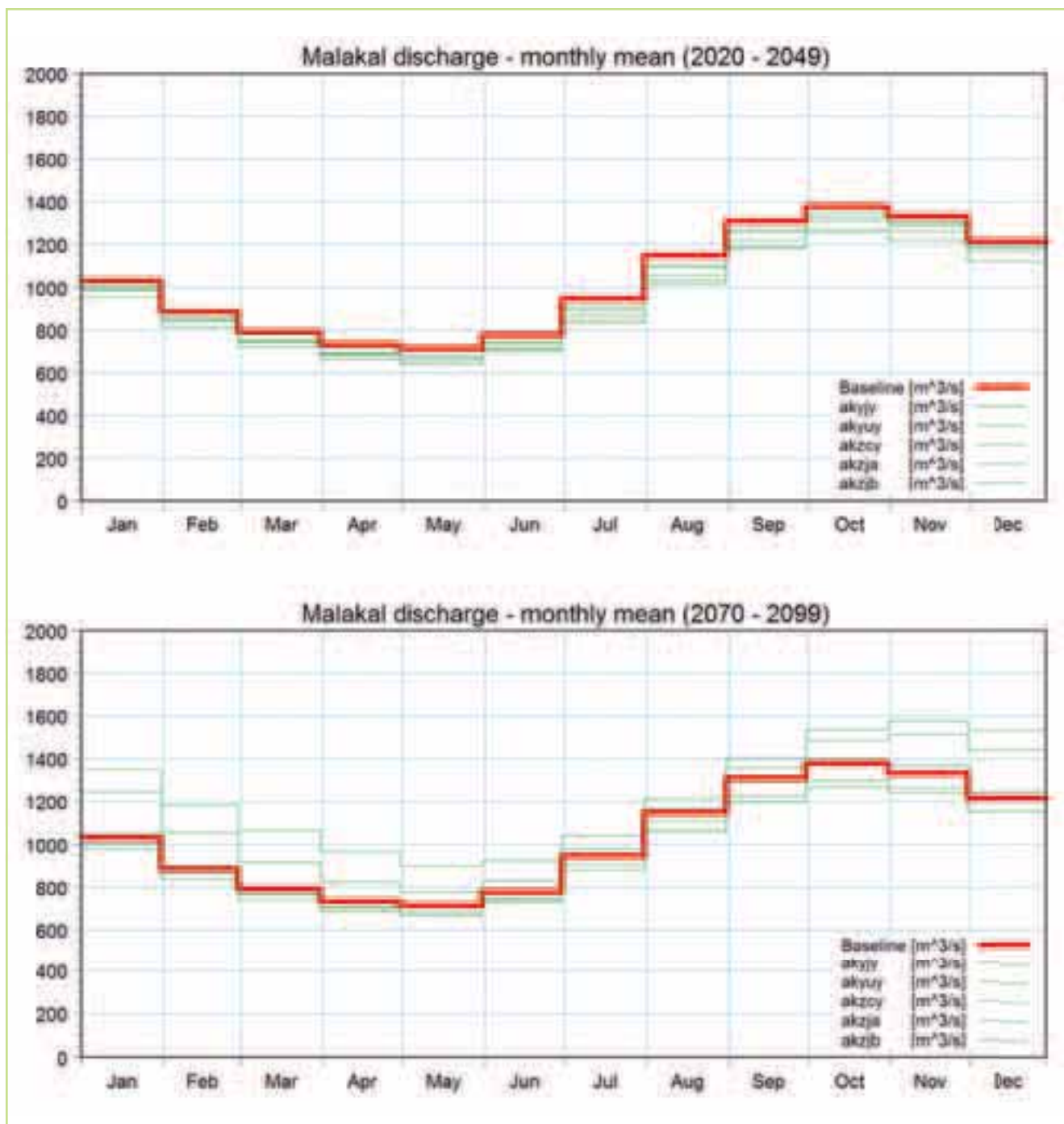
Figure 1. Projected changes in the average monthly flows in the Nile at Malakal, South Sudan. Projections are shown for two periods; 2020-2049 (top) & 2070-2099 (bottom). The solid (red) line shows the baseline levels (1961-1990) & the thin green lines the different RCM ensemble member projections

are expected to be critical only in the areas where agriculture is already marginal.

For the far future scenarios (2070-2099) the projected changes in flow at Malakal are not as clear, with both significant increases and smaller decreases amongst the ensemble members. A large uncertainty in both the sign and magnitude of the change in flow make the impacts in the far future period more difficult to adapt to. Here, a robust adaptation strategy that accounts for a wide range of possible future conditions is required.

Blue Nile

Interestingly, the precipitation changes over the Blue Nile are expected to be quite different from the White Nile. Together the Blue Nile and Atbara rivers represent a significant part of the water resource generation in the Nile, and as they account for more than 70% of the main Nile peak flows, they are critical to the downstream water resources management.

The near future RCM projections show both increases and decreases in flow during the important

wet season from June to September. The reductions appear in the most western parts of these two catchments, while the increases appear in the south and east and suggest a general increase at the end of the wet season.

Although the present methodology is designed to explicitly account for uncertainty in model projections, our findings indicate an underestimation of the overall level of uncertainty. This is most pronounced for the Western Ethiopian Plateau in summer (June, July and August). During these months the UK Met Office GCM ensemble describes a general increase in rainfall for the region while some of the other CMIP3 GCMs describe possible reductions

in precipitation. The lack of these drier runs in the present simulations implies that some likely climate scenarios for this region may be underrepresented in the present study.

By contrast, the far future projections (2070-2099) show a consistent increase in precipitation during most of the year, including the rainy season. It should be noted that this study seems to project less reduction in precipitation compared to some CMIP3 GCMs for this region during the summer months.

The projected changes in rainfall are clearly reflected in the simulated river flows for the Blue Nile at Khartoum (Figure 2). There is a general tendency toward increased flows from August to December for
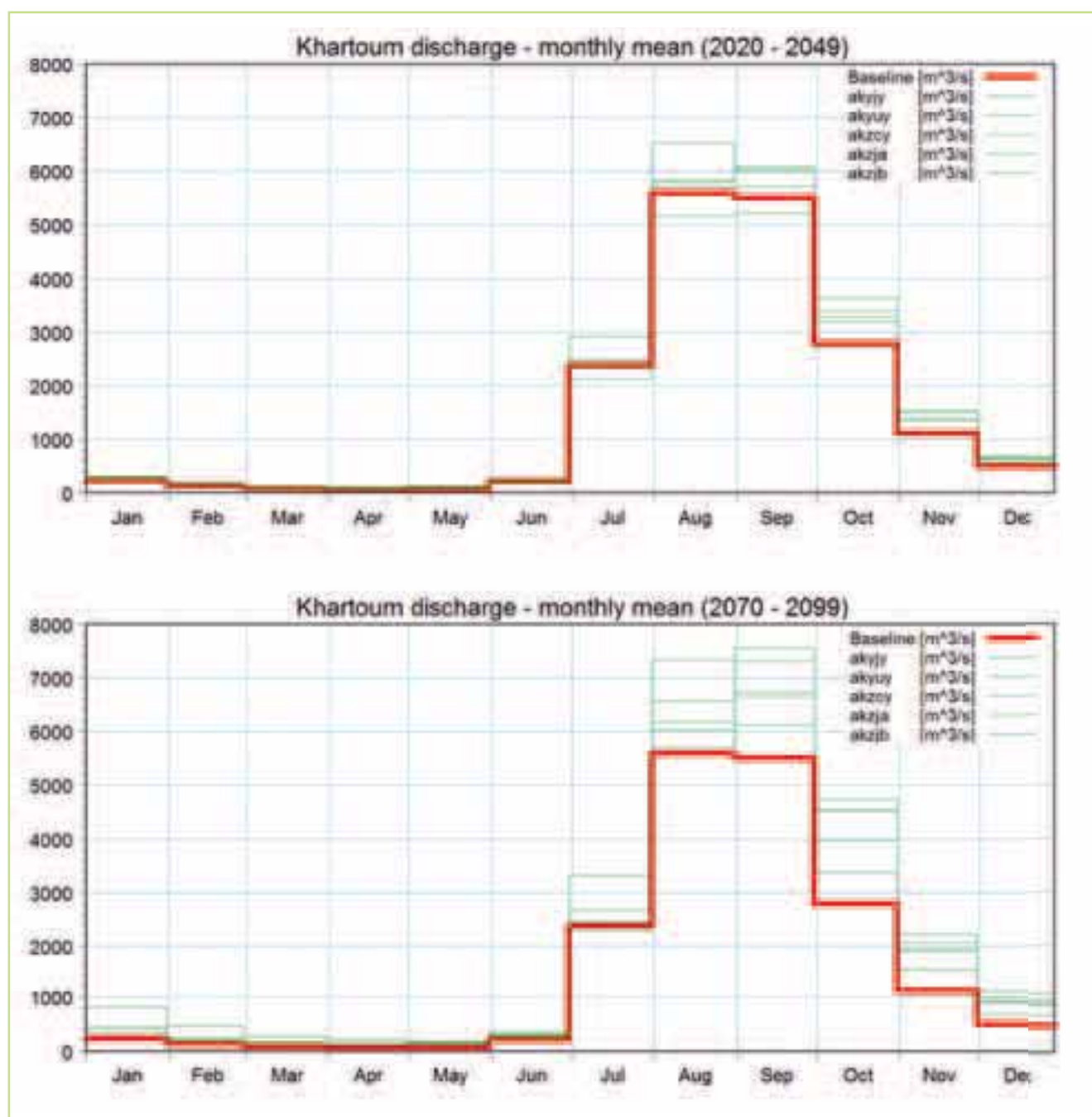
Figure 2. Projected changes in the average monthly flows for the Nile at Khartoum, Sudan. Projections are shown for two periods; 2020-2049 (top) & 2070-2099 (bottom). The solid (red) line shows the baseline levels (1961-1990) & the thin green lines the different RCM ensemble member projections
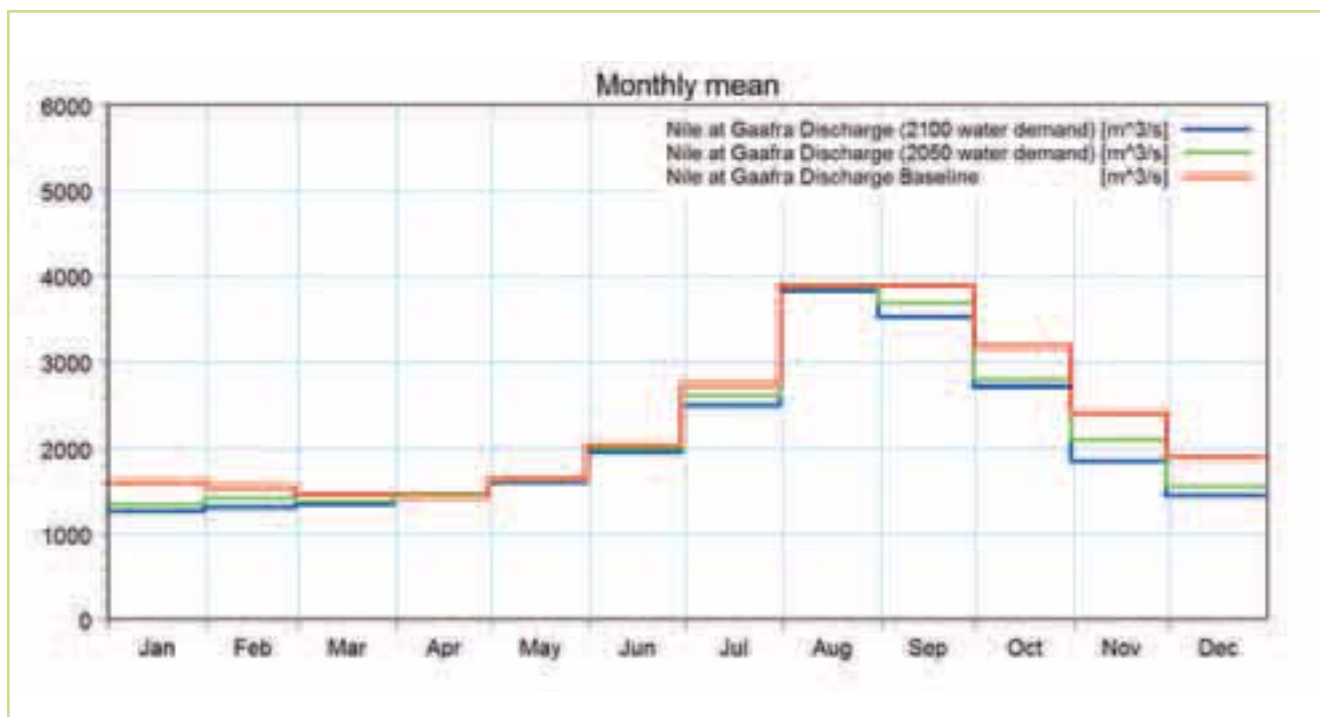
Figure 3. Mean monthly discharges for the Gaafra (El-Ga'Afra) gauge for baseline, 2050 & 2100 water demand scenarios

the 2020-2049 projections with both increases and decreases in simulated flows in July. The 2070-2099 projections show consistently higher flows, with some ensemble members showing significant increases, but their variation across the ensemble are large. This is consistent with previous studies (e.g. Elshamy et al., 2009) that indicate that the Blue Nile is extremely sensitive to small changes in rainfall and PET. Since relatively small changes in either rainfall or PET are amplified in the flow calculations by the developed hydrological models (which are based on a limited amount of available data, with low spatial and temporal resolution for this region), these projections are uncertain and should be interpreted with caution.

Climate adaptation measures in this region will have to consider both increases and decreases in the high flow range. Increases in flood risk can be expected with increasing high flows.

Main Nile

The main influences on the water resources in this part of the Nile are expected to be the changes in climate upstream and the extraction of water for irrigation, industrial and domestic demands. The Ethiopian highlands alone contribute about 86% of the annual flow to the High Aswan Dam in Egypt. Any changes in the high flows will be the direct result of changes in the Blue Nile and to a lesser extent in

the Atbara. The lows flows, outside the peak flow season, are expected to be influenced by changes in the White Nile flows.

The Gaafra station represents flows downstream between the Aswan Dam and the coast. The simulations using the 2020-2049 water demand projections show significant reductions throughout the year, with the exception of April-June (Figure 3). The 2070-2099 projections amplify these reductions. Reductions in the peak flows (August-September) range from 6-16 %. Reductions in the low flows (January-February) range from 7-15%. It should be noted that the projected water demands are highly uncertain and it was not possible in this project to reliably quantify this uncertainty.

Comparison with the range of flow simulations from the RCM climate projections (Figure 4)) show that the flow changes for the 2020-2049 period are likely to be dominated by the increase in water demands and increasing water stress. Even for the RCM projections with the largest increases in flow, the magnitude of the water demands will still exceed these increases in some months. The changes in flow due to climate change at this site during should be viewed with some caution as the reference period includes flows during the construction of the High Aswan Dam and some two years where the actual operation of the dam appears to be different from the operation in the hydrological model. Furthermore, these figures represent changes in the mean flow.

Vulnerability to water stress in dry years or a sequence of dry years will be even larger. Future work should address this issue of dry year sequences, but a robust assessment is likely to require analyses of data for 50 year periods.

For the far future projection a general increase in flow is projected. However, the large variation among the projections and the larger degree of uncertainty in the ability of the model to represent the reservoir-controlled flows prohibits clear-cut conclusions.

Estimates of projected population for Egypt for 2050 range from 115 to 179 million which indicate how uncertain the future water demands may be, with consequences on water stress in all sectors, including food production. Agriculture consumes about 85% of the water resource and contributes 20% of GDP in Egypt making it highly vulnerable to changes in Nile flows.
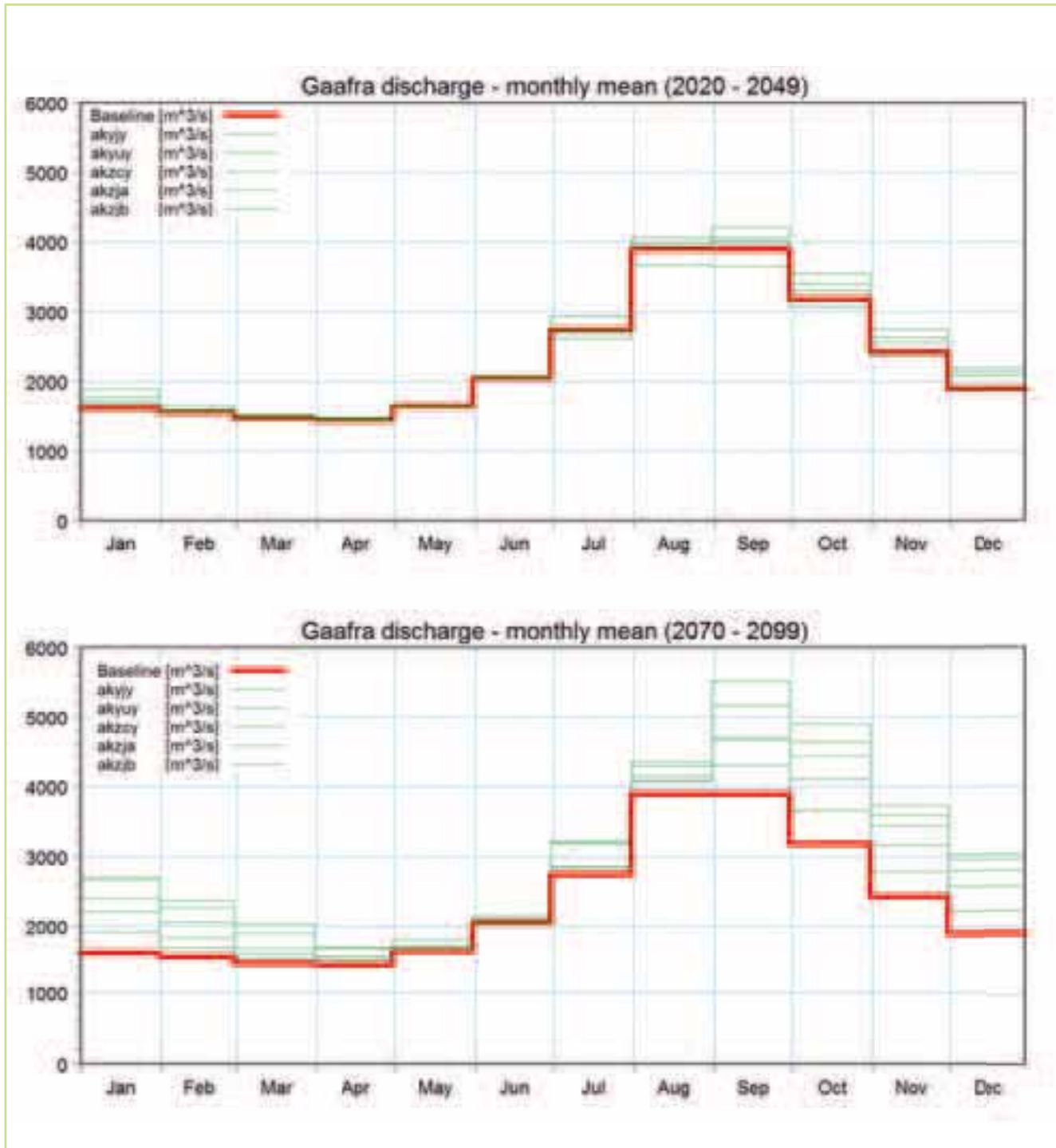
Figure 4. Projected changes in the average monthly flows for the Nile at Gaafra (El-Ga'Afra). Projections are shown for two periods; 2020-2049 (top) & 2070-2099 (bottom). The solid (red) line shows the baseline levels (1961-1990) & the thin green lines the different RCM ensemble member projections

Recommendations

While a number of recommendations are made in throughout the report, the key recommendations can be summarised as:

- Improve the availability and consistency of socio-economic data to allow socio-economic evaluations to be incorporated into the water resources analyses.
- Assess the impact of current and planned water infrastructure (reservoirs, irrigation schemes, etc.) development and their impact on water supply deficit
- Quantify the uncertainties in water demand projections.
- Future work to assess the impact of climate change on rain-fed agriculture and on crop water demand
- Incorporate the models developed here into the Nile Decision Support System (DSS) to support the evaluation of alternative measures for water resources management and climate adaptation.
- Incorporate additional data to further improve the regional hydrological models or sub-models.
- Improve hydro-climatic observation data (and access to this data).

Main conclusions

The water resources in the Nile River Basin are strongly linked to the flows in the river. One of the unusual characteristics of the basin is the contrast between the size of the basin and the relatively small volume of runoff, compared to other large basins.

This characteristic means that the flow in the Nile is sensitive to changes in precipitation and therefore climate change. The effects of climate variability, principally rainfall variability, in the Ethiopian highlands and Lake Victoria Basin, are known to have caused significant inter-annual and inter-decadal variability in Nile flows.

From the flow projections derived here we can see that both future water demands and climate change will have significant impacts in the basin but in different parts to different degrees. For the

White Nile, reductions in the precipitation and flows are projected for the near future 2020-2049 which is an important time horizon for the planning and implementation of infrastructure projects. It should be noted that the RCM in the "short" rainy season (October, November and December) seems to over-estimate the projections, exhibiting a strong positive bias directly over Lake Victoria. A clear trend for the 2070-2099 is not found for the White Nile. The reverse is the case for the Blue Nile. No clear trend is found for the 2020-2049 horizon while the climate projections for the far future 2070-2099 indicate a consistent increase in precipitation and therefore flows over this region. However, the uncertainty in these projections is large and should be viewed with caution.

The water demand projections have the largest impact at the regional scale on the Main Nile where the existing demands are largest. Our results indicate increasing water stress however the quantification of the future demands are highly uncertain and increasing irrigation efficiency, changes in cropping practices and the variability in population growth estimates can all affect these estimates.

Uncertainty is a major issue in climate change studies and important information for climate adaption decision-making. We have addressed this in a number of ways, both reducing and quantifying some of the largest contributions to uncertainty. However, it not feasible to quantify all aspects of uncertainty in both the flow and climate projections and there will always be a risk of future climates outside the range of futures simulated by current climate models.

It is recommended that in order to achieve its full potential the regional hydrological model and assessment framework developed for this study be taken up by NBI and incorporated in the Nile DSS to assess water resource management and climate adaptation scenarios. Finally, the assessment framework tool developed in this project could have important implications for planning and assessing the potential impacts of climate change adaptation measures in other basins, particularly large transboundary basins.

1.0 Introduction

This document is a contribution to the United Nations Environment Programme (UNEP) project "Adapting to climate change induced water stress in the Nile River Basin"[3]. It summarises the technical developments and assessments carried out under work package (WP) 1.1 "Comprehensive Assessments of Flood and Drought Prone Areas" by DHI and the UK Met Office in collaboration with the Nile Basin Initiative (NBI)[4].

The project was launched in March 2010 as a partnership between UNEP and the Nile Basin Initiative (NBI), sponsored by the Swedish International Development Cooperation Agency (SIDA). The overall project goal is to build the resilience of ecosystems and economies that are most vulnerable to climate change induced water stress in the Nile Basin countries through building key adaptive capacity and piloting adaptation in "hotspots" with technical, policy and financial interventions.

The focus of "WP1.1 Comprehensive Assessments of Flood and Drought Prone Areas" has been to develop projections of climate change and water demand in order to assess projected changes in water stress, related to both floods and droughts. These assessments are then used to derive information to support and inform decision-making for climate adaptation at the regional scale, i.e. at the scale of the Nile Basin rather than the national or local scale. By linking these assessments to climate change adaptation science and policy this study will provide appropriate information to inform decision-making for water resources management under a changing climate.

1.1 Nile River Basin

The Nile basin is one of the most critical and perhaps most important shared water basins in Africa, hosting 25% of Africa's population (SEDAC, 2010) while accounting for only 10 % of its landmass. The Nile is a crucial resource for the economy of eastern and north-eastern Africa. Agriculture, energy production and livelihoods in general, all depend strongly on the river. Surrounding Lake Victoria in Kenya and Uganda, in the Ethiopian highlands surrounding the Blue Nile, and along the banks of the Nile in Egypt in the Nile Basin are considered as the three highest population concentrations in Africa (UNEP, 2010). Managing and developing the water resources within the basin must not only address different water uses but also the trade-off between developments upstream and water use downstream, often between countries. In addition, the region is facing rising

[3]http://www.unep.org/climatechange/adaptation/EcosystemBasedAdaptation/NileRiverBasin/tabid/29584/Default.aspx
[4]Project Contract Agreement between UNEP and DHI, Feb 2011.

levels of water scarcity, high population growth, watershed degradation and loss of environmental services. Any future changes in the water quantity and quality and their distribution in space and time will have important impacts on the local and basin-wide economies and environment. It is important therefore to obtain quantitative assessments of projected changes in climate and water demand as the basis for water resources management and climate adaptation strategies.

To understand the challenge of managing water resources within the Nile, it is necessary to examine the complex geography and hydrology of the basin. The Nile River is the longest river in the world (approx.

6,800 km (UNEP, 2010)) and is located in the east of Africa (Figure 1.1). It extends from approximately latitude 4°S to 32°N, and from longitude from 23° to 40°. In part due to the large range in latitude, the Nile basin's climate varies significantly from extreme aridity in the north region including Egypt and Sudan to the tropical rainforests in Central and East Africa and parts of Ethiopia. Furthermore, there are significant differences in the wet and dry period distribution over the Nile, with some of the areas in the tropical region of Nile Basin having two rainfall seasons. Due to its size and varying climate and topography, the Nile Basin constitutes one of the most complex river basins.

The distribution of the precipitation over the basin can be categorised into two distinct areas; the Equatorial (or East African) lakes and the Ethiopian highlands (Figure 1.2) and these are the most important contributions to the flow (Sutcliffe and Parks, 1999). As a result, one of the unusual characteristics of the basin is the contrast between the size of the basin and the relatively small volume of runoff, compared to other large basins.

This characteristic of the basin means that the flow in the Nile is sensitive to changes in precipitation, which in turn means that there is great variability in runoff from year to year. The effects of climate variability, principally rainfall variability in the Ethiopian highlands and Lake Victoria, are shown to have caused significant inter-annual and inter-decadal variability in Nile flows with major implications for water resources in Egypt (Conway, 2005).

While the historical variability is well studied, the implications in terms of the potential effects of future climate changes is less well known, though the Nile is expected to be critically sensitive to such changes (Conway, 2007). Several previous studies (e.g. Strzepek et al, 1996; Milly et al. 2005, Elshamy et al., 2009, Beyene et al., 2010) have examined the impacts of climate change on the temperature and precipitation across the region and the subsequent effects on flows within the Nile. For temperature, the current consensus seems to be that warming trends are expected, but projections for precipitation are much more variable. As a result, projections of changes in flows in the Nile due to climate change are associated with a large degree

Figure 1.1 Overview of the Nile Basin & the ten major sub-basins referred to in this report

of uncertainty. This uncertainty is inherent in climate projections and must be addressed and preferably quantified when assessing the impact of climate change on water resources and in developing climate change adaptation strategies. This assessment proposes an operational methodology to quantify part of this uncertainty. However a complete assessment of all contributions to the uncertainty is an extremely demanding task that continues to be the subject of a substantial amount of research effort in the climate community.

1.2 Climate adaptation at the regional scale

Climate adaptation is the process or outcome of a process that leads to a reduction in harm or risk of harm, or realization of benefits, associated with climate variability and climate change. The main focus of this study has been to develop relevant information for climate adaptation to water stress (floods and water scarcity) in the Nile Basin for 1) integration in policy making and 2) implementation of adaptation measures. These are both new disciplines and there are no accepted methodologies. Only recently, for example, has the European Union published a European framework for action related to adapting to climate change at the European level, (EU, 2009). Many national adaptation strategies are currently at an early stage.

A schematic of the adaptation process for water resources is shown in Figure 1.3 (Butts et al., 2010). The first three steps define the impact of climate change on water resources. The final step is in fact an iterative process where different options are explored. There are many different options for climate adaptation and their assessment in relation to both water resources and the corresponding cost-benefit analysis. Typical adaptation measures for floods and droughts are listed in Table 1.1 and Table 1.2, respectively. For floods, Butts (2000), listed a number of measures for flood mitigation split into structural and non-structural approaches (Table 1.1). For droughts and water scarcity, IPCC (2008) split climate adaptation measures into supply-side and demand-side options (Table 1.2).

While the tables presented here are by no means comprehensive, they illustrate the breadth of possible measures. This has some important consequences for the approach adopted in this study. Firstly it would not be possible to cover or assess all possible adaptation measures. Secondly, because of the wide range of choice, adaptations in particular sub-basins must be selected based on
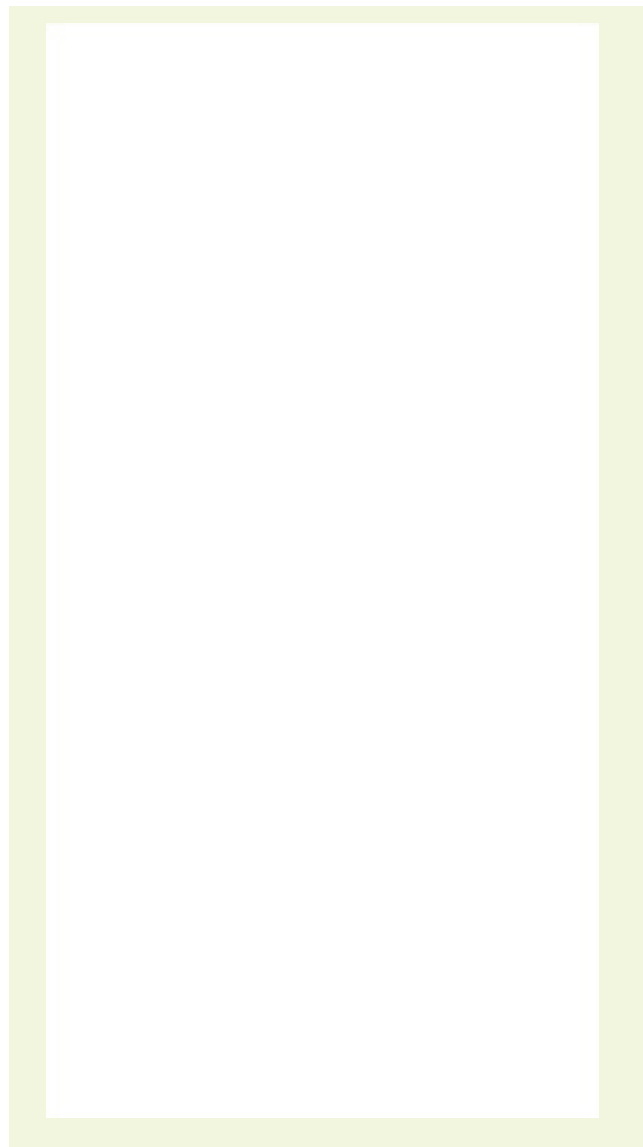
Figure 1.2 Distribution of annual rainfall over the Nile Basin (Source Africa Water Atlas, UNEP 2010)

what is feasible and appropriate for that particular sub-basin. It is therefore a good strategy to focus on a few carefully chosen demonstration sites and appropriate adaptation options. Finally, and perhaps most importantly for this project, different measures can be implemented, and will impact at, many scales, from local, to national, to regional (basin) (Figure 1.4). The range of potential interventions is large and the cost-benefit trade-offs amongst these options are complex.

The goals of this study are the provision of information and tools to inform climate adaptation at the regional scale. The motivation for this is the clear perception that tools to assess climate adaptation at the regional scale are missing. This is clearly a key gap in the current capability and knowledge. Adaptation measures, for example for floods, range from structural measures such as construction of embankments, flood diversion channels and reservoirs to non-structural measures

such as zoning controls, flood forecasting and flood preparedness. Some of these, like the construction of flood protection embankments, are implemented locally and have only local impacts. However, many measures, such as the construction of reservoirs or raising river banks upstream, can have regional impacts downstream. This is even more critical for transboundary basins, such as the Nile, where the implementation of national adaptation measures may have important downstream regional implications. Therefore, for improved water management at the regional scale, there is a need to provide tools to inform decisions regarding climate adaptation at the scale of the entire Nile Basin region and the overall approach adopted here is to develop and apply a regional scale framework for the assessment of climate change effects and adaptation.

1.3 Floods, high flows, droughts & water scarcity

Globally, the most recent analyses of observational records and climate projections provide abundant evidence that water resources are vulnerable and have the potential to be strongly impacted by climate change, with wide-ranging consequences for human societies and ecosystems (IPCC, 2008). Floods and droughts are the most prevalent and costly natural disasters (UN, 2003). In addition to the potential loss of life, flooding can cause substantial damage to crops and infrastructure. Droughts will directly affect the availability of water and food security for both rain-fed and irrigated agriculture. AR4 concludes that "Increased precipitation intensity and variability are projected to increase the risks of flooding and drought in many areas". Therefore it is natural to initially focus on floods and droughts in formulating a regional climate adaptation strategy as proposed in the objectives of this study.

While floods and droughts can both be viewed as water-related natural disasters based on extreme meteorological events they have quite different spatial and temporal scales. Droughts generally cover large areas that may include several basins and/or countries and occur over longer time scales (weeks to months). On the other hand, floods are generally more local, but can range from localized floods in urban areas, to extensive flooding over large-scale basins and occur predominantly at time scales of hours to days. These differences are important to bear in mind for this project as they will determine the time and space scales for the data and models required. For example water scarcity can be modelled using data and models at a monthly time scale, however floods should be modelled at daily or smaller time scales.

The terms droughts and water scarcity are often used interchangeably by laymen. Strictly speaking however, droughts can be considered as a temporary decrease of the average water availability and are therefore related to variability in climate and water demands. On the other hand water scarcity refers to long-term water imbalances, combining low water availability with a level of water demand exceeding the natural recharge.

Furthermore, some authors distinguish between meteorological droughts (precipitation well below average), hydrological droughts (low river flows and low water levels in rivers, lakes and groundwater which may be caused by changing demands as well as a lack of precipitation), agricultural drought (low soil moisture), and environmental drought (a combination of the above).

Similarly there are several different types of inland floods, including flash floods which are the result of local heavy rains producing flooding with little or no warning in urban areas or small upland catchments, fluvial flooding etc. The impacts of catastrophic flooding are however often quite local and the detailed assessments of the impact of flooding using modelling, especially where high value urban infrastructure is at risk requires detailed information about the local rainfall, river cross-sections, flood plain topography, flow paths, land use, etc. This type of local flood risk assessment must then be combined with detailed local information on property values and damage curves to assess the economic consequences.

At the regional scale, flood modelling should address the high flow regime in the basin rather than detailed local scale representations of the inundation patterns. This is illustrated in Figure 1.5 which shows the sources of inflows to the Aswan dam. At this regional scale flooding is a long term seasonal event for much of the basin. In addition to this seasonal flood pattern there are of course local flood events caused by local heavy rainfall events. While both are important the focus of this work is at the regional scale. A comprehensive assessment of the impact of local flooding would require more detailed local hydrological modelling at higher spatial and temporal resolutions. The regional model developed here is expected to the starting point for future local scale modelling.

These considerations of the appropriate spatial and temporal scales are used in formulating the regional scale framework adopted in this study and outlined in the next section.

Global Climate Projections
- Long term global development scenarios
- Emission (SRES) scenarios
- Global Circulation models
- Climate change with low spatial resolution

Regional Climate Projections
- Downscaling to river basin and catchment scale (dynamical or statistical)
- Time series representing local climate change

Hydrological climate assessments
- Assessment of hydrological effect effects of climate change on
  - flooding
  - severity and frequency of droughts
  - water availability
  - groundwater recharge and salinity intrusion
  - irrigation demands and domestic and industural water supply
  - environment and ecosystems
- Time series representing the changed local hydrology

Evaluation and implement of adaptation measures
- Assessment of Social, Economic and Environmental impacts
  - size of population
  - impact on economic sectors: agriculture, industry, energy,water supply, transport, etc.
  - Integratioin of cllimate change effects in long term planniig
- Information, education, preparedness and warning systems
- Structual measures
  - reservoir construction, design of infrastructure, more resistant crop type,s, allternative water sources, etc
- Non-structural measures
  - Water demand management, water reuse,. land use changes, resource savings, etc.

Figure 1.3 The climate change adaptation process for water resources systems (Source: Butts 2010)

Structural	Non-structural
Dikes	Zoning controls
Polders	Regulation of construction on flood plains
Flood Diversion channels	Flood proofing
Real time monitoring networks	Flood forecasting
Control structure e.g. gates	Optimization of reservoir and structure operations
Pumps	Flood preparedness
Reservoirs	Public education
	Flood insurance

Table 1.1 Climate adaptation measures for floods (Modified from Butts, 2000)

Table 1.2 Climate adaptation measures for water scarcity (IPCC, 2008)
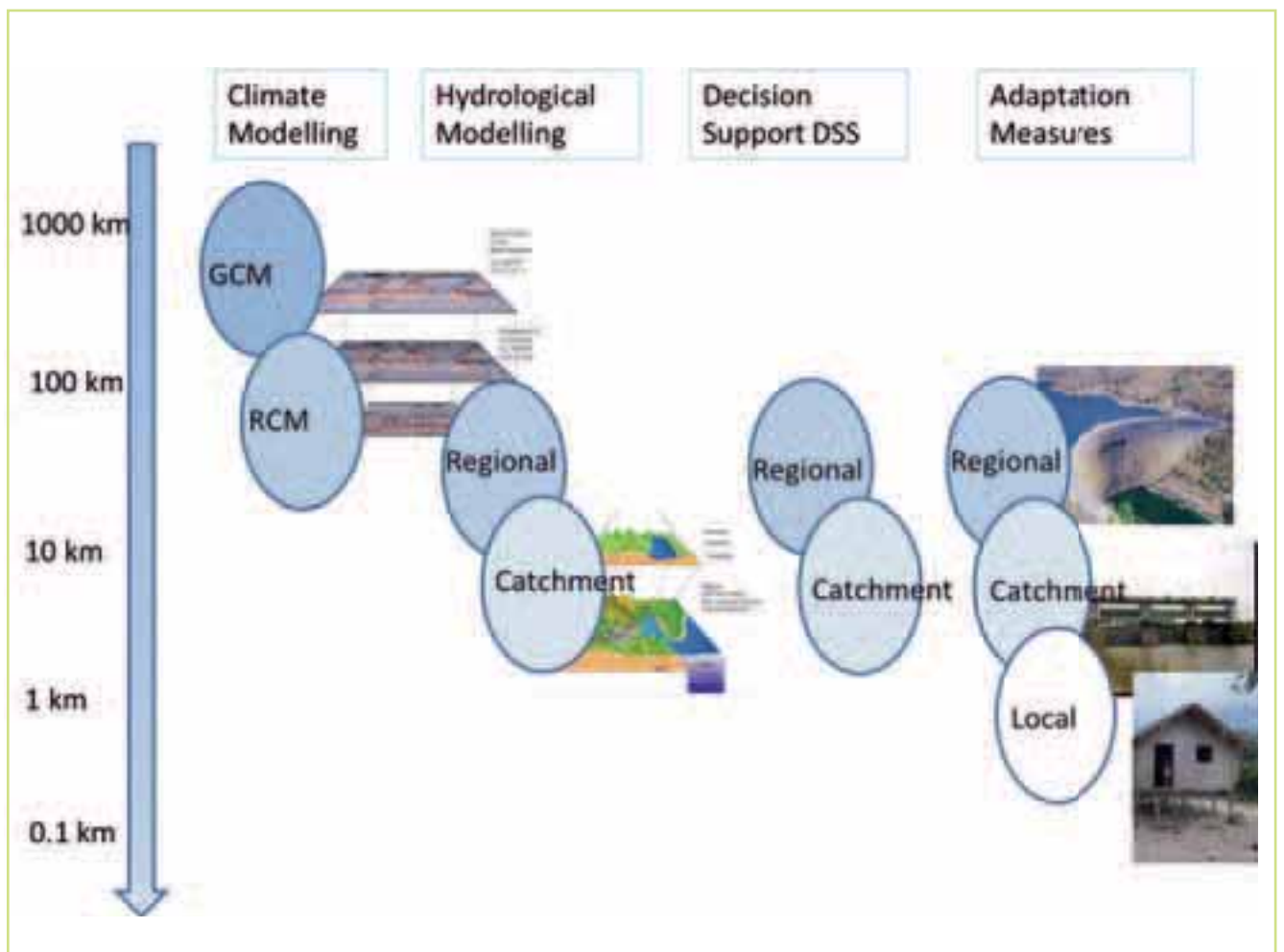
Figure 1.4 Spatial scales for climate modelling, hydrological modelling, decision-making & implementation of climate adaptation measures
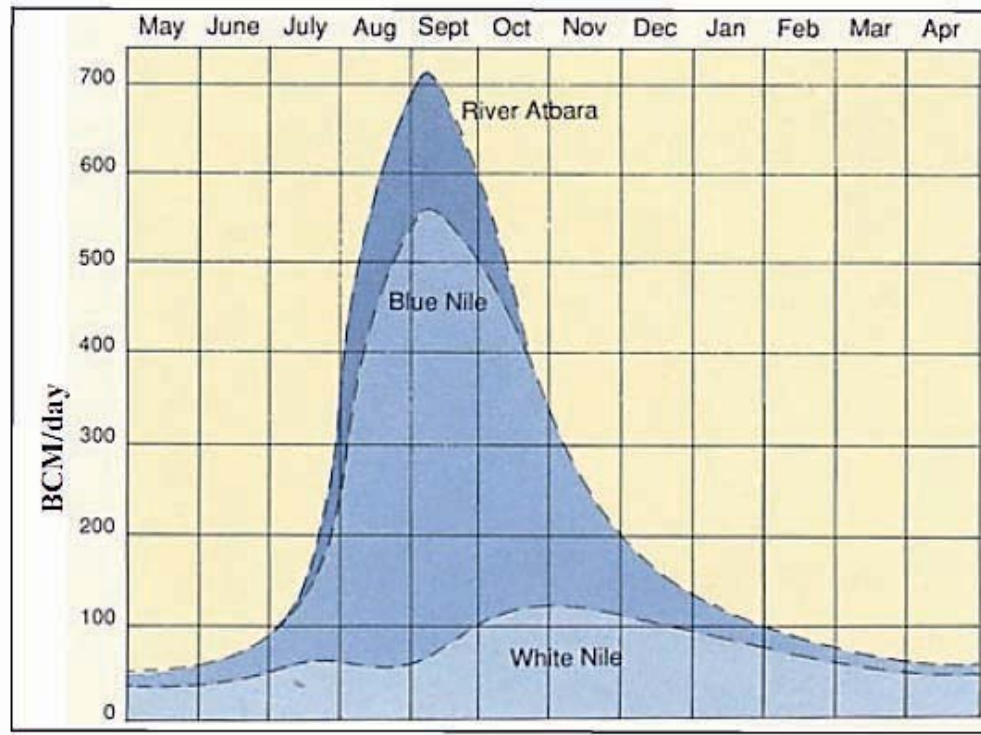
Figure 1.5 Sources of flow into the Aswan dam [BCM/ day] (Source: http://www.marefa.org)

2.0 Approach & methodology

The overall approach has been to develop and apply a regional scale framework for assessing climate change effects. This framework consists of combining regional scale climate modelling with hydrological modelling tool both to assess the impacts of climate change on the hydrology resources and to provide the capability to evaluate adaptation measures at the regional scale. This was motivated by the clear perception that such tools to assess climate adaptation climate at the regional scale are missing. This is particularly critical for transboundary rivers, such as the Nile where the water resources are shared between countries and where adaptation measures, depending on the type of interventions considered may have important implications downstream.

Here the concept of "hot spots" and in particular their scale is important. The original concept of this particular work package was concerned with the identification of "hot spots". The implication being that there are local areas with significant water resources, climate or other issues. While this is certainly the case in terms of for example population or local threat to water quality or ecosystem health, it became clear at the outset of the project that in terms of climate and water resources then the so-called "hot spots" identified were Egypt, the Blue

Nile, Sudan and Lake Victoria which are clearly much larger regions. As a result we have chosen to refer to these large scale "hot spots" as focus areas.

For the purposes of this study we will examine, the impacts of climate change and water demand scenarios at the regional scale and investigate particular aspects of the focus areas:

• The Equatorial Lakes basin
• The Ethiopian Highlands (Blue Nile and Atbara basins)
• The Egypt and Sudan water demand region.

2.1 General framework

The approach adopted here is based on a vulnerability assessment framework derived from an EU project called ATEAM (Advanced Terrestrial Ecosystem Analysis and Modelling). The advantage of the ATEAM methodology is that it provides an integrative framework for a wide range of potential ecosystem services and would provide a consistent approach not only for this study but for future applications as well. The methodology outlined below has been adapted and simplified from the ATEAM methodology (ATEAM, 2004). In particular, the ecosystem services to be addressed in this project

are limited to the water sector, focussed on floods and droughts and water scarcity. However, these have direct implications for agriculture, hydropower, etc. Furthermore, while vulnerability depends on adaptive capacity, estimating adaptive capacity is outside the scope of this particular study.

Vulnerability is defined as the undesirable state of being open to damage. By assessing future vulnerability under different scenarios this unpleasant state can perhaps be avoided by adaptation measures. ATEAM defined vulnerability as a combination of 3 elements:
• It's exposure to 'global' change
• The sensitivity of the ecosystem service to that change, and
• The adaptive capacity of the sector which relies on the ecosystem service.

Exposure and sensitivity of a region result in potential impacts which may to a certain extent be avoided or modified by adaptation. The last component is an assessment of the ability of that sector to react to changes and is highly dependent on a number of socio-economic factors. Different sectors and different countries or areas will exhibit different levels of adaptive capacity. While such an assessment may be useful, it would require the collection or derivation of a large amount of socio –economic data and is outside the scope of the current project.

The ecosystem services relevant to this project for the water sector are:
• Water supply (irrigation, hydropower, domestic and industrial use)
• Drought and flood prevention

Indicators for these services identified in the ATEAM project were
• Runoff quantity
• Runoff seasonality (variability)
• Water resources per capita
• Drought runoff
• Flood runoff

These indicators need to be quantified in relation to climate change. For example a flood runoff index could be the max monthly flow.

2.2 Scenario-based methodology

The scenario-based methodology is outlined in Figure 2.1.

Two sets of scenarios are formulated:
1. Projection of future water demand driven primarily by estimates of population growth
2. Climate projections derived from regional climate models driven by anthropogenic effects.

Changes in water demand and climate are expected to have the largest impact on water resources in the region. The development scenarios considered here are an assessment of changes in water demand over three sectors; agriculture, industry and domestic/municipal water supply. The climate projections are based on an ensemble of regional climate model simulations based on the SRES emission scenario (A1B). A detailed description of these two sets of scenarios is given in sections 3 and 6.

For both climate change and water demand, projections are made for the future time period: 2020-2049 and 2070-2099 allows a comparison
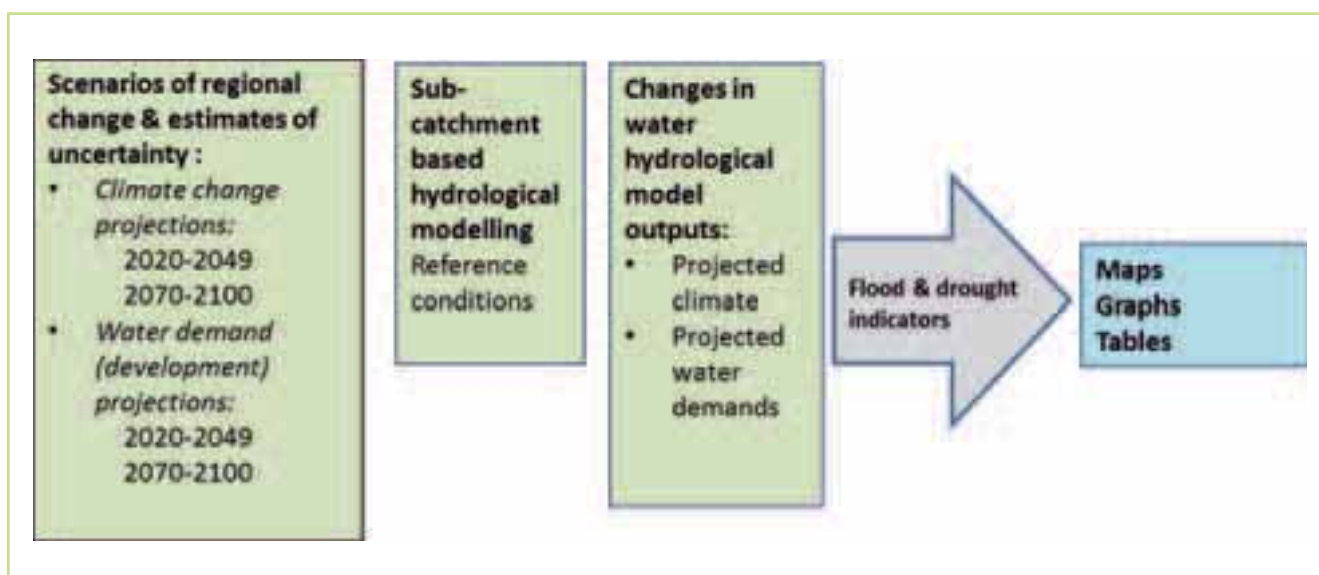
Figure 2.1 Schematic of the scenario-based methodology

of the relative impacts of climate change and increasing water demand. This selection also means that the climate change results developed here can be more directly compared to the global climate projections from IPCC. For the same reason the baseline or reference period used for the climate change downscaling is 1960-1989.

2.3 Regional climate modelling

The regional climate modelling performed here is based on dynamical downscaling from Met Office Hadley Centre global climate model to the regional climate HadRM3P (PRECIS). The climate model simulations are run from December 1949 to November 2099 at a 50 km resolution. The regional climate modelling presented here represents a completely new set of 5 regional climate simulations carried out for the project. Originally, it was proposed that this would simply be covered by the provision of an existing set of change factors, derived by DHI and UK Met Office for the project: "Regional Climate Modelling of the Nile Basin-Preparation of climate scenario outputs for assessment of impact on water resources in the Nile Basin", for UNEP and the Ministry of Water Resources and Irrigation (MWRI), Egypt.

The provision of a new set of PRECIS RCM simulations is a significant new undertaking and it is of course time-consuming to perform 5 new climate simulations covering 150 years. This has however also provided some innovations with respect to the earlier work. The key advances incorporated in these simulations are:

- New methodology for selecting GCM ensemble members to drive the RCM runs, which gives a better representation of uncertainty in the climate modelling
- New land surface scheme describing the exchange of water between the atmosphere and the land surface
- Investigation of an improved treatment of the climate of Lake Victoria based on Sea Surface Temperatures
- Extension of the climate simulations beyond 2050 to the end of the century (2100)

The result is a set of 5 selected RCM simulations chosen both to give the best possible representation of the current climate while capturing the variability exhibited by the full 17-member QUMP ensemble, see section 3.6. On the basis of these new RCM simulations the UK Met Office have derived the change factors for all 5 ensembles, for temperature,

potential evapotranspiration and precipitation and for two periods 2030-2049 and 2070-2099.

2.4 Water demand (development) scenarios

The water demands of three sectors are considered:
1. Agricultural: considers both groundwater and surface water withdrawals for irrigation.
2. Industry: considers water withdrawals for industrial use for self-supplied industries not connected to the public distribution network
3. Municipal: considers total water withdrawn by the public distribution network. It can include industrial withdrawals from the municipal network

The projections of current and future water demands are based on FAO (FAO, 2011a). These provide the most comprehensive and up-to-date data available on agricultural water demands for the Nile basin. This uses a 2005 baseline which is also used here as the baseline or reference case. Projected water withdrawals for irrigation are also derived from the same source. Significant expert judgement was involved in producing the projected withdrawals provided for 2030 and 2050. A conservative approach was adopted here using the 2050 figures throughout the period 2020-2049 and simple extrapolation to 2070-2099.

The industrial and domestic/municipal water demands were derived from AQUASTAT (2012) and national population data is downloaded from UNDESA 2010 to derive per capita values. Population projections were then used to estimate the future water demands. Changes in the spatial distribution of these water demands were neglected.

2.5 Regional hydrological modelling

The regional scale modelling over the Nile Basin has been carried out using the MIKE BASIN/MIKE HYDRO hydrological modelling tool. This choice was in part motivated by the implementation of this tool in the Nile Basin DSS. MIKE BASIN consists of a routing component and a sub-basin based rainfall-runoff component. The use of a sub-basin discretization is useful for modelling large basins where the data coverage is highly variable as the size of the sub-basins can be adapted to mount of data available. MIKE BASIN is well-suited to regional scale adaptation as it includes facilities for representing reservoirs and their operation, water users, water transfers, different types of irrigation and demands. MIKE HYDRO is the next generation

of MIKE BASIN and has the same numerical engine as MIKE BASIN but a completely new user interface. The regional models has been developed in MIKE BASIN and afterwards converted into MIKE HYDRO,

2.6 Indicators

Water indicators can be used for example to understand the current state of water resources, the changes in these resources and whether or not our interventions in a river basin produce the desired effect. A detailed review of the indicators in the literature has been carried out that highlighted the fact that there are potentially many such indicators. This is particularly the case for the socio-economic and sector-specific indicators not assessed in this study.

Since the main aim is to determine suitable indicators that could be applied to an assessment of the vulnerability to water stress (floods and droughts) to climate change at the regional scale, a set of selection criteria were used to define a suitable subset. The key selection criteria were:
- Need to reflect vulnerability to floods and drought to climate change
- Based on available and reliable data sets

- Reflect the data availability spatial coverage and temporal frequency in the observation data sets
- Appropriate at the regional scale
- Indicators representing similar characteristics are not replicated
- Can be applied as input to other indicators in the different water-related sectors.

Based on the these criteria the following indicators are proposed for this project
- Regional climate model consensus to reflect the climate projection variability
- Climate Moisture Index (CMI) as an aggregate measure of potential water availability imposed solely by climate
- Climate Moisture CV useful for identifying regions with highly variable climates as potentially vulnerable to periodic water stress and/or scarcity
- Average Monthly runoff at the key discharge stations for annual and seasonal changes in flow regimes
- Flow duration curves to assess changes in high and low flow distributions
- Water demands current and future (2030-2050) for domestic, industrial and agricultural purposes.

3.0 Regional climate change & modelling

The first step in a quantitative assessment of the impacts of climate change on water resources (Bates et al, 2008; DHI 2012) is the use of climate model projections based on Global Circulation Models (GCMs) and/or Regional Climate Models (RCM's). The 4th IPCC assessment (IPCC, 2007a, 2007b, 2007c) represents the current benchmark for climate change impact, adaptation and vulnerability (CCIAV) assessment and the 5th IPCC assessment is already underway (http://www.ipcc.ch/).

This chapter describes in detail the regional climate modelling approach used in this project. There are several innovative aspects to this work that should be highlighted. Firstly results are based on the novel "perturbed physics ensemble" method pioneered by the UK Met Office. This ensemble-based approach does not rely on a single model simulation but seeks instead to represent a range of climate model projections. Secondly, the results presented here are based on a completely new set of regional climate projections, not originally envisaged as part of this project and which completely replaces and improves

earlier work, Buontempo et al (2011). This provides the project with the most recent PRECIS RCM model simulations in the region and the results are also being formulated as journal papers (Buontempo et al, 2013a & b; Butts, Buontempo et al., 2013). It also involves the application of methodology for more effectively selecting ensemble members (McSweeney et al, 2012), some modification of the land surface scheme was introduced in the regional model and a novel treatment of the climate of Lake Victoria was also introduced. Furthermore, projections of the previous work (Buontempo et al., 2011) extend only to 2050, whereas these new simulations extend the PRECIS RCM climate projections to 2100.

3.1 Emission scenarios

Climate projections depend on future emissions which in turn depend on human interventions. It is common therefore to present projections that are conditional on scenarios, such as those detailed in the Special Report on Emissions Scenarios (SRES) (Nakicenovic

et al., 2000). In fact, there are three main sets of climate forcing scenarios; SRES scenarios, non-SRES scenarios and more recently Representative Concentration Pathways (RCP) scenarios.

There are 40 SRES scenarios grouped into four families (A1, B1, A2, B2) based on narratives of demographic, social, economic, technological, and environmental development. Of these, there are 6 widely used illustrative scenarios: A1B, A1F1, A1T, A2, B1, B2 (Table 3.1). The global greenhouse gas emissions and the corresponding projected increase in global surface temperature for the six SRES scenarios are shown in Figure 3.1. More information on SRES scenarios can be found in the IPCC Special report on emissions scenarios. (http://www.ipcc.ch/pdf/special-reports/spm/sres-en.pdf).

Studies which have focussed on comparing climate model projections have typically limited the number of scenarios used. This reduces the number of climate model runs as these simulations are computer resource-intensive and time-consuming. No single scenario has been developed as the "most likely" option, but rather the scenarios are designed to show the range of possible trajectories. If the focus is on changes in (air) temperature, differences between scenarios are small up to around 2050, depending on the region. In this case it may be sufficient to include only one scenario in the analysis. For longer projection horizons it is generally recommended to include more scenarios, e.g. median, low and high scenarios, which cover the range of scenarios. If focus is on changes in precipitation, differences between scenarios are, in general, smaller than differences between different climate models. In this case it may be sufficient to consider only one scenario up to 2100, depending on the region.

In this study the A1B emission scenario is used. A1B is a "business-as-usual" scenario which contains no mitigation and is a widely used reference. Only one emission scenario was used for three main reasons:1) The major differences between the emission scenarios are mainly seen after 2050, while the differences between scenarios are relatively small until 2050 which was the original scope of this study, 2) RCM simulations are very time consuming, and it was only possible to run one emission scenario within the current project framework, 3) as noted above the variation between climate models are often larger than the variations between scenarios and we are using a novel "perturbed physics ensemble" to represent these climate model variations.(Figure 3.1).

Non-SRES scenarios are not based on narratives but simulate various changes in concentrations. The Representative Concentration Pathways (RCPs) are the latest scenarios developed for the next IPCC assessment. There are 4 RCP pathways shown in Table 3.1. These are based on a range of radiative forcing scenarios rather than emissions. They provide a wider range of futures than the previous scenarios (Van Vuuren et al., 2011; Moss et al., 2010). A comparison of the CO_2 emission rates for the RCP scenarios with the emission rates for the
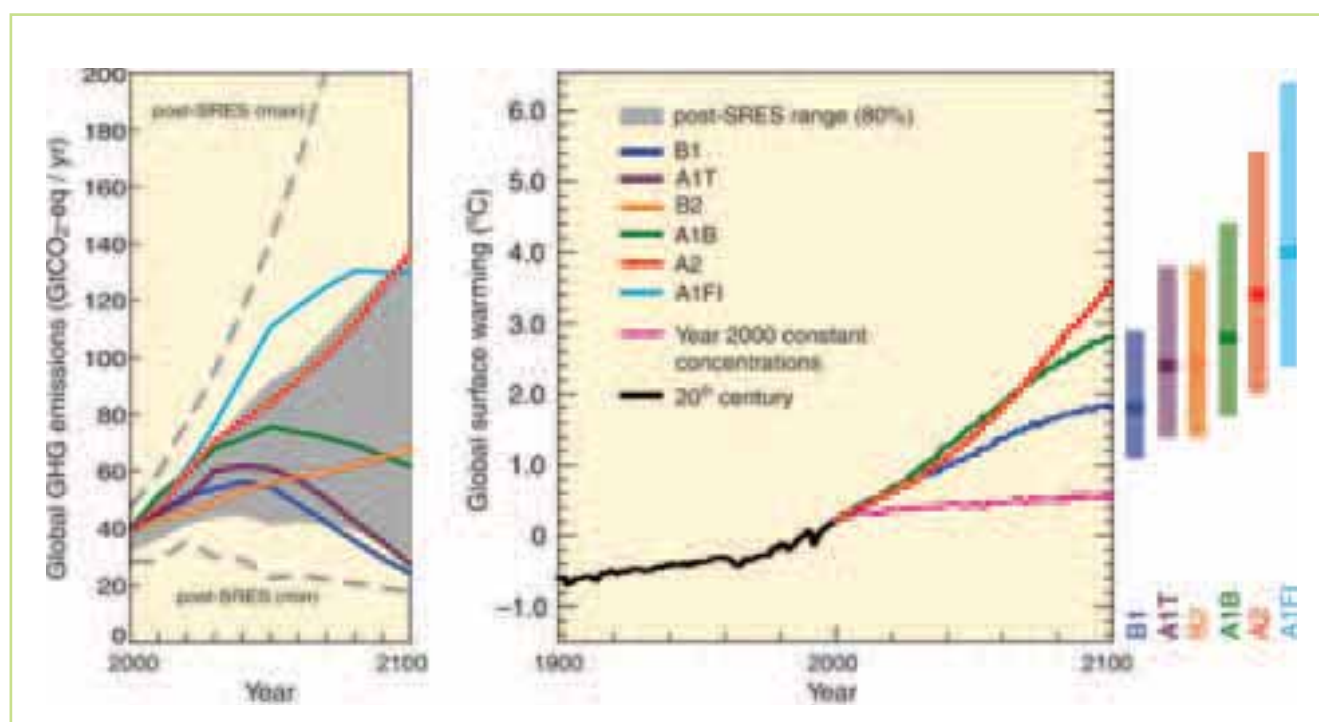
Figure 3.1 The range of global greenhouse gas emissions (left) & corresponding global warming (right) for different SRES scenarios. The bars on the right show the likely range of temperature increase in 2100 (relative to the period 1980-1999). Source: IPCC AR 4 report (http://www.ipcc.ch/publications_and_data/ar4/syr/en/contents.html)

SRES scenarios B1, A1B and A2 is given in Figure 3.2. The RCP6.0 scenario has similar emission rates to the A1B scenario and will allow comparison of the results of this study with future work using the RCP scenarios.

3.2 Regional & global climate modelling

Many current analyses of the impacts of climate change on water resources are based on Global Climate Models (GCMs). While GCMs are successful in simulating many features of present day climate and climate variability, the projection of robust regional changes in climate over the next 50 years still presents a considerable challenge for the current generation of climate models and this is still a rapidly developing field.

While their resolution continues to improve the current generation of GCMs is often too coarse to provide reliable estimates of localised changes or feed directly into local impact models. This is the case for hydrological processes where an accurate descriptions

of both orography and land use are essential to correctly capture the important hydrological elements of the water cycle, precipitation and evapotranspiration. GCM's generally are not designed for the application

Table 3.1 The main climate forcing scenarios & their assumptions

Scenario	Assumptions (Source IPCC website)
The SRES scenarios	
A1B	A future world of very rapid economic growth, low population growth and rapid introduction of new and more efficient technology. Major underlying themes are economic and cultural convergence and capacity building, with a substantial reduction in regional differences in per capita income. In this world, people pursue personal wealth rather than environmental quality. Energy technologies balanced across energy sources
A1FI	As A1B but with fossil-intensive energy technologies
A1T	As A1B but with predominantly non-fossil energy sources
B1	A convergent world with the same global population as in the A1 storylines but with rapid changes in economic structures toward a service and information economy, with reductions in materials intensity, and the introduction of clean and resource-efficient technologies
A2	A very heterogeneous world. The underlying theme is that of strengthening regional cultural identities, with an emphasis on family values and local traditions, high population growth, and less concern for rapid economic development
B2	A world in which the emphasis is on local solutions to economic, social, and environmental sustainability. It is again a heterogeneous world with less rapid, and more diverse technological change but a strong emphasis on community initiative and social innovation to find local solutions
RCPs	
RCP8.5	Rising radiative forcing pathway. Leading to 8.5 W/m2 in 2100
RCP6	Stabilization without overshoot pathway. Leading to 6 W/m2 at stabilization after 2100
RCP4.5	Stabilization without overshoot pathway. Leading to 4.5 W/m2 at stabilization after 2100
RCP2.6	Peak in radiative forcing at about 3 W/m2 before 2100 and then a decline

of hydrological response to climate change. The hydrological surface runoff processes are often highly simplified, without lateral flows on the land surface (Xu, 1999) and simplified representation of the subsurface. The spatial and temporal scales of GCM's are considerably larger than those used in hydrological modelling. The spatial patterns (Salathe, 2003) and variability in daily precipitation (Burger and Chen, 2003) are not adequately represented. The reliability of GCM output deceases with increases in temporal and spatial resolution and the representation of extremes is poor (Huth et al., 2003, Fowler et al. 2005). This is particularly the case for precipitation.

One widely applied method for achieving higher resolutions from global projections is to a use a regional climate model (RCM). This is sometimes referred to as dynamical downscaling, (Fowler et al., 2007) as dynamical boundary conditions from a GCM are used to drive the higher resolution RCM. In general, dynamical downscaling is well suited to simulating regional scale climate such as orographic precipitation and land-sea contrasts or regional scale effects such as those associated with the El Nino. A number studies have shown that dynamical downscaling improves predictions of regional climate (Leung et al., 2003; Frei et al., 2003, 2006; Fowler et al., 2005). Furthermore since they improve the description of meso-scale precipitation processes they can also simulate more plausibly the climate extremes and variability at the regional scale. The control simulations are improved with more accurate extreme event statistics and variability and can be readily applied to geographical diverse regions and sub-regions. However there are limits to how high a resolution can be achieved at present controlled by the representation of cloud physics in the precipitation process but also by other factors, van Roosmalen et al. (2010).

The approach adopted in this study is to use lateral boundary conditions from the Met Office Hadley Centre HadCM3 global model to drive the regional model HadRM3P on the 50km resolution Africa CORDEX (Giorgi et al, 2009) domain. The improvement in resolution is illustrated in Figure 3.3 which compares the spatial resolution of the RCM used here and one of the IPCC GCM,s. The HadRM3P simulations were made with the MOSES (Met Office Surface Exchange Scheme Version) 2.2 tiled land-surface scheme (Essery et al., 2001). The RCM simulations were made from December 1949 to November 2099 for the A1B SRES scenario.
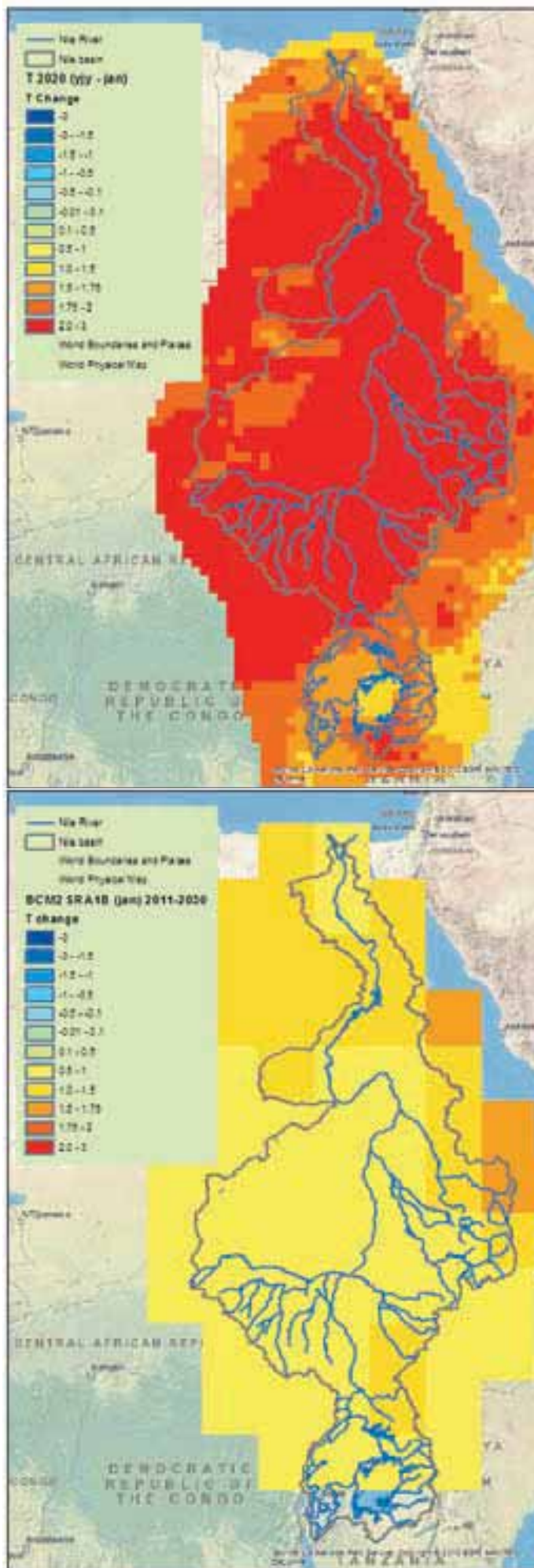
Figure 3.3 Comparison of the spatial resolution of temperature simulations from a regional climate model (top) & a global climate model (bottom) over the Nile Basin. Data courtesy of the UK Met Office

3.3 Ensemble modelling

It is now widely recognized within the climate community that assessments of climate change should be based on multiple model projections (ensembles) and their application in a probabilistic framework (Collins and Knight, 2007; Buontempo et al., 2011). This is motivated by the inherent uncertainty in climate projections. A single model simulation provides one representation of climate. However different GCM's project different responses to climate change (Giorgi and Francisco, 2000). This arises from the choice of which processes are represented and how they are represented including at what scale. For example in water resources applications an accurate representation of precipitation processes which range from convective systems (which can range in size from tens to hundreds of kilometres) to large-scale fronts may be difficult to achieve. One of the most challenging problems in both weather forecasting and climate modelling is the difficulty of accurately modelling cloud physics. This is due In part to the limits in our current understanding of how to represent the actual processes and in part because when representing these processes in a numerical grid, processes occurring at scales smaller than this grid (subgrid processes) must be approximated in some way. This leads both to biases in the model and to variations in the model simulations depending on, for example, how the cloud physics or land surface processes are represented in the different models. Similarly, the climate system depends on interactions, such as the interactions between the ocean and the atmosphere that are not fully understood or accurately represented in the models. These feedback mechanisms may amplify or suppress climate change impacts and different responses in climate will occur depending on how these feedbacks are represented. In some regions the different models even disagree on the sign of the changes in particular regions, (Giorgi and Francisco, 2000).

Recognising that there are numerous sources of uncertainty that affect the robustness and reliability of climate projections has led to the widespread use of ensemble modelling or probabilistic projections in an attempt to represent the range of likely future climates, (Collins and Knight, 2007). This has been possible in part due to the advances in computing power and in part by the availability of co-ordinated projects with the climate community (Palmer and Williams, 2008; UK Met Office 2009). While there exist methods for developing probabilistic predictions from a single model, such as fingerprinting (Allen et al., 2000, Stott and Kettleborough, 2002), the overriding view

is that no single "true" model can be found. Results from multiple global climate models (Benestad, 2004), multiple parameterisations of the same model (Murphy et al., 2004, Stainforth et al 2005) and multiple GCM-RCM combinations (Christensen et al., 2007, Hewitt, 2005) are now available and can be used to derive probabilistic predictions of climate change. These represent the current state of the art in terms of climate change assessment.

In this project the UK Met Office regional climate model HadRM3P (Jones et al., 2004) was run several times using different Global Climate model (GCM) members to provide driving lateral boundary conditions. This enabled the creation of an ensemble of regional (high resolution) RCM projections. As argued above, this is likely to be more informative than a simulation based on a single model projection. While there are a number of ways in which an ensemble of climate projections can be generated (e.g. multi-model ensembles, initial condition ensembles, emission scenario ensembles, etc.) we have adopted a Perturbed Physics Ensemble (PPE). The PPE approach (Collins et al., 2006) represents the uncertainties or variability in climate projections by perturbing uncertain parameters to create new versions of the climate model. Each of these versions was characterised by different values for a set of parameters that describe the basic unresolved physical processes (Collins and Knight, 2007; Palmer and Williams 2008). The Met Office Hadley Centre, in the project on Quantifying Uncertainty in Model Predictions (QUMP), pioneered the use of systematically designed Global Climate Model (GCM) ensembles using the HadCM3 global model to explore the uncertainties in climate projections (Murphy et al., 2009). This novel approach has however had to date seen only very limited application outside Europe.

The 17 members of the QUMP ensemble are referred to as HadCM3Q0-16, where HadCM3Q0 is the unperturbed member. The members Q1-Q16 are numbers according to their global climate sensitivity, where Q1 has the lowest global average temperature response to a given increase in atmospheric CO_2 and Q16 the highest.

These GCM simulations are used as lateral boundary conditions for the RCM simulations. However performing such simulations for an ensemble of 17 members would be highly computer resource intensive. Indeed, running a high resolution RCM for 150 years for each available ensemble member of QUMP was impractical. An alternative approach, used here, is to select a subset of the full ensemble but which represents a similar range

of outcomes. A recently published systematic methodology to achieve this (McSweeney et al, 2012) is applied here to select 5 ensemble members based on their ability to reproduce important features of the present-day climate over Africa while capturing the range of outcomes from the GCM ensemble.

3.4 Bias corrections & change factors

As described above, the difficulty in accurately modelling the complexity of the climate means that both GCMs and RCMs are subject to systematic biases and errors. These biases are found by comparing simulated meteorological variables for the current climate to observations and these biases can affect hydrological simulations considerably. Andréasson et al. (2004) point out that these biases are particularly pronounced for precipitation, but that they also exist for temperature even though

climate models are able to simulation this variable more accurately.

The most widely used method to correct for these biases is the delta-change method (Fowler et al., 2007). For change factor methods like the delta-change method, the difference between control (historical) climate model simulations and future projections are used to modify baseline by adding (in the case of temperature) or multiplying in the case of precipitation and evapotranspiration).

3.4.1 Derivation of the delta change factors
The delta change method uses the change in selected variables by comparing climate model simulations for a control or reference period (typically a 30-year period, e.g. 1961-1990) to simulations of a future (scenario) climate for a similar period. In this study we perform the change factor calculations for both the period 2020-2049 and 2070-2099.

For temperature, this calculation is straightforward. The time series of future temperature $T_{future}(i)$ for each time step i is defined by adding the changes in monthly average temperature between the control and scenario period to the observed temperature time series $T_{obs}(i)$.

$$T_{future}(i) = T_{obs}(i) + CF^T(j) \qquad (3.1)$$

$CF^T(j)$ is the temperature change factor for month j calculated as

$$CF^T(j) = \tilde{T}_{scenario}(j) - \tilde{T}_{control}(j), \quad j = 1,12 \qquad (3.2)$$

The ^ (tilde) sign denotes an average over the entire period, either control or scenario. The subscript control denotes the control period (e.g. 1961-1990) and the subscript scenario denotes the future period considered (e.g. 2020-2049).

The time series of future precipitation $P_{future}(i)$ for each time step i is defined by multiplying the observed precipitation time series $P_{obs}(i)$ by the change factor.

$$P_{future}(i) = P_{obs}(i) \cdot CF^P(j) \qquad (3.3)$$

$CF^P(j)$ is the precipitation change factor for month j calculated using the same notation conventions above as

$$CF^P(j) = \frac{\tilde{P}_{scenario}(j)}{\tilde{P}_{control}(j)}, \quad j = 1,12 \qquad (3.4)$$

Which can be written alternatively as

$$CF^P(j) = [1 + \Delta^r(j)], \quad j = 1,12 \qquad (3.5)$$

Where $\Delta^r(j)$ is the relative change in precipitation.

$$\Delta^r(j) = \frac{\tilde{P}_{scenario}(j) - \tilde{P}_{control}(j)}{\tilde{P}_{control}(j)}, \quad j = 1,12 \qquad (3.6)$$

The time series of future reference or potential evapotranspiration $PET_{future}(i)$ for each time step i is calculated in a similar manner to precipitation by multiplying the observed PET time series $PET_{obs}(i)$ by the change factor.

$$CF^{PET}(j) = \frac{\tilde{PET}_{scenario}(j)}{\tilde{PET}_{control}(j)}, \quad j = 1,12 \qquad (3.7)$$

While for precipitation and temperature, the change factors can be estimated directly from the output from the RCM simulations, potential evapotranspiration (PET) which is required by the hydrological model is not a direct output from the RCM simulations and a different approach therefore had to be used. Firstly, mean monthly PET maps for the baseline and future periods are calculated using the FAO Penman-Montheith method (Allen et al., 1998) from the mean monthly RCM outputs of temperature, humidity, surface wind speed, and shortwave radiation for each ensemble member. Then, the PET change factors for each ensemble member are calculated from equation (3.7).

3.5 Evaluation & validation of the African climate simulations

To evaluate and validate the performance of the climate models, we have compared the observed and simulated annual cycles of temperature and precipitation and the geographical patterns of precipitation and 850hpa winds (both speed and direction) in the simulations to those in observed datasets. The climatic sub-regions used in the evaluation presented here are shown in Figure 3.4. The observed datasets used are listed in Table 3.2. The annual cycles for each of these sub-regions for 1961-1990 are shown in Figure 3.5, Figure 3.6 and Figure 3.7.

Figure 3.4 Regions used in the validation of the QUMP GCM ensemble members
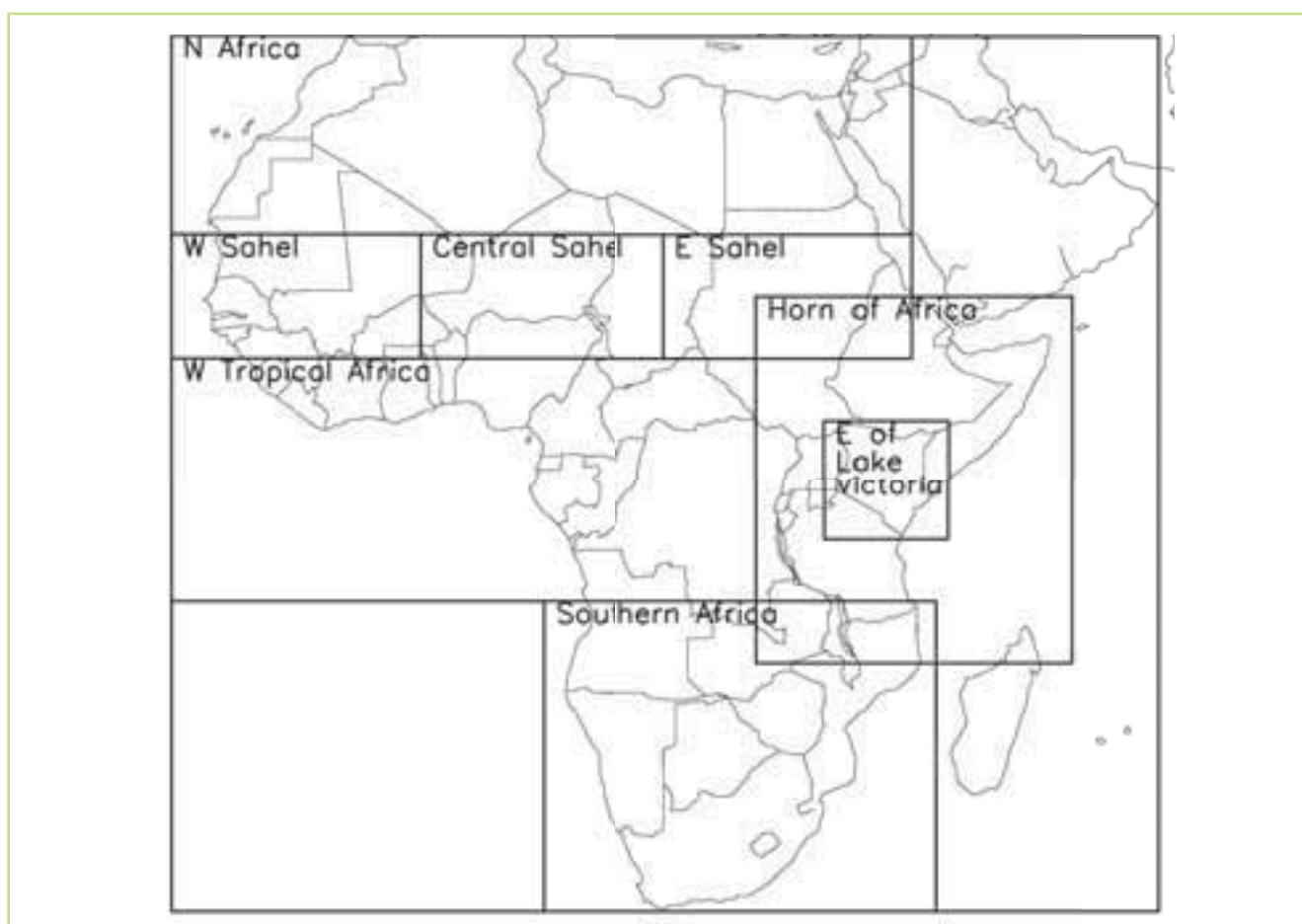
Table 3.2 Observed data sets used for evaluation of the climate model simulations for Africa

Data set	Variable	Resolution	Description	Reference
CRU 3.0	1.5m Temperature	0.50° monthly, 1900-2006	Gridded station data, land only	Mitchell and Jones (2005)
ERA40	850hPa Winds	2.5° monthly, 1979-1996	Reanalysis	Uppala et al. (2005)
CMAP	Precipitation	2.5° monthly, 1979-1998	Gridded station data merged with satellite data	Xie and Arkin (1997)
CPC-FEWS	Precipitation	0.1° daily, Jan 1983 - March 2013	Gauge data, geostationary IR, and polar orbiting microwave SSM/I and AMSU-B satellite data. (RFE 2.0)	Love et al., (2004)
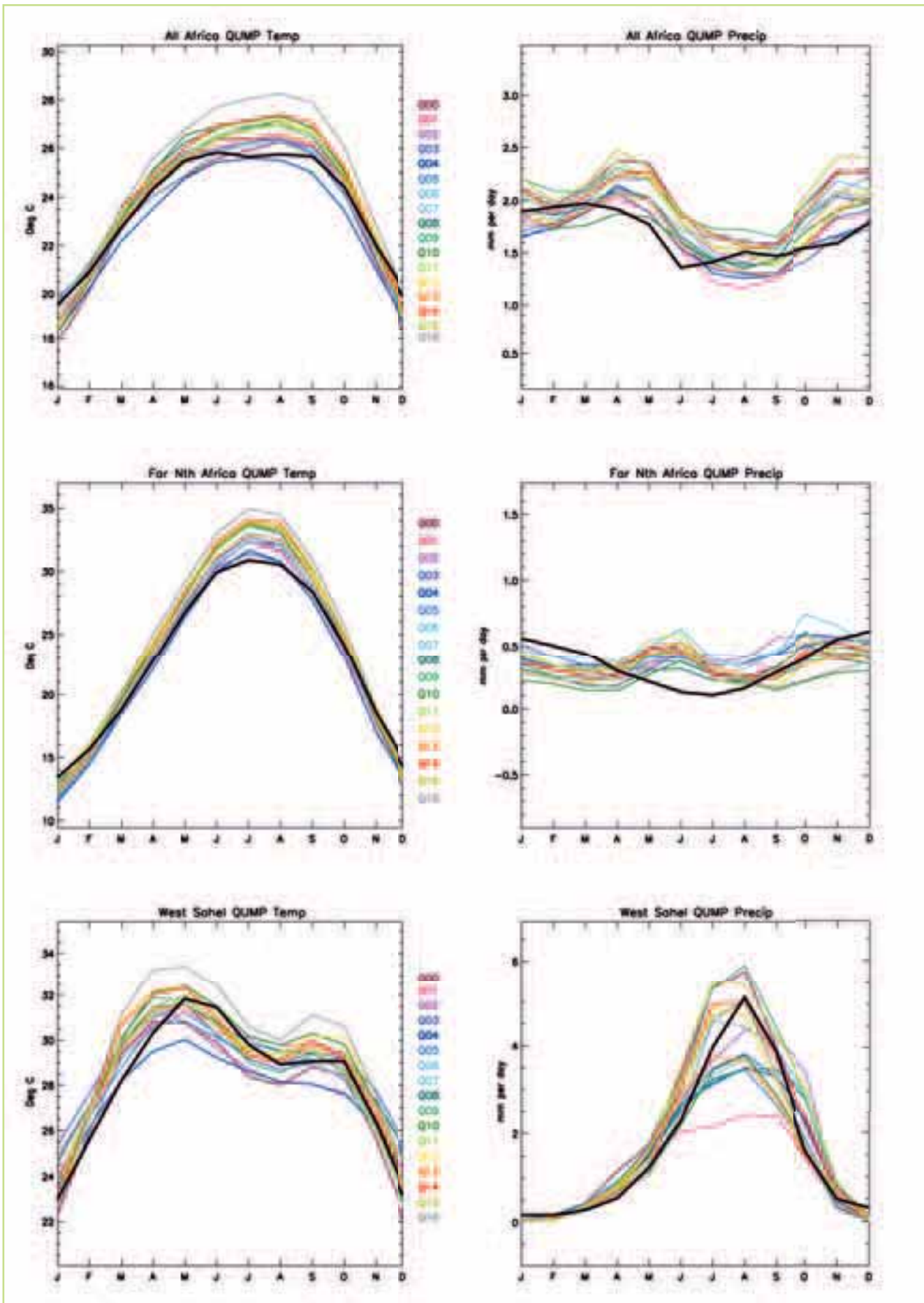
Figure 3.5 The annual variation of temperature (left) & precipitation (right) for Africa, North Africa & West Sahel. The black line shows the observed values of temperature & precipitation from CRU 3.0 & CMAP, respectively, while the coloured lines show the model outcomes. Note the differences in y-axis scaling, especially for precipitation
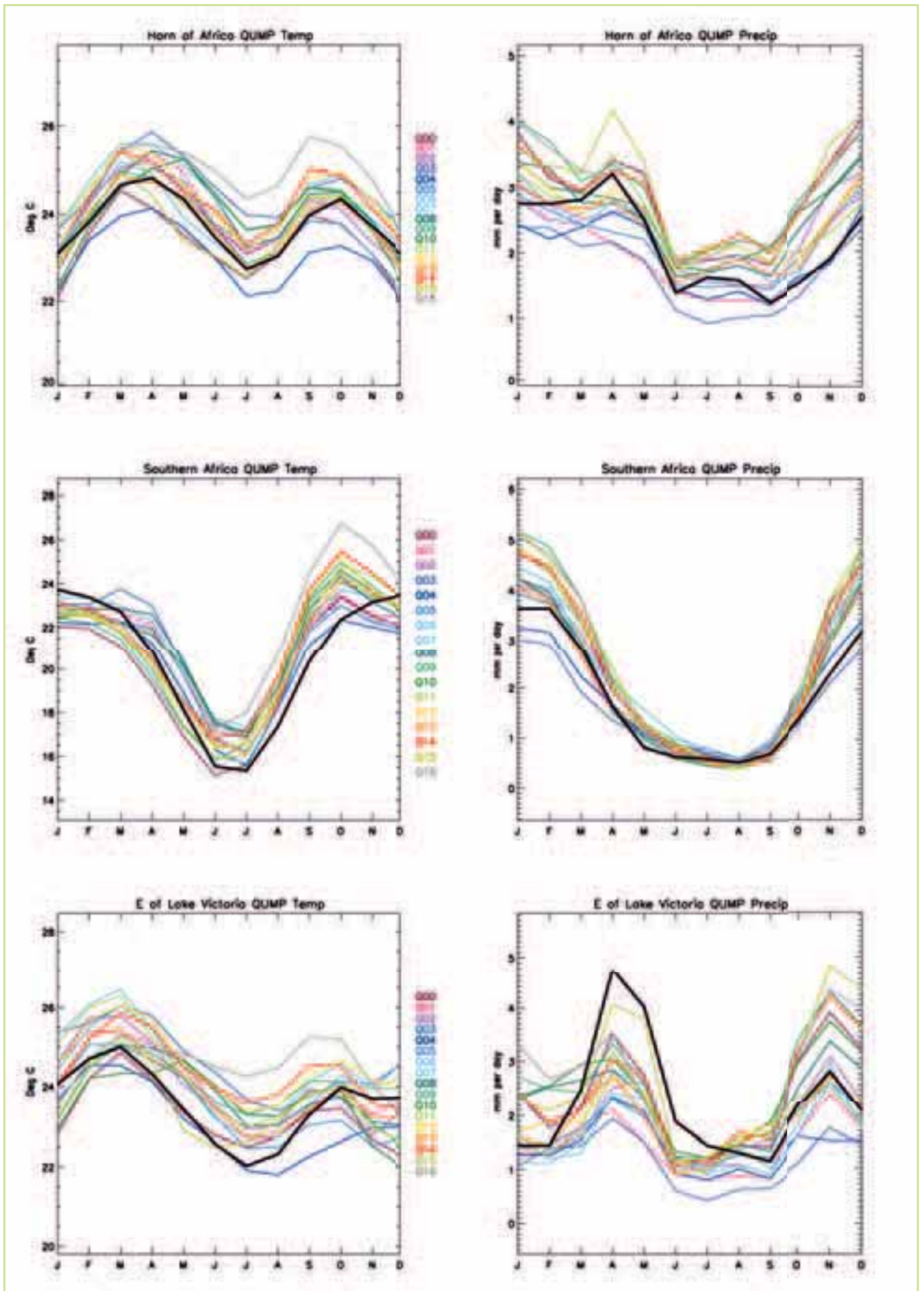
Figure 3.6 The annual variation of temperature (left) & precipitation (right) for Horn of Africa, Southern Africa & East of Lake Victoria. The black line shows the observed values of temperature & precipitation from CRU 3.0 & CMAP, respectively, while the coloured lines show the model outcomes
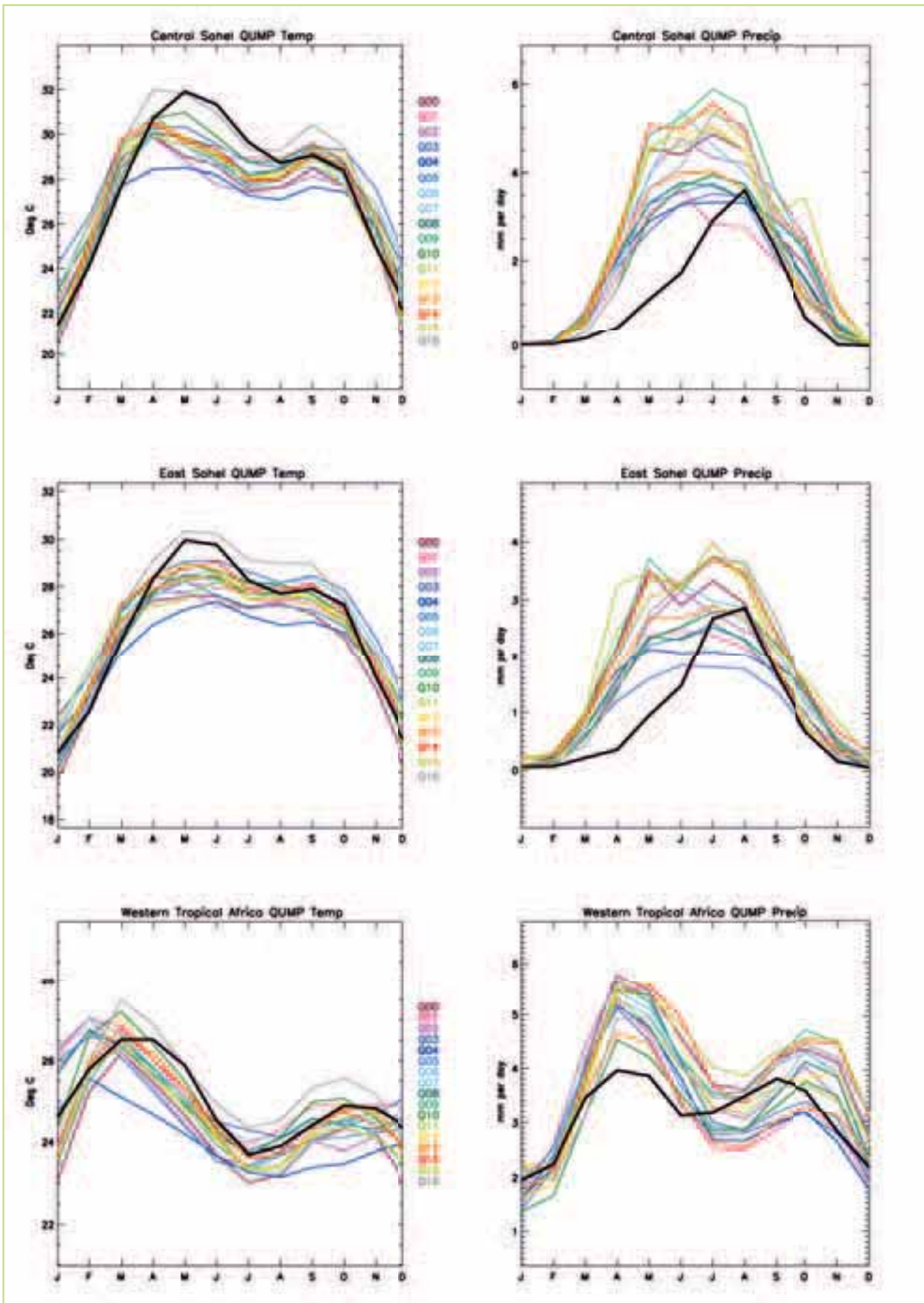
Figure 3.7 The annual variation in temperature (left) & precipitation (right) for Central Sahel, East Sahel & Western Tropical Africa. The black line shows the observed values of temperature & precipitation from CRU 3.0 & CMAP, respectively, while the coloured lines show the model outcomes

Table 3.3 Co-ordinates of the corners of sub-regions of Africa used in the validation of the climate models

Region	Western longitude (W)	Eastern longitude (E)	Northern latitude(N)	Southern latitude (S)
Africa	-20°	60°	36°	-35°
Northern Africa	-20°	40°	36°	20°
West Sahel	-20°	0°	20°	10°
Central Sahel	0°	20°	20°	10°
East Sahel	20°	40°	20°	10°
Western Tropical Africa	-20°	27.5°	10°	-10°
Horn of Africa	27.5°	52°	15°	-15°
Southern Africa	10°	42°	-10°	-35°
East of Lake Victoria	33°	43°	5°	-5°

The annual cycle of temperature for the whole of Africa suggests that the UK Met Office GCM models capture the seasonal cycle of temperature realistically, although the majority of members slightly over-estimate temperatures between May and September (Figure 3.5, top left). Most of the models also capture the different seasonal temperature cycles in the sub-regions similarly, although for some regions there is a greater spread in the model simulations skill (e.g. Horn of Africa). Model Q16 tends to be consistently the warmest model, and lies apart from the other models while Q4 the coolest. The temperatures for the Central Sahel and East Sahel are generally under-estimated by most of the models for the period between April and June.

In terms of temperatures in the Nile Basin, the most important sub-regions are the Horn of Africa, East of Lake Victoria as well as East Sahel and North Africa. At this scale the GCM results reproduce the temperature behaviour satisfactorily but as described above over-estimation of the average for the summer in North Africa and under-estimation in Central and East Sahel as mentioned above The double peak pattern over the Horn of Africa is well captured but with substantial variation amongst the different GCM ensemble members. The double peak in temperature over the East of Lake Victoria is captured but is generally over-estimated.

In general the ensemble members capture the annual cycle of rainfall for many of the regions of Africa shown here (however there are differences in spread between ensemble members for different regions and how close the simulations are to observations. The models capture the main rainy season in the Sahelian regions in JAS, although the rainy season begins two months too early in most of the models, and the range of magnitudes of wet-season rainfall is large.

In terms of sources of precipitation in the Nile Basin, the most important sub-region is the Horn of Africa, containing the Equatorial Lakes and Ethiopian highlands and East of Lake Victoria For the Horn of Africa, the QUMP GCM ensemble captures the seasonal pattern here but with a large spread in simulated precipitation, as was found for the temperature. In terms of water scarcity it is also of interest to examine simulation the North Africa and East Sahel subregions. The two wet seasons observed over the East of Lake Victoria are simulated by the ensemble but the first (March, April, May) is under-estimated and the second (September, October November) is over-estimated by some ensemble members.

The simulations of precipitation for these sub-regions do not, at first glance appear to compare well with observations, for example the northern Africa region seasonal cycle is not captured at all. However, there are two aspects to the analysis of precipitation that should be noted; firstly modelling the climate of Africa is a challenge in itself, this is highlighted in the IPCC 4th assessment, which shows the systematic errors that occur in and around Africa in many of the GCMs included in the assessment. In 90 percent of IPCC 4th assessment models there is excessive rainfall (by on average 20 percent) for southern Africa and the Inter-Tropical Convergence zone is displaced towards to equator. In fact several of the IPCC GCMs have no representation of the

West African Monsoon at all (Meehl et al, 2007b). So it is not surprising that there is some difference in the HadCM3 model ensemble studied here compared with observations and actually this model does reasonably well in comparison. Secondly the amounts of precipitation that occur in some of these sub-regions are very small therefore errors in the

simulations could appear more significant than they actually are. This is particularly the case for North Africa. In this case it is helpful to refer also to the geographical patterns of precipitation and compare these with observations to establish if the ensemble members capture the observed synoptic picture.

Figure 3.8 and Figure 3.9 show the precipitation
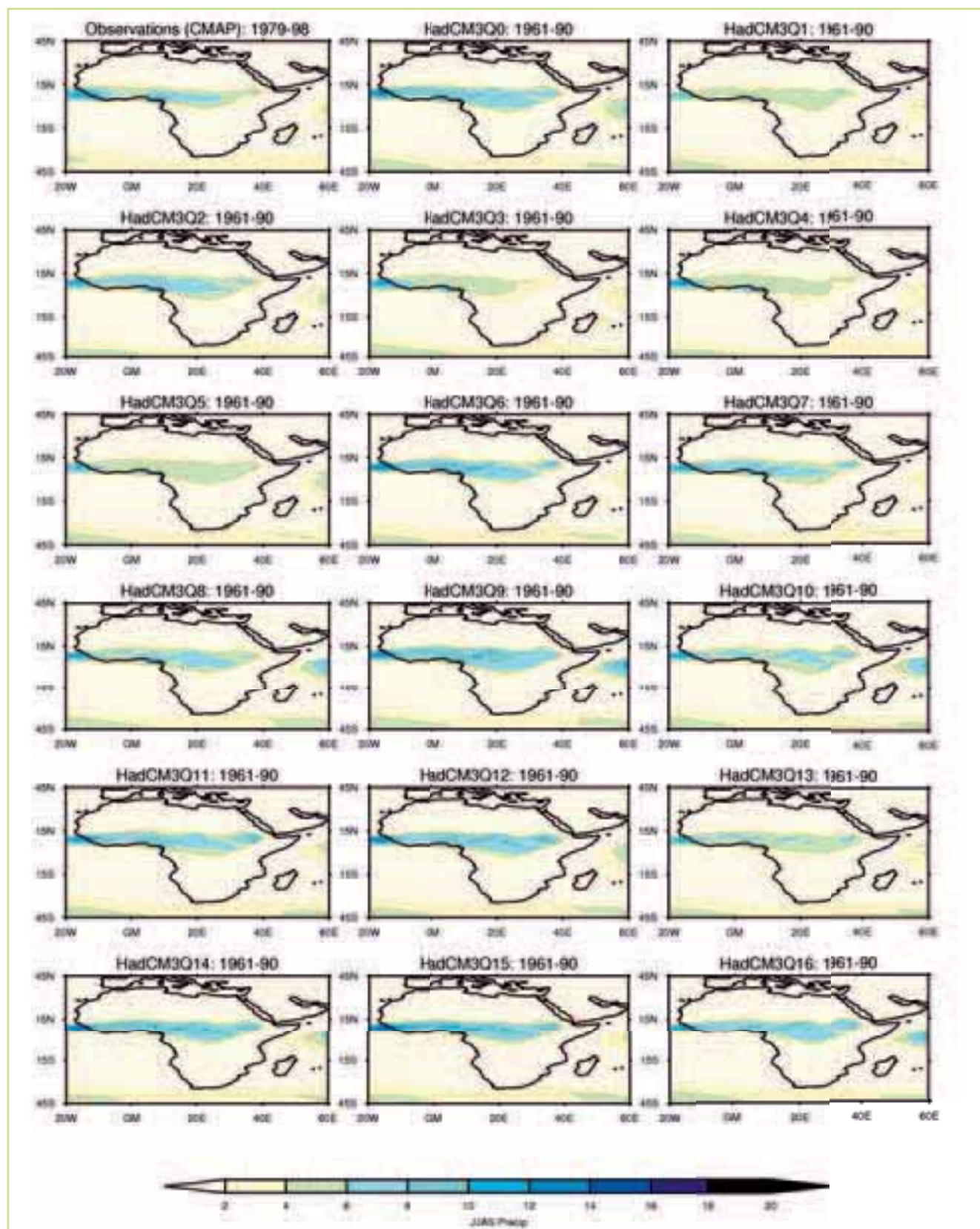
Figure 3.8 Comparison of the observed (CMAP) & simulated precipitation for Africa during JJAS. The observations were taken during the period 1979-1998 & the simulation data during the period 1961-1990. All values are in mm/d

for Africa for the seasons June, July, August and September (JJAS) and December, January, February (DJF) respectively. The large scale patterns are generally captured by all the ensemble members, however many over-estimate the magnitude of the precipitation over central southern Africa particularly during DJF. In Figure 3.9 the lower sensitivity models (Q1-Q5) tend to match the magnitude of the observed DJF precipitation climatology more closely than the higher sensitivity models (Q15 and Q16). The timings, and geographical location of wet periods and regions, however, are realistic.
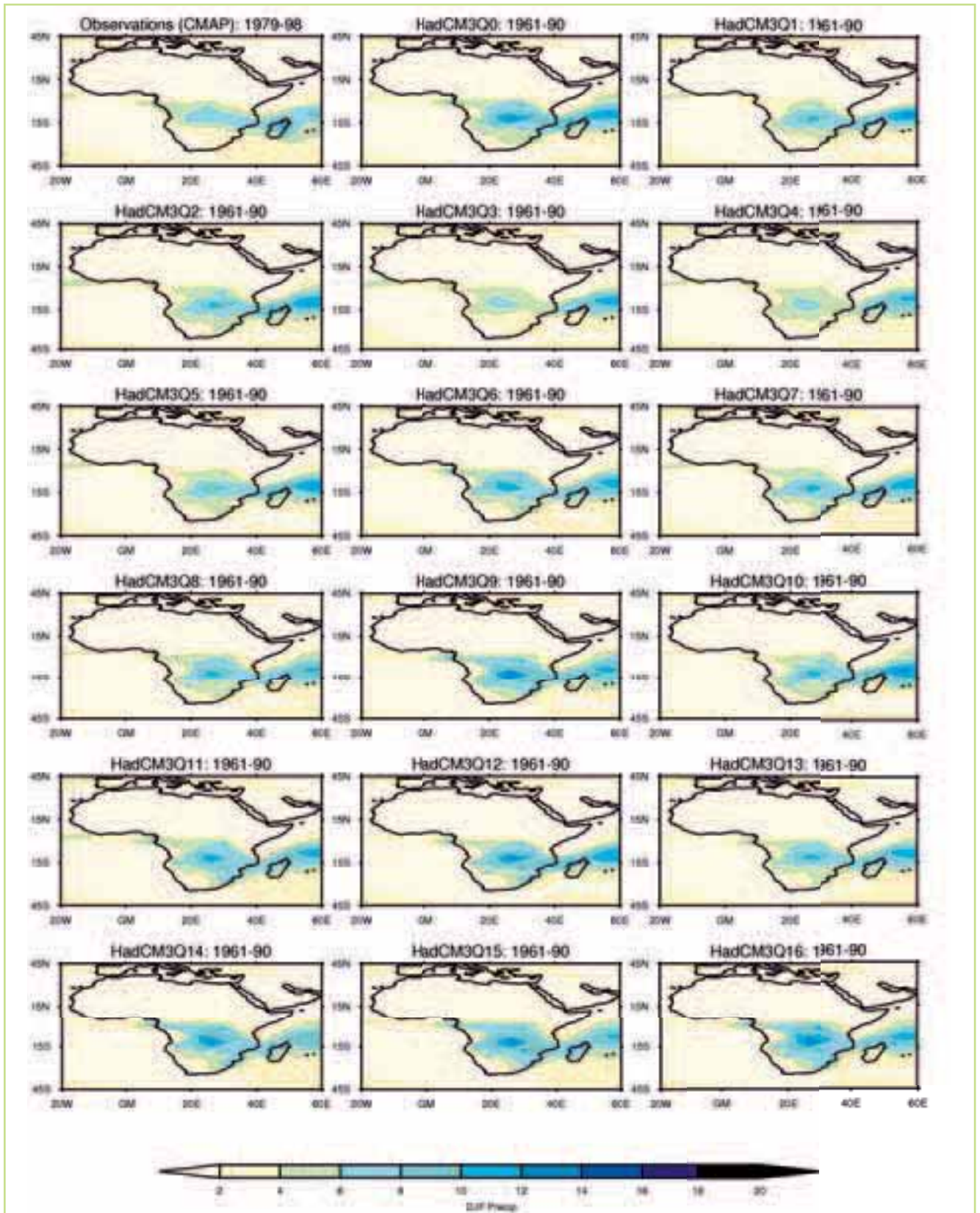
Figure 3.9 A comparison of observed & simulated precipitation for Africa during DJF. The observations were taken during the period 1979-1998 & the simulation data during the period 1961-1990. All values are in mm/d

Figure 3.10 and Figure 3.11 compare the simulated 850hPa winds during JJAS and DJF months respectively with ERA40 (Uppala et al 2005). As with the precipitation maps the models generally reproduce prevailing circulation patterns, including the direction of the trade winds (both north-east and south-east). During JJAS the region of higher wind-speeds over the Horn of Africa (referred to as the 'Somali Jet') are also captured. However there is some variation between the ensemble members in the magnitude of the Somali Jet, with Q2, Q3, Q6 and Q7 matching the observations more closely than the other ensemble members. The direction of the DJF trade winds are also captured in most of the ensemble members e.g. Q8, Q9, Q11 and Q13; however the magnitude of the winds over the Sahel and southern Africa are slightly over-estimated in most of the ensemble members. Of all the ensemble members Q3 is the closest match to the observed climatology for the magnitude of DJF wind-speed.

The surface temperature and sea surface temperature patterns (not shown) in general compare well with the CRU observations and HadISST datasets respectively. However some of the ensemble members, particularly the higher sensitivity ones (Q9- Q16) do overestimate the temperatures in regions where temperatures are high. The mean sea level pressure patterns (also not shown) for the ensemble members also compare well with observations.

Our validation of the 17 models shows that while all the models capture the broad seasonal and geographical pattern in key climate features, the range in magnitudes of features such as seasonal rainfalls, and the realism of those magnitudes, varies from across the models. However, it is not straightforward to identify a subset of models that perform better or worse across the whole region – models that do least well in some regions tend to be the most realistic in another.

Our approach, therefore, is to select the sub-set based mainly on representing the spread of future climate outcomes across the regions. When making this decision, however, we take into account the shortcomings of some of the models. For example, where two models project similar characteristics of change in the future, we can use the validation information to choose to include the better performing model.
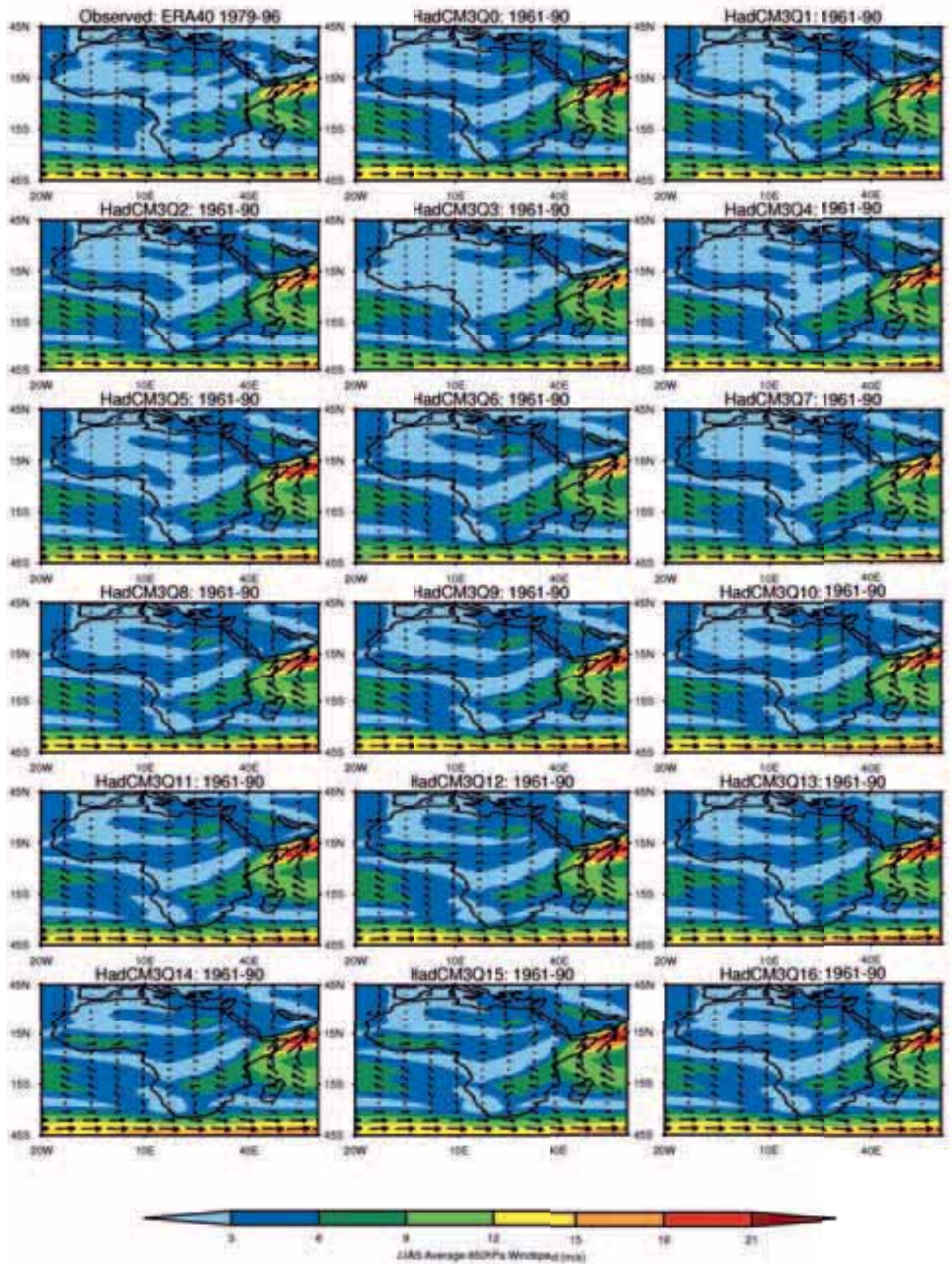
Figure 3.10 A comparison of observed & simulated 850 hPa winds for Africa during JJAS. The observations were taken during 1978-1998, & the simulated outcomes during the period 1961-1990
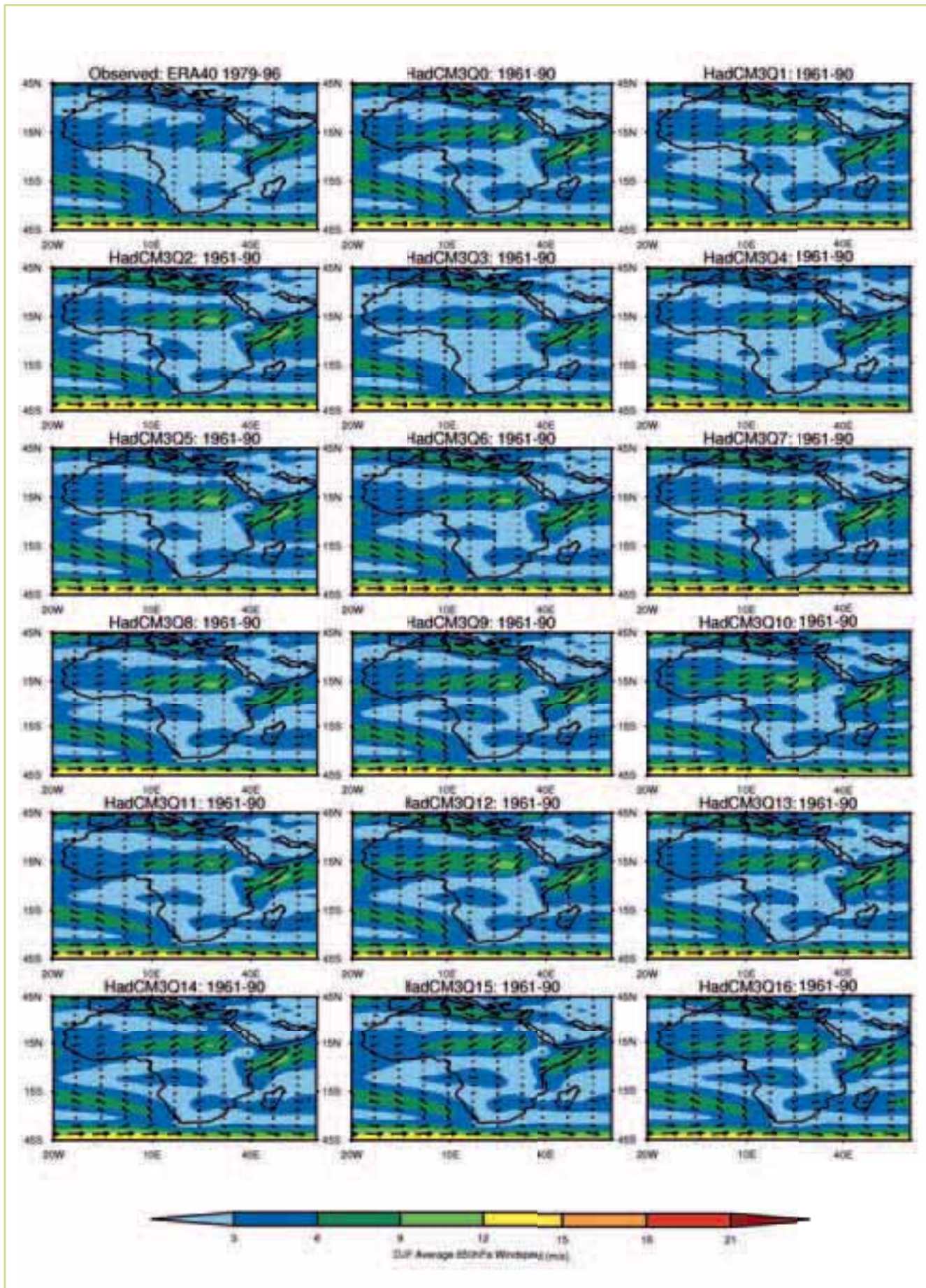
Figure 3.11 A comparison of observed & simulated 850 hPa winds for Africa during DJF. The observations were taken during 1978-1998, & the simulated outcomes during the period 1961-1990

3.6 Selection of ensemble members

The approach used here as described earlier is to select 5 ensemble members based on their ability to reproduce important features of the present-day climate over Africa while capturing the range of outcomes from the GCM ensemble. This selection process is carried out systematically based on McSweeney et al, 2012.

On the basis of the analysis shown above Q1, Q3, Q4, and Q16 are not considered further in this analysis because for many of the regions the seasonal cycle of both precipitation and temperature do not compare as well with observations as other ensembles. The final selection of ensemble members for Africa involves identifying the models which represent the range of the full ensemble in their change in precipitation (ΔP) and temperature (ΔT) for Africa and the climatic sub-regions (Figure 3.4) for the A1B scenario. These changes are evaluated from the 1970's and to the 2080's. More precisely, averages were taken over simulation periods 1961-1990 and 2070-2099 to allow in part for natural climate variability.

This analysis takes the form of scatter plots which the relevant sub-regions in Figure 3.12, Figure 3.13 and Figure 3.14. There is no particular model that consistently shows the largest change in precipitation for all regions throughout the year. For example for the Horn of Africa in DJF the largest change in precipitation is seen in Q14 but this model is not always the wettest model for the other seasons for this region. Q14 is for example close to the ensemble mean for the Horn of Africa for the JJA season. Q14 is also one of the driest models for some sub-regions, for example, some seasons (MAM, JJA, SON) in the West Sahel. On this basis the extremes of the ensemble distribution are classified in terms of which models consistently have the largest positive or negative change in precipitation across all the sub-regions and seasons. Therefore using this scoring system Q9 represents one of the wettest and Q0 represents one of the driest models in the range of the ensemble (but this does not mean these are the wettest and driest models in all sub-regions and seasons).

Although the models are numbered 1-16 according to their global temperature response, their regional responses will vary. Temperature response is more consistent, across the regions and the seasons, than the precipitation response, with the higher response models tending to capture the warmer end of the range. Q13, Q14, and Q16 tend to have the largest temperature response across the regions and seasons. While the lower-response models, tend to indicate smaller temperature responses. Q0, Q1, Q2, Q3 tend to be coolest. Therefore on the basis that, of the lower response models, Q1 and Q3 do not validate as well as Q0 and Q2 compared with observations; thus Q0 and Q2 are selected to represent the colder end of the range. At the hotter end of the range, Q16 has already been discounted on the basis of validation results, thus Q13 and Q14 are selected to represent this part of the range of the ensemble. On the basis of this analysis we conclude that a sample which reproduces important characteristics of current the African climates and represents the spread in projected outcomes produced by the QUMP ensemble consists of the following models: Q0, Q2, Q9, Q13 and Q14.

3.6.1 Comparison of QUMP & CMIP3 climate simulations

As described earlier, the ensemble modelling approach used here is a novel perturbed-physics ensemble based on a single GCM with different parameterisations among the ensemble members.

It is therefore of interest to investigate whether the projections from the QUMP GCM ensemble represent the full range of climate futures predicted by other ensemble approaches. In particular we compare here the QUMP ensemble variability with the multi-model ensemble (MME) CMIP 3, (Meehl et al., 2007a). The WCRP CMIP3 multi-model dataset is a collection of results contributed by leading climate modelling centres around the world. The motivation for this was to serve IPCC's Working Group 1, which focuses on the physical climate system -- atmosphere, land surface, ocean and sea ice and to enable groups outside the major modelling centres to perform research of relevance to climate scientists preparing the Fourth Assessment Report (AR4) of the Intergovernmental Panel on Climate Change (IPCC).

The blue bars in Figure 3.12, Figure 3.13 and Figure 3.14 show the spread of the CMIP3 ensemble for each of the African sub-regions considered. The black bars show the corresponding spread in the QUMP GCM ensemble. In general, the spread of the projected temperature changes are of a comparable size, but with the QUMP distribution shifted to slightly higher values. The temperature projections in QUMP therefore do not sample the lower values of temperature changes sufficiently. The two sets of projected precipitation changes show greater disagreement. In the majority of regions and seasons, the range of CMIP3 projections is significantly different from the range of QUMP projections, e.g. East Sahel in JJA, where QUMP predicts wetter conditions across the ensemble, while the CMIP3 projections include both wetter and drier climates. Note also that, in many cases, the QUMP projections are outside the range of CMIP3 projections (e.g. West Sahel in JJA), indicating the importance of considering both MME and PPE ensembles.

In particular, 5 ensemble members chosen here represent the range of QUMP projections; however these QUMP ensemble members does not represent the full range of projections produced by other GCM models. Indeed, for many regions and seasons, the CMIP 3 multiple model ensemble produces projections outside this range.

In terms of sources of precipitation in the Nile Basin, the Horn of Africa is the most important sub-region. The general pattern here seems be that the PPE ensembles are cooler on average than the CMIP3 ensemble and slightly drier. The magnitude of the variations for temperature is comparable but, with exception of MAM, the spread in precipitation changes is significantly larger.
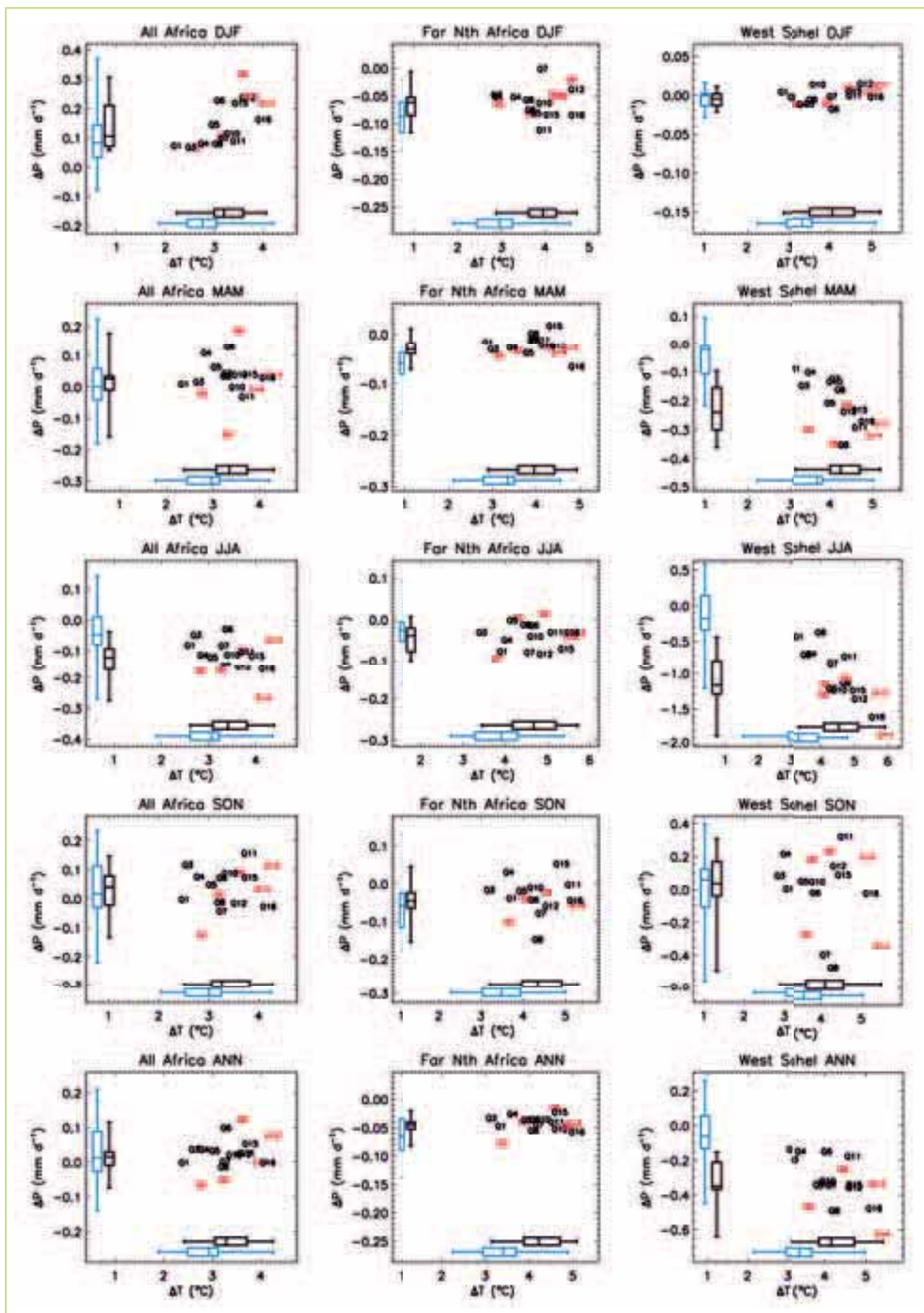
Figure 3.12 Plots for the QUMP ensemble showing projected change in precipitation versus change in the temperature for all Africa, North Africa & West Sahel. The panels show the spread in projected outcomes during DJF, MAM, JJA, SON & annual (ANN). The data point labels (Q#) identify the GCM models & the red data points indicate the selected sample
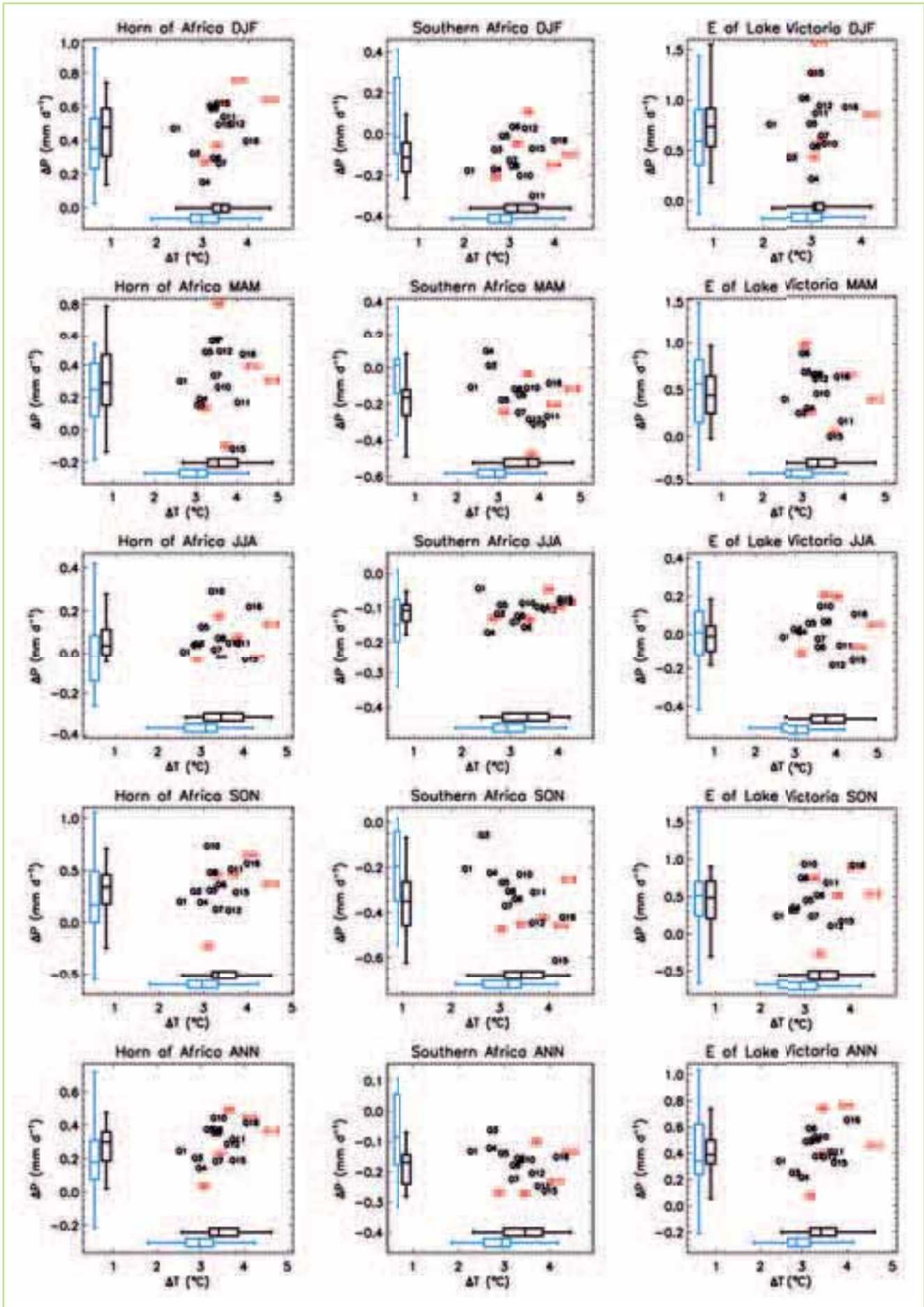
Figure 3.13 Plots for the QUMP ensemble showing projected change in precipitation versus change in the temperature for Horn of Africa, Southern Africa & East of Lake Victoria. The panels show the spread in projected outcomes during DJF, MAM, JJA, SON & annual (ANN). The data point labels (Q#) identify the models & the red data points indicate the selected sample
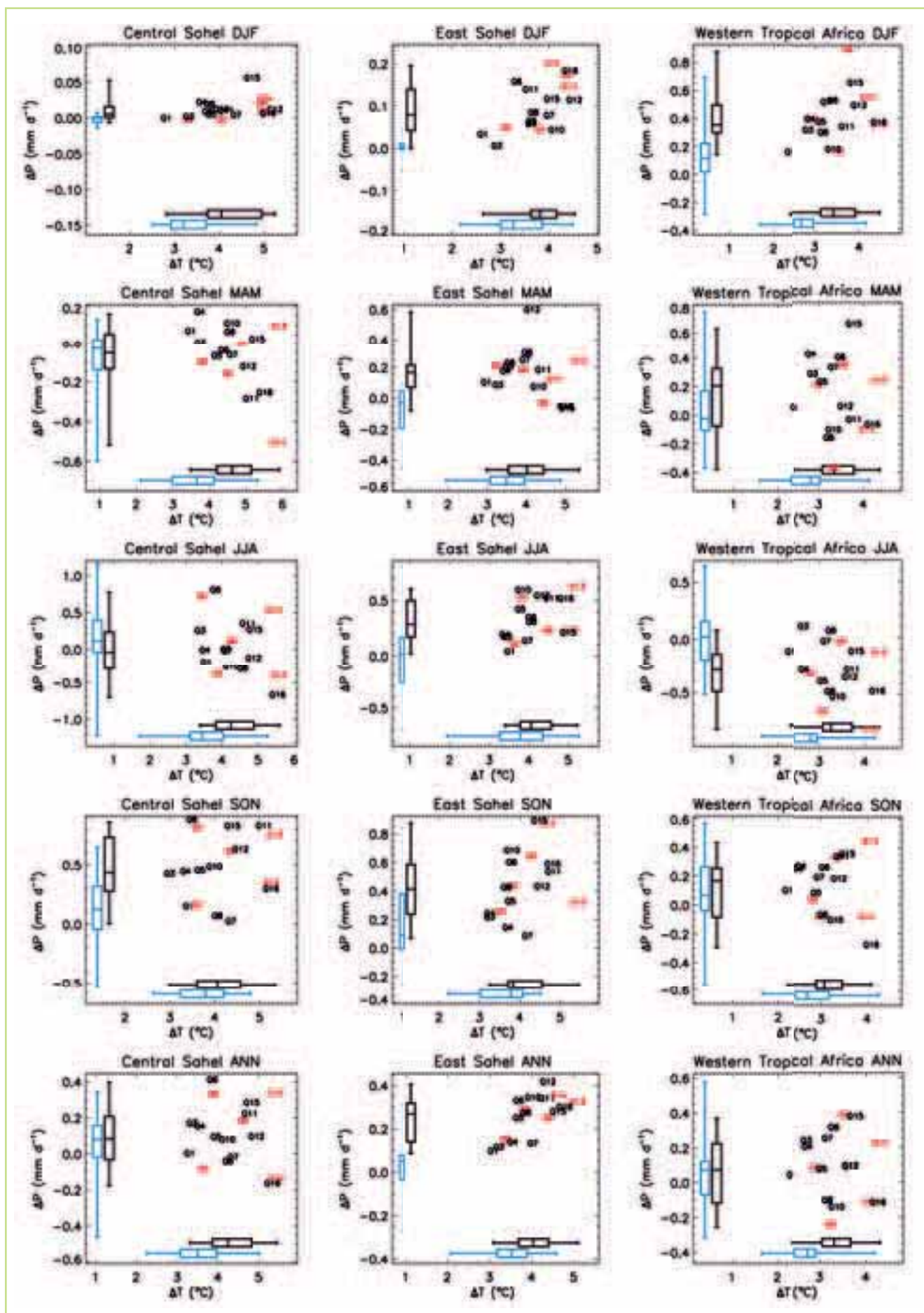
Figure 3.14 Plots for the QUMP ensemble showing projected change in precipitation versus change in the temperature for Central Sahel, East Sahel & Western tropical Africa. The panels show the spread in projected outcomes during DJF, MAM, JJA, SON & annual (ANN). The data point labels (Q#) identify the models & the red data points indicate the selected sample

3.6.2 Evaluation of the RCM simulations

Based on the selection procedure described above HadCM3 (QUMP) GCM ensemble consisting of the following models: Q0, Q2, Q9, Q13 and Q14 is used as driving boundary conditions for higher resolution (approx. 50 km) regional climate model (RCM) simulations.

The RCM ensemble in general captures the annual cycle of temperatures well both for Africa as a whole and the sub-regions, Figure 3.15, Figure 3.16 and Figure 3.17. In all regions, the RCM ensemble fits the observations better than the QUMP ensemble and the spread has been reduced, which is consistent with the selection criteria for the driving QUMP members, since we discarded those that were a poorer fit.

In general, N1 is the coolest and N2 is the warmest ensemble member. The RCM ensemble has a cold bias May-September in the East Sahel and West Sahel regions, which appears to be inherited from the driving GCM ensemble members.

One feature that emerges more clearly in the RCM ensemble than the QUMP ensemble is that while the GCM ensemble generally has a warm bias for the East of Lake Victoria compared to the observations, the RCM ensemble has a cold bias during October, November, December during the second of the two rainy seasons known as the "short rains".

The RCM ensemble shows a substantial improvement over the QUMP ensemble in many regions. This is particularly noticeable in the Sahelian regions, where the RCM does a much better job of reproducing both the magnitude and timing of the wet season. The magnitude of the peak in the East Sahel region is still over estimated in the model and the model wet season is still early compared to observations, but to a much lesser extent than the QUMP ensemble. In general, the RCM ensemble overestimates precipitation over Africa as a whole. In some regions, this positive bias is particularly pronounced, e.g. Western Tropical Africa April-June, the Horn of Africa October-December, East of Lake Victoria October-December.

Figure 3.18 and Figure 3.19 show the geographical patterns of precipitation in the RCM ensemble for JJAS and DJF respectively. The CPC-FEWS high resolution precipitation data set is shown for comparison. The RCM ensemble is better at reproducing the JJAS precipitation than the QUMP GCM ensemble. Both the magnitudes and spatial patterns are well represented well in comparison with QUMP, although some features, such as the observed peak in precipitation over the Cameroon highlands, are still not captured by the RCM ensemble. As discussed previously, the GCM ensemble represented the spatial patterns of DJF rainfall well, but overestimated its magnitude over central Southern Africa. The RCM ensemble performs significantly better over land - it reproduces both the spatial pattern and the magnitude well, as illustrated in Figure 3.19. The RCM has introduced a larger positive bias in precipitation over the Western Indian Ocean in DJF, consistently over the ensemble. A comparison of the RCM simulations with the ERA40 wind data (not shown) indicates that the general circulation in the RCM is not a significant improvement over the GCM simulations.

Table 3.4 Naming conventions for the RCM ensemble members & the sensitivity of the driving GCM ensemble member

RCM identifier	RCM Short Name	QUMP GCM driving run	Eq. Climate sensitivity
akyjy	N0	Q0	3.53
akyuy	N1	Q2	2.42
akzcy	N2	Q9	4.400
akzja	N3	Q14	4.88
akzjb	N4	Q13	4.80
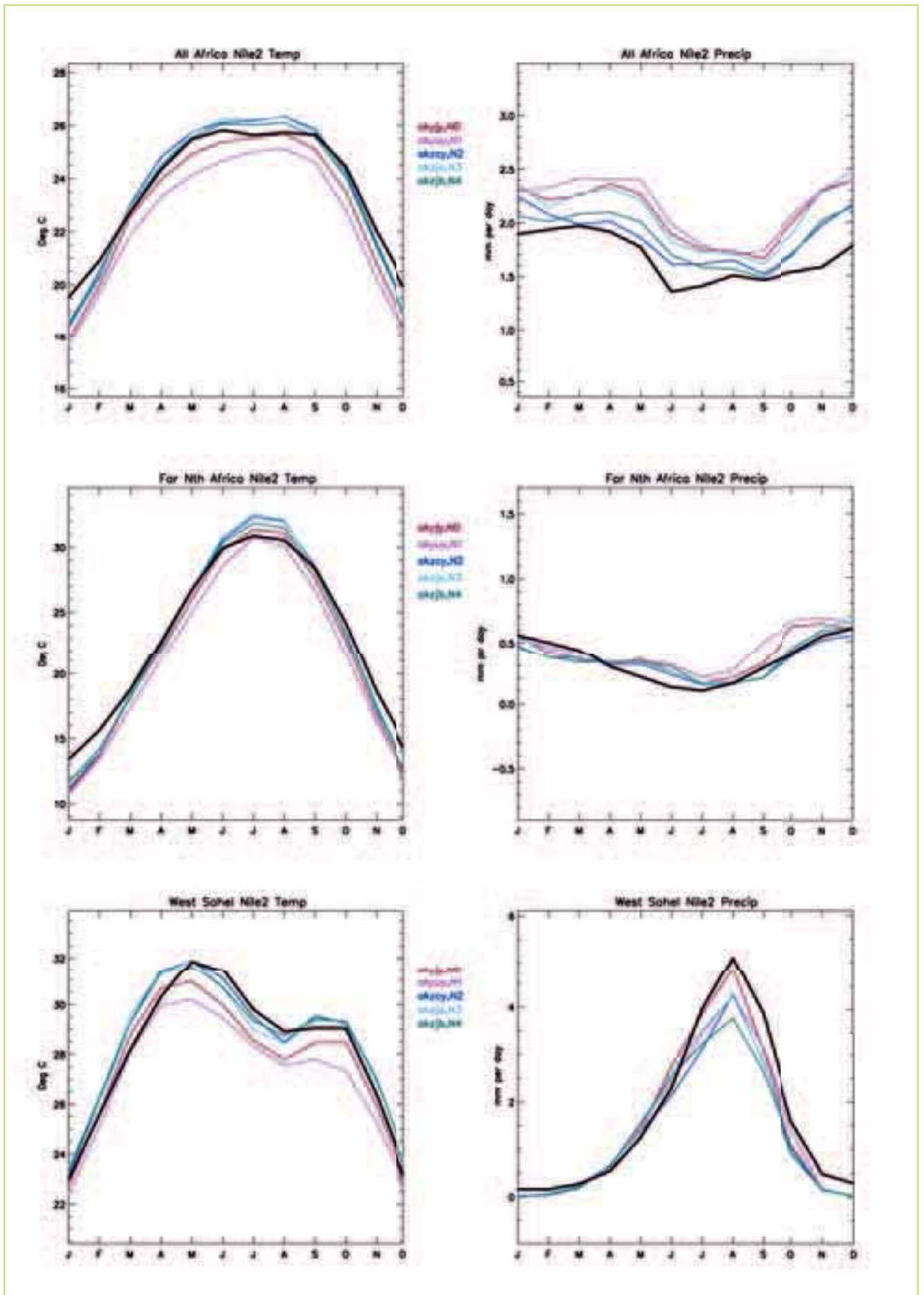
Figure 3.15 The annual variation in temperature (left) & precipitation (right) for Africa, North Africa & West Sahel. The black lines show the observed values of temperature & precipitation from CRU 3.0 & CMAP, respectively, while the coloured lines show the selected RCM ensemble member simulations
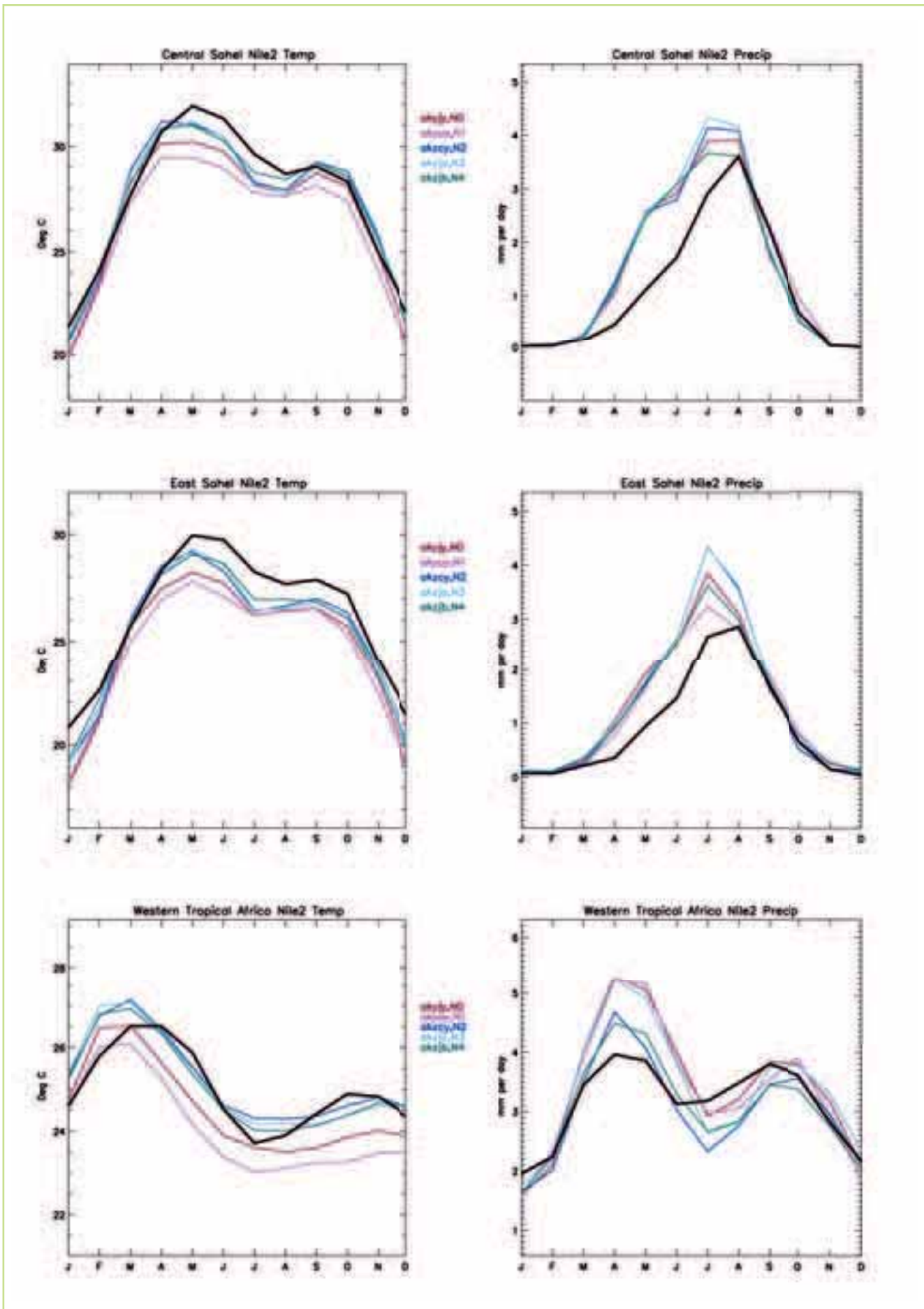
Figure 3.16 The annual variation in temperature (left) & precipitation (right) for central Sahel, East Sahel & Western Tropical Africa. The black lines show the observed values of temperature & precipitation from CRU 3.0 & CMAP, respectively, while the coloured lines show the selected RCM ensemble member simulations
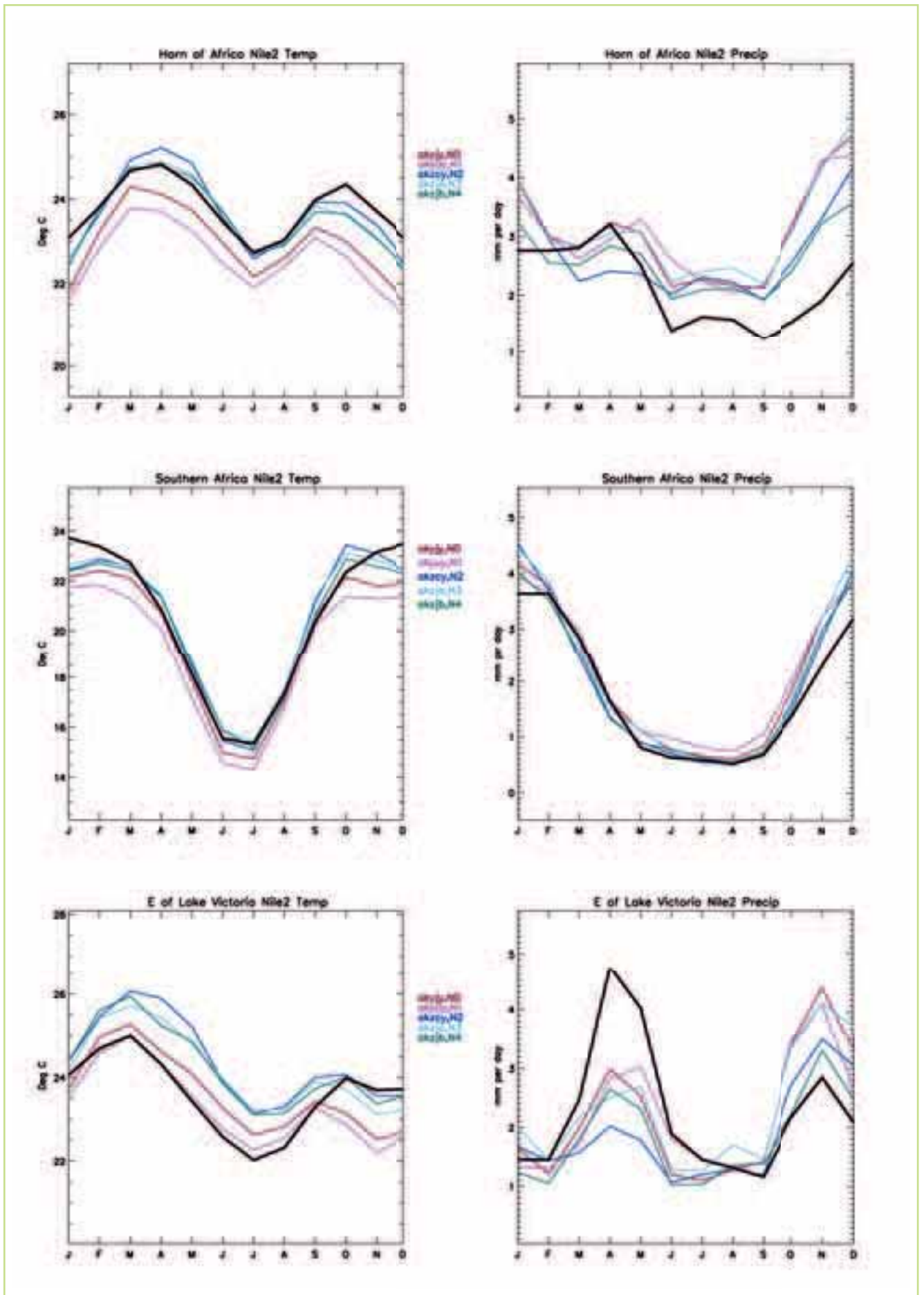
Figure 3.17 The annual variation in temperature (left) & precipitation (right) for the Horn of Africa, Southern Africa & East of Lake Victoria. The black lines show the observed values of temperature & precipitation from CRU 3.0 & CMAP, respectively, while the coloured lines show the selected RCM ensemble member simulations

An interesting feature is the apparently dramatic improvement in the rainfall distribution for North Africa using the RCM. The likely cause of this is not known, Since the North African precipitation is dominated by the contributions along the Mediterranean coast. The precipitation along this narrow strip may be controlled by processes along the sea-land contrast. Since the RCM,'s have a better representation of the land-sea mask and an improved representation of the topography, this may improve model fit. Conversely, the low resolution of the GCM may misrepresent the coastal mountains and atmospheric flows into the desert. However, this is currently speculative.
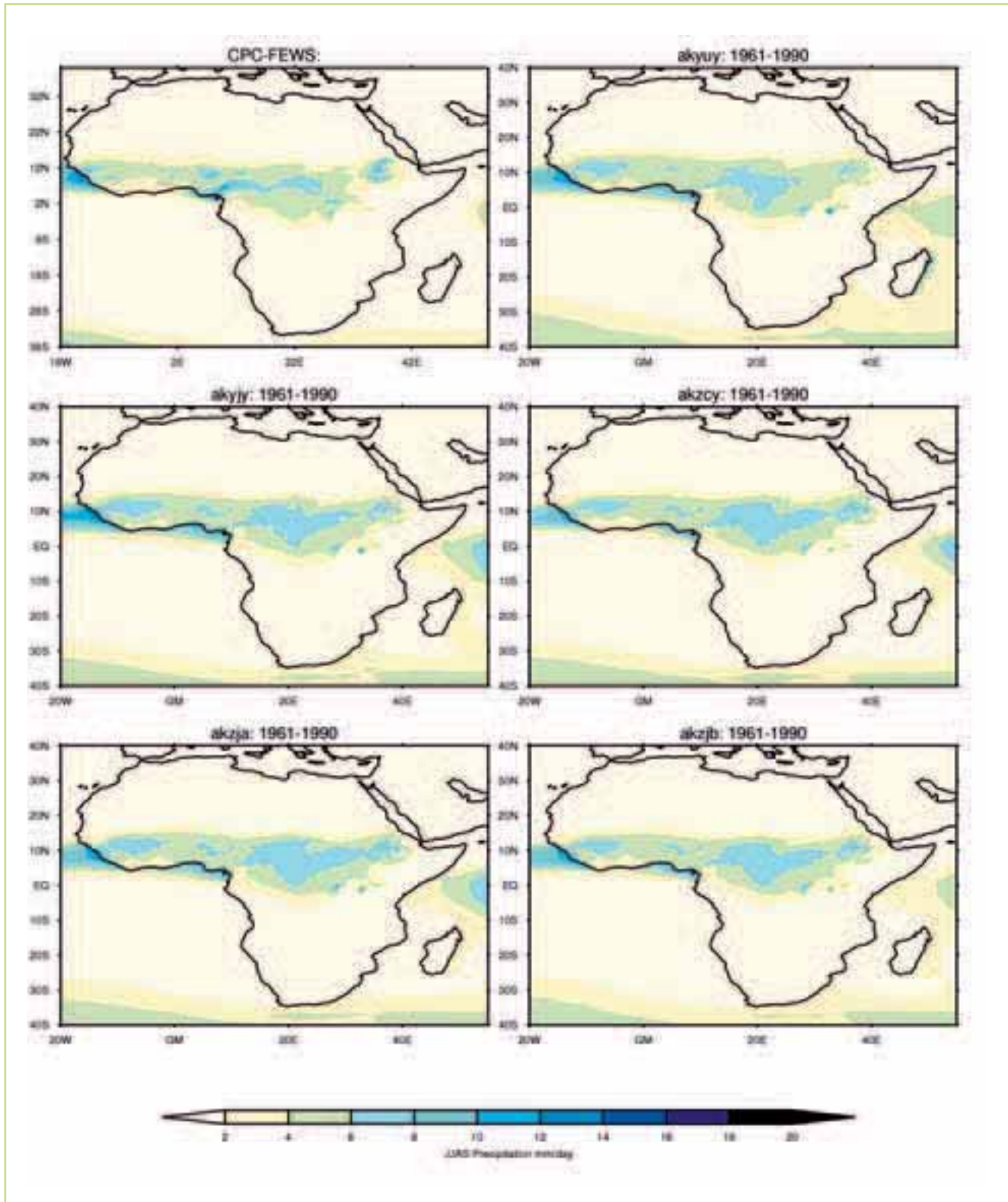
Figure 3.18 Comparison of the observed & simulated precipitation for Africa during JJAS. The observations cover the period 1983-2012 (CPC-FEWS) while the simulations cover the 1961-1990 period. All values are in mm/day
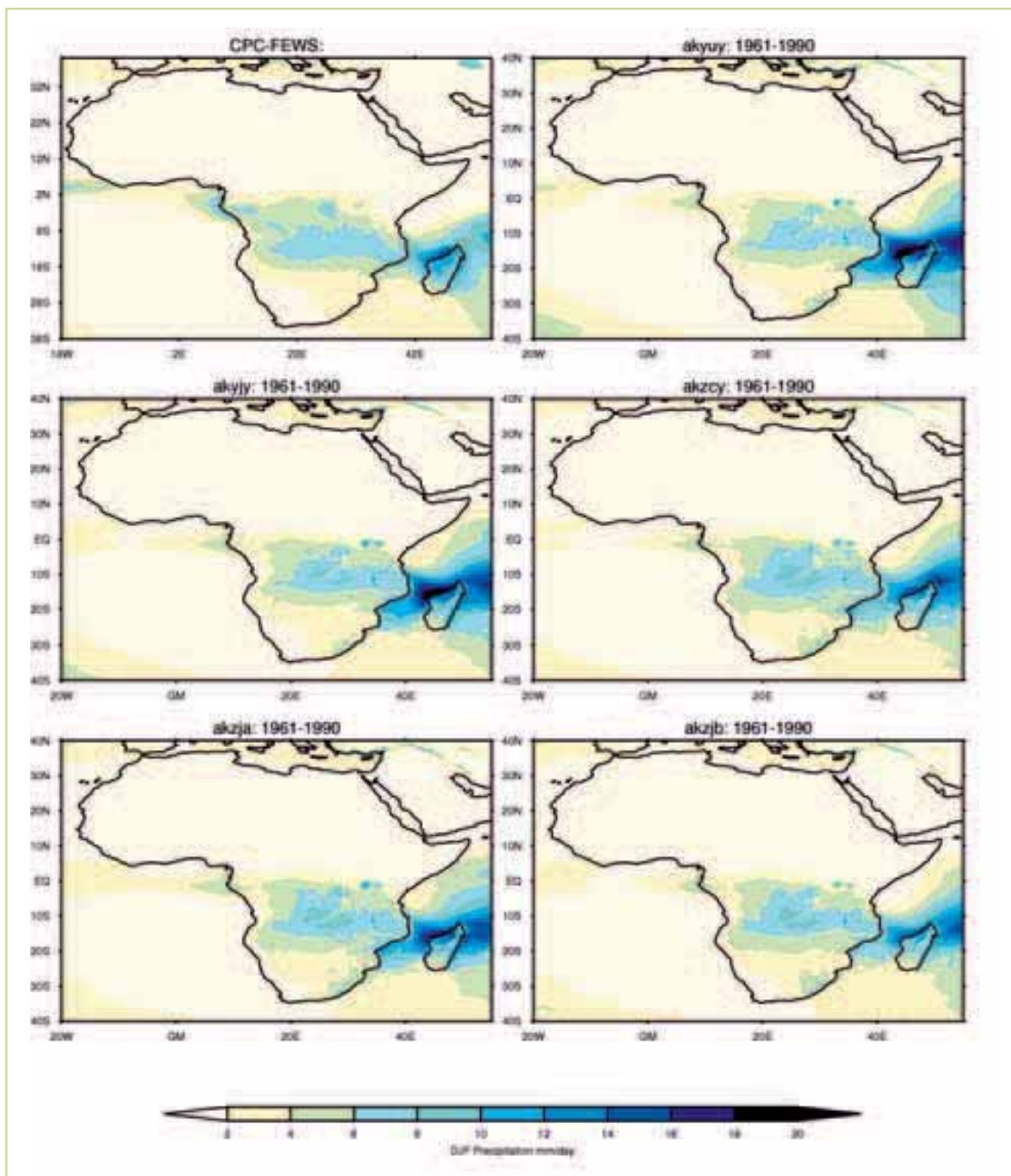
Figure 3.19 Comparison of the observed & simulated precipitation for Africa during DJF. The observations cover the period 1983-2012 (CPC-FEWS) while the simulations cover the 1961-1990 period. All values are in mm/day

3.6.3 Regional climate modelling of Lake Victoria

Lake Victoria is the second largest body of freshwater in the world. Its drainage basin extends into Uganda, Tanzania, Kenya, Rwanda and Burundi and forms the southern part of the Nile. One of the key features that determine the hydrology of the lake is the high contribution (85%) to the total lake inflow by rainfall falling directly on the lake. This suggests that lake levels and the long-term outflow will be highly sensitive to climatic change.

The climate processes in this region are dominated by the migration of the Inter-Tropical Convergence Zone (ITCZ). This is an area of intense convection that marches between its northernmost and southernmost locations following the position of the sun. As the ITCZ travels northwards over the Lake Victoria region during March, April and May, the

region experiences the "long rains" and as it travels southwards during October, November, December the region experiences the "short rains". The land/lake breezes driven by the thermal gradients between the lake surface and the surrounding land dominate the diurnal cycle. In addition, there are a number of large scale phenomena that influence the climate (Buontempo et al, 2013b).

Climate modelling in the Lake Victoria basin is challenging because of the complex nature of the climate and the variety of influences. The model resolution should be sufficiently fine to resolve both the lake itself and the mountain ranges to the east and west. The downscaled RCM model used here over the CORDEX domain used here represents an improvement in resolution in comparison to the GCM's.

The other major challenge is that while much of rainfall occurs directly over the Lake observation data over the lake are few and obtaining a reliable estimate of rainfall over the lake is difficult.

In HadRM3P and MOSES2.2 there is no specific lake model. In an attempt to improve the description of climate processes in this region the lake surface temperatures of Lake Nyasa, Tanganyiki and Victoria have been prescribed as a lower boundary condition. The prescribed values were obtained by bias correcting the temperature of the nearest sea point, (Buontempo et al, 2013). The bias correction was obtained by calculating the mean temperature of the nearest sea point in the unperturbed QUMP run for each month over a baseline period. This gives the climatology of the model lake without bias correction. The difference between this and the climatological mean lake temperature given by the ARClake project for that month (based on observations from 1995-2009) represents the bias correction which is then applied in the climate projections.

To validate the RCM precipitation in this region, four observation datasets have been used.
1. Climate Research Unit (CRU): :Mitchell and Jones (2005)
2. Global Precipitation Climatology Project (GPCP): Adler et al. (2003)
3. Climate Prediction Center Merged Analysis of Precipitation (CMAP): Xie and Arkin (1997)
4. Climate Prediction Center – Famine Early Warning System (CPC-FEWS): Love et al. (2004)

Figure 3.20 shows the average daily precipitation for the Lake Victoria region. There are clearly a number of differences between the datasets. The CPC-FEWS dataset, for example, shows an enhancement of precipitation over the lake in all seasons that is absent from the other precipitation observations. CRU dataset shows a precipitation enhancement on the north-east coast of the lake. It is interesting to notice that this specific feature is absent in the other rainfall datasets, which rely mainly on satellite observations. On the other hand the lack of reporting station over the lake inevitably makes the rainfall estimation over the lake less constrained by observation and potentially more dependent on the calibration of the satellite sensors.

As we have seen, the RCM ensemble captures the spatial distribution of precipitation across the continent African continent well, and also the seasonal migration of the ITCZ. This is reflected in the RCM ensemble mean (Figure 3.21) which has a bias of less than 2mm/day over most of the African Continent compared to the CPC-FEWS dataset. There are two main areas with a greater bias. The first is along the Northern edge of the rain belt in June-August, where previous studies (Butts et al., 2011) have noted that the QUMP ensemble also has a positive bias compared to both CRU and the CMIP3 ensemble mean. The second area is directly over Lake Victoria, where the model has biases as large as 8 mm/day compared to CPC-FEWS. This discrepancy between model and observation is particularly pronounced in the late rainfall season (September-November), but the bias is also present in the off-peak seasons. It is all worth noticing that no bias is noticed in MAM.

Given these comparisons, it seems that the regional climate model has a large rainfall bias in this region. It is not possible at this stage to satisfactorily attribute this bias to a specific cause. It is worth noting that precipitation estimates are under-constrained by observations in this region given that no report station exists over the lake itself and therefore a large uncertainty could be associated with rainfall estimates over the lake. However, the model representation of the lake as well as the processes controlling the diurnal cycle of temperature and humidity over the land surrounding the lake are likely to play an important role in explaining the rainfall discrepancies noticed here. Further investigation is required to fully understand all the processes contributing to this rainfall bias.

As described earlier, the rainfall in the region of Lake Victoria undergoes a strong diurnal cycle. Figure 3.22 shows the diurnal variation in the model convective rainfall rate in the region of Lake Victoria, averaged across the entire ensemble for the period 1961-1990. Between 14:00 and 20:00, the convective rainfall is concentrated in a region to the North East of the lake. The peak then moves

westwards over the lake, until by 05:00 - 08:00 it covers its surface and has substantially increased in magnitude, before reducing in size once more and continuing westwards. This compares very well with the spatial pattern of convection seen in the cold cloud fraction (the fraction of cloud with temperature below 210K) derived from satellite data, (see Buontempo et al., 2013b for further details). In addition, model precipitation in this region is found to be influenced by processes in the Indian Ocean and Pacific Ocean, properties seen in studies of observational data sets (Buontempo et al, 2013b).
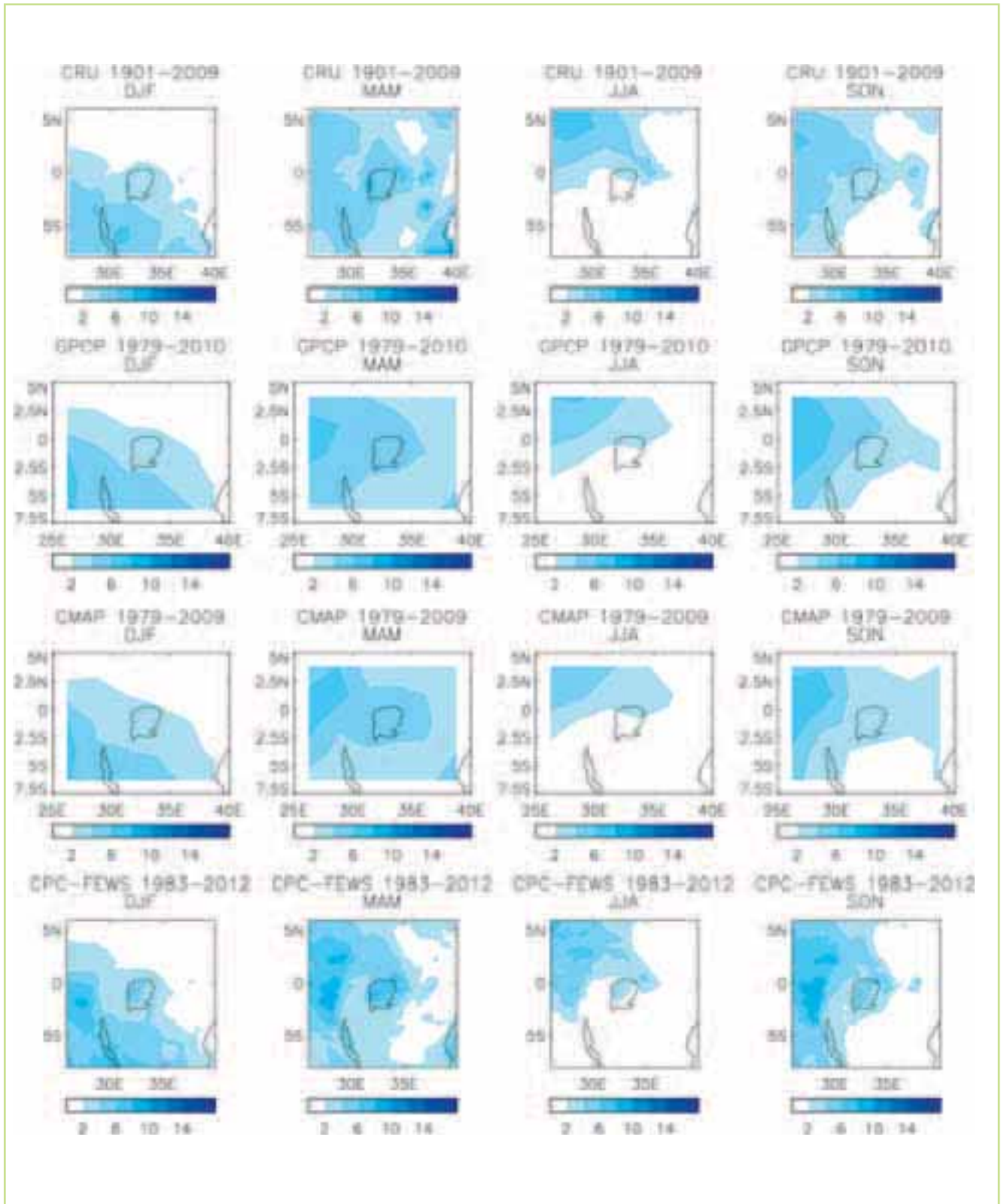
Figure 3.20 Daily precipitation averaged over each season over Africa (mm/day) for four observational datasets 1) CRU, 2) GPCP, 3) CMAP & 4) CPC-FEWS
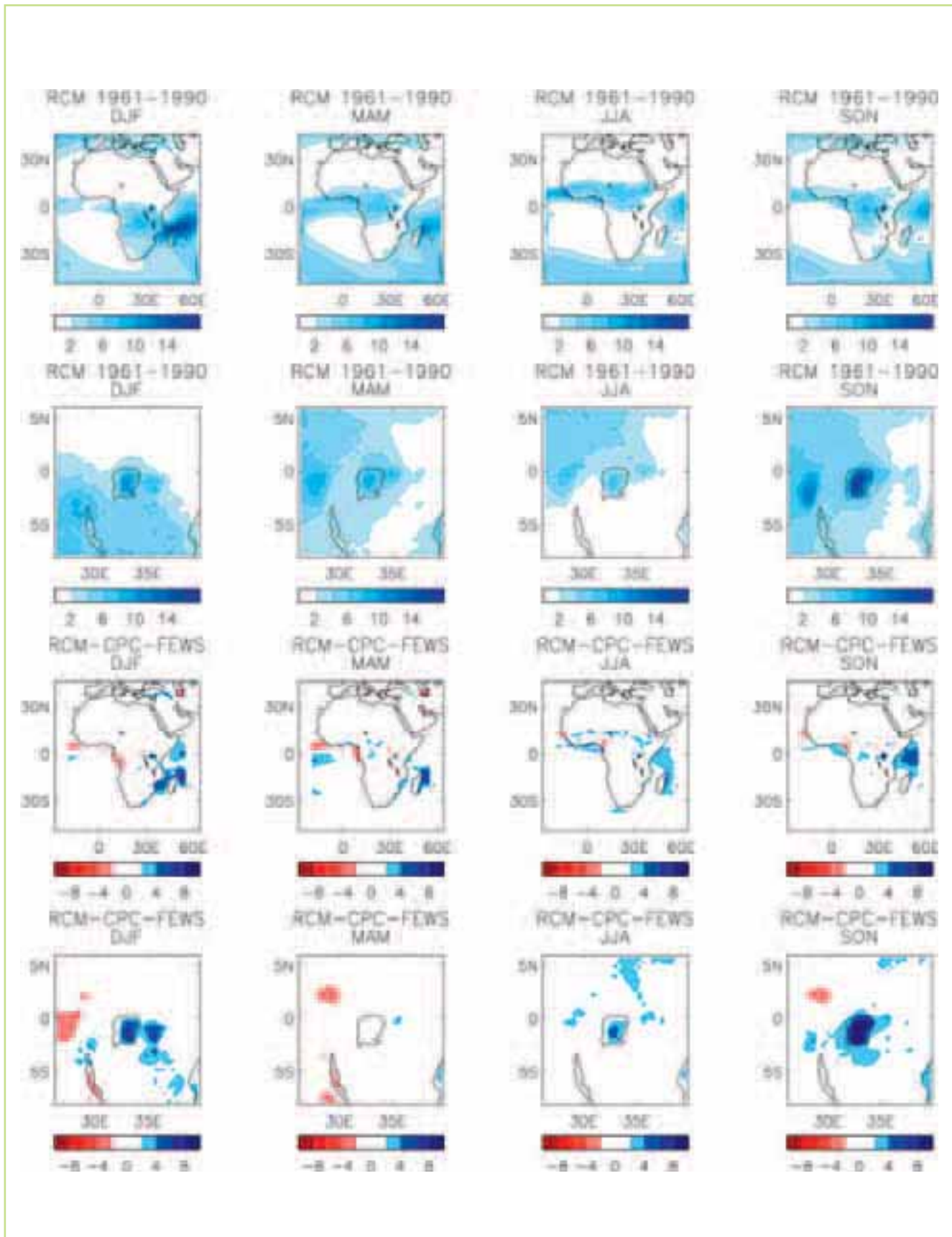
Figure 3.21 Average daily rainfall in mm/day for each season for the African continent (top) & the Lake Victoria region (second row) from the baseline model runs (average over 5 ensemble members) & model bias (bottom rows) when compared to CPC-FEWS
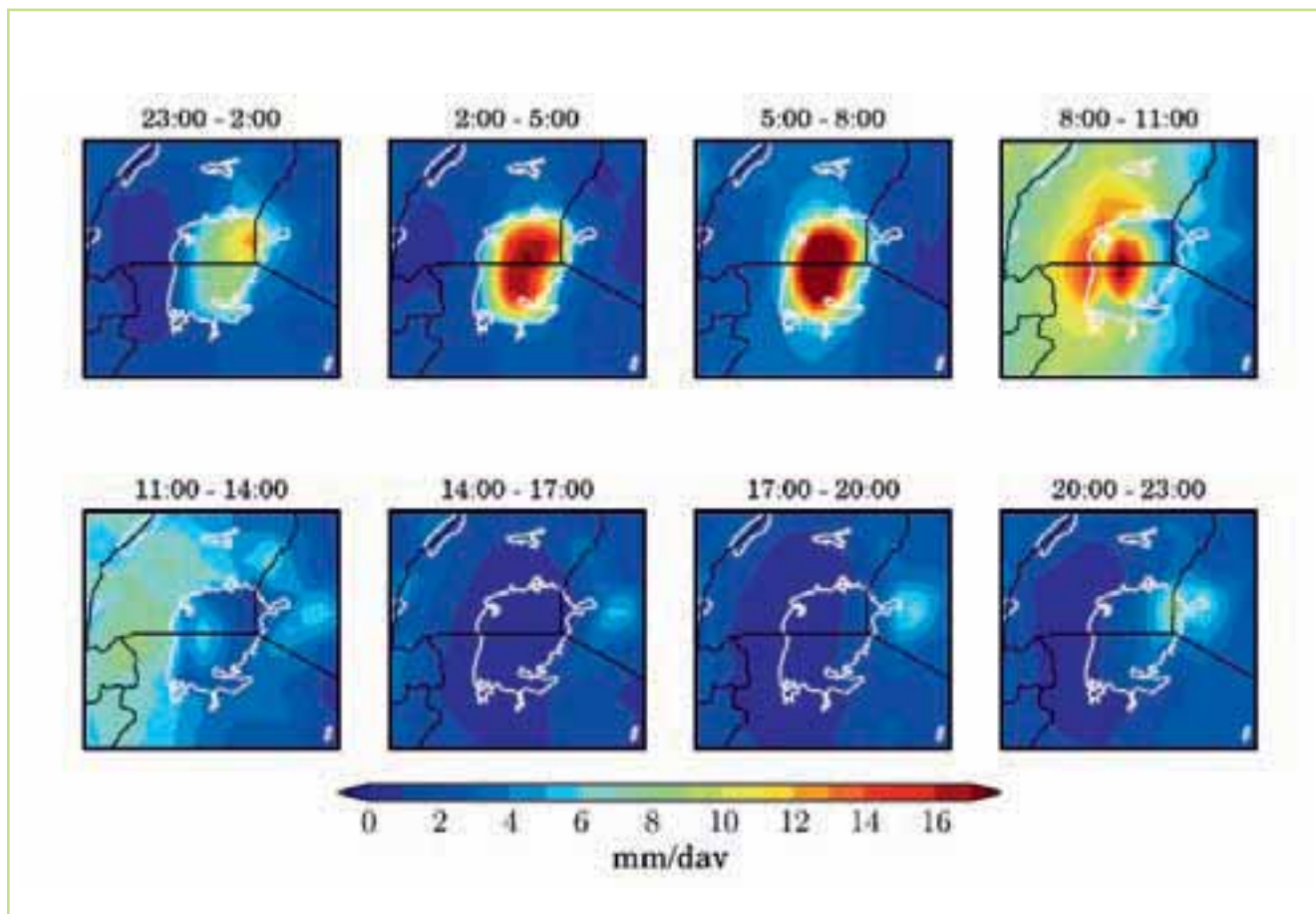
Figure 3.22 Convective rainfall in the model, averaged over each day in a baseline period of 1961-1990 & averaged over the RCM ensemble

3.6.4 Summary

In summary, the RCM ensemble derived in this study captures the annual cycle of temperatures across the whole of Africa and in the sub-regions. In general, the RCM ensemble slightly overestimates the precipitation as a whole but appears to capture the annual cycle of Africa for most of the sub-regions. The regional model ensemble shows a substantial improvement over the GCM ensemble in many regions. This is particularly noticeable in the Sahel, where the RCM does a much better job of reproducing both the magnitude and timing of the wet season.

For the Nile Basin, the relevant sub-regions are the Horn of Africa, East Sahel and North Africa. The RCM ensemble members capture satisfactorily both the dynamics and magnitude of the temperature in these sub-regions, although some relatively small biases remain. For precipitation, the most important sub-region is the Horn of Africa. Here there appears to be a consistent over-estimation both in the period from June to December and this is a consistent pattern for all ensemble members.

The RCM simulations over Lake Victoria are particularly challenging. Nevertheless each RCM model run contains a land and lake breeze and reproduces the spatial and temporal pattern of precipitation well, which represents a significant improvement on the global climate model results. In comparing the model precipitation with observed values, we find that there is a large positive bias in the model in most seasons which is closely tied to the location of the lake. However further investigation is required to fully understand all the processes contributing to this bias.

As stated at the outset of this section, the projection of robust regional changes in climate over the next 50-100 years still presents a considerable challenge for the current generation of climate models and this is still a rapidly developing field. The approach adopted here has been to exploit the novel perturbed physics ensemble approach as the basis for an assessment of variability in climate projections. The systematic selection procedure used has the advantages that the smaller ensemble is better conditioned, i.e. better able to represent current climate in most regions of Africa and at the same time also represent the range of variability expressed in a larger ensemble.

The assessment of changes in water resources at the regional scale for the Nile basin will therefore be carried out using these, bias-corrected RCM climate simulations.

4.0 Water demand (development) scenarios

Sections 4.1 and 4.2 describe the development of the estimates of water demand as indicators introduced in Section 2.6. The objectives for developing these scenarios are to assess the vulnerability to changes in water demand in the region and to compare the magnitude of these projected changes in demand to climate change. The approach to representing these demands in the model is described in Section 4.3. The water demands of three sectors are considered:

- Agricultural: considers total crop water requirements (including groundwater and surface water withdrawals, as well as considering direct precipitation) in irrigated areas.
- Industrial: considers water withdrawals for industrial use for self-supplied industries not connected to the public distribution network (Aquastat 2012)
- Municipal: considers total water withdrawn by the public distribution network. It can include industrial withdrawals from the municipal network (Aquastat 2012).

A baseline water demand scenario is established as a reference level for water demand. As described in Section 2, the two projection periods are 2020-2049 and 2070-2099, in accordance with the projected climate periods. However, a conservative approach has been taken for estimating the demands for these two periods. Thus, 2050 represents the period 2020-2049, and 2100 represents the period 2070-2099.

4.1 Agricultural water demand

4.1.1 Baseline
The most comprehensive and up-to-date data publically available on basin-scale agricultural water use in the Nile basin is the FAO Nile project, which developed a number of "information products" intended to support water resources management in the basin. These products include an effort to project future agricultural water use from a 2005 baseline (FAO 2011a). The FAO study considers water use by both rain-fed and irrigated agriculture (in other words, crop evapotranspiration).

However, the focus of this project is on the management of freshwater resources. As the evapotranspiration (ET) from rain-fed cultivated land is unlikely to be significantly different from the ET from uncultivated land, the impact of rain-fed

cultivation on the overall water balance of the Nile is considered negligible (FAO 2011a), and is not included in the scenarios of water demand developed here. Nevertheless, changes in precipitation and evaporative demand from future changes in climate are expected to have a direct impact on the viability and sustainability of rain-fed agriculture. Some indications of these changes are given by the Climate Moisture Index (CMI) presented in section 6.2.

The 2005 baseline agricultural water demand based developed here was also used to estimate water demands for the control period used for regional hydrological baseline. While it can be argued that the expected demands are likely to be lower for the period 1961-1990 extrapolating backwards in time is highly uncertain. The actual demands during the control period may be smaller because of the lower population levels but may be larger because of reduced irrigation efficiency, crop choice, etc. The baseline estimates for 2005 from FAO are based on expert knowledge of these factors but have not been made for the control period. National estimates of irrigation from FAO appear first in the 1990's. Thus rather than introducing additional uncertainty the FAO 2005 agriculture water demands are used as a reference level in this study rather than a historically accurate representation of the actual demands during the control period. This study focuses on the magnitude of changes in the water demand when compared to the changes in flows as a result of climate change.

The overall approach to developing the baseline estimates was firstly to use the volumes of water demand were derived from the FAO 2011. To develop indicator maps of the spatial distribution of water demand the Global Map of Irrigated Areas (GMIA) developed in collaboration with FAO was used (Siebert et al., 2007) as the FAO Nile data did not include the spatial distribution data. The spatial distribution of these demands in the regional model is described in section 4.3. The seasonal distribution of these demands throughout the year is made according to FAO (2000). The derivation of the maps of baseline and projected agricultural water demands is presented in detail below.

In the FAO study, irrigation demands are estimated using cropping calendar data compiled at district level throughout the basin. ET demands are translated into water withdrawals by using the

national 'water requirement ratio' (WRR) calculated by FAO in AQUASTAT. The WRR is the ratio between the estimated irrigation water requirements and the actual irrigation water withdrawal. This assumes that the same ratio can be applied to the entire portion of the country in the basin. The estimate gives an upper limit to agricultural water withdrawals based on reference ET. Actual ET and actual withdrawals will always be below this limit. Therefore the estimates of agricultural water demand will represent an upper bound.

In order to include the agricultural water demand in the model, it is necessary to distribute demands spatially. The country level data is compiled from 216 irrigation districts throughout the basin (FAO 2011a). Unfortunately, data released by FAO in accordance with the data-sharing agreement with the Nile countries does not contain the spatial data for the irrigation districts for all countries. As an alternative, the Global Map of Irrigated Areas (GMIA), developed in collaboration with FAO, can be used to distribute national-level demands over the basin. The GMIA (Siebert et. al. 2007) defines the percentage of each 5 minute pixel equipped for irrigation. The GMIA is considered the most up to date, readily available data source for distributing irrigation demands throughout the Nile Basin.

The areas equipped for irrigation according to the GMIA are not exactly consistent with harvested irrigated areas presented in the FAO Nile report (2011a), as shown in Table 4.1. While the overall difference in irrigated area varies by 3%; considerable differences exist from country to country. The FAO (2011a) dataset is considered to be more accurate as the data collection effort was focussed on the Nile basin and is more up to date. Therefore, the spatially distributed irrigated areas presented in the GMIA were scaled to match national totals presented by FAO (2011a) (Table 4.1). This was done as follows, with the column numbers referring to those in Table 4.1:

1. The area equipped for irrigation, according to GMIA, was determined for each country in ArcGIS based on the GMIA grid (column 3).
2. The harvested irrigated areas (FAO 2011a, column 2) was divided by the area equipped for irrigation (GMIA, column 3), to give a scaling factor (column 4).
3. The GMIA grid was then multiplied by the scaling factor in ArcGIS to produce a scaled grid.

Table 4.1 Irrigated areas by country

1 2		3	4	5	6
	Harvested irrigated areas	Area equipped for irrigation	Scaling factor (GMIA to FAO 2011a)	Harvested irrigated areas check	Harvested irrigated areas difference check
Unit	km²	km²	Factor	km²	%
Source	FAO 2011a	GMIA (Siebert et al. 2007)	(FAO 2011a) / GMIA	Calculated in ArcGIS using the scaled GMIA distribution.	% difference between original FAO 2011a data and rescaled area using GMIA distribution
Egypt	39,270	30,732	1.28	39,338	0.2%
Sudan[6]	11,567	18,240	0.63	11,491	-0.7%
Eritrea	41	54	0.77	42	0.5%
Ethiopia	142	906	0.16	145	2.3%
Uganda	332	90	3.69	332	-0.1%
Kenya	417	144	2.90	417	0.0%
Tanzania	1	12	0.10	1	-4.4%
Rwanda	156	82	1.90	156	-0.2%
Burundi	32	26	1.19	31	-0.3%
Total	51,959	50,288		51,953	0.0%

[5]South Sudan became an independent state on 9 July 2011. The data on which these estimates were made predates this event. The available irrigation information contains therefore values including both South Sudan (Republic of South Sudan) & Sudan (Republic of Sudan)

[6]South Sudan became an independent state on 9 July 2011. The data on which these estimates were made predates this event. The available irrigation information contains therefore values including both South Sudan (Republic of South Sudan) and Sudan (Republic of Sudan)

Table 4.2 Water withdrawal for irrigation, based on crop ET (FAO 2011a)

Country	Irrigation water
Egypt	68.80
Sudan	27.51
Eritrea	0.127
Ethiopia	0.483
Uganda	0.829
Kenya	1.076
Tanzania	0.003
Rwanda	0.317
Burundi	0.048
Total	99.19

4. The new harvested irrigated areas within each country portion of the basin was then determined in ArcGIS from the scaled grid (column 5), and checked against the country portions from FAO 2011a (column 2), giving the differences in percent (column 6).

Both datasets indicate that areas under irrigation in Egypt and Sudan exceed irrigated areas in other basin countries by two to three orders of magnitude. Using the scaled GMIA estimates, the differences between the two estimates of irrigated area for Egypt and Sudan[5] are less than 1%.

FAO 2011a specifies the estimated annual water withdrawn for irrigation for the harvested irrigated areas (Table 4.2), based on crop ET as described on previous page.

Table 4.3 Crop area as proportion of the total area equipped for irrigation by month (FAO 2000)

	Jan	Feb	Mar	Apr	May	Jun	Jul	Aug	Sep	Oct	Nov	Dec
Egypt	1	0.93	0.99	0.98	0.67	0.79	0.86	0.86	0.8	0.79	1	1
Sudan	0.48	0.48	0.48	0.39	0.39	0.48	0.48	0.48	0.48	0.48	0.48	0.48
Eritrea	0.36	0.36	0.36	0.36	0.07	0.07	0.39	0.39	0.39	0.39	0.39	0.36
Ethiopia	0.63	0.63	0.63	0.4	0.4	0.66	0.66	0.66	0.66	0.66	0.63	0.63
Uganda	0.44	0.44	0.44	1	1	1	1	1	0.44	0.44	0.44	0.44
Kenya	0.81	0.81	0.43	0.71	0.71	0.71	0.71	0.71	0.43	0.81	0.81	0.81
Tanzania	0.36	0.36	0.36	0.24	0.24	0.49	0.49	0.49	0.39	0.39	0.36	0.36
Rwanda	0.17	0.67	0.67	0.67	0.67	0.67	0.17	0.17	0.17	0.17	0.17	0.17
Burundi	0.9	0.9	0.9	0.9	0.9	0.9	0.12	0.12	0.9	0.9	0.9	0.9

Table 4.4 Water withdrawals per month per unit irrigated area (thousand m^3/km^2) (FAO 2011)[7]

	Jan	Feb	Mar	Apr	May	Jun	Jul	Aug	Sep	Oct	Nov	Dec
Egypt	160	150	160	160	110	130	140	140	130	130	160	160
Sudan	200	200	200	170	170	200	200	200	200	200	200	200
Eritrea	280	280	280	280	60	60	310	310	310	310	310	280
Ethiopia	300	300	300	190	190	310	310	310	310	310	300	300
Uganda	140	140	140	310	310	310	310	310	140	140	140	140
Kenya	250	250	130	220	220	220	220	220	130	250	250	250
Tanzania	180	180	180	120	120	250	250	250	200	200	180	180
Rwanda	80	300	300	300	300	300	80	80	80	80	80	80
Burundi	150	150	150	150	150	150	20	20	150	150	150	150

[7]Note the values in the table have been rounded to the nearest ten thousand m^3/km^2 for clarity of presentation.
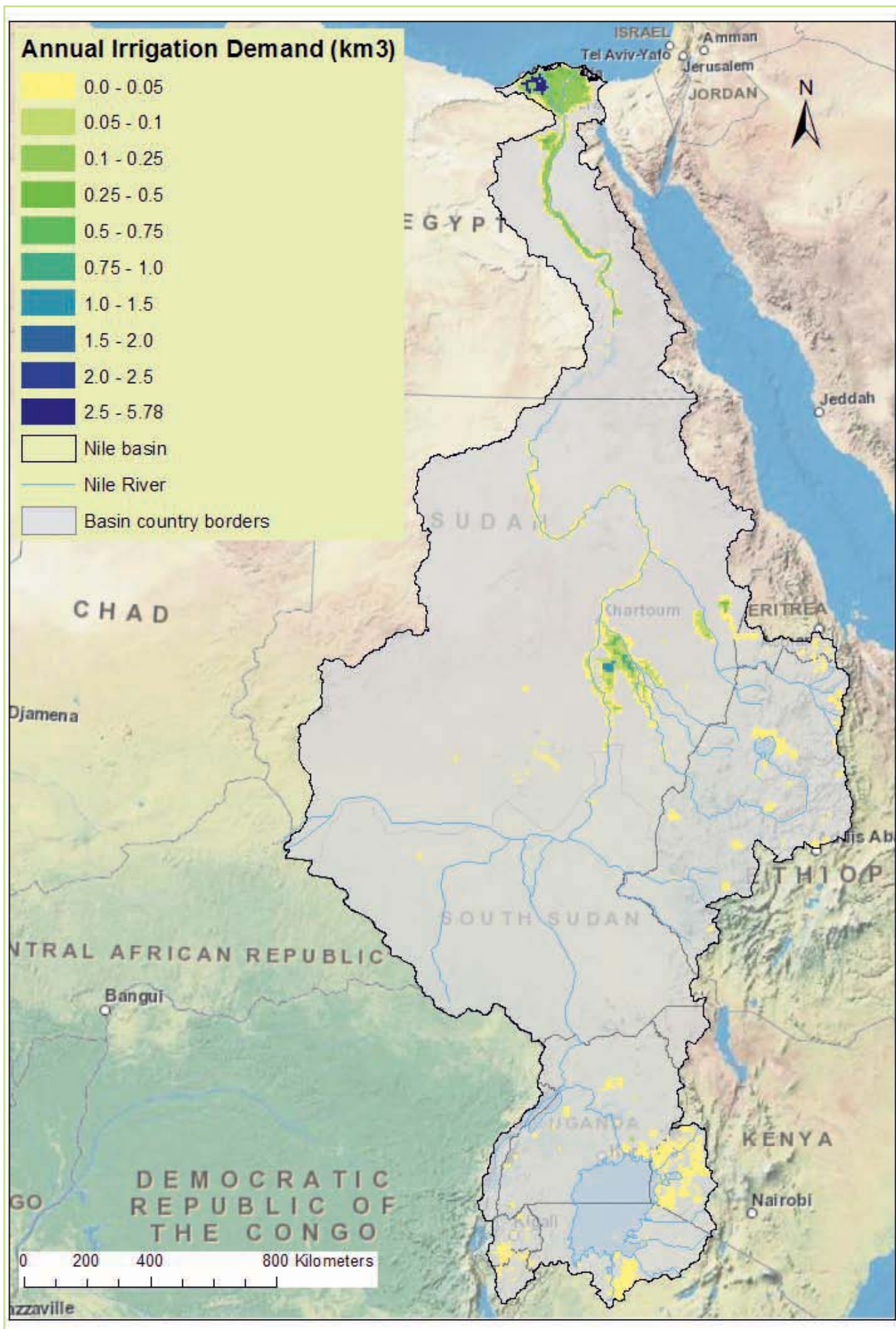
Figure 4.1 Baseline spatial distribution of annual irrigation withdrawals (2005)

In order to obtain a monthly irrigation demand, the annual, national values from Table 4.2 are distributed through the year using the proportion of total area equipped for irrigation in each month (FAO 2000) (Table 4.3).

The derived monthly irrigation withdrawals are then divided by the harvested irrigated area (Table 4.1, column 2), to give the irrigation withdrawals per unit area (Table 4.4).

In ArcGIS, the areas equipped for irrigation, according to GMIA, are multiplied by the scaling factor (Table 4.1), as described above. Finally, these scaled areas are multiplied by the monthly water withdrawals per unit of irrigated area (described in Table 4.4), to give a spatial distribution of water withdrawal per month.

Figure 4.1 shows the spatial distribution of annual irrigation withdrawals for the 2005 baseline using the FAO 2011a volumes and the GMIA irrigated areas

After the irrigation demands were spatially distributed in ArcGIS, a check was undertaken to compare the irrigation demands for each country according to FAO (2011a) and those aggregated to the country level in ArcGIS (Table 4.5). The percentage differences are considered well within the bounds of uncertainty for other inputs, and are therefore acceptable for the purposes of this study.

The above methodology includes the following main assumptions:

- The proportions of irrigation withdrawals for each month are distributed evenly throughout each country (FAO 2000, Table 4.3). This was the most detailed source of publicly available information that could be found on the monthly distribution of irrigation that covered all countries.
- The Global Map of Irrigated Areas (GMIA) is the most accurate spatial distribution of irrigated areas publically available.

Table 4.5 Water withdrawal for irrigation by country after spatial distribution

	Irrigation withdrawals		Percentage difference
Unit	km³	km³	%
Source	FAO 2011a	After redistribution using GMIA and aggregation in ArcGIS	Calculation
Egypt	68.80	68.91	0.2%
Sudan	27.51	27.33	-0.7%
Eritrea	0.127	0.128	0.5%
Ethiopia	0.483	0.494	2.3%
Uganda	0.829	0.828	-0.1%
Kenya	1.076	1.076	0.0%
Tanzania	0.003	0.003	-4.4%
Rwanda	0.317	0.316	-0.2%
Burundi	0.048	0.048	-0.3%
Total	99.19	99.14	-0.1%

Table 4.6 Projected water withdrawal for irrigation (FAO 2011a)

	Weighted mean unit irrigation withdrawals (m³/ha)	2005		2030			2050		
		Water use requirement ratio	Irrigation withdrawals (km³)	Water use requirement ratio	Irrigation withdrawals (km³)	% increase in withdrawals from 2005	Water use requirement ratio	Irrigation withdrawals (km³)	% increase from 2005
Egypt	9,285	0.53	68.80	0.61	71.74	4.3%	0.64	73.64	7.0%
Sudan	9,513	0.40	27.51	0.43	30.18	9.7%	0.50	34.64	25.9%
Eritrea	9,847	0.32	0.13	0.33	0.22	70.1%	0.33	0.25	94.5%
Ethiopia	7,498	0.22	0.48	0.22	0.66	37.3%	0.22	1.08	124.2%
Eastern Nile Total	-	-	96.92	-	102.80	6.1%	-	109.60	13.1%
Uganda	7,493	0.30	0.83	0.30	2.26	173.0%	0.31	2.69	224.8%
Kenya	7,746	0.30	1.08	0.31	1.48	37.9%	0.31	1.89	75.8%
Tanzania	8,071	0.30	0.00	0.31	0.01	66.7%	0.30	0.01	133.3%
Rwanda	6,076	0.30	0.32	0.30	0.38	20.2%	0.31	0.45	41.0%
Burundi	4,557	0.30	0.05	0.31	0.09	77.1%	0.30	0.13	172.9%
Equatorial Lakes Total	-	-	2.27	-	4.22	85.5%	-	5.17	127.4%
Nile Basin Total	-		99.19		107.02	7.9%		114.77	15.7%

4.1.2   Projections of future irrigation demand

FAO (2011a) have produced projections for irrigation withdrawals for 2030 and 2050. These assume:

- The annual cropping calendar remains the same as the baseline scenario,
- The water use requirement ratio considers projected responses to climate change and the capacity to adopt more progressive irrigation technology and management.

The projections for the portion of each country within the Nile basin are given in Table 4.6.

A conservative approach has been used to estimate the irrigation water demand values for the period 2020 - 2049 by applying the 2050 irrigation withdrawal estimates throughout this period.

As with the baseline scenario, it was not possible to obtain GIS files corresponding to the projections in the report from FAO. Estimating the spatial distribution of the projected withdrawals is not a straightforward task. Therefore, it was assumed that the projected withdrawals have the same spatial

Table 4.7 Irrigated areas by country 2050 (km²)

	Area equipped for irrigation (ca. 2000)	Harvested irrigated areas 2050	Scaling factor (GMIA to FAO 2050)
Unit	km³	km³	
Source	GMIA (Siebert et al. 2007)	FAO 2011a	Calculation
Egypt	30,732	50,758	1.65
Sudan	18,240	18,204	1.00
Eritrea	54	83	1.53
Ethiopia	906	318	0.35
Uganda	90	1,114	12.39
Kenya	144	757	5.26
Tanzania	12	3	0.21
Rwanda	82	228	2.78
Burundi	26	87	3.27
Total	50,288	71,550	

Table 4.8 2050 water withdrawals per month per unit irrigated area (m^3/km^2)

	Jan	Feb	Mar	Apr	May	Jun	Jul	Aug	Sep	Oct	Nov	Dec
Egypt	135,964	126,446	134,604	133,244	91,096	107,411	116,929	116,929	108,771	107,411	135,964	135,964
Sudan	163,664	163,664	163,664	132,977	132,977	163,664	163,664	163,664	163,664	163,664	163,664	163,664
Eritrea	276,404	276,404	276,404	276,404	53,745	53,745	299,438	299,438	299,438	299,438	299,438	276,404
Ethiopia	296,276	296,276	296,276	188,111	188,111	310,384	310,384	310,384	310,384	310,384	296,276	296,276
Uganda	131,633	131,633	131,633	299,166	299,166	299,166	299,166	299,166	131,633	131,633	131,633	131,633
Kenya	239,295	239,295	127,033	209,753	209,753	209,753	209,753	209,753	127,033	239,295	239,295	239,295
Tanzania	209,132	209,132	209,132	139,421	139,421	284,652	284,652	284,652	226,560	226,560	209,132	209,132
Rwanda	73,425	289,380	289,380	289,380	289,380	289,380	73,425	73,425	73,425	73,425	73,425	73,425
Burundi	147,443	147,443	147,443	147,443	147,443	147,443	19,659	19,659	147,443	147,443	147,443	147,443

distribution as the baseline scenario, using the global map of irrigated areas. This was deemed sufficient given the main focus of the study is regional scale impacts.

Initially, the irrigated area defined by the Global Map of Irrigated Areas (GMIA) was multiplied by a scaling factor to match the irrigated area for each country as defined by FAO (2011a) (Table 4.7). The harvested irrigated areas shown in shown in Table 4.7 are the projected harvested areas for 2050 within the Nile basin from the FAO (2011a) projections report (Table 4) rather than the country wide estimates.

The annual country irrigation withdrawals shown in Table 4.6 were distributed monthly using the same factors as in Table 4.3, giving monthly irrigation demands per unit of irrigated area (Table 4.8). It is important to note that baseline withdrawals per unit area shown in Table 4.4 for the baseline are generally larger than those shown in Table 4.8 for 2050 however the total withdrawals increase because of the increase in irrigated area (Table 4.1 and Table 4.7).

The monthly irrigation withdrawals per unit area in Table 4.8 were multiplied by the irrigated areas in Table 4.7, spatially distributed in ArcGIS using the GMIA distribution (Figure 4.2).

After the projected 2050 irrigation demands were spatially distributed in ArcGIS, a check was undertaken to compare the irrigation demands for each country according to FAO (2011a) and those aggregated to the country level in ArcGIS. There is an exact match between the two.

Table 4.9 Projected water withdrawal for irrigation 2030, 2050 & 2100 (km^2) (FAO 2011a)

	Irrigation withdrawals (km^3)		
	2030 2050		2100
Egypt 71,740		73,636	78,376
Sudan 30,182		34,635	45,7675
Eritrea 0,216		0,247	0,3245
Ethiopia 0,663		1,083	2,133
Uganda 2,263		2,693	3,768
Kenya 1,484		1,892	2,912
Tanzania 0,005		0,007	0,012
Rwanda 0,381		0,447	0,612
Burundi 0,085		0,131	0,246
Total	107,02	114,77	134,15
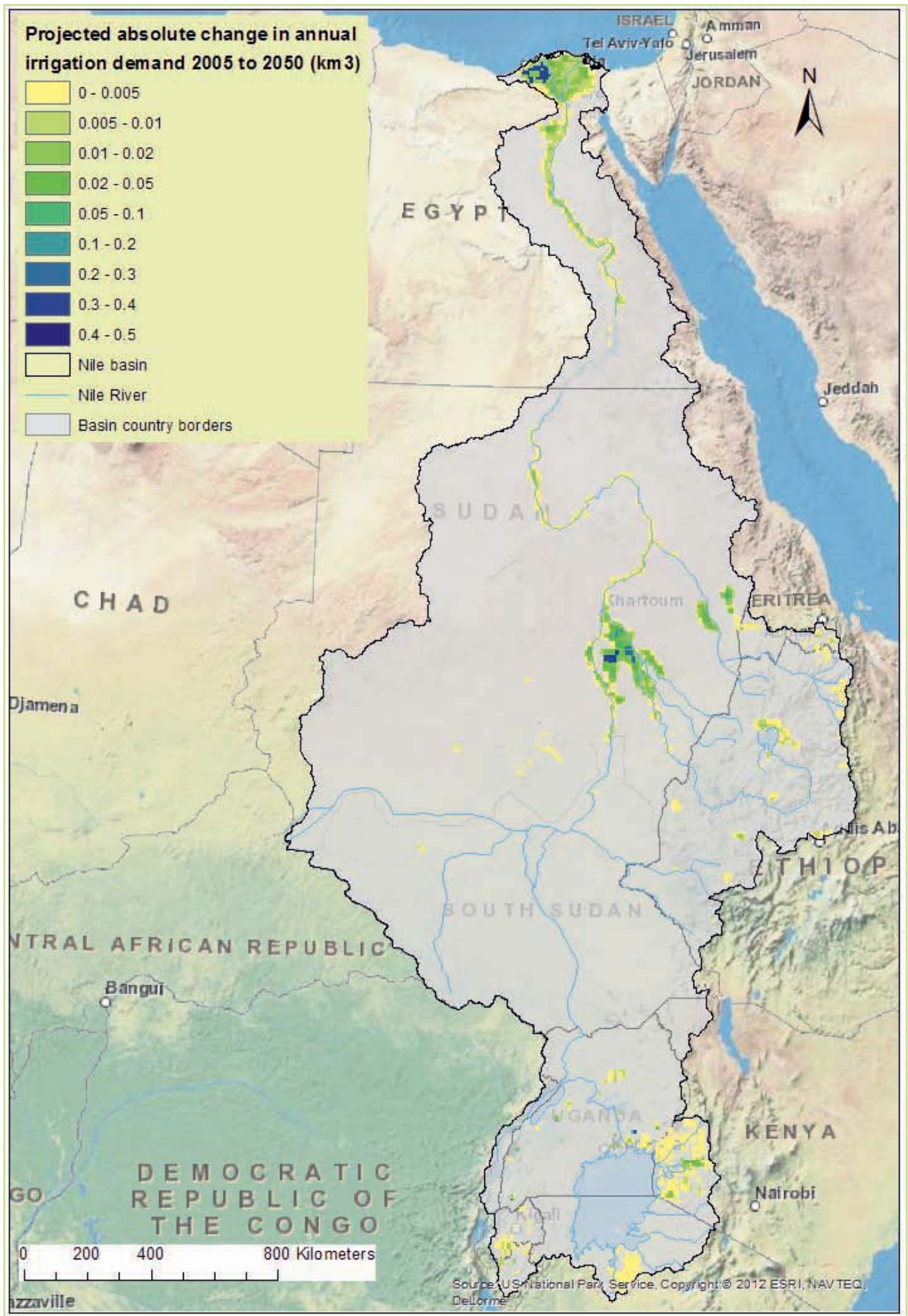
Figure 4.2 Projected changes in the annual irrigation withdrawals from the baseline to the 2020-2049 period represented by 2050 projection

The legend of the figure reads:

Projected absolute change in annual irrigation demand 2005 to 2050 (km3)

- 0 - 0.005
- 0.005 - 0.01
- 0.01 - 0.02
- 0.02 - 0.05
- 0.05 - 0.1
- 0.1 - 0.2
- 0.2 - 0.3
- 0.3 - 0.4
- 0.4 - 0.5
- Nile basin
- Nile River
- Basin country borders

For the period 2070 to 2099, a conservative approach has been adopted. Based on the 2030 and 2050 irrigation water demands published in FAO (2011), 2100 demands have been projected using the same spatial distribution and a straightforward linear extrapolation (Table 4.9). There is no basis for a more sophisticated estimation approach based on the information available.

4.2 Industrial & municipal water demand

4.2.1 Baseline

It was not possible to identify an existing source of spatially-distributed, up-to-date industrial and municipal water demand estimates suitable for the purposes of this project. Instead, estimates were developed from data aggregated at the national level and spatially distributed using population distribution.

National industrial and municipal water withdrawals were downloaded from AQUASTAT (2012). National population data were downloaded from UNDESA[8] (2010). Annual per capita demands

were derived by dividing the AQUASTAT water use estimates by the UNDESA population estimates (Table 4.10). The annual demands were distributed monthly by assuming an equal proportion of use each month.

In order to distribute per capita demands spatially, a 2005 population raster dataset developed as part of the FAO Nile project (FAONile 2011) was used. However, the raster data set appeared to underrepresent the population in each country when compared to the FAO Nile Synthesis Report (2011b) (see column 4 in Table 4.11). As the FAO Nile population raster was believed to be the best spatially distributed dataset available, the raster was multiplied by a unique scaling factor for each country (column 5) to obtain values comparable to FAO (2011b) (column 6). The differences between the FAO Synthesis Report (2011b, column 3) and the scaled population raster (column 6) are shown in column 7. These differences are minor (generally less than 1%), and are likely to be due to rounding errors in applying the scaling factor to a large number of cells.

Table 4.10 National* Industrial and municipal annual per capita withdrawals

	2005 Water withdrawals (km³/yr)		2005 Population (1000s)	Annual per capita water demand (m³/cap/yr)	
	Industrial	Municipal		Industrial	Municipal
Burundi	0.02	0.04	7,251	2.07	5.94
Congo DR	0.15	0.46	57,421	2.56	8.10
Egypt	3.57	6.87	74,203	48.12	92.60
Eritrea	0.00	0.03	4,486	0.22	6.91
Ethiopia	0.05	0.81	74,264	0.69	10.91
Kenya	0.10	0.47	35,615	2.81	13.20
Rwanda	0.02	0.06	9,202	2.23	6.67
Sudan	0.30	1.14	38,410	7.81	29.76
Tanzania	0.03	0.53	38,831	0.64	13.57
Uganda	0.04	0.11	28,431	1.55	4.04
Total	4.13	10.07	310,693		

* NB. The data in this table considers the whole country, not just the portion of each country within the Nile Basin.

[8] The United Nations Department of Economic & Social Affairs

Table 4.11 Nile Basin population calculation: baseline scenario

1	2 2005 basin population in each country		4 Population difference (%)	5 Scaling factor	6 Final population	7 Population difference check (%)
	Calculated from FAO Nile 2005 population raster*	From FAO (2011b)	Between FAO 2011b & pop2005 raster*	From FAO Nile raster to 2011b	Calculated from scaled population raster	Difference between FAO 2011b and scaled raster.
Burundi 3,531,298		4,615,000	-23%	1.31	4,605,960	-0.2%
Congo DR 1,768,508		1,851,000	-4%	1.05	1,887,950	2.0%
Egypt 54,650,880		72,617,000	-25%	1.33	71,763,536	-1.2%
Eritrea 880,413		1,721,000	-49%	1.95	1,699,999	-1.2%
Ethiopia 21,987,056		31,044,000	-29%	1.41	31,052,474	0.0%
Kenya 11,341,000		13,359,000	-15%	1.18	13,366,891	0.1%
Rwanda 5,920,502		7,685,000	-23%	1.30	7,686,111	0.0%
Sudan 23,657,744		32,406,000	-27%	1.37	32,401,010	0.0%
Tanzania 6,817,895		7,933,000	-14%	1.16	7,942,274	0.1%
Uganda 21,373,236		28,477,000	-25%	1.33	28,414,016	-0.2%
Total 151,928,532		201,708,000	-25%	1.33	200,820,222	-0.4%

* Based on the FAONile catchment boundary 'bas_hydrosheds_v2'

The municipal and industrial per capita demands (Table 4.10) were then multiplied by the scaled population raster (Table 4.11) to give spatially distributed industrial and municipal demands throughout the basin (Figure 4.3 and Figure 4.4).

The municipal and industrial per capita demands (Table 4.10) were then multiplied by the scaled population raster (Table 4.11) to give spatially distributed industrial and municipal demands throughout the basin (Figure 4.3 and Figure 4.4).

4.2.2 Industrial & municipal water demand projections

Industrial and municipal water use projections were assumed to be a function of population growth only (in other words, per capita water use is assumed not to change). Although per capita use may be expected to increase due to increases in water supply and wealth, these trends maybe offset to some extent by increases in efficiency. Given the lack of literature on changes in per capita municipal and industrial water demand globally and within the Nile Basin to 2050, it is assumed that the per capita municipal and industrial withdrawals used in the baseline scenario are still appropriate for the projections.

Population projections are based on projections made by UNDESA (2010). UNDESA has made 5-yearly national population projections till 2100, with low, medium, high, and constant fertility variants. The medium variant was chosen for this study.

The UNDESA projections are aggregated at the national level and must be distributed spatially. To maintain consistency with the baseline scenario, the FAO Nile 2030 population raster for the Nile Basin countries was used to estimate the spatial distribution of population (FAO Nile 2011). However, similar to the 2005 raster, there appear to be inconsistencies with the data in the raster file when aggregated nationally compared to the national data from UNDESA (Table 4.12, columns 2-4). A scaling factor was therefore used to produce 2050 and 2100 population rasters with aggregate national population totals comparable to UNDESA national population projections for 2050 and 2100. This scaling method assumes a uniform increase in population across each country. The percentage differences given in columns 8 and 12 of Table 4.12 are within the bounds of uncertainty for other inputs.

The municipal and industrial per capita demands (Table 4.10) were then multiplied by the scaled population raster (Table 4.12) to give spatially distributed industrial and municipal demands throughout the basin for 2050 and 2100 (Figure 4.5 to Figure 4.8).

Industrial demand
m3

	0 - 1,000
	1,000 - 6,048
	6,048 - 9,866
	9,866 - 13,684
	13,684 - 17,501
	17,501 - 21,319
	21,319 - 25,136
	25,136 - 28,954
	28,954 - 32,771
	32,771 - 36,589
	36,589 - 40,407
	40,407 - 44,224
	44,224 - 6,631,266

Nile River
Nile Basin
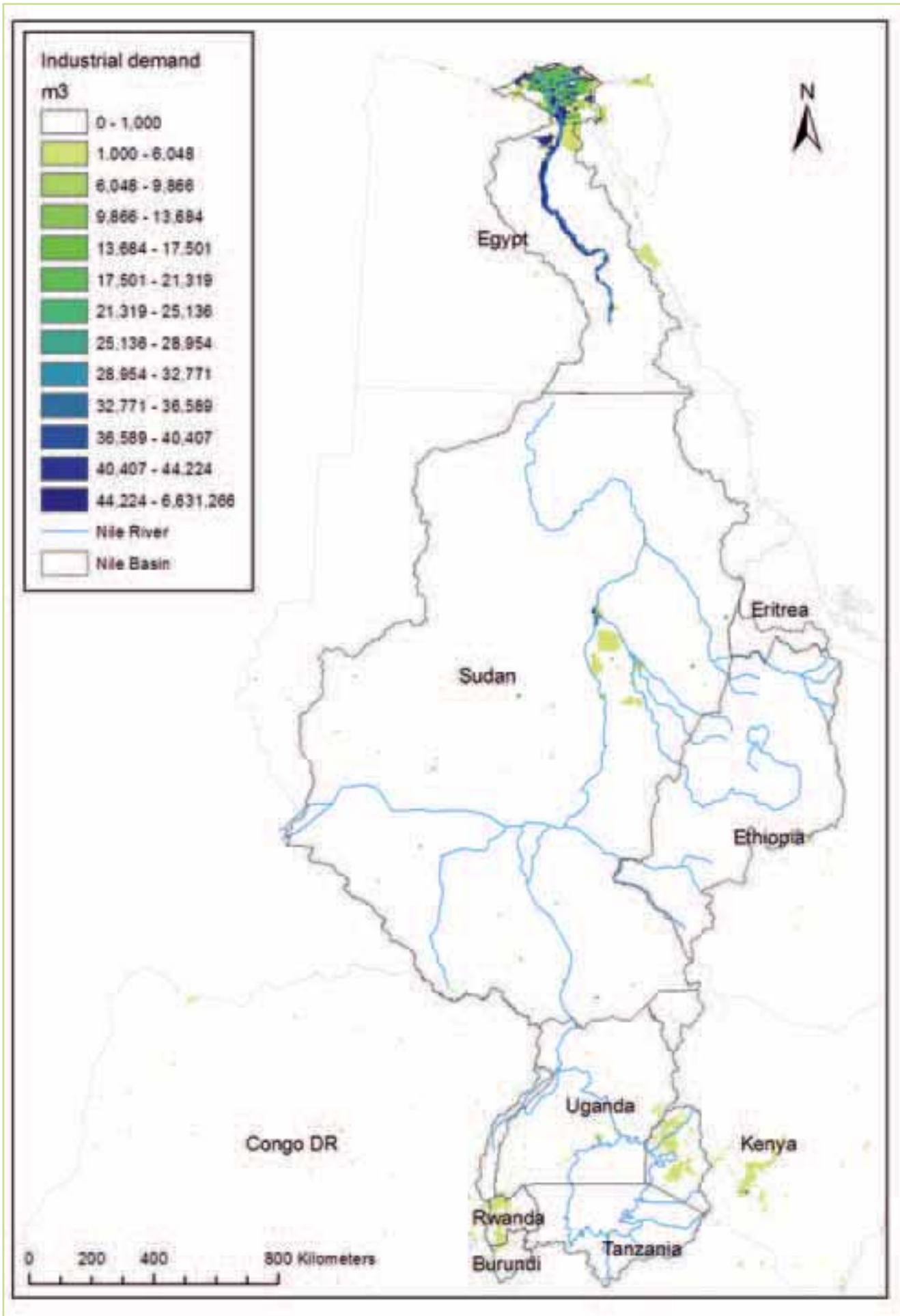
Figure 4.3 Spatial distribution of baseline annual industrial withdrawals (2005)
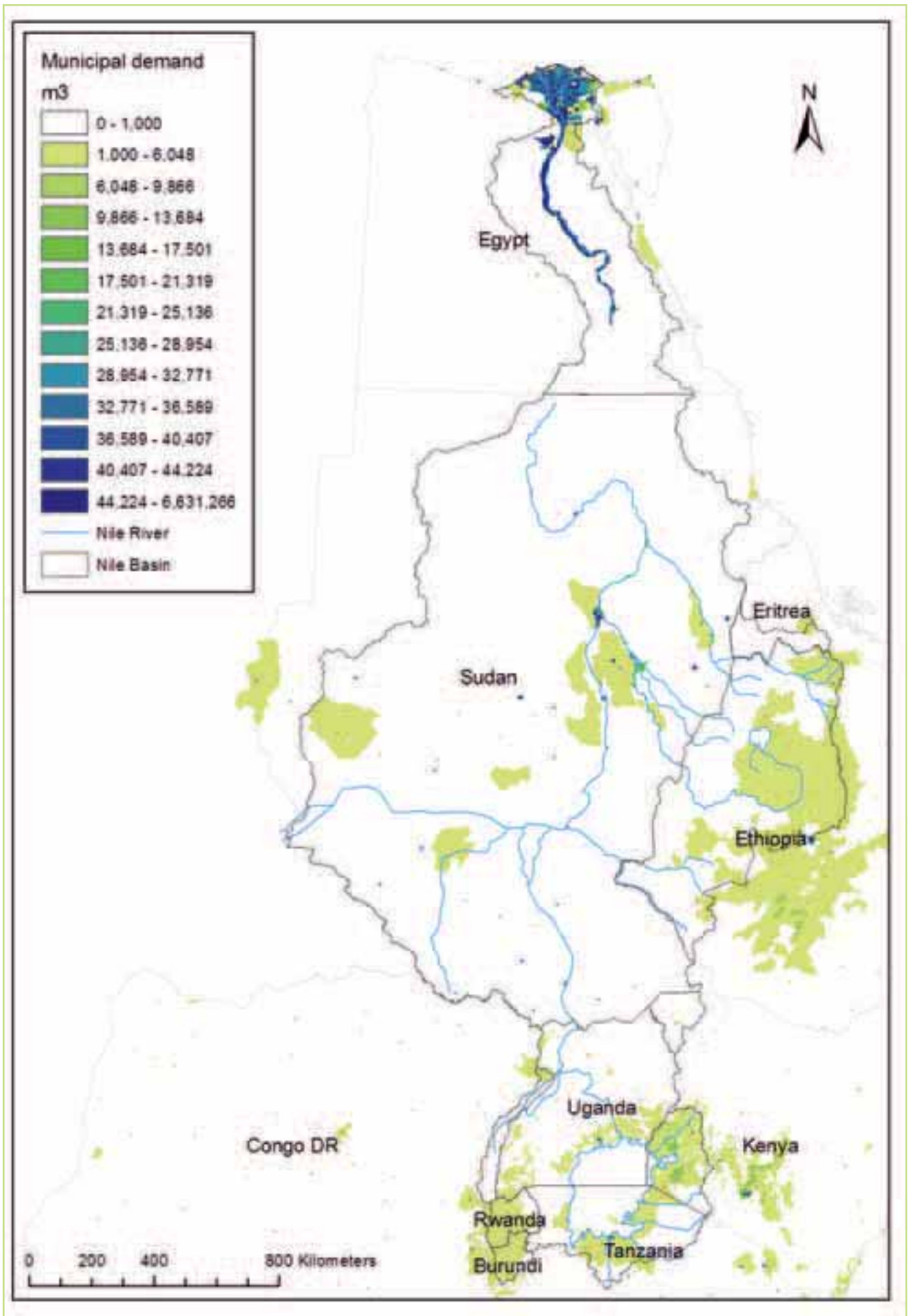
Figure 4.4 Spatial distribution of baseline annual municipal withdrawals (2005)

1 2		3	4	5	6	7	8	9	10	11	12
Parameter	2030 national population	2030 national population	Population difference (%)	2050 national population	Scaling factor	Final national population (whole country)	2050 Population difference check (%)	2100 national population	Scaling factor	Final national population (whole country)	2100 Population difference check (%)
Source	Calculated from FAO Nile 2030 population raster	UNDESA (2010)	UNDESA (2010) & pop2030 raster (FAONile 2011)	UNDESA (2010)	From FAO Nile raster to UNDESA (2010)	Calculated from scaled population raster based on national boundaries	Difference between UNDESA (2010) & scaled raster	UNDESA (2010)	From FAO Nile raster to UNDESA (2010)	Calculated from scaled population raster based on national boundaries	Difference between UNDESA 2010 & scaled raster
Burundi	6,109,885	11,441,000	-47%	13,703,000	2.24	13,076,072	-4.6%	14,587,000	2.39	13,919,631	-4.6%
Congo DR	97,392,424	105,956,000	-8%	148,523,000	1.52	146,966,430	-1.0%	212,113,000	2.18	209,750,220	-1.1%
Egypt	55,998,124	106,498,000	-47%	123,452,000	2.20	117,357,450	-4.9%	123,227,000	2.20	117,143,550	-4.9%
Eritrea	6,185,818	8,394,000	-26%	11,568,000	1.87	12,162,701	5.1%	15,496,000	2.51	16,292,637	5.1%
Ethiopia	109,744,420	118,515,000	-7%	145,187,000	1.32	152,212,700	4.8%	150,140,000	1.37	157,366,590	4.8%
Kenya	55,964,768	65,928,000	-15%	96,887,000	1.73	95,528,712	-1.4%	160,009,000	2.86	157,685,380	-1.5%
Rwanda	14,285,408	17,579,000	-19%	26,003,000	1.82	25,247,532	-2.9%	42,316,000	2.96	40,987,792	-3.1%
Sudan	53,009,408	66,856,000	-21%	90,962,000	1.72	95,002,552	4.4%	127,621,000	2.41	133,280,130	4.4%
Tanzania	68,189,704	81,852,000	-17%	138,312,000	2.03	128,967,290	-6.8%	316,338,000	4.64	294,942,910	-6.8%
Uganda	42,840,016	59,846,000	-28%	94,259,000	2.20	93,4e06,728	-0.9%	171,190,000	4.00	169,642,110	-0.9%
Total	509,719,975	642,865,000	-21%	888,856,000	1.74	879,928,167	-1.0%	1,333,037,000	2.62	1,311,010,950	-1.7%

Table 4.12   Nile Basin population calculation: projected scenarios
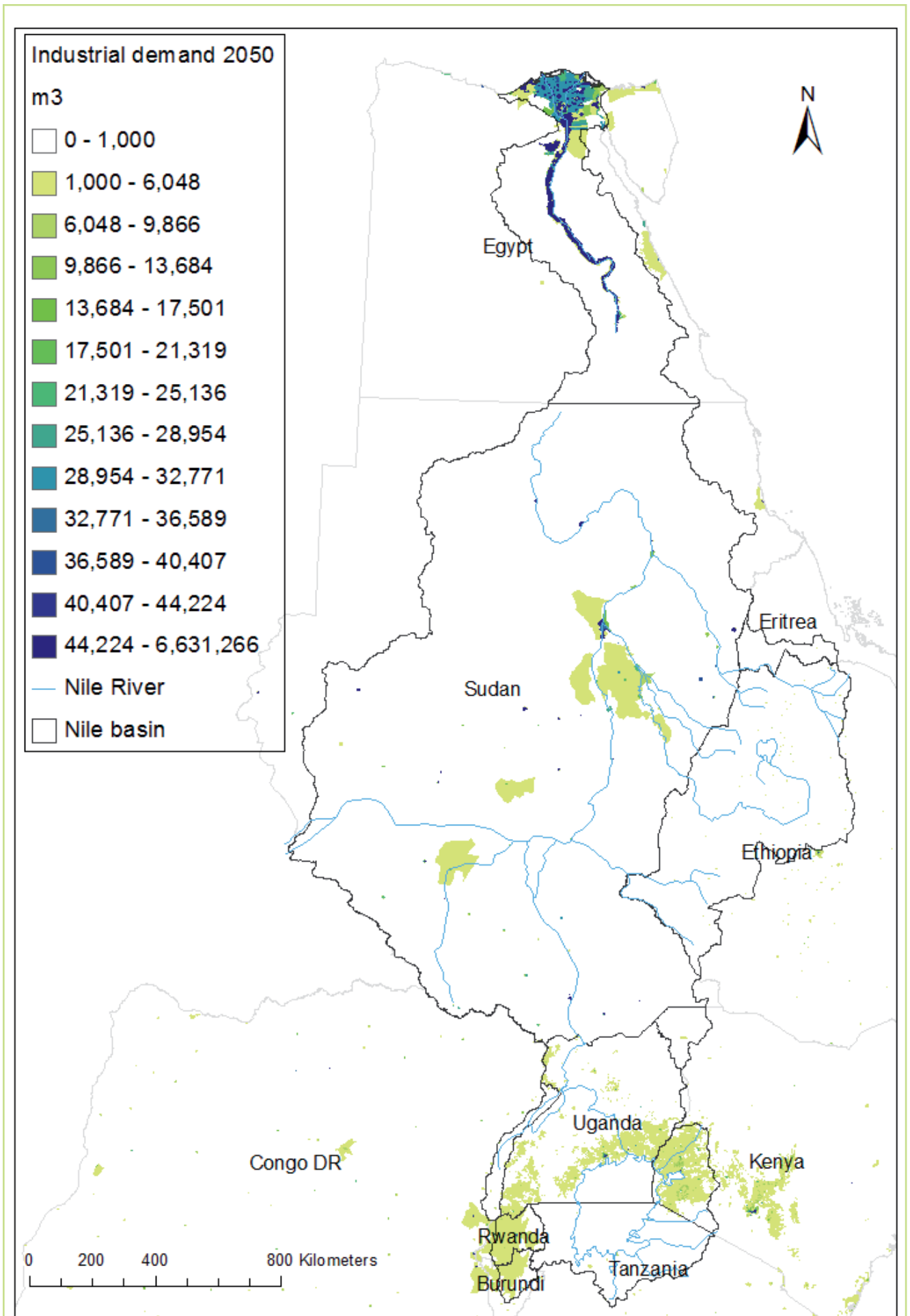
Figure 4.5 Spatial distribution of projected annual industrial withdrawals (2020-2049 period represented by 2050 projection)

Municipal demand 2050 m3

- 0 - 1,000
- 1,000 - 6,048
- 6,048 - 9,866
- 9,866 - 13,684
- 13,684 - 17,501
- 17,501 - 21,319
- 21,319 - 25,136
- 25,136 - 28,954
- 28,954 - 32,771
- 32,771 - 36,589
- 36,589 - 40,407
- 40,407 - 44,224
- 44,224 - 6,631,266
- Nile River
- Nile basin
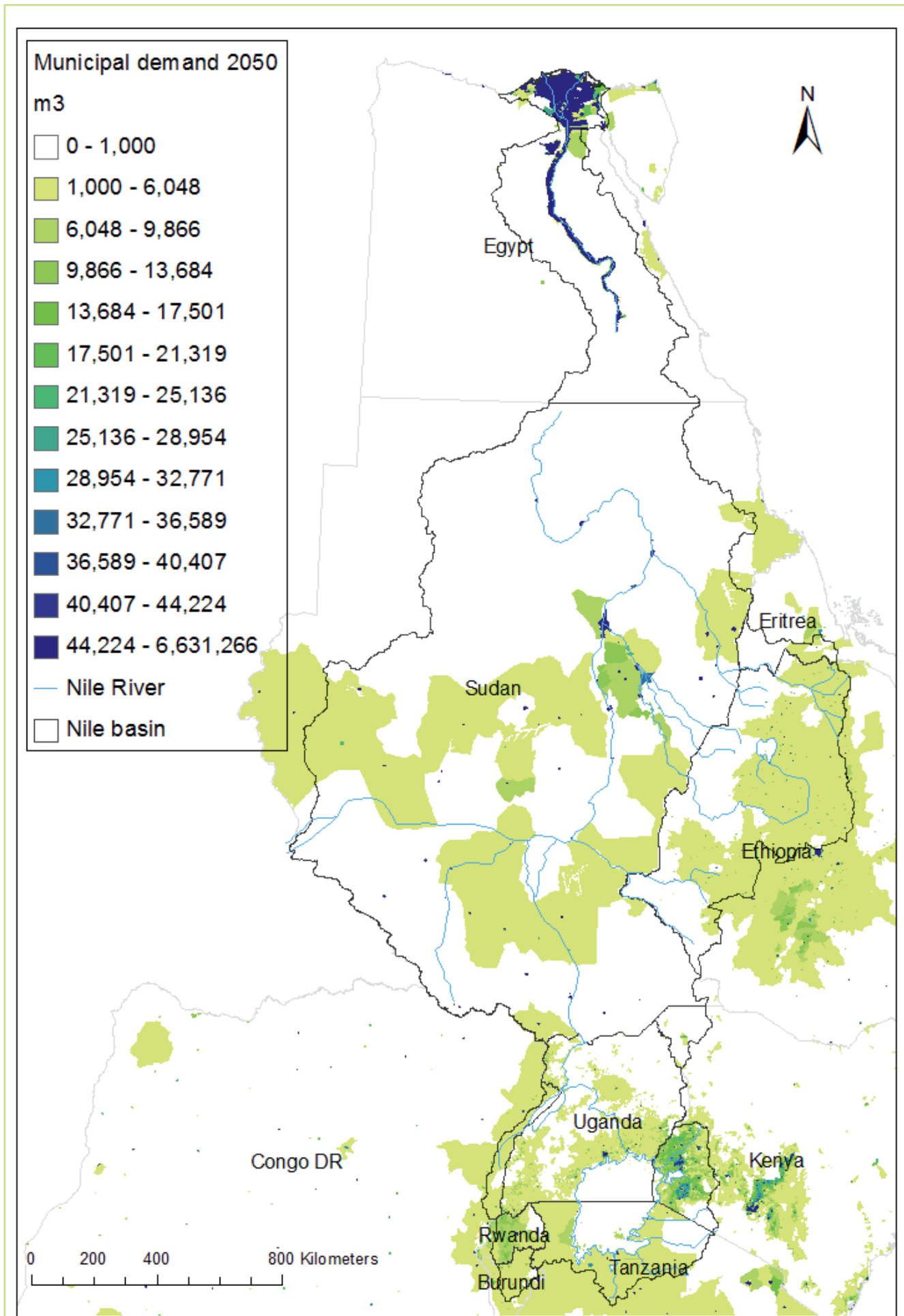
Figure 4.6 Spatial distribution of projected annual municipal withdrawals (2020-2049 period represented by 2050 projection)
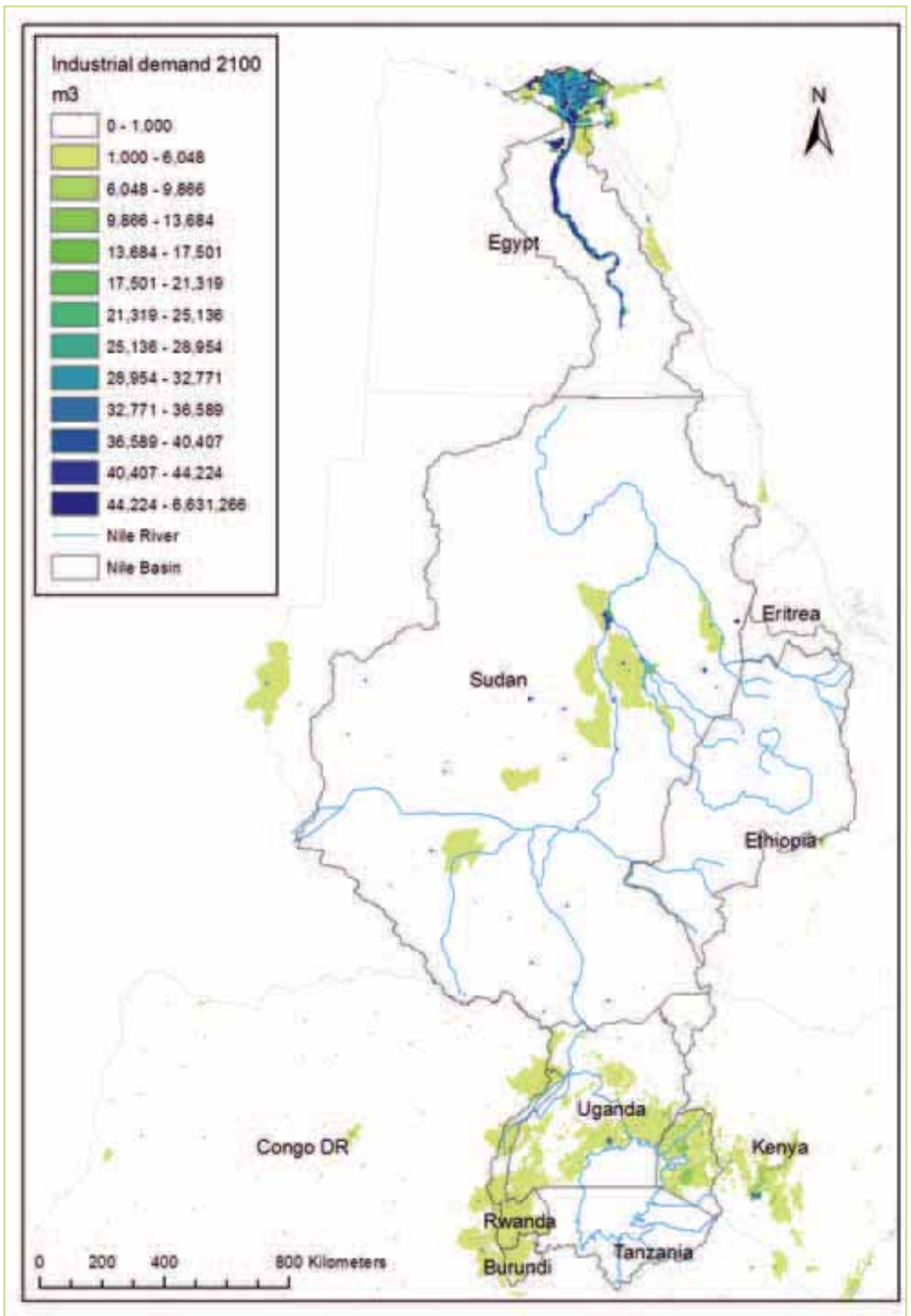
Figure 4.7 Spatial distribution of projected annual industrial withdrawals (2070-2099 period represented by 2100 projection)
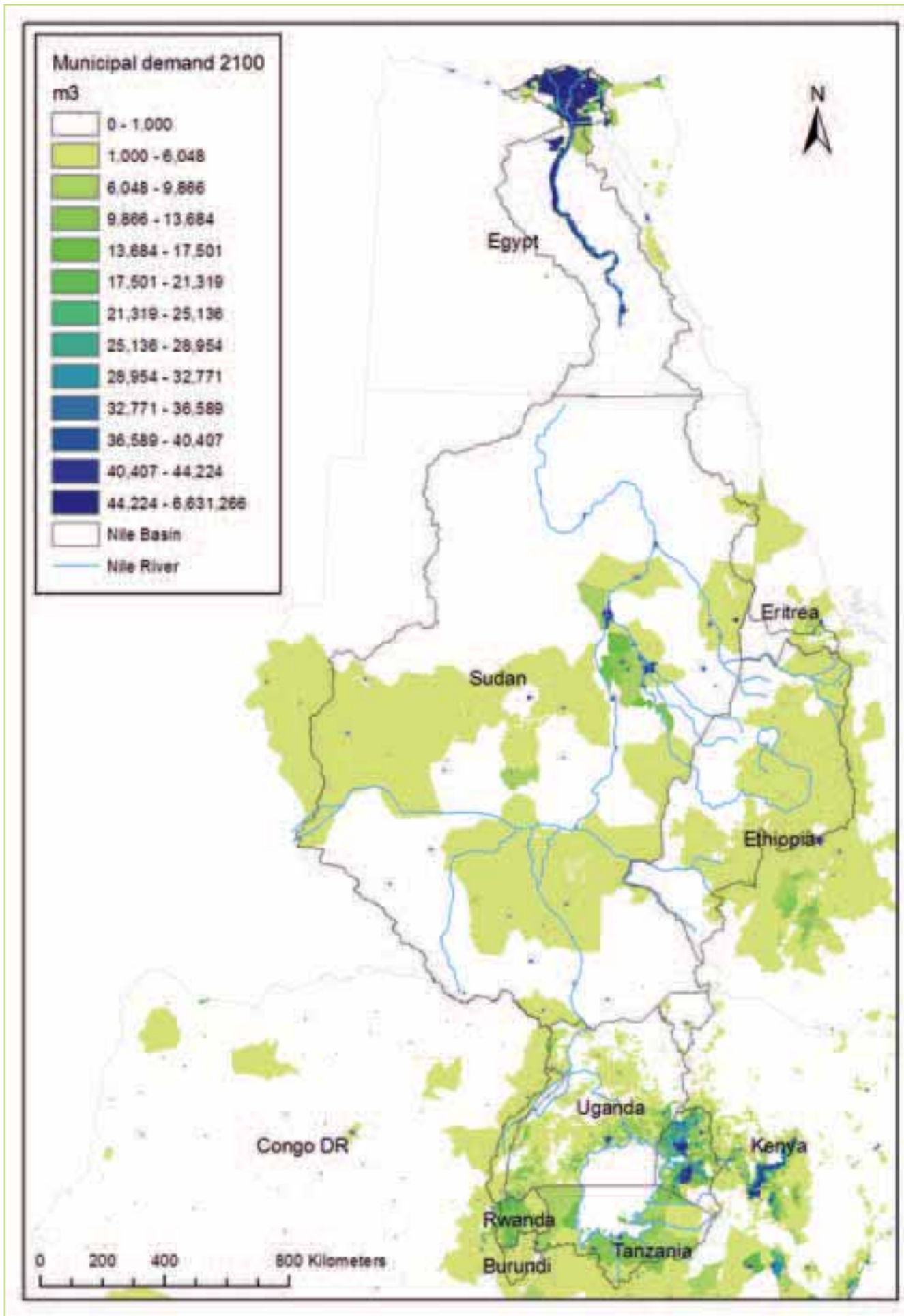
Figure 4.8 Spatial distribution of projected annual municipal withdrawals (2070-2099 period represented by 2100 projection)

4.3 Representing water demands in a regional hydrological model

4.3.1 FAO Nile Information

The low rainfall over Egypt and Sudan (Republic of Sudan) and their location at the downstream end of the Nile River makes this area highly vulnerable to climate variability, climate change and interventions upstream. Furthermore, the delta area represents one of the highest populations in the region.

The largest water use by far in the Nile is the irrigation water. Table 4.13 shows the relative proportion of irrigation demand from each country compared to the irrigation demand of the basin. It can be seen from Table 4.13 that Egypt and Sudan account for more than 97% of total irrigation withdrawals in the basin, compared with less than 3% for the other 7 countries. Similarly Egypt and Sudan account for more than 96% of the estimated total water demand (irrigation, industrial, and municipal) in basin (Table 7.2). Given the regional (basin-wide) focus of this project, it is reasonable to focus on the demands that are likely to have impacts on the regional scale, rather than in any one country.

Therefore, the water use demands implemented in the regional hydrological model are limited to the irrigation, industrial and municipal water demands in Egypt and Sudan.

Irrigation demands are based on the FAO Nile project described at the beginning of Section 4.1.1 (FAO 2011a).

Table 4.13 Proportion of estimated irrigation water withdrawals per country (FAO 2011a)

	Irrigation water withdrawals (km³)	Percentage of overall irrigation withdrawals (%)
Egypt 68.80		69.4%
Sudan 27.51		27.7%
Eritrea 0.13		0.1%
Ethiopia 0.48		0.5%
Uganda 0.83		0.8%
Kenya 1.08		1.1%
Tanzania 0.003		0.003%
Rwanda 0.32		0.3%
Burundi 0.05		0.05%
Total 99.19		

Industrial and municipal demands were derived as described in Section 4.2. These demands were spatially distributed in the model as follows:
- 1 location representing the demands for Sudan immediately downstream of Khartoum
- 1 location representing the demands for Egypt immediately downstream of Gaafra.

The industrial and municipal demands make up only 11% of demands for the entire basin. The combined estimates of industrial and municipal water demands for Egypt and Sudan together represent 84% of this was considered a reasonable representation of demands in a regional model.

4.3.2 NBI baseline model irrigation locations

Irrigation demand locations used in this study are consistent with irrigation demand locations used in the NBI baseline model of the Nile Basin (A. H. Seid, pers. comm.). The NBI baseline model includes 11 water demand locations. Three are located in Egypt:
1. Aswan
2. Upstream of El Akhsas
3. Downstream of El Akhsas

The Aswan demand location is connected directly to Lake Nasser and is assumed to represent withdrawals taken directly from the reservoir. The demand location called "Upstream of El Akhsas" is assumed to represent all demands on the Nile River between Aswan Dam and the Nile Delta. The demand location called "Downstream of El Akhsas" is assumed to represent all demands on the Nile River downstream of the entrance to the Nile Delta.

Eight of the water demand locations in the NBI baseline model are located in Sudan. These locations are summarized in Table 4.14.

A comparison showed many differences between the NBI baseline estimates of water demands and our interpretation of the FAO Nile (FAO 2011a) estimates. The most striking difference is that the NBI baseline model estimates generally show water use peaks in the wet season in the autumn, while the FAO Nile estimates show water use peaks during the winter/spring months. Since the FAO Nile estimates appear to be more in line with observed cropping patterns and crop evapotranspiration requirements, these were used as the basis for the demand volumes implemented in the regional hydrological model.

Table 4.14 NBI baseline demand locations in Sudan

Name Physical	location
Hassanab-Dongola	Main Nile between Atbara mouth and Lake Nasser
Tamaniat-Hassanab	Main Nile between Khartoum and Atbara mouth
Jebel Aulia	White Nile at Jebel Aulia Reservoir
Upstream of Jebel Aulia	White Nile upstream of Jebel Aulia Reservoir
Downstream of Sennar	Blue Nile between Rahad River and Khartoum
Gezira-Managil	Blue Nile at Sennar Reservoir
Upstream of Sennar	Blue Nile between Roseires and Sennar reservoirs
Khashm El Girba	Atbara at Khashm El Girba Reservoir
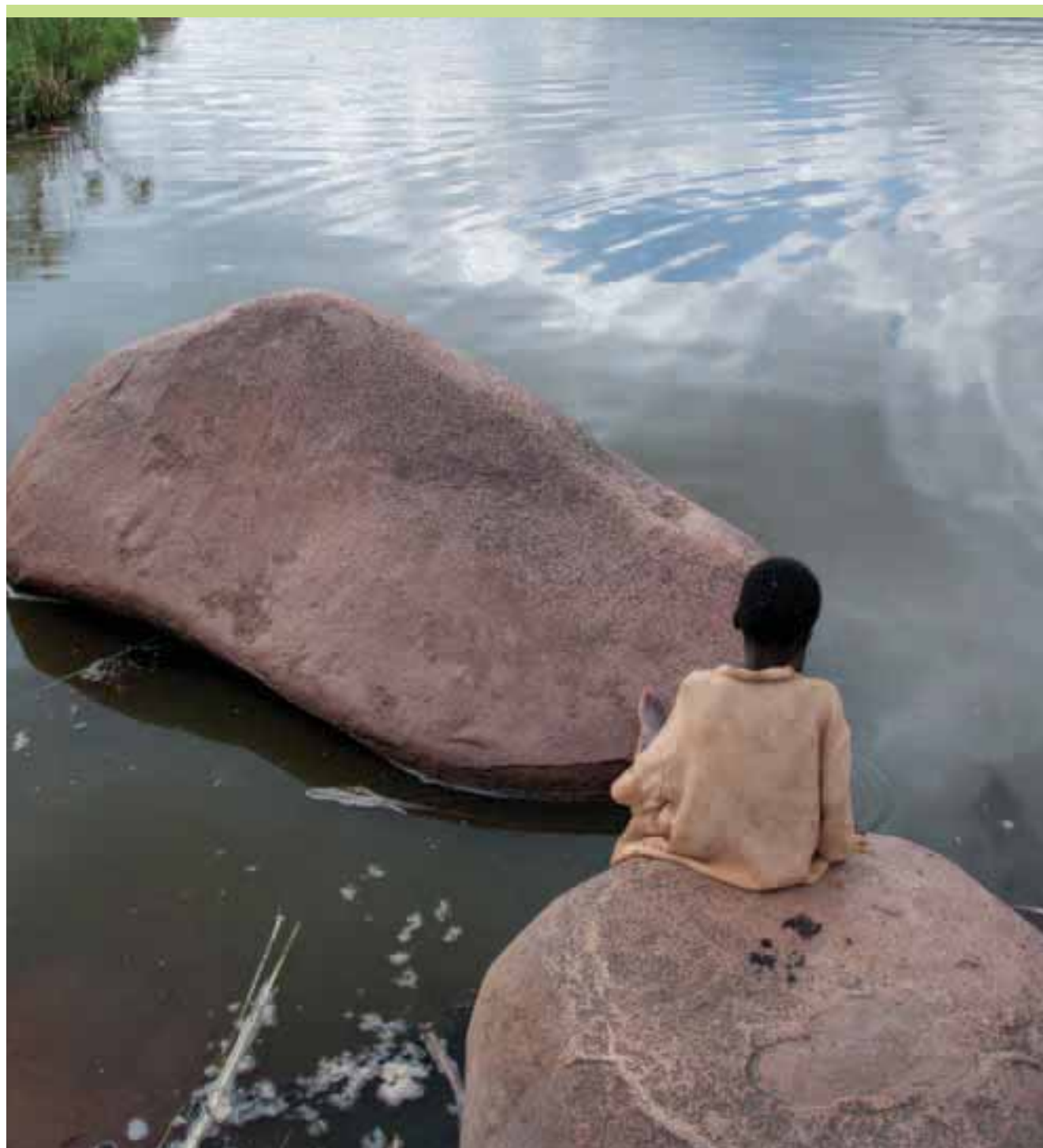
4.3.3 Spatial disaggregation of the FAO Nile data set

The FAO Nile estimates of crop water requirements for Egypt and Sudan are disaggregated by region, crop type, and month. The crop area estimates are disaggregated by region and crop type. The crop area estimates include baseline estimates and projections to 2030 and 2050. Crop water requirements are not projected to the future (in other words, the analysis assumes that crop evapotranspiration requirements will not change).

The FAO Nile water use estimates are disaggregated spatially by government administrative district. In Egypt, the disaggregation corresponds to the boundaries of Egypt's governorates. The boundaries of the governorates in Egypt are given in Figure 4.9. The names of the governorates are not given because of the density of governorates in the Nile Delta region.

In Sudan, the spatial disaggregation of water demand corresponds to the boundaries of Sudan's states. The boundaries of the states of Sudan are shown in Figure 4.10.

0   50   100   200 Kilometers

Figure 4.9   Egyptian governorate boundaries
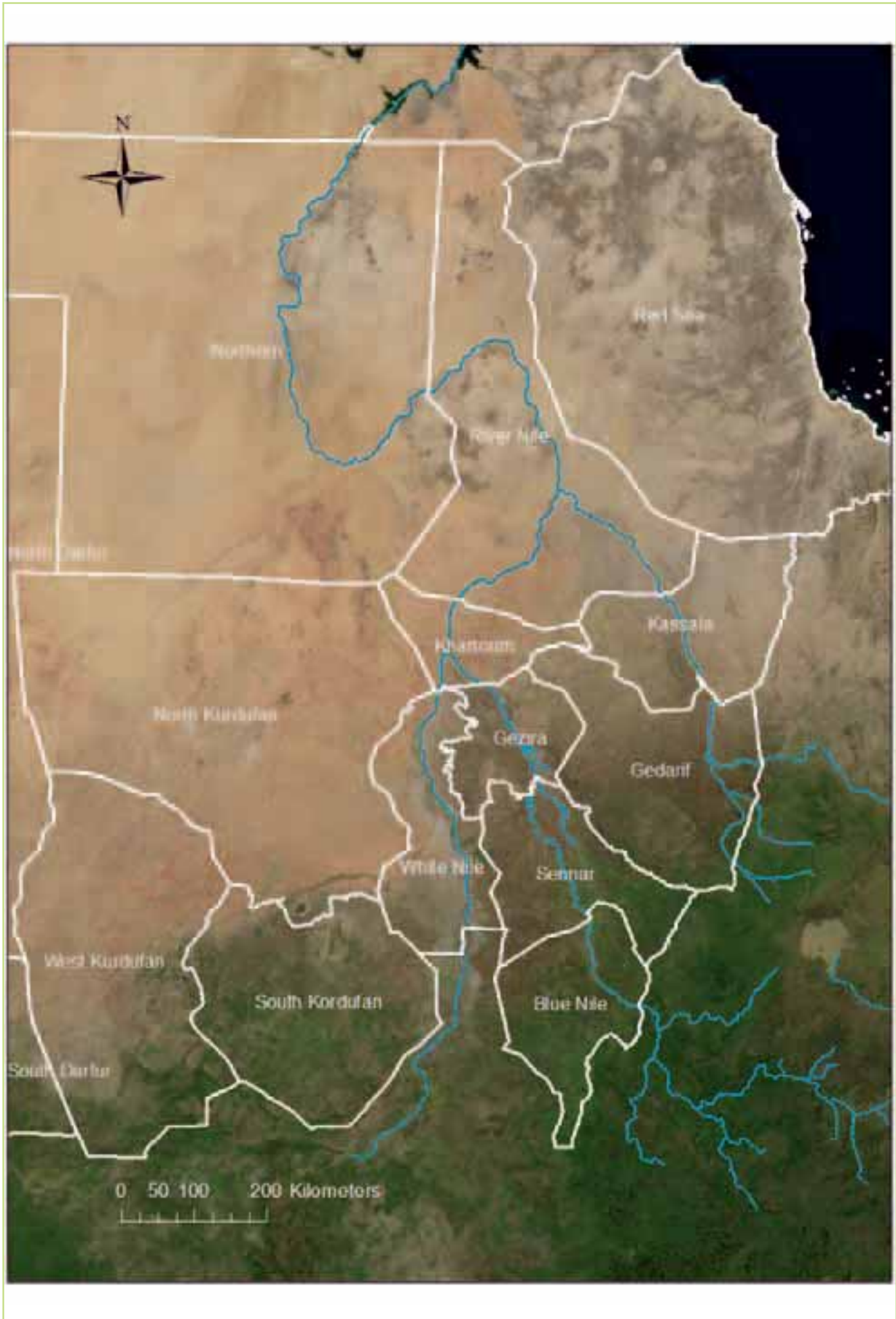
Figure 4.10 States of Sudan
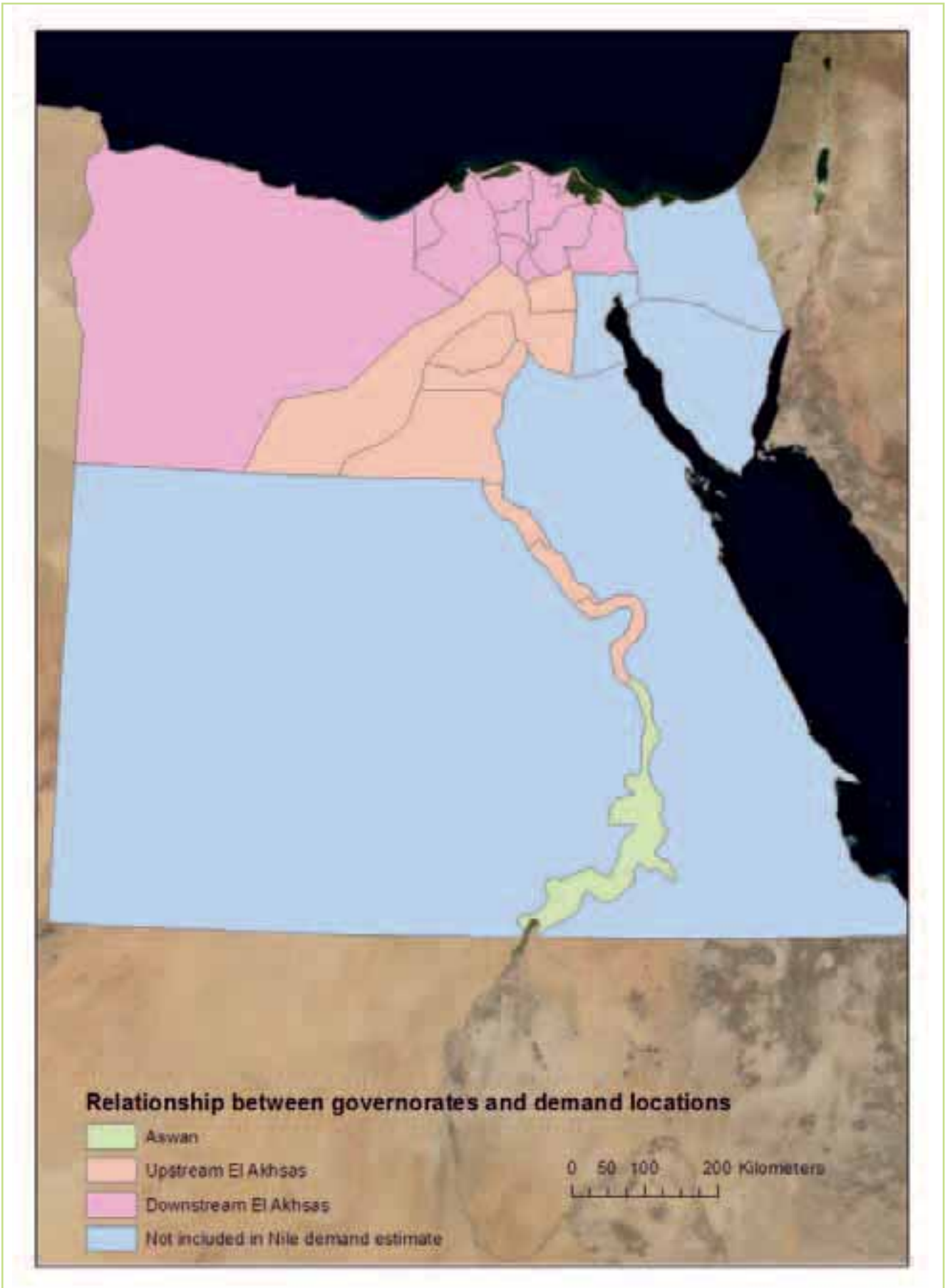
Figure 4.11 Relationship between governorates & demand locations

4.3.3.1 Demand locations in Egypt

Each governorate in Egypt has been assigned to one of the three demand locations in the NBI baseline model, with the exception of governorates for which water demand estimates are unavailable or for which no hydraulic connection to the Nile River appears to exist. Figure 4.11 shows which governorates have been assigned to each demand location.

According to the 1959 agreement with Sudan, Egypt is entitled to the use of 55.5*109 m^3/year from the Nile River. Figure 4.12 compares annual water use estimates from the FAO Nile baseline and the 2050 projection. The figure suggests that the baseline water use estimate is in line with Egypt's annual entitlement. The FAO water use estimates presented here are net water requirements and do not include losses from inefficient irrigation practices or flushing. Because a considerable amount of diversions to irrigation in Egypt are reused downstream, the FAO Nile baseline estimate may be reasonable.

4.3.3.2 Demand locations in Sudan: Main Nile

In the FAO Nile data set, irrigation water use data in Sudan are aggregated at the state level. The FAO Nile data set also provides information about the spatial extent of irrigation and the principal source of water for each irrigated area. Figure 4.13 shows the spatial extent of irrigation in Sudan, along with the principal source of water for each area.

According to Figure 4.13, most of the irrigation between the mouth of the Atbara and Lake Nasser is located in the Northern state. Therefore, it is assumed that all irrigation in the Northern state can be assigned to the "Hassanab-Dongola" demand location (see Table 4.14).

According to Figure 4.13, most of the irrigation between Khartoum and the mouth of the Atbara is located in the River Nile state. Therefore, it is assumed that all irrigation in the River Nile state can be assigned to the "Tamaniat-Hassanab" demand location (see Table 4.14).
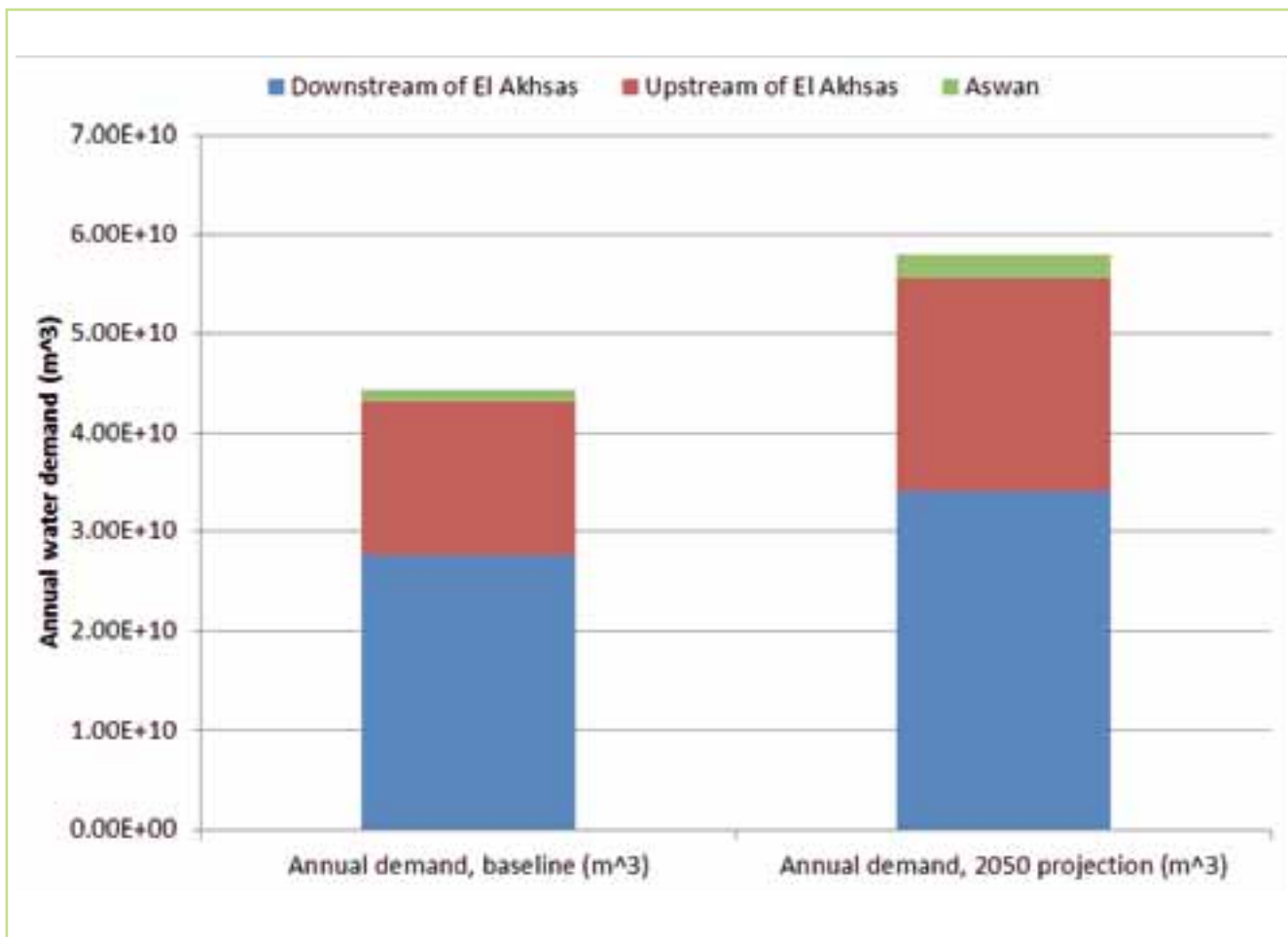
Figure 4.12 FAO Nile annual water demand estimates for Egypt
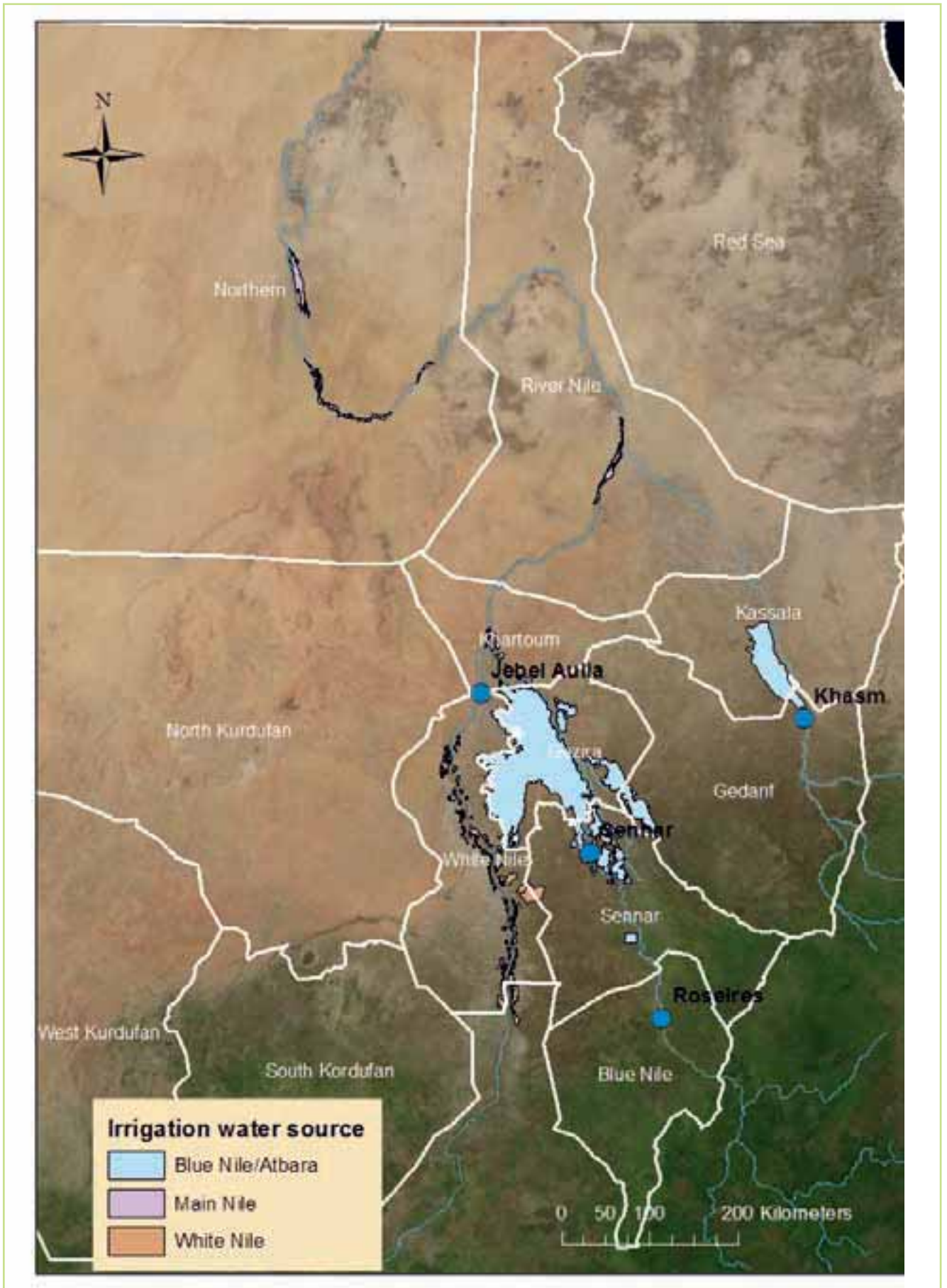
Figure 4.13 Map of irrigation locations in Sudan, with water sources (Reservoir locations shown in as blue circles)

4.3.3.3 Demand locations in Sudan: White Nile & Blue Nile

The NBI baseline model includes two water demand locations on the White Nile: one that diverts water directly from Jebel Aulia Reservoir, and one that diverts water upstream of the reservoir. Three water demand locations are present on the Blue Nile: one that diverts water directly from Sennar Reservoir (Gezira-Managil), one that diverts water upstream of Sennar Reservoir but below Roseires Reservoir, and one that diverts water downstream of Sennar Reservoir and downstream of the Rahad River. In Figure 4.14, an interpretation is provided of which irrigated areas in the FAO Nile report are served by each NBI baseline model diversion point.
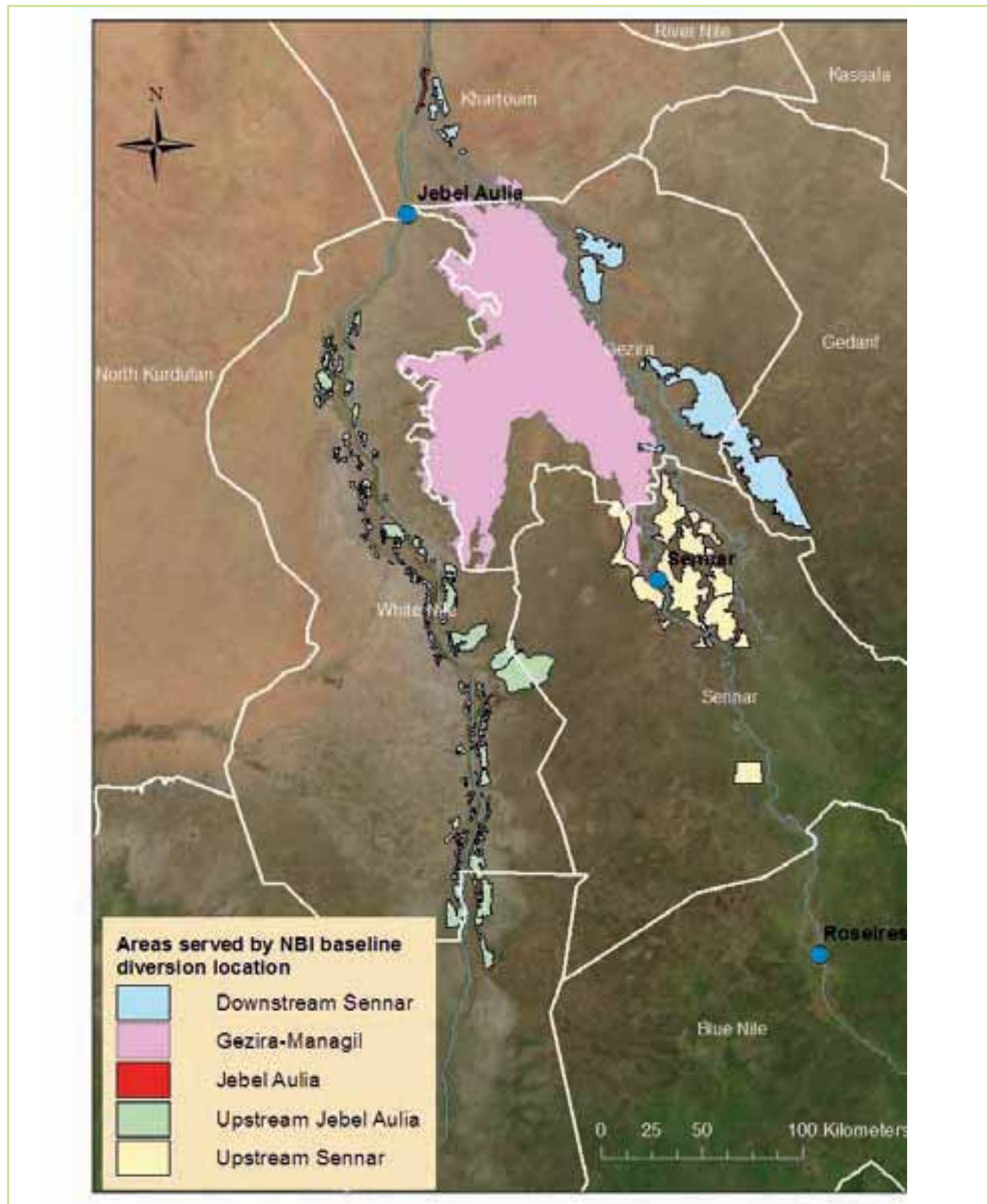
Figure 4.14 Interpretation of link between NBI baseline diversion locations & FAO Nile crop areas for Blue Nile & White Nile (reservoir locations shown as blue circles) for the 2005 baseline
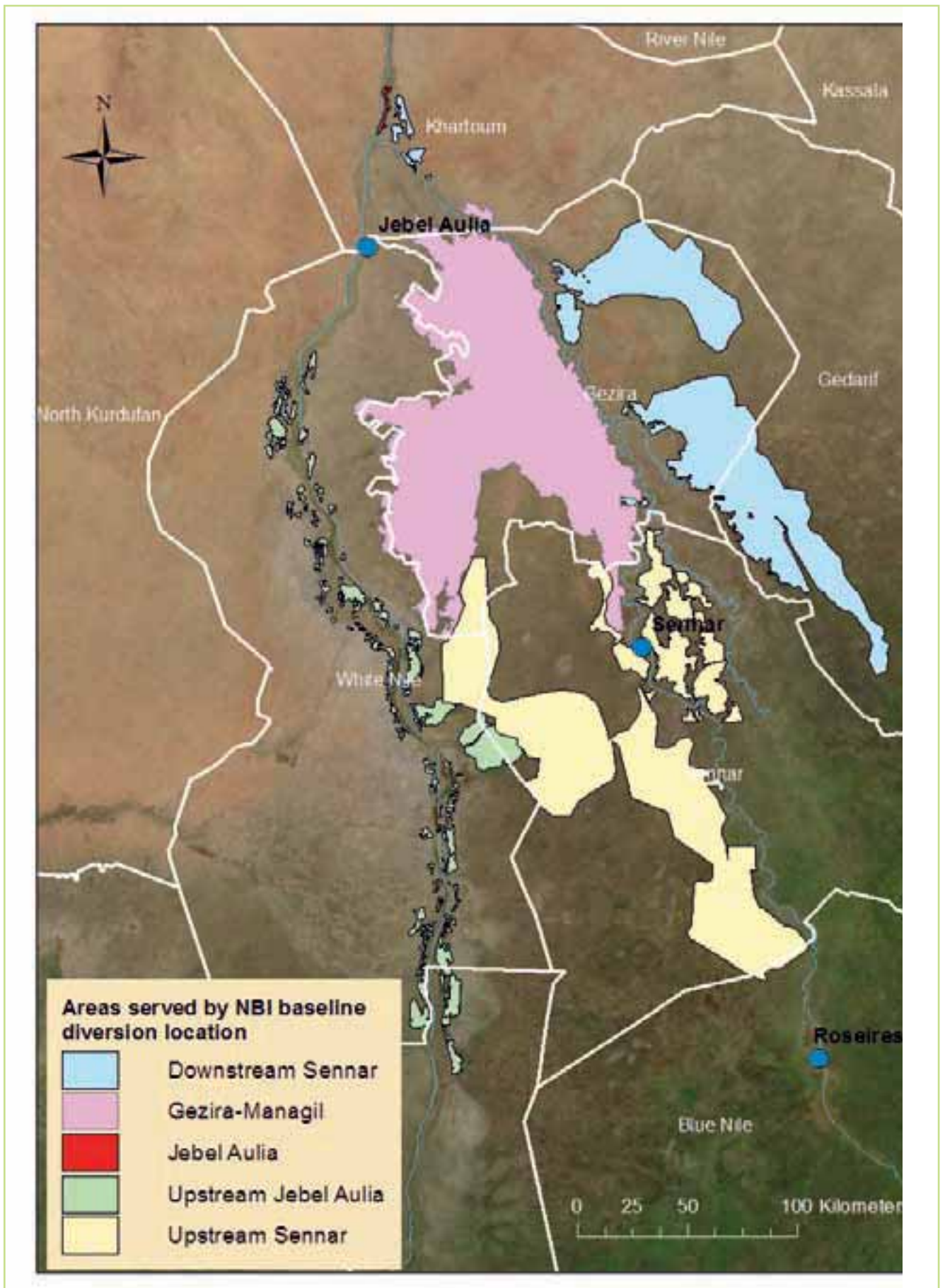
Figure 4.15 Interpretation of link between NBI baseline diversion locations & projected FAO Nile crop areas for Blue Nile & White Nile (reservoir locations shown as blue circles) for the 2050 projection

The FAO Nile report also includes projections of how irrigated areas will change in the Blue Nile and White Nile regions of Sudan. In Figure 4.15, an interpretation is provided of how the projected areas are linked to the NBI baseline diversion locations.

Because the FAO Nile report aggregates irrigation water use data in Sudan at the state level, a method is needed for estimating water use in each of the areas assigned to each of the NBI baseline demand locations. In this analysis, an area-weighted method is used to assign water use information to each NBI baseline demand location. The method assumes that the portion of water use from each state that can be assigned to a particular demand location is proportional to that state's share of the total land area assigned to the demand location. For example, the total irrigated area inside the Gezira state is ~14,100 km² (in the baseline estimate). The portion of this area that lies within the area assigned to the Gezira-Managil diversion location is 70%. Therefore, 70% of the water use attributed to the Gezira state in the FAO Nile report is assigned to the Gezira-Managil demand location.

4.3.3.4 Demand Locations in Sudan: Atbara

Figure 4.13 shows an irrigation location downstream of the Khashm El Girba reservoir location. All of this area has been assigned to the "Khashm El Girba" demand location. Figure 4 13 also shows that this area is divided between the Kassala and Gedarif states. FAO Nile water use estimates for the two states are allocated to the "Khashm El Girba" demand site using the same methodology that was used to distribute water use estimates in the White Nile and Blue Nile regions.

5.0 Regional hydrological modelling

To simulate flows and water levels on the regional scale, both for climate change assessment and for climate adaptation scenarios, a distributed hydrological modelling approach is required. Because of the diversity of hydrological processes in the Nile Basin, the basin was delineated into major sub-basins that share common hydrological characteristics; different modelling approaches were then used in each major sub-basin (Figure 5 1). Models for each of the sub-basins were developed and calibrated separately and then combined into a single regional hydrological model.

For the purposes of this report the basins are referred to (Figure 5 1) as:
• Lake Victoria (actually the Equatorial Lakes including Lake Victoria)
• Sobat
• Sudd
• Bahr El Ghazal
• White Nile
• Blue Nile
• Atbara
• Main Nile
• Egypt

Each major sub-basin was then further divided into smaller sub-basins. Once the regional scale model was calibrated it was then used together with projections derived for future climate change and water demand to determine changes in water resource availability.

5.1 Types of models used

Two different model types were used to develop the hydrologic representation. The NAM rainfall-runoff model (Havnø et al., 1995) was used to simulate rainfall-runoff processes. A rainfall-runoff model is necessary in order to translate climate model projections of changes in rainfall and evaporation into projections of changes in runoff. The rainfall-runoff model provided inputs to a river basin planning model that was used to simulate other major factors affecting water availability in the basin. The MIKE BASIN river basin modelling package (DHI, 2009) was used to simulate reservoir and hydropower operations, anthropogenic water use, river routing, evaporative losses, and wetland processes.

A separate rainfall-runoff model was developed for each runoff-generating catchment in the basin. Runoff-generating catchment areas were delineated as described below. Individual MIKE BASIN models were then developed for each of the major sub-basins described above. Finally, the individual MIKE BASIN models were combined into a single MIKE BASIN model of the entire basin. In fact, the regional model was finalised using MIKE HYDRO the latest version of the MIKE BASIN model.
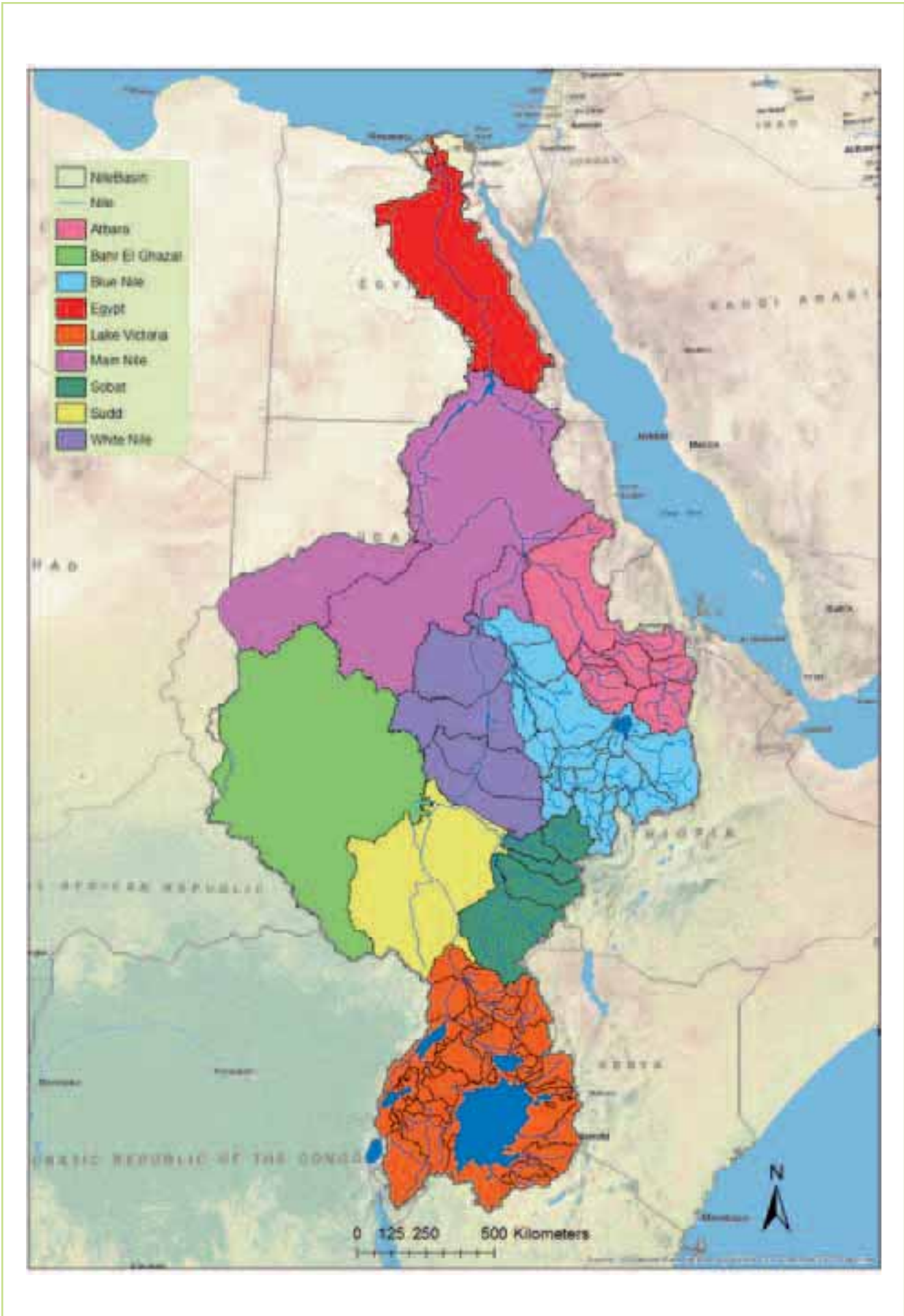
Figure 5.1 The Nile River Basin showing the major sub-basins, the minor sub-basins within each these sub-basins & showing the model river network linking the sub-basins that was used to represent the Nile river system

5.2 Modelling scales

The spatial scale appropriate for hydrological modelling depends on the scale of interest for the modelling objectives, including the spatial variability of important phenomena like precipitation, and also on the resolution and availability of modelling data. While the hydrological modelling tools proposed can be applied across the entire range of spatial and temporal scales, they are no better than the data available for running and calibrating the model.

For the purposes of this study we are interested in developing a regional scale hydrological model suitable for assessing the effectiveness of regional scale adaptation measures. Therefore the focus has been on developing the best representation of the rainfall-runoff and routing processes appropriate to this regional scale.

In general the spatial distribution and availability of climate and hydrological information is highly variable and in this respect, the Nile River Basin is no exception. Some parts of the Nile Basin are characterized by sparse data availability and therefore modelling is best carried out at a larger scale as no new information is gained by further refinement. For other areas, more data are available to support modelling at a higher spatial resolution. One advantage of the sub-basin based modelling approach used here is the flexibility to adapt the modelling scale to available data and the variability in hydrological and climatic characteristics across the whole region. The regional model developed consists of more than 120 rainfall-runoff sub-basins. These range in area from less than 100 km2 (for example in the Lake Victoria catchment) to sub-basins of approximately 80,000 km2 used in the Sobat major sub-basin, Figure 5 1.

Similarly, the appropriate temporal scale depends on the time scales of the phenomena of interest and also on the temporal resolution of the data available for modelling. If the phenomena of interest are droughts and/or long-term water scarcity, For analysis of changes in the frequency and intensity of droughts, as well as the extent to which water scarcity may be expected in the future, hydrological modelling is required to determine how changes in the climatic conditions will affect the supply of water available to meet the water demands and in turn how changes in the demand will affect the hydrological response. For flooding, hydrological modelling is required to predict the expected changes in flood hydrographs and peak flows. While water scarcity can be addressed using monthly values, it is more appropriate to carry out flood modelling at smaller time scales in order to properly capture the dynamics of flood behaviour. Appropriate time scales for flooding range from hours in urban catchments and upland catchments in mountainous areas to days or weeks for large scale rivers like the Nile, Ganges, etc. Usually however the most appropriate time scale for flood modelling at the catchment scale is hours or days and the final choice is often governed by the temporal resolution of the available data.

The regional model we have developed and calibrated here is then used in this study to assess the hydrological impacts of climate change and for comparison an assessment of the changes in water demand.

This regional model has a number of potential applications in future work including:

- To be used as the basis for more local studies, where the regional model forms the regional boundary conditions for the local studies.
- To be used for further regional studies
- To investigate the potential impacts of different climate adaptation measures at the regional scale

The remainder of this section is organized as follows: first, general approaches to rainfall-runoff modelling and river basin modelling are described; next, we describe modifications to the general approaches that were necessary in individual sub-basins because of data constraints, distinctive hydrological features, or both; finally, we present key results from the river basin model of the entire basin.

5.3 Rainfall-runoff modelling

This section describes the rainfall-runoff modelling approach. The section begins with a general description of the NAM rainfall-runoff model. This is followed by a description of the approach used to develop inputs to the model, including river discharge estimates used for model calibration. The section concludes with a description of the calibration process.

5.3.1 The NAM rainfall-runoff model

For many hydrological applications where continuous rainfall-runoff modelling is required the NAM model has been widely used, (Butts et al., 2007; Butts et al., 2004; Madsen, 2000; Refsgaard and Knudsen, 1996; Havnø et al., 1995). When applied to a single catchment this model can be characterised as a deterministic, lumped conceptual model that operates by continuously accounting for the moisture content in a number of different but mutually interrelated storages, Figure 5.2.
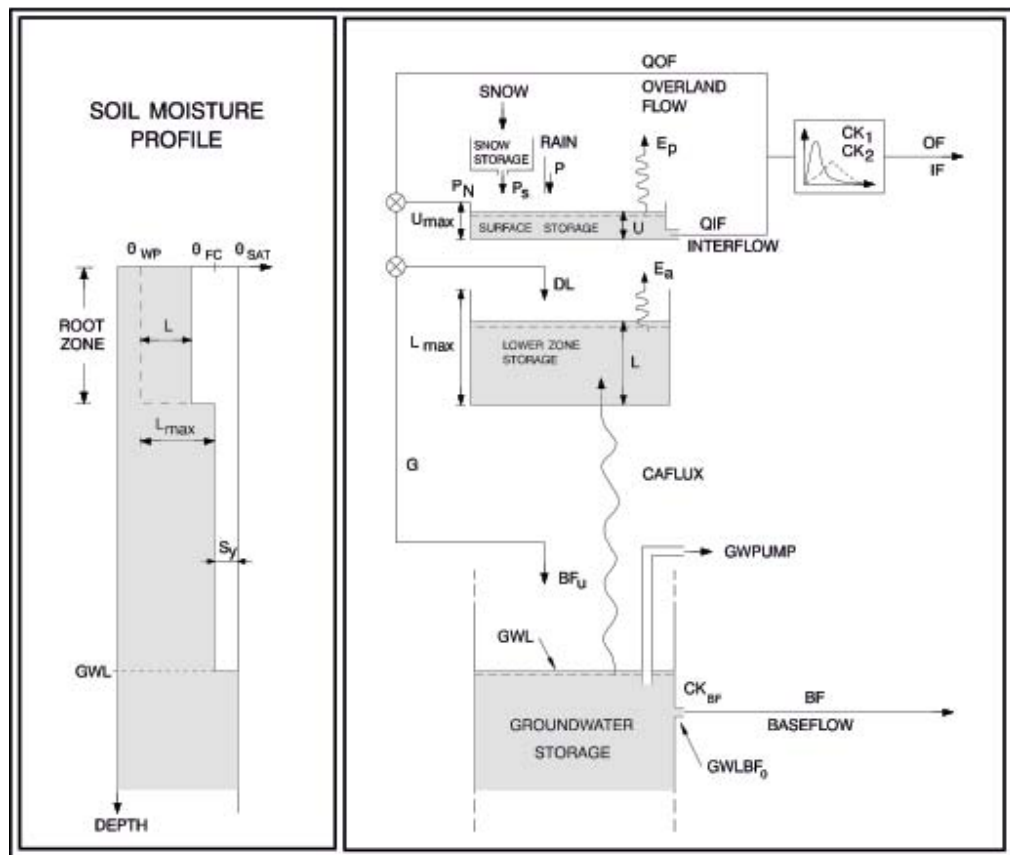
Figure 5.2 The conceptual model structure of the NAM model
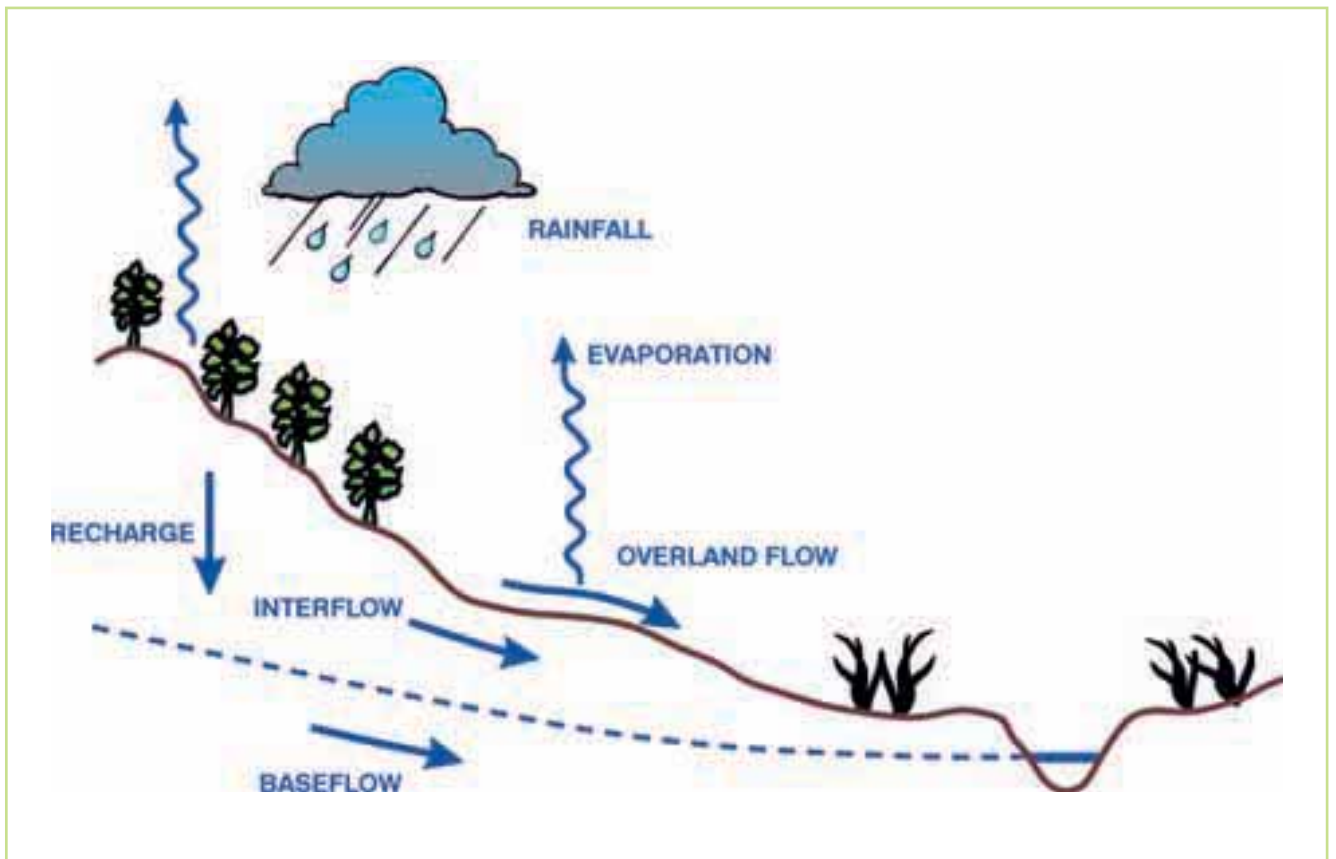
Figure 5.3 The major rainfall-runoff processes modelled in NAM hydrological model

The basic data input requirements for the NAM rainfall-runoff model are meteorological data, stream flow stage and discharge data for model calibration and verification, definition of the catchment parameters, and definition of initial conditions. The basic meteorological data requirements are precipitation time-series, potential evapotranspiration time-series, and temperature and radiation time-series if snow accumulation and melt are to be modelled. Based on these meteorological inputs, NAM simulates catchment runoff as well as information about other elements of the land phase of the hydrological cycle, such as the temporal variation of the evapotranspiration, soil moisture content, groundwater recharge, and groundwater levels. The resulting catchment runoff is split conceptually into overland flow, interflow and base flow components.

The amount of infiltrating water recharging the groundwater storage depends on the soil moisture content in the root zone. Base flow from the groundwater storage is calculated as the outflow from a linear reservoir using a time constant. The groundwater level is calculated from a continuity consideration accounting for recharge, capillary flux, net groundwater abstraction, and base flow. The inclusion of capillary flux and groundwater pumping are optional.

The parameters of the NAM model are described briefly in Table 5.1. The parameters of conceptual models like NAM cannot, in general, be obtained directly from measurable quantities of catchment characteristics, and hence model calibration is needed. The calibration procedures used here are described in more detail in section 5.3.6. The recommended procedure for calibration is firstly to make an initial approximate calibration of key parameters:

- Lmax and Umax for water balance
- CQof and CK1,2 for peaks
- CKBF for baseflow

Once the water balance and the large scale features of the flow hydrograph are well reproduced then the following iterative procedure should allow rapid calibration.

- identify a parameter change, likely to improve the calibration
- change this parameter only
- make significant changes the first time
- repeat until the calibration objectives are reached

The main parameters used in the calibration of the NAM model are listed in Table 5.1 and a more detailed description of this model can be found in the NAM references cited above. Manual and automatic calibration approaches for the NAM model are described in Madsen (2000) and Madsen et al., (2002).

5.3.2 Major sub-basins in which rainfall-runoff models were developed

Hydrological modelling is carried out for all of the major sub-basins with the exception of Bahr el Ghazal. The Bahr el Ghazal is unique among the Nile tributaries in that its outflow to the White Nile is almost negligible as a result of evaporation losses from the swamps at the lower end of the basin (Sutcliffe and Parks, 1999). For this reason the Bahr el Ghazal basin is not included in the regional model. Rainfall-runoff modelling

Table 5.1 Summary of the NAM model parameters & their physical interpretation

Parameter	Units	Description
U max	mm	Maximum water content in the surface storage. This storage can be interpreted as including the water content in the interception storage, in surface depression storages, & in the uppermost few cm's of the soil
L max	mm	Maximum water content in the lower root zone storage. Lmax can be interpreted as the maximum soil water content in the root zone available for the vegetative transpiration
CQOF	-	Overland flow runoff coefficient. CQOF determines the distribution of excess rainfall into overland flow & infiltration
TOF	-	Threshold value for overland flow. Overland flow is only generated if the relative moisture content in the lower zone storage is larger than TOF
TIF	-	Threshold value for interflow. Interflow is only generated if the relative moisture content in the lower zone storage is larger than TIF
TG	-	Threshold value for recharge. Recharge to the groundwater storage is only generated if the relative moisture content in the lower zone storage is larger than TG
CKIF	hours	Time constant for interflow from the surface storage. It is the dominant routing parameter of the interflow because CKIF >> CK1,2
CK1.2	hours	Time constant for overland flow and interflow routing. Overland flow and interflow are routed through two linear reservoirs in series with the same time constant CK1,2
CKBF	hours	Baseflow time constant. Baseflow from the groundwater storage is generated using a linear reservoir model with time constant CKBF

Figure 5.4 Catchments delineated for rainfall-runoff modelling of Blue Nile and Atbara basins

using NAM was not carried out in all of the major sub-basins. In some basins, rainfall does not make a substantial contribution to the water balance. In other basins, rainfall makes a substantial contribution but evaporative losses are so great that little runoff reaches the main channel of the Nile. In particular rainfall-runoff models were developed using NAM for the following major sub-basins:

- Lake Victoria (Equatorial Lakes including Lake Victoria)
- Sobat
- Sudd
- White Nile
- Blue Nile
- Atbara

For the Sudd a simplified water balance model was developed to represent the swamps within the region. The conceptual model of the Sudd is based on a series of reservoirs, where each reservoir will describe the relationship between the water level and the flooded area, and the subsequent rainfall and evaporation on these areas. Only the direct rainfall and evaporation are considered. Similar conceptual models were developed where the influence of swamps and wetlands are important. Finally for the Main Nile and Egypt the rainfall is very low and the corresponding rainfall-runoff contributions to the Nile flow are very low. For these two sub-basins, a simplified hydrological model representing flow routing, reservoir operations and water balances, water use and irrigation demands was developed. The details of the hydrological modelling approaches used in each sub-basin are discussed in the remainder of section 5.

5.3.3 Delineation of catchments
To develop rainfall-runoff models, it is necessary to delineate catchment areas for rainfall-runoff simulation. Catchments were delineated based on the availability of discharge data for model calibration at catchment outflow points. Some additional catchments were delineated at outflow points that lack discharge data, either to estimate water supply at existing or proposed reservoir locations, or because these catchments are thought to have distinctive hydrological characteristics that make them unsuitable for merger with nearby catchment areas. The various reasons for catchment delineation can be grouped into the following categories:
1. Gauged headwater catchments: Gauged headwater catchments have downstream boundaries defined by gauging stations and do not have inflows from other catchments or

significant lake or reservoir storage.
2. Gauged downstream catchments: Gauged downstream catchments have downstream boundaries defined by gauging stations as well as inflows from other catchments but do not feature significant lake or reservoir storage
3. Existing lake or reservoir catchments: Existing lake or reservoir catchments have downstream boundaries defined by the outlets of existing lakes or reservoirs. Existing lake or reservoir catchments can be headwater catchments but can also have inflows from other catchments.
4. Proposed reservoir catchments: Proposed reservoir catchments have downstream boundaries defined by the outlets of proposed reservoirs. Proposed reservoir catchments can be headwater catchments but can also have inflows from other catchments.
5. Ungauged catchments with distinctive features: Ungauged catchments with distinctive features that make them unsuitable for aggregation with other nearby catchment areas.

An example of this grouping for the Atbara and Blue Nile is shown in Figure 5.4.

5.3.4 Catchment precipitation & potential evapotranspiration
This section summarizes available precipitation and potential evaporation data and then explains how catchment-level estimates were developed for input into NAM

5.3.4.1 Precipitation data
The main sources of precipitation information available across the region are:
- Reanalysis data
- Satellite-based remote sensing (RS) products
- Gauge-based data

In this project, only gauge-based data were used. The motivation for this is outlined below.

Reanalysis data are usually obtained by combining time series of past observations with numerical weather prediction models using data assimilation techniques. By conditioning the weather model using observations, the model results are better suited studies of long-term variability in climate. Alternatively this can be viewed as applying numerical weather models to interpolate/extrapolate precipitation observations dynamically in space and time. Several sources of reanalysis data are available including global datasets from NCEP/NCAR, the National Centers for Environmental Prediction (NCEP), and

the National Centre for Atmospheric Research (NCAR), as well as the ERA datasets produced by the European Centre for Medium Range Forecasting (ECMWF). There are several important limitations in using these data for hydrological simulation for climate change. First, using one weather forecasting model for re-analysis and another for climate projections will lead potentially to inconsistencies and accumulation of model error. Secondly, the data are often only available at large grid sizes based on global gauge data rather than local gauges. Thirdly, while reanalysis can be used to generate daily data from monthly datasets, (for example the Princeton reanalysis datasets use monthly CRU data to provide daily rainfall), a comparison of the data generated in this way with observations over Ethiopia showed that while the monthly totals were preserved the daily patterns produced are markedly different from actual observations making this data unsuitable for model calibration.

Satellite remote sensing (RS) as a source of precipitation information over the Nile is of interest for several reasons. While station data over the region is quite sparse, RS data provide grids across the whole region. There is a global decline in point station climate observations since the early 1990s in part due to the infrastructure costs of maintaining traditional gauge networks. RS data exhibits an opposing trend with increasing numbers of satellites, at higher resolution and higher frequency and these are becoming more widely available at little or no cost. Therefore these data can provide a highly useful and sustainable data sources. Furthermore, these can be obtained at quite

high spatial resolution (Figure 5.5) and most have daily time resolution or smaller. Several such sources of remote sensing data were examined at the outset of the project (Table 5.2).

The most interesting of these were TRMM 3B42, which uses a combination of infrared sensor, microwave sensor, and precipitation radar, and RFE 2.0, which uses an infrared based sensor and 2 specialised microwave sensors, with reference over GTS gauge data to remove the bias. While both gauge data and RS data are subject to systematic errors and biases, remote sensing is an indirect measurement and therefore considered less accurate although this depends on the region. Dinku et al., (2008) compared several remote sensing rainfall datasets (RFE, PERSIANN, TRMM and CMORPH) with a reference dataset using gridded station data interpolated (using kriging and angular–distance weighting interpolation) from over 120 stations data over Ethiopia. The results showed poor performance especially for correlation at the daily time scale for this region

Unfortunately, the majority of the measured discharge data made available to the project for model calibration covered the period from the late 1950's to the early 1980's. In order to carry out a consistent calibration across the Nile at a regional scale it is necessary to have several years where both precipitation and discharge are available. Therefore the precipitation data used in the regional hydrological model consist of gauge data from a variety of sources.

Publicly available sources of remotely-sensed data and gauge data are listed below:

Rainfall Data	Passive-IR	VIRS	GPI - IR	MW	SSM/I	AMSU	PR	GTS	GCOS	SRDC	Type
RFE 2.0			x		x	x		x			REMOTE SENSING
CMORPH – 3 hourly	x			x							
TRMM 3B42		x		x			x				
PERSIANN – 6 hourly	x			x							
GPCP	x			x						x	
CPC-GLB								x			STATION BASED
CRU 3.1									GHCN V2, MCDW, CLIMAT		
GHCN Daily V2.7									x		

Legend:	RS Sensor:	INFRARED		MICROWAVE		RADAR
		IR: Infrared **VIRS**: Visible Infrared Scanner **GPI**: Global Precipitation Index		**MW**: Microwave **SSM/I**: Special Sensor Microwave/Imager **AMSU**: Advanced Microwave Sounding Unit		**PR**: Precipitation Radar
	Station Data:	**GTS**: WMO Global Telecommunication System (station data)		**GCOS**: Global Climate Observing System (station data)		**SRDC**: Surface Reference Data Centre (Gridded)

Table 5.2 Summary of RS and gauge data sources examined
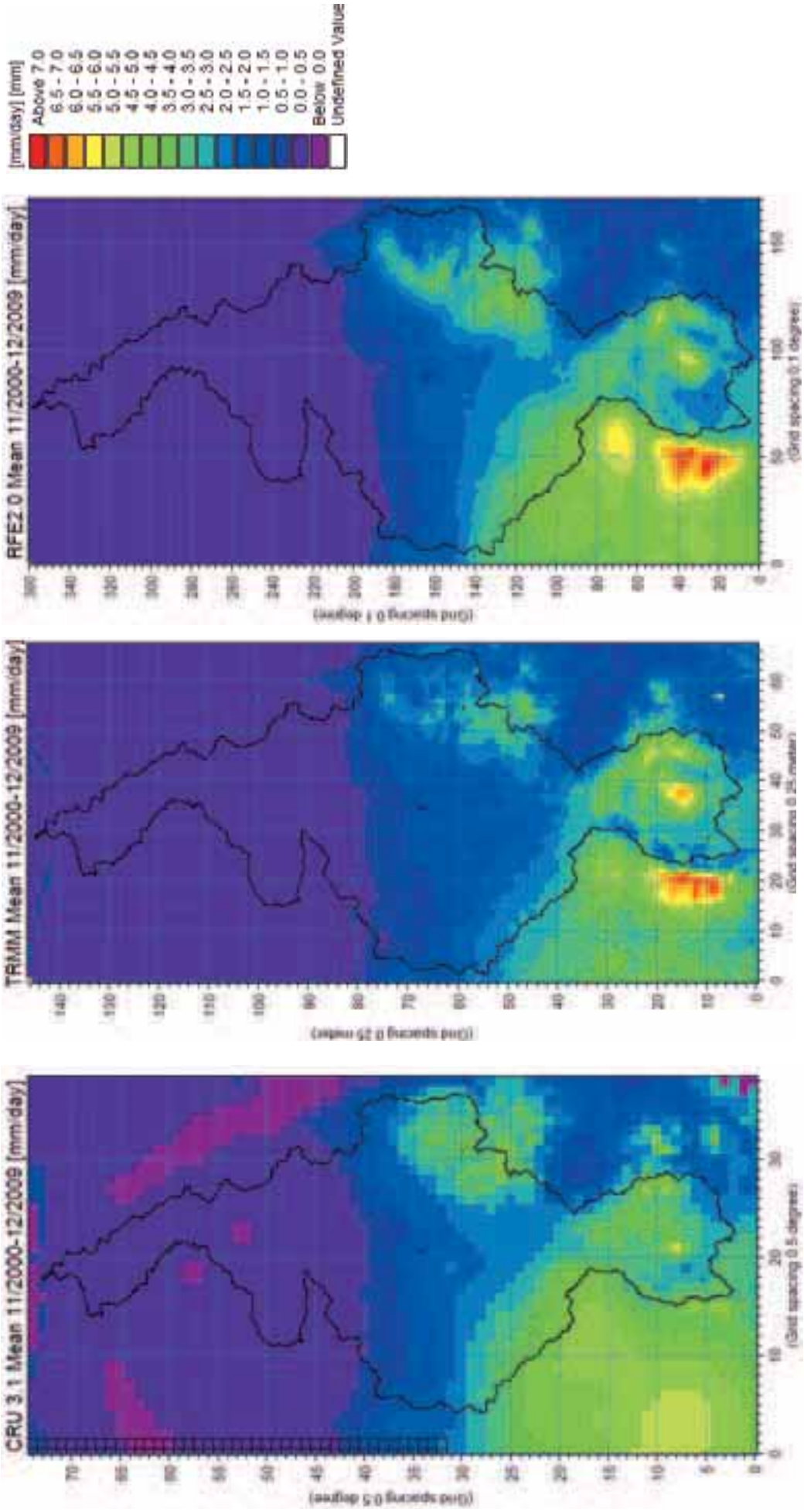
Figure 5.5 Spatial distribution of mean precipitation grids for the period 11/2000–12/2009 estimated from a) CRU 3.1, b) TRMM 3B42, & c) RFE2.0 for the Nile basin

Several sources of precipitation gauge data were used in formulating the regional hydrological model. The most useful data for modelling at the regional scale in order to capture both the high and low flows are daily data. This is certainly the case if the rainfall-runoff model is to be able to capture the high flows in the upper catchments. Experience has also shown that even if the objective of a modelling study is to reproduce monthly flows then using daily precipitation data shows better performance than for example monthly data as input. Therefore considerable efforts have been made to acquire as much daily precipitation as possible. Sources of precipitation gauge data used in the model are listed below. These include both the publicly available sources listed in Table 5-3 and confidential sources obtained from project partners.

Global Historical Climatology Network: (GHCN) is a publicly available data set which has daily rainfall data from a limited number of stations (approximately 70) throughout the region. This network is therefore quite sparse has a number of gaps or missing data and highly variable coverage. Therefore while this data is useful it is alone insufficient for modelling across the region.

Nile DST: This data set was provided to DHI for the purposes of this project including more than 1400 daily stations throughout the region. The time period covered is highly variable and there also a number of gaps and periods of missing data with a number of cases where 20-50% of data is missing over the period of record. This provides an important additional data set however required extensive quality checking for application in hydrological modelling. It should be noted however that this data set does not include any stations in Ethiopia. This dataset is confidential and is not permitted to be used outside of this project.

ENTRO: have provided monthly data to DHI for the purposes of this project for a number of stations located in Sudan and Ethiopia. The dataset has had limited use in this project because it consists of a small number of monthly stations. This dataset is confidential and is not permitted to be used outside of this project.

CRU 3.1: The University of East Anglia Climate Research Unit (CRU) data set is a global gridded data set that includes monthly rainfall estimates for each grid cell for the period 1901-2009. The CRU 3.1 grid is a 0.5 degree by 0.5 degree latitude-longitude grid, (Harris et al., 2012). The resolution over the Nile

Basin can be seen in Figure 5 5. There are several versions of the CRU dataset, the first derived initially for the International Water Management Institute's (IWMI) World Water and Climate Atlas. The gridded data is based on daily data, however as pointed out by New et al. (2002), the station data represents only a subset of the available stations. These point data are gridded spatially using spline interpolation as a function of latitude, longitude and elevation. This data set provides complete and long term coverage in the region but with a monthly time resolution. This dataset is publicly available.

In addition to the sources outlined above, a number of other sources of rainfall gauge data were used in the Equatorial Lakes region. These sources are described in section 5.5.

5.3.4.2 Estimating catchment-scale precipitation

For each rainfall-runoff catchment, it is necessary to estimate a catchment-level precipitation time series that is used to represent average precipitation over the catchment. The process of estimating an average catchment precipitation time series consists of two steps. In the first step, appropriate gauge records are selected. In the second step, these gauges are averaged over the catchment area.

In the Lake Victoria (Equatorial Lakes), Sobat, and White Nile sub-basins, only station gauge records were used to develop catchment averages. In the Blue Nile and Atbara sub-basins, a hybrid approach was used that combined station records with the gridded CRU data set (that is in turn based on gauge data). A thorough checking of rainfall stations has been undertaken prior to the selection of the stations to be used. The following three key criteria have been used to select the rainfall stations to be used for the rainfall-runoff modelling:
1. Data coverage for the modelling period
2. Data quality
3. Spatial location.

In the Lake Victoria (Equatorial Lakes), Sobat, and White Nile sub-basins, the Thiessen polygon method has been used as the point of departure for estimation of the mean areal rainfall. However, some subsequent weighting of the stations have been necessary for some of the catchments, e.g. if the selected / available station do not give a good representation of the rainfall within the catchment. In the Blue Nile and Atbara basins, a hybrid approach has been used that combines the Thiessen polygon method with a weighted averaging of CRU cells.

Details of the methods used in each basin are provided in section 5.5.

5.3.4.3 Potential Evapotranspiration (PET) data

In general, PET data are sparse. One reason is that while direct measurements using newer methods such as flux towers are now available, traditionally PET is difficult to observe directly as it depends on several meteorological parameters which are observed only at major stations. Several approximate methods are available if only part of the necessary information is available however these approximations have only been validated in certain regions and climates and therefore may be of limited validity. In reviewing the available estimates of potential evapotranspiration several sources were found:

Satellite remote sensing (RS) is an interesting source of PET data over the Nile. However, as for precipitation, these are only available for the last 10-15 years. The measured discharge data made available to the project for model calibration covered the period from the late 1950's to the early 1980's and therefore these data were not suitable.

CLIMWAT: The FAO database CLIMWAT contains observed agro-climatic data (rainfall, temperature, etc.) from over 5000 stations worldwide and global maps of reference PET at a monthly time scale. The dataset has been prepared according to the FAO Penman - Monteith method with limited climatic data as described in FAO Irrigation and Drainage Paper 56 (Allen et al, 1998). The dataset consists of 12 ASCII-grids with mean monthly data in mm/day * 10, and one ASCII-grid with yearly data in mm/year. A disadvantage of the CLIMWAT data set is that only average values are available (in other words, it is not possible to obtain time series estimates for a period that aligns with available runoff time series).

GDAS: An alternative dataset is available from GDAS (Global Data Assimilation System) that estimates PET from climate model variables including air temperature, atmospheric pressure, wind speed, relative humidity, and solar radiation. PET is calculated on a spatial basis using Penman-Monteith equation (Shuttleworth, 1992). The GDAS has similar limitations to other re-analysis data.

CRU 3.1: This dataset consists of gridded monthly PET estimates for the period 1901-2009 over a 0.5 degree by 0.5 degree latitude-longitude grid (Harris et al., 2012). PET is calculated from a variant of the Penman-Montieth formula derived from gridded data of; temperature, minimum and maximum temperature, vapour pressure and cloud cover (Mitchell and Jones, 2005). The CRU PET data are publicly available and information about permitted uses of the data is available at the CRU web-site. This data set provides complete and long term coverage in the region but with a monthly time resolution.

The CRU dataset is used to estimate PET for most rainfall-runoff catchments represented in the model. In general, PET exhibits less spatial and temporal variability than precipitation. Therefore, in many hydrological studies, monthly data for PET provide satisfactory results for rainfall-runoff modelling. The PET dataset from CRU 3.1 provides one of the most up to data station-based datasets and provides complete and long-term coverage over the whole basin.

Station measurements of evaporation have been used for a limited number of catchments in the Equatorial Lakes sub-basin. The sources of these data are described in section 5.5.

5.3.4.4 Estimating catchment-scale PET

Monthly time series estimates of PET for each catchment are estimated using a weighted average of all CRU grid cells that are located either fully or partially in that catchment. The weight attached to each value is equal to the fraction of the grid cell area located within the catchment. The procedure is outlined in Equation 5.1.

For a limited number of catchments in the Equatorial Lakes sub-basin, PET is estimated from station data. Details of procedures used to estimate PET for these catchments are provided in section 5.5.

Equation 5.1

$$PET_{i,t} = \frac{\sum_{j=1}^{n} w_j \cdot PET_{j,t}}{\sum_{j=1}^{n} w_j} \text{ where } w_j = \frac{A_{i,j}}{A_j}$$

and i = catchment index

j = index of CRU grid cells located fully or partially in catchment i

t = time index

n = number of CRU grid cells located fully or partially in grid cell k

$PET_{i,t}$ = rainfall in catchment i at time step t

$PET_{j,t}$ = rainfall in grid cell j at time step t

w = weight

A_j = area of grid cell j

$A_{i,j}$ = area of grid cell j located within catchment i

5.3.5 Catchment discharge

Discharge estimates are required for all rainfall-runoff catchments for model calibration.

Discharge data are obtained from the following sources: i) NBI (Nile Encyclopaedia and Ethiopia master plan), (ii) ENTRO and iii) Global Runoff Date centre (GRDC).

Nile Encyclopaedia: Discharge records from the Nile Encyclopaedia have been provided by NBI. It should be noted that this data set does not include any measurements in Ethiopia, with the exception of one station at the outlet of Lake Tana. The Nile Encyclopaedia data are confidential and are not permitted to be used outside of this project.
Ethiopian Master Plan: Discharge data from the Ethiopia Master Plan have been provided by NBI. The Ethiopia Master Plan data set includes both monthly and daily records. Most of the stations in the data set are located in Ethiopia, although a few are located in Sudan. These data are all confidential and are not allowed to be used or distributed outside of this project.

ENTRO: The available discharge records received from ENTRO consist of a limited number of monthly records. The ENTRO data are not used because these records duplicate other records in the Nile Encyclopaedia and Ethiopia Master Plan data sets. The ENTRO data are confidential and are not permitted to be used outside of this project.

GRDC: The GRDC discharge data are public and are downloaded from the GRDC web-page. For conditions for using and distributing these data please refer to the GRDC web-page. The GRDC data include both monthly and daily records. Many of these data duplicate other sources of discharge.

In the Equatorial Lakes sub-basin, some additional discharge data have been obtained from other sources. These data are described in section 5.5.

In the Equatorial Lakes, Blue Nile, and Atbara sub-basins, it was necessary to delineate rainfall-runoff catchments for which discharge data are not available, for the reasons outlined in section 0. Details of procedures used for these catchments are described in section 5.5.

5.3.6 Calibration

The parameters of conceptual rainfall-runoff models like NAM cannot, in general, be obtained directly from measurable quantities of catchment characteristics, and hence model calibration is needed. The calibration procedures consists of adjusting the model parameters until a good fit between the simulated flow contributions, (overland flow, interflow and base flow) and gauged stream flow is attained. The main aim of the study was to ensure the highest accuracy of the water balance and a good representation of the general flow regime. The low flow regime is important to address water scarcity but at the same time, a good representation of the high flow regime is also needed.

Calibration of rainfall-runoff models requires performance measures to assess whether calibrated values are reasonable. There exist numerous methods to evaluate the performance of mathematical models depending on the type of model, the data available for testing, and the ultimate purpose of the modelling (ASCE Task Committee, 1993). Any one particular criterion, however, may give more weight to certain aspects of disagreement between simulated output and observed data than others (Green and Stephenson, 1986). Thus, as stated by Diskin and Simon (1977), there should be a definite link between the selected criteria and the application for which the model is intended. Although it is not advisable to rely on one single criterion, two reviews of criteria for model validation (Martinec and Rango, 1989; ASCE Task Committee, 1993) proposed that only a very few quantitative measures should be used in combination with graphical plots.

In this study, calibration was carried out with the

Table 5.3 Rainfall-runoff model performance measures

Performance indicator	Graphical measure(s)	Quantitative measure(s)
Overall water balance	Accumulated flow plot	Difference between total accumulated flow volumes over calibration period
Seasonal flow pattern	Daily and monthly hydrographs, plot of average monthly flows over simulation period	R2 and Nash-Sutcliffe measures
Frequency distribution of flow volumes	Flow duration curve	Not used

goal of obtaining reasonable representations of the following:

1. Overall water balance
2. Seasonal flow pattern
3. Frequency distribution of flow volumes

Measures used to evaluate model performance for each of the above criteria are summarized in Table 5.3.

Both automatic and manual calibration methods were used in the calibration. There are advantages and disadvantages in both methods and these are discussed in detail elsewhere (Duan et al., 1992; Madsen, 2000, 2003; Butts et al., 2004). In general automatic methods were used to provide an initial calibration and then expert judgement was applied for further manual calibration. Only quantitative performance measures can be used in model calibration. The methods used for model calibration vary according to sub-basin and are described in section 5.5.

Uncertainty in hydrological model simulations is dependent on uncertainty in the climate forcing terms (precipitation and PET), the model parameters, the model structure and the uncertainty in the discharge data used for calibration (Butts et al., 2004; Rajaram and Georgakakos, 1989).

In calibrating against discharge it should be noted that many instances river gauging stations in the basin have few discharge measurements for high to very high flows and therefore the reliability of the rating curves for this flow range is low and are often need to be extrapolated beyond the range of measurements. It is also worth noting that a reasonable estimate of the uncertainty in measured discharge for normal flows lies in the range 5-10%. For standard stream gauging methods World Meteorological Organisation (WMO, 1994) estimate the measurement uncertainty of gauged streamflows as 5% standard error at 95% but other sources of errors increase this estimate. These uncertainties should also be borne in mind when assessing calibration performance.

In some basins, it was also necessary to estimate parameters for ungauged catchments. Methods that were used to estimate parameters for ungauged catchments vary according to sub-basin. Details of these methods are outlined in section 5.5.

5.4 River basin modelling

This section describes the river basin modelling approach. The section begins with a general description of the MIKE BASIN rainfall-runoff model. This is followed by a general descriptions of MIKE BASIN was used to simulate factors affecting water availability in the basin, including reservoir and hydropower operations, anthropogenic water use, river routing, evaporative losses, and wetland processes.
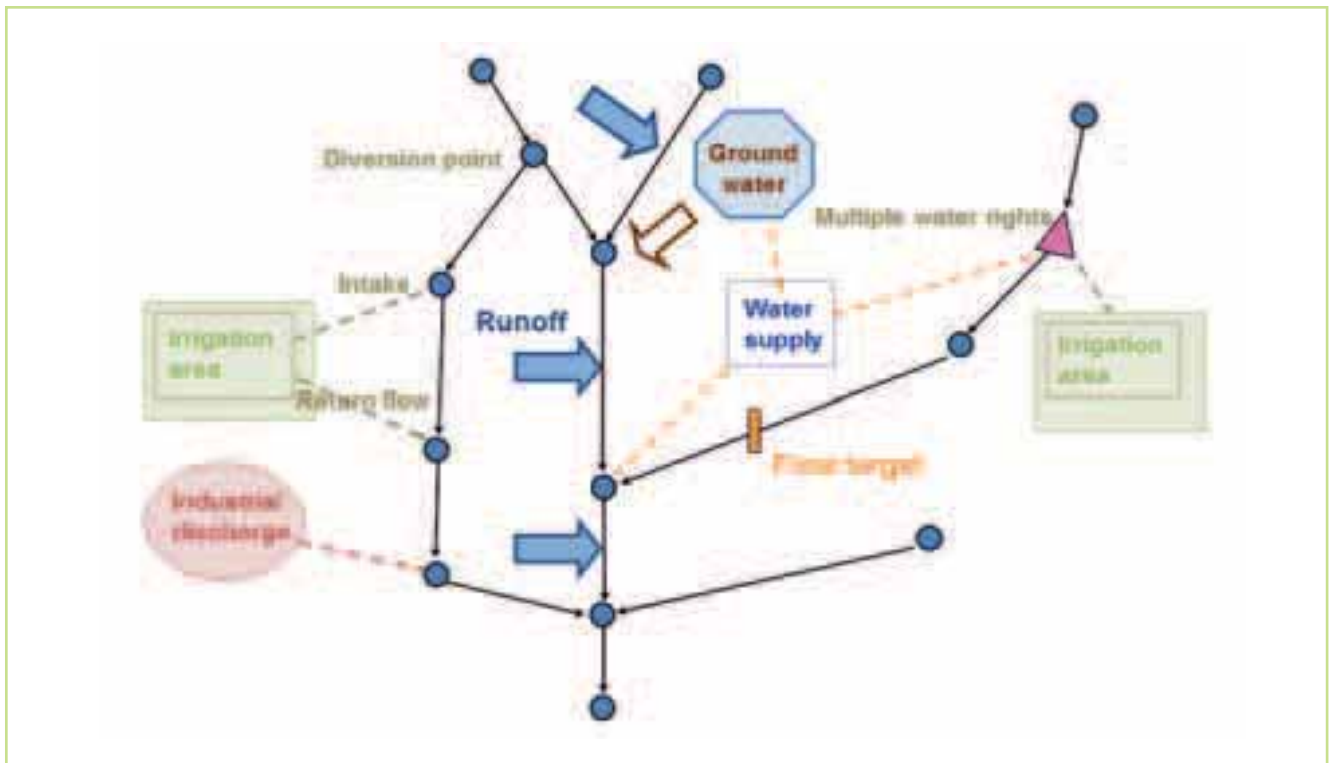
Figure 5.6 Schematic of the MIKE BASIN network model including different water activities

5.4.1 MIKE BASIN

MIKE BASIN (DHI, 2009) is a general water resources modelling framework developed specifically to identify and assess water resource management measures and constraints. This model simulates a river network that links catchment inflows from different sub-basins to the river and links the different tributaries to the main river, routing along the river reaches. NAM rainfall-runoff models can be included in a MIKE BASIN model set-up as a pre-processing step. MIKE BASIN was used to develop and calibrate the major sub-basin models.

Recent research suggests that focussing on the "best" model is inappropriate and that models must first and foremost be "fit-for-purpose". Simply stated, models must be suited to study objectives, which in this project are to represent on a regional scale the impact of climate change on high flow and low flow processes and to be able to the impact of adaptation measures also at the regional scale such as the construction and operation of reservoirs. MIKE BASIN is well-suited to this type of application and is one of the modelling tools currently available in the Nile Basin DSS system.

A short description of this model is given here but further details can be found in DHI (2009). The water resource system is represented as a network as shown in Figure 5.6.

This framework represents rivers and their main tributaries as a network consisting of branches and nodes. Branches represent the individual river sections, while nodes represent either a confluence or a location where certain water activities occur. These include, for instance, multipurpose reservoirs, withdrawals for water supply or irrigation, effluent discharges, diversion canals and systems, gauging stations or low flow control points, and priority-based allocations. Simple routing along the branches is used between these nodes (Figure 5.6).

The available routing schemes include; 1) Linear reservoir routing, 2) Muskingum routing, and 3) Wave translation. The linear reservoir routing scheme is used throughout this study. Losses (seepage or evaporation) along the different reaches can be specified as either as time series of the (absolute) fluxes or as a fraction of the flow or as an (absolute) flux. The runoff components can be specified as time series or can be modelled either using the NAM rainfall-runoff model in a pre-processing or by using a simplified representation of the groundwater discharge to the river system. Withdrawals from the river or reservoir can be represented using an irrigation module that computes crop water requirements or using time series estimates of water demands.

MIKE BASIN accommodates multiple multi-purpose reservoir systems. Individual reservoirs can simulate the performance of specified operating policies using associated operating rule curves. These define the desired storage volumes, water levels and releases at any time as a function of current water level, the time of the year, demand for water, and losses and gains.

The MIKE BASIN irrigation module can be used to simulate agricultural water use (e.g., Riegels et al., 2011). The MIKE BASIN irrigation module is based on the FAO-56 irrigation water use methodology (FAO, 1998). Crop water requirements are calculated based on meteorological data and user-specified crop information such as crop coefficients and growth stage lengths. Soil water storage and uptake of water from soil are also modelled based on the FAO-56 methodology. Crop yields as a function of water use are modelled according to FAO-33 methodology (FAO, 1979), which links yields to cumulative water supply over the growing season.

In summary, MIKE BASIN is designed for integrated river basin analysis, planning and management and for investigating options as the basis for decision-making. It is also part of the modelling tools provided to NBI within the Nile Basin DSS. Therefore MIKE BASIN is well-suited for both assessing the impacts the impacts of climate change on regional water resources and for subsequent assessment of regional scale climate adaptation options.

MIKE HYDRO is the next generation of MIKE BASIN and has the same numerical engine as MIKE BASIN but a completely new user interface. The regional models has been developed in MIKE BASIN and afterwards converted into MIKE HYDRO.

5.4.2 Reservoir & hydropower operations

Reservoir and hydropower operations have a significant impact on flow regimes in the Nile basin. Reservoirs in the basin are operated for flood control, water supply, hydropower, and conservation of wet-year flows for use in dry years.

MIKE BASIN facilitates reservoir and hydropower operations through the use of operating rules and demand time series. The following rule types are implemented for reservoirs and hydropower facilities in the basin:

* Dead storage rule: This rule specifies the minimum operational volume of the reservoir.
* Flood control rule: This rule specifies the maximum operational volume of the reservoir. If storage exceeds this level, the reservoir spills until storage is less than or equal to the flood control level. The purpose of the flood control rule is to maintain space in the reservoir for attenuation of flood flows.
* Minimum release rule: This rule gives the minimum required downstream release from reservoir during each time step.
* Maximum release rule: This rule gives the maximum downstream release. Maximum release rules can be implemented to prevent unrealistically high

releases that might be triggered, for example, during an abrupt transition to a lower flood control level.
* Demand time series rules: Demand time series give the amount of water to be delivered to hydropower facilities or other water use locations directly connected to the reservoir. In the case of hydropower demand time series, these demands can specified using either flow or energy units.
* Allocation rules: Allocation rules can be implemented when demand time series are associated with a reservoir. Allocation rules specify the extent to which deliveries to demand locations should be reduced when reservoir storage falls below threshold levels.
* Hydropower capacity constraints: Capacity constraints are used to limit flows that can be delivered to hydropower facilities. These constraints are given in both flow and energy units.

In the case of the High Aswan Dam, additional rules and other features are implemented because of the complexity of the operation. Details of the simulation of High Aswan Dam and other reservoir and hydropower operations in the basin are provided in section 5.5.

5.4.3 Irrigation, domestic, & industry water use

Irrigation water use is significant in the Nile Basin, particularly in Egypt and Sudan, where irrigation withdrawals have a significant impact on the flow regime. Domestic and industry water uses are less important for the overall water balance, but can be significant, particularly in Egypt.

The irrigation, domestic, and industry water uses implemented in the regional model are represented using demand time series that specify the amount of water to be delivered during each time step. The MIKE BASIN irrigation module is not used in this study as this would require additional detailed crop information. Water deliveries can take place from rivers or from reservoirs, as described above. If a water delivery takes place from a river, MIKE BASIN will attempt to deliver the entire demand amount unless the river flow is insufficient. If a water delivery takes place from a reservoir, the delivery can be reduced depending on the reservoir level.

5.4.4 River routing & losses

The use of river routing in the model depends on estimated travel times in each river reach. In shorter mountain reaches, it was assumed that travel times are less than the model time step (one day), so routing

was not used. In downstream reaches with smaller gradients and longer travel times, linear reservoir routing was used to attenuate reach outflows.

The approach used to simulate river losses is similar to the routing approach. In upstream and mountain catchments, it was assumed that no losses take place. In downstream reaches, it was assumed that significant evaporation losses occur. These losses are represented in the model as a time-varying percentage of river flows. No seepage losses are assumed to occur, primarily because it was not possible to estimate the magnitude of these losses or distinguish these from evaporation losses from the available data.

5.4.5 Wetland processes

Wetland processes have an important impact on flow regimes in the Nile basin. The two most important wetland areas in the basin are the Sudd and the Machar marshes in the Sobat basin. In both locations, significant seasonal flooding takes place, with resulting evaporative losses.

MIKE BASIN does not have explicit capabilities for representing wetland processes. Wetlands are either represented as reservoirs along the main reach, which have the effect of delaying travel times and facilitate surface evaporation, or using bifurcation nodes, which can be used to simulate overflow from the river channel to wetland areas where flows are subsequently lost to evaporation.

In this study, wetland processes in the Sudd are simulated using reservoirs, while the Machar marshes are represented using a bifurcation node. More details are provided in section 5.5.

5.5 Hydrological modelling of the major sub-basins

This section describes the basin-specific aspects of the hydrological modelling for the major sub-basins in the regional model. In particular, a more detailed description is given for the focus areas identified previously.

5.5.1 Focus areas

The focus of this study has been to develop and apply models to address climate change and water resource issues at the regional scale. The original concept of this particular work package was concerned with the identification of "hot spots". While the implication is that there are local areas with significant water resources, climate or other issues. At the outset of the project it quickly became clear that the "hot spots" most easily identified within the Nile Basin were often

quite large areas, rather than localised points. As a result we have chosen to refer to these large scale "hot spots" as focus areas.

In this project we have chosen to make additional effort to ensure that the regional hydrological models represent the climate and hydrology in three focus areas:
- The Equatorial Lakes basin (called the Lake Victoria basin in the model)
- The Ethiopian Highlands (Blue Nile and Atbara basins)
- The Egypt and Sudan water demand region

These are undeniably the most crucial areas in term of hydrology. The Equatorial lakes and the Ethiopian highlands are the main source areas of precipitation that generate runoff to the rest of the Nile Basin. The largest water use by far in the Nile is the irrigation water demands and the analysis of these demands across the whole Nile Basin (section 4) show quite clearly that the irrigation water requirements in Egypt and Sudan are 2-3 orders of magnitude greater than the other countries. Examination of the inflows to the Aswan Dam presented in Figure 1.5 shows the hydrological connection between these three regions. In terms of the inflows the White Nile contribution, with its source in the Lake Victoria sub-basin, provides the background flow, much like baseflow, throughout the year. Changes in these flows will more likely affect the flows during the drier period. The Blue Nile and Atbara provide the peak flows and the inflows to the Aswan are particularly sensitive to changes in these contributions because of their magnitude, corresponding to more than two thirds of the overall flow.

5.5.2 The Equatorial Lakes Basin (Lake Victoria Basin)

The Equatorial Lakes Basin is dominated physical as well as hydrologically by the existence of the five major equatorial lakes, with Lake Victoria and the outflow from Lake Albert being the dominating factors for the flow in the Nile down to the Sudd.

Lake Victoria is the second largest body of fresh water in the world with a surface area of 68,800 km2 and it is shared by Kenya (6%), Tanzania (49%), and Uganda (45%). Its drainage basin extends over 184,000 km2 and includes parts of Burundi and Rwanda. There are concerns about eutrophication and pollution in the lake. Coastal towns and cities discharge untreated sewages into the lake, while soil erosion caused by deforestation and poor farming methods is increasing sediment loads in the rivers flowing into the lake.
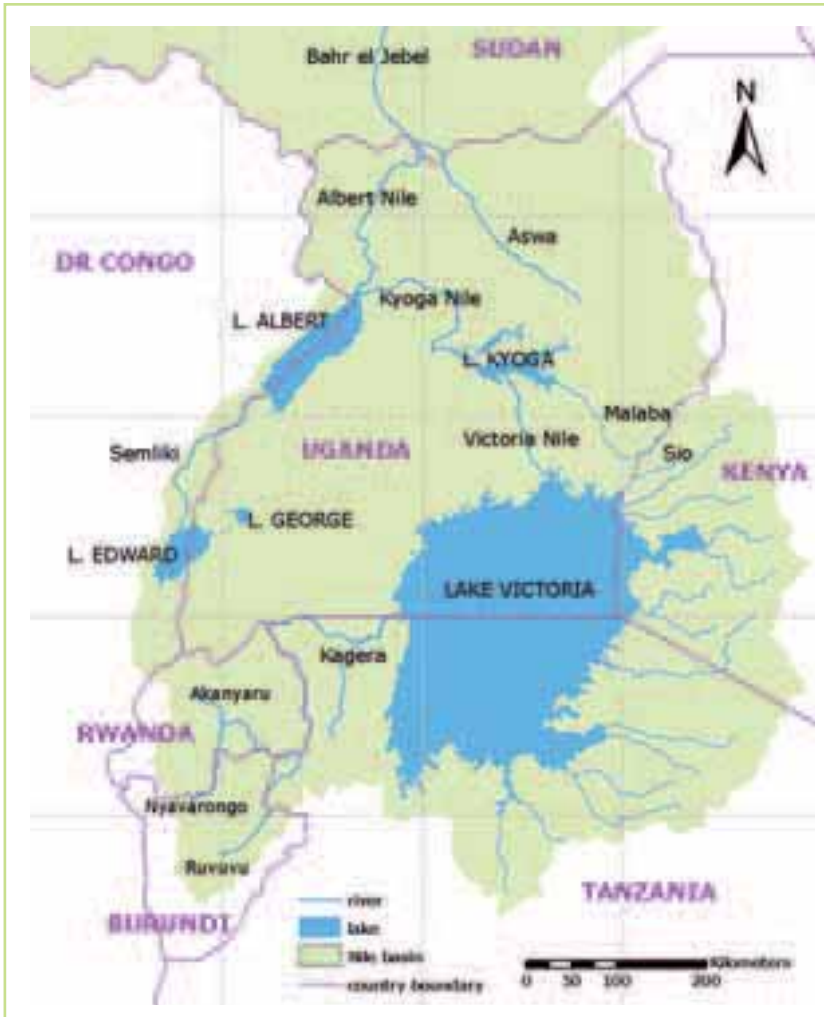
Figure 5.7 The main lakes & rivers in the Equatorial Lakes Basin

Lake Edward has a surface area of 2,325 km² and a mean depth of 33.5 m, and is located on the border between Uganda and the Democratic Republic of Congo. Its catchment area measures 12,000 km² and includes Lake George which drains into Lake Edward through the Kazinga channel. The whole system is drained by the Semliki River.

Situated in the western Rift Valley, Lake Albert has a surface area of 5,800 km² and is shared by Uganda and the Democratic Republic of Congo. It is an important part of the Nile system and most of its inflow comes from the Kyoga Nile followed by the Semliki. In spite of its large surface area it is the shallowest of the large Rift Valley lakes, with a mean depth of only 20.5 m. Because of its relatively steep banks, Lake Albert has an attractive surface-to-volume ratio. The discovery of exploitable quantities of oil in the Albertine Rift could have adverse implications for the water quality of the lake.

The key features that determine the hydrology of the lake include the high contribution (85%) of rainfall falling directly on the lake contributing to the total lake inflow. This suggests that lake levels and the long-term outflow will be highly sensitive to climatic change. The operational policies of the Kiira and Nalubaale hydropower stations at Jinja control the outflow from the lake and effectively limit lake level fluctuations to a relatively narrow band of some 3 m, giving a live storage volume of over 200 km³. This attenuates seasonal and annual variability in lake inflows and has led to a relatively stable outflow down the Nile. With an average depth of only 40 m, Lake Victoria is extremely shallow in relation to its surface area and lake dynamics are affected in various ways, such as high evaporation, and are likely to have an effect on aspects relating to water quality. The outflow from Lake Victoria is presently determined by the 'agreed curve', which represents the natural outflow, based on a ten-day average flow of the Victoria Nile at Ripon Falls prior to the construction of the Owen Falls Dam, as a function of lake level.

5.5.2.1 Data

Compared to other parts of the Nile system there is generally a good coverage and in many cases good quality of data not least for the period (1960-80) covered in this study. This is not least due to the achievements of the HYDROMET project (Hydro Meteorological Surveys Project of the Upper Nile - Equatorial Lakes Catchments) which took place from 1967-92.

Similar to the other parts of the Nile Basin data from the following sources have been used: 1) Nile Encyclopaedia, 2) Global Runoff Data Centre (GRDC), 3) CRU data, 4) Nile DST and 5) NBI baseline model (provided by NBI; A.H: Seid, pers. comm.). The GRDC and CRU data are publically available and the conditions of use for these data can be found on the corresponding web sites. The Nile Encyclopaedia and Nile DST data have been provided by NBI under a confidentiality agreement. For this reason only processed data or model results will be delivered as part of the project, the actual observed data are confidential. However, the data made available through these sources provides a reasonable coverage for this region but only includes a minor part of the data actually collected in the region during the modelling period 1960-80.

Table 5.4 List of data used for the NAM & MIKE BASIN (MB) modelling work for the Equatorial Lakes Basin. Where more than one source is mentioned the first is the main / most important source

Type of model	Country	Area[3] / Catchments	Type of data[1] Data	sources[2] used
NAM	Kenya	All	Q	LVEMP I
NAM	Kenya	All	P	LVEMP I
WRMA K	enya	All	Ep	CRU LVEMP I
NAM T	anzania	Kagera	Q	LVDB /Hydromet
NAM T	anzania	Kagera	P	NileDST
NAM T	anzania	Kagera	Ep	CRU
NAM	Tanzania	Other TZ catchments	Q	LVEMP I
NAM	Tanzania	Other TZ catchments	P	NileDST LVEMP I
NAM	Tanzania	Other TZ catchments	Ep	CRU
NAM	Uganda	Lake Victoria Basin	Q	LVEMP I
NAM	Uganda	Lake Victoria Basin	P	DWRM LVEMP I
NAM	Uganda	Lake Victoria WMZ	Ep	CRU
NAM Uganda		Kyoga WMZ	Q	DWRM
NAM Uganda		Kyoga WMZ	P	DWRM
NAM Uganda		Kyoga WMZ	Ep	CRU
NAM Uganda		Albert WMZ	Q	DWRM
NAM Uganda		Albert WMZ	P	DWRM
NAM Uganda		Albert WMZ	Ep	CRU
NAM Uganda		Upper Nile	Q	DWRM
NAM Uganda		Upper Nile	P	DWRM
NAM Uganda		Upper Nile	Ep	CRU
MB	LV Basin	Lake Victoria	HVA curves	DWRM
MB	LV Basin	Lake Victoria	P & Ep	LVEMP I
MB	LV Basin	Lake Victoria	Releases	DWRM
MB	LV Basin	Lake Victoria	"Agreed curve"	DWRM
MB	Uganda	Lake Kyoga, Albert, George & Edward	P	DWMR
MB	Uganda	Lake Kyoga, Albert, George & Edward	Ep	DWMR
MB	Uganda	Lake Kyoga	HVA curve	DWRM
MB	Uganda	Lake Kyoga	Rating curve outlet	DWRM
MB Sudan		Mongalla	Q	GRDC

[1] Type of data: Q = Discharge, P = Precipitation and Ep = Potential Evapotranspiration

[2] Data sources: LVEMP I: Data generated in relation to Lake Victoria Environmental Management Project I, WRMA: Water Resources Management Authority, Kenya, DWRM: Directorate of Water Resources Management, Uganda, LVDB: Lake Victoria Database: Data primarily collected during the HYDROMET project.

[3] WMZ: Water Management Zone (Uganda is now divided into 4 WMZs: 1) Albert, 2) Kyoga, 3) Upper Nile and 4) Victoria

For the catchments draining into Lake Victoria the data used in relation to Lake Victoria Environmental Management Project (LVEMP I) has been an important source of information. For the Ugandan catchments, which in numbers, constitute the major part of the NAM catchments included in the MIKE BASIN setup, the Directorate of Water Resources Development (DWRM) in Uganda, have been extremely cooperative and have made their precipitation, discharge and evaporation data available for the study. This has substantially improved the modelling work in the Ugandan part of the model and DWRM is gratefully acknowledged for making the data available for the modelling work. For Tanzania a substantial part of the daily data from the catchments draining into Lake Victoria was not made available for this project.

Table 5.4 provides a more detailed list of the different types of data used for the setting up the NAM models and the MIKE BASIN model for the Equatorial Lakes system covering all the Nile system upstream of Mongalla in Southern Sudan. This includes almost the entire Uganda and those parts of Kenya, Tanzania, Burundi and Rwanda which drains into Lake Victoria.

5.5.2.2 Rainfall-runoff modelling

The majority of catchments in the basin are gauged, especially the headwater catchments. However, for some of them, including some of the catchments in the very north-western part of Uganda, the periods with data are either too short, contain too many gaps or are of too poor quality.

The main ungauged areas in the basin are: 1) The areas around the shore of the lakes, 2) Northern part of the Semliki valley and 3) The area south and west of Lake Edward from both Uganda and Congo, see Figure 5.7. The hydrology of the area from Lake Albert down to Laropi is also not well understood.

The estimation of discharge from ungauged areas has been carried out either directly by rainfall-runoff modelling (cf. section 5.3.2) or for some intermediate catchments by further calibrating the overall MIKE BASIN model once the subcatchment models have been linked together.

Precipitation

The sources of rainfall data used in the study are listed in Table 5.4. For most catchments, with the exception of just a few, more than one rainfall station has been used to estimate the mean areal rainfall over the catchment. For some of the major catchments up to 8-10 rainfall stations has been used. A thorough check of the rainfall stations has been undertaken prior to the selection of the stations to be used. The following three key criteria have been used to select the rainfall stations to be used for the rainfall-runoff modelling: 1) Data coverage for the modelling period, 2) Data quality and 3) Spatial location.

The Thiessen polygon method has been used as the point of departure for estimation of the mean areal rainfall. However, modification of the station weights has been necessary for some of the catchments. For example if the station does not give a good representation of the rainfall within the catchment. This has particularly been the case for the gauged catchments draining the eastern side of the Rwenzori Mountains as most of the rainfall stations are located in the lower part of the catchments and receive less rainfall than the central and upper parts of the catchments.

Potential evapotranspiration (PET)

The amount of evaporation data within the basin is limited compared to the amount of rainfall data. Most of the data collected are from evaporation pans which often are of relatively poor quality. The thorough studies of evaporation based on meteorological data using the Penman-formula carried out by Rijks & Owens (1970) for Uganda and by Woodhead (1968) for Kenya and the Uganda study only included a few stations. It was therefore decided to use the CRU evaporation data for the majority of catchments in the basin, while only a few catchments in Kenya are based on ground data. An important exception is directly over Lake Victoria where the CRU data has set evapotranspiration to be zero. Instead the PET directly over the lake was derived from the LVEMP 1 data.

Based on the CRU grid data and the shape of the catchments the mean areal potential evapotranspiration has been estimated. These estimates have been used as the point of departure for the NAM rainfall-runoff calibrations. In some cases it has been assessed that the figures needed to be increased or reduced slightly to provide a proper estimate of the mean areal potential evapotranspiration.

5.5.2.3 Calibration of gauged headwater catchments

Gauged headwater catchments are calibrated by comparing the measured flows at the outlet of the catchment with the simulated flow from the model. As described above both manual and automatic calibration methods based on the shuffled complex evolution (SCE) method (Duan et al., 1992; Madsen, 2000, 2003) using bounds on the calibration parameters. The following objectives are usually considered during the model calibration; 1) reasonable agreement between the average simulated and average observed catchment runoff, (i.e., a reasonable and realistic water balance.), 2) reasonable overall agreement of the shape of the hydrograph, 3) reasonable agreement of the peak flows with respect to timing, rate and volume and 4) reasonable agreement for base flows. These were
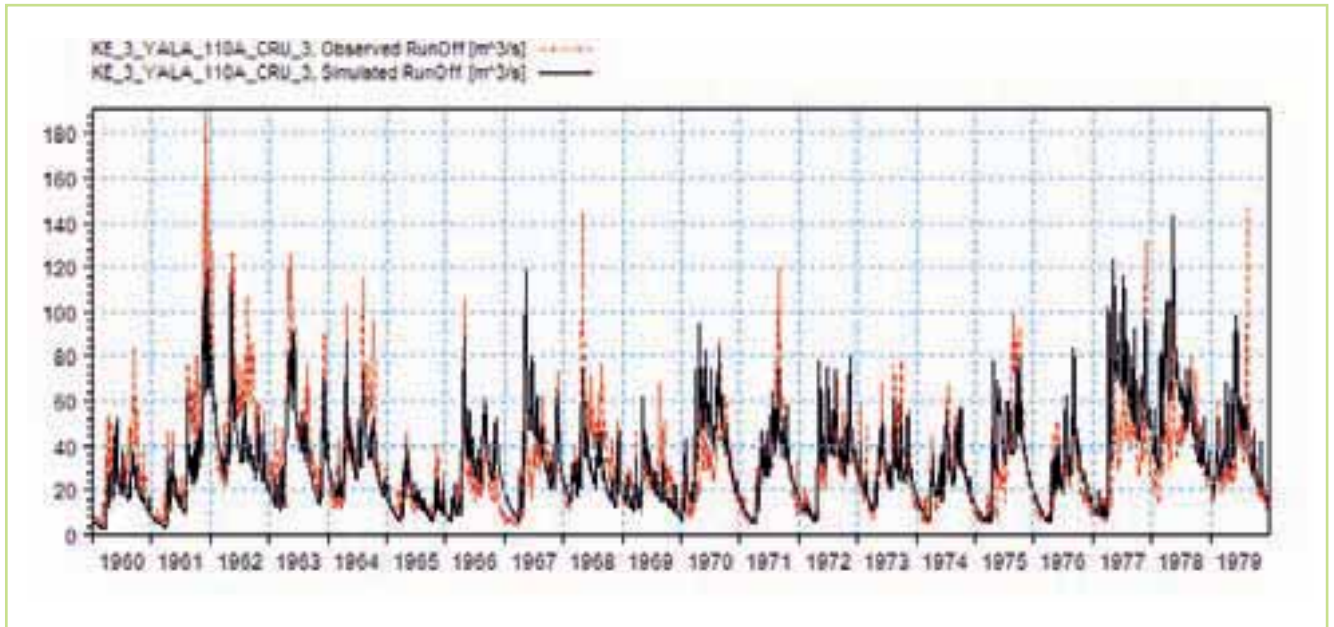
Figure 5.8 Example of calibration plot from the Yala catchment in the Lake Victoria Basin. Comparison of the observed (red) & simulated (black) discharge for the KE03 - Yala catchment for the period 1960-1979. It is possible to obtain a consistent calibration throughout the 20 year period indicating good data quality
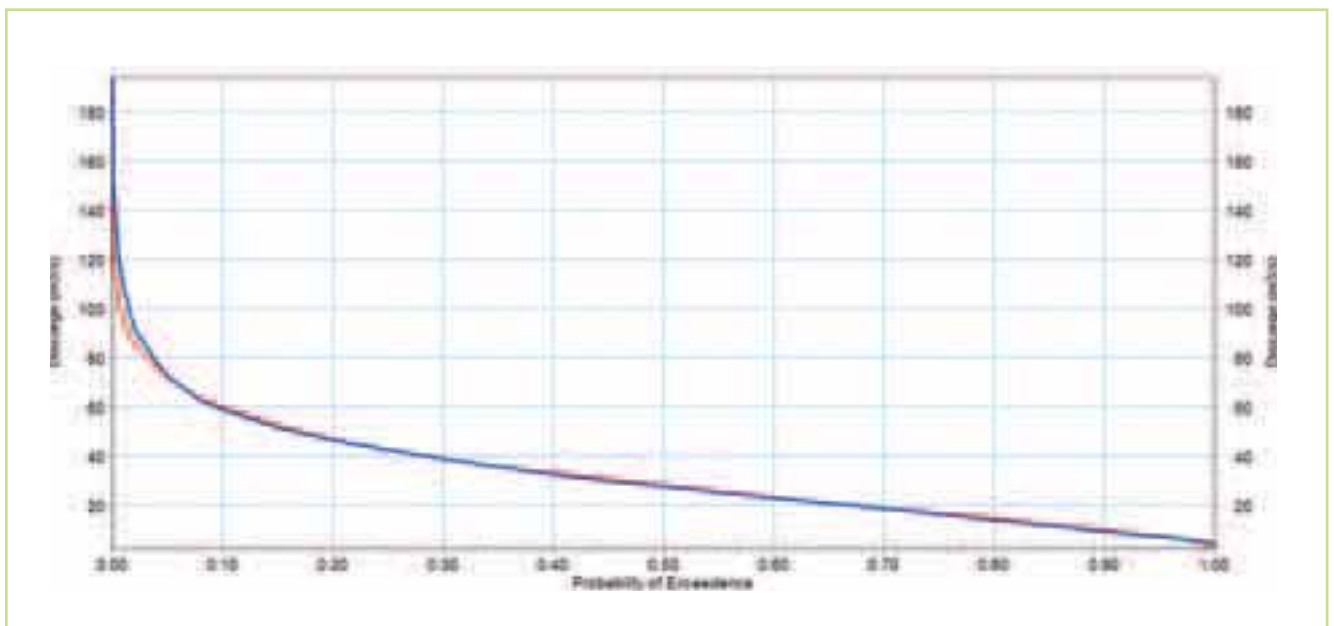
Figure 5.9 Example of calibration plot with duration curve from the Yala catchment in the Lake Victoria basin. Comparison of flow duration curves for the observed (blue) & simulated (red) discharge for KE03 – Yala for the period 1960-1979. There is reasonable reproduction of flows throughout the flow regime except for minor differences for very high flows where the uncertainty in observed flows is expected to be high

assessed during the calibration process primarily by examining comparing the flow hydrographs, the accumulated mass curves and flow duration curves. Examples of such comparisons are given below.

In general, the quality of the calibration reflects the quality and reliability of the data used. The best calibration results are obtained where there is good coverage of precipitation data and continuous and good quality discharge data. Generally the rainfall-runoff models have also been better at representing catchments with relatively high runoff coefficients where the baseflow constitutes a significant part of the total runoff, while it has been more difficult for the models to reproduce runoff from arid to semi-arid catchments with little runoff or where runoff occurs during just a few events each year.
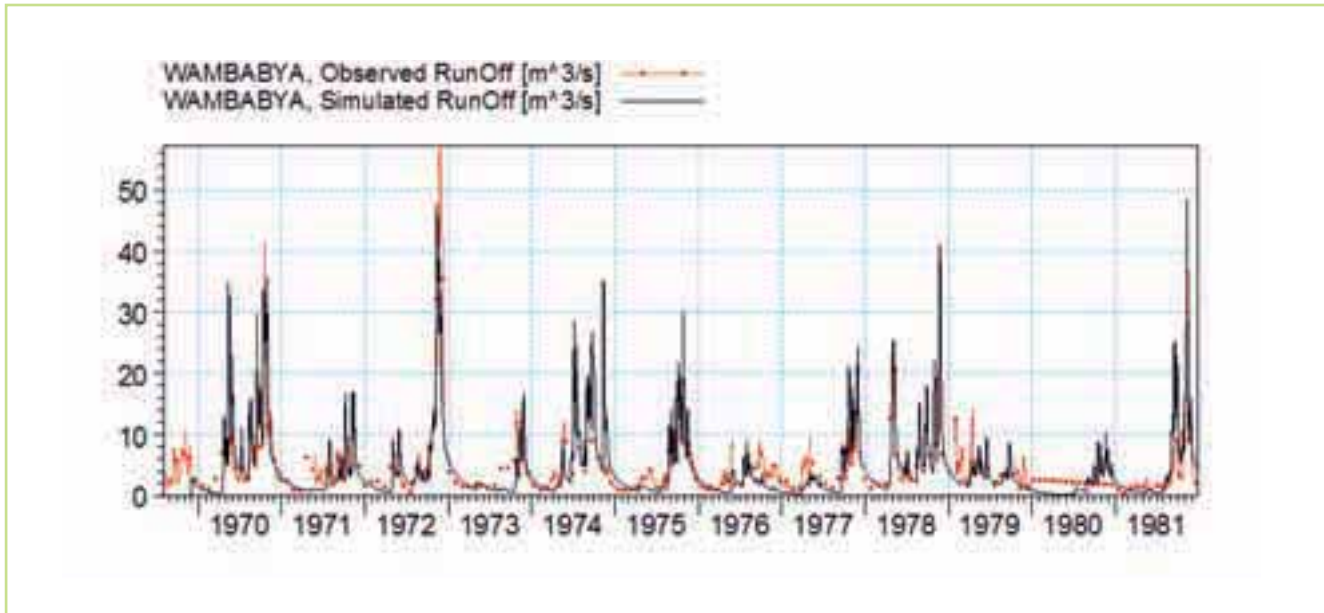
Figure 5.10 An example of a calibration plot from the Wambabya catchment in the Lake Victoria Basin. Comparison of the observed (red) & simulated (black) discharge for the Wambabya catchment, for the period 1970-1981. There is a reasonable agreement between the two hydrographs with the exception of 1980 where the observed data is probably not reliable. It should also be noted that for this particular station the model has difficulties in representing the flow pattern during the dry period

Figure 5.11 Example of accumulated mass curves for the observed (red) and simulated (black) discharge for the Wambabya catchment. There is a reasonable agreement between the two hydrographs with the exception of 1980 where the observed data is probably not reliable

Calibration results from gauged catchments

The best calibration results have generally been obtained for catchments with good spatial coverage of continuous and high quality input (where the climate data is the most important). Generally the models have also been better in representing catchments with relatively high runoff coefficients where the baseflow constitutes a substantial part of the total runoff, while it has been more difficult for the models to reproduce runoff from arid to semi-arid catchments. For the same reason the uncertainty related to estimated change in runoff as a consequence of climate change is also expected to be higher from these catchments.

The calibration results for a number of selected catchments in the Equatorial Lakes (Lake Victoria) basin are presented below.
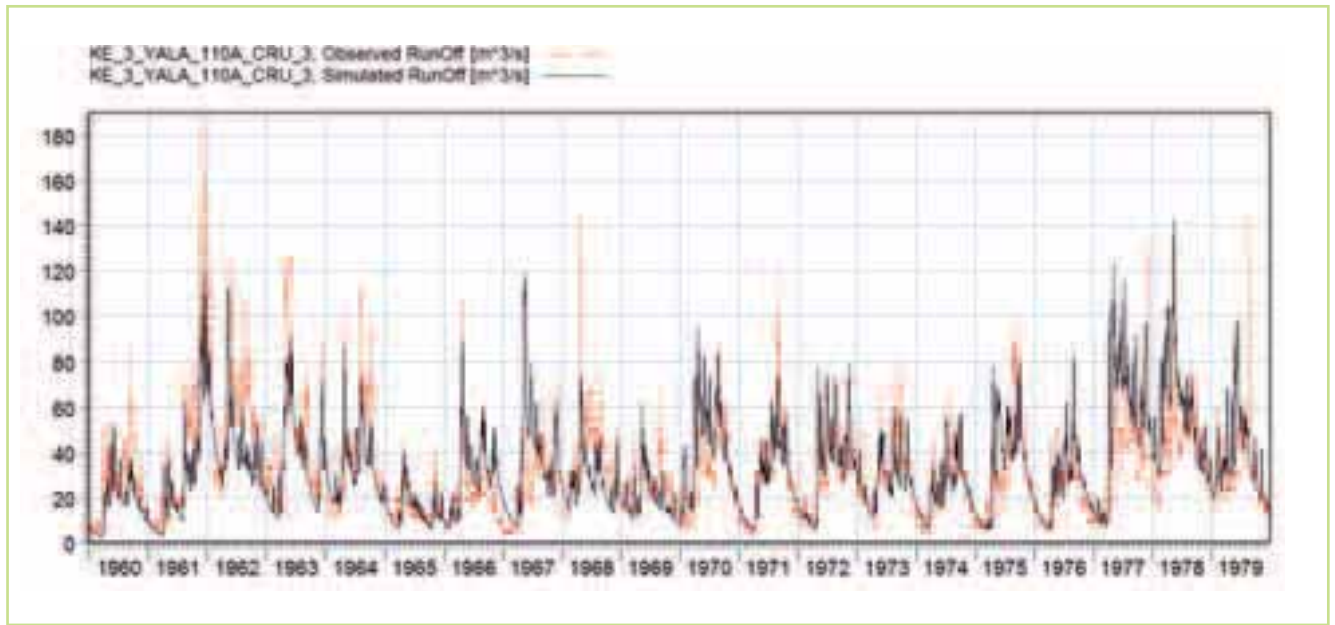
Figure 5.12 Comparison between simulated (black) & observed discharge (red) for KE03 – Yala for the period 1970-1988. It has been possible to obtain a reasonable an realistic representation thoughout the 20 years period, indicating good data quality

Figure 5.13 Comparison between flow duration curves for simulated (red) & observed discharge (blue) for KE03 – Yala for the period 1960-80. It has been possible to obtain a reasonable reproduction of the flows throughout the flow regime except for some minor differences for the very high flows where the uncertainty related to the observed flows are substantial
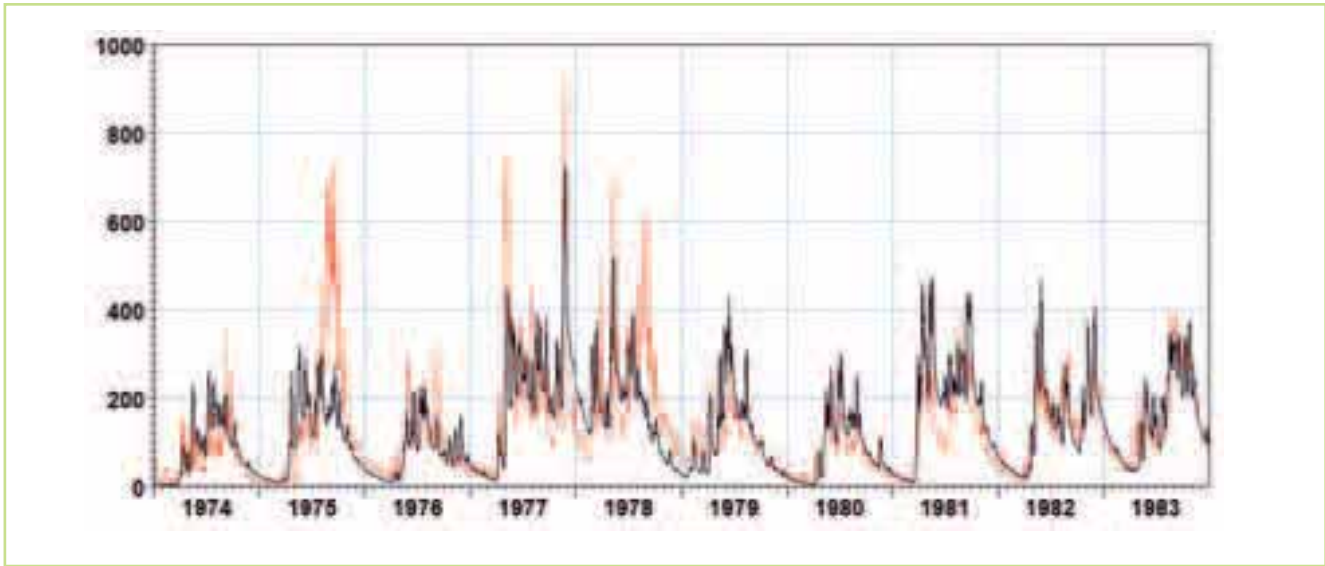
Figure 5.14 Comparison between simulated (black) & observed discharge (red) for KE02 – Nzoia for the period 1974-1983. Due to lack of observed discharge for other periods, 1974-83 was selected as the calibration period
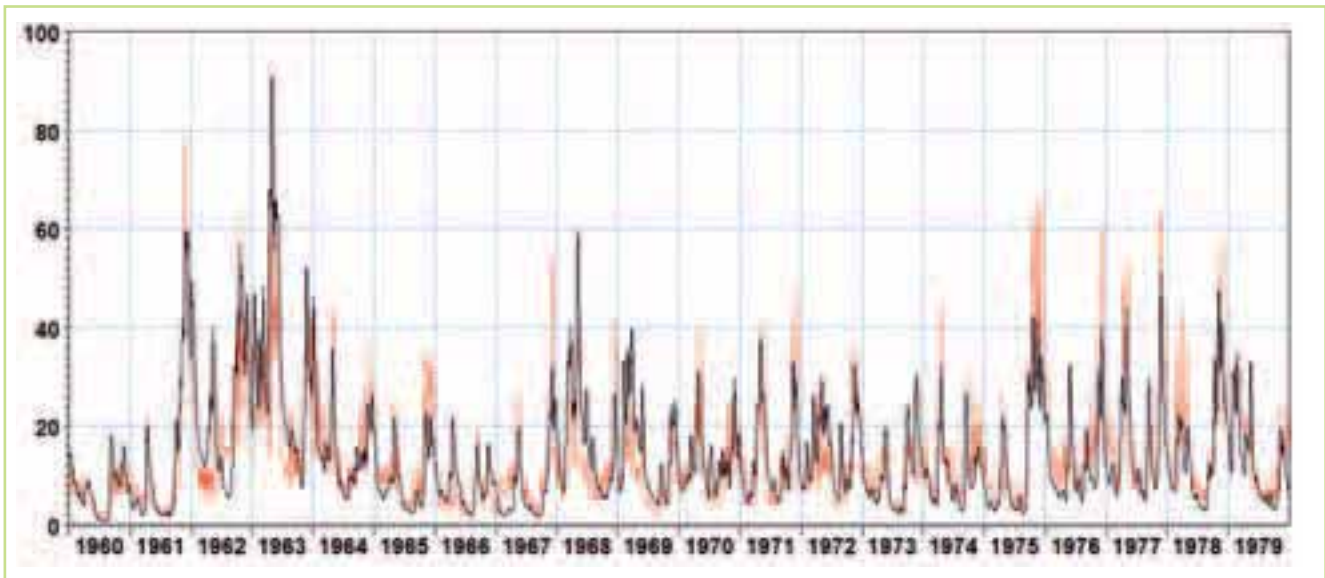
Figure 5.15 Comparison between simulated (black) & observed discharge (red) for UG20_84267_Mitano for the period 1960-1980. It has been possible to obtain a reasonable & realistic representation throughout the 20 years period, indicating good data quality as well as the RR-models ability to reproduce the flow regime
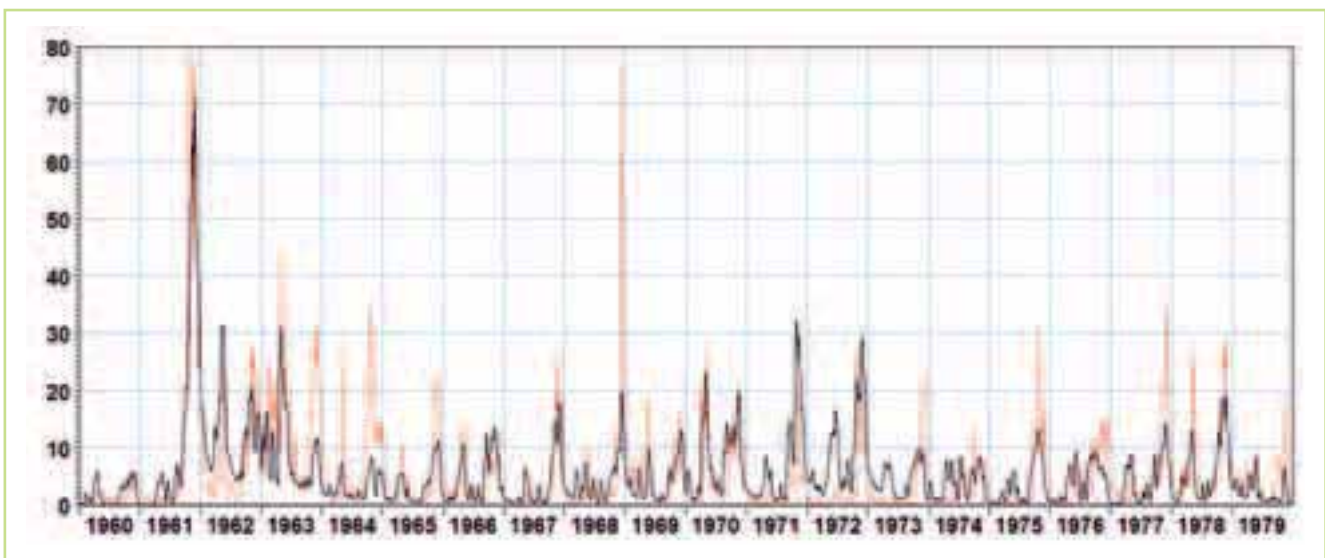
Figure 5.16 Comparison between simulated (black) & observed discharge (red) for UG13_85211_Muzizi for the period 1960-1980
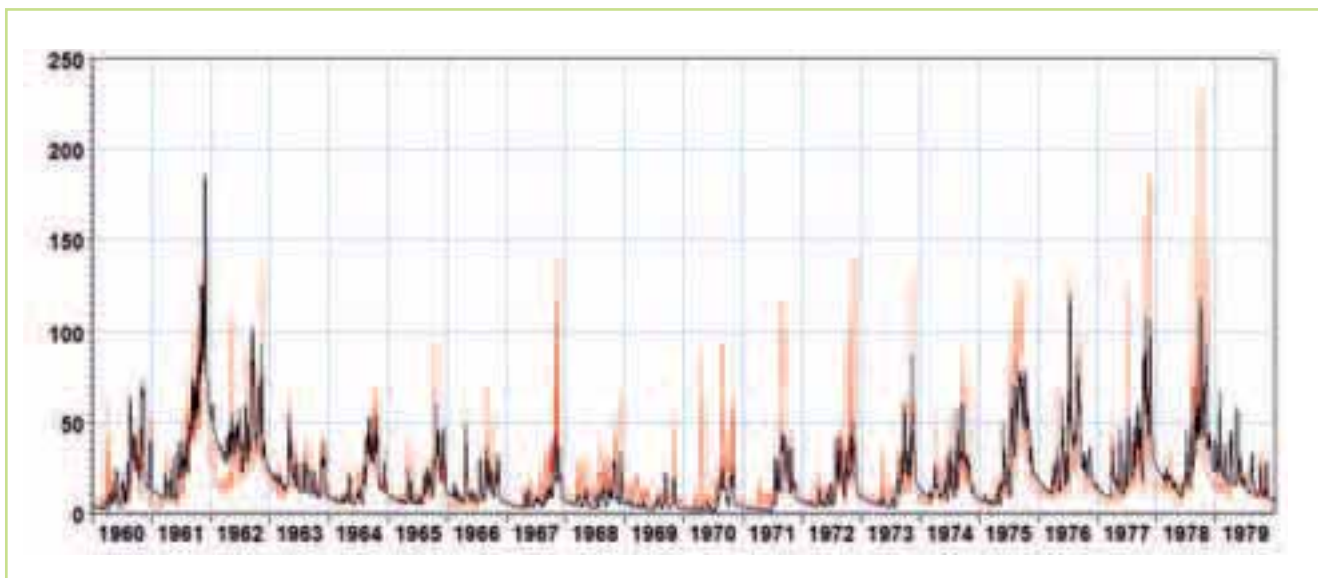
Figure 5.17 Comparison between simulated (black) & observed discharge (red) for UG41_87212_OraAtInde for the period 1960-1980

5.5.2.4 Ungauged catchments

In general model parameters for ungauged catchments were estimated using a proxy basin approach (Refsgaard and Knudsen, 1996) where parameters from hydrologically similar (rainfall, PET, topography, land cover) catchments were used to provide a first estimate of the NAM parameters. These parameters were then reviewed when the major subcatchment models were assembled by assessing their impact at downstream gauges.

The ungauged basins were treated in two different ways depending on: 1) the size of the catchments, 2) the difference in rainfall regime as compared to the proxy basin catchment, 3) the availability of data of precipitation data, and 4) the type of catchment.

a. The specific runoff from a nearby NAM catchment (proxy basin) was used to generate the runoff. In reality this means that the parameter setup in input data from the proxy basin was used and the catchment area was adjusted to compensate for the difference in area between the ungauged catchment and the gauged proxy basin This was, generally,' done for the following types of headwater catchments:

- the ungauged catchment is small and adjacent to the original gauged catchment
- the ungauged catchment is close to the gauged catchment and has a rainfall regime very similar to the gauged catchments
- only poor or no rainfall data are available for the ungauged catchment.

b. The parameter setup for a nearby gauged NAM catchment (proxy basin) was used but with new input data for precipitation and potential evapotranspiration representing the ungauged catchment. This was, generally, done for the following types of headwater catchments:

- the ungauged catchment is close to the original catchment but large in size
- the ungauged catchment has a rainfall regime which is substantially different from the gauged NAM catchment.

5.5.2.5 MIKE BASIN modelling
Model setup

The basin is dominated by the existence of the five Equatorial lakes, namely Lake Victoria, Lake Kyoga, Lake Albert, Lake Edward and Lake George, the two latter being immediately connected through the Kazinga Channel. These lakes have a very dominant impact on the hydrology on the Nile in this part of the Nile Basin upstream of Mongalla. The lakes have two major impacts on the flow in the Nile:

1. The magnitude of the flow, through direct input (rainfall) and outputs (evaporation from the lakes).
2. The timing of the flow through the routing / storage effect on the flow.

Regarding the magnitude of the flow, Lake Victoria receives on average substantially more rainfall on the lake itself than evaporation from the lake corresponding to 350-400 m3/s while there is a net loss in the balance between rainfall on and evaporation for the four other lakes.

The dominant factor determining the amount of flow in Nile upstream of Mongalla is the releases from the Lake Victoria. The outflows from the lake have only a small seasonal variation as the inflows

from adjacent catchments and the direct rainfall on the lake are attenuated by the large lake storage. The flow is further attenuated by Lake Kyoga and Lake Albert before it flows down the Albert Nile towards Mongalla, where contributions from local catchments in the upper part of Uganda which adds some seasonal variation to the total flow before the Nile reaches Mongalla.

Setting up the lakes in the model

The dominance by the lakes in the basin poses a number of challenges in creating a realistic model setup of the system. Among other things, the following three key issues had to be addressed due to the existence of the lakes:

1. Establishment of HVA (Height-Volume-Area) curves for each of the lakes: While good estimates of the HVA-curve exist for Lake Victoria and Lake Kyoga, approximate HVA-curves had to be established for Lake Albert, Lake Edward and Lake George based on the available information about the lakes. The well-established HVA-curves for Lake Victoria and Lake Kyoga made it possible to calibrate the model against the measured water levels in the two lakes but not for the other lakes

2. Estimation of evaporation from the lakes and rainfall on the lake: This also poses a challenge as there are no measurements available from the lakes themselves except from Lake Victoria where there are measurements from a number of islands in the lake. The estimates therefore had to be based on measurements from stations around the lake. For Lake Victoria the rainfall input and

evaporation from the lake was based on the results of the LVEMP I project.

3. Outflow from the lakes: The perhaps greatest challenge was to determine the outflow from the lakes as the outflow should be the natural outflow based on a rating curve rather than forced outflow based on e.g. the releases at the Owen Falls Dam. This is discussed in further detail below.

The outflow from Lake Victoria

The outflow from Lake Victoria determines to a large extent the flow volume in the Nile down to Mongalla is therefore crucial for the whole system.

From a calibration point of view, the outflow should be the actual releases from the lake to ensure that the correct figures are used for the calibration of the model and establishing the water balance for the Lake Victoria. However, from the perspective of assessing the impact of climate change on the whole system it is important that the outflow from the lake is the "natural" outflow determined by a rating curve where the outflow from the lake is a function of the water level in the lake. With the construction of the Owens Falls Dam it was agreed that the releases from the Dam should follow the old rating curve as the original "Rippon Falls" – the so-called "Agreed Curve". The first thing to investigate was therefore if the actual releases during the modelling period 1960-80 had followed the agreed curve. Figure 5 18 compares the actual releases at Owens Falls dam and the outflow from the Lake according the "agreed curve". We find that the release follow the Agreed Curve for most of the period, with the exception of 1968-70.
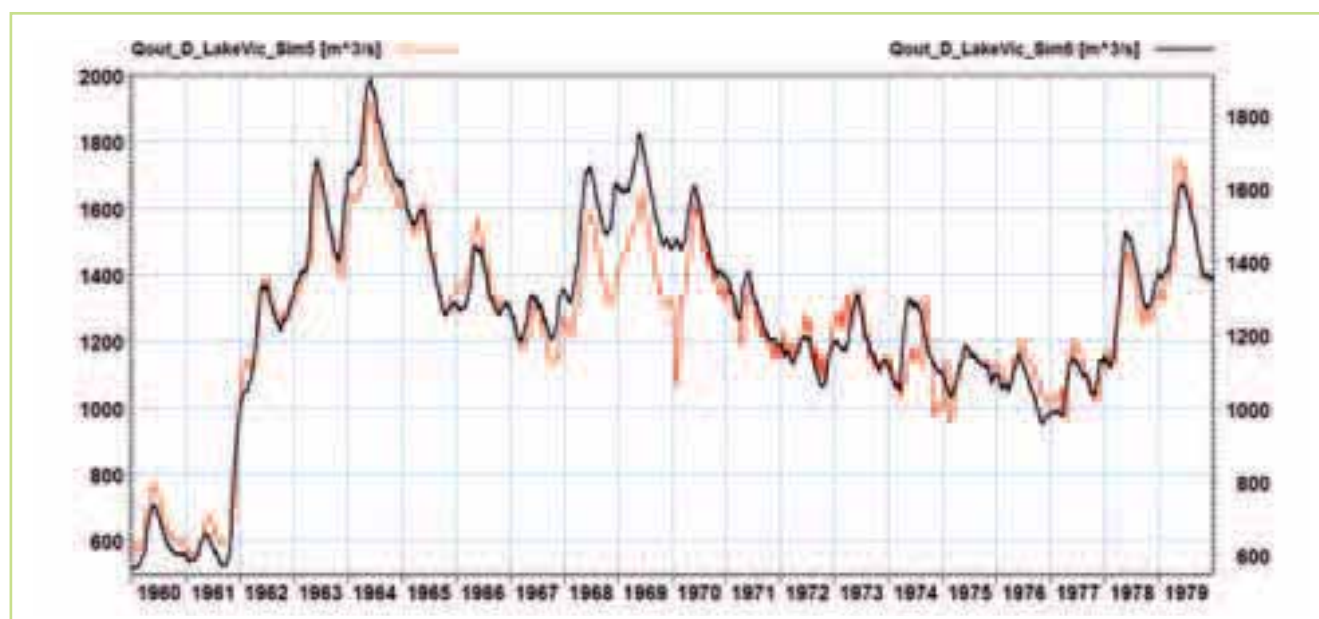
Figure 5.18 Comparison between the actual releases at Owens Falls Dam (red) & the outflow from Lake Victoria as it would have been according to the agreed curve (black). Generally, there is an acceptable agreement between the observed & simulated hydrographs except for a few major deviations, mainly in 1968-69

Key calibration results

A comprehensive presentation of the calibration results is outside the scope of this report. However, some of the key calibration results are shown including those used in the subsequent regional assessments. Model variables at key locations were prioritized when minimizing the deviation from the observed flow in time and magnitude. Some of these are listed in Table 5.5.

Table 5.5 List of prioritized variables at key locations during model calibration

	Variable	Location	Hydrological aspect to address
1	Discharge	Jinja / Outlet of Lake Victoria	The contribution from the Lake Victoria Basin to the overall water balance
2	Water level	Lake Victoria	Contribution of catchments to and water balance of Lake Victoria
3	Water level	Lake Kyoga	Contribution to Lake Kyoga from local catchments and water balance of Lake Kyoga
4	Discharge	Kamdini (83206)	Contribution from intermediate catchments along the Kyoga Nile and the discharge from the Kyoga Nile to Lake Albert
5	Discharge	Semliki (85205)	The contribution from local catchments between Lake Edward and Lake Albert, including contributions from the western part of the Rwenzori mountains.
6	Discharge	Laropi (87217)	This represents to a large extent the inflow to the Sudd.
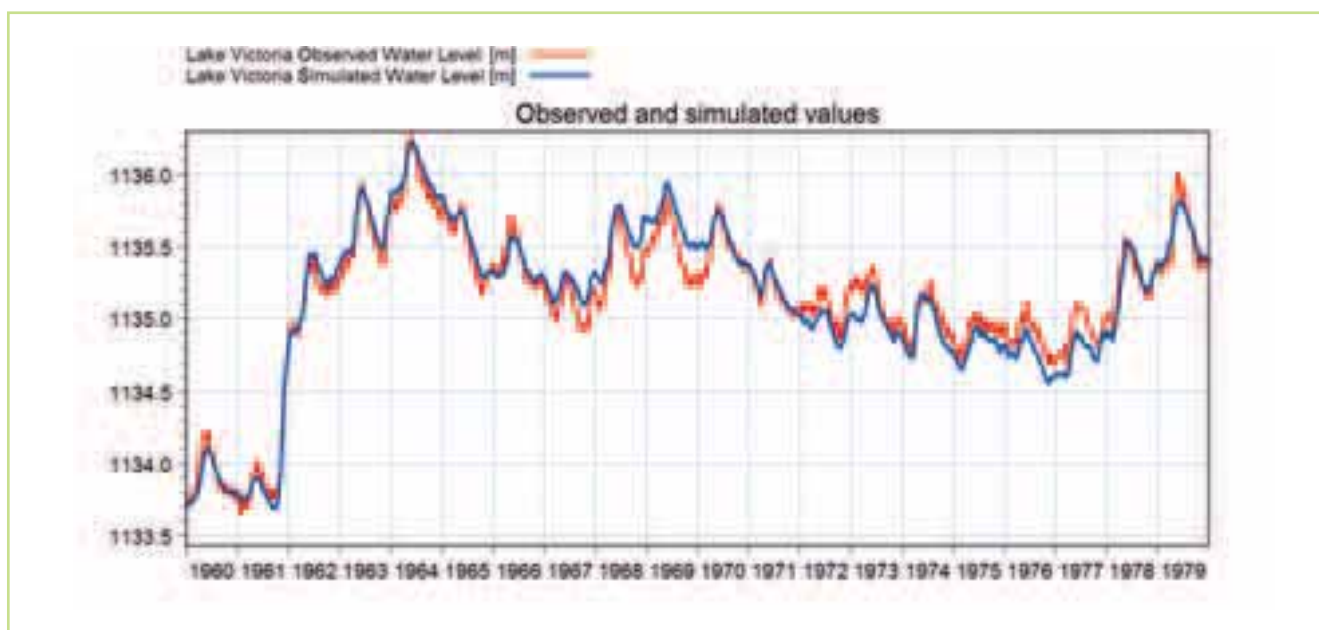
Figure 5.19 Comparison between observed (red) & simulated (blue) water levels at Lake Victoria for the modelling period 1960-80
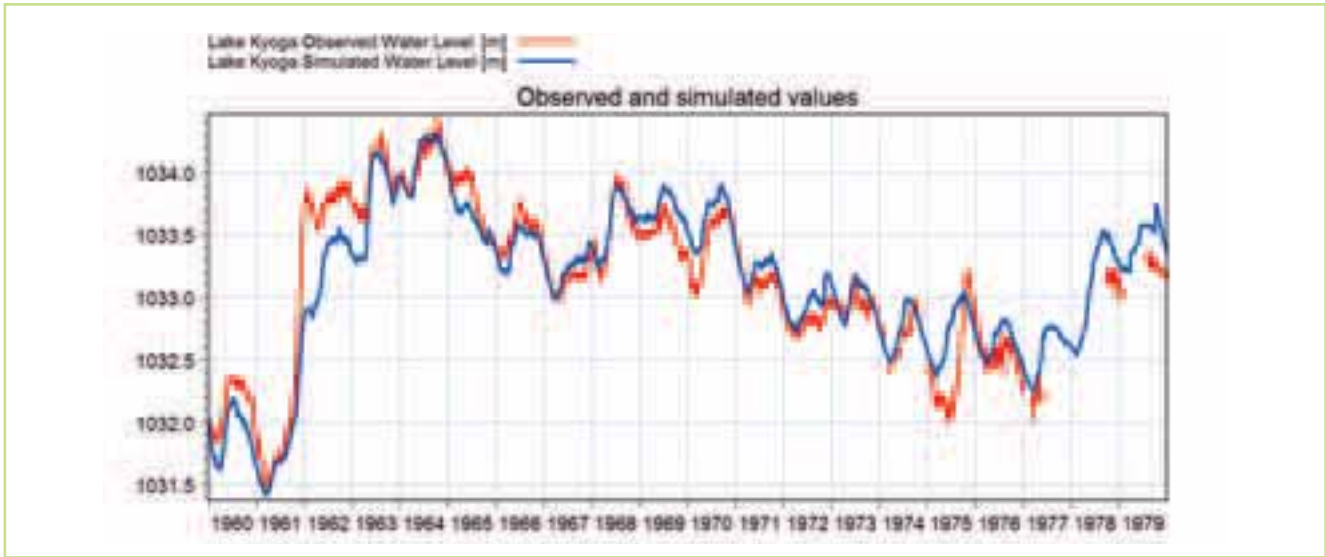
Figure 5.20 Comparison between observed (red) & simulated (blue) water levels at Lake Kyoga for the modelling period 1960-80
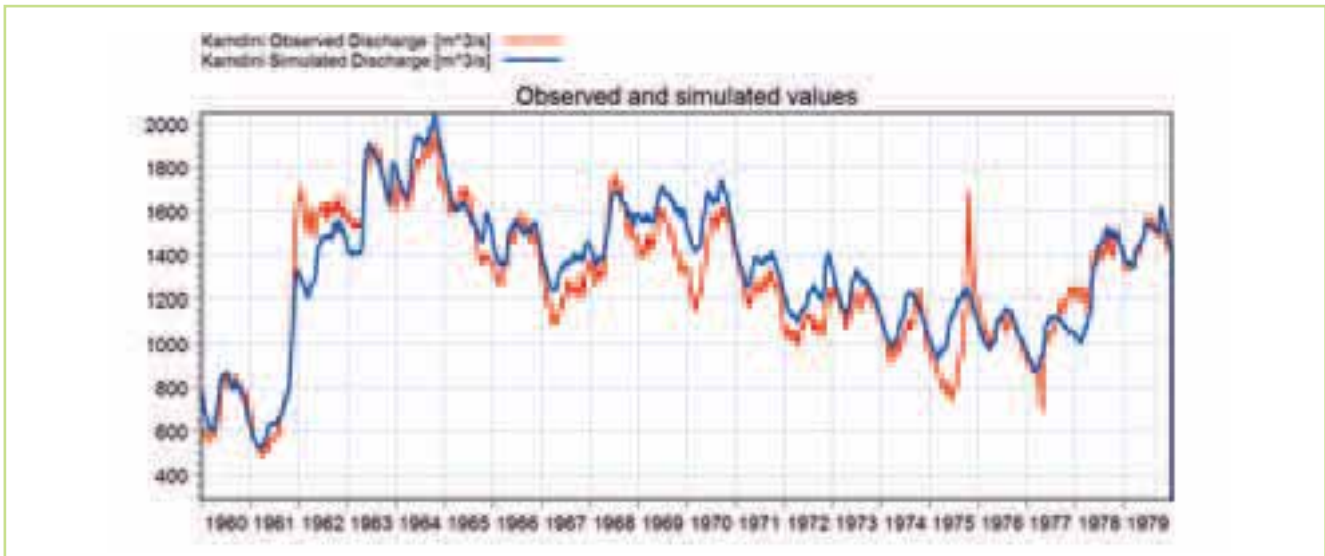
Figure 5.21 Comparison between observed (red) & simulated (blue) discharge at Kamdini (83206) for the modelling period 1960-80
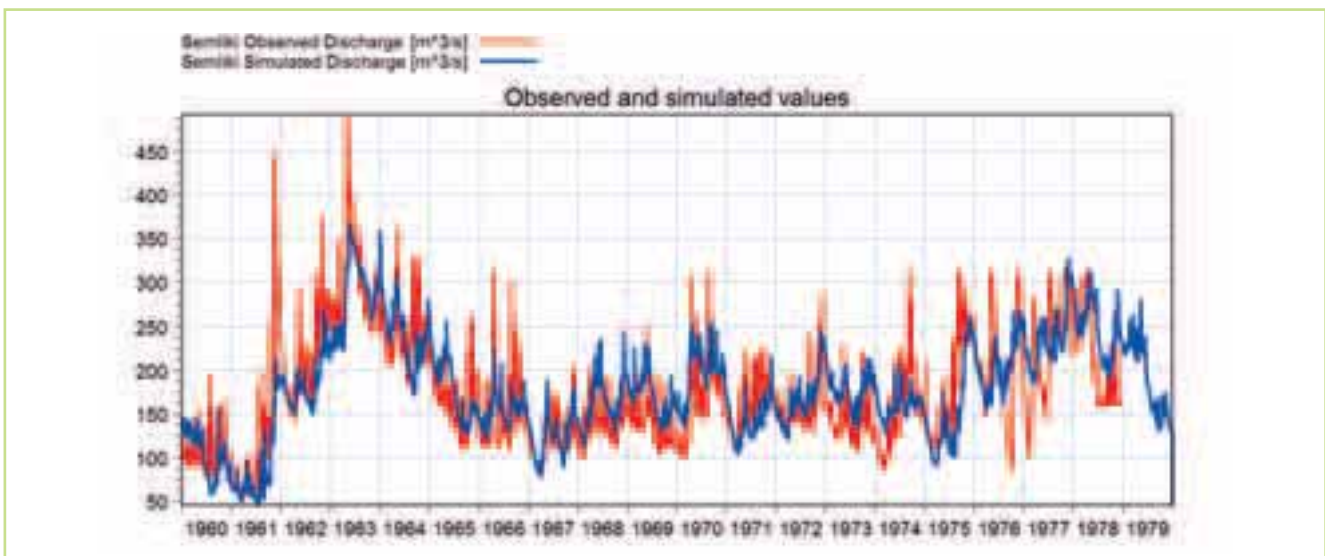
Figure 5.22 Comparison between observed (red) & simulated (blue) discharge at Semliki for the modelling period 1960-80
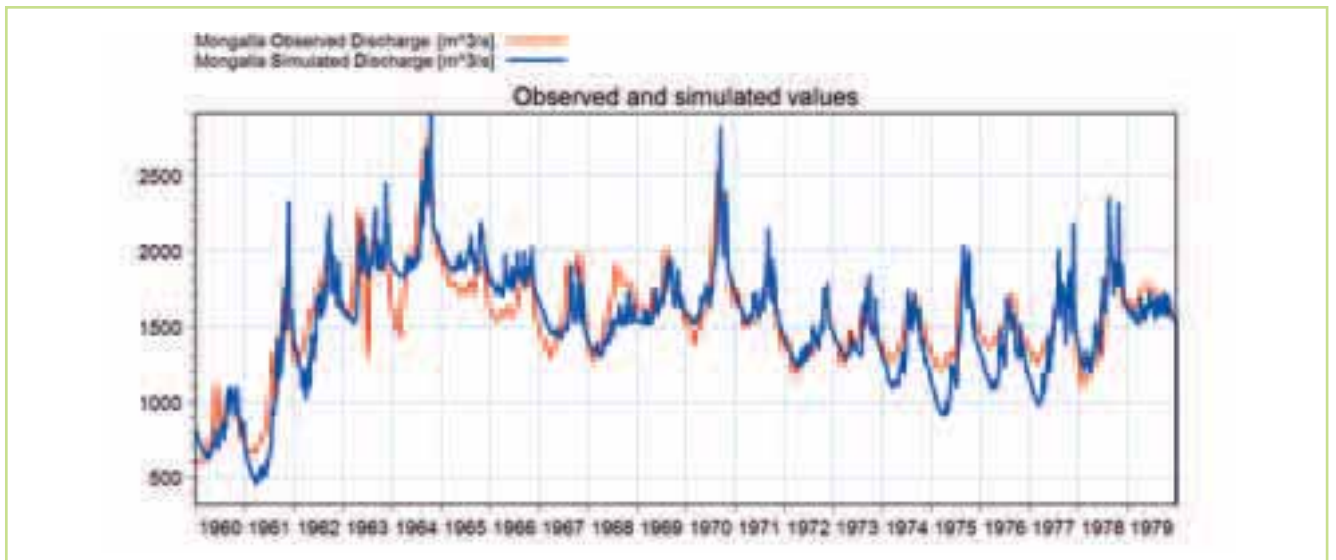
Figure 5.23 Comparison between observed (red) & simulated (blue) discharge at Mongalla for the modelling period 1960-80

Figure 5.24 The Sudd

The simulations of the water levels for Lake Victoria and Kyoga are of very good quality and given that there are good estimates of the HVA curves for these lakes, it is expected that the overall water balance for these lakes is well represented in the model. The simulations presented for the discharge are also satisfactory and the main features and dynamics are well captured by the simulations. In light of the overall quality of the data available, the overall quality of the calibration for the Lake Victoria Basin is very good and an excellent starting point for the assessment of the impacts of climate change.

5.5.3 The Sudd

The Sudd is a series of wetlands in the southern part of Sudan, extending along the Bahr el Jebel from Mongalla in the south to the confluence with the White Nile in the north. The Sudd receives water from Lake Albert in the south (Lake Victoria region), and due to evapotranspiration from flooded areas the outflow is, on average, less than half of the inflow. The Bahr el Jebel contributes with around 14% of the total annual flow in the Nile. As the evaporation losses in the Sudd accounts for around 50% of the total inflow to the Sudd, this area has an important impact on the water balance for the whole Nile Basin.

Figure 5.24 illustrates the Sudd and some of the main observation stations.
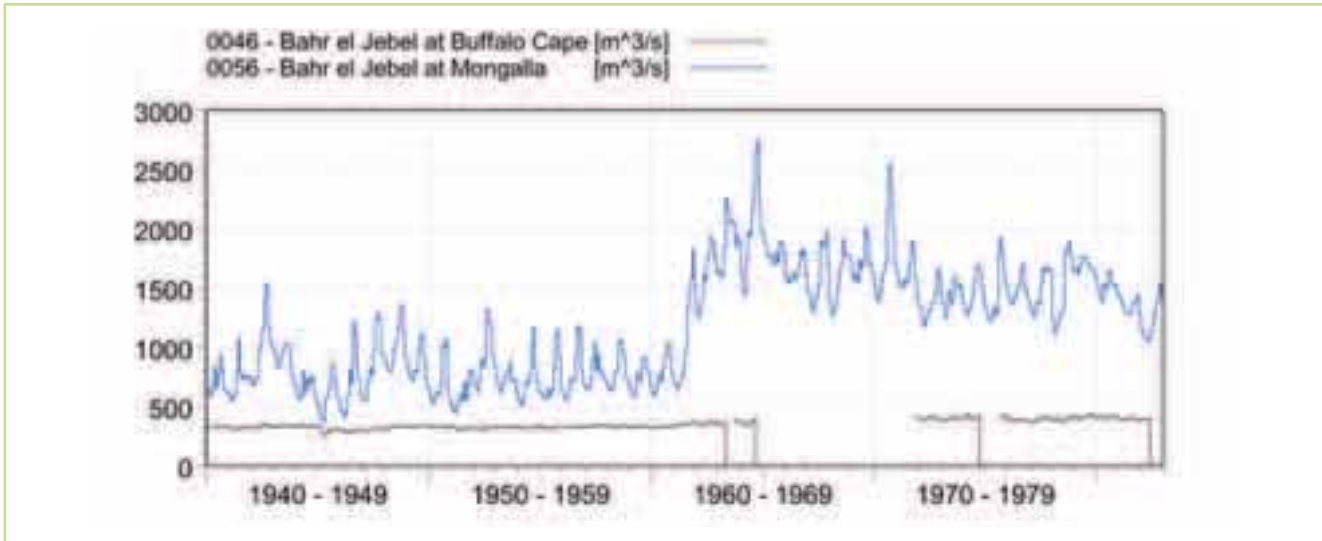
Figure 5.25 Observed discharge at Mongalla & Buffalo Cape

The part of the Nile between Mongalla and the confluence with the White Nile and the Sobat is named Bahr el Jebel, or just the Sudd. This part of the Nile is, in hydrological terms, one of the most complex part of the Nile reaches, as a large part of the area gets inundated every season, and significant water losses occurs due to open water evaporation and transpiration from the vegetation in the wetlands. The below figure illustrates the observed discharge at Mongalla and Buffalo Cape. The following is observed:

- The inflow to the Sudd is controlled by the outflow from Lake Albert (Lake Victoria re-gion), where a significant seasonal pattern is visible at the observed discharge at Mongalla.
- The observed discharge at Buffalo Cape is a factor 2 to 5 lower than the inflow, and the seasonal variation observed at the inflow is almost disappeared. The outflow from the Sudd is more or less constant throughout the season.
- The observed discharge at Buffalo Cape is varying between 350 and 450 m3/s, while the inflow at Mongalla is varying between 1050 and 2750 m3/s, all values for the period 1940 to 1983.
- The increase in the discharge in the period around 1961, caused by higher water levels in Lake Victoria, is visible at the Mongalla station, but there is no significant change at the observed discharge at Buffalo Cape. Note that the station at Buffalo Cape is missing data in the period from 1963 to 1972.

The observed discharge at Mongalla and Buffalo Cape illustrates some of the significant hydro-logical processes in the Sudd, resulting in a significant water loss and a change and dampening of the river hydrograph. The main reason for this is the seasonal

flooding of large areas within the Sudd resulting in retaining of large volumes of water on the flood plains, and subsequently evaporation loses from the flooded areas.

5.5.3.1 Bahr el Zeraf

The Bahr el Zeraf diverges from the Bahr el Jebel about 200km downstream of Bor and re-joins the main river, about 100km downstream of Lake No. The below figure illustrates the location of Bahr el Zeraf and the inlet and outlet to the Bahr el Jebel.

The Bahr el Zeraf is connected to the Bahr el Jebel through a channel, see the above figure, where a part of the flow in Bahr el Jebel is diverted. Approx. 30 pct. of the flow run through the Bahr el Zeraf and approx. 70 pct. runs through the Bahr el Jebel. The distribution to the Bahr el Zeraf is according to the available flow observations data slightly higher; 35-36 pct. during March through May and 40-42 pct. in October and November.

The hydrology in the area of the Bahr el Jebel-Bahr el Zeraf diversion is rather complex as the water flows in several parallel channels. The total discharge in such systems has to be found by summing over discharge measurements in multiple channels, and there could potentially be large errors in the observed flow. Further downstream of the 'actual' diversion the total discharges of the Bahr el Jebel and the Bahr el Zeraf can be measured with sufficient accuracy in a single main channel.

5.5.3.2 Model development

The main purpose has been to model the water losses and transformation of the inflow hydrograph when passing through the Sudd, where the hydrological processes should be conceptualised using the MIKE BASIN model. The main processes to
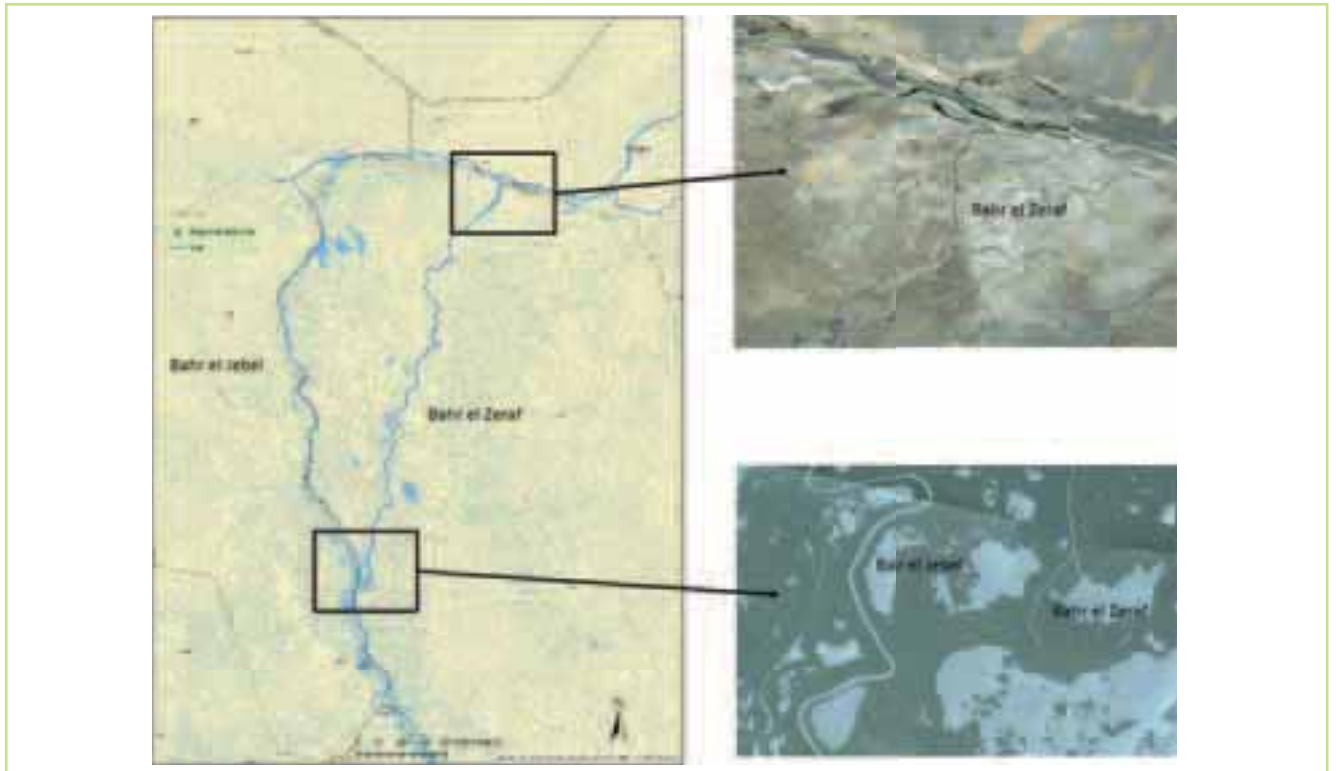
Figure 5.26 Location of Bahr el Zeraf with GOOGLE Earth images of the inlet & outlet to the Bahr el Jebel

be conceptualised in the developed model are:

- Evaporation losses and the correlation between discharge and evaporation losses.
- Dampening of the hydrograph caused by the detention of the water as it flows across the flood plains.
- The influence of local rainfall, as local rainfall events normally coincide with the release of water from the Lake Victoria region.
- The flow in the Bahr el Zeraf is represented using a simple rule of 30 % of the flow in the Bahr el Jebel is diverted into the Bahr el Zeraf.

As MIKE BASIN is a lumped water resource model, it will not be possible to make a distributed description of the processes along the whole Bahr el Jebel from Mongalla to the confluence with the White Nile. For this reason it has been decided to divide the stretch into a number of sections, based on the changes on the observed hydrograph.

5.5.3.3 Conceptual representation of the hydrological processes

The flooding, evaporation and rainfall processes are represented in the model by a simple reservoir description, where the relationship between the water level and the surface area is used to describe the evaporation from the open water bodies.

The rainfall is expected to have some effect on the flooding processes if the rainfall coincides with the large discharge events from the Lake Victoria region.

It is expected that the rainfall has the following effect on the hydrology in the Sudd:

- Rainfall occurring in areas that are inundated is expected to increase the flood, and should be included as water that potentially could contribute to the flow in the Bahr el Jebel.
- Rainfall occurring outside of the inundated areas is not expected to create run-off, as it most likely would evaporate or infiltrate into the ground. For this reason rainfall outside of the inundated areas are not seen as water that could contribute to the flow in the Bahr el Jebel.

Rainfall is handled in the way that rainfall time series are added to the reservoir description, meaning that rainfall will only occur on the area that are defined as open water bodies.

The evapotranspiration will be handled in the same way, meaning that evapotranspiration occurring outside of the inundated areas will not be described by the model. Hence only evaporation (including transpiration from swamp vegetation) from the open water bodies will be described by the model.

The conceptual model of the Sudd will be based on a series of reservoirs, where each reservoir will describe the relationship between the water level and the flooded area, and the subsequent rainfall and evaporation on these areas. In order to describe the change in the hydrograph one or two reservoirs are used on each stretch of the river, where:

- The first reservoir describes the loss during a situation with normal or little flow. Minor water loos and almost no change to the hydrograph.
- The second reservoir describes the water loss during a situation with high and extreme discharge. The level/area/volume relationship is designed in order to describe the water loss during periods with high and extreme discharge, and with no change in periods with low discharge. For this reservoir the level/area/volume curve is designed so that there are no area for small water levels, but a steep increase in the area when the water level exceeds an elevation which described the bank elevation, where flooding occurs.

It should be noted that all the levels used in the reservoirs are empirical, and are not based on actual values from the DEM. The reason for this is that the models works on a volume basis and as should is describes the relative change in volume and elevation, more than the actual elevation values. The rainfall and evaporation values are based on CRU values as the available climate data for the Sudd is not sufficient.

5.5.3.4 Calibration

In the model the Bahr el Jebel has been divided into three stretches i) Malakal to Bor, ii) Bor to Kenisa and iii) Kenisa to Buffalo Cape. The hydrological processes within each of the stretches are conceptualised based on the changes in the hydrograph on each of the starches. The main approach is as follows:

- The hydrological processes are conceptualised using two reservoirs
- The first reservoir describes the loss during a situation with normal or little flow. Minor water losses and almost no change to the hydrograph.

- The second reservoir describes the water loss during a situation with high and extreme discharge. The level/area/volume relationship is designed in order to describe the water loss during periods with high and extreme discharge, and with no change in periods with low discharge.

The reservoirs are inserted at Bor, Kenisa and Buffalo Cape. The processes along the stretch to Buffalo Cape are represented using a single reservoir, as the loss on this stretch is small.

It should be noted that the description is based on the analysis of the available discharge hydrographs, and is not an exact description of the actual situation. Especially the evaporation losses and the level/area/volume curve could be refined in order to achieve a better match.

The changes on the hydrograph on the stretch from Bro to Kenisa are shown in Figure 5 27. There are significant reduction in the discharge values and the variation between the dry and the wet season is reduced, compared to the stretch between Malakal and Bor.

The simulated discharge at the Kenisa station is presented at and the following could be noted:
- The model captures the general level of the discharge, and the low and high events are in sync with the observed values.
- The model generally overestimates the high flows and underestimates the low flow. This could be modified by looking closer into the reservoir representation.
- The change in the discharge around 1961 is represented by the model.
- On this stretch the model could be used to evaluate both flood and drought issues.
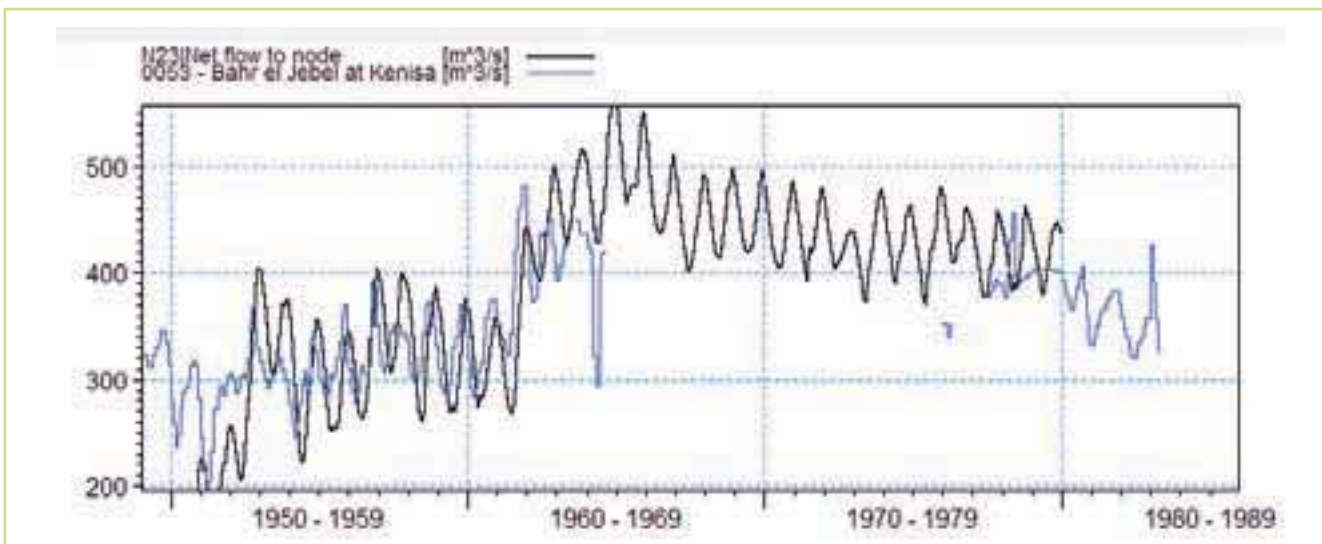
Figure 5.27 Simulated (black line) & observed (blue line) discharge at Kenisa
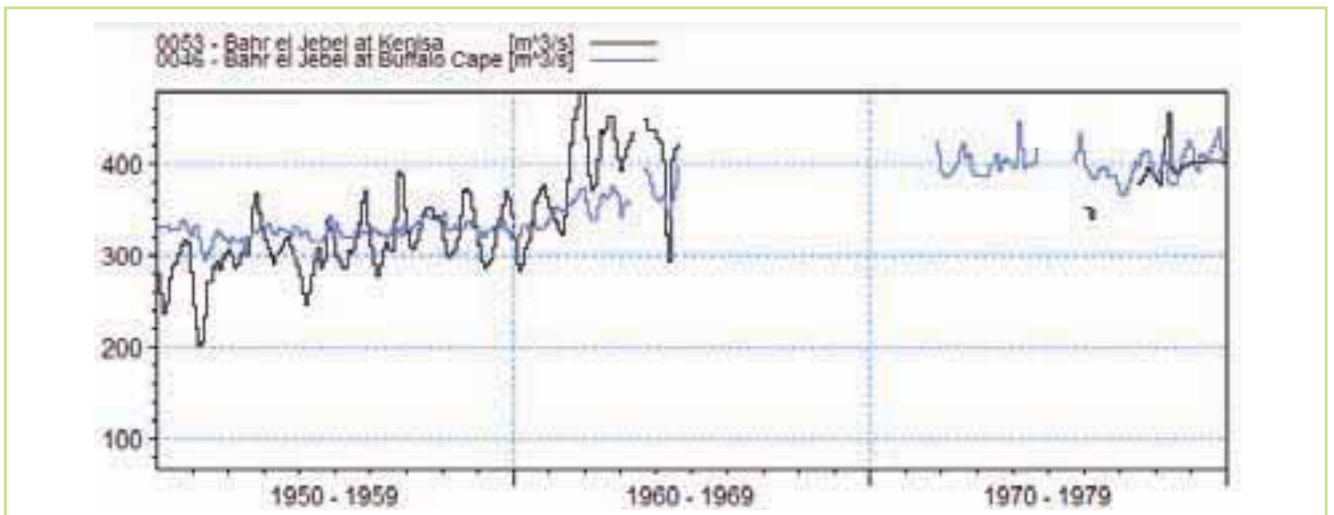
Figure 5.28 Observed discharge at Kenisa (black line) & Buffalo Cape (blue line)
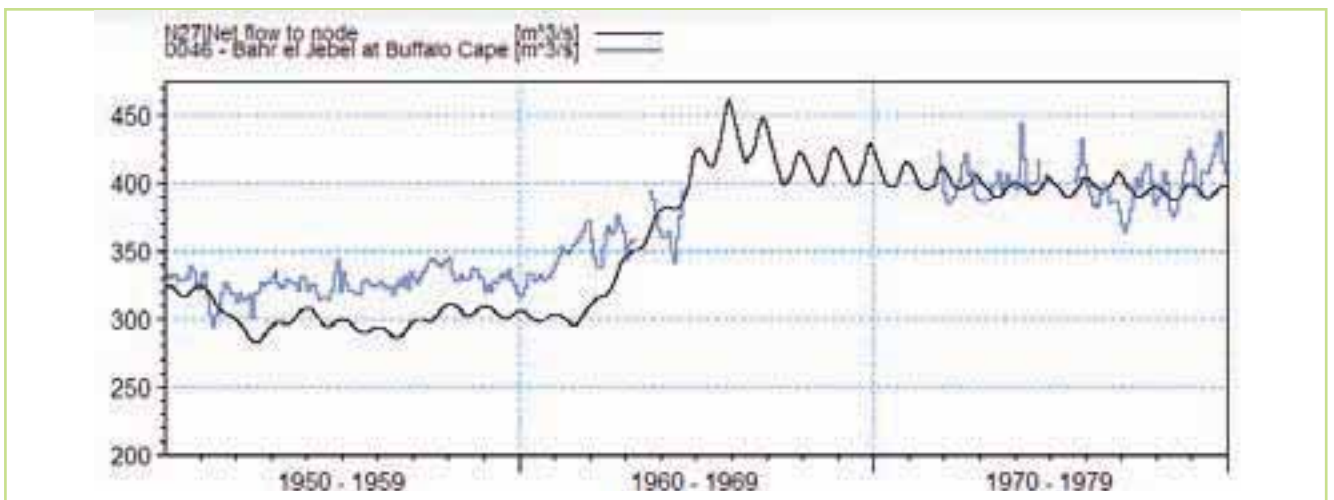
Figure 5.29 Simulated (black line) & observed (blue line) discharge at Buffalo Cape

The changes on the hydrograph on the stretch from Kenisa to Buffalo Cape are shown in Figure 5.28. There are limited losses on this stretch, especially during the dry period, where the discharge in some cases is higher than at Kenisa. It is presently unknown if this is caused by additional flow to Bahr el Jebel on this stretch or if the observed discharge values at Buffalo Cape are uncertain.

During the wet period the high events are further dampened, and the seasonal variation in the flow at Bahr el Jebel is almost gone at this station. Hence the flow is almost constant throughout the year. It could also be noted that the impact on the increased discharge from the Lake Victoria region is very limited at this station. This implies that any climate change impact in the Lake Victoria region has a limited impact on the downstream flow regime.

The simulated discharge at the Buffalo Cape station is presented at Figure 5.29 and the following could be noted:

- The model underestimates the discharge prior to 1961.
- During the period after 1961 the model simulates

the discharge in the same magnitude as the observed values.
- The model doesn't simulate the fast response that is noticeable in the observed data. Local rainfall events are most likely causing the fluctuations in the observed data, and this is not captured accurately in the model.

5.5.4 Bahr-El-Ghazal

The Bahr el Ghazal catchment drains the western part of the highlands in Sudan, and due to areas with rainfall rates of more than 1000 mm/year the upper part of the catchment contributes with significant flow to the lower basin. In this part of the basin almost all the water is lost due to evaporation, and the contribution to the Nile is almost negligible. For that reason it has been decided not to represent the Bahr el Ghazal basin in the model, and as such the internal hydrological processes in the basin are not represented by the model.

5.5.5 Sobat

The Sobat basin is located upstream of the White

Figure 5.30 The Sobat catchment

ranging from the Ethiopian highland in the upstream part of the Baro, the Marchar wetlands in the downstream part of the Baro, the large plains in the southern part of the Pibor basin, and the flood plains along the Sobat river.

As the hydrological processes within the basin varies, the basin are divided into the following sections:

1. Sobat river downstream the confluence of Baro and Pibor rivers.
2. Pibor basin
3. Baro river from the confluence with Pibor, and upstream to Gambeila.
4. The part of the Baro catchment upstream of Gambeila.

Each of the sections are briefly described in the following sections.

5.5.5.2 Sobat River between Nasir & the outlet in White Nile

The downstream part of the Sobat basin, comprises of the Sobat river which flows from the con-fluence between Baro and Pibor River down to the outlet in the White Nile. This part of the basin is fairly well described in earlier studies. There a few tributaries along the Sobat River, where Twalor and Wakau are the only measures tributaries. The main hydrological processes in this part are conveyance of the water until the White Nile, and flooding of the surrounding areas during periods of high flow. Some of the key findings in earlier studies are:

- Apart from rainfall and evaporation over flooded areas, and absorption on newly flooded land, the river loses and gains some water through the tributaries Wakau and Twalor, but otherwise the river is self-contained and acts aimply as a reservoir. It's principal effect is to delay the passage of the flood by about a month.
- The Sobat has fairly limited losses and gains in normal years, and the main effect is the attenuation of the flow hydrograph by storage within the flood plan.

5.5.5.3 Pibor catchment

The Pibor basin drains an area of around 109,000km2, including part of the Ethiopian highland south of the Baro basin, but also a wide area of plain east of the Sudd. Although this basin is almost 2.5 times larger than the Baro basin, the average flow is around three times smaller than the average flow from the Baro basin. The main contribution to the Pibor rivers comes from the three tributaries Khor Makwai, Khor

Nile, and connects with the White Nile at Malakal. The flow from the Sobat is in the same order as the flow from the Sudd, and is an important part of the total flow in the White Nile. The Sobat has the Baro and the Pibor as the largest tributaries. The Baro (41 400 km2) drains an area of the Ethiopian mountains east of Gambeila rising to peaks of 3300 m. The Pibor (109 000 km2) receives the Gila and Akobo from the mountains south of the Baro basin, but also drains a wide area of the plains east of the Bahr el Jebel, from which there is little runoff in most years but high flows in some years. During years of heavy rainfall on the Baro and other Ethiopian tributaries, high flows are spilled from the river system to the Machar marshes and other wetlands. In general the hydrology of Sobat has not been studied in detail, and only sparse data and information exist. The belown figure illustrates the Sobat and some of the main rivers.

5.5.5.1 Hydrological processes in the Sobat

The hydrology of the Sobat basin is complicated as the area consists of a number of significant features,

Gila and Akobo, which all drains part of the Ethiopian highland. During years with rainfall equalling the average or below the average most of the annual flow in the lower part of the Pibor is supplied by the Ethiopian tributaries. During exceptional years the southern part of the Pibor basin seems to have a large contribution to the flow.

In general the hydrological processes in the Pibor basin is controlled by the climate and runoff from the Ethiopian highlands, while there in some years will be some contribution from the southern part of the basin. The main processes in the basin will be runoff and conveyance throughout the system.

5.5.5.4 Baro River downstream of Gambeila

The part of the Baro River between Gambeila and the outlet to the Sobat is probably the area with the most complicated hydrology. This part has been investigated in several studies but is still an area that is not fully understood, mainly caused by the lack of hydrological data.

Downstream of Gambeila the Baro loses around 10 % of the flow to the Adura River. This leaves from the left bank of the Baro, and returns to the Baro downstream. The most significant spill from the Baro is towards the Machar marshes. This spill is concentrated in June to November, which are the months with high flow values in the Baro river.

The Machar marshes are connected to the White Nile through the Khor Adar, but it's not clear if any or how much of the water that is spilled from the Baro that reaches the White Nile

5.5.5.5 Baro River upstream of Gambeila

The area upstream of Gambeila is draining the Ethiopian highland, and this area is the main contributor of water from the Sobat basin.

The hydrological processes are dominated by runoff processes from the highland, and conveyance through the river system. The flow is well defined from the observations at the station at Gambeila.

5.5.5.6 Model development

The main purpose of the model is to describe the runoff and flooding processes in the basin to such a level that the model could be used to evaluate impacts from climate changes.

The main processes to be conceptualised in the developed model are:
- Runoff processes from the Ethiopian highlands
- Runoff processes from the plains east of the Sudd

- Dampening of the hydrograph caused by the detention of the water as it flows across the flood plains
- Losses due to evaporation from wetlands and flooded areas

As MIKE BASIN is a lumped water resource model, it will not be possible to make a distributed description of the processes ain the Sobat basin. For this reason it has been decided to divide the basin into a number of sections, and the model development will be described for the following sections:
- Ethiopian highlands upstream of Gambeila
- Baro river downstream of Gambeila
- Pibor basin
- Sobat river between Nasir and the outlet in the White Nile

The model development for each of the above areas will be described in the following sections.

5.5.5.7 Ethiopian highlands upstream of Gambeila

The upstream part of the Baro river, upstream Gambeila, is modelled as a single runn-off catchment. The catchment is shown on the below figure.

Figure 5.31 Catchment for the part upstream of Gambeila
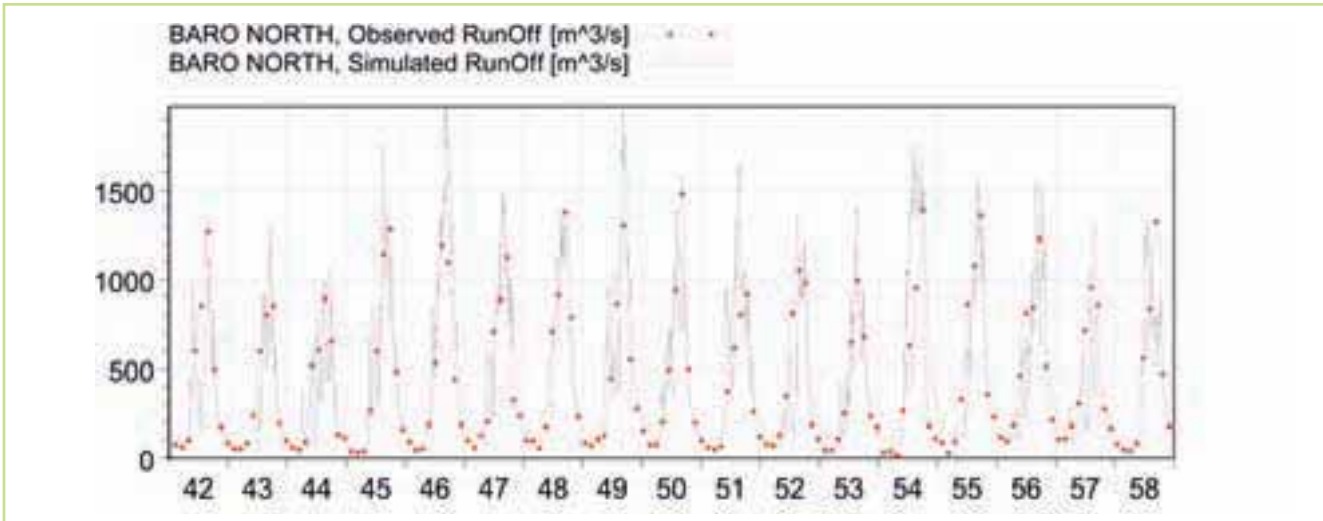
Figure 5.32 Simulated & observed runoff

The run-off modelling is performed with the following input:

- Catchment area is 23,543 km2
- Nile DST rainfall record from the station at Gambeila. Daily records for the period 1905 until 1980
- Runoff observation from the Nile Encyclopedia station at Gambeila. 10-daily records for the period 1928 until 1959.
- PET is extracted from the CRU dataset as monthly data for the period 1901 until 2009.

The runoff model is calibrated for the period 1942 to 1959, as this period has sufficient runoff and rainfall data.

This catchment is where the main part of the runoff from the Sobat catchment is generated, and it is vital for a good description of the runoff processes in the Sobat. The runoff model yields acceptable results, and this part of the model could be used in scenario evaluations.

5.5.5.8 Baro river downstream of Gambeila

This part of the Baro river is complicated as there are spill to the Marchar wetland and the Adura river. Figure 5 33shows the recorded flow at Gambeila and the outlet into the Sobat. When looking at the observed discharge records at Gambeila and the confluence with the Sobat river, it's evident that the spill limits any flow above 50,000,000 m3/day or 580 m3/s. A closer look at the flow records shows that there is some delay in the flow, which is probably caused by flooding. To simplify the processes on this stretch, the following is implemented:

- As the physical description of the spill on this stretch is poorly described and understood, the model is developed based on a simple approach that does not allow any flow above 580 m3/s. This is implemented in the MIKE BASIN model using a bifurcation node, where the flow above 580 m3/s is diverted, and a water user which removes all the flow above 580 m3/s.
- The delay of the flow is modelled using a routing with a time delay of 1 month.
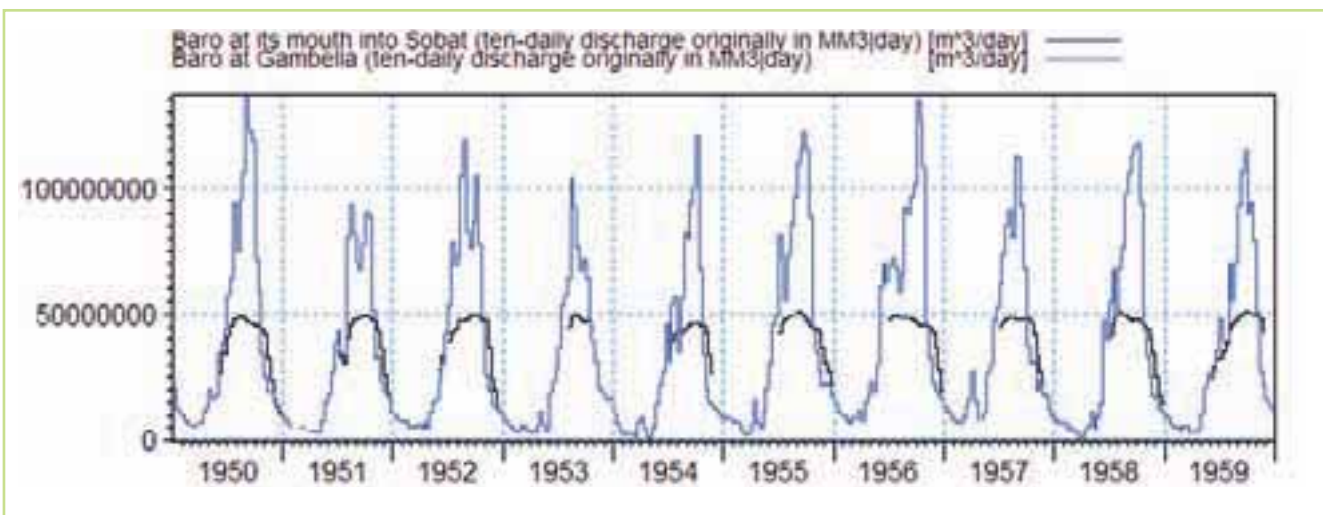
Figure 5.33 Flow record at Gambeila & at the outlet to the Baro river
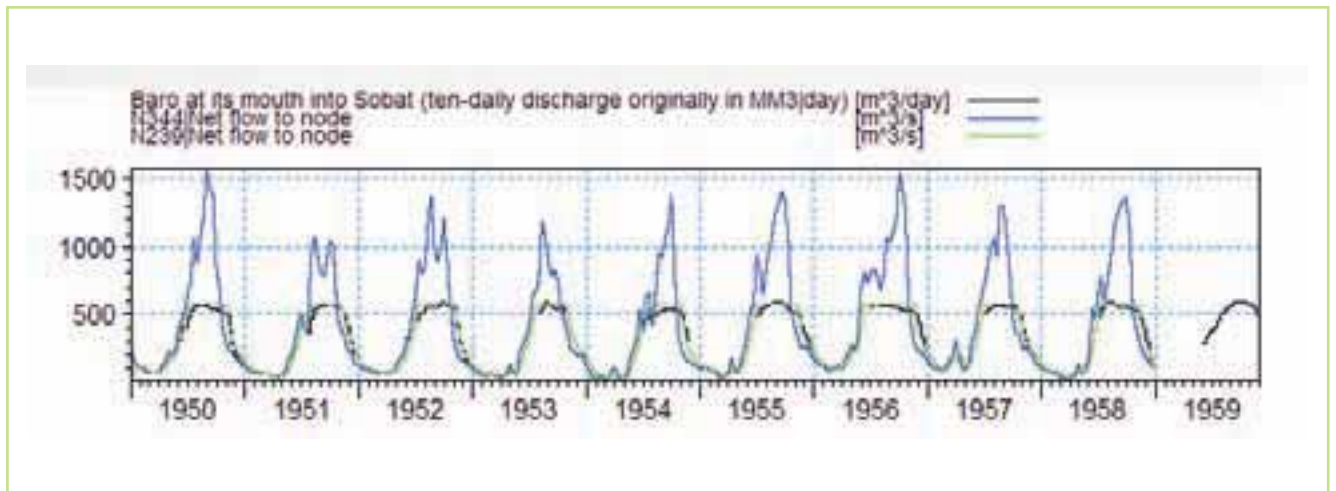
Figure 5.34 Observed flow at Gambeila (blue line), observed flow at the outlet to the Sobat river (black line) & the simulated flow at the outlet to the Sobat (green line)

Based on the simulated flow at the outlet from the Baro, the simple approach seems to represent the hydrological processes and the spill on this stretch, to a degree where the model could be used for climate scenarios.

5.5.5.9 Pibor basin

The Pibor basin drains the southern part of the Ethiopian highlands, and the plains in the southern part of the Sobat basin. The Pibor basin contributes with approximately 25 % of the total flow from the Sobat basin.

The model is developed based on the available flow records, and a runoff model is developed for the Akobo, Mokwai and Pibor rivers, as there are no flow records for the Gila river. For the Gila river the runoff processes are described using the same parameters as for the Akobo river. The runoff is calibrated against observed flow records for the period 1929 to 1934, as this is the only period with reasonable data. Nile DST stations are used to describe the rainfall, and CRU data is used for the PET values.

The simulated runoff from the sub-catchments within the Pibor basin are added to the MIKE BASIN model. The flood processes and subsequently changes to the hydrograph and loss by evaporation, is conceptualised by the use of a simple reservoir.

The correlation between observed and simulated flow at the Pibor basin is not very good. The reason is mainly the lack of rainfall data, and missing description of the hydrological processes in this part of the basin.

5.5.5.10 Sobat river between Nasir & the outlet in the White Nile

The downstream part of the Sobat river is described using a routing method with a delay factor of 15 days. The simulated and observed flow from is shown on the below figure.

In general the model has a reasonable representation of the flow from the Sobat basin, and the model is evaluated as being acceptable for climate simulations.

5.5.6 The White Nile

The White Nile is defined as the stretch between the
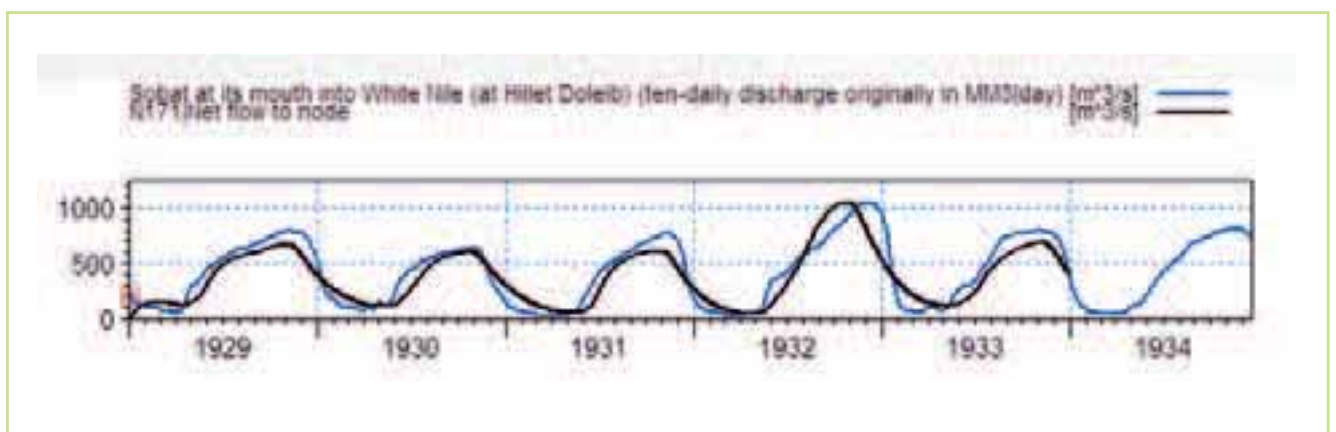
Figure 5.35 Simulated (black line) & observed (blue line) from Sobat river (at the outlet to the White Nile)

outlet from the Sobat and the junction with the Blue Nile at Khartoum. The stretch is around 840km long, and is almost flat. The White Nile has a fall of 13 meters over the 840km strech.

There are no major tributaries on this stretch, and the inflows are sporadic and relatively small.

5.5.6.1 Hydrological processes in the White Nile
The White Nile, between Malakal and the junction with the Blue Nile, is 840km long, and the river has a fall of around 13m along the stretch. The White Nile receives the outflow from the Sudd, which provides the baseflow component, as the outflow from the Sudd is almost constant throughout the year. The more seasonal contribution comes from the Sobat basin. There is no significant inflow along the White Nile, and the main hydrological processes are conveyance through the system, and attenuation and evaporation loses from the flood plain storage.

5.5.6.2 Model development
The main purpose of the model is to describe the runoff and flooding processes in the White Nile to such a level that the model could be used to evaluate impacts from climate changes.

The main processes to be conceptualised in the developed model are:
- Dampening of the hydrograph caused by the detention of the water as it flows across the flood plains.
- Losses due to evaporation from wetlands and flooded areas

As MIKE BASIN is a lumped water resource model, it will not be possible to make a distributed description of the processes in the basin to the White Nile. For this reason it has been decided to divide the basin into a number of sections, and the model development will be described for the following sections:
- Malakal to Melut
- Melut to Renk
- Renk to Kosti
- Kosto to Jebel Aulia
- Jebel Aulia to Mogren

It could be noted that the limited observation data for the Kosti and the Renk catchment makes it difficult to evaluate the hydrological processes in these catchments, and it could be argued that they should be treated as a single catchment. It has however been decided to keep them as separate catchments in case more detailed data from the flow stations should appear.

A total of five catchments have been delineated in the sub-basin. The representation includes five catchments, one reservoir, one hydropower station, and two water use locations. Rainfall-runoff processes are active in all catchments. All rainfall-runoff processes are simulated using the NAM model with a single-layer representation of groundwater. Linear reservoir routing is active for all river reaches except those just downstream of the Jebel Aulia Reservoir. Evaporation and flood processes are conceptualized using a reservoir where the level – area – volume relationship represents the flooding and the subsequent evaporation loss.

5.5.6.3 Malakal to Melut
The Melut catchment is the southernmost catchment in the White Nile sub-basin, located just downstream of the Malakal flow gauge.

The model development for the Melut catchment is done with the following input:
- Area of delineated catchment is 50109 km2
- Rainfall runoff modeling using 6 Nile DSF rainfall stations. Weighthed rainfall calculated based on Thiessen polygons.
- Potential evapotranspiration is based on CRU
- NAM model is calibrated to get zero runoff during the period 1960 to 1980
- ET and flood processes are represented using a reservoir in MIKE BASIN. Average monthly values are used to describe the ET losses. The area - level – volume curve are fitted to give a reasonable ET response.
- The MIKE BASIN model is calibrated against the flow station at Melut.

Figure 5.36 shows the observed flow at Malakal (black line), the observed flow at Melut (red line) and the simulated flow at Melut (blue line). The following could be observed:
- The model has an acceptable description of the flow in the dry season. During this period there is limited change to the hydrograph.
- The model captures the high events well during most of the years but are simulating too high flow during the highest events. This is due to how the flood area is described, and it should be noted that the relationship between the flow and the flood area is not known, and is one of the parameters that are adjusted during the calibration.
- In general the model is evaluated as being able to capture the flow regime making the model able to be used for climate simulations.
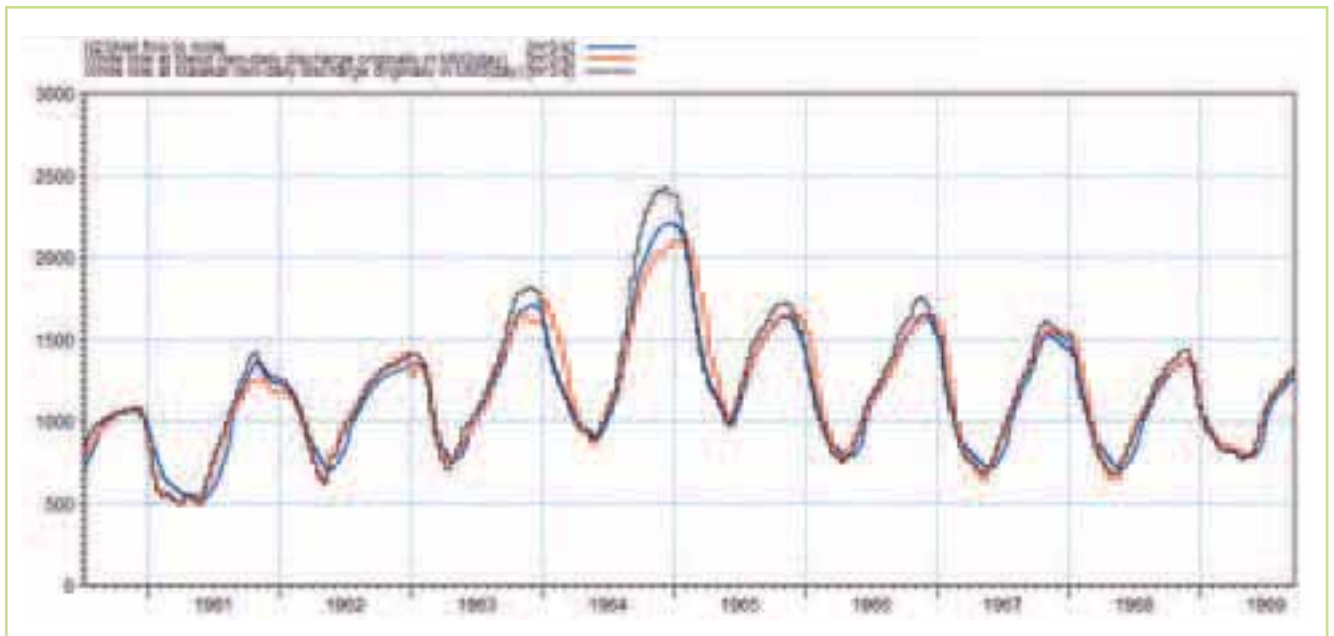
Figure 5.36 Observed flow at Malakal (black line), observed flow at Melut (red line) & simulated flow at Melut (blue line)

5.5.6.4 Melut to Renk

The stretch between Melut and Renk is difficult to evaluate as the available flow records at Renk only covers the period between 1928 and 1947. As the available rainfall do not have a good coverage in this period, this stretch is not calibrated in the MIKE BASN model.

5.5.6.5 Renk to Kosti & Kosti to Jebel Aulia

The stretch from Renk to Jebel Aulia contains two flow stations. The flow stations at Kosti only contains flow records for the period 1912 to 1913, and is not suitable for analyzing the hydro-logical processes on the stretch, and will not be used to calibrate the model. Downstream of Jebel Aulia there is another flow stations with flow observation for the period 1944 to 1998 (ten-daily), but as the flow at this stations is influenced by the release from the Jebel Aulia Dam, it's not possible to use this station for evaluation of the hydrological processes on the stretch. The following conceptual approach will be used to simulate the hydrology between Renk and Jebel Aulia:

- The catchment to Renk (70,628 km2) and Jebel Aulia (77,544 km2) are digitized and rainfall runoff models are developed for both catchments.
- The rainfall runoff models are calibrated based on an assumption of zero flow during the current climate. The same parameters are used for both catchments.
- The Jebel Aulia reservoir is added and the evaporation losses on this stretch are handled at the reservoir.

- The irrigation loss upstream and at the Jebel Aulia reservoir is added to the model.
- The operation rules of Jebel Aulia are implemented in the model and control the operation and outflow from the dam.

The Jebel Aulia Reservoir is operated as a rule curve reservoir with three rules active: a flood control rule, and two rules controlling releases to demand sites that are directly connected to the reservoir (irrigation and hydropower). All rules are implemented as monthly time series. The flood control rule is the same as the flood control rule used in the NBI/ENTRO Nile Basin baseline model.

The following could be noted:
- The model captures the trends in the observed hydrograph well, and both the low and high periods are captured.
- There are deviations from the observed hydrograph throughout the period. This probably implies that the actual used flood control rule is not used as strict as it is in the model. Meaning that the real flood control operation might deviate from the one used in the model.
- In general the model captures the outflow from Jebel Aulia well, and it's considered ac-ceptable for use in the climate scenarios.

5.5.6.6 Jebel Aulia to Mogren

The Mogren catchment is located on the White Nile between the Jebel Aulia dam and the confluence with the Blue Nile. The model development for the
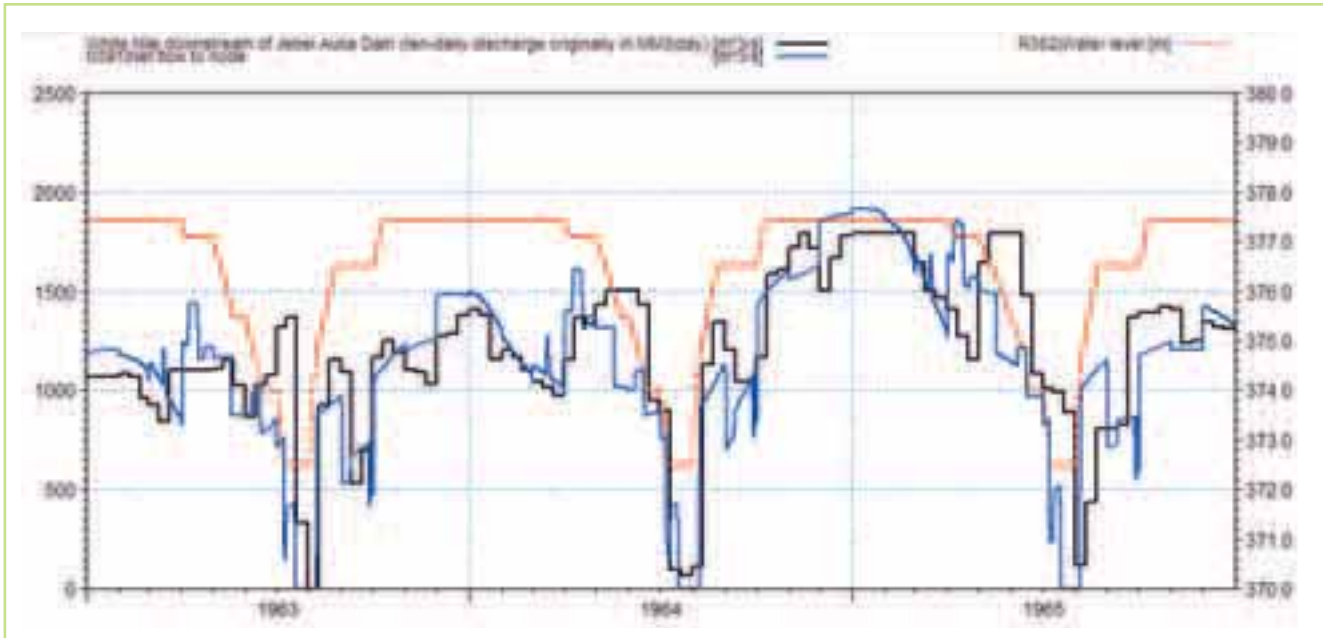
Figure 5.37 Observed outflow from Jebel Aulia (black line), simulated outflow from Jebel Aulia (blue line) & simulated water level at Jebel Aulia (red line)

Mogren catchment is done with the following input:

- Area of delineated catchment is 3109 km2
- Rainfall runoff modeling using 3 Nile DSF rainfall stations. Weighthed rainfall calculated based on Thiessen polygons.
- Potential evapotranspiration is based on CRU
- NAM model is calibrated to get zero runoff during the period 1960 to 1980
- As the hydrological processes on this stretch is not clearly understood and as the stretch is fairly short, the water flow is modeled using a linear

reservoir routing with a delay of 2 days.

The above figure illustrates the observed (black line) and simulated (blue line) flow at Mogren. The deviations between the observed and simulated flow are mainly caused by the operation rules applied in the Jebel Aulia reservoir.

In general the model has a reasonable representation of the flow on the White Nile, and the model is evaluated as acceptable for use in climate scenarios.
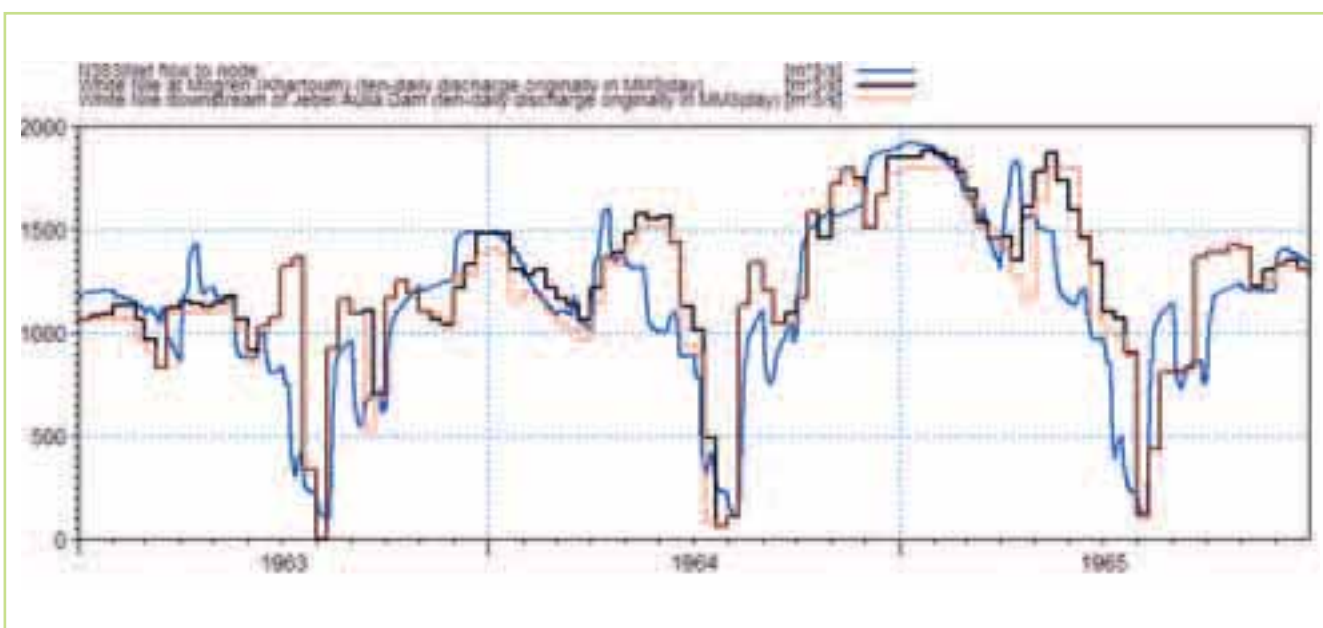
Figure 5.38 Observed flow at Mogren (black line), simulated flow at Mogren (blue line) & observed flow at Jebel Aulia (red line)

5.5.7 The Ethopian Highlands (Blue Nile & Atbara sub-basins)

The Blue Nile and Atbara basins are located in the Ethiopian highlands and in eastern Sudan. A small portion of the Atbara basin is located in Eritrea. The Blue Nile originates near Lake Tana, flows south and then west through Ethiopia, and then turns north and enters Sudan, where it joins the White Nile at Khartoum to form the Main Nile. The Atbara originates in the Ethiopian highlands north and east of Lake Tana and flows northeast through Sudan to join the Main Nile approximately 300 km downstream of Khartoum. The Atbara is the last significant tributary to the Nile River before its outlet to the Mediterranean Sea.

The Blue Nile and Atbara basins are characterized by highly seasonal runoff regimes, and both make substantial contributions to the total flow of the Nile River. The Blue Nile contributes about 55% of the total flow of the Nile, with more than 80% of this contribution concentrated between July and October. The Atbara provides about 10% of the total flow of the Nile, with more than 90% between July and September. The runoff season is more concentrated in the northern portion of the Ethiopian highlands, which results from the relation between the rainy season and the position of the ITCZ.

5.5.7.1 Data

The Ethiopian Highlands is the other main contributing area to the flows in the Nile River and contributes substantially to the high flow regime downstream, Figure 1.5. In terms of hydrological modelling it was noted earlier that water scarcity can be modelled using data and models at a monthly time scale, however high flows should be modelled using rainfall and discharge data on time scale of one day or less. Despite best efforts only a limited amount of daily data was made available to the project. Therefore and because of the importance of this basin a robust disaggregation method has been developed to generate daily precipitation data in order to achieve an acceptable hydrological model of this important area. The data made available and the disaggregation method are described in more detail below.

Data used to model these two major sub-basins include discharge, rainfall, lake level, and evapotranspiration data. Discharge data are obtained from the following sources: i) NBI (Nile Encyclopaedia and Ethiopia master plan), (ii) ENTRO and iii) Global Runoff Date centre (GRDC). Rainfall data sources include NBI, ENTRO, the Global Historical Climatology Network (GHCN), and the University of East Anglia Climatic Research Unit (CRU). Lake level data have been obtained from NBI. Evaporation data have been obtained from CRU. The available data are presented in the following sections.

Discharge

The discharge data from the Nile Encyclopaedia were provided by NBI under confidentiality agreement. This consists of 10-day flows values for 15 stations. These data are the main data source used in Sudan. The Nile Encyclopaedia data set does not include any measurements in Ethiopia, with the exception of one station at the outlet of Lake Tana.

The discharge data available from GRDC consist of 16 monthly and 6 daily

Figure 5.39 Blue Nile & Atbara basins

stations, however the daily data only covers 3 years from 1978-80. For conditions for using and distributing these data please refer to the GRDC web-page. None of the GRDC data are used for model calibration because these data duplicate data available from other sources.

The Ethiopia Master Plan data set includes both monthly and daily records. Most of the stations in the data set are located in Ethiopia, although a few are located in Sudan. These data were also provided under a confidentially agreement. This consists primarily of monthly discharge values from more than 80 stations and daily data from 11 stations.

Discharge data was also received from ENTRO under a confidentiality agreement. However these are all monthly data and were not used because these records duplicate other records in the Nile Encyclopaedia and Ethiopia Master Plan data sets

Precipitation

The precipitation data available from the Global Historical Climatology Network (GHCN) consists of 13 stations with daily records. For conditions for using and distributing these data please refer to the GHCN web-page.

Precipitation from the Nile DST data were provided under a confidentiality agreement however these data were not used in the Blue Nile or Atbara representations because most of the rainfall in these basins is generated in Ethiopia, which is not covered by the Nile DST. Instead a method combing the GHCN and CRU was developed ensuring a consistent approach over both basins.

The precipitation data obtained from ENTRO under a confidentiality agreement consists of monthly data from 13 stations. However the ENTRO data were not used in the Blue Nile or Atbara representations because of the need to develop daily rainfall inputs.

Potential Evapotranspiration (PET)

As described earlier, the potential evapotranspiration data used across the region is the CRU data set. The CRU data set includes estimates of potential evaporation (PET) for each grid cell for the period 1901-2009. The CRU PET data are secondary data computed from estimates of temperature, vapour pressure, and cloud cover. The CRU PET data are publicly available and information about permitted uses of the data is available from the CRU web-site.

While the CRU data is only monthly, this is often sufficient for hydrological modelling in many instances. One of the advantages of using the CRU dataset is that it represents the spatial variability in PET.
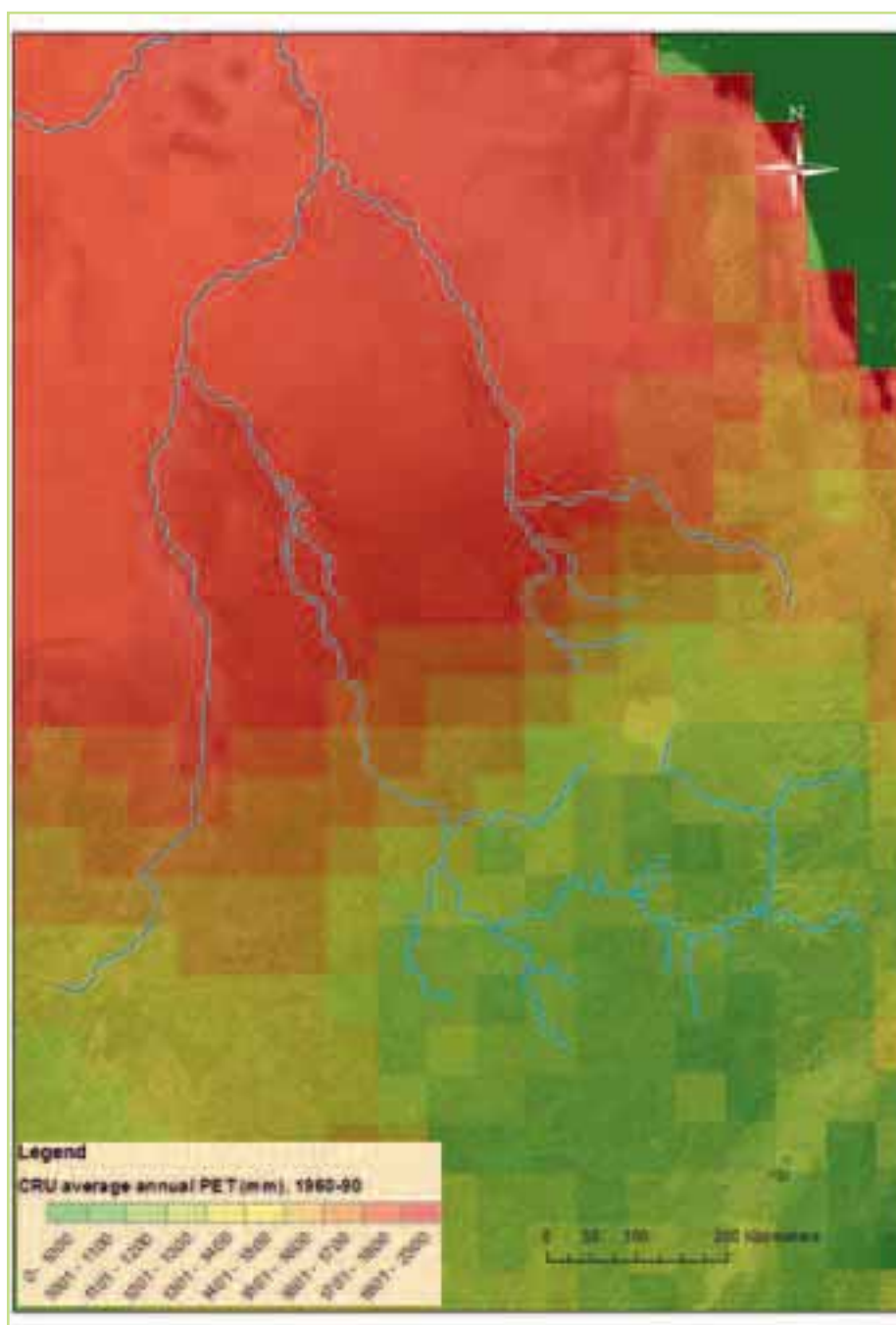
Figure 5.40 Spatial distribution of average annual PET (1960-90) for the Blue Nile & Atbara sub-basins from the CRU gridded dataset

5.5.7.2 Rainfall-runoff modelling
Catchment delineation

To develop rainfall-runoff models of the Blue Nile and Atbara basins, it is necessary to delineate catchment areas for rainfall-runoff model development. Catchments are delineated based on the availability of discharge data for model calibration at catchment outflow points. Some additional catchments are delineated at outflow points that lack discharge data, either to estimate water supply at existing or proposed reservoir locations, or because these catchments are thought to have distinctive hydrological characteristics that make them unsuitable for merger with nearby catchment areas. The various reasons for catchment delineation can be grouped into the following categories:

1. Gauged headwater catchments: Gauged headwater catchments have downstream boundaries defined by gauging stations and do not have inflows from other catchments or significant lake or reservoir storage. In the Blue Nile basin, gauged headwater catchments include the Rahad, Dinder, Upper Beles, Upper Didessa, Upper Dabus, and Angar catchments. In the Atbara basin, the Upper Atbara catchment is classified as a gauged headwater catchment.

2. Gauged downstream catchments: Gauged downstream catchments have downstream boundaries defined by gauging stations as well as inflows from other catchments but do not feature significant lake or reservoir storage. In the Blue Nile basin, gauged downstream catchments include the Lower Blue Nile, Border-Lower Beles, Shegoli, and Kessie catchments. In the Atbara basin, gauged downstream catchments include the Lower Atbara, Humera, and Ambamadre catchments.

3. Existing lake or reservoir catchments: Existing lake or reservoir catchments have downstream boundaries defined by the outlets of existing lakes or reservoirs. Existing lake or reservoir catchments can be headwater catchments but can also have inflows from other catchments. In the Blue Nile basin, existing lake or reservoir catchments include the Sennar, Roseires, and Lake Tana catchments. In the Atbara basin, existing lake or reservoir catchments include the Khashm El Girba and Tekeze catchments.

4. Proposed reservoir catchments: Proposed reservoir catchments have downstream boundaries defined by the outlets of proposed reservoirs. Proposed reservoir catchments can be headwater catchments but can also have inflows from other catchments. In the Blue Nile basin, the Mandaya, Bako-Abo, and Karadobi catchments are classified as proposed reservoir catchments. There are no proposed reservoir catchments in the Atbara representation.

5. Ungauged catchments with distinctive features: Ungauged catchments with distinctive features have distinctive hydrological features that make them unsuitable for aggregation with other nearby catchment areas. In the Blue Nile basin, the Lower Dabus, Lower Didessa, and Finchaa catchments are considered ungauged catchments with distinctive features. In the Atbara representation, no catchments are classified as ungauged catchments with distinctive features.

Rainfall estimation

It is necessary to develop daily rainfall estimates for each catchment area in the model representation for the purpose of rainfall-runoff modelling. However, the only daily rainfall data set covering Ethiopia that is available to the project team is the GHCN data set. The GHCN network is thought to be too sparse to develop an adequate representation of rainfall in the Ethiopian highlands, which are characterized by considerable spatial variability. To address this concern, a hybrid approach combining the GHCN and CRU data sets is developed.

Equation 5.2

$$R_{i,t} = \frac{\sum_{j=1}^{n} w_j \cdot R_{j,t}}{\sum_{j=1}^{n} w_j} \text{ where } w_j = \frac{A_{i,j}}{A_j}$$

and i = catchment index

j = index of CRU grid cells located fully or partially in catchment i

t = time index

n = number of CRU grid cells located fully or partially in grid cell k

$R_{i,t}$ = rainfall in catchment i at time step t

$R_{j,t}$ = rainfall in grid cell j at time step t

w = weight

A_j = area of grid cell j

$A_{i,j}$ = area of grid cell j located within catchment i

The hybrid approach consists of two steps.

1. Monthly time series estimates of rainfall for each catchment are estimated from the CRU data set. The estimate for each catchment is a weighted average of all of the CRU grid cells that are located either fully or partially in that catchment. The weight attached to each value is equal to the fraction of the grid cell area located within the catchment. The procedure is summarized in Equation 5.2.

Average annual estimates for sub-basin rainfall obtained using the procedure given in step 1 are presented in Figure 5.41. The figure shows that rainfall is highest in the Dabus and Didessa sub-basins, and decreases from south to north.

Estimates of rainfall during the July/August summer rainy season are presented in Figure 5.42. The figure shows the impact of the position of the ITCZ on summer rainfall, with higher totals observed in more northern catchments.
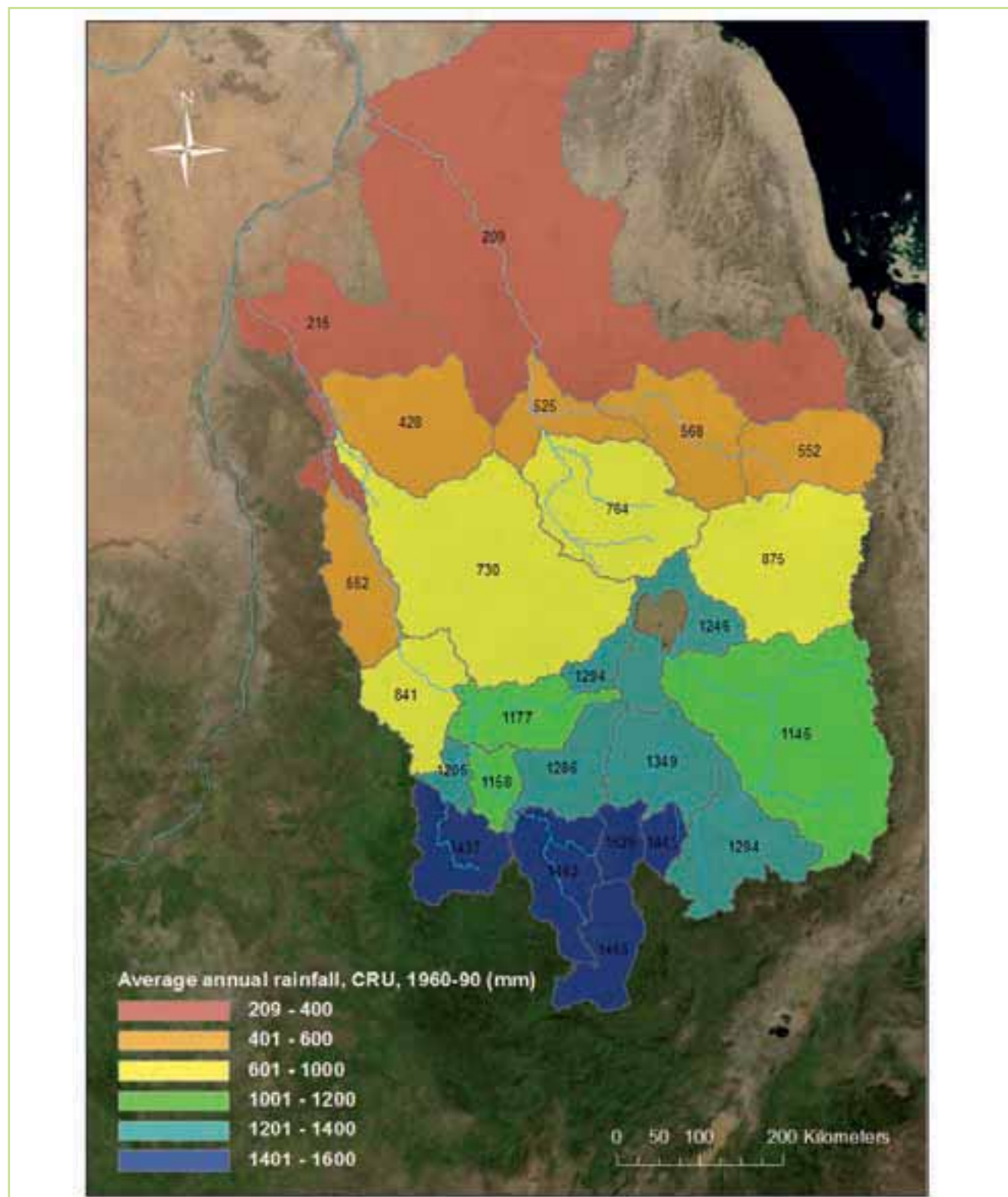
Figure 5.41 Average annual rainfall estimated from CRU data set for period 1960-90
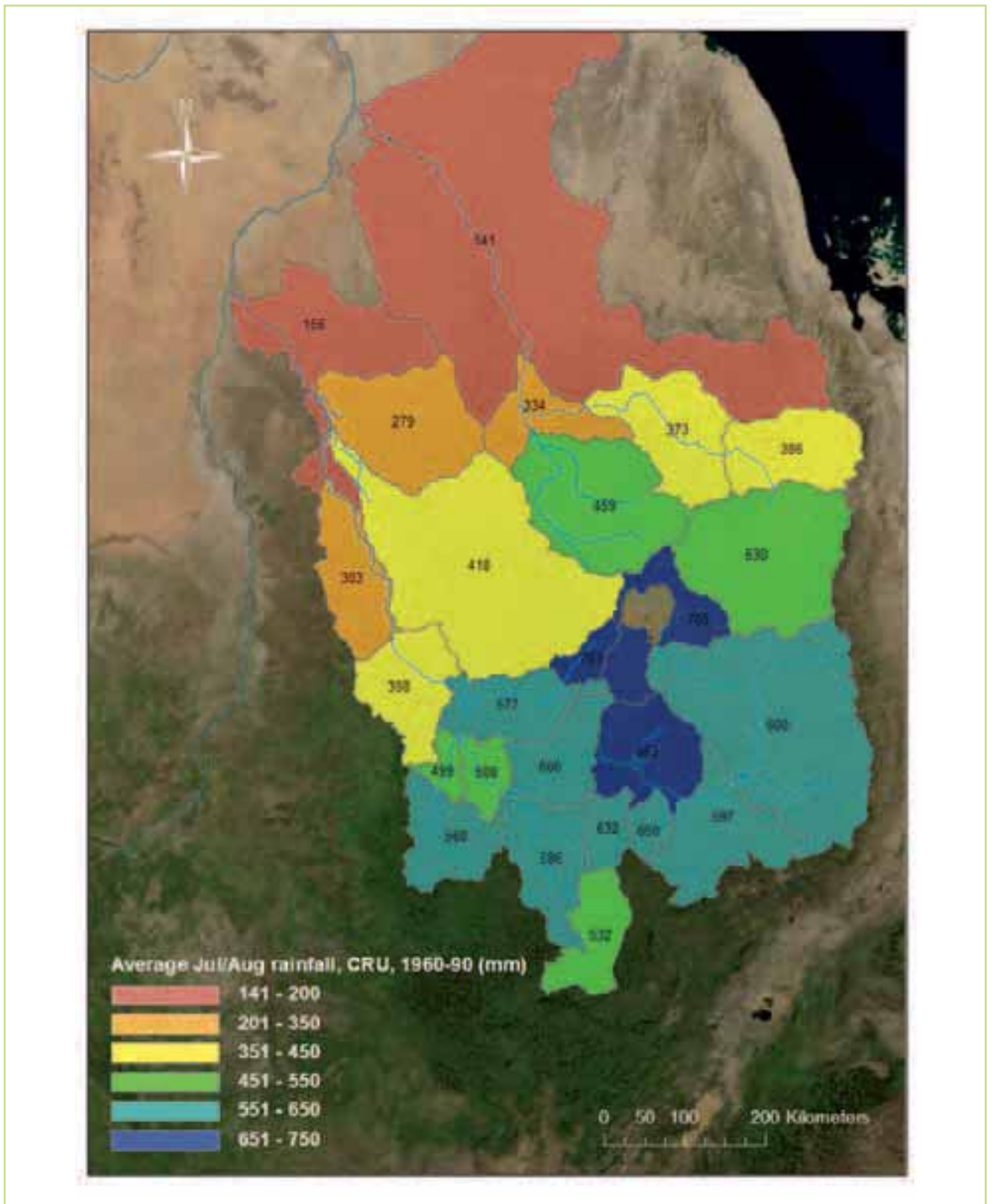
Figure 5.42 Average July/August rainfall estimated from CRU data set, 1960-90

Equation 5.3

$$R_{i,d,t} = \sum_{k=1}^{m} R_{k,d,t} \cdot w_k \cdot \frac{R_{i,t}}{\sum_{d=1}^{D} R_{k,d,t}}$$

where $w_k = \frac{A_{k,i}}{A_i}$

k = index of GHCN stations with Thiessen polygons located partly in catchment i

m = # of GHCN stations with Thiessen polygons located partly in catchment i

d = day of month index

D = number of days in month

$R_{i,d,t}$ = rainfall in catchment i during day d of month t

$R_{k,d,t}$ = rainfall recorded at station k during day d of month t

$A_{k,i}$ = area of catchment i located within Thiessen polygon k

A_i = area of catchment i

2. In the second step, GHCN rainfall records are used to distribute the CRU monthly estimates over the days of the month. A weighting procedure that uses Thiessen polygons is used to assign GHCN rainfall stations to individual catchments. The weighting procedure is summarized in Equation 5.3.

PET estimation

The sub-basin estimates of PET for rainfall-runoff modelling were developed using the same procedure as step 1 using the procedure outlined in step 1 for rainfall estimation. Average annual PET estimates are presented in Figure 5.43. The figure shows that PET is lower in southern and mountain areas.
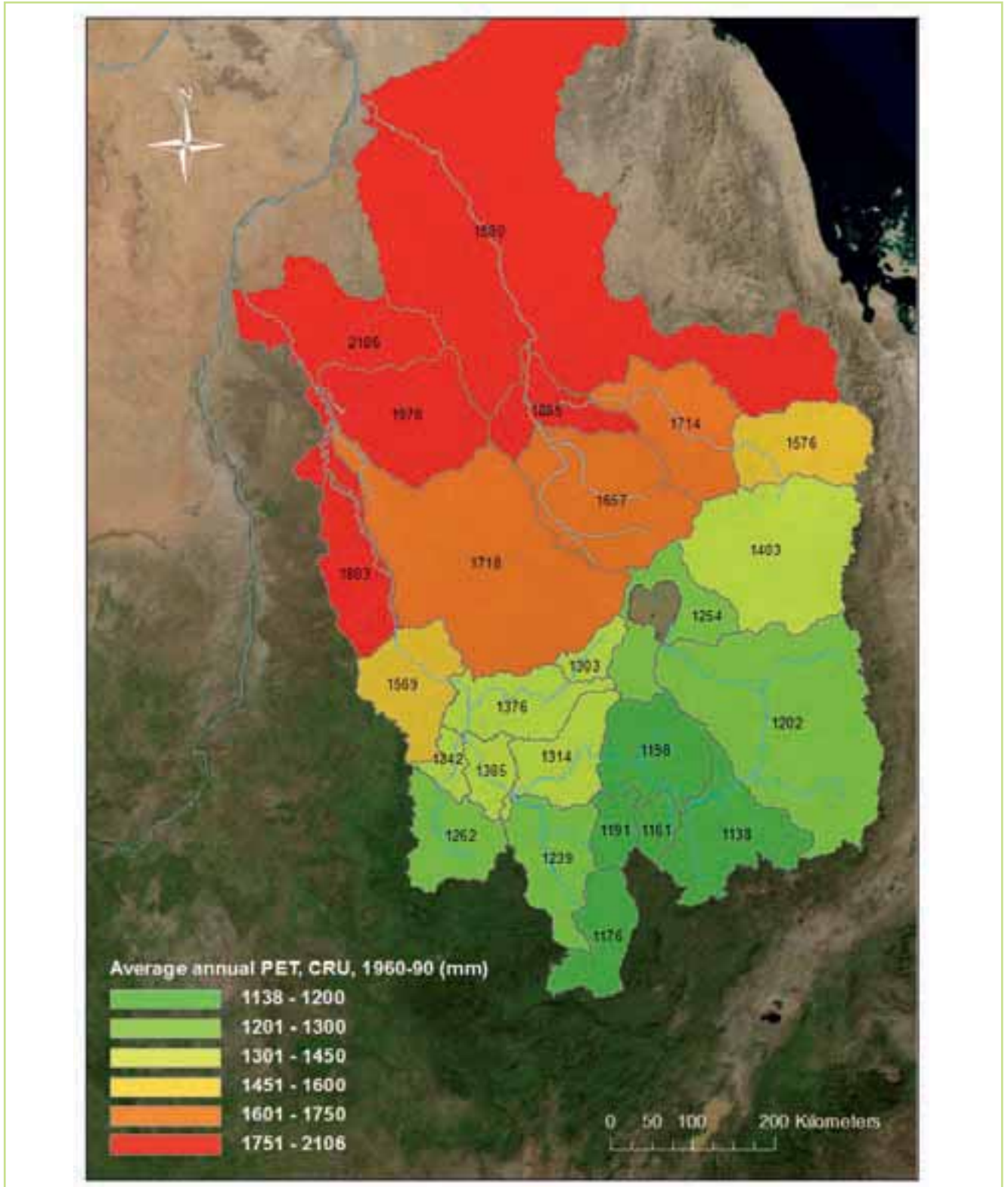
Figure 5.43 Average annual PET estimated from CRU data set, 1960-90

Runoff estimation

The Blue Nile and Atbara representation includes both gauged and ungauged catchments. For ungauged catchments, it is necessary to estimate runoff for model calibration, or else transfer rainfall-runoff model parameters from other catchments. In some catchments, runoff was thought to be insignificant and rainfall-runoff models were not developed. Out of 25 catchments in the Blue Nile and Atbara representation, gauge data are used for model calibration in 8 catchments, runoff estimates are used in 10 catchments, transferred parameters are used in 4 catchments, and no rainfall-runoff models are developed in the 3 remaining catchments. A map showing where the different approaches to using runoff data for model calibration are used is presented in Figure 1.1.

Figure 5.44 Approaches to estimating runoff for model calibration

Table 5.6 Catchments calibrated to gauge data

Catchment	Downstream gauge	Downstream gauge time step	Downstream gauge data source	Upstream gauge	Upstream gauge time step	Upstream gauge data source
Lake Tana	Abay at Bahir Dar (Monthly Discharge originally in Mm3) - Observed [10^6m^3]	Monthly	Ethiopia master plan (NBI)	None, headwater catchment	None, headwater catchment	None, headwater catchment
Rahad	Rahad near its mouth into Blue Nile (at Abu Haraz) [m^3/day]	10-day	Nile Encyclopedia (NBI)	None, headwater catchment	None, headwater catchment	None, headwater catchment
Dinder	Dinder near its mouth into Blue Nile (at Hillet Idreis) [m^3/day]	10-day	Nile Encyclopedia (NBI)	None, headwater catchment	None, headwater catchment	None, headwater catchment
Upper Dabus	Dabus near Assosa (Monthly Discharge originally in m3|s) - Infilled [m^3/s]	Monthly	Ethiopia master plan (NBI)	None, headwater catchment	None, headwater catchment	None, headwater catchment
Upper Beles	Beles near Metekel (Monthly Discharge originally in m3|s) - Infilled [m^3/s]	Monthly	Ethiopia master plan (NBI)	None, h eadwater catchment	None, headwater catchment	None, headwater catchment
Upper Didessa	Didessa near Arjo (Monthly Discharge originally in m3|s) - Infilled [m^3/s]	Monthly	Ethiopia master plan (NBI)	None, headwater catchment	None, headwater catchment	None, headwater catchment
Angar	Angar near Nekemte (Monthly Discharge originally in m3|s) - Infilled [m^3/s]	Monthly	Ethiopia master plan (NBI)	None, headwater catchment	None, headwater catchment	None, headwater catchment
Kessie	Abay at Kessie (Monthly Discharge originally in Mm3) - Observed [10^6m^3]	Monthly	Ethiopia master plan (NBI)	Abay at Bahir Dar (Monthly Discharge originally in Mm3) - Observed [10^6m^3]	Monthly	Ethiopia master plan (NBI)

Ten catchments in the Blue Nile and Atbara representation are calibrated to estimated data. These catchments can be grouped into the following categories:

1. Catchments located between the Shegoli and Kessie gauges on the Blue Nile.
2. Catchments located between the Border and Shegoli gauges on the Blue Nile.
3. Catchments located upstream of the Ambamadre gauge on the Atbara.

The runoff estimates in the above mentioned areas are only described in brief in the following sections.

The eight catchments for which gauge data are used for model calibration are listed in Table 1.10 Catchments calibrated to gauge data. For each catchment, the table presents the gauge(s) used for calibration.

Runoff estimation: Blue Nile between Shegoli & Kessie gauges:

No gauge records are available on the Blue Nile between the Shegoli and Kessie gauge locations. This region covers a large portion of the runoff-generating area of the Blue Nile basin. Important tributary rivers in the region include the Dabus, Didessa, Finchaa, Guder, Muger, Birr, Fattam, and Dura rivers. Because the area covered by this region is so large, significant variation in rainfall patterns exist. In addition, the Dabus and Finchaa catchments feature large wetland areas that delay hydrological response in comparison to other catchments in the region. Three large dams are planned for the main stem of the Blue Nile between the Shegoli and Kessie gauge locations: Mandaya, Bako-Abo, and Karadobi. A map showing the positions of the Shegoli and Kessie gauges, the major tributaries, and the locations of the proposed dams is presented in Figure 5.45.

No gauge records are available for any of the tributary catchment areas shown in Figure 5 45. A number of gauge records are available for smaller upstream portions of the tributary catchments. Some of these records are used to delineate and calibrate upstream areas. Other upstream records are not used because these locations delineate catchments areas that are thought to be too small to develop reasonable estimates of local rainfall using the CRU and GHCN data sets. As a general rule, gauge records are only used for catchment delineation and calibration if the area of the resulting catchment area is greater than or equal to the area of one CRU grid cell (~ 2500 km^2). Upstream areas between the Shegoli and Kessie gauges that are delineated and calibrated using gauge data include the Angar, Upper Didessa, and Upper Dabus catchments (Figure 5.44).

Because of the diversity of the hydrology of the area and because of the need to estimate available water supply at each of the proposed reservoir locations, it is not possible to aggregate the remaining area between the Shegoli and Kessie gauges into a single catchment. The remaining area between the Shegoli and Kessie gauges is divided into seven catchment areas (Figure 5 44). The Lower Dabus, Lower Didessa, and Finchaa catchment areas are delineated because of each of these areas have unique hydrological features that prevent aggregation with nearby catchments. The Mandaya, Bako-Abo, and Karadobi catchments are delineated in order to estimate water supply at the proposed reservoir locations. The Shegoli catchment

area is delineated to estimate runoff generated by the remainder of the area between the gauges.

The method used to estimate runoff for each of these seven catchment areas depends on a group of records in the Ethiopia Master Plan data set that are labelled "generated". These records all cover a uniform time period (1960-92) and are thought to represent output from a statistical or hydrological model of the basin. Although not appropriate for calibrating hydrological models, these records are thought to provide insight into how the gain between the Shegoli and Kessie gauges is distributed in space and time. The "generated" records in the Ethiopia Master Plan data set provide estimates of outflows from all of the tributary catchment areas shown in Figure 5.45 with the exception of the Dura River.

Runoff estimation: Blue Nile between Border & Shegoli gauges:

The region between the Border and Shegoli gauges is divided into two catchment areas: Upper Beles and Border-Lower Beles (Figure 5 44). The Upper Beles catchment is calibrated to gauge data as described above. The Border-Lower Beles catchment area includes small tributaries to the Blue Nile between the Border and Shegoli gauges as well as the Beles catchment area downstream of the Upper Beles catchment. Runoff from the Border-Lower Beles is estimated to be equal to an area-weighted multiple of runoff from the Shegoli catchment. It is not possible to estimate runoff from the Border-Lower Beles catchment from the difference between downstream and upstream gauge records because

Figure 5.45 Tributary catchment areas & proposed dam locations between the Shegoli and Kessie gauges

this difference is not positive in all months. The three records that define the upstream and downstream boundaries of the Border-Lower Beles catchment are all characterized as "infilled" records in the Ethiopia Master Plan data set. These records are thought to consist of a combination of observed data and other data that have been estimated using statistical methods to "infill" gaps in the observed record. Perhaps because of inconsistencies between procedures used to fill in data gaps, these records may not be consistent with one another. Therefore, runoff from the nearby Shegoli catchment was used to estimate runoff from the Border-Lower Beles catchment.

Runoff estimation: Atbara above Ambamadre gauge:

The Ambamadre gauge is the uppermost observed gauge record in the Tekeze River basin, which is the major tributary to the Atbara River. It is not possible to delineate a headwater catchment with a downstream boundary at the gauge because the gauge is located downstream of the Tekeze (TK-5) Dam. Because of the need to estimate water supply at the dam location, the area upstream of the gauge is delineated into two catchments (Figure 5 44): the Tekeze catchment is a headwater catchment bounded by the Tekeze Dam location at the downstream end, while Ambamadre catchment consists of the area between the Tekeze Dam and the Ambamadre gauge.

The flow measured at the Ambamadre gauge is partitioned between the Tekeze and Ambamadre catchments using a method similar to the method used to partition flow between the Shegoli and Kessie gauges on the Blue Nile. The method uses records labelled as "generated" to partition flows measured at the Ambamadre gauge in space and time.

Catchments simulated using parameters transferred from other catchments:

Rainfall-runoff processes in four catchments were simulated using parameters transferred from other catchments. These catchments include the Roseires catchment on the Blue Nile and the Humera, Upper Atbara, and Khashm El Girba catchments on the Atbara.

The Roseires catchment occupies the catchment area of the Blue Nile between Roseires Dam and the Border gauge. Estimating runoff from this region requires an estimate of inflow to Roseires Reservoir, which is not available to thsi project. attempted to estimate inflow to Roseires Reservoir using outflow and storage change records. The difference between the resulting inflow estimate and the flow at the Border gauge location is not always positive, which

led the project team to conclude that the records associated with Roseires Reservoir are not consistent with the record at the Border gauge location. The project team chose not to estimate runoff using runoff estimates from the nearby Border-Lower Beles catchment because the runoff from the Border-Lower Beles catchment is in turn based on estimated runoff from the Shegoli catchment. Instead, rainfall-runoff model parameters estimated during calibration of the Border-Lower Beles catchment are transferred to the Roseires catchment. Transfer of parameters from the Border-Lower Beles catchment to the Roseires catchment is justified by similar rainfall, PET, and topography. The same justification is used for the three other catchments.

The Humera catchment occupies the catchment area of the Tekeze River between the Humera and Ambamadre gauge locations. The Humera gauge record was not used for model calibration because the period of record for the Humera gauge runs from 1981 to 1987. This period lies outside the 1960-80 baseline simulation period and parameters calibrated to the 1981-87 period do not produce a reasonable simulation of rainfall-runoff processes during the 1960-80 period. Instead, rainfall-runoff model parameters were transferred from the nearby Ambamadre catchment.

The Upper Atbara catchment occupies the catchment area of the Atbara River upstream of the Kubur gauge location. The Kubur gauge record was not used for model calibration because the period of record for the Kubur gauge runs from 1985 to 1992. This period lies outside the 1960-80 baseline simulation period and parameters calibrated to the 1985-92 period do not produce a reasonable simulation of rainfall-runoff processes during the 1960-80 period. Instead, rainfall-runoff model parameters were transferred from the nearby Ambamadre catchment.

The Khashm El Girba catchment occupies the catchment area of the Tekeze and Atbara rivers upstream of the Khashm El Girba dam and downstream of the Kubur and Humera gauge locations. A record of inflow to the Khashm El Girba Reservoir is not available to the project team. It is possible to estimate reservoir inflow using reservoir storage and outflow records; however, the resulting inflow estimate cannot be used to estimate catchment runoff because there is no common period of overlap between the reservoir storage and outflow records and the gauge records that define the upstream boundaries of the catchment. In addition, the upstream boundary gauge records are not available until after 1980, so the problem of calibrating to a

period outside the baseline simulation period also applies to this catchment. Rainfall-runoff model parameters were transferred to the Khashm El Girba catchment from the Ambamadre catchment.

Catchment areas for which no rainfall-runoff models are developed:

Catchment areas for which no rainfall-runoff models are developed include the Sennar, Lower Blue Nile, and Lower Atbara catchments. The Sennar catchment consists of the catchment area of the Blue Nile between the Sennar and Roseires dams. The Lower Blue Nile catchment consists of the catchment area of the Blue Nile upstream of Khartoum and downstream of Sennar Dam (not including the Rahad and Dinder catchments). The Lower Atbara catchment consists of the catchment area of the Atbara between Khashm El Girba Dam and the confluence with the Main Nile. All three catchment areas are located in areas characterized by flat topography, low rainfall and high evapotranspiration rates and because of these factors, it is considered that runoff generation in these catchments is not significant enough to justify the development of rainfall-runoff models. In addition, comparison of gauged river flows at the upstream and downstream boundaries of these catchments suggests that any runoff generated in these catchment areas does not make a significant contribution to the total flow of either the Blue Nile or Atbara Rivers.

5.5.7.3 MIKE BASIN modelling in the Blue Nile & Atbara sub-basins

The basin-scale model is developed using MIKE BASIN to integrate the rainfall-runoff models with reservoir, hydropower, and irrigation diversion operations as these activities existed during the 1960-80 baseline simulation period.

Reservoir and hydropower operations

Three reservoirs are included in the MIKE BASIN representation of the Blue Nile and Atbara basins: Roseires and Sennar on the Blue Nile, and Khashm El Girba on the Atbara. All three reservoirs are multi-purpose facilities operated for both irrigation and hydropower.

Roseires Reservoir

Roseires Reservoir is operated for hydropower and for downstream irrigation. The reservoir began operation in 1965, and is active beginning in 1965 in the 1960-80 baseline MIKE BASIN simulation. Roseires Reservoir is operated using a flood control rule, a minimum release time series, a hydropower demand time series, and an allocation rule that adjusts hydropower releases depending on the surface elevation of the reservoir. The flood control elevation is constant throughout the simulation period. The hydropower demand is also constant but is given in power units, so the release required to meet the demand varies depending on reservoir storage. The minimum release time series is time-varying but generally follows the same pattern from year to year. Minimum releases and flood control releases are routed through hydropower facilities unless turbine capacity is exceeded. Some different components of the total simulated release from Roseires are shown in Figure 5.46.
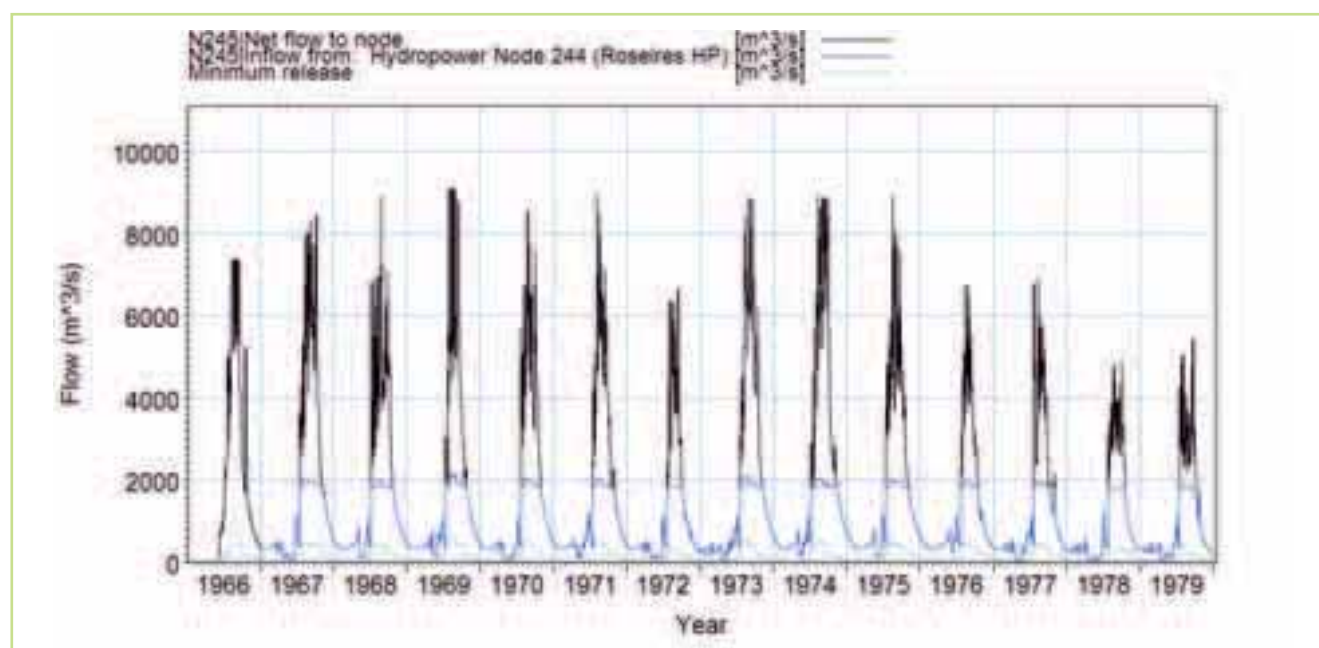
Figure 5.46 Simulated Roseires outflows ("Net flow to node" = total release, minimum release is routed through hydropower and therefore is a component of the hydropower release)
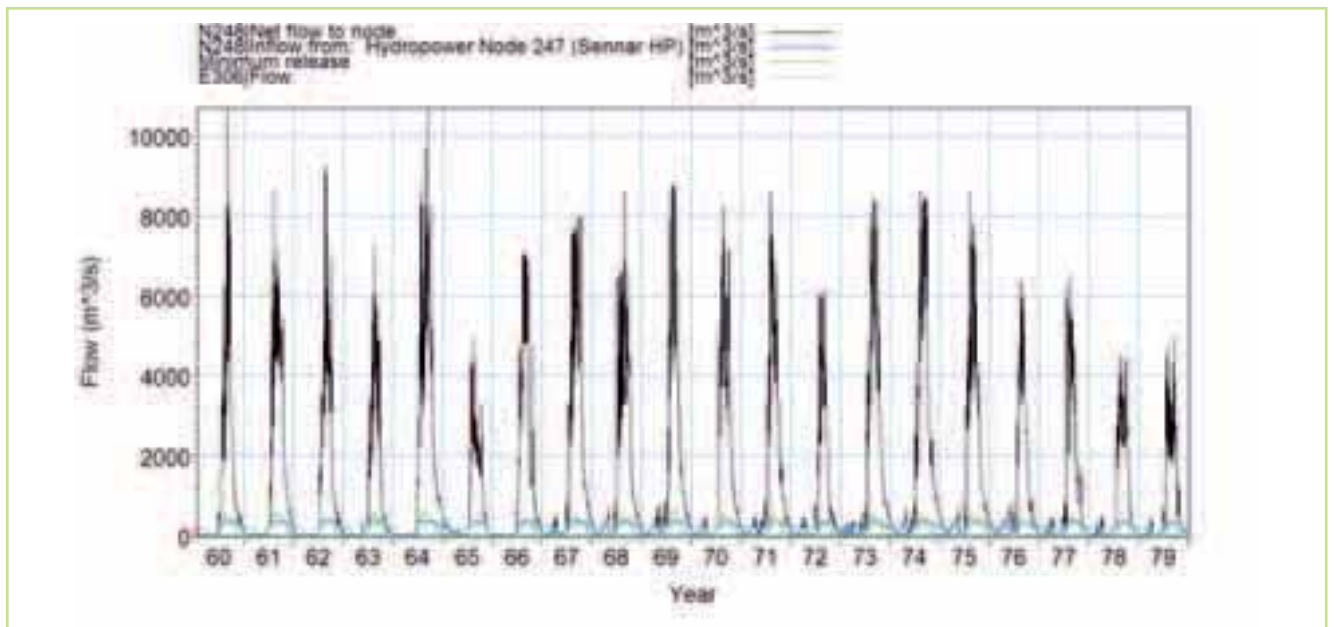
Figure 5.47 Simulated Sennar outflows ("Net flow to node" = total downstream release, minimum release is routed through hydropower and therefore is a component of the hydropower release, E306 = delivery to Gezira-Managil scheme)

Sennar Reservoir

Sennar Reservoir is operated to supply water to the Gezira-Managil irrigation scheme and also to provide water for downstream irrigation use. Hydropower is produced incidentally. Sennar Reservoir began operation in the 1930s and is active throughout the 1960-80 baseline simulation period. Sennar Reservoir is operated using a flood control rule, a minimum release time series, and a demand time series for the Gezira-Managil irrigation scheme. The flood control elevation is constant throughout the simulation period. The minimum release time series is time-varying but generally follows the same pattern from year to year. Minimum releases and flood control releases are routed through hydropower facilities unless turbine capacity is exceeded. The demand time series for the Gezira-Managil irrigation scheme is presented in Figure 5 49. Some different components of the total simulated release from Sennar are shown in Figure 5 47.

Khashm El Girba Reservoir

Khashm El Girba Reservoir is operated for irrigation and hydropower. The reservoir began operation in 1964 and is active beginning in 1964 in the 1960-80 baseline simulation. The capacity of the reservoir has been reduced substantially by sedimentation; the reservoir capacity used in the 1960-80 MIKE BASIN simulation is equal to the current capacity. Khashm El Girba Reservoir is operated using a flood control rule, a hydropower demand time series, and an allocation rule that adjusts hydropower releases depending on the surface elevation of the reservoir.

No minimum release rule is used. The flood control elevation is constant throughout the simulation period. The hydropower demand is also constant, but is given in power units, so the release required to meet the demand varies depending on reservoir storage. Flood control releases are routed through hydropower facilities unless turbine capacity is exceeded. The demand time series for the Khashm El Girba irrigation scheme is presented in Figure 5 49. Some different components of the total simulated release from Khashm El Girba are presented in Figure 5.48.

Irrigation operations

Four irrigation water use locations are included in the MIKE BASIN representation of the Blue Nile and Atbara basins. These locations are labelled as follows: Downstream of Sennar, Gezira-Managil, Upstream of Sennar, and Khashm El Girba.

1. Downstream of Sennar: This location aggregates all irrigation water use in the Blue Nile basin downstream of Sennar Dam and upstream of the confluence with the White Nile at Khartoum. In the MIKE BASIN model, diversions to this location are made from a point downstream of the confluence of the Blue Nile with the Rahad River and upstream of the confluence of the Blue Nile with the White Nile.

2. Gezira-Managil: This location represents the Gezira-Managil irrigation scheme on the Blue Nile in Sudan. In the MIKE BASIN model, diversions to this location are made from Sennar Reservoir.

3. Upstream of Sennar: This location aggregates
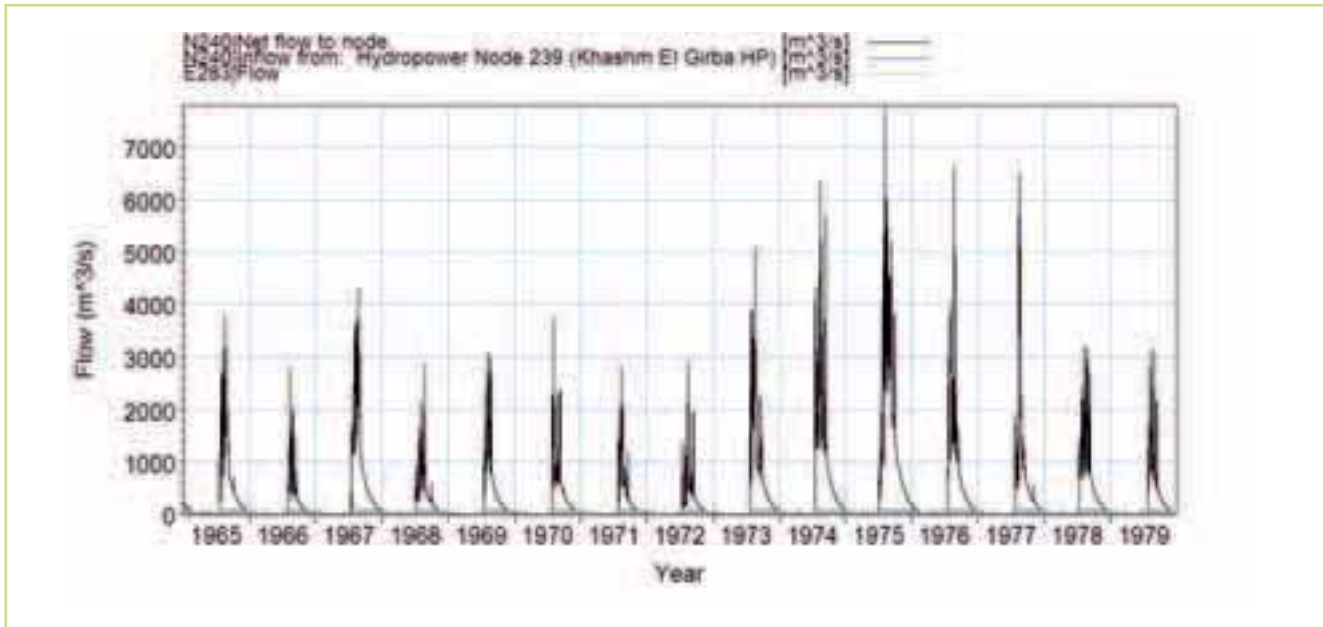
Figure 5.48 Simulated Khashm El Girba outflows ("Net flow to node" = total downstream release, E283 = delivery to Khashm El Girba scheme)

all irrigation water use in the Blue Nile basin upstream of Sennar Reservoir and downstream of Roseires Reservoir. In the MIKE BASIN model, diversions to this location are made from a point upstream of Sennar Reservoir and downstream of Roseires Reservoir.

4. Khashm El Girba: This location represents irrigation water use supplied from the Khashm El Girba Reservoir on the Atbara River. In the MIKE

BASIN model representation, diversions to this location are made from the Khashm El Girba Reservoir.

Demand time series used to represent the four locations above are summarized in Figure 5.49. All four locations are represented using constant annual time series (in other words, demands do not change from year to year).
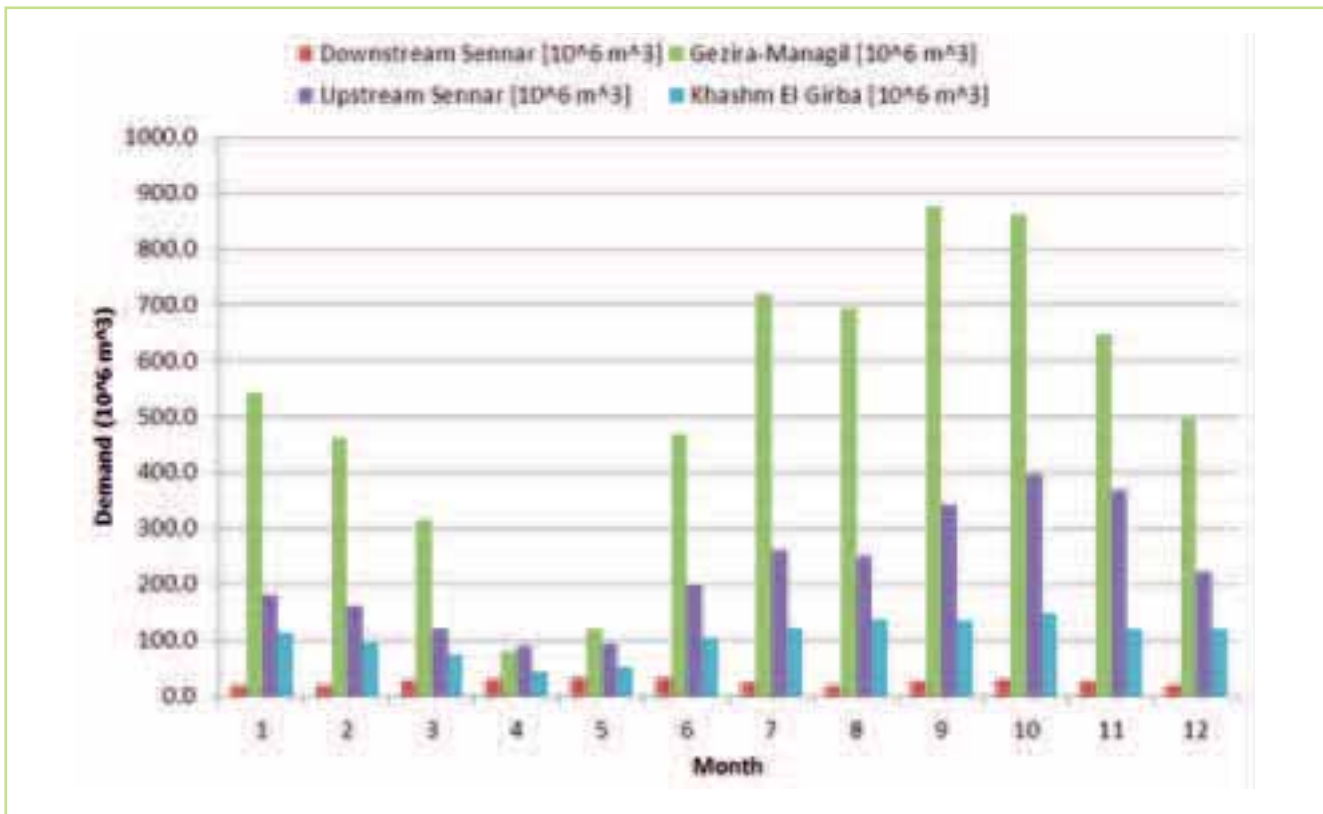
Figure 5.49 Irrigation water demands in Blue Nile & Atbara representation

5.5.7.4 Model performance

The integrated model of the Blue Nile and Atbara basins is used to check flow accumulations at important gauging locations on the Blue Nile and Atbara rivers. A check of accumulated flows against the gauge records indicated an underestimation of flow in Blue Nile at the border between Sudan and Ethiopia. This occurred in the process of calibrating individual model catchments, where rainfall was reduced for many of the catchments on the Blue Nile. Because many of these catchments are calibrated to estimated runoff data and not measured data, it is thought that perhaps rainfall was reduced too much in some catchment areas. As a result, the minimum rainfall reduction percentage in the Blue Nile basin is used as a final calibration parameter to close the water balance at the Sudan/Ethiopia border. In the final version of the model, the minimum rainfall reduction percentage is 83%. No rainfall estimates were reduced in the Atbara representation.

Simulated flows on the Blue Nile and Atbara are evaluated using monthly Nash-Sutcliffe and accumulated water balance measures. Model performance measures for the gauge locations are summarized in Table 5.7.

In summary, a consistent disaggregation technique has been developed across the Blue Nile and Atbara sub-basins in order to develop spatially distributed estimates of daily rainfall. This was motivated by the sparse raingauge data provided to this project and the strong spatial patterns in the rainfall in this sub-basin. Similarly, because of the corresponding spatial distribution in the runoff and sparse discharge data network, distributed estimates of runoff were also made for calibration. From Table 5.7 it appears that the Blue Nile model provides satisfactory simulation results when compared to the observed flow records with low water balance errors and satisfactory Nash-Sutcliffe values. Applying the same approach to the Atbara sub-basin is not as successful in Atbara with good Nash-Sutcliffe values but larger water balance errors. The performance of the Atbara model is strongly limited by the scarcity of observed flow records in upper catchment areas, which requires the use of transferred parameters in many catchments. More observed data in upper catchment areas during the 1960-80 baseline period would enable calibration of rainfall-runoff model parameters for these catchments, improving the Atbara representation.

Table 5.7 Model performance measures for calibration locations on the Blue Nile & Atbara rivers

Basin	Gauge	Calibration period start	Calibration period end	Water balance	Monthly NS
Blue Nile	Abay at Kessie (Monthly Discharge originally in Mm3) - Observed [10^6m^3]	1/1/1961	1/1/1980	1.6%	0.86
Blue Nile	Abay at Shegolie (Monthly Discharge originally in m3|s) - Infilled [m^3/s]	1/1/1961	1/1/1980	0.1%	0.88
Blue Nile	Abay at Ethio-Sudan Border (Monthly Discharge originally in m3|s) - Infilled [m^3/s]	1/1/1961	1/1/1980	0.9%	0.89
Blue Nile	Blue Nile at Roseires Dam	1/1/1973	1/1/1980	-2.1%	0.78
Blue Nile	Blue Nile at Mokwar (downstream of Sennar Dam)	1/1/1961	1/1/1980	-0.5%	0.86
Blue Nile	Blue Nile at Khartoum & Soba	1/1/1961	1/1/1980	-5.0%	0.88
Atbara	Tekeze at Ambamadre (Monthly Discharge originally in m3|s) - Observed [m^3/s]	6/1/1967	11/1/1976	1.4%	0.78
Atbara	Atbara at Khasm el Girba (Monthly Discharge originally in Mm3) - Infilled [10^6m^3]	1/1/1965	6/1/1973	17.6%	0.87
Atbara	Atbara downstream of Khashm el Girba Dam	1/1/1977	6/1/1981	-13.0%	0.86
Atbara	Atbara at Kilo 3	1/1/1965	1/1/1980	-22.3%	0.77
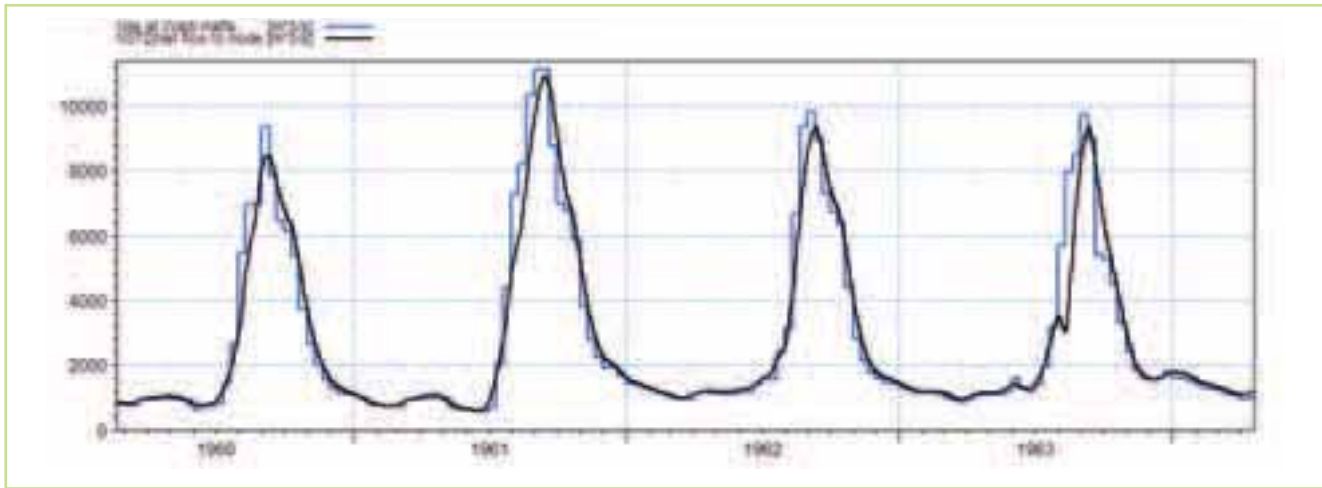
Figure 5.50 Observed (blue line) & simulated flow (black line) at Wadi Halfa

5.5.8 The Main Nile

The reach from Khartoum to Wadi Halfa is around 1,500 km long, where the only major tributary is the Atbara river.

The Main Nile is well described in a number of studies, where some of the main conclusions are:

- The main hydrological interest of this reach is in the time of travel, which varies according to flow, and the losses due to evaporation and irrigation.
- The travel times from Khartoum to Atbara were found to vary from 1 day at high levels to 5 days at low levels.
- The travel time from Atbara to Wadi Halfa, a distance of 1,170 km, was found to vary between 5 and 12 days.
- The evaporation losses are estimated to around 2.4 km³/year, or 76 m³/s on average
- The irrigation losses have increased from 0 In 1950 to around 1.1 km³/year in 1980. This is equivalent to 35 m³/s in 1980.
- The losses to evaporation and irrigation comprises of 2 to 4 % of the total flow.
- The Nile profile has a fall from around 360 meters at Atbara to around 110 meters at Wadi Halfa.

The overall conclusion is that the reach acts as a transmission channel conveying flow from Khartoum to Wadi Halfa with limited channel losses and irrigation abstraction.

5.5.8.1 Model development

The main purpose of the model is to describe the travel through the system and the losses to irrigation and evaporation.

The model is developed based on the following:

- The conveyance of water through the system is calculated using the linear reservoir routing with

a delay factor
- The irrigation losses are implemented based on the values from the NBI baseline model
- The losses to evaporation are added as a constant value throughput the year. The value reported in "The Hydrology of Nile" is used.

Figure 5.50 shows the observed and simulated flow at Wadi Halfa.

5.5.9 Egypt

The water demands for Egypt are described in Section 4.3. This section focuses on the operation of the High Aswan Dam and Lake Nasser.

The primary source of information on Lake Nasser operations is the 2005 Egypt National Water Plan (MWRI 2005). This has been supplemented with information from the PhD thesis of Amir Mohamed Akl Mobasher (2010).

The main operating rules governing the operation of High Aswan Dam and Lake Nasser are the following:

1. The surface elevation of Lake Nasser should be reduced to 175 m on August 1, which is considered the beginning of the flood season.
2. The maximum downstream release should not exceed 2,890m³/s.
3. When the surface elevation of Lake Nasser exceeds 178m, the volume of water above this level is spilled to the Toshka depression.
4. Downstream releases are reduced when storage in Lake Nasser is less than 60 E^{+9} m³ (~160m).

To implement the above rules and provide reservoir releases sufficient to meet downstream demands, the following implementation is made:

1. Downstream releases from Lake Nasser are generally controlled using hydropower timeseries

demands. The hydropower timeseries demands vary by simulation as follows:

- In the simulation used for model calibration and validation, the hydropower demand is set equal to the observed release downstream of the High Aswan Dam location. Lake Nasser began to fill in 1964 and hydropower operations began in 1967. From 1964 to 1967, the release from High Aswan is controlled using a minimum flow timeseries that is set equal to the observed flow downstream of High Aswan Dam. From 1967 until the end of the simulation period, the release from Lake Nasser is controlled using a timeseries of hydropower demand. The timeseries of hydropower demand is given in flow units (m^3/s).

- In the baseline and projected climate change simulation, demands have been set to equal estimates developed from the FAO Nile projection, as described in section 4.3. The hydropower demand at High Aswan dam is set equal to the sum of downstream demands: net water demand at "Upstream El Akhsas" plus gross water demand at "Downstream El Akhsas" minus return flow from the "Aswan" location.

2. Drought operations are simulated by reducing downstream releases when storage in Lake Nasser is less than 60 E^{+9} m^3. This allocation rule reduces hydropower demand in the following increments:

- If Lake Nasser storage is >55 E^{+9} m^3 and <60 E^{+9} m^3, hydropower demand is reduced by 5%.
- If Lake Nasser storage is >50 E^{+9} m^3 and <55 E^{+9} m^3, hydropower demand is reduced by 10%.
- If Lake Nasser storage is <50 $^{E+}9$ m^3, hydropower demand is reduced by 15%.

3. Flood operations are simulated by setting the flood release elevation of Lake Nasser to 178m in all months except July, when the flood release elevation is set to 175 m.

4. Spillway operations are now included, with the spillway characteristics set equal to those of the spillway to the Toshka depression. The bottom level of the spillway is set equal to 178m, and dimensions of the spillway capacity table are set equal to a Q-h relationship described in Mobasher (2010).

5. The diversion to hydropower from Aswan Dam is constrained to be less than or equal to 2890m^3/s. Because flood releases are routed to hydropower when excess capacity exists, this has the effect of constraining flood releases to 2890m^3/s unless the surface elevation reaches 178m, the bottom level of the spillway to the Toshka depression.

6. Spills from Lake Nasser are routed to the Toshka depression using a bifurcation node located downstream of High Aswan Dam. Of the total flow reaching the bifurcation node, all flows between 0 and 2890 m^3/s are routed to the Nile River, and all flows greater than 2890 m^3/s are routed to the Toshka depression. Because hydropower releases are constrained to be less than or equal to 2890m^3/s, this has the effect of routing all spills to the Toshka depression.

7. Return flow rules have been added for all demand locations. For the "Aswan" and "Upstream El Akhsas" locations, the return flow fraction is 47%, which is the return flow fraction given in the FAO Nile report (FAO 2011a). For the "Dowstream El Akhsas" location, a return flow fraction of 30% has been estimated. A smaller return flow fraction is used at this location because it covers a very large area (it is the largest demand location in the Nile basin), and it is likely that a considerable amount of water reuse takes place within the demand site. Reducing the return flow fraction for the "Downstream El Akhsas" location also reduces total demand at High Aswan demand to levels that are more in line with historical releases.

8. Because of technical constraints in MIKE BASIN/HYDRO, it is not possible to use a flood control level that is different from the spillway bottom level. This means that it is not possible to release water through hydropower for flood control and at the same time prevent spillway releases. There are some times in July when it is not possible to meet the 175m flood control target through HP releases alone without exceeding the 2890m^3/s downstream release limit. In these cases, water would be released using the spillway, as the spillway bottom level is assumed to equal the flood control level (even though the bottom elevation of the Toshka spillway is actually 178m). To prevent simulation of spills to the Toshka depression when the level of Lake Nasser is less that 178m, diversions to the Toshka depression (at the bifurcation node) are prevented during the month of July and unlimited HP releases (up to turbine capacity) are allowed during that month.

5.6 Results from the regional model

A regional hydrological model covering the entire Nile Basin was developed by linking together the calibrated models derived for each of the major sub-basins. The regional model was developed in MIKE HYDRO and the overall procedure was as follows:

- The calibrated sub-basin models (MIKE BASIN models) were exported into MIKE HYDRO

- The sub-basin models were joined at their boundaries, e.g. the Lake Victoria sub-basin model ends at Mongalla, where the Sudd model begins.
- The regional model was use to simulate flows in the Nile for the period 1960 to 1980 and the performance of the regional model was evaluated at 15 regional stations
- Minor parameter adjustments were made to the regional model in order to improve the performance at the regional stations.

One of the considerations made during development of the regional model was how to handle the deviations between observed and calibrated flow from the sub-basin models in the regional model. Considerable effort has been made to achieve the best possible calibration of the major sub-basin models based on the available information. There is the risk that if all the sub-models were to systematically under- or overestimate the flows, this bias would accumulate downstream and lead to significant errors. The strategy adopted here was to keep adjustments to the regional model to a minimum and to maintain the parameters developed during the calibration of the sub-models in the regional model. The argument being that having strived to obtain the best possible calibration any adjustments in the regional model would be inappropriate. Where limitations in the regional model are identified in this analysis the best approach would be to address these in future work based on new data and information in the appropriate sub-basin model.

To evaluate the overall performance of the model at the regional scale and the model performance in the different parts of the Nile Basin, the calibration results are assessed at selected regional key stations. For each station the following plots are shown:

- Hydrographs: The plots show a comparison between the simulated and observed discharges for the modelling period 1960 to 1980. Where possible the comparison is made on a daily basis, otherwise on a monthly basis.
- Mean monthly discharges: The plots show a comparison between the observed and simulated mean monthly discharges. The monthly mean value for the observed and simulated values. The mean monthly discharges are calculated for the period 1960 to 1980.
- Flow duration curves. The plots show a comparison between the observed and simulated flow duration curves for the modelling period 1960-1980 A flow duration curves ranks all the flows in a given period, from the lowest to the highest, where the rank is the percentage of time the flow value is equalled or exceeded. Flow duration curves are useful for evaluating the performance of a model and in particular how the model represents the flow regime and the different parts of the hydrograph.

The main goal is to ensure that the regional model captures both the flow dynamics (flow regime) and the flow magnitudes so that it can be used to assess the changes in flow in the Nile as a result of projected climate change. For this reason the changes in flow are assessed against model reference simulations in section 6 rather than the observations.

5.6.1 Semliki

The flow at Semliki represents the flow from Lake Edward and George. It also includes the entire flow from the Ruwenzori as well as the flow from the mountains in the Democratic Republic of Congo draining into Lake Edward and Lake Albert. As such the station is important for evaluating the flow from the western part of the Equatorial Lakes basin.

The data coverage and quality in this part of the model varies significantly. There is a good coverage of data in the Ugandan part of the area, i.e. the area draining into Lake Albert from the eastern side as well as the area draining into Lake George including the eastern side of the Rwenzori. On the other hand the coverage of discharge as well as hydro-climatic data is poor in that part of the area located within the DR Congo., i.e. the area south and west of Lake Edward, most of Semliki valley and the mountains west of Lake Albert.

The model generally provides a good representation of variation in the observed flows throughout the period, Figure 5.51. However, generally the simulated flows exhibit fewer fluctuations resulting in underestimation of the high flows and generally an overestimation of the medium to low flows (except the lowest flows), which is also reflected in the flow duration curves Figure 5.53. The model also provides a reasonable representation of the variation in the mean monthly flow with the main deviations appearing in January, February and June, Figure 5.52. Despite the reasonable model performance at Semliki, it is crucial for a better understanding of the hydrology in this area to improve the provision of data in the south-western part of the area located inside DR Congo. Similarly while there is a relatively good coverage in the Ugandan part of the area for the modelling period 1960-80, there is also a need to improve the present day monitoring in this area, including updating of the rating curves.
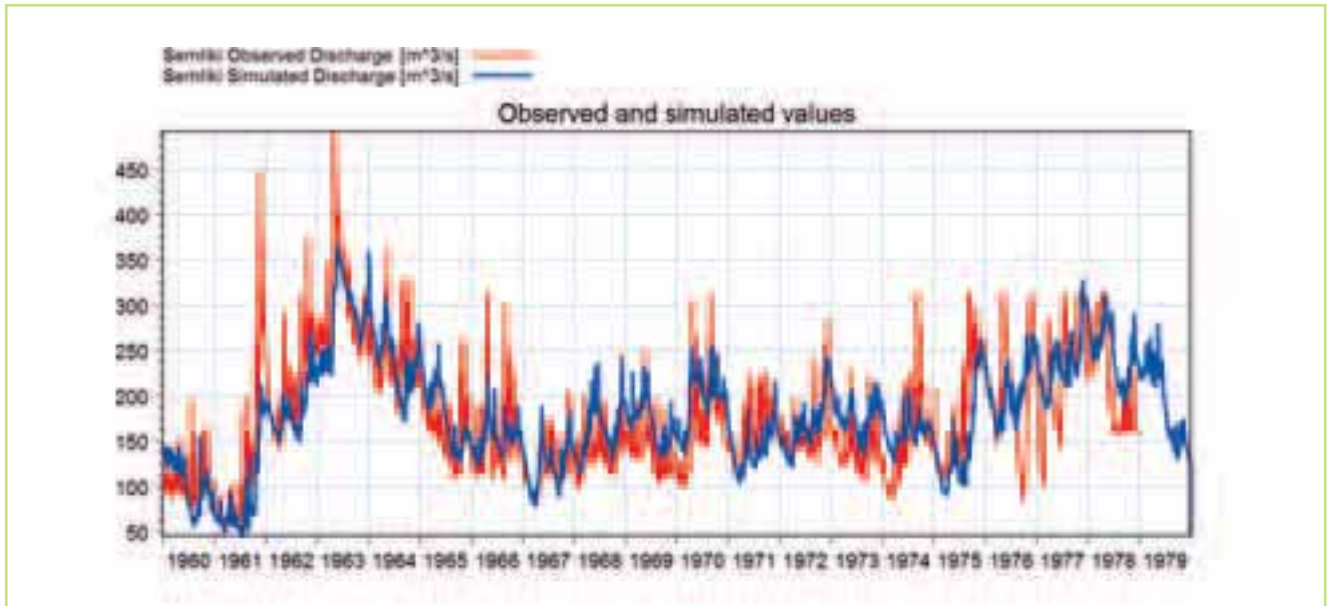
Figure 5.51 Comparison of the observed (red) & simulated (blue) flow hydrographs at the Semliki station for the period 1960-1980
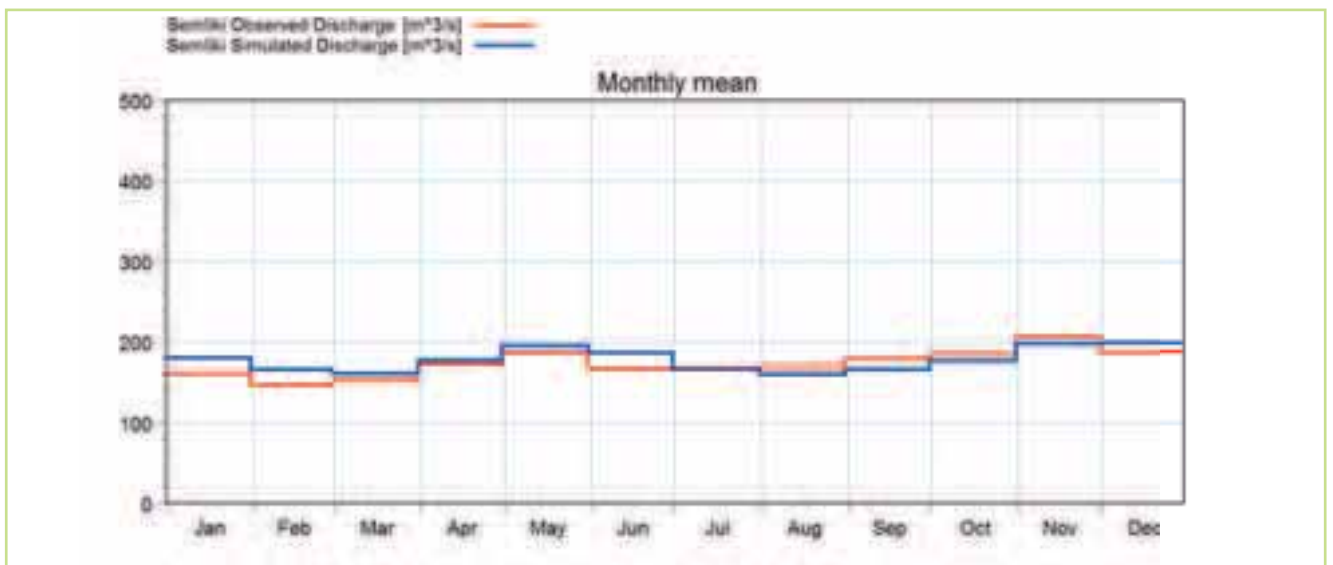
Figure 5.52 Comparison of the observed (red) & simulated (blue) mean monthly flows at the Semliki station for the period 1960-1980
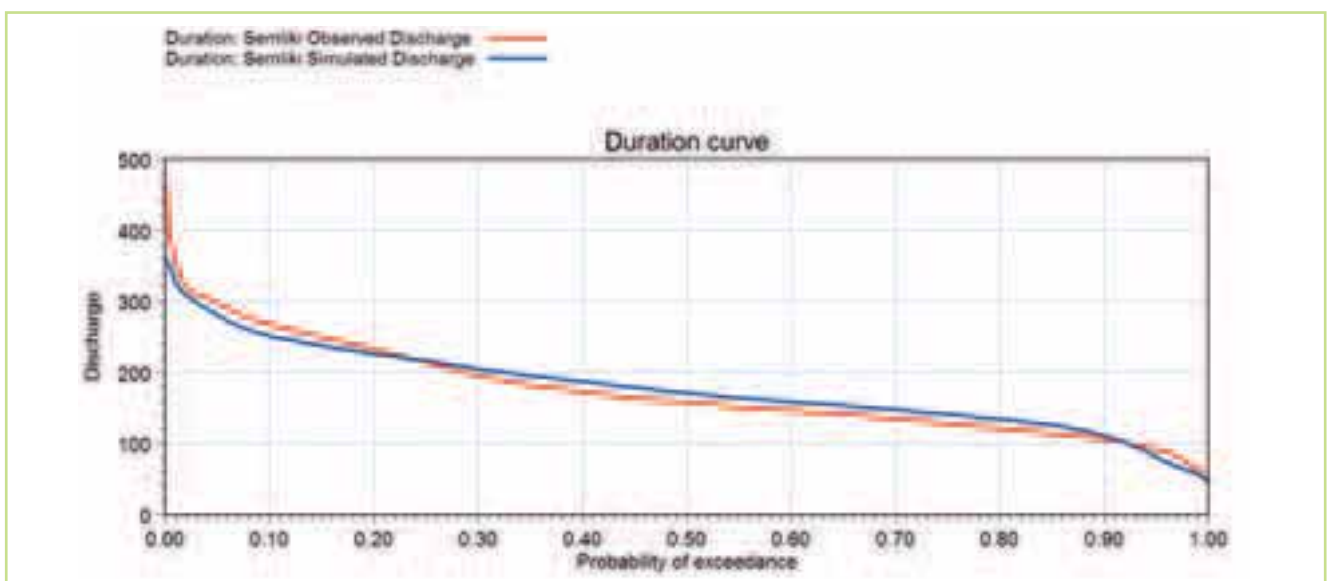
Figure 5.53 Comparison of the observed (red) & simulated (blue) flow duration curves at the Semliki station for the period 1960-1980

5.6.2 Lake Victoria (Water level)

Lake Victoria is represented as a lake-type reservoir in the MIKE BASIN hydrological model. The level-area-volume relationship is relatively well-defined. The so-called "agreed curve" is used as the rating curve which determines the relationship between the water level in the lake and the outflow from the lake. A comparison made prior to the calibration, showed good agreement between the actual measured outflow and outflow determined by the agreed curve from the water levels for the modelling period (1960-80). Following the NAM calibration of the catchments surrounding the lake, only minor calibration was needed when setting up the MIKE Basin model. As the flow data for the catchments around the lake appears to be reasonably good while the rainfall over the lake is less well known, some adjustments (+/-1-2% for a few years) were made to the estimated rainfall over the lake to improve the calibration, Figure 5.54.

The model is able to represent the monthly means with a deviation of only few centimetres, Figure 5.55. The highest error is seen during May and June where the highest water levels occur. The model is able to represent the increased water level during 1961 to 1964 and has a reasonable representation of the water level in the period after this event. The fact that the model is able to capture the increased water levels during 1961 to 1964 provides some confidence for using this model under projected climate change.
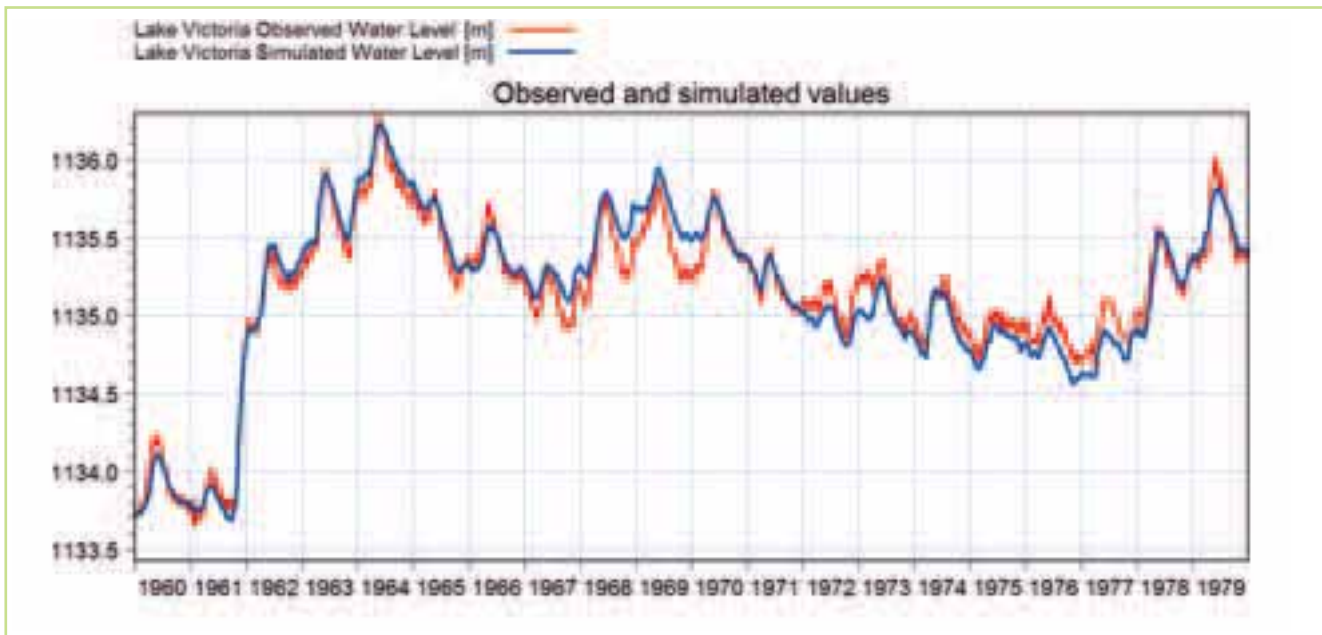
Figure 5 54 Comparison of the observed (red) & simulated (blue) water level hydrographs at the Lake Victoria station for the period 1960-1980
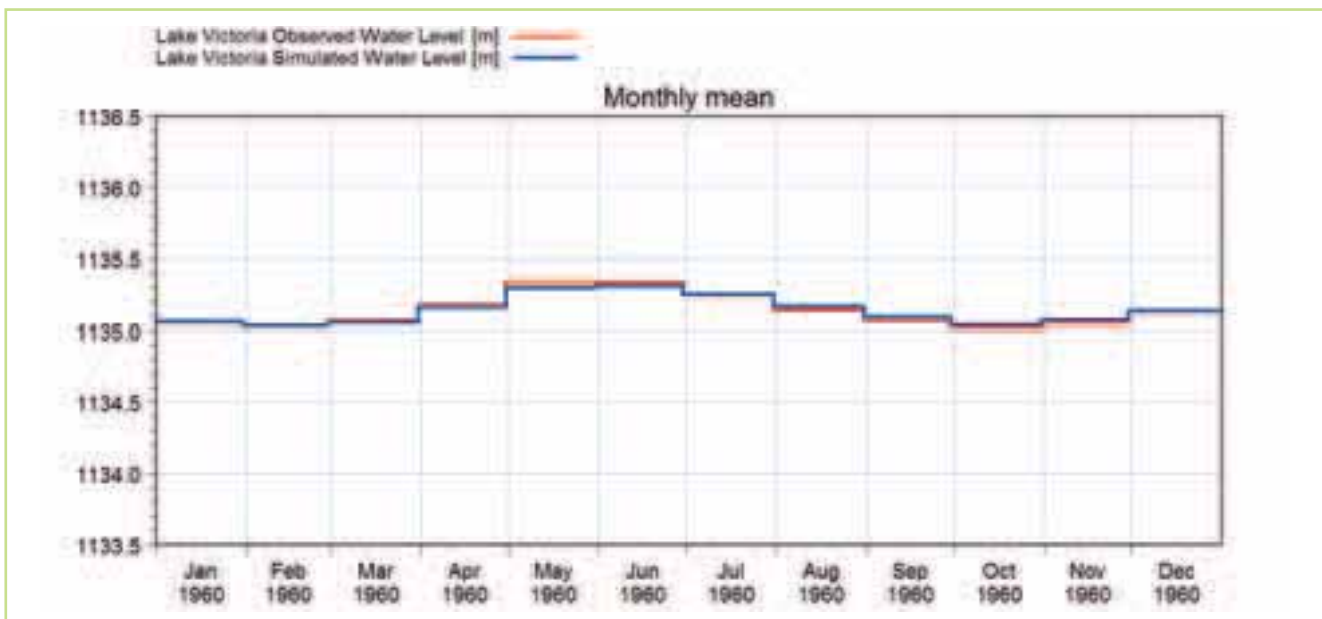
Figure 5.55 Comparison of the observed (red) & simulated (blue) mean monthly water levels at the Lake Victoria station for the period 1960-1980

5.6.3 Lake Kyoga (Water level)

Lake Kyoga is represented in the same way as Lake Victoria in the hydrological model, i.e. as a lake-type reservoir. The inflow from the Victoria Nile and the local catchments primarily east and north-east of the lake that drain into Lake Kyoga are represented in this part of the model. While the well-defined "agreed-curve" was used for Lake Victoria, the rating curve for the outflow from Lake Kyoga is less well-defined and fitting of this rating curve was part of the calibration of the lake.

The model is able to represent the monthly means with a deviation of a few centimetres, Figure 5.57. In examining the water level hydrograph, the model is generally able to capture the variation in the observed water levels including the increased water level during the period 1961 to 1964, with the exception of 1962 where the water level is under-estimated, Figure 5.56. For the remaining period the model gives a reasonable representation of the water level. The deviations for the mean monthly water levels are generally less than 10 centimetres, so the ability of the model to represent the observed water level is considered reasonable.
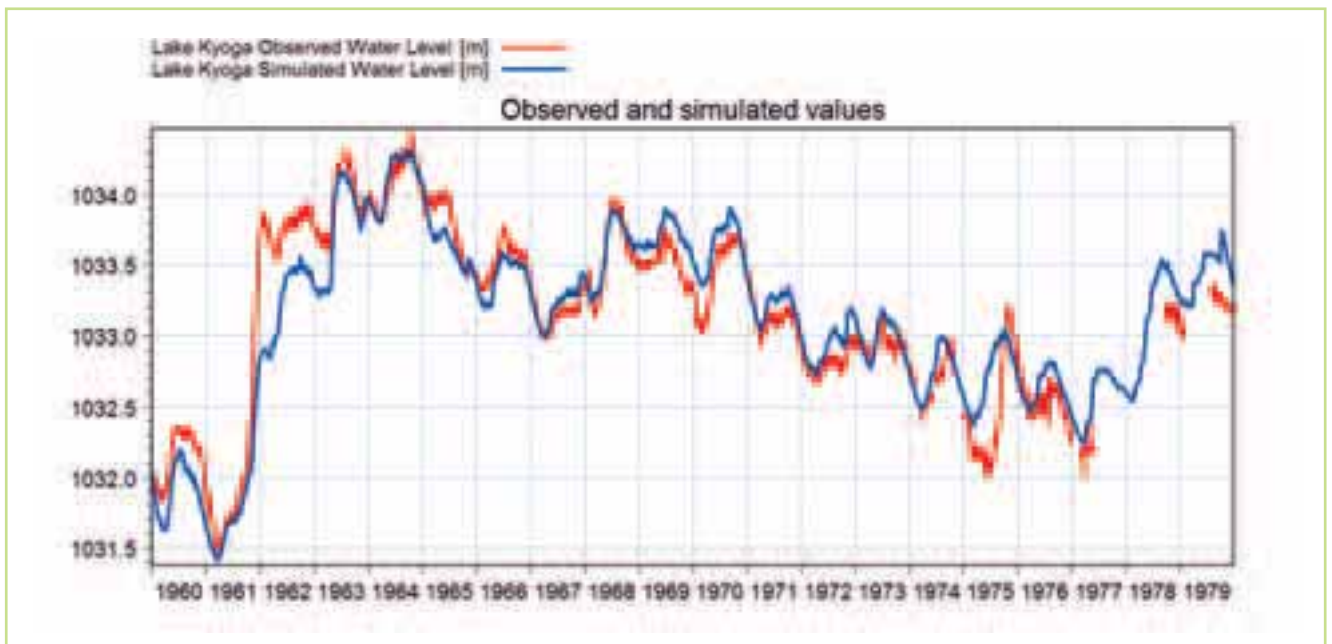
Figure 5.56 Comparison of the observed (red) & simulated (blue) water level hydrographs at the Lake Kyoga station for the period 1960-1980
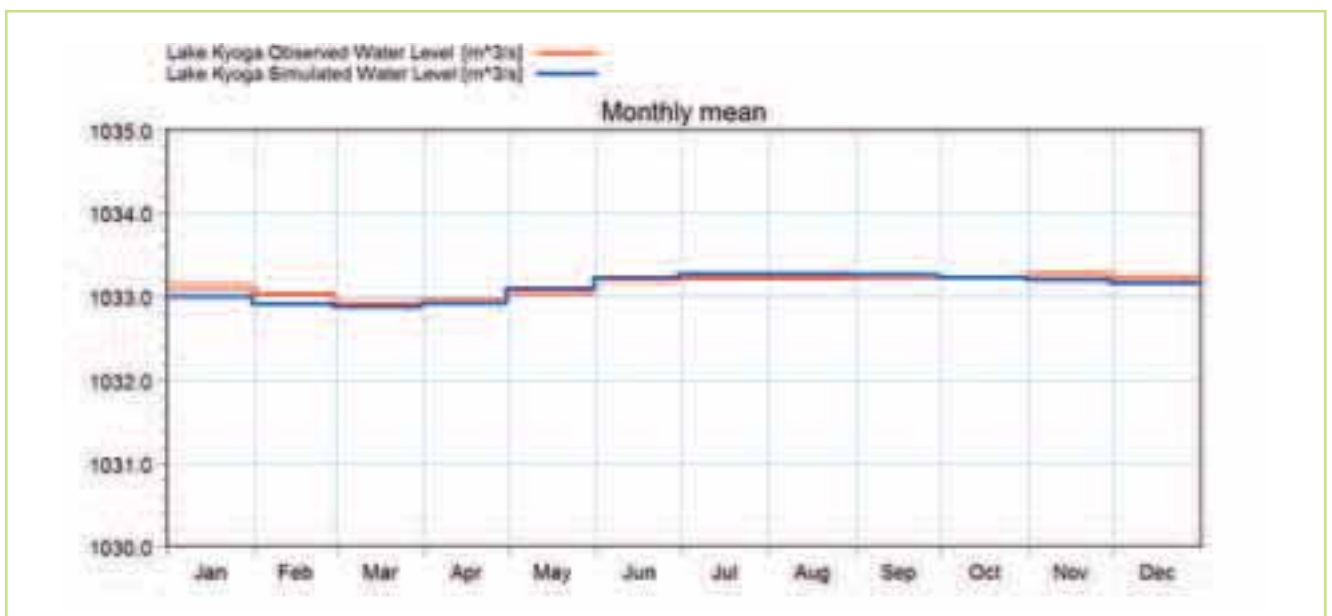
Figure 5.57 Comparison of the observed (red) & simulated (blue) mean monthly water levels at the Lake Kyoga station for the period 1960-1980

5.6.4 Jinja

The flow at Jinja represents the outflow from Lake Victoria and is one of the key stations in the basin. The outflow at Owens dam is calculated using a rating curve where the outflow from the lake is a function of the water level in the lake. With the construction of the Owens Falls Dam it was agreed that the releases from the Dam should follow the old rating curve the so-called "Agreed Curve". This rating curve is used in the model as mentioned earlier.

The model provides a good representation of the variation in the observed outflow including the major increases in the outflow during 1961-64, which is not surprising considering the good agreement between the simulated and observed water levels for the lake and the fact that the outflow is determined by the agreed curve, Figure 5.58. The main deviation in 1969-70 is due to the fact that the actual outflow during this period does not follow the agreed curve so well. When comparing the observed and simulated mean monthly discharge, it appears that the model tends to slightly overestimate the outflow from Lake Victoria, especially for the months of April, November and December, Figure 5.59. However, since the model follows the agreed curve and the actual outflow deviates slightly from the agreed curve for shorter periods only, the simulated outflow is reasonable, and gives confidence in the model's ability to represent the outflow from Lake Victoria.
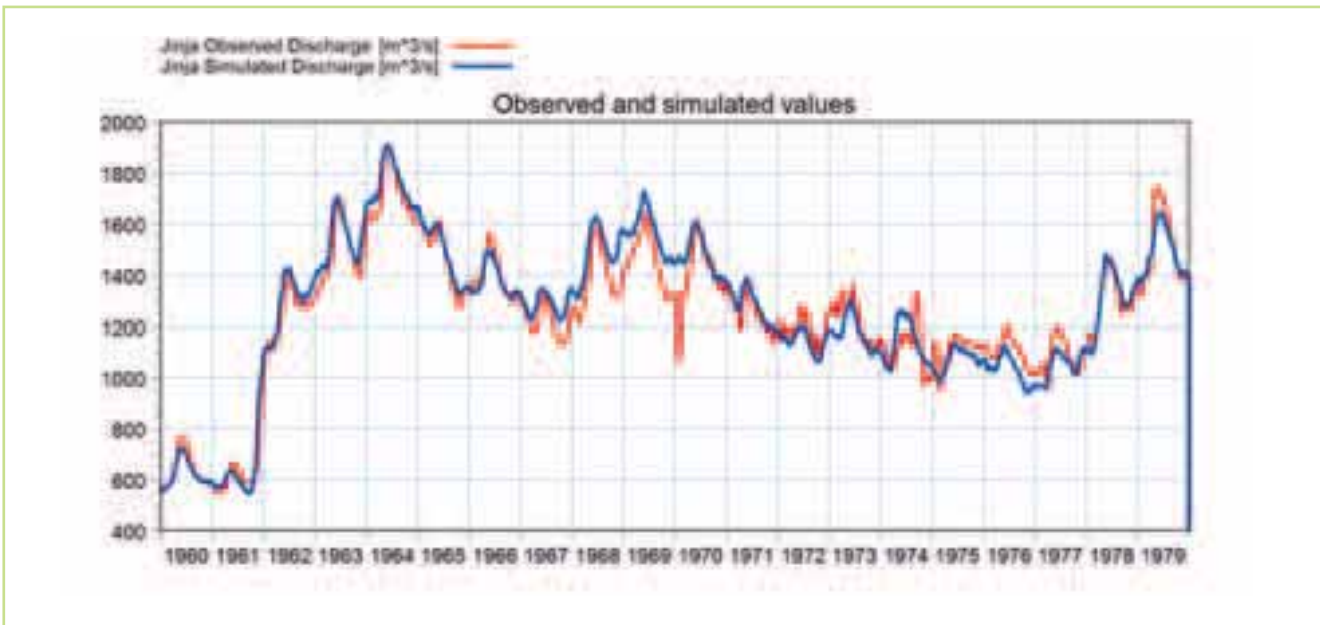
Figure 5.58 Comparison of the observed (red) & simulated (blue) flow hydrographs at the Jinja station for the period 1960-1980

Figure 5.59 Comparison of the observed (red) & simulated (blue) mean monthly flows at the Jinja station for the period 1960-1980.
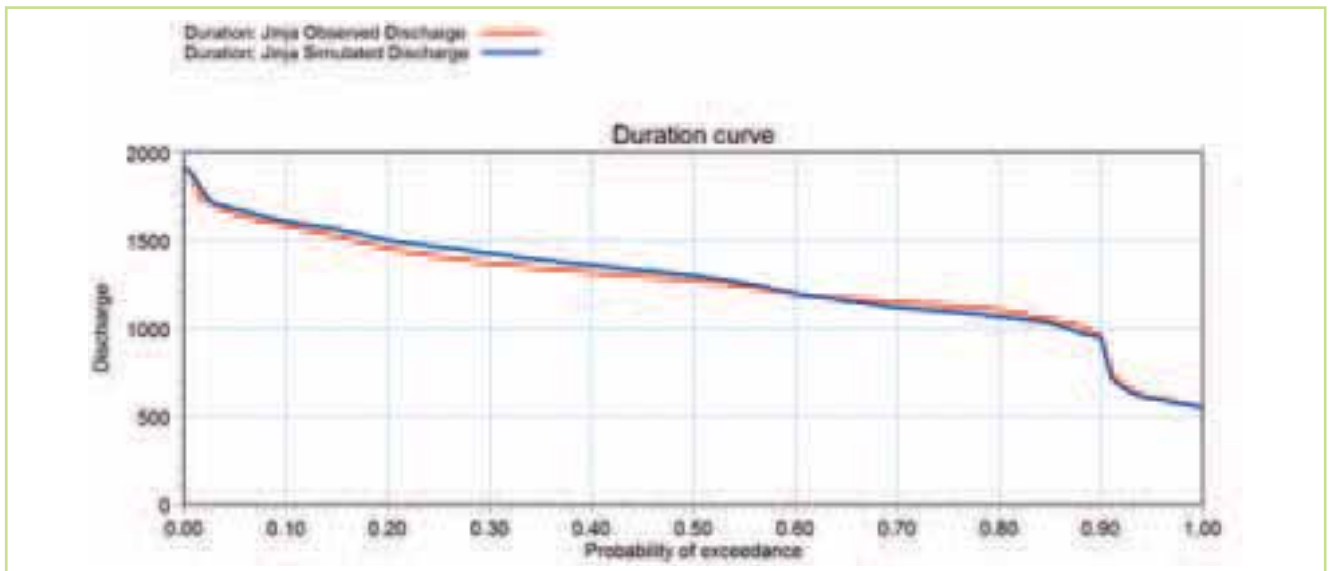
Figure 5.60 Comparison of the observed (red) & simulated (blue) flow duration curves at the Jinja station for the period 1960-1980

5.6.5 Kamdini

The Kamdini station represents the flow from Lake Kyoga, Lake Victoria and the Kafu catchment. Kamdini is one of the most important stations on the Kyoga Nile and substantial effort was put into detailed checking and gap-filling of the observed time series based on the information from Masindi Port and other stations on the Kyoga Nile.

As for the outflow from Lake Victoria at Jinja, the model generally provides a reasonable representation of the variation in discharge over the modelling period. The model slightly overestimates the flow during most of the flow events with 1961-63 being and exception which corresponds to the period with underestimation of the water level in Lake Kyoga, Figure 5.61.

The model gives a reasonable representation of the mean monthly discharge during most of the year,

with the largest deviations occurring from April to August, Figure 5.62. The slight overestimation of the flow at Kamdini is also reflected in the comparison of the flow duration curves where the simulated discharge is slightly higher than the observed discharge for almost the whole flow regime, Figure 5.63. The likely reason for these deviations is the lack of good quality discharge data for a major part of the catchments draining into Lake Kyoga. This is caused in part by the existence of large wetland areas around the lake which complicates both the understanding of the hydrology in the area and makes it a challenge to set up good quality river gauging stations. To improve the model representation in this area an improved hydrometric network and a better understanding of the hydrological impact of the wetland area is required.
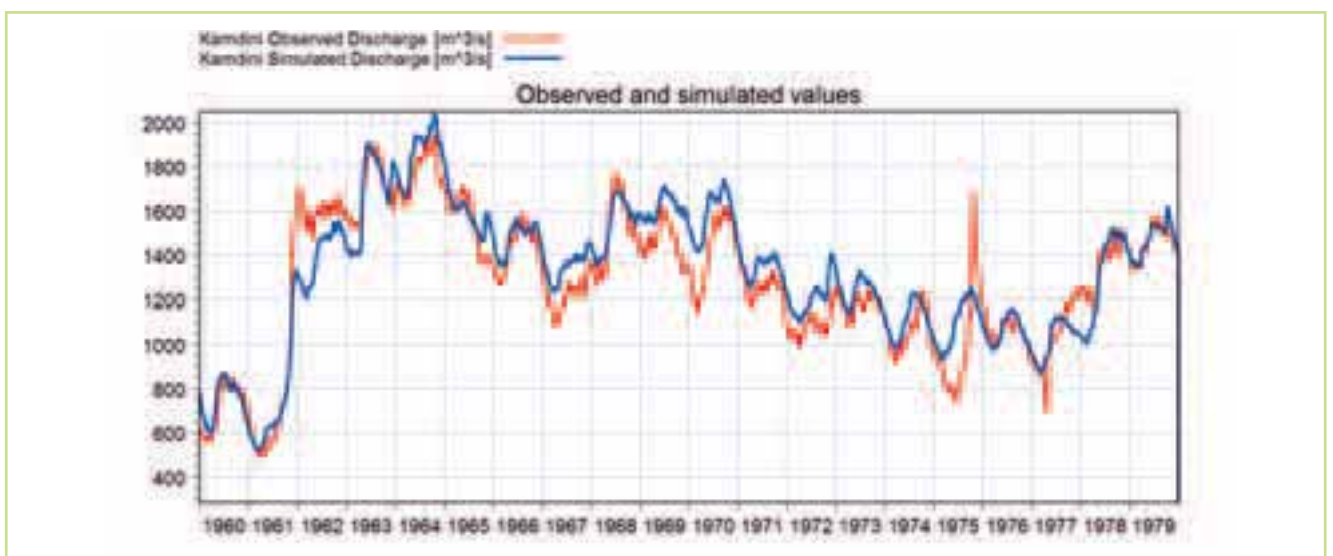
Figure 5.61 Comparison of the observed (red) and simulated (blue) flow hydrographs at the Kamdini station for the period 1960-1980

Figure 5.62 Comparison of the observed (red) & simulated (blue) mean monthly flows at the Kamdini station for the period 1960-1980
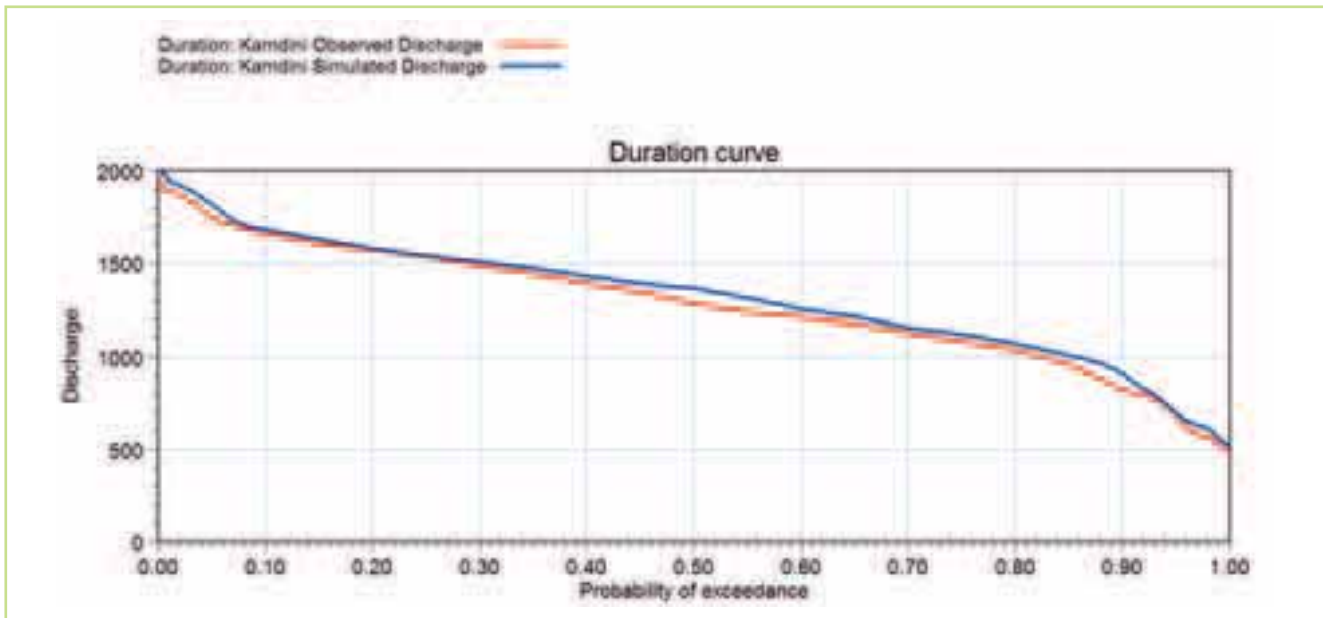
Figure 5.63 Comparison of the observed (red) & simulated (blue) flow duration curves at the Kamdini station for the period 1960-1980

5.6.6 Mongalla

The flow at Mongalla station represents the total outflow from the Equatorial Lakes basin. Thus, it also represents the outflow from the Lake Victoria sub-model and the inflow to the Sudd sub-model.

The model gives a reasonable representation of the variation in the observed flow in the model period. A few larger deviations exist, including an under-estimation of the flows for part of 1975-77.

Examining the mean monthly flow as well as the flow duration curve, there is a good agreement between the simulated and observed discharge. In fact the flow duration curves for observed and simulated flows are very similar except at the low flows. In general, it is our evaluation that the regional model provides a reasonable representation of the dynamics and magnitude of the flow for the Equatorial Lakes basin.
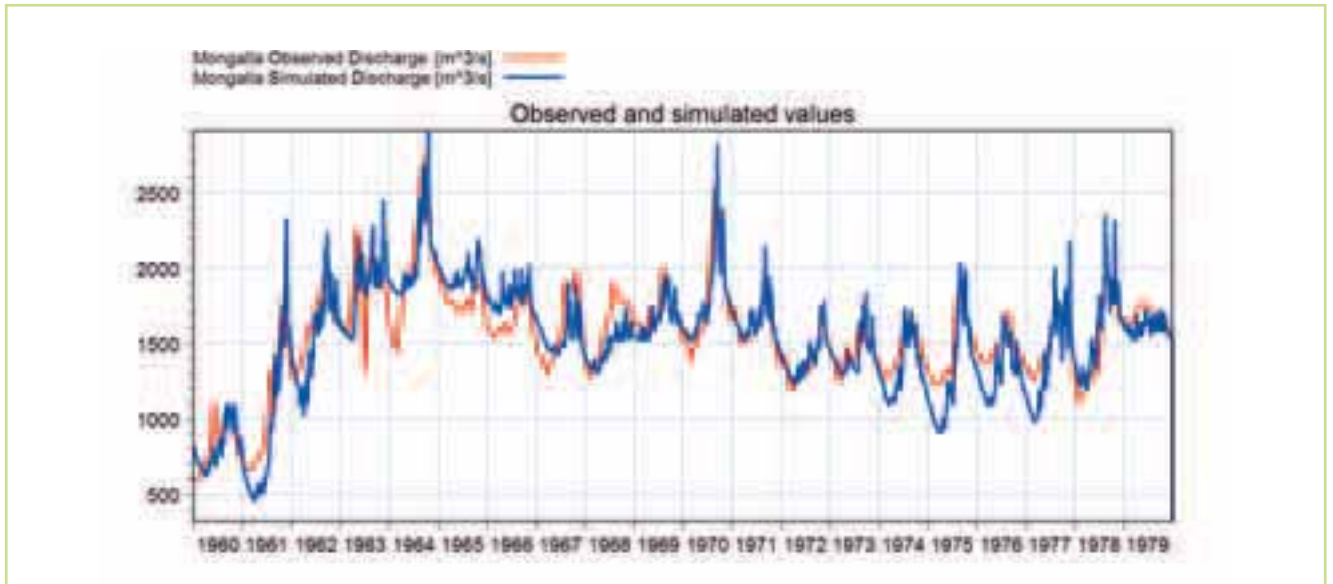
Figure 5.64 Comparison of the observed (red) & simulated (blue) flow hydrographs at the Mongalla station for the period 1960-1980
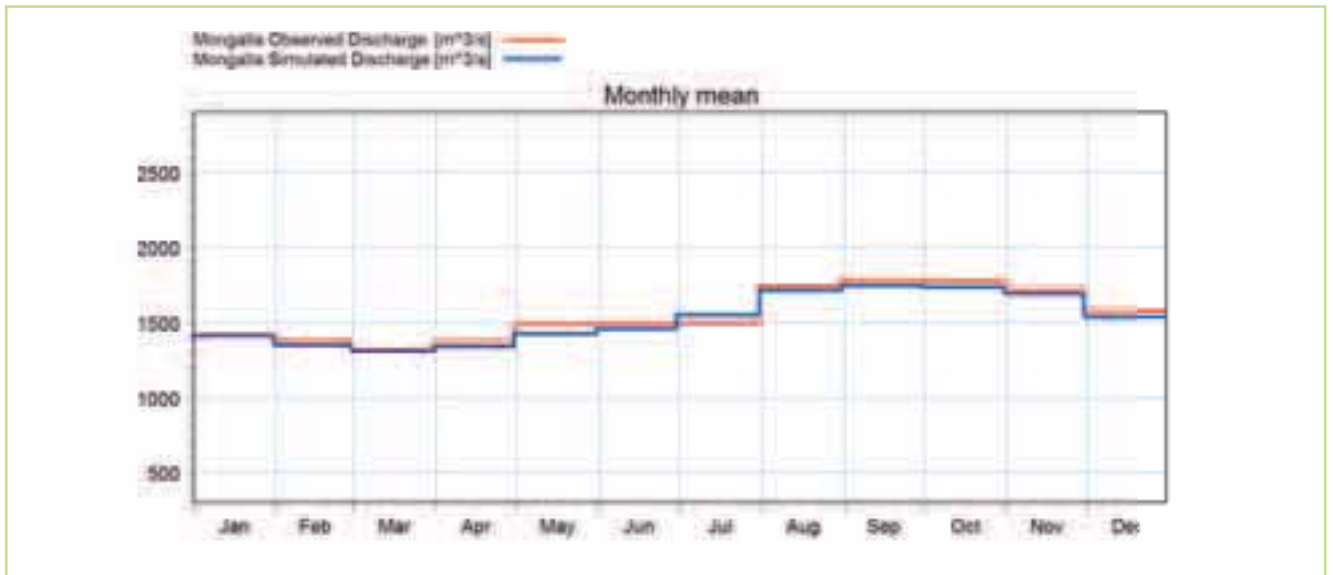
Figure 5.65 Comparison of the observed (red) & simulated (blue) mean monthly flows at the Mongalla station for the period 1960-1980
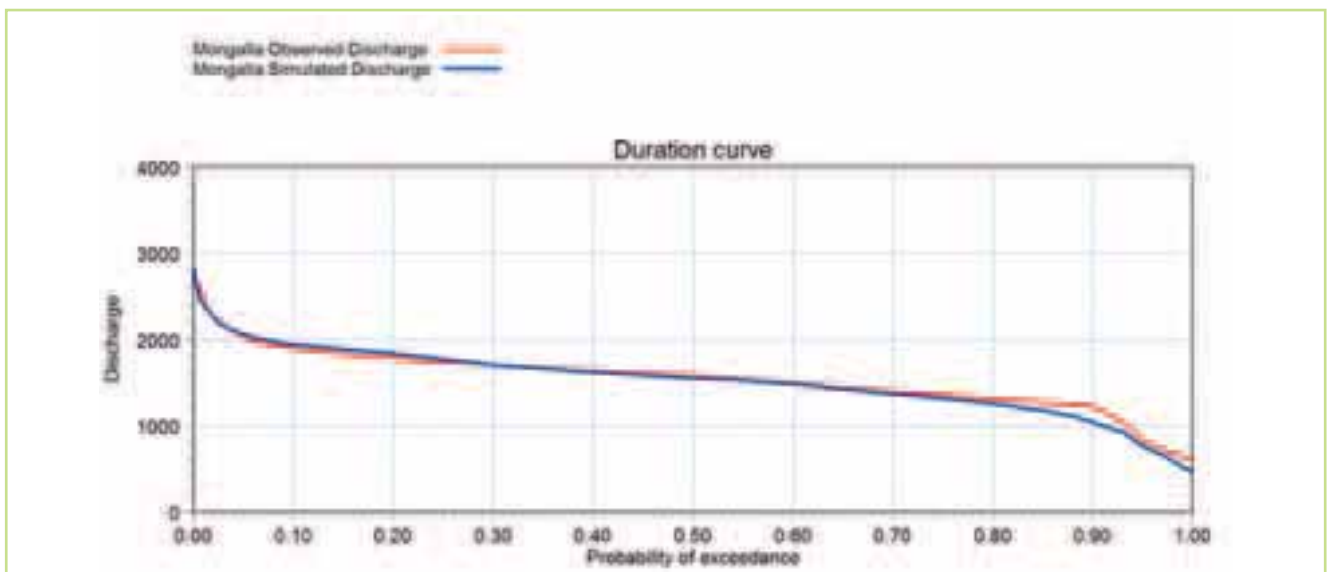
Figure 5.66 Comparison of the observed (red) & simulated (blue) flow duration curves at the Mongalla station for the period 1960-1980

5.6.7 Buffalo Cape

The Buffalo Cape station is located in the Bahr el Jebel, just upstream of Lake No, South Sudan, and represents the fraction of the flow through the Sudd that is not flowing in the Bahr el Zeraf. The flow through the Bahr el Zeraf is around 30 % of the flow in the Bahr el Jebel, (Shahin, 1985).

This station was included in this analysis despite the limited quality and quantity of observed data because it is one of the few stations that could provide information about flows within the Sudd and the potential effects of climate change. It is difficult to determine any seasonal variation in the flow at the Buffalo Cape station from this period of record and there is a large period of missing data from 1965-1971. The increased discharges from the Lake Victoria region (during the 1961 to 1964) appear to have limited impact. While this might suggest that any climate change in the Lake Victoria region has a limited impact on the downstream flow regime but it is difficult to make any conclusions given the amount of missing flow data.

At present the best that can be said is that the model simulates the order of magnitude of the flows for the Buffalo Cape station. Published data from Sutcliffe and Parks (1999) for 1927-37 show flows of approximately 500 m³/s (450-550), with seasonal variations of up to 5%. Additional discharge observations in this region are required if the model is to better represent the complex hydrology of the Sudd and thereafter assess the potential impacts of climate change. Nevertheless we have chosen to retain this station in our analysis in order to provide some preliminary conclusions on the impact of climate change on the Sudd.
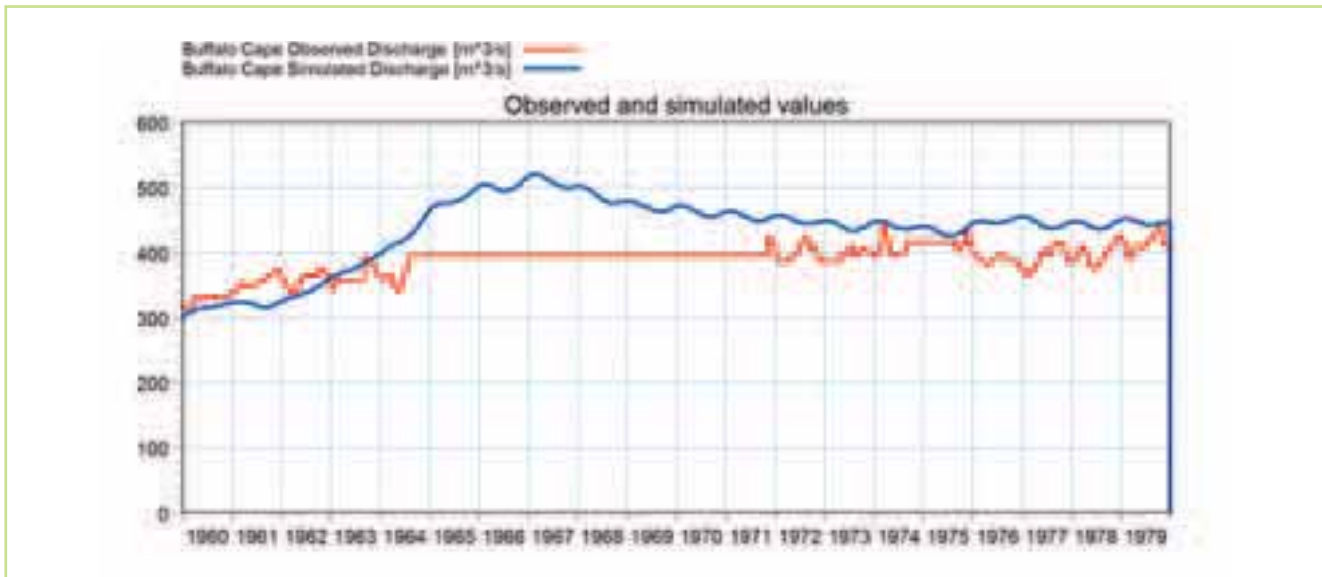
Figure 5.67 Comparison of the observed (red) & simulated (blue) flow hydrographs at the Buffalo Cape station for the period 1960-1980
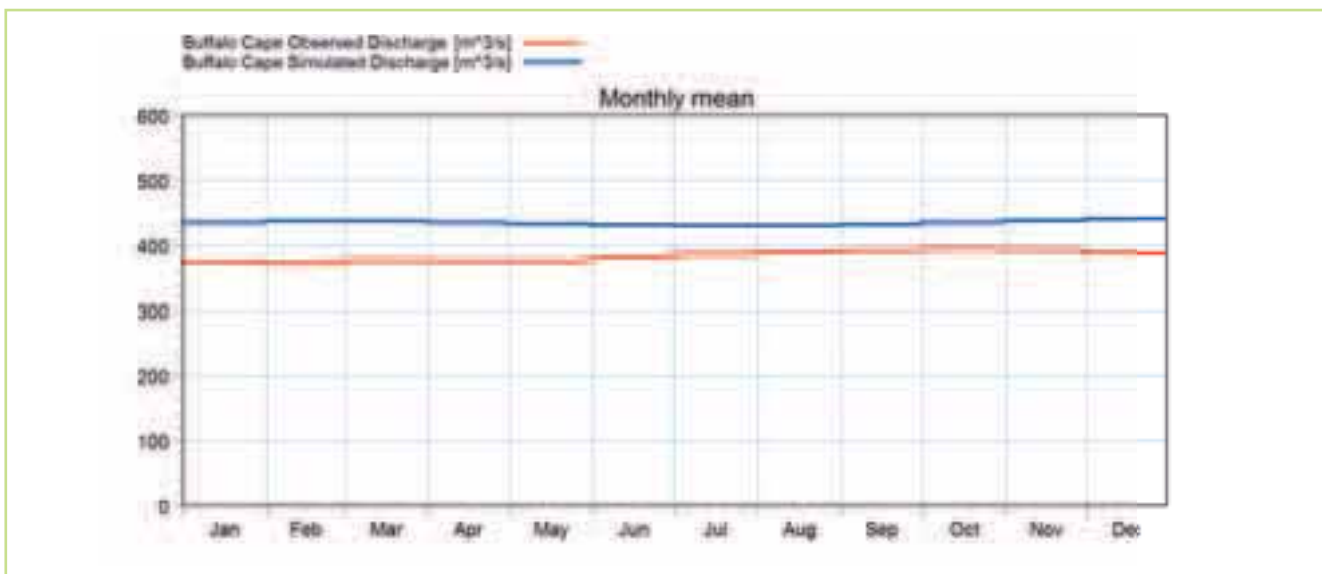
Figure 5.68 Comparison of the observed (red) & simulated (blue) mean monthly flows at the Buffalo Cape station for the period 1960-1980
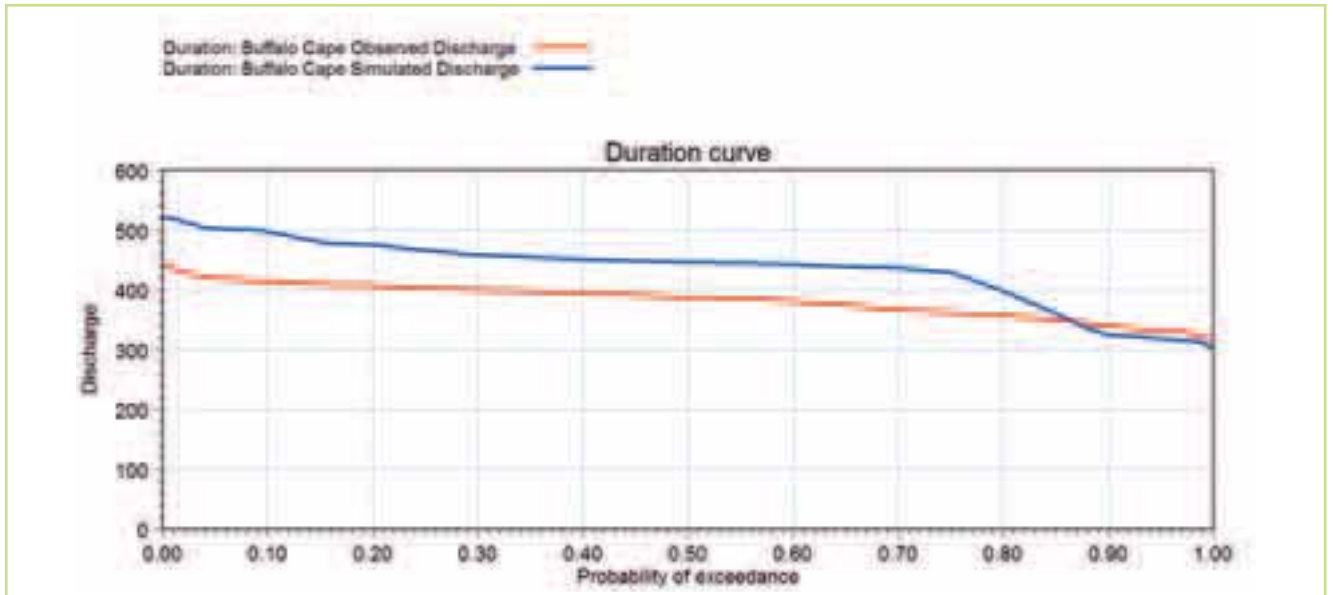
Figure 5.69 Comparison of the observed (red) & simulated (blue) flow duration curves at the Semliki station for the period 1960-1980

5.6.8 Sobat

The Sobat is a tributary of White Nile which connects with the White Nile at Malakal and it contributes an important part of the total flow in the White Nile. The flow from the Sobat has the same order of magnitude as the flow from the Sudd but in contrast to the Sudd the flow from Sobat is highly variable.

The Sobat has the Baro and the Pibor as the largest tributaries. The Baro (41 400 km2) drains an area of the Ethiopian mountains east of Gambeila rising to peaks of 3300 m. The Pibor (109 000 km2) receives the Gila and Akobo from the mountains south of the Baro basin, but also drains a wide area of the plains east of the Bahr el Jebel.

Figure 5.70 shows a comparison between the observed and simulated discharge at Sobat just upstream of the confluence with the White Nile. The model has a reasonable representation of the flow from the Baro basin, which represents the main part of the baseflow at the Sobat station. The peak flow originates mainly from the Pibor basin, and due to very poor data in this area (the model is calibrated against data from the 1930's), the model has a poor representation of the flow from the Pibor basin. This can be seen at the Sobat station where there are deviations between the observed and simulated during the peak flows, while the low-flow values are represented reasonably well.
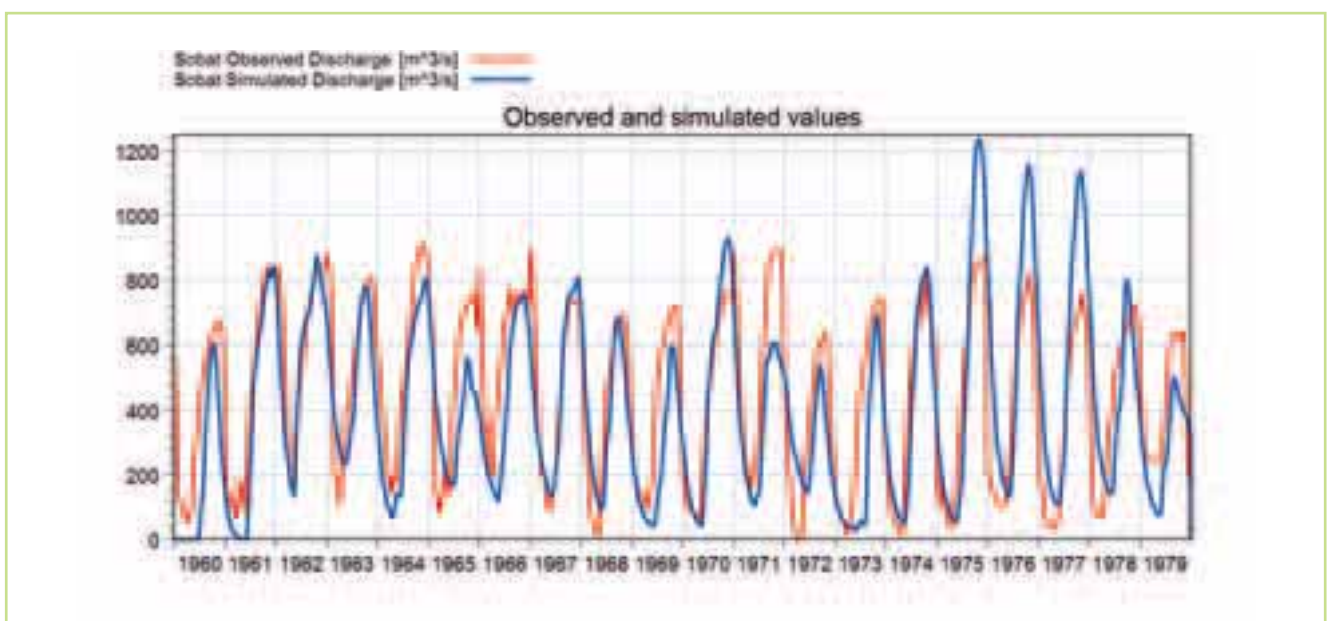
Figure 5.70 Comparison of the observed (red) & simulated (blue) flow hydrographs at the Sobat station for the period 1960-1980

Figure 5.71 Comparison of the observed (red) & simulated (blue) mean monthly flows at the Sobat station for the period 1960-1980
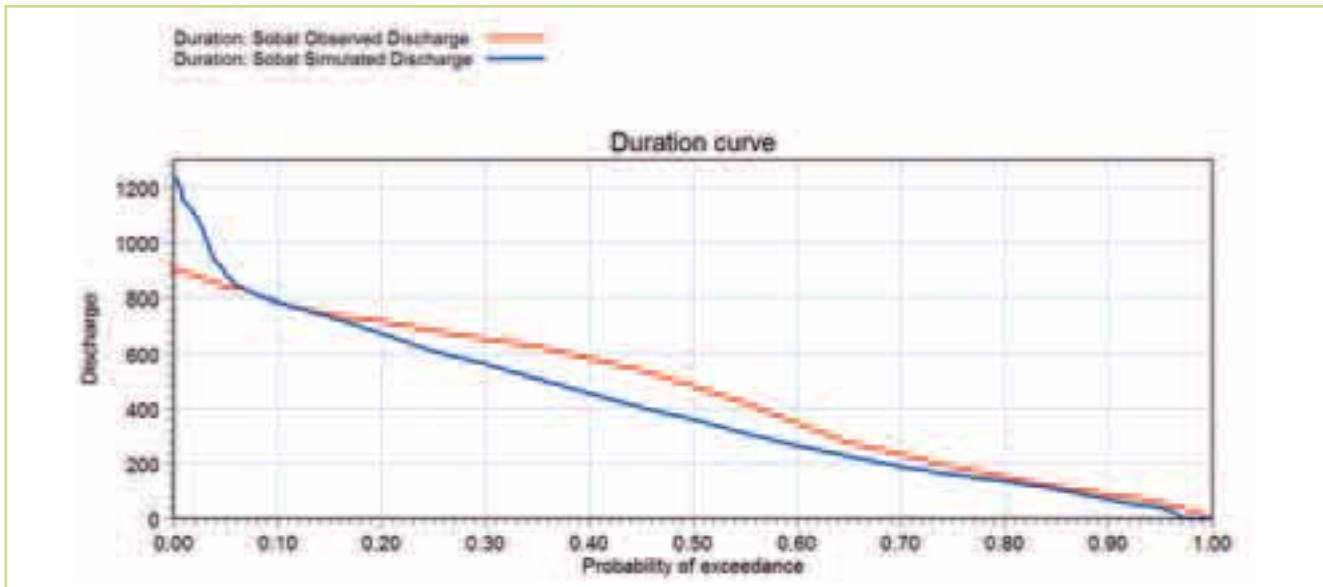
Figure 5.72 Comparison of the observed (red) & simulated (blue) flow duration curves at the Sobat station for the period 1960-1980

The model has a reasonable representation of the monthly average values during the dry period, where most of the flow originates from the Baro basin, while the model has a poor representation during transition to the wettest months. Further information from the Pibor basin, both climate and discharge information, could significantly improve the representation of the flow from this basin.

5.6.9 Malakal

The station at Malakal is a key station as the flow at this location represents the sum of the flows from the Sudd together with the Sobat, and Bahr el Ghazal tributaries.

While the overall behaviour of the model is reasonable the peak flows are consistently under-estimated in the period 1963-5, Figure 5.73,

indicating additional inflows unaccounted for in the model. This corresponds to the very wet period seen in the Equatorial Lakes region.

The Sobat is the main contributor to the total flow at Malakal (during the peak months) and it would be expected that such a significant increase in the discharge peaks at Malakal would result from elevated runoff in the Sobat region; however, the discharge peaks at the Sobat flows do not increase by the same magnitude as observed at Malakal. The good agreement between the observed and simulated discharges at Sobat during the same period suggests that this cannot be the cause of the deviations.

The Bahr el Ghazal is unique among the Nile tributaries in that its outflow to the White Nile is almost negligible as a result of evaporation losses from the swamps at the lower end of the basin (Sutcliffe and
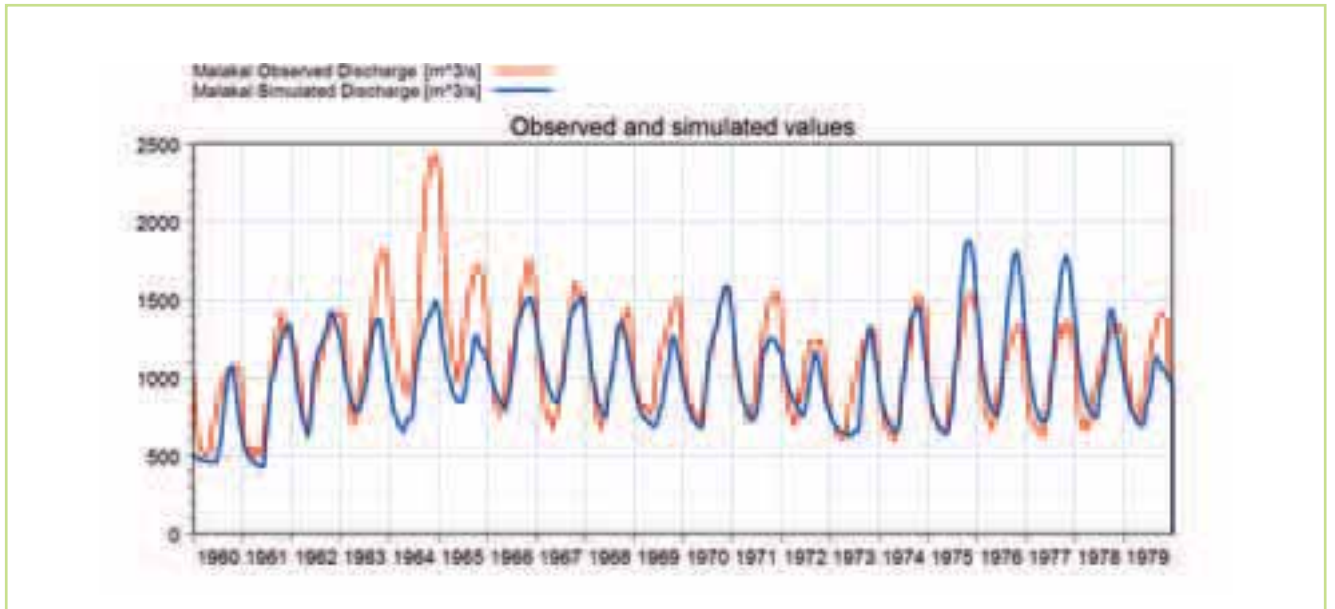
Figure 5.73 Comparison of the observed (red) & simulated (blue) flow hydrographs at the Malakal station for the period 1960-1980
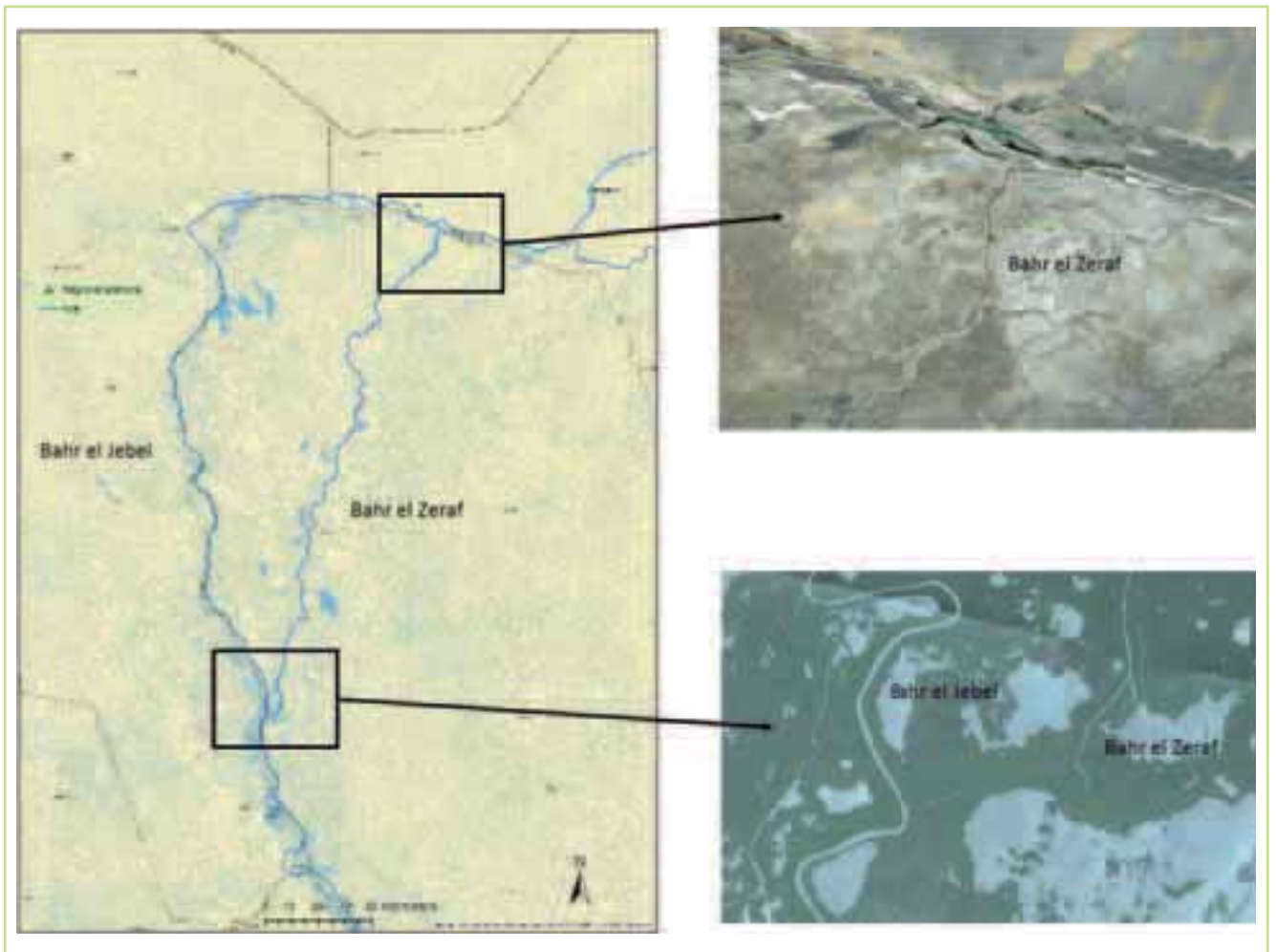
Figure 5.74 Location of Bahr el Zeraf with GOOGLE Earth images of the inlet & outlet to the Bahr el Jebel.

Parks, 1999). For this reason the Bahr el Ghazal basin is not included in the regional model. One possible explanation is that during the same period unusually heavy rainfall in the Bahr el Ghazal led exceptionally to outflows from the basin into the White Nile.

An alternative explanation may be that this is caused by how the Sudd is described in the model. The simulations of the flows at Buffalo Cape are highly uncertain given the quality and quantity of the measured discharge. However it is expected that the order of magnitude is correct and that the significant increase in the flow, observed at Malakal, does not originate from the Bahr el Jabel upstream of the Buffalo Cape station.

The Bahr el Zeraf diverges from the Bahr el Jebel about 200 km downstream of Bor and re-joins the main river, about 100 km downstream of Lake No,

Figure 5.74. The Bahr el Zeraf is connected to the Bahr el Jebel through a channel, where a part of the flow in Bahr el Jebel is diverted. Previous work (Shahin, 1985) suggests that approximately 30 percent of the flow during peak water levels runs through the Bahr el Zeraf and approximately 70 percent runs through the Bahr el Jebel. This percentage may vary however while this will changes the dynamics it is not expected to impact the water balance.

However in this portion of the model the rainfall-runoff processes are highly simplified. The swamps are represented as reservoirs and only direct rainfall on the estimated swamp area and evaporation are used in the water balance. If additional rainfall falls over this area for the period 1963-65 and increases the swamp area, this might also explain part of the missing water volume.
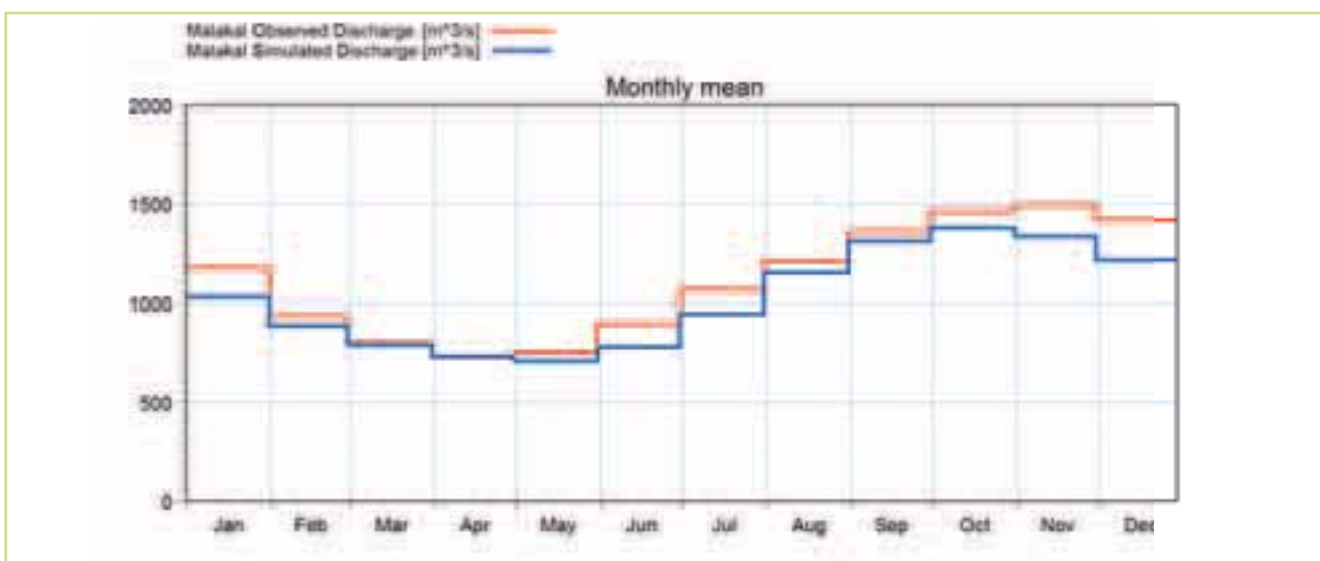
Figure 5.75 Comparison of the observed (red) & simulated (blue) mean monthly flows at the Malakal station for the period 1960-1980
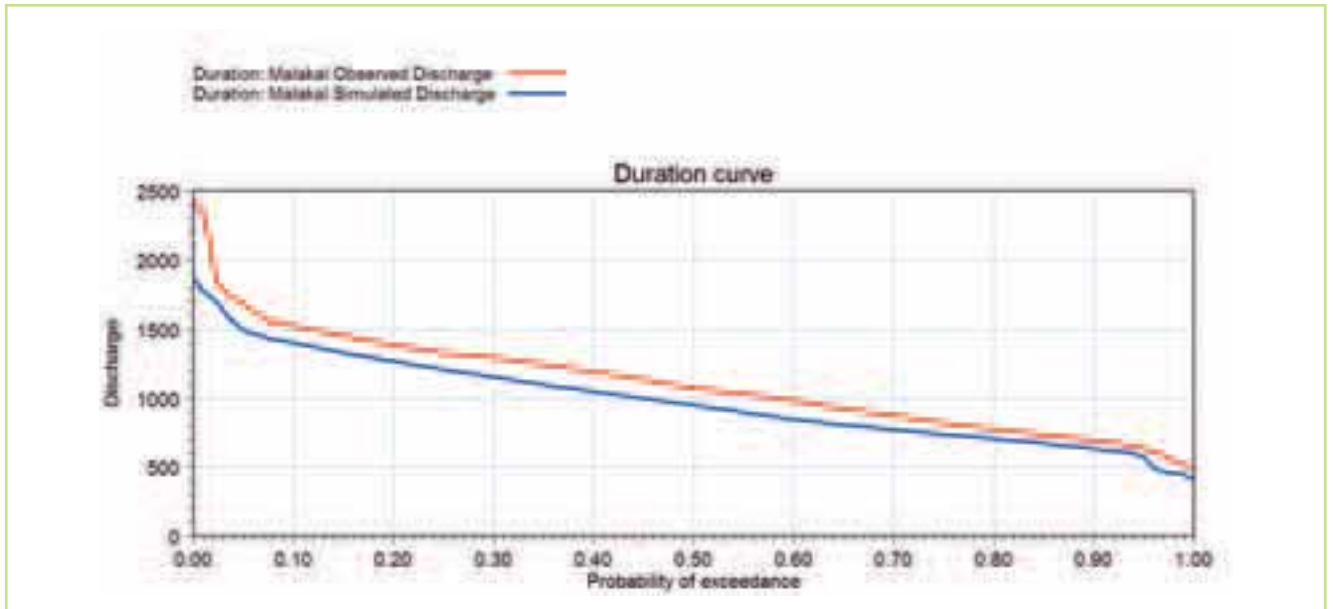
Figure 5.76 Comparison of the observed (red) & simulated (blue) flow duration curves at the Malakal station for the period 1960-1980

5.6.10 Jebel Aulia

The outflow of the White Nile is controlled by the Jebel Aulia Reservoir which was built to prolong the natural White Nile recession for irrigation downstream. Examining the performance of the model at this station we find:

- The model captures the trends in the observed hydrograph well, and both the low and high periods are captured.
- There are deviations from the observed hydrograph throughout the period, which is also

reflected in the comparison of the mean monthly discharge. This is probably arises from differences in the actual flood control operations from those used in the model.

- In general the model captures the outflow from Jebel Aulia reasonably well including a good match between the observed and simulated flow duration curves for most of the flow regime. Therefore it is considered acceptable for use in the climate scenarios.
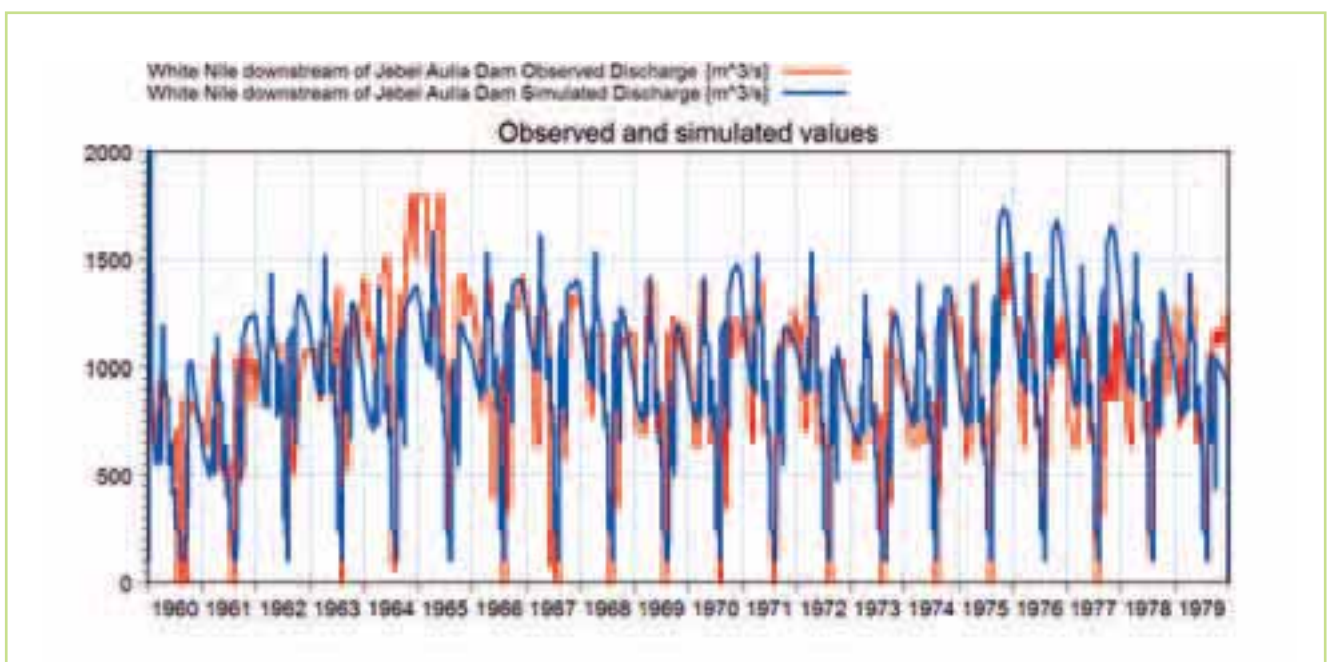
Figure 5.77 Comparison of the observed (red) & simulated (blue) flow hydrographs at the Jebel Aulia station for the period 1960-1980
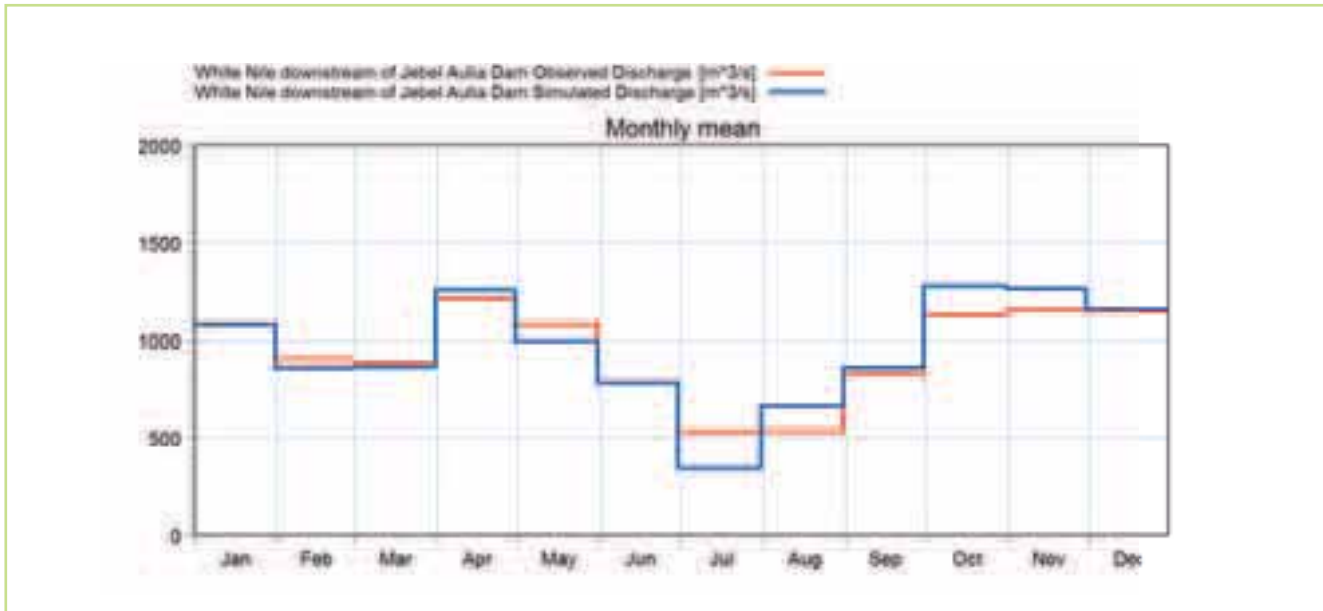
Figure 5.78 Comparison of the observed (red) & simulated (blue) mean monthly flows at the Jebel Aulia station for the period 1960-1980.
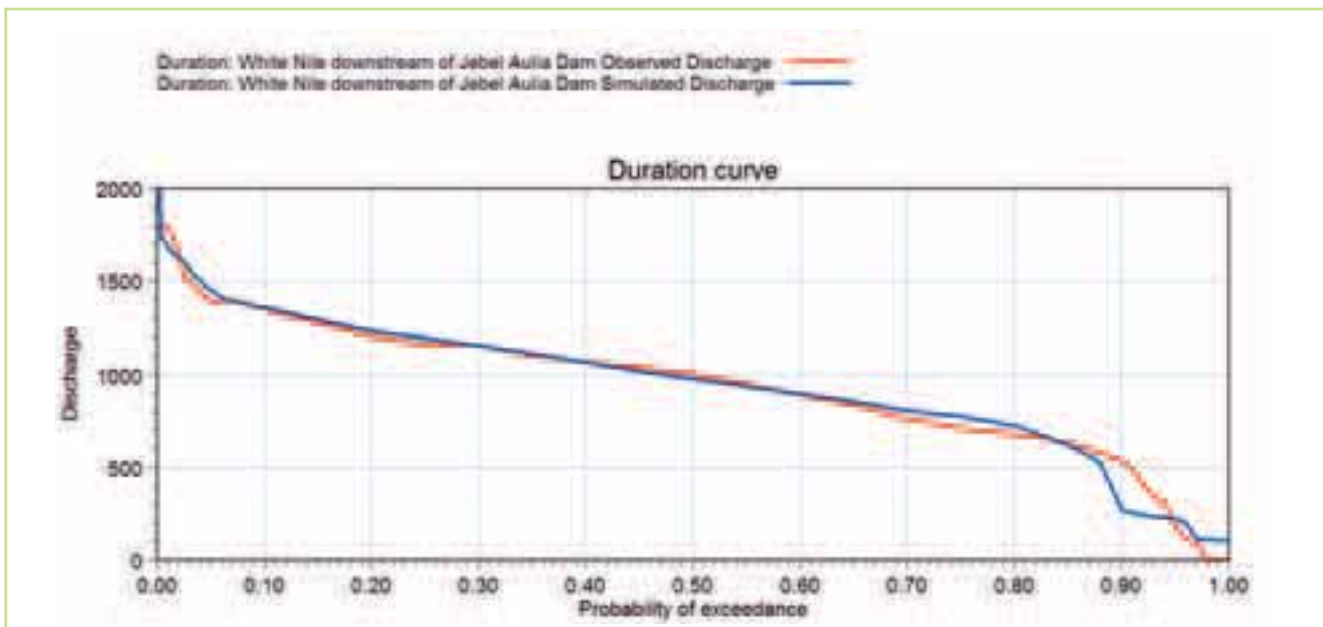
Figure 5.79 Comparison of the observed (red) & simulated (blue) flow duration curves at the Jebel Aulia station for the period 1960-1980

5.6.11 Abay

The Abay station is located at the border between Ethiopia and Sudan and represents the flow from Lake Tana and the part of the Ethiopian highlands draining to the Blue Nile. The flow at this station is highly seasonal with flows greater than 10.000m3/s during the wet season and almost no flow during the dry season.

In general, the model represents the inter-annual as well as intra-annual flow patterns well throughout the modelling period. From the monthly flows the model appears to have a reasonable representation of the flow during the dry season. There is a tendency to underestimate the flow in the beginning at the wet season and overestimate the flow at the end of the wet season and the following recession. The seasonal pattern of the flow is therefore captured reasonably well by the model. The recession from the wet season to the dry season seems to be slightly delayed. This could be caused by irrigation uptake or groundwater recharge that is not fully understood.

While reasonable results were obtained for the Abay, it should be re-iterated that the rainfall-runoff modelling throughout the Blue Nile has been based on limited climate information. There is no doubt that better information of the daily rainfall patterns would increase the performance of the model. Future effort should include the provision of more comprehensive daily observation data for both rainfall and flow from Ethiopia.
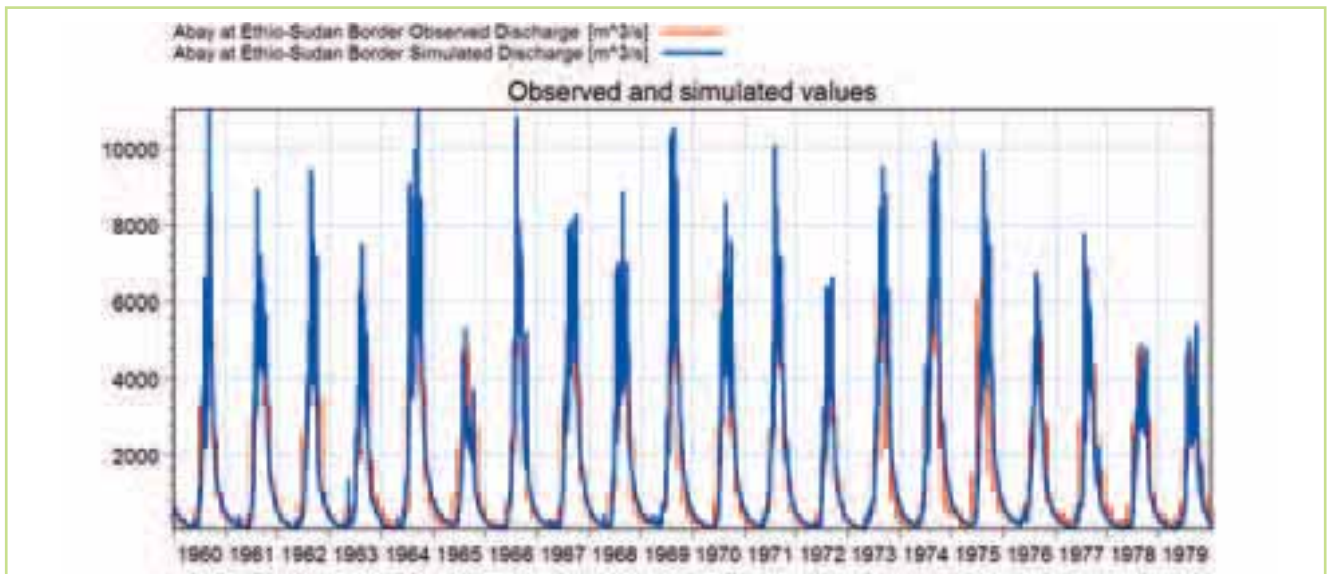
Figure 5.80 Comparison of the observed (red) & simulated (blue) flow hydrographs at the Abay station for the period 1960-1980

Figure 5.81 Comparison of the observed (red) & simulated (blue) mean monthly flows at the Abay station for the period 1960-1980
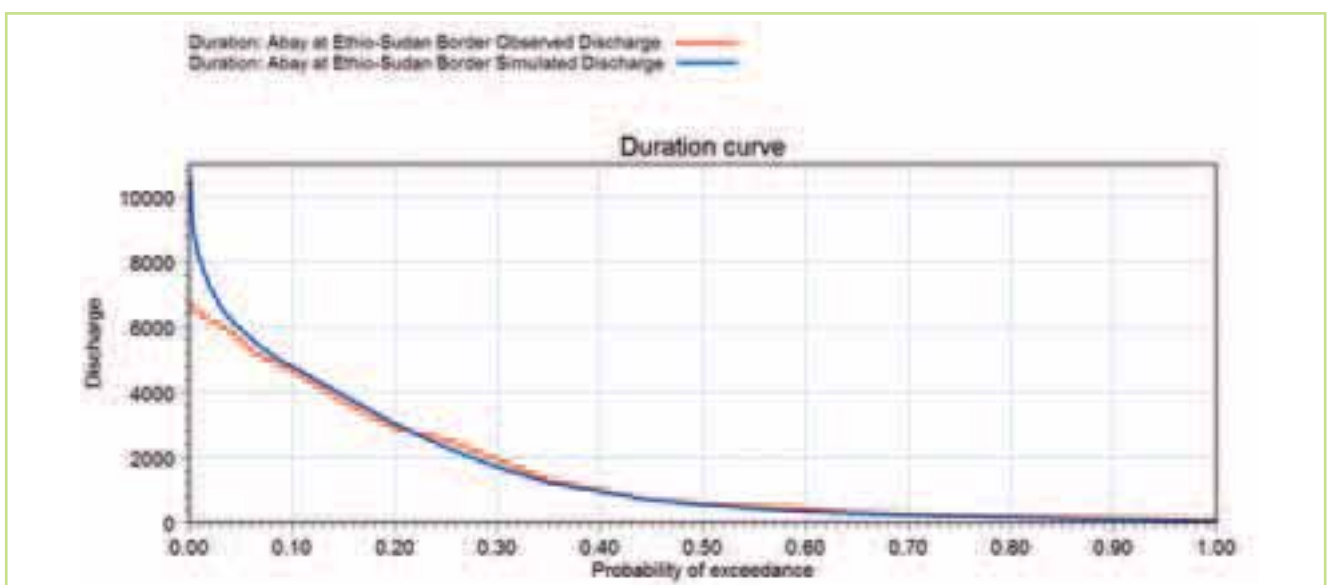
Figure 5.82 Comparison of the observed (red) & simulated (blue) flow duration curves at the Abay station for the period 1960-1980

5.6.12 Khartoum (Blue Nile)

The station at Khartoum represents the total flow in the Blue Nile just before it joins the White Nile. The flow is highly seasonal but the model appears to capture the inter-annual as well as intra-annual flow patterns reasonably well, Figure 5.83.

Examination of the monthly average shows the low flow distribution is reasonably well captured but the peak flows are in general are overestimated with the exception of the highest peaks in August, Figure 5.84. This is clearly reflected in the flow duration curves, Figure 5.85. This general tendency to over-estimate flows in the Blue Nile should be examined in detail in future work. As described in detail in section 5.5.7, limited rainfall and discharge data were available to the project and this has been a limiting factor in achieving a more accurate calibration. Several reasons for these biases can be envisaged including biases in the CRU data used to estimate both rainfall and PET, in the contributing sub-catchments. It is recommended that additional data should be acquired before further calibration work is undertaken.

These biases in the peak simulation should be kept in mind when evaluating the impacts of climate change. Nevertheless, as the model captures the seasonal behaviour and the largest peaks reasonably well it should provide a reasonable basis for assessing changes in flows (rather than the absolute value) as a result of climate change.
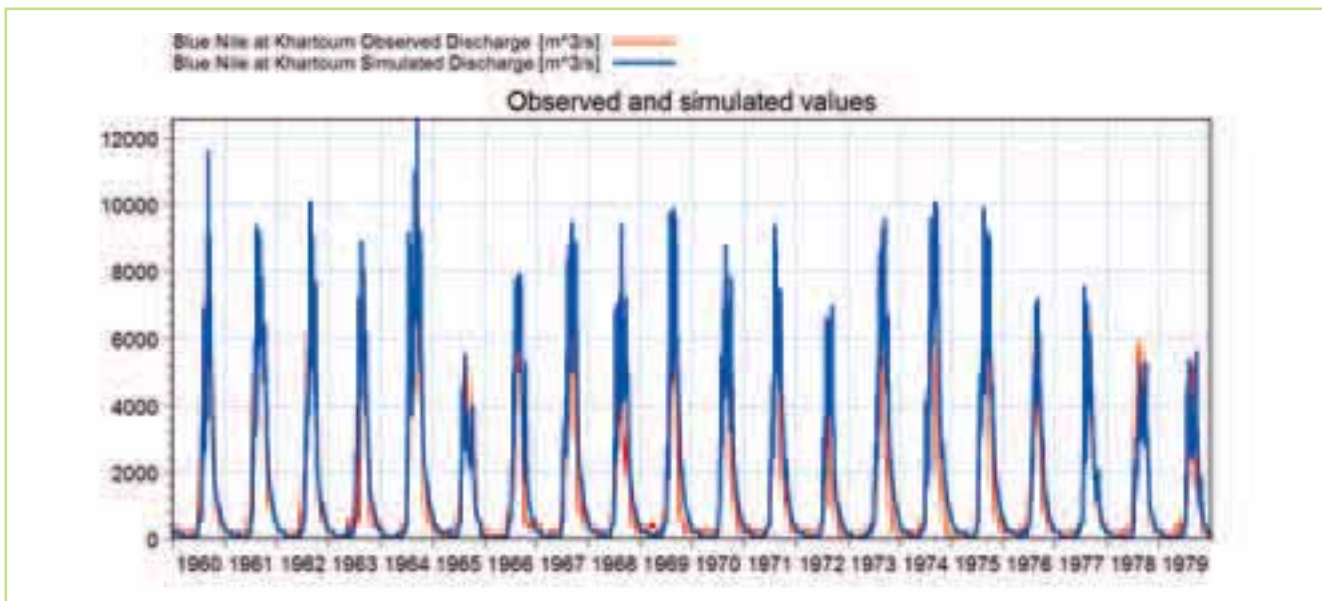
Figure 5.83 Comparison of the observed (red) & simulated (blue) flow hydrographs at the Khartoum station for the period 1960-1980

Figure 5.84 Comparison of the observed (red) & simulated (blue) mean monthly flows at the Khartoum station for the period 1960-1980
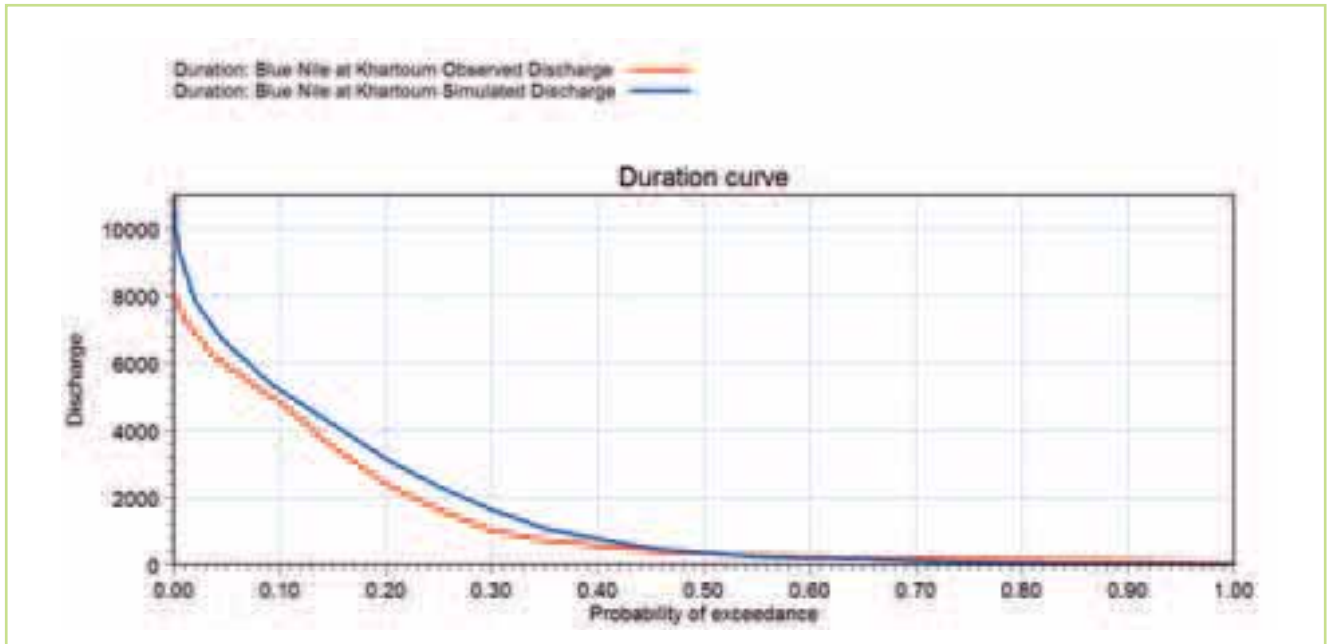
Figure 5.85 Comparison of the observed (red) & simulated (blue) flow duration curves at the Khartoum station for the period 1960-1980.

5.6.13 Atbara

The Atbara station represents the flow from the entire Atbara basin. The observed flow has the same highly seasonal pattern as observed in the Blue Nile, with peak values of more than 7000 m^3/s and almost no flow during the dry season.

The model captures the seasonal patterns, but overestimates the flow during the wet season, and also overestimates the recession from the wet to the dry season. As with the Blue Nile, there was only a limited amounted of data, rainfall in particular and

the same methods of estimating daily patterns used in the Blue Nile were applied here. It is therefore not surprising that similar biases in the peak flows were found and similar recommendations for improving the calibration apply.

As with the Blue Nile, the over-estimation of the peak flows should be kept in mind when assessing the impacts of climate change on the flows in Atbara. These simulations should however provide a reasonable basis for an assessment of the changes in flow as a result of climate change.
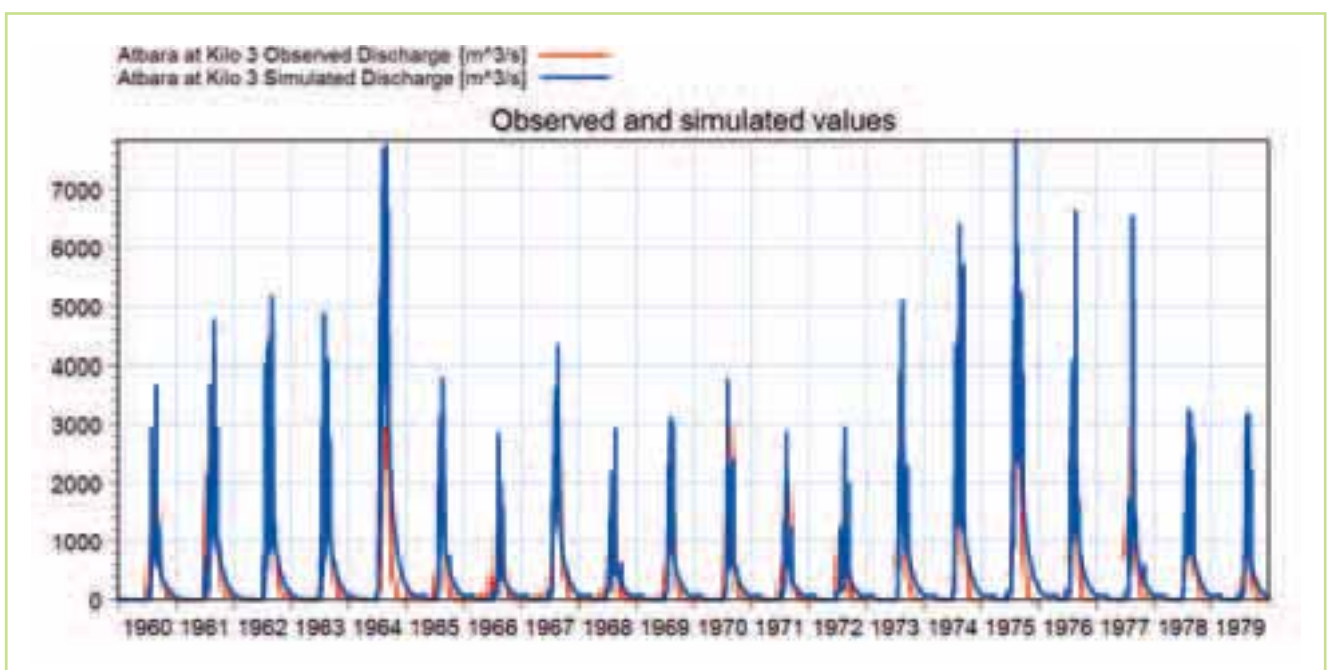
Figure 5.86 Comparison of the observed (red) & simulated (blue) flow hydrographs at the Atbara station for the period 1960-1980

Figure 5.87 Comparison of the observed (red) & simulated (blue) mean monthly flows at the Atbara station for the period 1960-1980
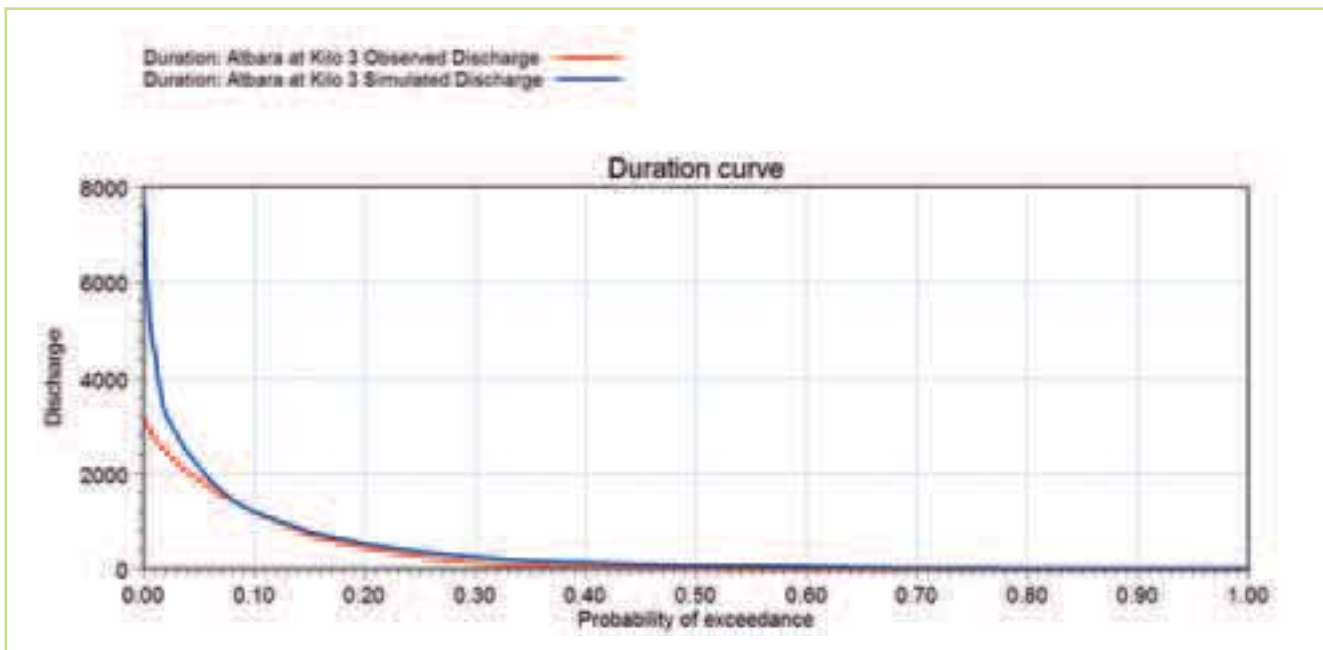
Figure 5.88 Comparison of the observed (red) & simulated (blue) flow duration curves at the Atbara station for the period 1960-1980

5.6.14 Dongola

The Dongala station represents the outlet of the whole of the Nile River; White Nile, Blue Nile and Atbara before the Nile flows into Lake Nasser. The flows are also affected by the routing along the Nile which varies according to flow, and the losses due to evaporation and irrigation.

The model captures the seasonal pattern, but with some deviations during the dry season. This part of the hydrograph originates from the White Nile, and the reason for the deviation is most likely that the operation of the Jebel Aulia is not fully understood and accurately represented in the current model.

Examining the monthly average flows it appears that the model captures the dry season flow, but generally overestimates the flows during July to November. The over-estimation of the peak flows arise from the over-estimation of the peak flows found for both Atbara and the Blue Nile.
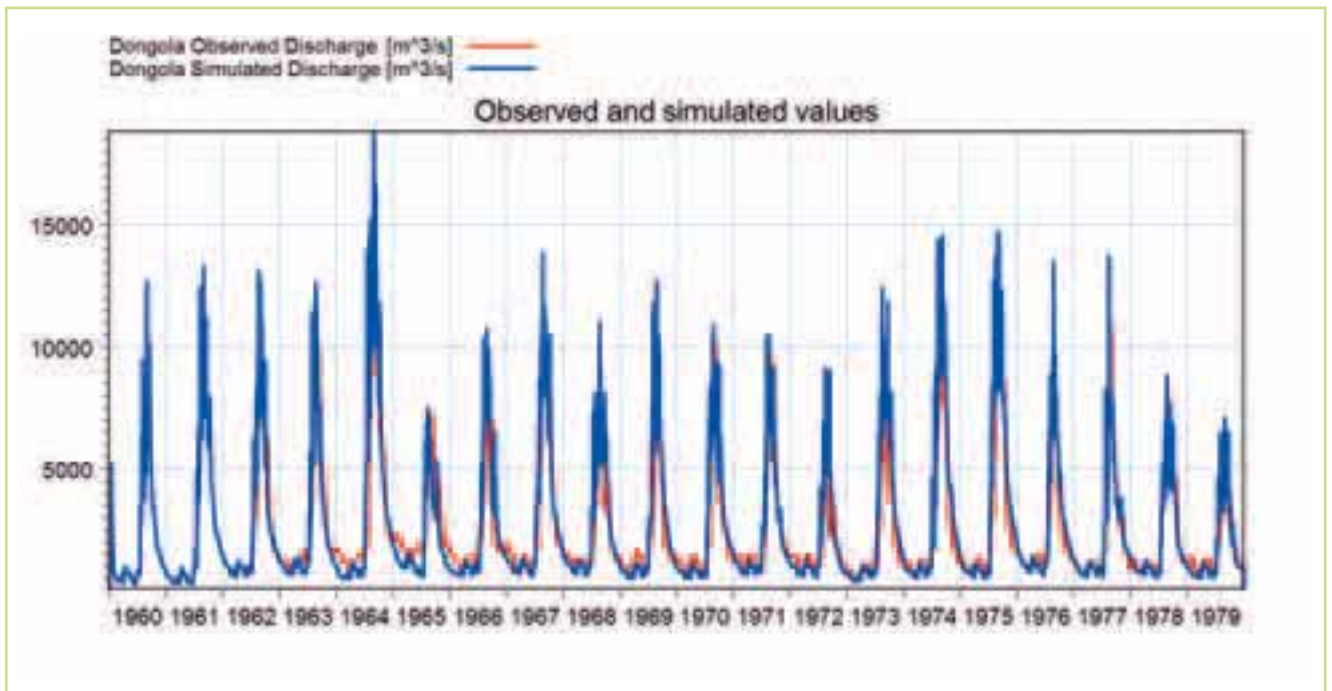
Figure 5.89 Comparison of the observed (red) & simulated (blue) flow hydrographs at the Dongola station for the period 1960-1980

Figure 5.90 Comparison of the observed (red) & simulated (blue) mean monthly flows at the Abay station for the period 1960-1980
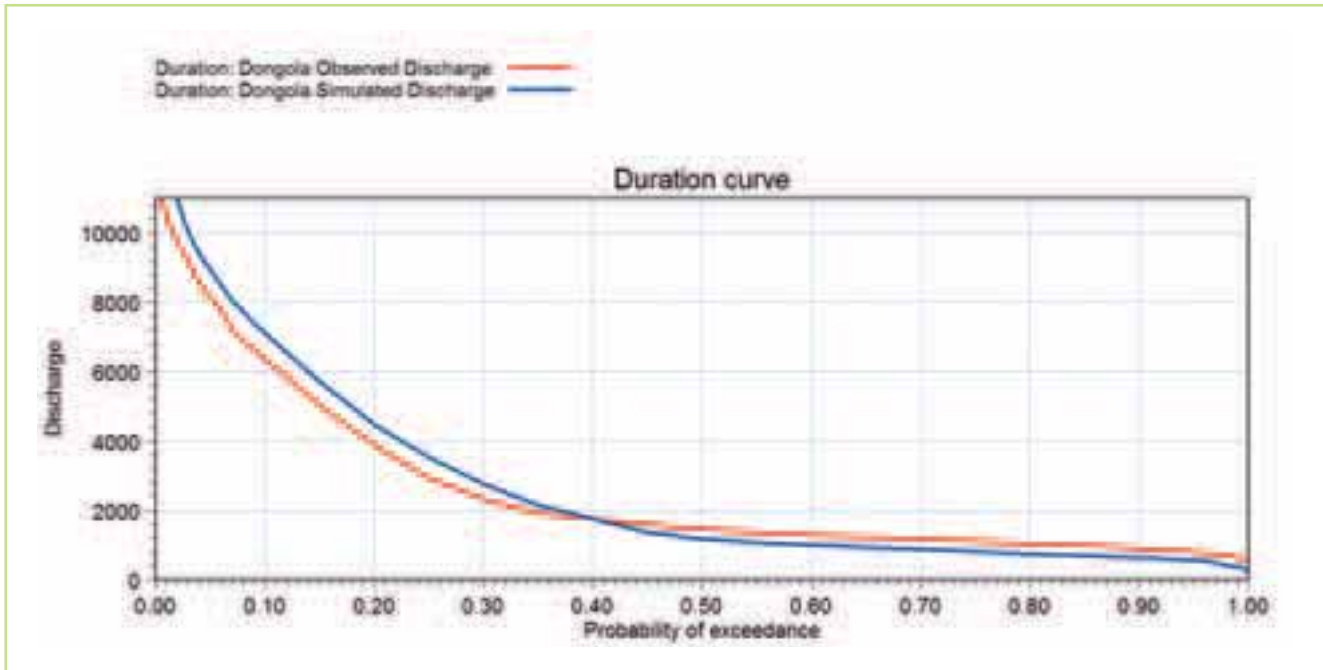
Figure 5.91 Comparison of the observed (red) & simulated (blue) flow duration curves at the Abay station for the period 1960-1980

5.6.15 Gaafra

The Gaafra station is the furthest downstream station used in this study. The flow regime is affected by the large irrigation withdrawals along the Nile and the operation of the Aswan dam. It was decided to conceptualise this part of the Nile in a relatively simple way, with an overall description of the Aswan Dam operation and the irrigation withdrawals in Egypt. These are described in detail in section 5.5.9.

Despite these relatively simple descriptions the model represents the flow reasonably well with the exception of 1974-75 where the flows are over-estimated, Figure 5 92. This is most likely as a result of the description of the Aswan dam operation used in the model. These two years seem to have a major impact on the monthly flows and care should be taken in interpreting the averages as it includes the construction (commenced 1960, completed 1970) and the filling (commenced 1964, completed 1976) of the Aswan dam.
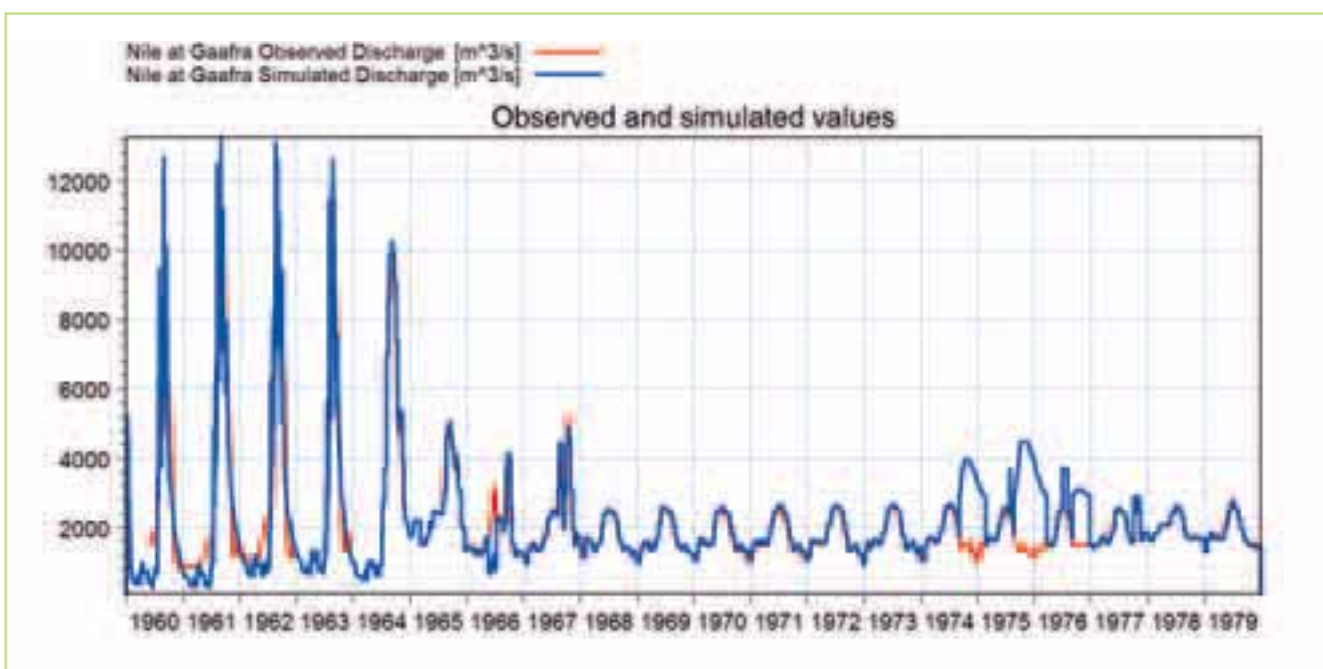
Figure 5.92 Comparison of the observed (red) & simulated (blue) flow hydrographs at the Gaafra station for the period 1960-1980

Figure 5.93 Comparison of the observed (red) & simulated (blue) mean monthly flows at the Abay station for the period 1960-1980
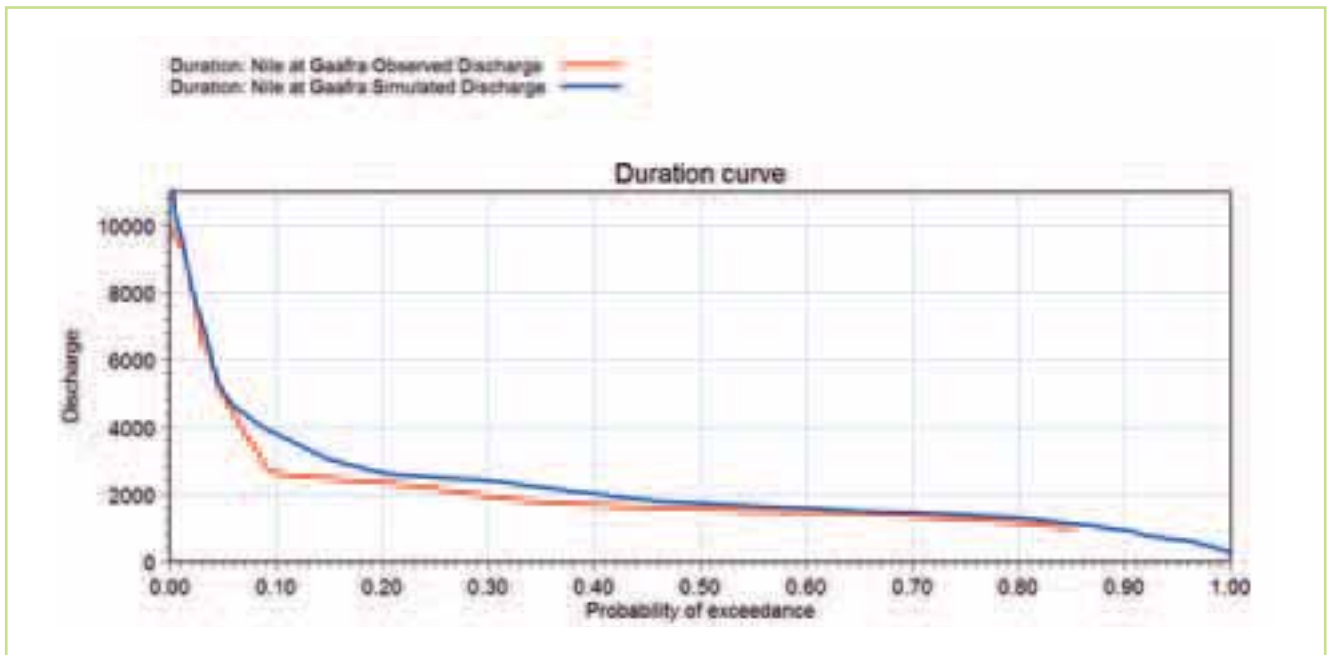
Figure 5.94 Comparison of the observed (red) & simulated (blue) flow duration curves at the Abay station for the period 1960-1980

5.6.16 Summary

The development of a regional hydrological model has been a necessary pre-requisite for an assessment of climate change impacts on Nile flows and water balance at the regional scale. The main goal was to develop a regional model captures both the flow dynamics (flow regime) and the flow magnitudes to the extent possible given the data available.

There have been a number of challenges, in particular, the comprehensive and complex nature of this task and the limitations concerning the quality and quantity of the data. Within each major

sub-basin we have identified the most important limitations and suggestions for future improvement. The interested reader is referred to the individual sections.

In summarising this assessment the most important limitation of the current regional model is the lack of daily observation data, particularly rainfall for the Blue Nile and Atbara catchments that both have a tremendous influence on the peak flows in the Nile. To address this limitation we developed a straightforward estimation procedure combining the few gauge data with the CRU monthly totals. While this

is a practical and viable approach we are convinced that improvements could be readily achieved with the provision of daily observation data for flow and discharge. The regional hydrological model developed for these two catchments satisfactorily captures the flow dynamics, the model tends to over-estimate the peak flows in these catchment. The biases for these two catchment must be kept in mind in assessing the resulting effect of climate changes within these stations and downstream. We strongly recommend that while further improvement to the calibration may be possible this should not be attempted until additional daily data are incorporated in the model. Nevertheless, the model should provide a reasonable basis for examining the changes in flows (rather than the absolute values) as a result of projected climatic change.

Overall, the White Nile seems to be well represented in the model, especially the Equatorial Lakes. While we have identified areas within the White Nile where additional data or information would be advantageous, the most important issues that we recommend be addressed in future work are the development of a local model for the Bahr el Ghazal basin and more detailed modelling investigations of the Sudd. It can be argued as we have done here that the outflow of this catchment has a negligible contribution to the regional Nile flows. However, this may not be the case for very large flows. More importantly however, we would recommend developing velop a local model, to support water resources management within the basin and subsequently to address the local impacts of climate change which was not carried out here.

The hydrological processes in the Sudd are recognised as having a controlling influence on the contribution of the White Nile to the Nile River flows. The hydrology of the swamps are represented in the regional a straightforward way as dynamic storages where the main contributions to the water balance are the direct rainfall and evaporation from the storages and other rainfall-runoff processes were neglected. The presence of the swamps and out-of-bank flows along the floodplain make it difficult to determine flow and water balances within the Sudd. However such data is seen as the only way forward for a better understanding and model representation of the process.

Accepting these limitations, we argue that the overall performance of hydrological model at the regional scale is satisfactory and an appropriate basis for the assessment of changes in the Nile as a result of projected climate change. In particular, the regional model should be used to assess the changes in flow as opposed to the absolute values. For this reason the climate change impacts are assessed against model reference simulations in section 6 rather than the observations.

6.0 Regional impact assessment for climate & water resources

To assess the impact of climate change at the regional scale on the climate, water resources and extremes of the flow regime we take as the starting point a set indicators (section 2.6).The key selection criteria used to identify these indicators were:

- Need to reflect vulnerability to floods and drought to climate change
- Based on available and reliable data sets
- Reflect the data availability spatial coverage and temporal frequency in the observation data sets
- Appropriate at the regional scale
- Indicators representing similar characteristics are not replicated.
- Can be applied as input to other indicators in the different water-related sectors

Based on the these criteria the following indicators are utilised in this project;
1. Climate Moisture Index (CMI)

2. Coefficient of variation of the Climate Moisture Index (CV CMI)
3. Regional climate model consensus
4. Average monthly runoff at key regional stations
5. Flow duration curves also at these key regional stations
6. Water demands for domestic, industrial and irrigation purposes.

In each case, changes in these indicators are assessed against a control or reference data set. For climate change a thirty year control period 1961-1990 is used. The IPCC assessments include both twenty and thirty year periods. A period of thirty 30 years is considered to be the shortest period in which one can reliably estimate changes in variability (Jones et al., 1997). This period was chosen to be consistent with control periods used in the climate literature to support comparison with previous work.

This choice is also consistent with the period for which we have gauge observation data (1960-1980) used in the regional hydrological modelling. The changes are then derived by applying the projected changes in climate derived from the regional climate simulations. The impacts changes in water demand are assessed in a similar manner in section 7.

The Climate Moisture Index (CMI) reflects the regional water balance. It is an aggregate measure of potential water availability imposed solely by climate. The coefficient of variation of the Climate Moisture Index (CV CMI) has been applied in earlier studies for identifying regions with highly variable climates as potentially vulnerable to periodic water stress and/or scarcity. The regional climate model consensus data are used to determine where clear signals regarding the magnitude and/or direction of projected climate change. These data are also used to examine the changes in seasonality of the driving climate variables.

The remaining indicators are used to assess the impacts of changes on water resources. The changes in average monthly runoff at the key discharge stations reflect how the changes in the driving climate variables affect the water balance at the regional/catchment scale and also the annual and seasonal changes in flow regimes. The flow duration curves are used to identify any shift in the flow regime and to assess changes in high and low flow distributions. Assessments of reference and projected water demands for domestic, industrial and irrigation purposes presented in next section provide an assessment of the changes in water stress driven by population growth.

6.1 Hydro-climatic setting

The regional hydro-climatic setting of the Nile Basin, Figure 6.1, is characterised by strong north-south trends in both the rainfall and potential evapotranspiration (PET). The annual rainfall distribution clearly shows the two major contributing areas to flow in the Nile; the Equatorial lakes and the Ethiopian highlands. It also highlights the extreme aridity in the north with large areas receiving less 10 mm per month on average throughout the year. It should be noted that these annual average values of course do not reflect the seasonal variations throughout the year.

Potential or reference evapotranspiration (PET) measures the amount of water that potentially can be lost via direct evaporation and plant transpiration under conditions where water is not a limiting factor. Therefore this is not a measure of the actual evapotranspiration but rather reflects the amount of energy available to drive the evapotranspiration process expressed in terms of water quantity. The regional PET distribution reflects the regional distribution of temperature, net radiation and humidity and therefore shows similar patterns to the temperature. The gradients are reversed when compared to rainfall with lower values in the south and the Equatorial lakes and the Ethiopian highlands and larger values to the north.

6.2 Regional climate projections – annual averages

Examining the climate change projections across the entire regional climate model domain provides some context for the climate change projections within the Nile.

The projected changes in annual average temperature over the whole domain for the two horizons, 2020-2049 and 2070-2099 are shown in Figure 6.2. All the RCM simulations project temperature increases. The changes shown represent the ensemble average of the 5 RCM simulations used in this study. For 2020-2049 increases of 1.5-2.0 degrees Celsius are seen on average across the Nile Basin in comparison to the control period. The largest increases are found in the northern parts of the basin. Even greater increases (3.5-4.5 degrees Celsius) are found over the basin for the 2070-2099 horizon. These projected changes are consistent with those made by the IPCC multi-model ensemble average for 2100 (see Figure 11.2, IPCC 2007b).

Figure 6.3 shows the corresponding percentage changes in precipitation for the two periods. For 2020-2049, large percentage changes are indicated in the northern part of the Nile, however as noted in the previous section the annual rainfall in this portion of the Nile is very low, Figure 6 1. Therefore the actual changes in terms of rainfall amounts are quite small. Reductions in rainfall are shown directly over Lake Victoria however it should be noted that the RCM in the "short" rainy season (October, November and December) seems to over-estimate the projections, exhibiting a strong positive bias directly over the lake. Stronger increases in precipitation across much more of the basin are seen for 2070-2099 suggesting a wetter future climate.

It should be recognised, however, that these projected changes in the annual averages mask the significant seasonal variations in climate in the Nile, particularly for the precipitation. To investigate these seasonal variations the climate projections presented in the subsequent sections.
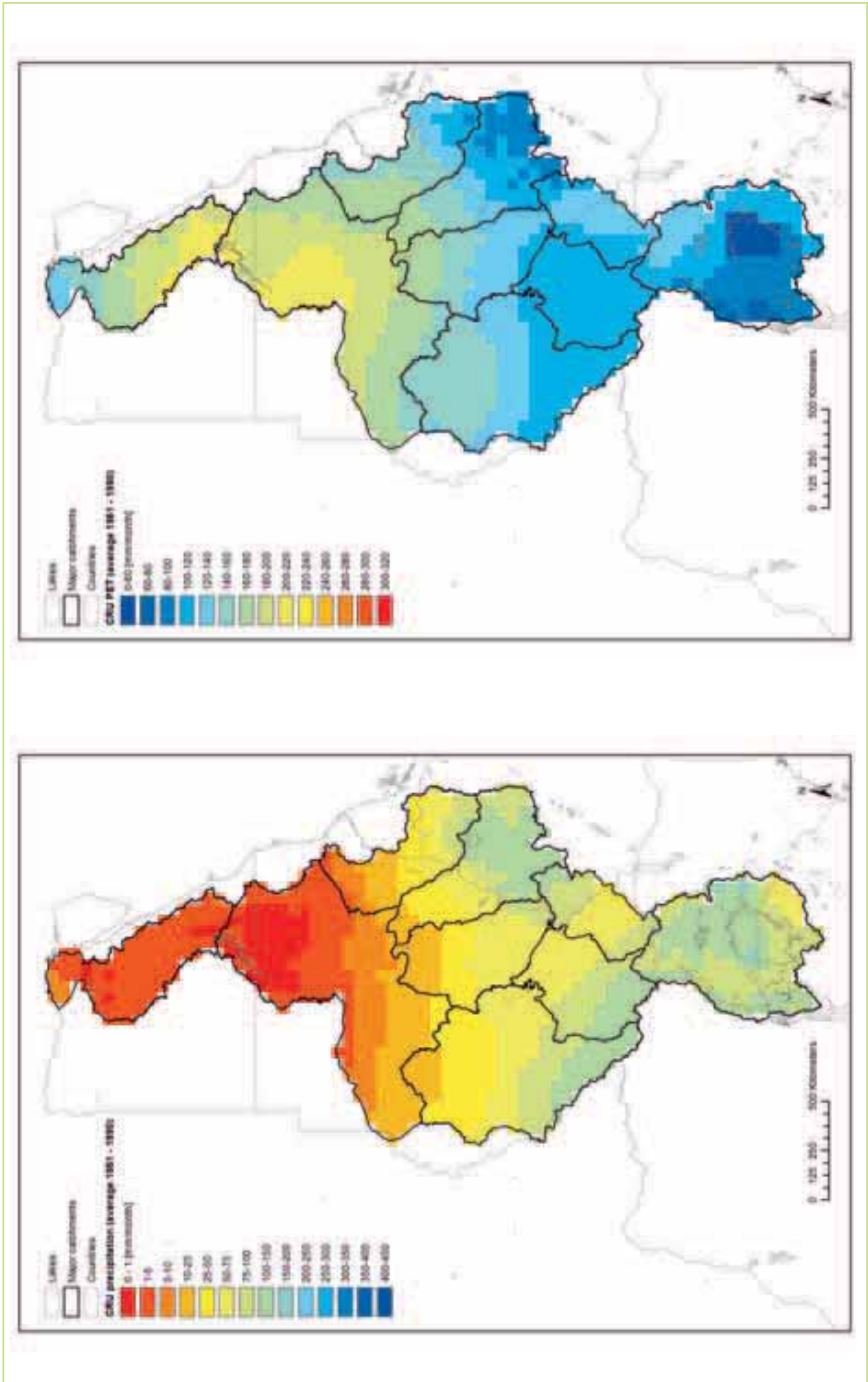
Figure 6.1 The distribution of annual average rainfall (left) & potential evapotranspiration (right) expressed in mm/month. The figures are derived from the CRU data for the reference period 1961-90. Note that the PET has been set to zero over Lake Victoria in the Cru dataset
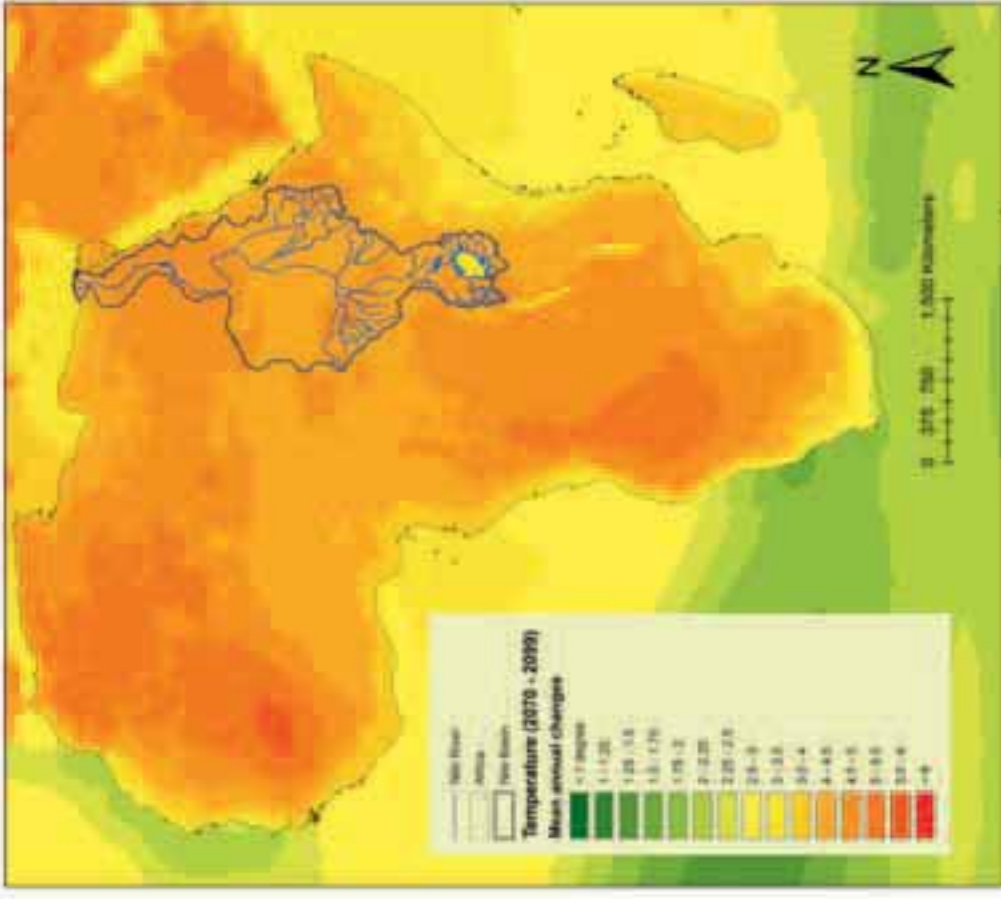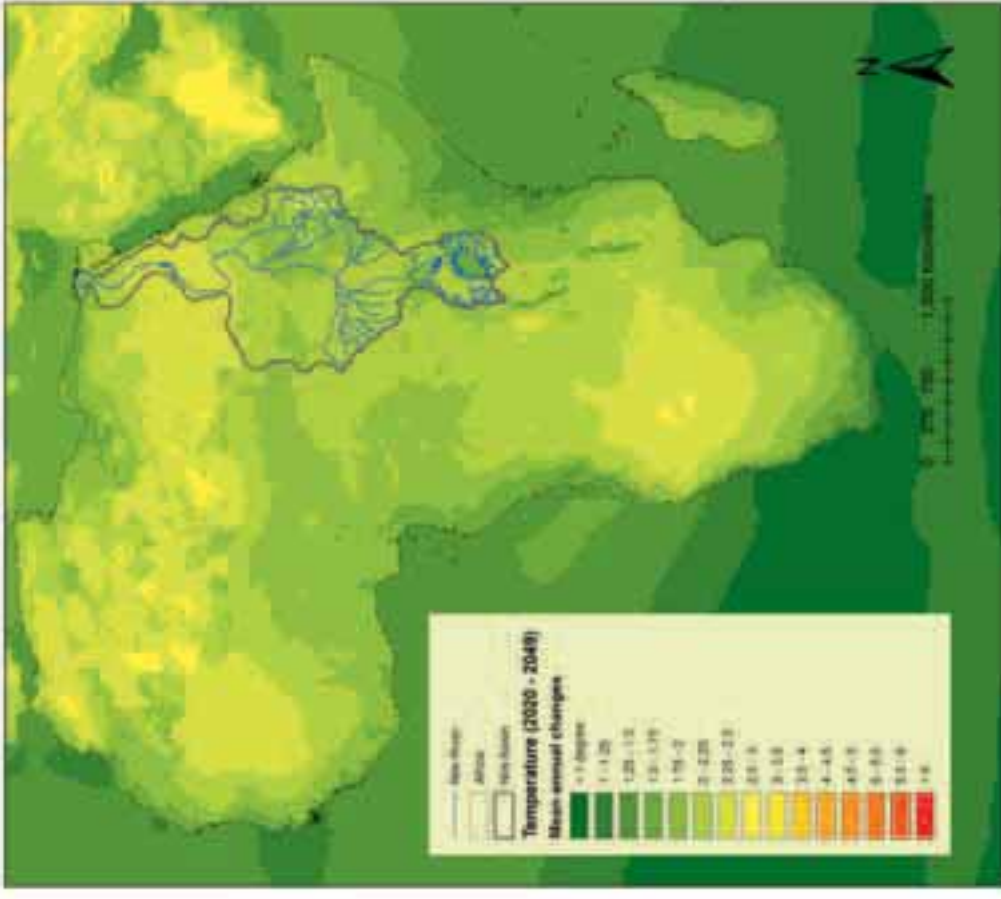
Figure 6.2 Projected changes in the annual temperature for 2020-2049 (left) & 2070-2099 (right). The projections are derived from the RCM ensemble average
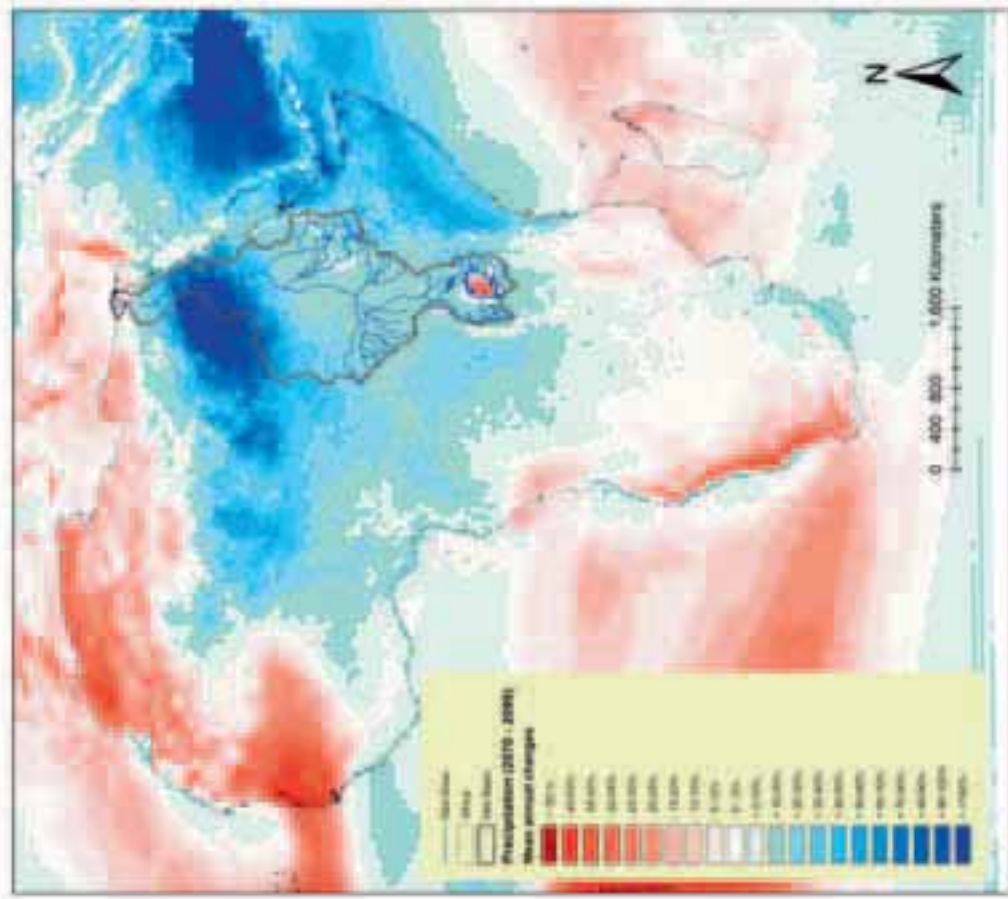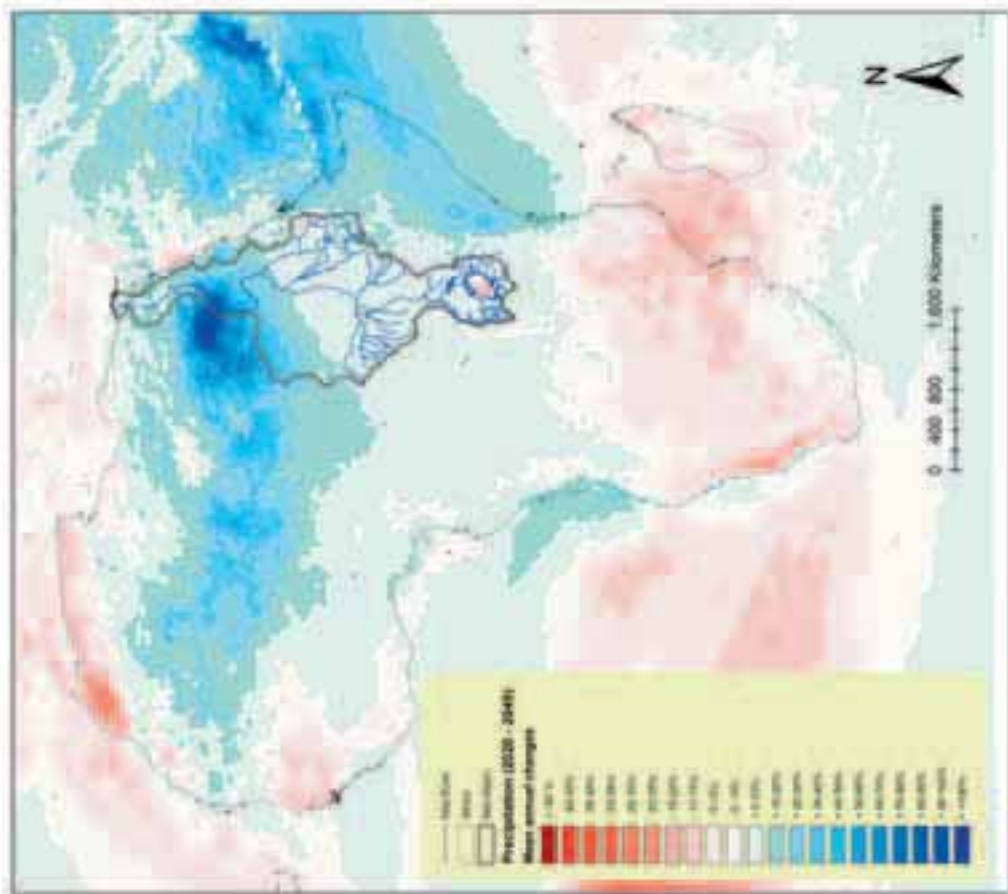
Figure 6.3 Projected changes in the annual precipitation 2020-2049 (left) & 2070-2099 (right). The projections are derived from the RCM ensemble average
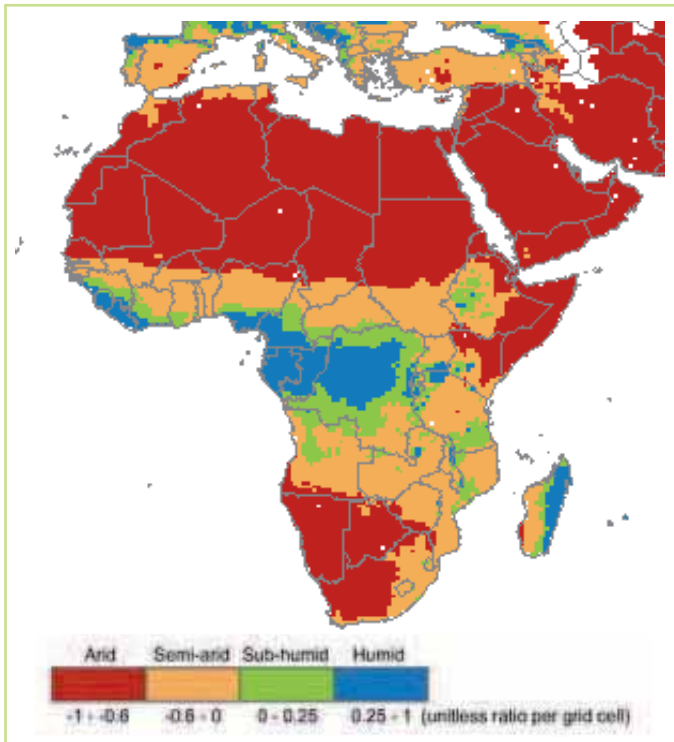
Figure 6.4 CMI Annual Mean for Africa from GWSP Digital Water Atlas (2008). Map 40: Climate Moisture Index (V1.0). Available online at http://atlas.gwsp.org

6.3 Climate Moisture Index (CMI)

The annual average climate moisture index (CMI) (Willmott and Feddema, 1992) is computed using the ratio of annual precipitation (P) to annual potential evapotranspiration (PET). This reflects the relationship between plant water demand and available precipitation.

CMI is defined by the equations:

- CMI = (P / PET) −1 when P < PET; and
- CMI = 1- (PET / P) when P ≥ PET

The CMI is an aggregate measure of potential water availability imposed solely by climate. Negative CMI values show potential evapotranspiration in excess of precipitation and thus the potential for climate-based water scarcity for resident populations and rain-fed agriculture. Areas with CMI values exceeding 0 generally represent humid or water abundant areas. Arid regions with very low rainfall show CMI values less than -0.5 where semi-arid regions have CMI values ranging from 0 to -0.5. These semi-arid transitional zones regions are most vulnerable to impacts from climate change.

Vorosmarty et al. 2005 present a global data set for CMI on a 0.5 x 0.5 degree grid in support of the World Water Development Report II, Indicators for the World Water Assessment Program (http://wwdrii. sr.unh.edu/index.html), which is available on-line. (Figure 6.4).

It should be noted that the values shown in Figure 6.4 are derived from other sources. To be consistent with the other data applications in this study, the CMI indicator for this analysis is calculated using the Climatic Research Unit CRU) , University of East Anglia (http://www.cru.uea.ac.uk/data) observation data sets for precipitation and potential evapotranspiration (PET) for the reference period 1961-1990. This is a reasonable approach as it is the changes in CMI that are of interest.

The changes in the CMI indicator are derived from changes in the climate predicted by the PRECIS regional climate model by applying the appropriate change factors to rainfall and PET respectively for the two periods 2020-2049 and 2070-2099.

Figure 6.5 and Figure 6.6 show the changes in CMI for these two periods respectively. Each figure shows the CMI values corresponding to the 5 RCM ensemble members used here to make projection of the future climate (section 3). The corresponding CMI distribution, for the 1961-1990 reference period, is shown in the bottom right panel in each figure for comparison. There appears to be good consistency between the CMI derived here and that presented in the GWSP Digital Water Atlas using other data sources, (Figure 6.4).

The overall spatial pattern for the CMI as it is defined above is essentially determined by the differences between the rainfall and PET (Figure 6.1). These overall patterns do not appear to be changed significantly under a future climate. A closer examination of the results for the period 2070-2099 indicates that the extent of the arid region appears to be unchanged and in particular the transition from arid to semi-arid conditions. The changes in CMI do not reveal any overall trends for the climate impact in the region.

The largest changes in relation to the reference period occur in the Ethiopian highlands, the Equatorial lakes and along the western part of South Sudan. Generally more humid conditions appear to the west of Lake Victoria around Kagera. The CMI directly over Lake Victoria is one for the reference period and remains unchanged. This arises directly from the definition of CMI and the fact that PET is set to zero over the lake in the CRU data set.

An increase in the extent of sub-humid and humid areas in the western part of the South Sudan seems to be a robust signal consistent across all 5 ensemble members. This corresponds to the upper part of the Bahr El Ghazal basin. The high rainfall in this region gives rise to a number of seasonal tributaries which converge towards the confluence of the Bahr el Ghaszal on the White Nile. The increase in

extent particularly pronounced for the two ensemble members; akzja (bottom left) & akzcy (top right) which is the warmest ensemble member. This can be seen as an increase in the area with potentially more plant available water which may have direct implications for rain-fed agriculture in this area. Similar comments can be made for the period 2020-2049 however the signal is not as strong. The contribution of the Bahr el Ghazal to the White Nile is almost negligible as a result of high evaporation losses from the swamps in the lower basin (Sutcliffe and Parks, 1999). The impact on flows in the White Nile therefore cannot be assessed directly from these maps.

For both periods four out of the five ensemble members also indicate an increase in CMI and humidity over the Ethiopian highlands. This is more clearly indicated in the period 2070-2099. However there appears to be considerable uncertainty regarding the areal extent of changes in the humid and sub-humid conditions.

It can be argued that the pattern exhibited by the CMI indicator is strongly constrained by the hydro-climate conditions of the basin. To the north precipitation is extremely low and PET is high, therefore only dramatic large-scale shifts in the regional climate patterns can be expected to affect the extent of the arid region. Similarly in the two source regions, the Equatorial Lakes and the Ethiopian highlands, the regional pattern of humid areas will only be changed by dramatic climate shifts. Nevertheless there are some changes especially in the transition from semi-arid to sub-humid. As mentioned above these are the vulnerable areas and so changes here should be examined carefully.

In terms of climate impacts and adaptation, these results suggest some reduction in the areas classified as semi-arid (or conversely increase in the sub-humid areas). This may potentially lead to beneficial effects in terms of rain-fed agriculture and where relevant an increase in the sustainability of groundwater recharge. However, these results should be interpreted with caution. In particular, the effects occur along the fringes of the two source areas where there are strong gradients in the precipitation and evapotranspiration. A simple cell-by cell assessment of the water balance using either observed or model data will be highly uncertain unless further constrained by flow measurements in a model calibration.

However, the CMI indicator also has some limitations. In particular, it is based on annual averages and therefore does not reflect seasonal changes or changes in variability. For example decreases in the amount of available water in the dry season may have more significant impacts than increases during the wet season. To examine changes in variability of the overall water balance, the CV CMI indicator which was developed as a regional scale indicator of variability in potential available water will be examined next.

As well as being an aggregated measure, the CMI indicator is also a measure of potential water availability rather than a direct measure of the actual water balance. A logical extension of the CMI indicator would be to examine the actual water balance, the difference between rainfall and the actual evapotranspiration in each cell.

The actual evapotranspiration depends on the soil and atmosphere humidity, soil and vegetation type, antecedent conditions and a number of other variables. Point measurements using lysimeters, evaporation pans, flux towers, etc. can be made but are relatively scarce and therefore most appropriate for local scale assessments.

Satellite-based methods may be used for estimating regional evapotranspiration. They have the disadvantage in the context of this study is that there is only limited coverage compared to the climate reference period (1961-1990), which is also the period for which point data climate and flow data have been made available for hydrological modelling. Although regional evapotranspiration can be estimated from satellite images by applying a range of methods (Ridler et al., 2012; Sandholt and Andersen, 1993; Norman et al., 2003; Nishida et al., 2003; Boegh et al., 2002), they are limited to snapshots during clear sky conditions. Therefore, they are usually combined with other data and hydrological models. Furthermore while methods like the Normalised Difference Vegetation Index (NDVI) method appear to provide satisfactory results under arid and semi-arid conditions, they do not work as well under in more humid areas.

A more robust method for estimating the regional water balance is to develop a regional hydrological model. This is the approach adopted here. One of the key advantages of this approach is that the water balance can be constrained by flow measurements. Some hydrological models are based on a simple water balance for a single column. This approach is widely used for example in assessing plant water demands at the field scale. However this approach has to be modified to estimate lateral surface flows and to properly distinguish between surface runoff and infiltration to the subsurface. The approach adopted in this study is to use regional estimates of potential evapotranspiration using the CRU 3.1 data, combined with MIKE BASIN/HYDRO hydrological model which has been calibrated against measured discharge.
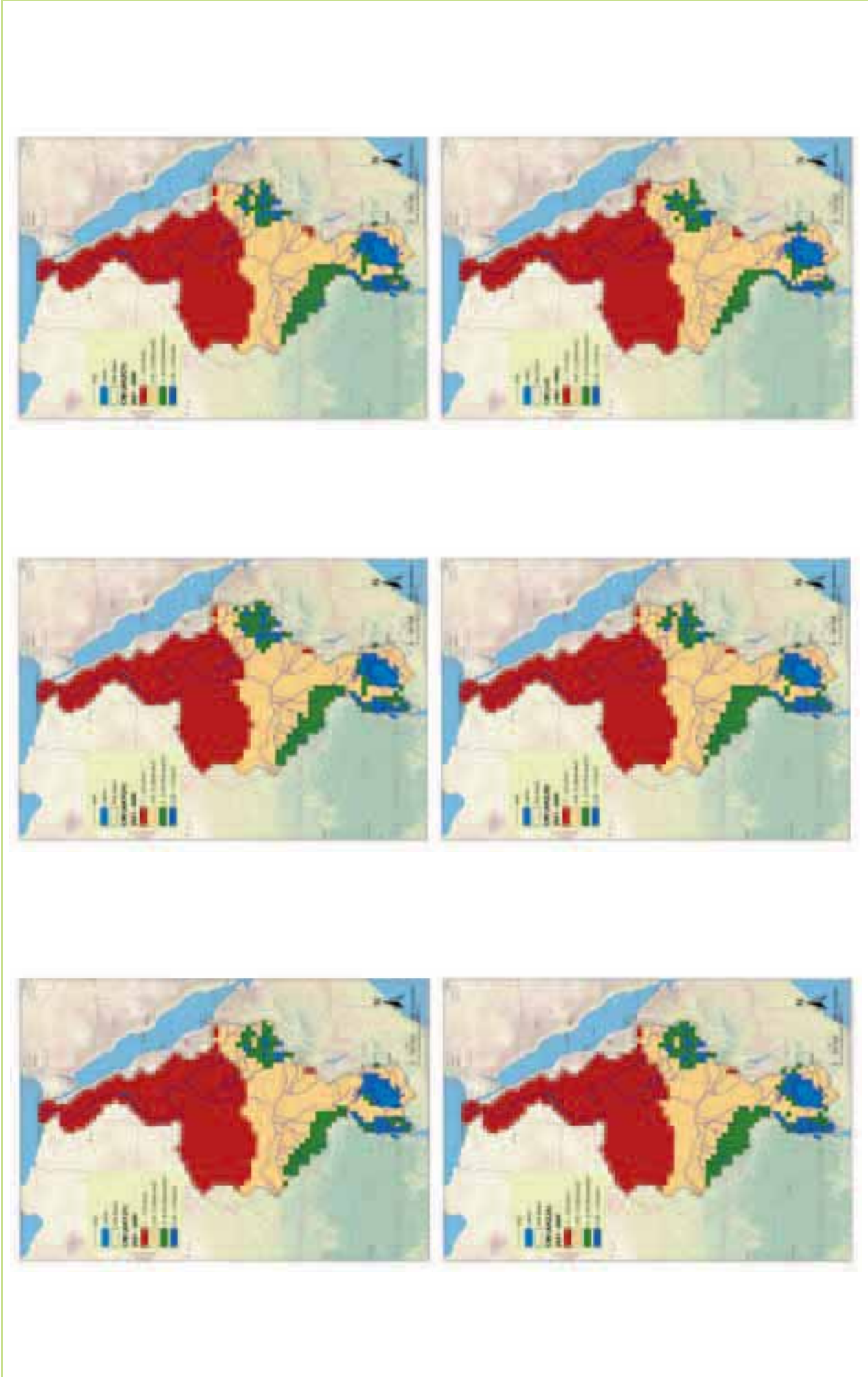
Figure 6.5 Climate Moisture Index (CMI) for the period 2020-2049 derived from the CRU data for rainfall & PET & projected for the 5 RCM ensemble members. The CMI for the reference period 1961-1990 is shown for comparison (bottom right)

Figure 6.6 Climate Moisture Index (CMI) for the period 2070-2099 derived from the CRU data for rainfall & PET & projected for the 5 RCM ensemble members. The CMI for the reference period 1961-1990 is shown for comparison (bottom right)
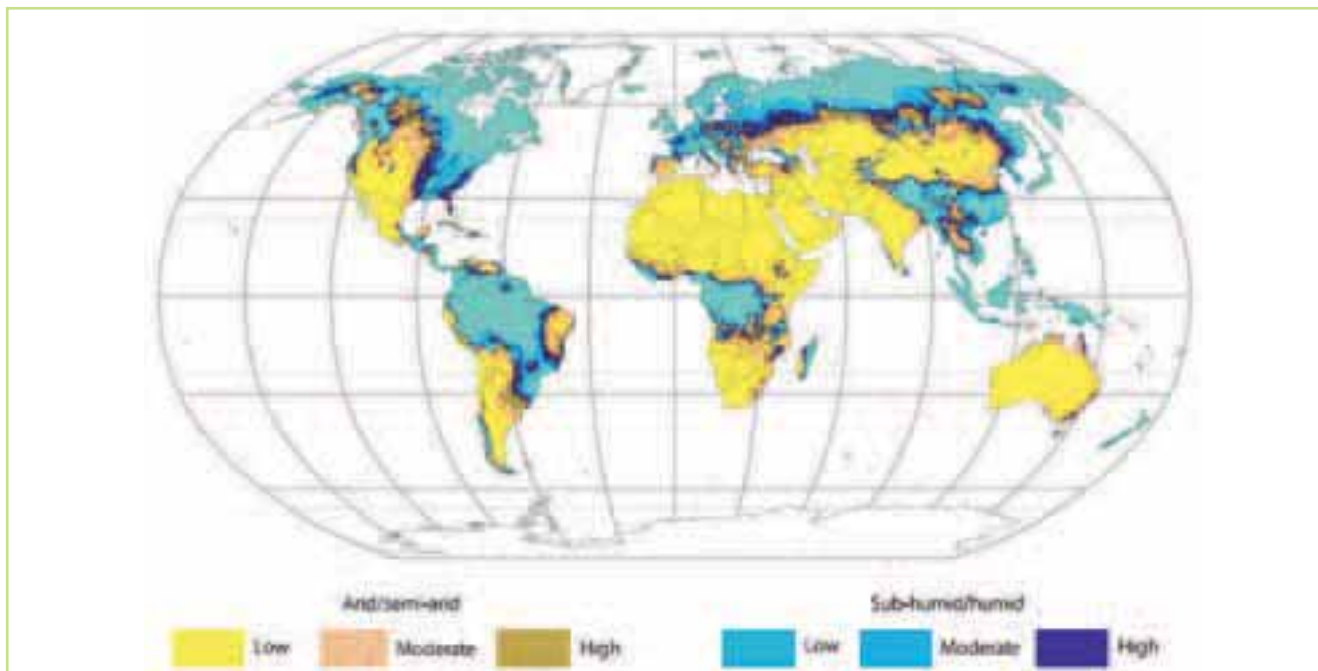
Figure 6.7 Coefficient of variation for climate moisture index for the globe[10]

6.4 Coefficient of variation of the Climate Moisture Index (CV CMI)

The coefficient of variation (CV) Index for the climate moisture index (CMI) is a statistical measure of variability in the ratio of plant water demand to precipitation. It is useful for identifying regions with highly variable climates as potentially vulnerable to periodic water stress and/or scarcity. The indicator is calculated as:

CMI CV = StdDev(CMI) / Mean(CMI)

In the World Water Assessment Programme (WWAP)[9] this indicator was derived from gridded time series of precipitation and potential evapotranspiration (Figure 6.7). The precipitation time series used in the WWAP assessment covers 1971-2010 and was derived from a reanalysis dataset (GPCC full data reanalysis product v5). The potential evapotranspiration time series from 1971-2010 was derived from a water balance/transport model, WBM plus, in combination with GPCC full data reanalysis product climate data.

As with the CMI, the CMI CV indicator developed in this study was calculated using the Climatic Research Unit, University of East Anglia (http://www.cru.uea.ac.uk/data) observation data sets for precipitation and potential evapotranspiration for the reference period 1961-1990. The CMI CV indicator

is a statistical measure derived directly from the CMI calculations.

From its definition the CV CMI can be expected to highlight areas where there is a strong inter-annual variation in water availability. Increased climate variability indicates larger year-to-year fluctuations, and hence, less predictability in the climate. Increased CMI CV often occurs along the interfaces between humid and dry areas such as the Sahelian region of Africa and in the North American Great Plains. These are areas known for periodic, severe droughts and water scarcity.

While the CMI indicator reflects the regional scale water balance, its variability over multiple years is also important in defining reliable water supplies (Vorosomarty et al. 2005). This is measured by the coefficient of variation (CV), defined as the ratio of year-to-year deviations around a long-term annual mean. A value of CV < 0.25 is classified as low variability, 0.25 to 0.75 moderate variability and > 0.75 high variability.

Figure 6.8 and Figure 6.9 show the changes in CV CMI for the two periods 2020-2049 and 2050-2099 respectively. Each figure shows the CMI values corresponding to the 5 RCM ensemble members used here to make projection of the future climate (Section 6.5). The corresponding CMI distribution, for the 1961-1990 reference period, is shown in the bottom right panel in each figure for comparison. There appears to be good consistency between the CMI derived here and that presented in the GWSP Digital Water Atlas (Figure 6.7).

The CVCMI for the reference period shows, perhaps

[9]http://www.unesco.org/new/en/natural-sciences/environment/water/wwap/

[10]http://www.unesco.org/new/fileadmin/MULTIMEDIA/HQ/SC/pdf/wwap_A7_Coefficient_of_variation_for_climate_moisture.pdf

not surprisingly that the inter-annual variability is located along the fringes of the two main sources of precipitation in the Nile, the Equatorial Lakes and the Ethiopian Highlands. Correspondingly, the variations in CV CMI for the RCM climate projections follow the changes in the CMI for each ensemble member. These results and the CMI result indicate that these fringe areas are vulnerable to both climate change and climate variability. While they reflect local vulnerability to water stress based on climatic conditions, these areas are on the other hand close

to areas with surplus rainfall with the corresponding opportunity to implement water management measures to protect against this variability.

The CMI and CV CMI reflect the annual average potential (plant) water availability and the inter-annual variability respectively, but not the seasonal changes. In the following section we will examine the variability and seasonal changes in climate (Section 6.5) and river flows (Section 6.6) at the monthly time scale using the regional climate model consensus data and average monthly discharge respectively.
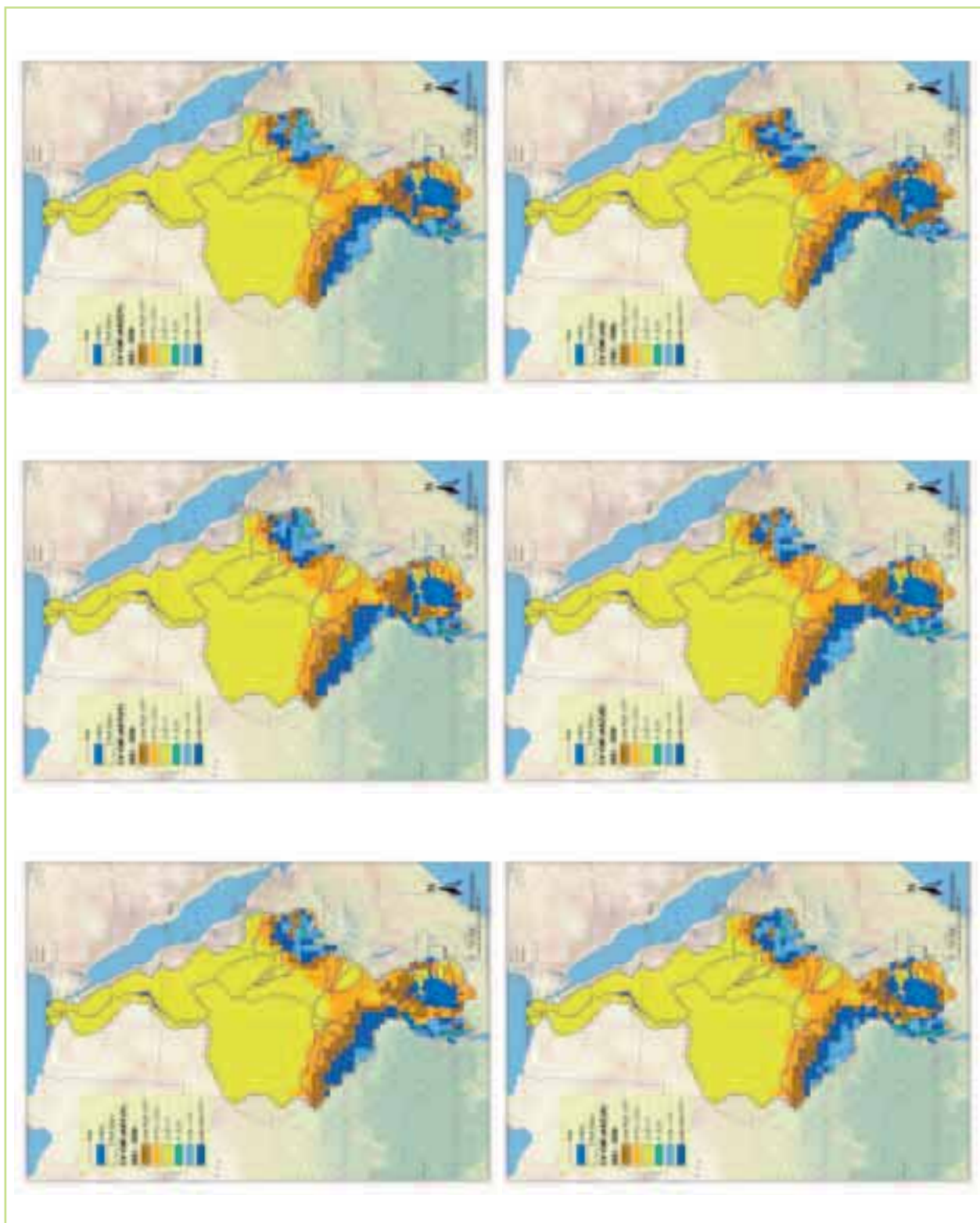
Figure 6.8. Coefficient of variation of the Climate Moisture Index (CMI) for the period 2020-2049 derived from the CRU data for rainfall & PET & projected for the 5 RCM ensemble members. The CMI for the reference period 1961-1990 is shown for comparison (bottom right)
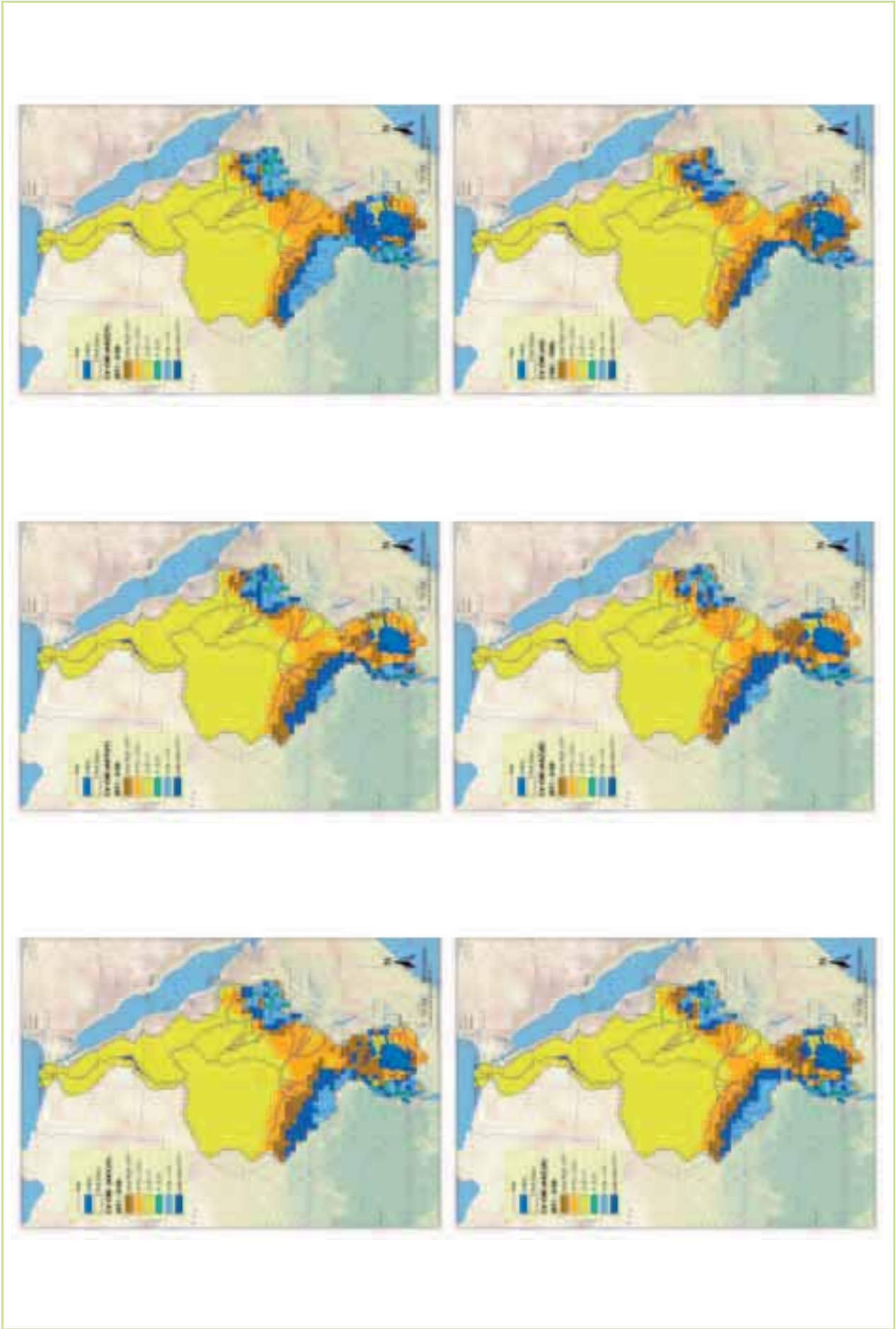
Figure 6.9 Coefficient of variation of the Climate Moisture Index (CMI) for the period 2070-2099 derived from the CRU data for rainfall & PET & projected for the 5 RCM ensemble members. The CMI for the reference period 1961-1990 is shown for comparison (bottom right)

6.5 Regional climate maps

In this section, the results of the Regional Climate Model (RCM) projections are presented. As the precipitation and potential evapotranspiration are the key driving variables in relation to the generation of flows in the Nile and the overall water balance, we will focus primarily on these in the subsequent analysis. However, for completeness we will present some observations on temperature changes in the region.

6.5.1 Reference or baseline climate

To examine the changes in seasonal behaviour, we present firstly comprehensive maps showing the monthly average values of rainfall (Figure 6.10 & Figure 6.11) and PET (Figure 6.12 & Figure 6.13) across the Nile Basin for the reference period (1961-1990). Monthly values rather than seasonal values are presented here in part because of the different seasons in the region and in part to allow for the possibility of any shifts in seasonal variations in climate.

In terms of precipitation, two key regions can be identified: the Equatorial Lakes and the Ethiopian Highlands (Figure 6.1). The most important seasons for precipitation are:

- The main rainy season from March to June in the Equatorial Lakes, referred to locally as the "long" rains.

- The secondary rainy season from October to December in the Equatorial Lakes, referred to locally as the "short" rains.
- The Kiremt rainy season from June to September in the Ethiopian Highlands (and the Belg rainy season from February to May in the southern part of Ethiopia)

These are clearly reflected in the monthly maps (Figure 6.10 to Figure 6.13) for the reference period derived from the CRU data.

The climate over the Nile Basin is determined by the interplay of a number of large-scale phenomena. For example the spatial distribution of rainfall over Ethiopia and its overall amount over the long rain season is not just a function of topography. The position and the intensity of the tropical easterly jet (TEJ), East African Low Level Jet (EALLJ) and the African easterly jet (AEJ), the phase of the Quasi Biennial Oscillation (QBO), the location of the inter tropical convergence zone (ICTZ), the strength of Azores high, the humidity anomaly over the Red Sea and the Gulf of Guinea, low level wind anomalies from the Atlantic Ocean and Indian Ocean to Africa and ENSO, (Diro et al., 2011) all play a role in controlling the rainfall pattern over the highlands. It is beyond the scope of this study to provide a physical understanding of the many climate processes affecting the Nile Basin and the interested reader is referred to the climate literature.
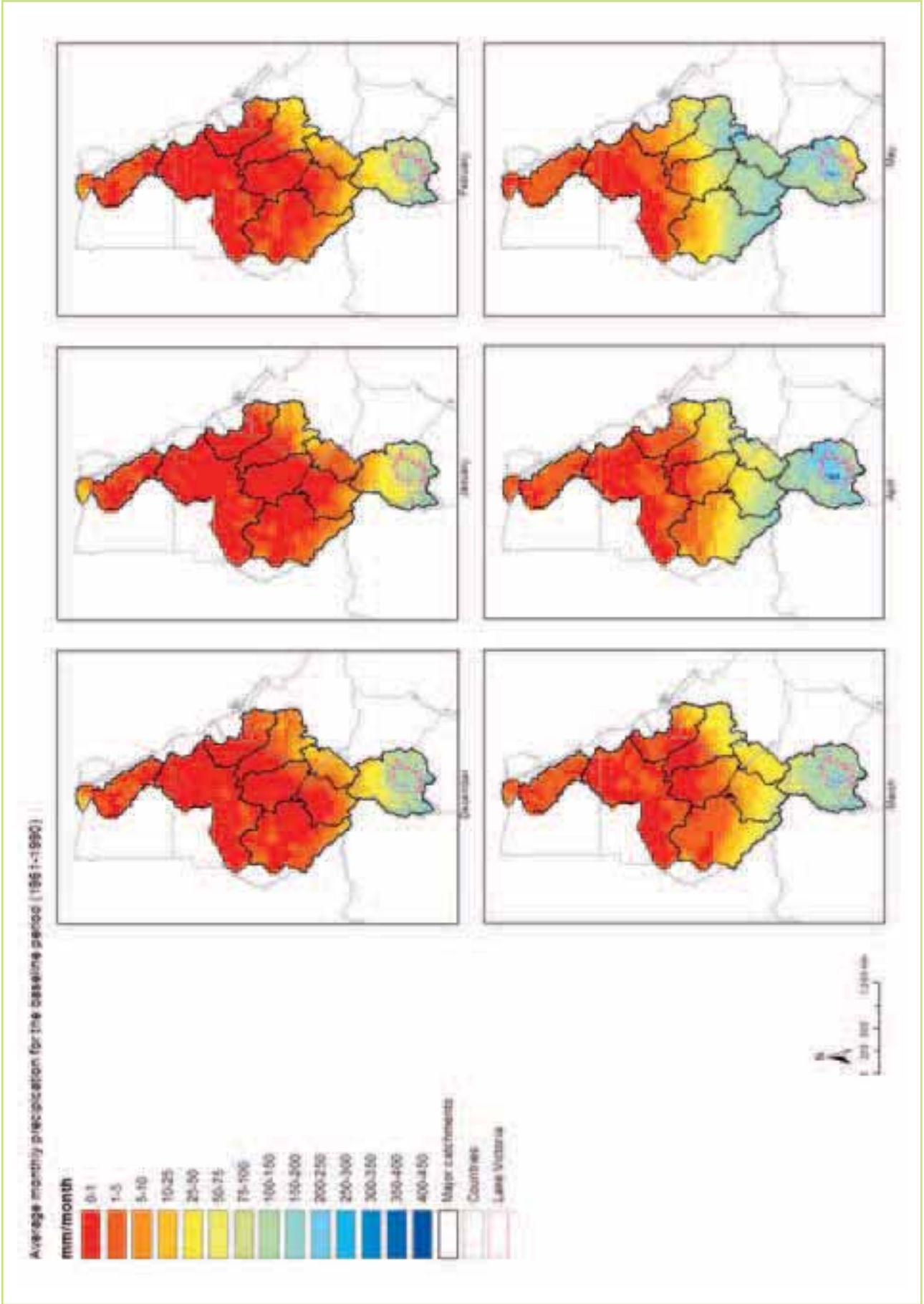
Figure 6..10 Average monthly precipitation for baseline period: 1961-1990, from CRU, December to May
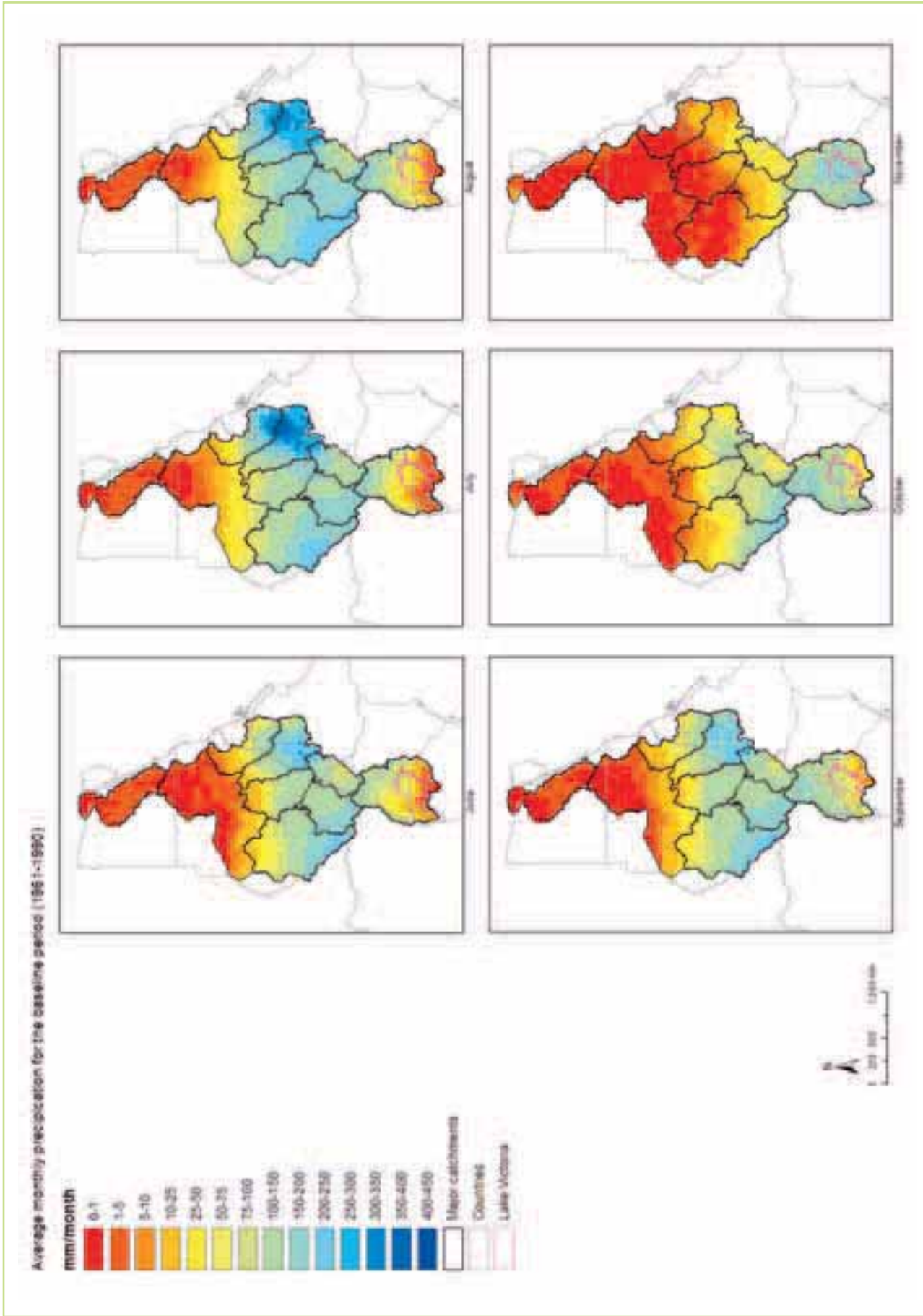
Figure 6.11 Average monthly precipitation for baseline period: 1961-1990, from CRU, June to November
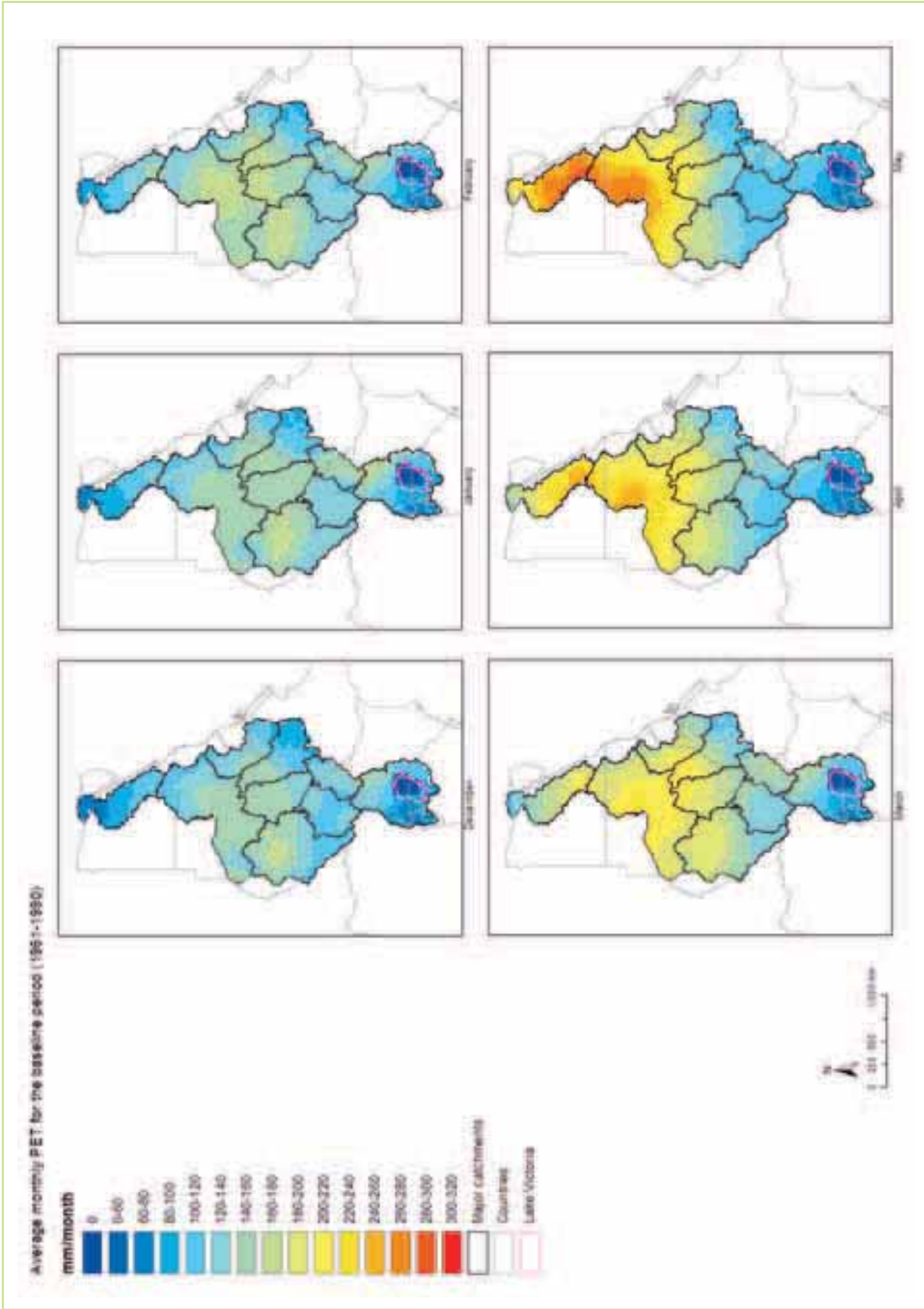
Figure 6.12 Average monthly PET for baseline period: 1961-1990, from CRU, December to May. Note that CRU values are given as zero over Lake Victoria
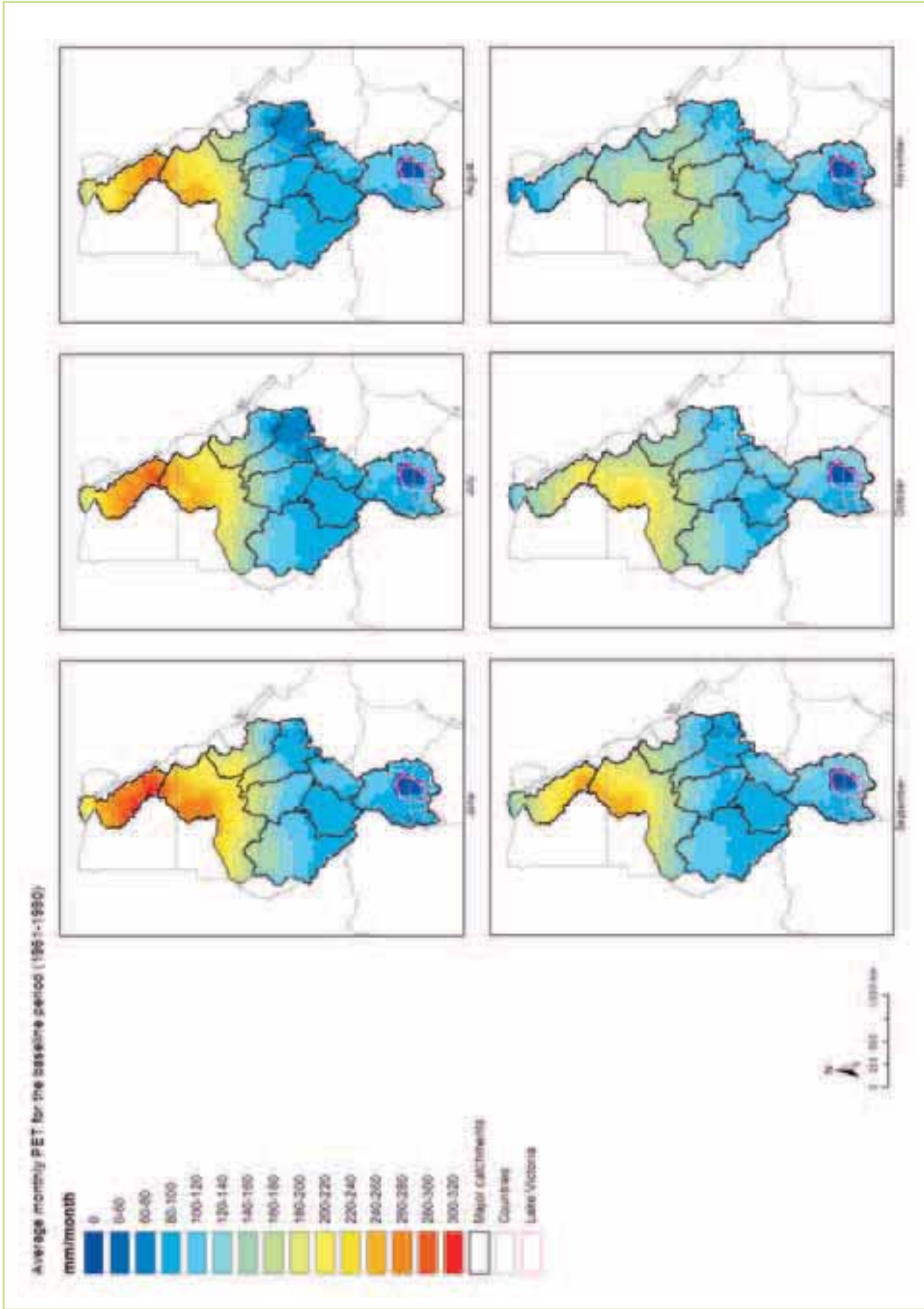
Figure 6.13 Average monthly PET for baseline period: 1961-1990, from CRU, June to November. Note that CRU PET values are given as zero over Lake Victoria.

6.5.2 Regional changes in temperature (2020-2049)

The projected regional changes in temperature show consistent increases for most of the Nile Basin and most of the year (Figure 6.14 and Figure 6.15). These figures show the median change in temperature at 1.5 m derived from the 5 RCM ensemble members.

There are however substantial variations both in space and time. There are significant increases in the southern part of the basin from April-June. The largest persistent increases occur over Egypt and the northern part of Sudan during the summer (June-October) with consistent increase of more than 2 degrees and close to 3 degrees in some locations. These large increases will occur during what are already the hottest months. This may be expected to affect water demand in both
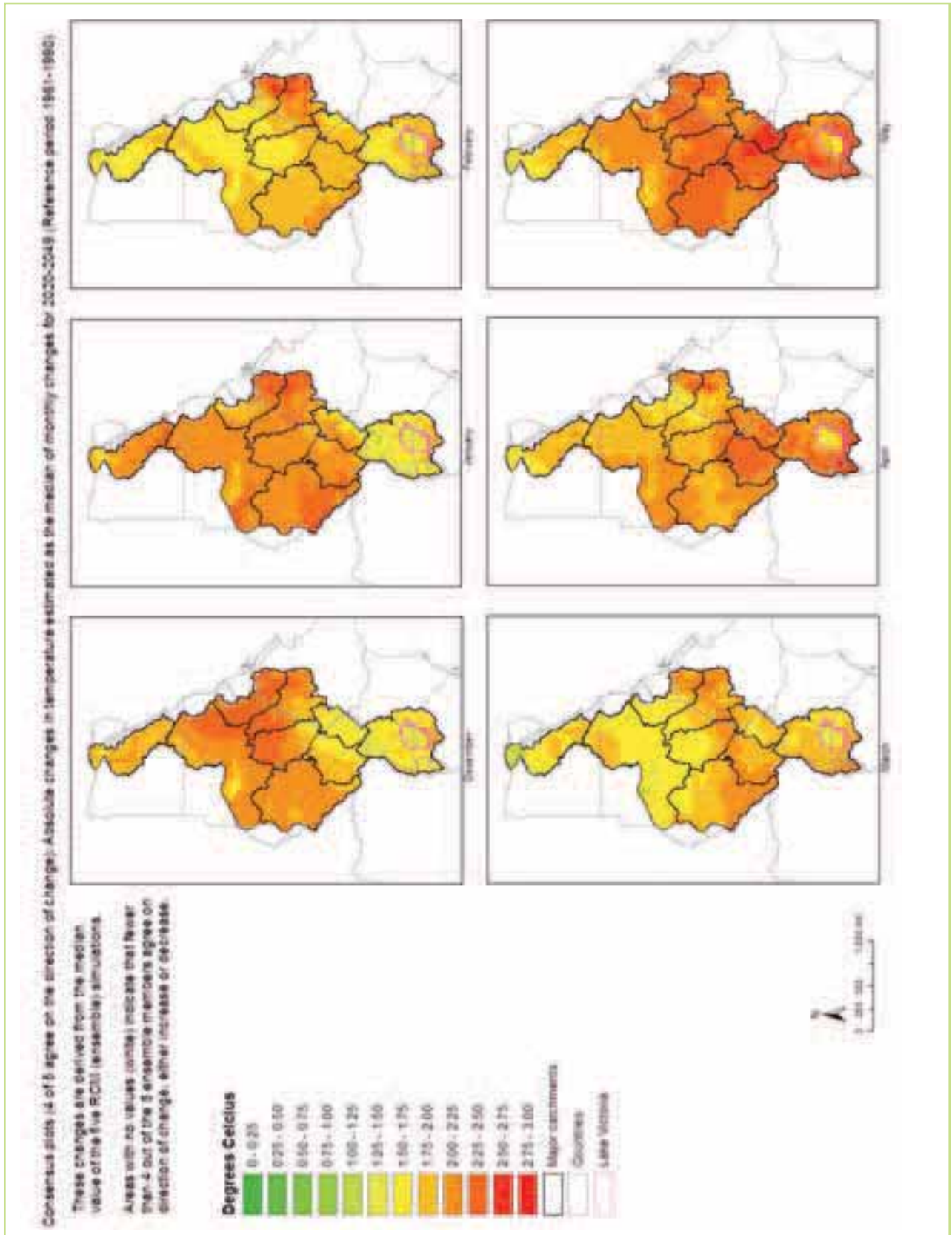
Figure 6.14 Absolute change in monthly temperature: 2020-2049, December to May

the agricultural and domestic sectors in these areas. The changes over Egypt and north Sudan for the winter (December to March) are lower by comparison and the smallest changes occur during this period at the Nile delta presumably controlled by coastal and ocean processes. There also appears to be a strong north south gradient in the temperature changes in the warmest months, July, August and September.

For the Ethiopian highlands, the temperature increase during the rainy season, especially July, August and September, appears to be limited to around 1.5 degrees. It is expected that the increases in temperature are moderated by the rainfall and cloud cover during this season.

A similar pattern of relatively low changes is seen over the Equatorial Lakes for November to December coinciding with the short rains.
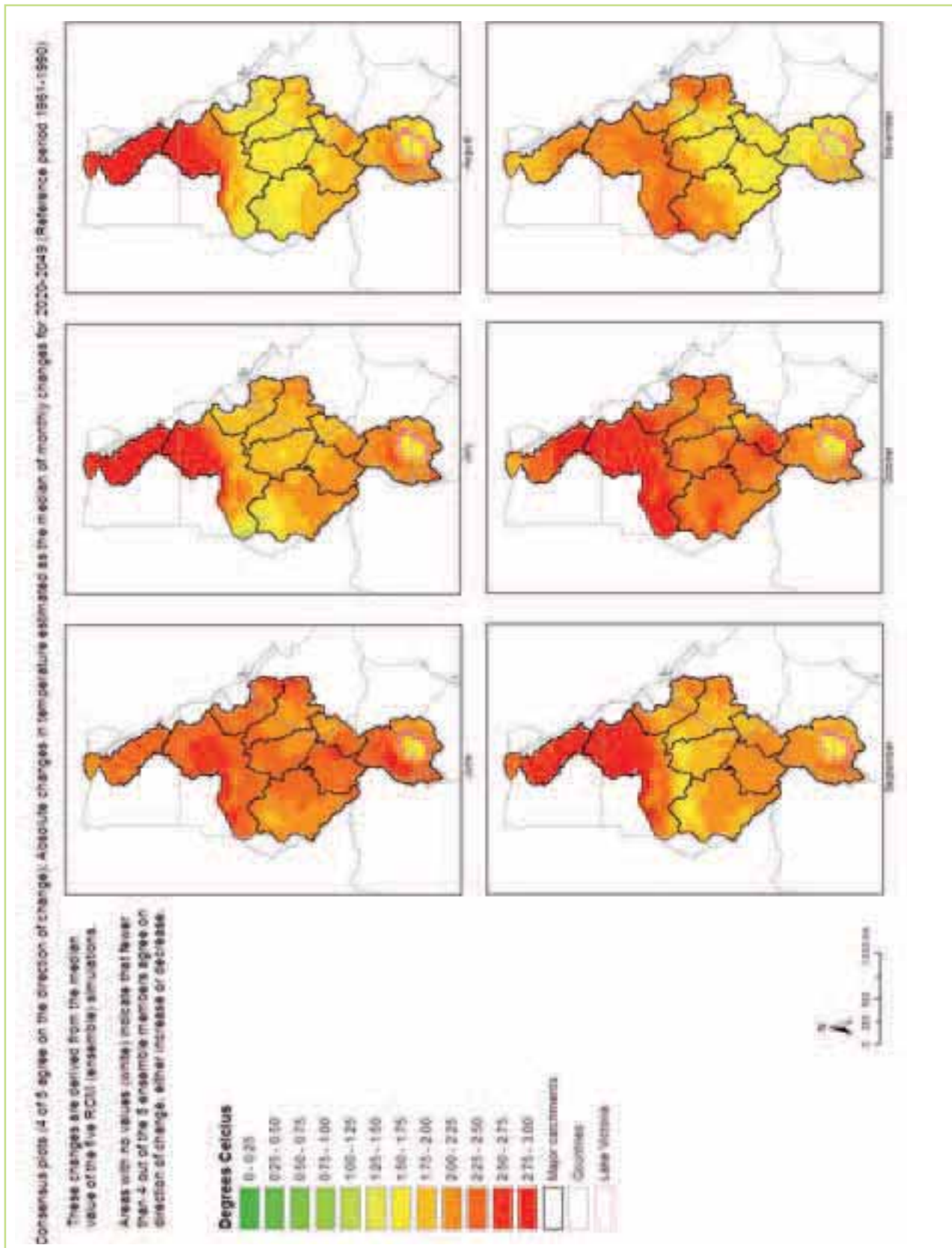
Figure 6.15 Absolute change in monthly temperature: 2020-2049, June to November

6.5.3 Regional changes in rainfall (2020-2049)

The projected regional changes in precipitation as percentages are presented in Figure 6.16 and Figure 6.17. The projections of precipitation from climate models in general are less reliable and exhibit less consistency and greater variability than the temperature projections. For example, although global models do agree on drying over Africa for the twentieth century, there is no robust agreement in their predictions of twenty-first-century rainfall (Giannini et al. 2008). Within the Nile Basin several previous studies indicate that there are large uncertainties in both the direction and magnitude of climate changes (e.g. IPCC 2007; Boko et al 2007; Elshamy et al. 2008; Beyene et al., 2010).

A review of the various indicators in relation to climate change highlighted an important limitation of many of the traditional indicators in relation to climate change which is that most are deterministic indices that do not reflect the uncertainties in the underlying data and calculations. This is particularly relevant for the Nile Basin as the water resources in the Nile are critically sensitive to climate change (e.g. Conway et al., 2007).

One approach to identify areas where consistent changes in precipitation can be found is to map the median value of precipitation at each cell where at least 4 out of the 5 ensemble members agree on the sign (direction) of the change. We refer to these maps as consensus maps. These consensus maps highlight regions where the regional climate models provide consistent (at least 4 out of 5 agree on the direction) projections and conversely areas where the regional models don't agree on the direction of change. This will support judgements on the impact of regional climate model uncertainty on floods and droughts. A consensus among the RCM projections for the direction of change provides useful information for decision-makers even if the magnitude of the change is uncertain. More robust approaches to climate change adaptation are needed in areas where the direction and magnitude of climate change are highly uncertain.

Figure 6.16 and Figure 6.17 present the consensus maps for precipitation for December-May and June-November, respectively. Care must be taken in the proper interpretation of these maps. The areas with no colour within the Nile Basin indicate the parts of the basin where fewer than 4 out of 5 RCM ensemble members agree on the direction of change in precipitation, i.e. the RCM projections give both increases and decreases in the precipitation in these areas. The areas in grey represent areas where the simulated precipitation amounts are less than 1 mm/month for that month in the RCM simulations of the baseline period. These correspond to areas of extremely low rainfall and thus estimates of percentage changes may be misleading. The colours indicate cells where at least 4 out of the 5 RCM ensemble members agree on the direction of change and the strength of colour indicates the magnitude of the change. The magnitude of change is estimated as the median of the 5 ensemble members. As the median of neighbouring cells can arise from different ensemble members these maps do not provide a physically coherent rainfall field but rather a graphical indication of areas of model consensus and the magnitude of the change.

The first point worth noting is that there are large areas for many months where fewer than 4 out of 5 RCM ensemble members agree on the direction of precipitation change. This reflects the inherent uncertainty in projections of precipitation and is consistent with previous studies based on global models. Nevertheless the coloured cells highlight areas where at least 4 out of 5 RCM projections are consistent and provide a strong signal as to the direction of future change.

The Nile Equatorial Lakes are the source areas for the White Nile and provide a major part of the Nile flows during the dry season of the Ethiopian Highlands. The projections indicate consistent reductions in the rainfall during part of the "long" rainy season (March to June) and the decrease continues until October. From November to January the results indicate increases in rainfall covering part of the "short" rainy season. Clear reductions are seen over Lake Victoria for most of the year, which is important to note as the rainfall falling directly on the lake itself corresponds to 80-85% of the water balance (Sutcliffe and Parks, 1999).

In developing the new set of RCM simulations for this project an alternative approach was used over Lake Victoria. As the HadRM3P and MOSES2.2 have no specific lake model, in earlier work, simulations have assumed the lakes to be at sea level, and the lake temperatures are interpolated from the nearest sea point. This leads to a warm bias in the lake temperatures and subsequently excessive evaporation. To address this in the climate model, the larger Great Lakes (Lake Victoria, Lake Nyasa and Lake Tanganyiki) were set to land points in the domain orography at the correct elevation. Secondly, observations of lake-surface temperatures

were used to bias correct the model temperatures (Buontempo et al., 2013a).

It should be noted that the resulting RCM projections developed for this study exhibit a strong positive bias in precipitation over the lake and closer examination of this effect has shown that the precipitation in the "short" rainy season in particular is over- estimated (Buontempo et al., 2013a). On the one hand, this effect is local to the lake but on the other hand the rainfall directly over the lake is large fraction of the total water entering the lake. The exact cause of this are not yet fully understood. It is worth noting however that previous work using a different description of processes for Lake Victoria also showed a significant drying during the northern hemisphere summer (JJAS) (Butts et al, 2011). No clear consensus is found regarding the changes over Lake Victoria for in the part of the "short" rainy season, but increases are projected north and west of the Lake Victoria during November-January.

An examination of the spatial patterns show an increase in precipitation over central Africa (Buontempo et al., 2013a) which appears to lead to increases in precipitation over southern part of Sudan and the northern part of the White Nile during August and September.

The most critical region for the high "flood" flow season in the lower part of the Nile is the western edge of the Ethiopian Highlands, where the Blue Nile and the Atbara rivers have their source. Together they contribute as much as 75% of the discharge in the main Nile. The RCM consensus maps show both increases and decreases in the region during the wet season, June to September. The reductions appear in the eastern most parts of these two model sub-basins, while the increases appear in the south and west and suggest a general increase at the end of the wet season. No clear patterns emerge for the other seasons.

Over Egypt, the results exhibit either very low rainfall or reductions for many months of the year. From November to March there are large parts of Egypt and Sudan that receive very little rainfall (<1 mm/month).

These consensus plots clearly indicate areas where the RCM simulations make consistent projections of the direction of change. However the distribution of rainfall in the Nile basin on a regional scale is localised around the Equatorial Lakes and the Ethiopian highlands. So small relative changes in rainfall here may lead to large increases in the absolute volume of rainfall whereas large relative changes in arid or semi-arid regions may have little effect on the water balance and river flows. To get a better indication of the absolute changes, the estimated relative median changes have been applied to the baseline monthly rainfall totals obtained from CRU (Figure 6.10 and Figure 6.11).

The resulting absolute changes in rainfall are shown in Figure 6.18 and Figure 6.19. Again it needs to be emphasised that care must be taken in interpreting these patterns and they do not represent a physically consistent rainfall field. The changes represent median values which may arise from different ensemble members in neighbouring cells which is reflected in the flecked or dotted appearance of these maps. Nevertheless these maps highlight the significant reductions in rainfall over Lake Victoria from April to October but also show increases in the rainfall north and west of Lake Victoria from November to January corresponding to the "short" rains. It should be recalled that the underlying RCM's simulations have a wet bias during this period. The spatial distribution of both the increases and decreases over the Ethiopian Highlands are also more clearly highlighted. There also appears to be a clear general increase in rainfall over Sudan at the end of the wet season.
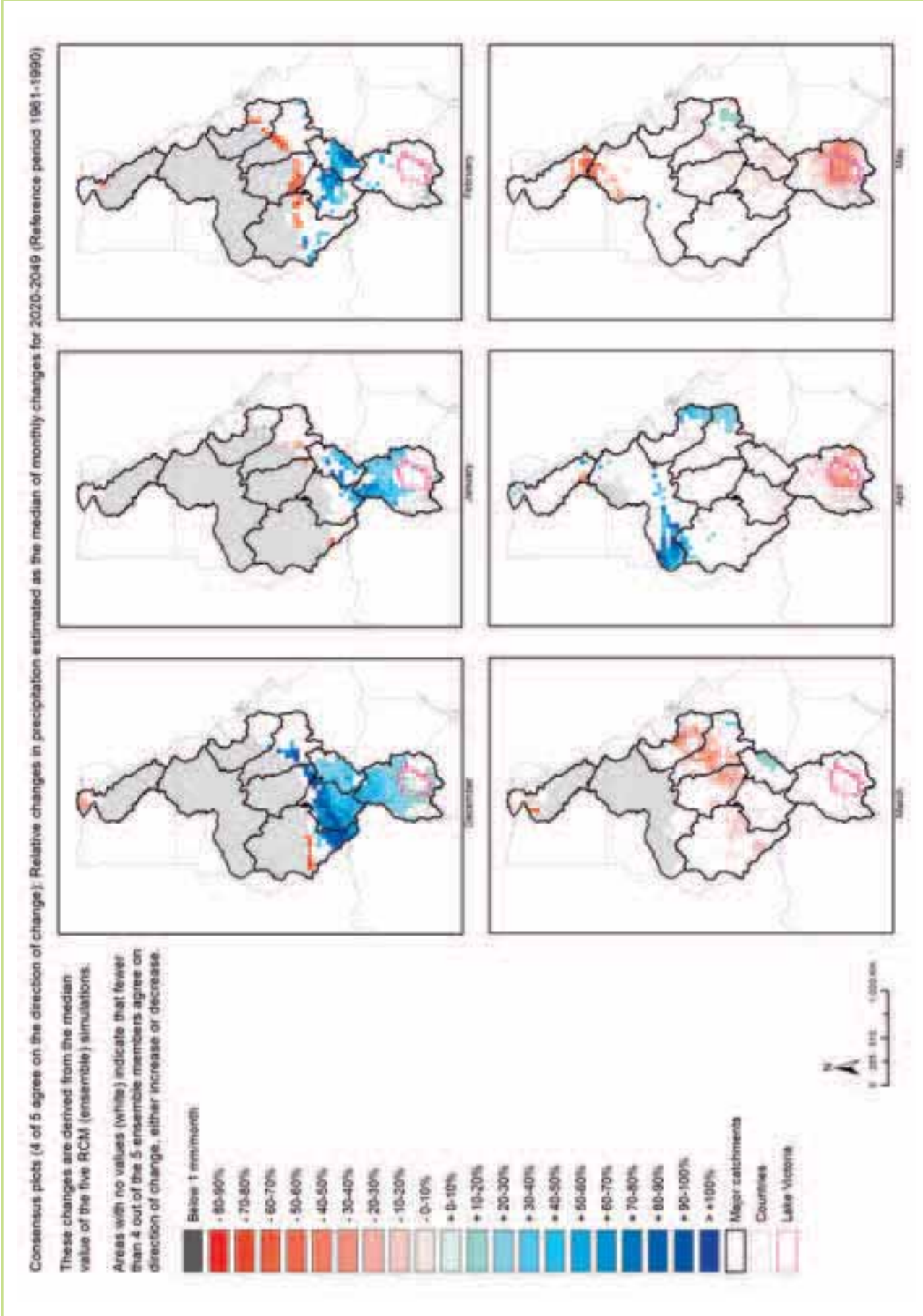
Figure 6.16 Relative change in monthly precipitation: 2020-2049, December to May
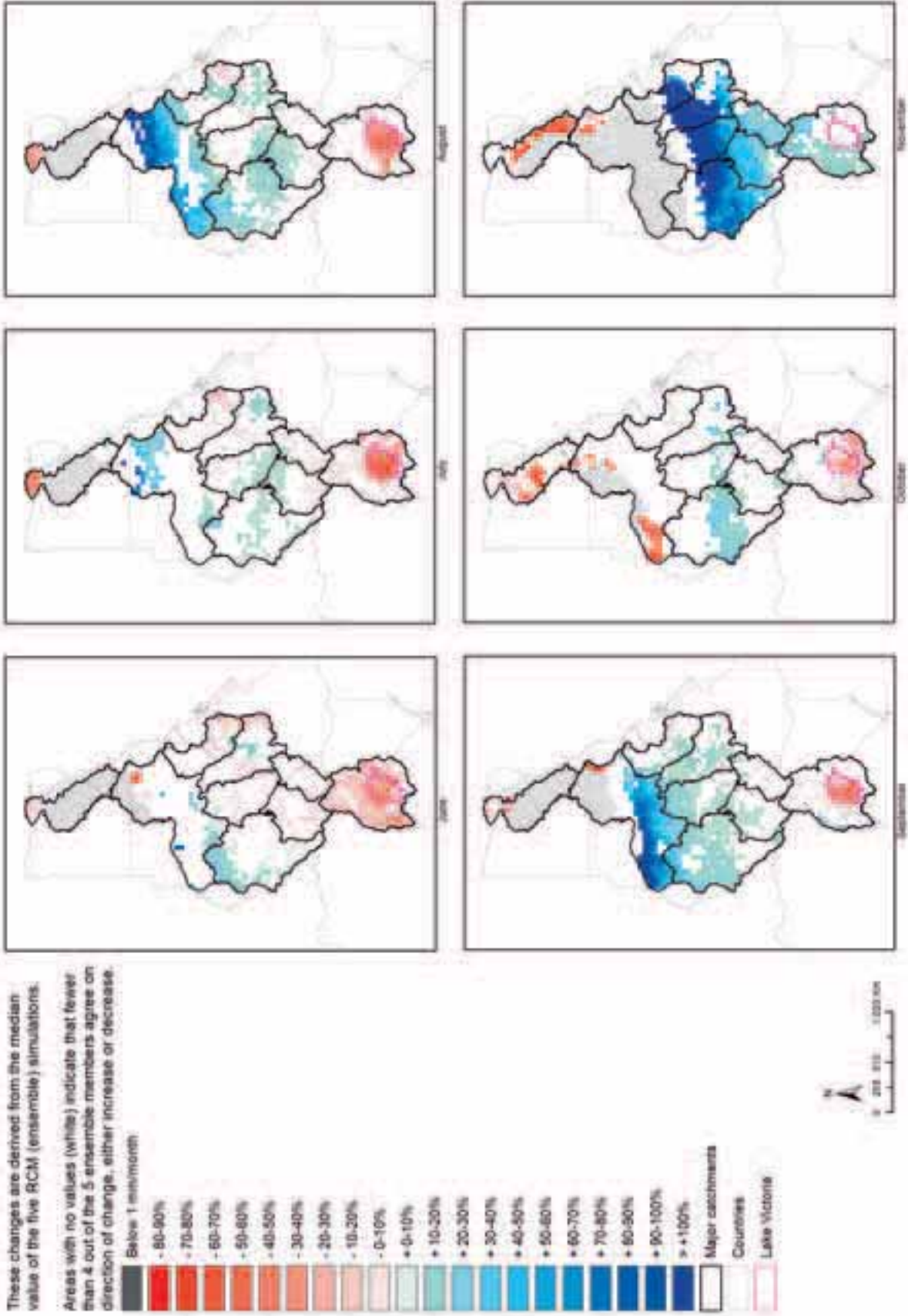
Figure 6.17 Relative change in monthly precipitation: 2020-2049, June to November
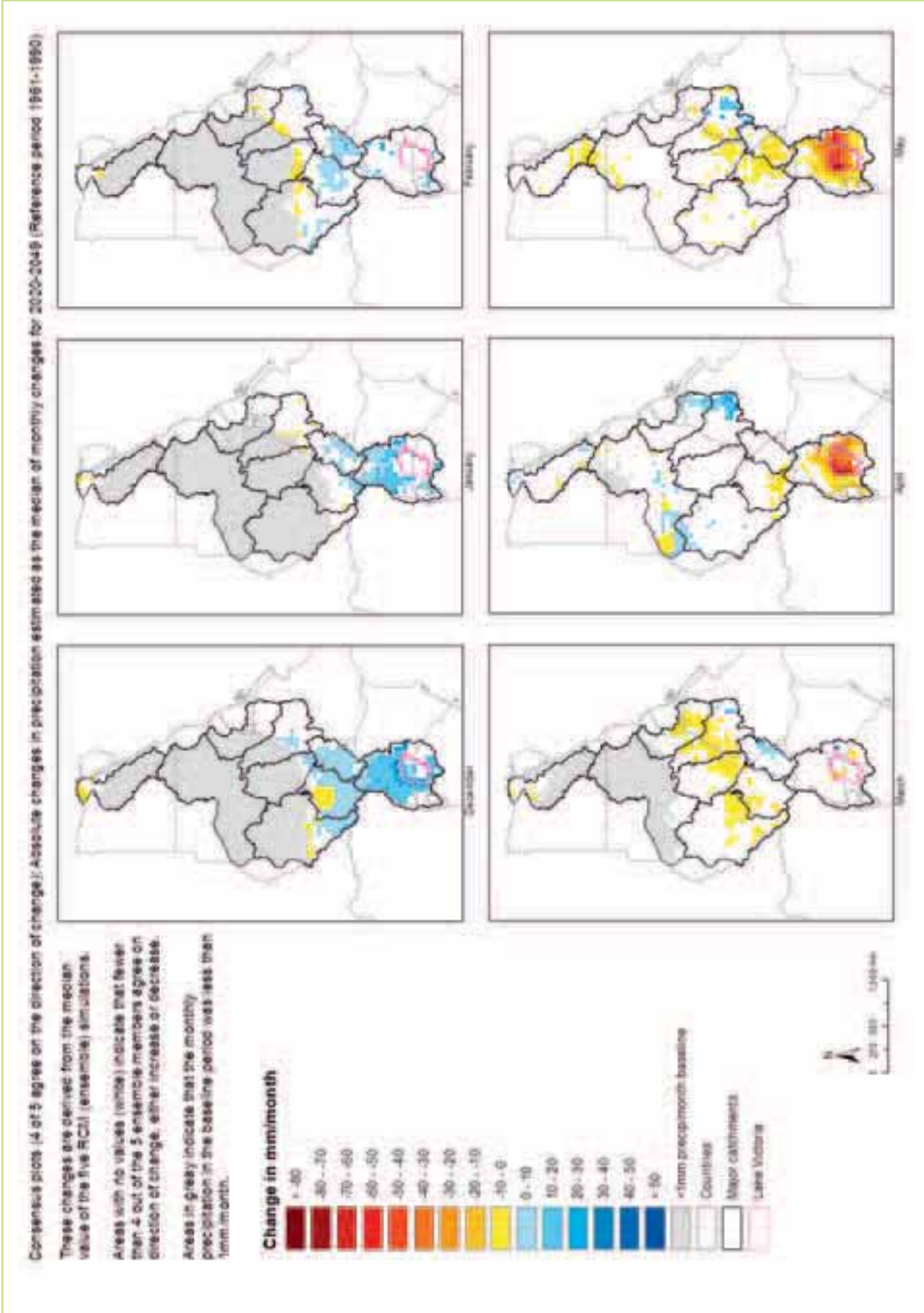
Figure 6.18 Absolute changes in monthly precipitation: 2020-2049, December to May
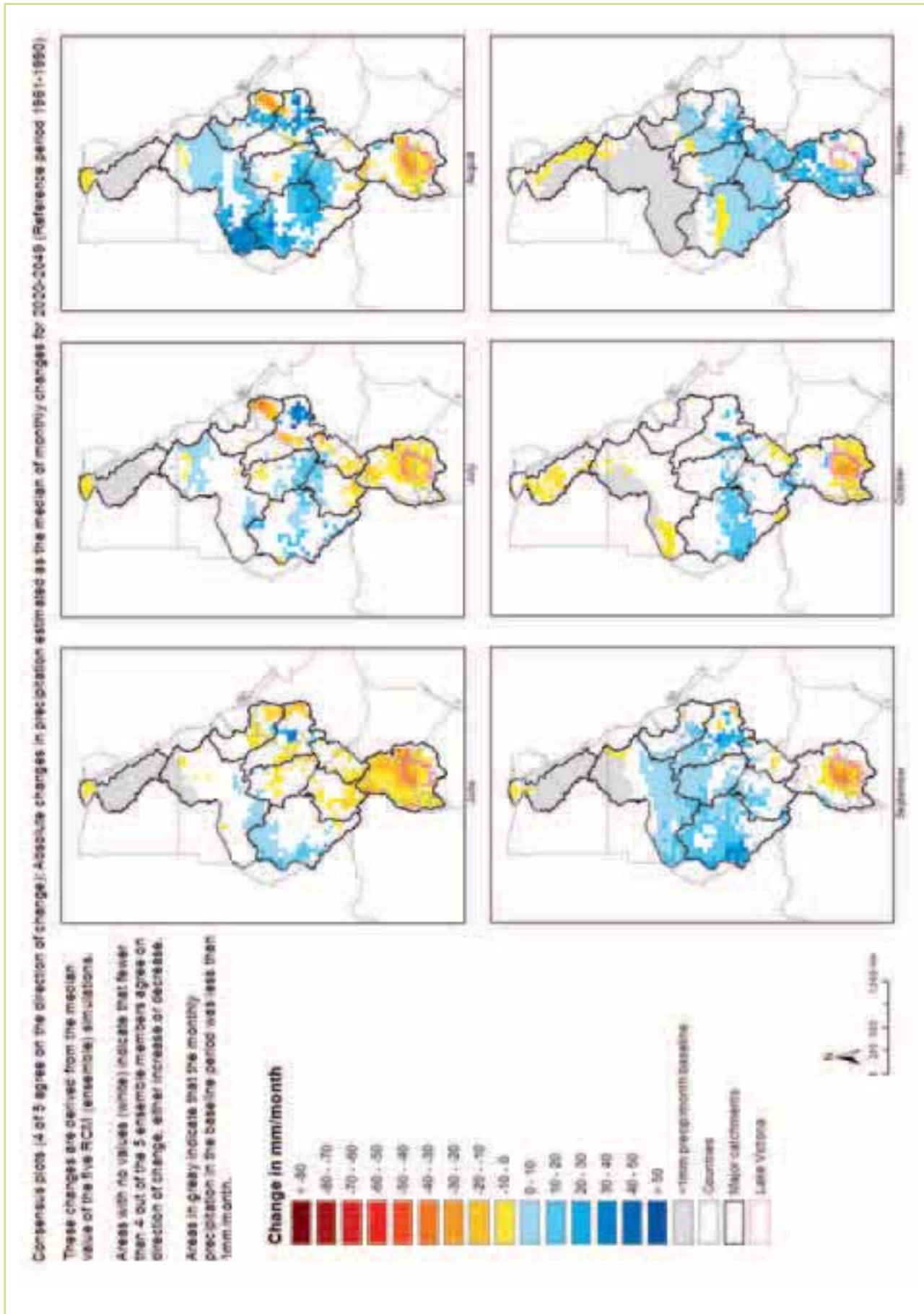
Figure 6.19 Absolute change in monthly precipitation: 2020-2049, June to November

191

6.5.4 Regional changes in potential evapotranspiration PET (2020-2049)

Potential evapotranspiration is the other main hydrological variable in assessing the water balance and estimating flows. It generally exhibits less spatial variability than rainfall. The projected regional changes in PET as percentages are presented in Figure 6 20 and Figure 6 21. These figures show that the overall trend is increasing PET which is consistent with increasing temperatures. However, there are large areas where no consistent direction of change is seen and the size and location of these areas are highly seasonal.

Nevertheless, there are some areas, where reductions in PET are projected, for example, north of Lake Victoria during December and January corresponding to the projected increases in rainfall. It is expected that this is a result of increases in cloud cover and humidity and the corresponding reductions in temperature. The projections also suggest some decreases in PET over the Sudd, White Nile and Sobat catchments of the regional model. More notably for these catchments there appears to be no clear agreement as to the direction of change in PET in the period from November to March. This is an important observation as potential evaporation over South Sudan plays a key role in the water balance of the White Nile. The evaporation losses in the Sudd control the amount of water reaching the main Nile.

There are significant increases in PET over the Blue Nile and Atbara catchment during June and July. The pattern for the rest of the year is less clear with slight increases or no consistent indication of the direction of change.

These figures show the relative change in PET and as described earlier there are strong north gradients in PET (Figure 6 1). To get a better indication of the absolute changes, the estimated rmedian changes have been applied to the baseline monthly PET totals obtained from CRU (Figure 6 22 and Figure 6 23).

These figures highlight the main features we found in the maps of relative change. There appears to be a small increase in PET around Lake Victoria for most of the year including the rainy seasons. The method used to calculate the PET change factors was designed for land points in the RCM and therefore not suitable for calculating PET directly over Lake Victoria, which was treated in the land surface model as a sea point. Therefore, the assumption was made that the change in PET over the lake was not significant (particularly considering the high uncertainty in the precipitation modelling directly over the lake, as demonstrated by the large bias in some seasons of the model precipitation compared to available observational datasets). For this reason Lake Victoria is shown in grey."

Figure 6.20 Relative change in monthly PET: 2020-2049, December to May

Consensus plots (4 of 5 agree on the direction of change): Relative changes in PET estimated as the median of monthly changes for 2020-2049 (Reference period 1961-1990)

These changes are derived from the median value of the five RCM (ensemble) simulations.

Areas with no values (white) indicate that fewer than 4 out of the 5 ensemble members agree on direction of change: either increase or decrease.

-10-12%
-8-10%
-7-8%
-6-7%
-5-6%
-4-5%
-3-4%
-2-3%
-1-2%
-0-1%
+ 0-2%
+ 2-4%
+ 4-6%
+ 6-8%
+ 8-10%
+ 10-12%
+ 12-14%
+ 14-16%
+ 16-18%
+ 18-20%
Major catchments
Countries
Lake_Victoria

August
July
June
September
October
November
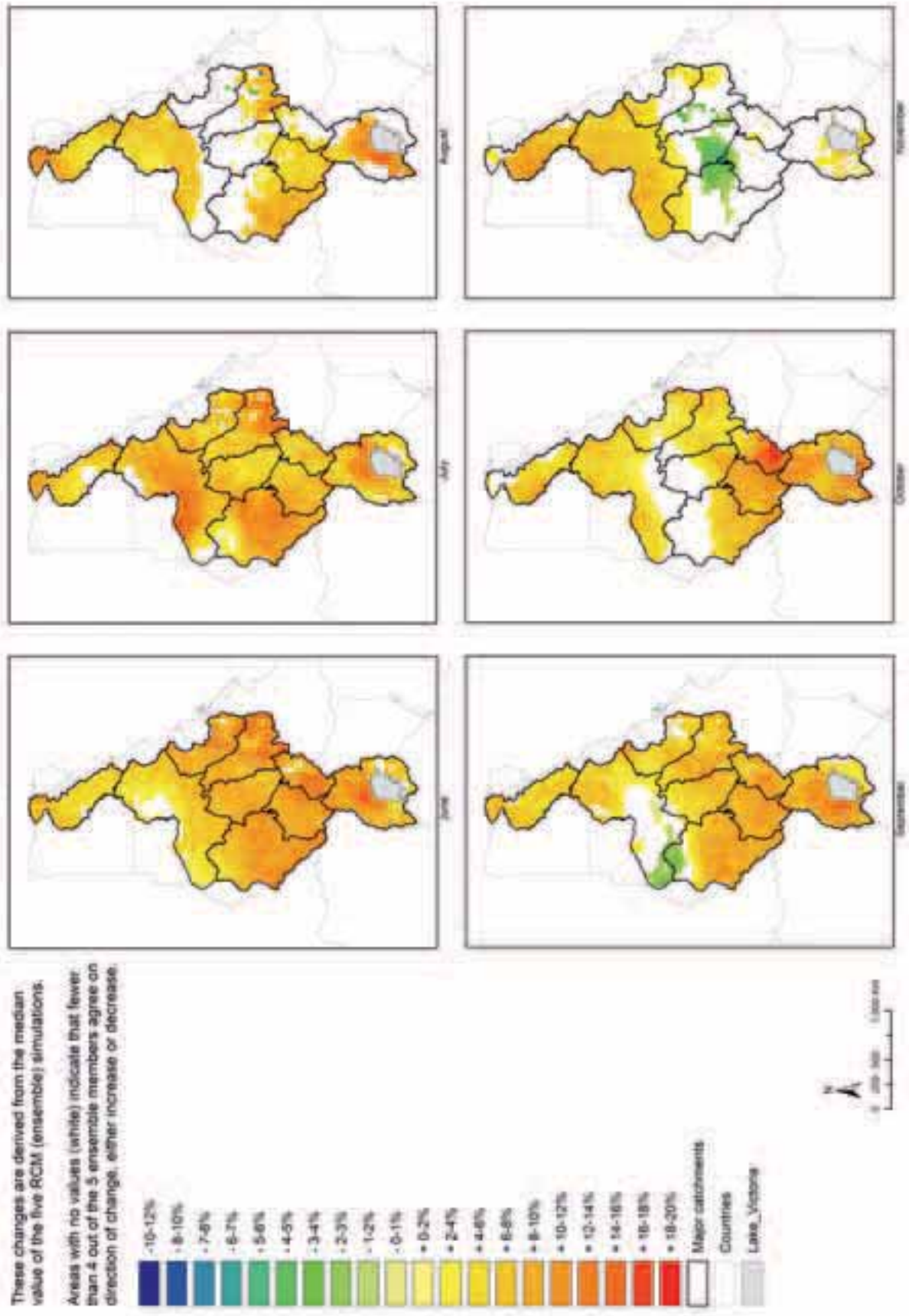
Figure 6.21 Relative change in monthly PET: 2020-2049, June to November

Figure 6.22 Absolute change in monthly PET: 2020-2049, December to May. Note that CRU baseline PET values are given as zero over Lake Victoria

Consensus plots (4 of 5 agree on the direction of change): Absolute changes in PET estimated as the median of monthly changes for 2020-2049 (Reference period 1961-1990).

These changes are derived from the median value of the five RCM (ensemble) simulations.

Areas with no values (white) indicate that fewer than 4 out of the 5 ensemble members agree on direction of change, either increase or decrease.
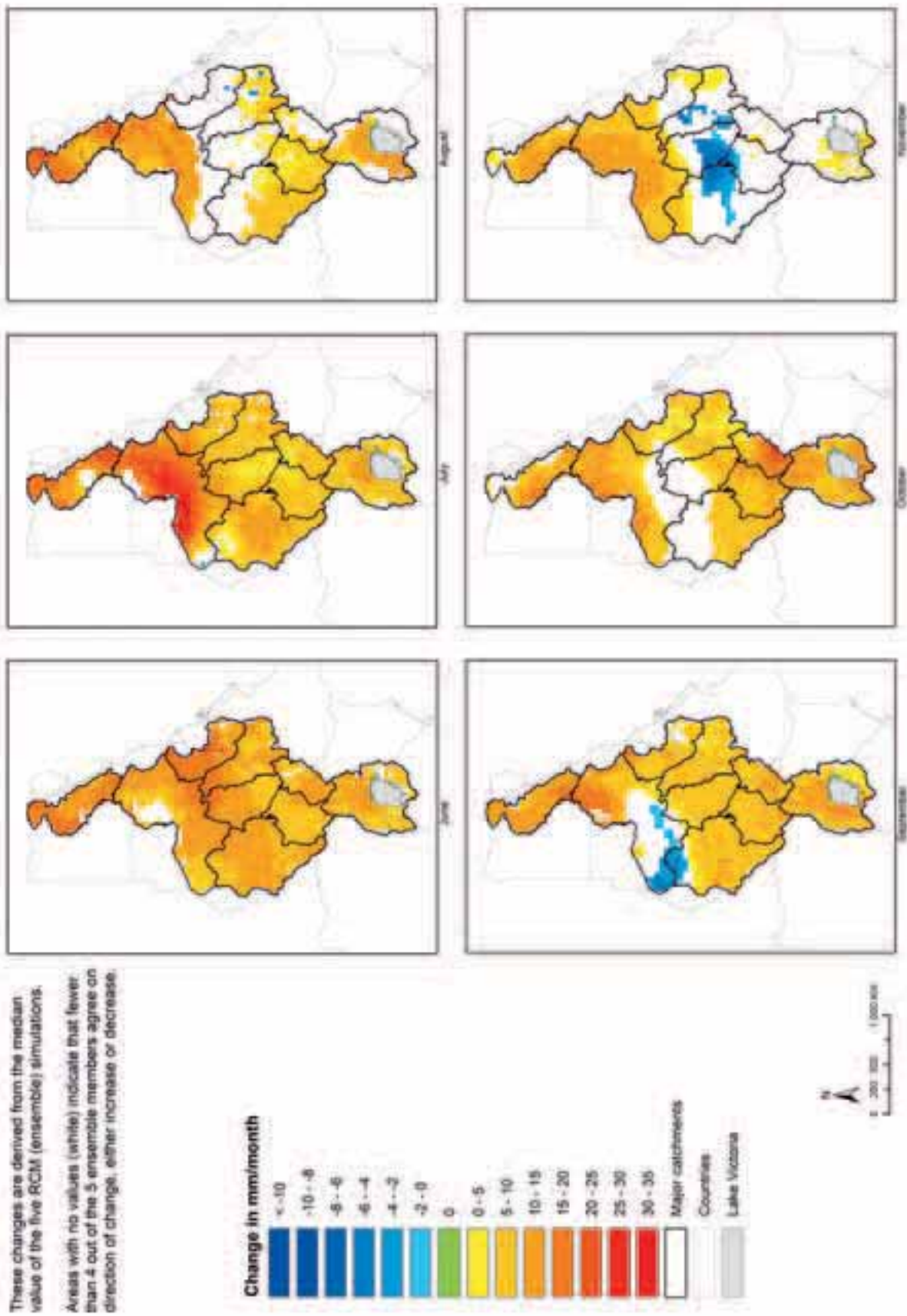
Change in mm/month

Figure 6.23   Absolute change in monthly PET: 2020-2049, June to November. Note that CRU baseline PET values are given as zero over Lake Victoria.

6.5.5 Regional changes in temperature (2070-2099)

The projected regional changes in temperature for 2070-2099 show significant and consistent increases for most of the Nile Basin (Figure 6 24 and Figure 6 25). Increases of 4-5 degrees are seen particularly for May-July and September-October for most of the Nile. Once again the largest increases occur in the hottest months. It is also important to recall that the figures shown here are median values of the 5 RCM ensemble members. This means that while a consistent increase in temperature is shown, the extent of the increases varies in the RCM ensemble projections. In general, the patterns for 2020-2049 and 2070-2099 are similar, with a substantial intensification of the increase in temperature between the two periods. While the temperature increases for 2020-2049 are mainly within the range of 1-3 oC, the projected temperature increases for 2070-2099 are mostly within the range of 2.5-6.0 oC.

In hydrological terms these large increases in temperature can be expected to result in increases in the potential evapotranspiration demands and may be expected to affect water demand in both the agricultural and domestic sectors in the populated centres. This large increase in temperature can therefore be expected to have significant socio-economic consequences in other sectors. A detailed discussion of these is outside the scope of the current study.

6.5.6 Regional changes in precipitation (2070-2099)

The projected regional changes in precipitation for the period 2070-2099 are shown in Figure 6.26 and Figure 6.27. Comparing these consensus maps with the corresponding maps for 2020-2049, a number of observations can be made.

One major difference from the 2020-2049 maps appears for the Ethiopian Highlands where the 2070-2099 projections show a consistent increase in the eastern most parts of the Blue Nile and Atbara catchments for most of the year including the rainy season. This is expected to have a significant impact on the flows in these two catchments and downstream as together they represent around 75% of the flows into the main Nile under current conditions.

Examining the behaviour over Lake Victoria, the projected changes show to a large extent the same trends as the 2020-49 projections: There is little agreement between the five ensembles from December to February, while there is a clear decrease in the rainfall over the lake from April to October. Around the lake the decrease in rainfall during May to August is also similar to 2020-2049. However, for the remaining part of the year there is an increase in rainfall which is generally more pronounced than during 2020-2049, particularly for December-March. The most obvious difference can be seen in March where there is a very substantial increase in the rainfall around almost all of the lake while there was either no agreement or a slight decrease in some parts for 2020-2049.

Figure 6.28 and Figure 6.29 provide an indication of the absolute changes in monthly rainfall. These changes are estimated by multiplying the median changes in rainfall with the baseline monthly rainfall totals obtained from CRU. These show clear increases in rainfall, from July to September in both the Ethiopian highlands and South Sudan. The increases in this area during these months are much higher than for the 2020-2049. Such increases in monthly rainfall are not unlikely during this period. While the increased rainfall over South Sudan may be lost through evaporation further downstream the other increases particularly over the Blue Nile and Atbara sub-basin are likely to lead to increased flows from these catchments and the Main Nile.

6.5.7 Regional changes in potential evapotranspiration PET (2070-2099)

The projected regional changes in PET as percentages are presented in Figure 6.30 and Figure 6.31. These figures show that the overall trend towards increasing PET, seen for the 2020-2049 period continues, which is consistent with the corresponding increase in temperatures. In comparison with the 2020-2049 projections, the increases are generally larger, sometimes up to twice as large. The areas where no consistent direction of change are seen are now generally smaller and there are only very few pixels where reductions in PET appear.

Estimates of monthly absolute changes in PET were obtained by multiplying the median relative projected changes by the baseline monthly PET obtained from CRU (Figure 6.32 and Figure 6.33). These figures show clear increases over most of the Nile including the Ethiopian Highlands and the Equatorial Lakes and the Sudd. Comparing the absolute changes for 2070-2099 (Figure 6.32 and Figure 6.33) with the absolute changes for 2020-2049 (Figure 6.22 and Figure 6.23), we find that for the areas showing increases, the absolute changes for 2070-2099 are roughly twice as large as for 2020-2049.

Figure 6.24 Absolute changes in monthly temperature: 2070-2099, December to May

Figure 6.25 Absolute changes in monthly temperature: 2070-2099, June to November

Figure 6.26 Relative changes in monthly precipitation: 2070-2099, December to May

Consensus plots (4 of 5 agrees on the direction of change). Relative changes in precipitation estimated as the median of monthly changes for 2070-2099 (Reference period 1961-1990)

These changes are derived from the median value of the five RCM (ensemble) simulations.

Areas with no values (white) indicate that fewer than 4 out of the 5 ensemble members agree on direction of change, either increase or decrease.
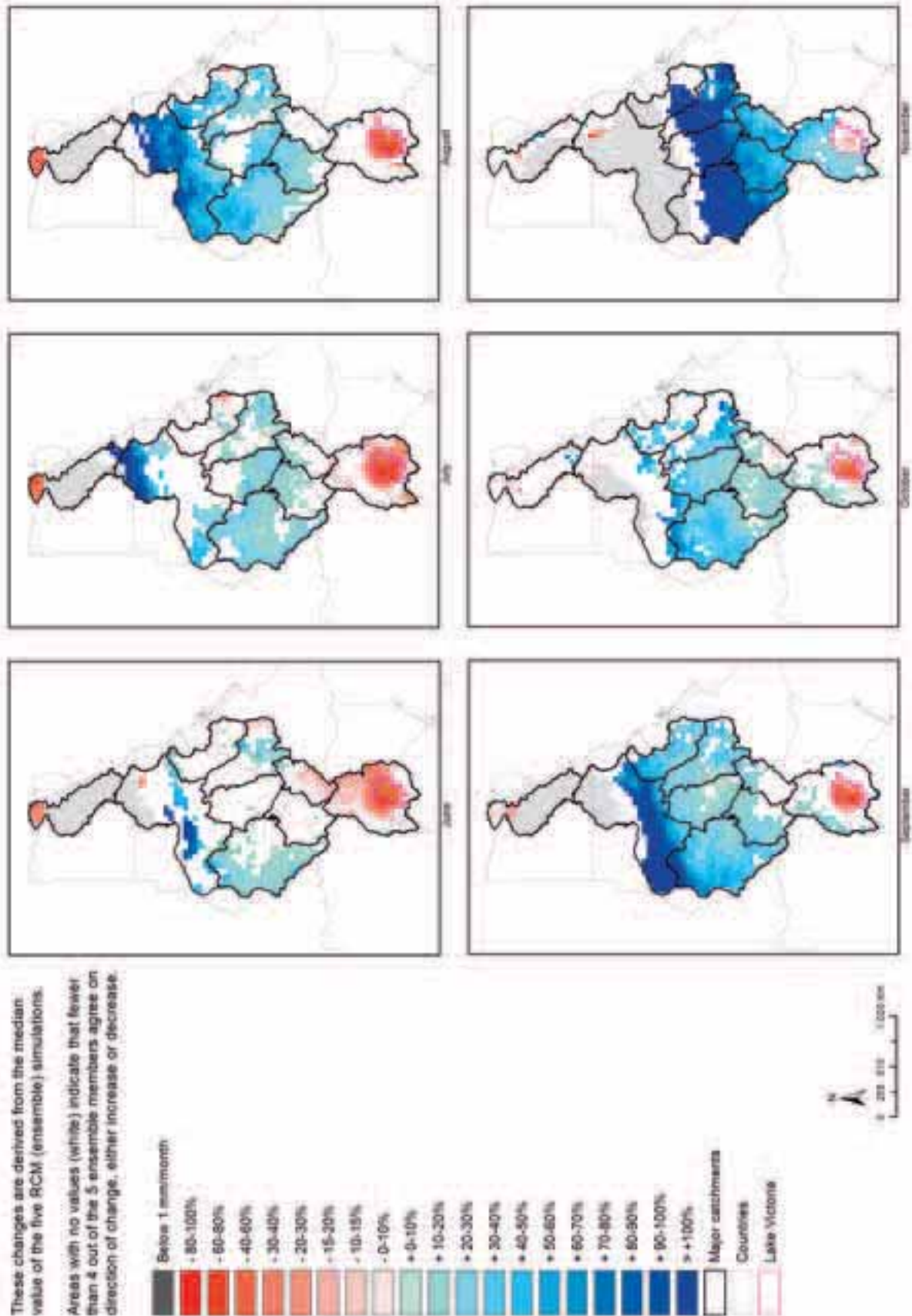
Figure 6.27 Relative change in monthly precipitation: 2070-2099, June to November
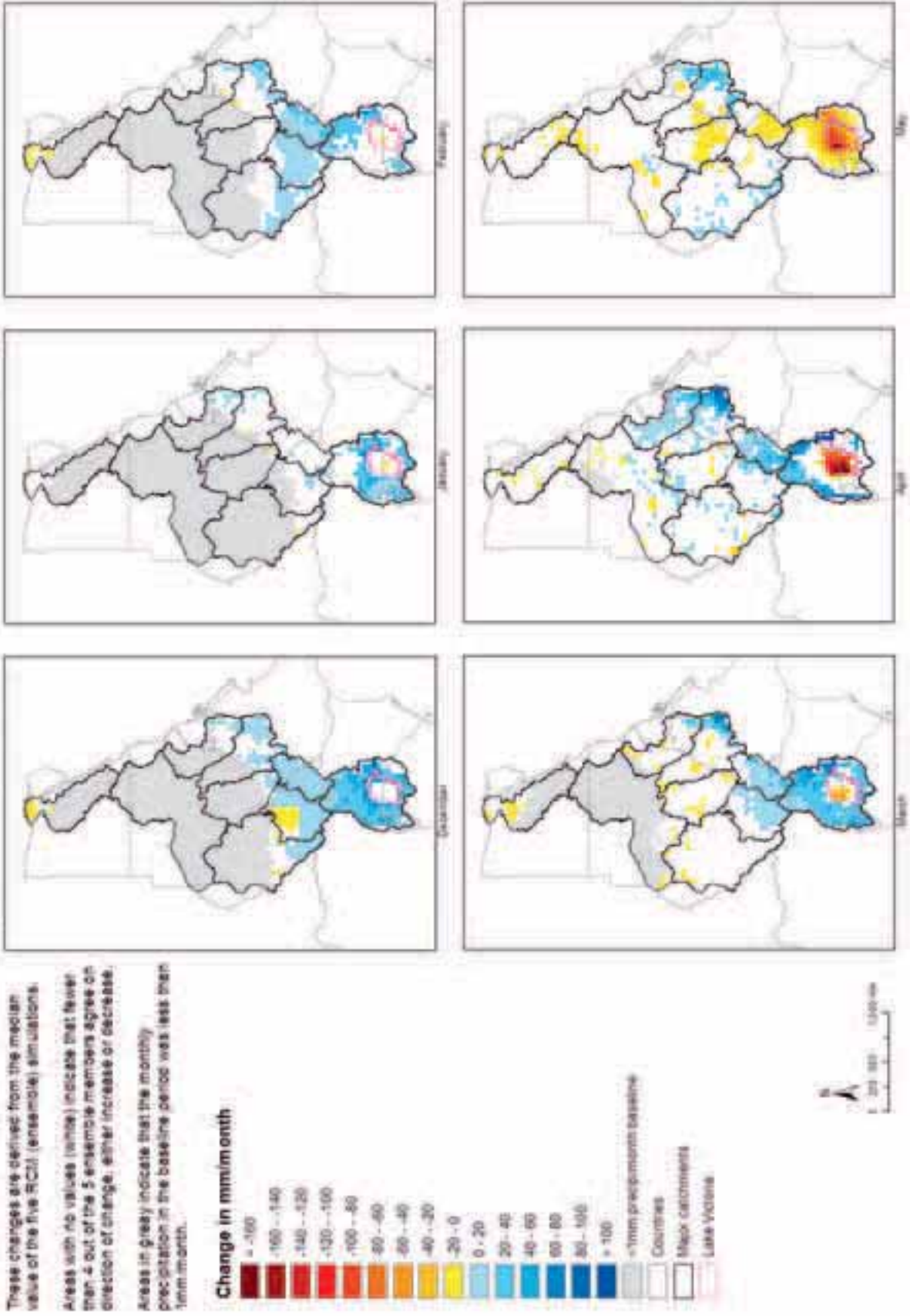
Figure 6.28 Absolute change in monthly precipitation: 2070-2099, December to May

Figure 6.29 Absolute change in monthly precipitation: 2070-2099, June to November

203

Figure 6.30 Relative change in monthly PET: 2070-2099, December to May
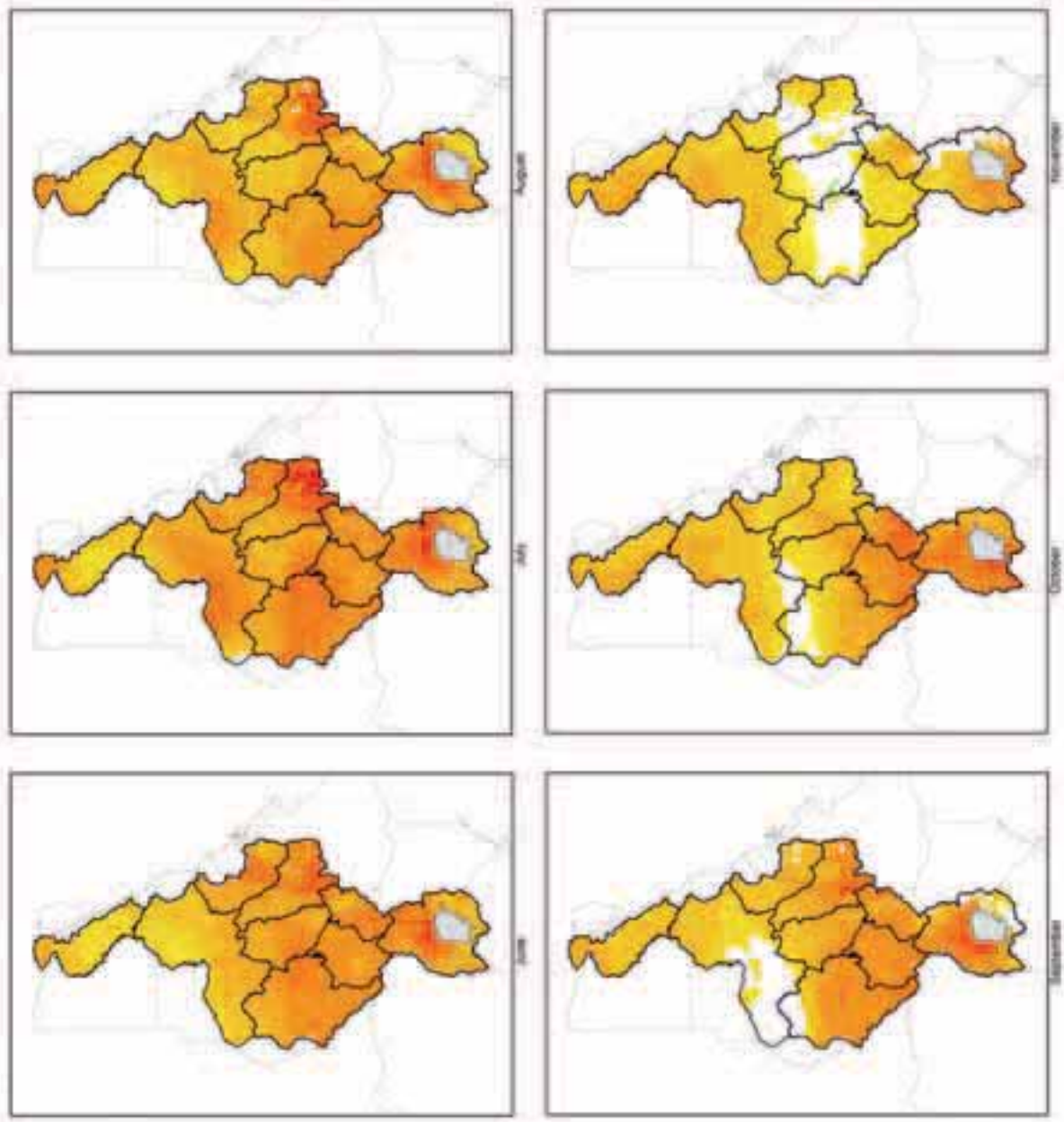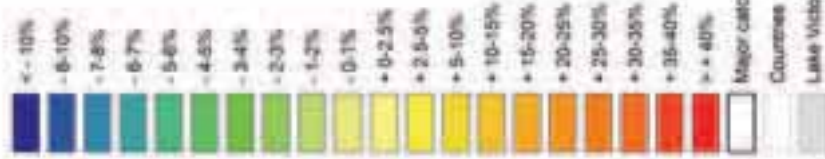
Figure 6.31 Relative change in monthly PET: 2070-2099, June to November

Consensus plots (4 of 5 agree on the direction of change): Absolute changes in PET estimated as the median of monthly changes for 2020-2049 (Reference period 1961-1990).

These changes are derived from the median value of the five RCM (ensemble) simulations.

Areas with no values (white) indicate that fewer than 4 out of the 5 ensemble members agree on direction of change: either increase or decrease.

Change in mm/month
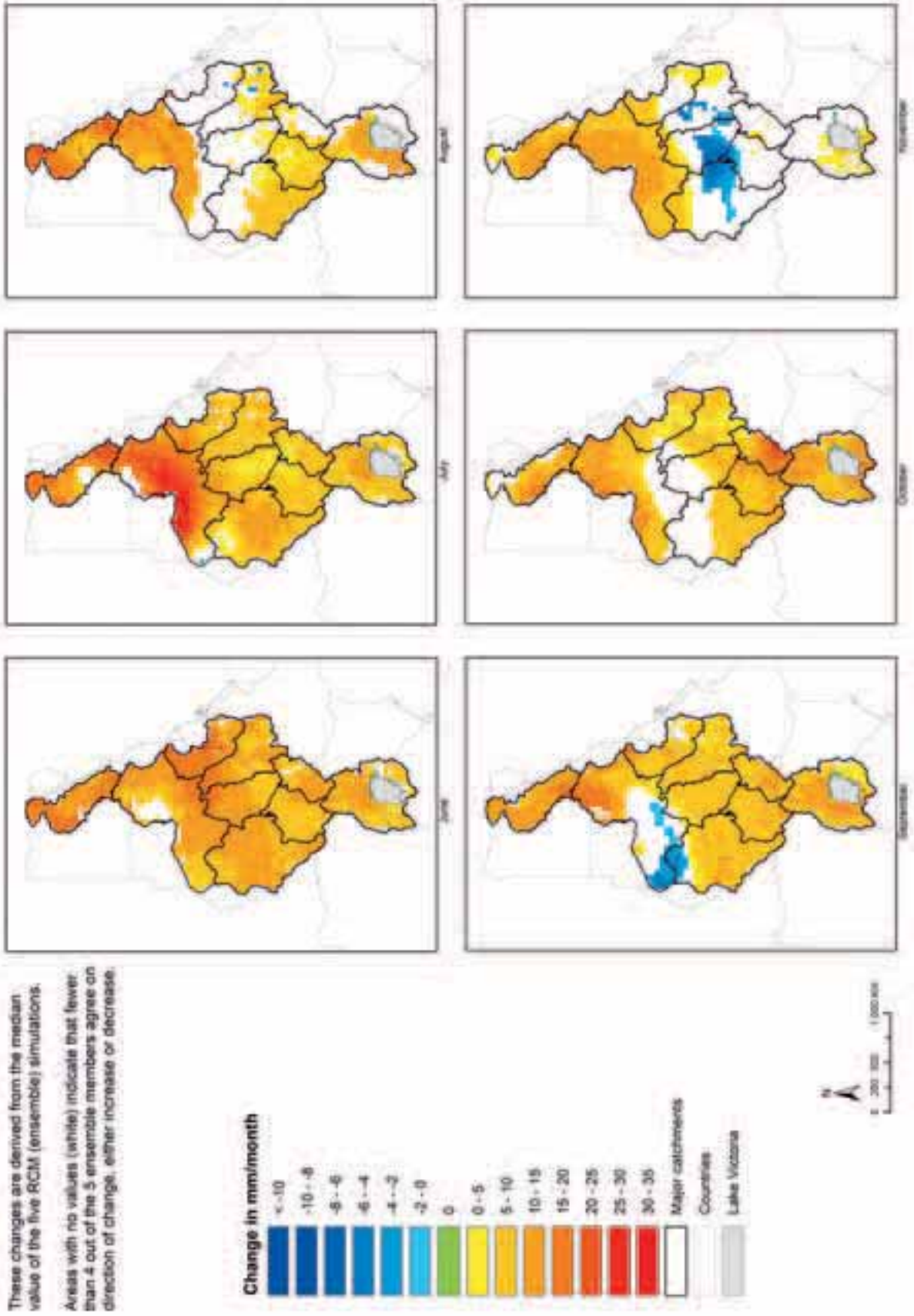
Figure 6.32 Absolute changes in monthly change in PET: 2070-2099, December to May. Note that CRU baseline PET values are given as zero over Lake Victoria.

Figure 6.33 Absolute changes in monthly PET: 2070-2099, June to November. Note that CRU baseline PET values are given as zero over Lake Victoria.

Table 6.1 Summary of selected locations for assessing the impact of climate change on the water resources in the Nile Basin. Note that Q refers discharge & WL to water level

	Variable	Location	Major Sub-basin	Hydrological relevance
1	Q	Semliki	Equatorial Lakes	Flow from Lake Edward and Lake George sub-basins including contributions from Rwenzori.
2	WL	Lake Victoria	Equatorial Lakes	The water level in Lake Victoria which determines the outflow at Jinja
3	WL	Lake Kyoga	Equatorial Lakes	The water level in Lake Kyoga representative of the other Equatorial lakes
4	Q	Jinja	Equatorial Lakes	The outflow from Lake Victoria which is the main contribution to the flow in the White Nile
5	Q	Kamdini	Equatorial Lakes	Key station on the Kyoga Nile between Lake Kyoga and Lake Albert
6	Q	Mongalla	Equatorial Lakes	A good measure for the inflow to the Sudd as it is the last key station before the Sudd
7	Q	Buffalo Cape	The Sudd	A measure of the flow in the main river in the Sudd. Approximately 70% (on average) of the flow through the Sudd is expected to pass this station
8	Q	Sobat confluence	Sobat	The outflow from Sobat into the White Nile
9	Q	Malakal	White Nile	Flow on the White Nile just downstream of the Sobat confluence, including input from Sobat, The Sudd and Bahr El Ghazal.
10	Q	Jebel Aulia Dam	White Nile	The regulated flow downstream of Jebel Aulia Dam which to a large extent represent the contribution of the White Nile to the Main Nile
11	Q	Abay	Blue Nile	Flow in the Blue Nile at the border between Ethiopia and Sudan
12	Q	Khartoum	Blue Nile	The Blue Nile at Khartoum just upstream of the confluence with the White Nile
13	Q	Atbara	Atbara	Atbara just upstream of the confluence with the Main Nile
14	Q	Dongala	Main Nile	The last key station before the inflow to the High Aswan Dam (HAD)
15	Q	Gaafra	Main Nile	Flow on the Main Nile downstream of HAD

6.6 Regional flow impacts

One of unique characteristics of the Nile basin is the unusually low specific discharge (discharge per unit area). This arises from the large size of the basin, its location and the fact that the major sources of rainfall are confined to two regions, the Equatorial Lakes and the Ethiopian Highlands while rainfall is relatively low over much of the rest of the basin at least compared to the PET. As a consequence, much of the water resource downstream of these sources is connected directly to the Nile River itself and the flows therefore are an important indicator of the water resource. In particular, how the flow moves down the river, the losses such as the evaporation losses from the Sudd swamps, the storage in lakes and reservoir and the

operation and release strategies can all potentially affect the downstream flows. Therefore the basin-wide impacts of projected climate changes on water resources are best assessed at key locations along the river using a basin-wide model that captures these processes.

In this regional assessment we have chosen to focus on the 15 locations shown in Figure 6.34 and listed in Table 6.1.

The analysis of the previous sections shows how projected changes in the driving climatic variables might affect the local water balance. However these analyses are based on the potential evapotranspiration, rather than the actual evapotranspiration together with the precipitation of course. A hydrological model is required to determine

the actual evapotranspiration and thereby the actual changes in the net water balance. In addition, the hydrological model must also describe the routing of flows, the losses where they are significant and the effects of lakes and reservoirs on the routing and losses and gains in order to properly determine the consequences downstream.

One of the most important advantages in examining the climate change impacts in terms of flow is that despite the noise or variability in precipitation and potential evapotranspiration, the catchment runoff response is often much smoother. The catchment acts in effect as a low pass filter. In the same manner while the hydro-climatic responses (precipitation and potential evapotranspiration) to climate change may also be noisy the hydrological response may exhibit a clearer signal and therefore better information for decision-makers.

It should be re-iterated here that the hydrological model was developed for application at the regional scale. This means that the focus has been on representing to the extent possible with the available data, the dynamics and the water balance at this regional scale rather than formulating a detailed high fidelity model to represent local conditions. Local scale modelling would require substantially more information and data than those provided to the project. On the other hand, unless these local conditions have regional impacts this is presumed to be a good approach for such a regional scale assessment. It should be highlighted that it was envisaged from the outset that this regional model would provide a strong platform for the development of local models for local water resources and climate adaptation assessments.

Finally, the key criterion for determining the quality of a hydrological model is whether it is suitable for its intended purpose. The main goal here is to develop information and tools to support decision-making for water resource management in the context of regional climate change. Just as in climate modelling science, the philosophy adopted here is that provided the hydrological model is reasonably sound then it will be suitable for assessing the size and magnitude of changes in the river flows as a result of climate change. This is more important than exact representation of the observed flows during the reference period.

The impacts of climate change on flows, throughout the Nile are obtained by using the basin wide hydrological model MIKE HYDRO. A summary of the development and calibration of this model is given in section 5. This model was calibrated within the major sub-basins (Figure 5 1) against available

discharge data within the period 1960 to 1980. These major basins were then combined and a reference or baseline simulation carried out for the period 1/1/1960 to the 1/1/1980, which is the period for which we have been provided with the most consistent and continuous climate data (rainfall and PET) when considering the entire basin. However, even for this period there is a shortage of data for certain periods and catchments for many of the sub-basins. The best data coverage exists for the Equatorial Lakes region because of the provision of additional data by the Directorate of Water Resources Management (DWRM) in Uganda. The data coverage is limited for some of the other sub-basins, including Sobat and the Sudd, and only extremely few daily data were made available for the Blue Nile.

This period of twenty years is assumed in this analysis to be representative of the flow variability of the 1961-1990 reference period. A cursory examination of the climate trends suggests that this is a reasonable approximation for much of the basin and it was not possible to extend these simulations for the entire period because of the lack of available data.

To assess climate change impacts on flow the MIKE HYDRO model was then run using perturbed (downscaled) values for rainfall and PET over the same period. All other factors such as the operation and operation strategies of the reservoirs, the extractions for irrigation, industrial and domestic water supply in Egypt and Sudan were kept fixed. The resulting changes are therefore solely as a results of projected changes in the climate. These changes are compared directly with the effect of projected changes in water demand in section 7.

The changes in the Nile flows as a result of the RCM climate projections used in the regional hydrological model are presented in two ways; the mean monthly flows and the flow duration curves. The monthly flows at key locations show the regional distribution of seasonal flows and the impacts on these introduced by climate change.

A flow duration curve represents the relationship between magnitude and frequency of daily, weekly, monthly (or some other time interval) stream flow for a river basin. It provides an estimate of the percentage of time a given flow was equalled or exceeded during a specific period. It provides a simple but comprehensive view of the historical variability in flow in a river basin, (Vogel and Fennessey, 1994). Flow duration curves are used in hydropower planning, water quality management, river and reservoir sedimentation, habitat suitability, low flows, etc.

Figure 6.34 Key stations used for the assessment of climate change on the Nile river flows

of the climate system at shorter time scales. More importantly, to simulate these extremes using a hydrological model would require high resolution in both space and time of the rainfall and flows.

For a regional assessment such as the one conducted here on a large river system like the Nile, changes in the flow duration curves and the monthly average flows are expected to be more robust indicator of climate change impacts on high and low flow distributions.

The projected changes in flow will be presented for the White Nile stations first, then the Blue Nile and finally the main Nile. The stations presented were selected based on the length and quality of the discharge record and their location in terms of being able to represent the regional flows (Table 6.1).

6.6.1 White Nile stations

The White Nile contributes about 25% of the total flow at the Aswan Dam and represents a baseflow or minimum flow component that remains relatively constant throughout the year (the flow from the White Nile is highly controlled by the releases from the Jebel Aulia dam). Any changes in the flows here will have important consequences for the dry season flows and overall level of water stress (Figure 1.5). The White Nile consists of the Nile Equatorial Lakes, the Bhar El-Ghazal to the west, the Sudd, the Sobat basin to the east and Bahar-Jebel basin. In the regional hydrological model, this large basin has been split into the major sub-basins (Figure 5.1) called Lake Victoria (but which is actually the Equatorial Lakes), the Bhaar el-Ghazal, the Sobat, the Sudd and at the lower end, the White Nile.

Within the Equatorial Lakes (Lake Victoria) sub-basin, the changes in the discharges at Semliki, Jinja, Kamdini and Mongala and the changes in the lake levels for Lake Victoria and Lake Kyoga are evaluated. Each graph shows the baseline flows as

One of the strengths of the flow duration curve is that it depicts changes in both the high, low and middle flows. It can be argued that extreme value analysis could also be used to evaluate the high and low flows at these locations. It is worth noting however that extreme value analysis requires both high quality data and long-term records to represent properly the occurrence of extremes. Furthermore climate impacts on variability and extremes (i.e., changes in flood and drought frequencies) are harder to detect than changes in averages and may be impossible to separate from the natural variability

a bold red line. For discharge these are the average flows for the 20 years simulations of the baseline model. The upper figures present the projected changes for the period 2020-2049, referred to here as 2050 for convenience and the lower figures present the projected changes for the period 2070-2099, referred to as 2100. The green lines show the projected flows for each period derived from the 5 RCM model projections.

The Semliki station (Figure 6.35) is representative of the western part of the Equatorial Lakes sub-basin. The 2050 projections indicate both increases and decreases in the monthly flows of around 15-20% of the baseline flows but with predominantly lower flows for most of the year, especially July to December. This is reflected in the flow duration curves which lie below the baseline for most of the flow regime with the exception of a single ensemble member. This situation appears to be dramatically reversed for the 2100 projections, with substantial increases in the average flows in 3 out of the 5 RCM projections, while the two remaining are only slightly below the baseline. The projected flow duration curves now lie at or above the baseline with a single exception.

The Lake Victoria water levels show consistent reductions in the 2050 projections (Figure 6.36), which can be largely ascribed to the projected decrease in rainfall over the lake for most months combined with a slight increase in the evaporation losses for all months. However no clear trend appears in the 2100 projections with both consistent increases and consistent decreases throughout the year. The Lake Kyoga water levels exhibit a similar pattern. This can probably be ascribed to the fact that although the lake itself show similar trends as 2050 regarding decreasing rainfall and increasing evaporation losses, the catchments draining into Lake Victoria seems to experience a considerable increase in rainfall for the period November to March.

The Jinja station is located at the outlet of Lake Victoria. It is an important control point with the Owens Falls dam located just downstream. The releases follow the so-called "Agreed Curve" to provide releases that resemble the natural outflows from the lake prior to its construction, (Kite, 1982). Releases have shown deviations from this curve since 2005 (Sutcliffe and Petersen, 2007) but this is outside the period of simulation used here. Figure 6 37 shows a clear consensus among the ensemble members with flow reductions projected for the 2020-2049 period. The reductions range from almost zero up to 100-200 m^3/s or approx. 15% of

the monthly flows. The 2100 show no clear pattern with changes varying from +/- 15%. As the flow is determined by the water levels in the Lake Victoria, the same factors affecting the changes in the water levels in the lake described above can explain the changes in the outflow.

The projected changes at Kamdini and Mongalla repeat these patterns with reductions of different magnitudes for the 2020-2049 period and a wide spread of both increases and decreases in the flow for the 2070-2099 projections, Figure 6.38 and Figure 6.39. The Kamdini station is located around 80 km downstream of Lake Kyoga and the flow represents the flow from Lake Victoria and the entire catchment contributing to Lake Kyoga. Mongalla represents the accumulated flow of the entire Equatorial Lakes sub-basin. The projected reductions for 2050 are consistent through the year and can be as large as 20-25% of the baseline flows. As the flow distribution is highly controlled, this can result in large accumulated reductions of the volume of water leaving the Equatorial Lakes. However, large variability is exhibited among the ensemble members.

Further north and downstream of the Equatorial Lakes, these patterns in the climate change response are quite different.

The Buffalo Cape station is located in the Bahr el Jebel, just upstream of Lake No, South Sudan, and represents the fraction of the flow through the Sudd that is not flowing in the Bahr el Zeraf. This station was included in this analysis because it is one of the few stations available that represents the Sudd. It should be noted that in some years where there are significant flow through the Bahr el Zeraf channel, water flows to the White Nile around this station, hence the flow measured at the Buffalo Cape station does not include any flow through the Bahr el Zeraf. Previous studies suggest that up to 30 % of the flow through the Sudd goes through the Bahr el Zeraf, but there are very few available data. The flow through the Buffalo Cape station accounts for at least 70% of the flow through the Sudd, and it's estimated that the fraction will be higher during the dry periods (close to 100%) and probably lower during the very wet periods (where more water will flow through the Bahr el Zeraf).

The Buffalo Cape station flows are highly uniform as a result of the storage and evaporation losses within the Sudd. The outflow from the Sudd has only a small seasonal variation. Consistent reductions of 5-10% of the baseline flows are observed in the monthly flows for 2020-2049 projections which give

a direct shift in the flow duration curve, (Figure 6 38). Similar behaviour but with much greater variability is seen for the 2100 projections. Projections from a single ensemble member result in flow increases for the 2070-2099 period.

The results here suggest that there will be consistent reductions of the flows in the Sudd for the 2020-2049 horizon that match the reductions seen throughout the White Nile. This trend appears to continue for the 2070-2099 projections however a single ensemble member simulates an increase in flow.

The Sobat station represents the accumulated flow for the Sobat basin. The runoff originates from the Baro basin (41 400 km^2) which drains an area of the Ethiopian mountains east of Gambeila rising to peaks of 3300 m, and the Pibor basin (109 000 km^2) which receives the Gila and Akobo from the mountains south of the Baro basin, but also drains a wide area of the plains east of the Bahr el Jebel, from which there is little runoff in most years but high flows in some years. The flows from the Sobat exhibit a strong seasonal behaviour due the peak in rainfall during the summer (July to September). The 2050 projections suggest a consistent reduction in these peak flows from July to December, with the largest reduction during those months with the largest flows, Figure 6.41. The 2100 projections show a quite different behaviour. During peak flow period from July to December, the range of projected monthly flows covers includes both substantial increases and decreases. In contrast to the 2050 projections which tend to show relatively small but consistent decreases, the 2100 projections show a tendency to increase and in some cases quite dramatically. This different behaviour between the two periods can probably be ascribed to the fact that for 2050 decreases in rainfall during the main rainy season are predicted, while for 2100 both increases and decreases are predicted during this period.

The results for the Malakal station integrate the contributions from all parts of the White Nile, including two main peaks in the rainfall, corresponding to the rainy season over the Ethiopian sub-catchments which contribute to the Sobat flows and the "long" rainy season over the Equatorial lakes. This station also reflects the heavy evaporation losses in the White Nile in the Sudd swamps. For the 2050 projections we observe a clear reduction of flows throughout the year including the June to September rainy season. During the remainder of the year the reductions appear to vary dramatically in magnitude from almost no change up to 25% in the drier period. These are important as this will increase dry season water stress in these regions and further downstream. For 2100 there is very little agreement between the different ensembles as some simulate increases throughout the year while others simulate decreases and the range of changes quite large.

The Jebel Aulia dam is located at the downstream end of the White Nile, about 45km south of Khartoum. The observation station is located downstream of the dam. The flow duration curves for the site (Figure 6.43) show clearly that the flows are controlled. The resulting flow behaviour at this the most downstream discharge site for the White Nile shows a very clear climate signal for the 2050 projections. There is a clear indication of reductions in the period from August to November with the strongest reductions during August and September. For the period from December to July there is also a decreasing trend but this is less pronounced. This is shown clearly in the perturbations in the flow duration curve for the low flows. It is worth recalling that in these projections no changes have been made to the reservoirs or their operation strategies and any changes can have an important impact on the downstream flow regime.

For the 2100 projections, 2 of the 5 RCM projections result in large increases in the flow, which from the flow duration curves, appear to occur throughout the year. However, the 2 of the other ensemble members give reduced flow projections for August to November which includes flows at the high and the low end of the flow regime.
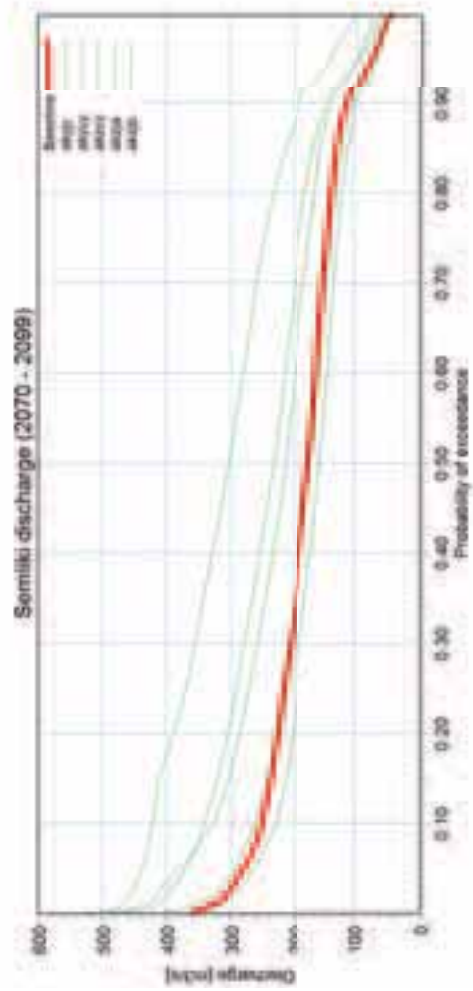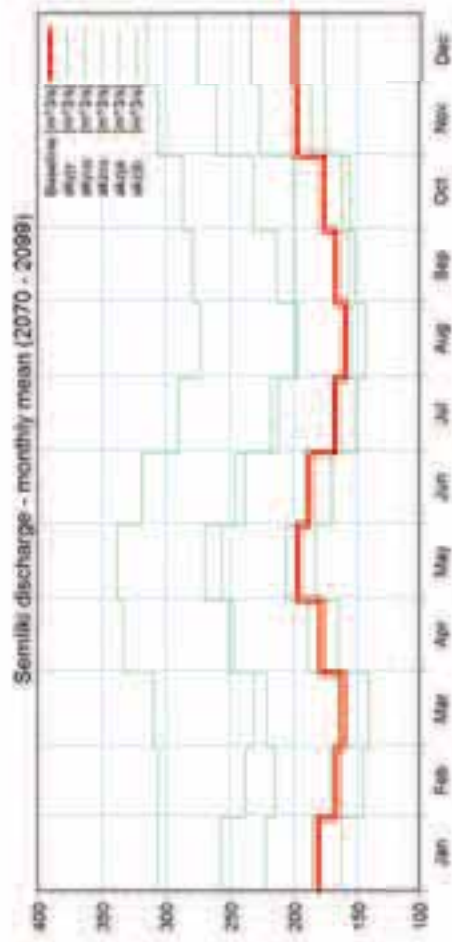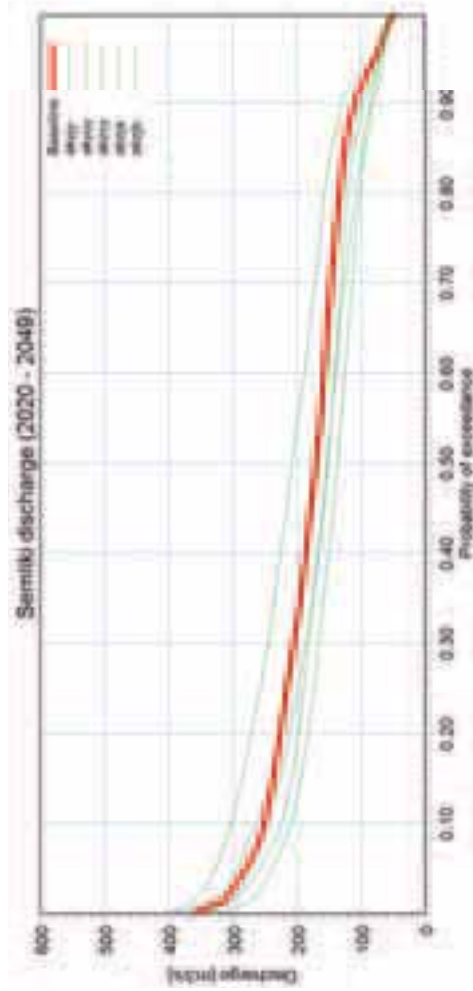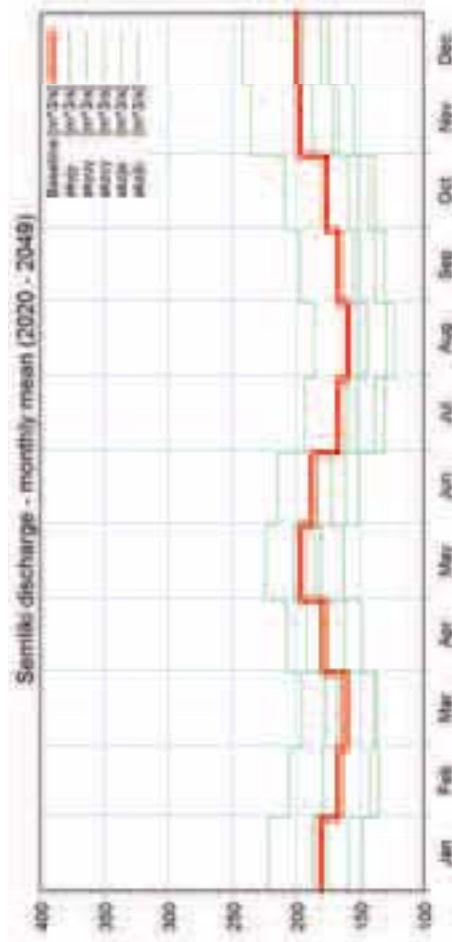
Figure 6.35 Projected changes in the average monthly flows (left) & flow duration curves (right) for the Semliki station. Projections are shown for two periods; 2020-2049 (top) & 2070-2099 (bottom). The solid (red) line shows the baseline levels (1961-1990) & the thin green lines the different RCM ensemble members
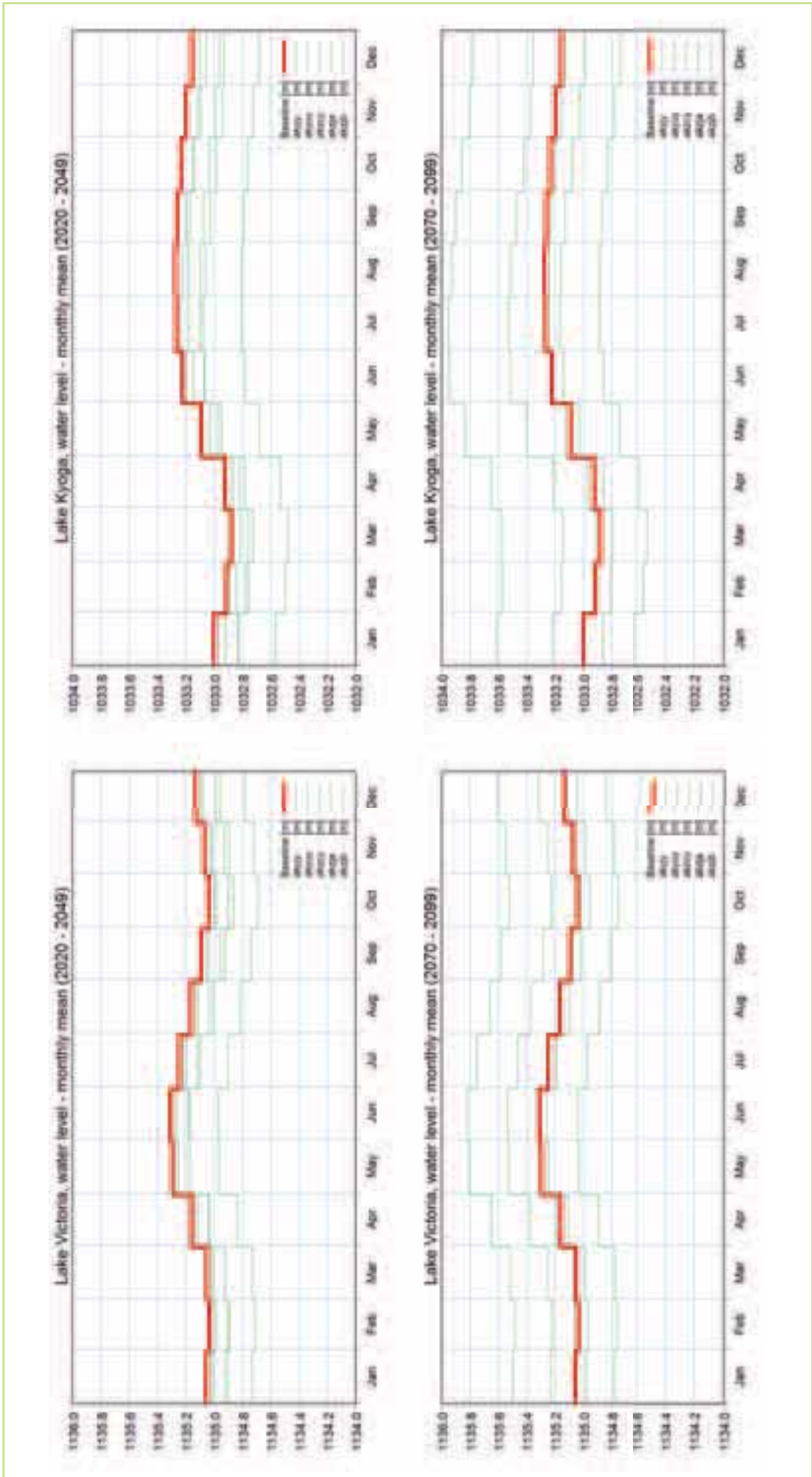
Figure 6.36 Projected changes in the average monthly water levels for Lake Victoria (left) & Lake Kyoga (right) . Projections are shown for two periods; 2020-2049 (top) & 2070-2099 (bottom). The solid (red) line shows the baseline levels (1961-1990) & the thin green lines the different RCM ensemble members
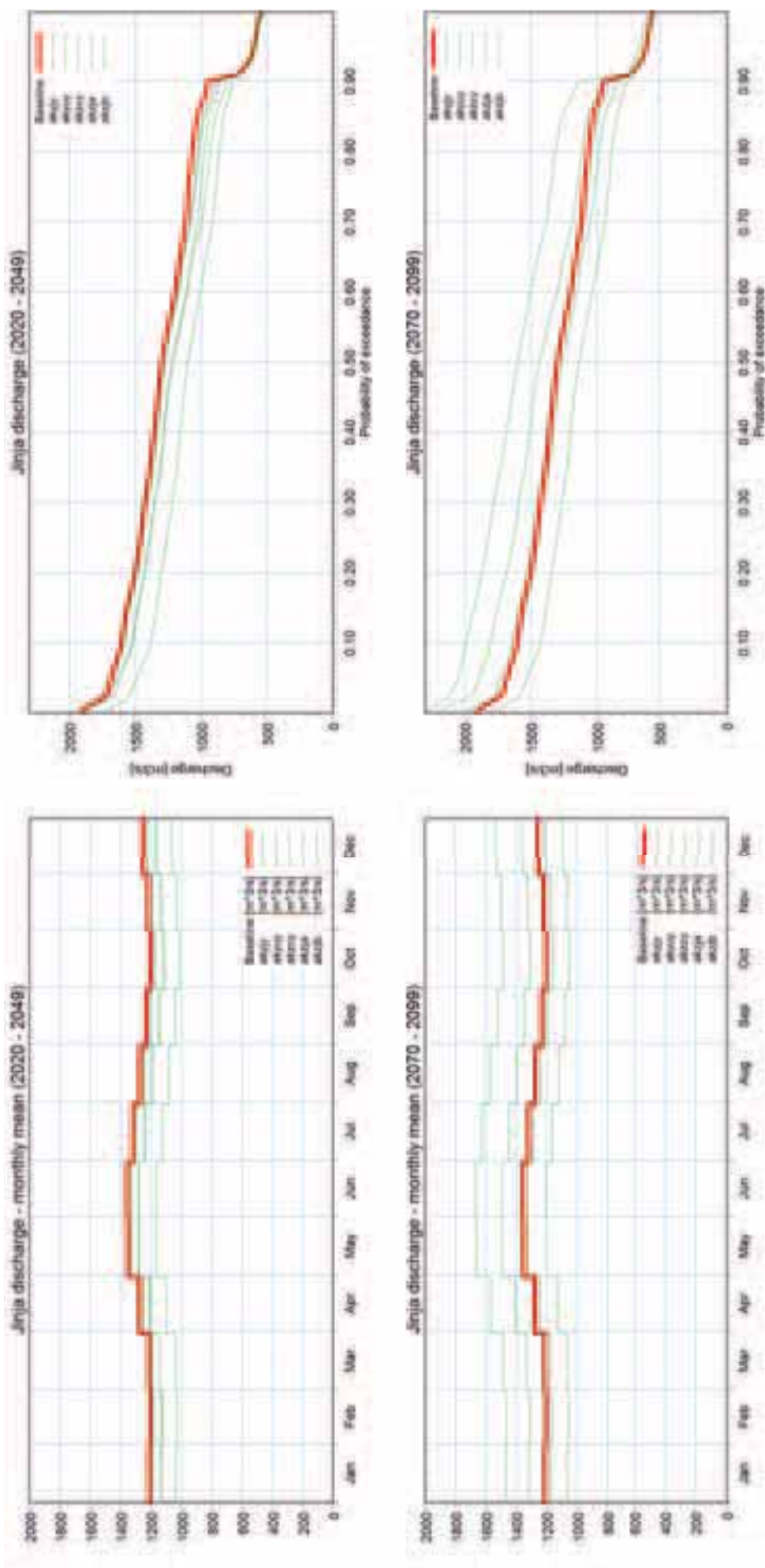
Figure 6.37 Projected changes in the average monthly flows (left) & flow duration curves (right) for the Jinja station. Projections are shown for two periods; 2020-2049 (top) & 2070-2099 (bottom). The solid (red) line shows the baseline levels (1961-1990) & the thin green lines the different RCM ensemble members
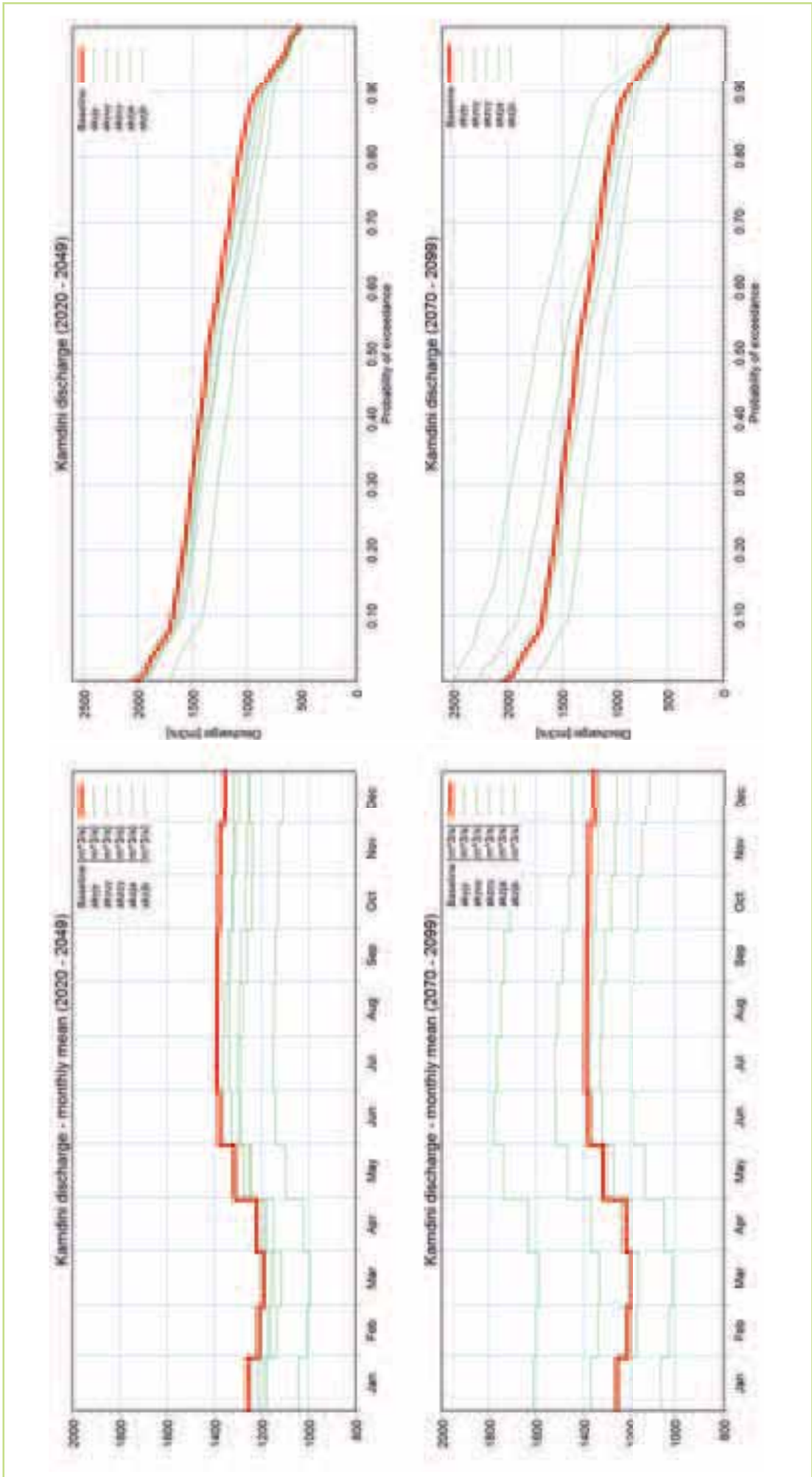
Figure 6.38 Projected changes in the average monthly flows (left) & flow duration curves (right) for the Kamdini station. Projections are shown for two periods; 2020-2049 (top) & 2070-2099 (bottom). The solid (red) line shows the baseline levels (1961-1990) & the thin green lines the different RCM ensemble members
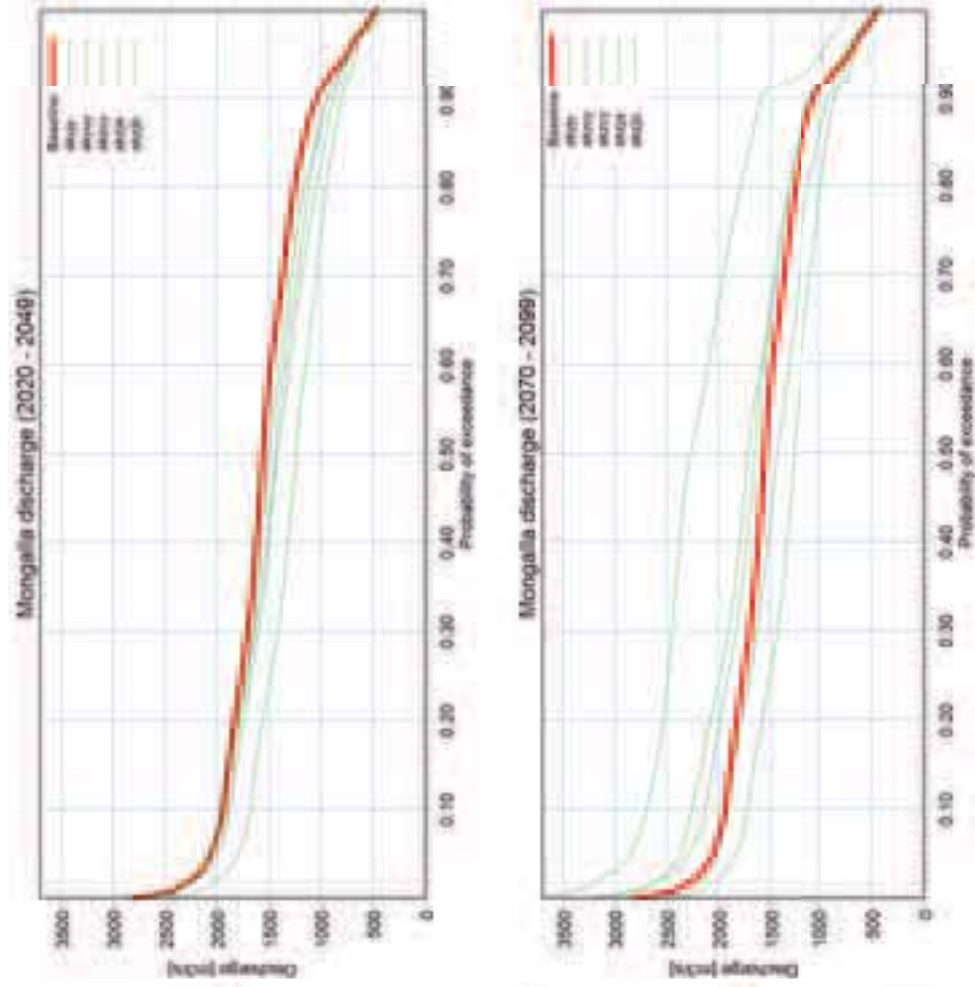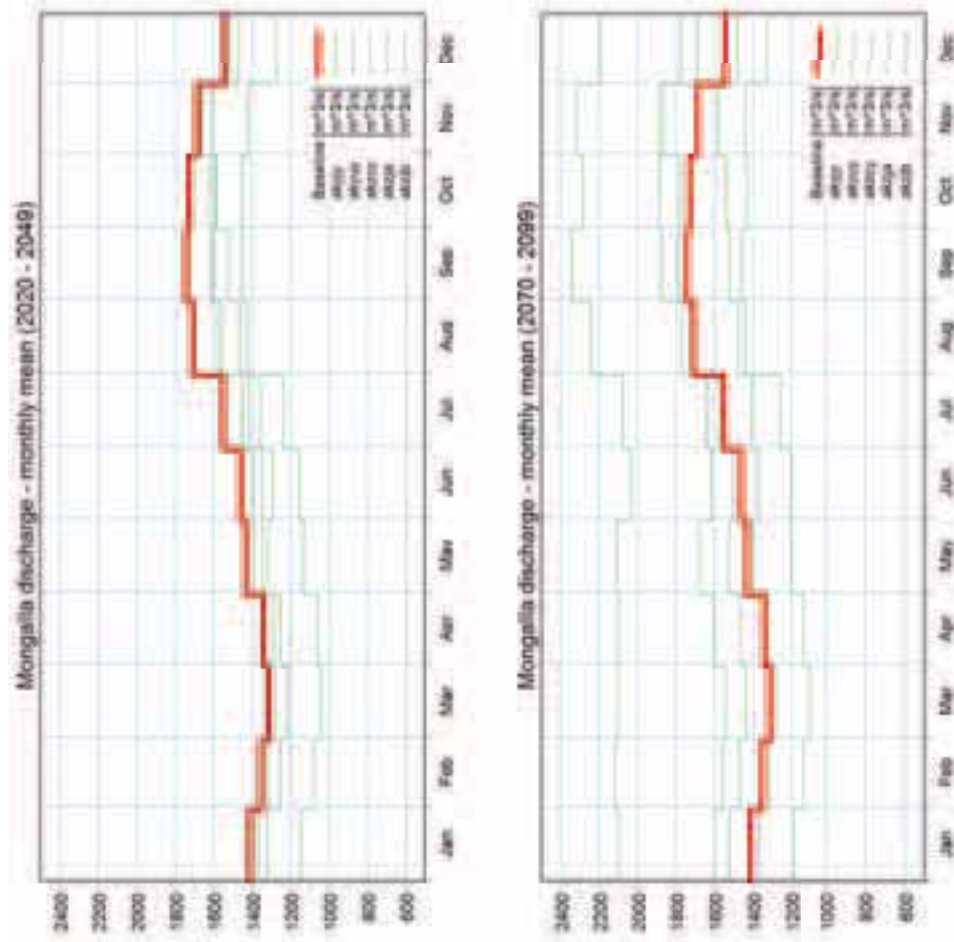
Figure 6.39 Projected changes in the average monthly flows (left) & flow duration curves (right) for the Mongalla station. Projections are shown for two periods; 2020-2049 (top) & 2070-2099
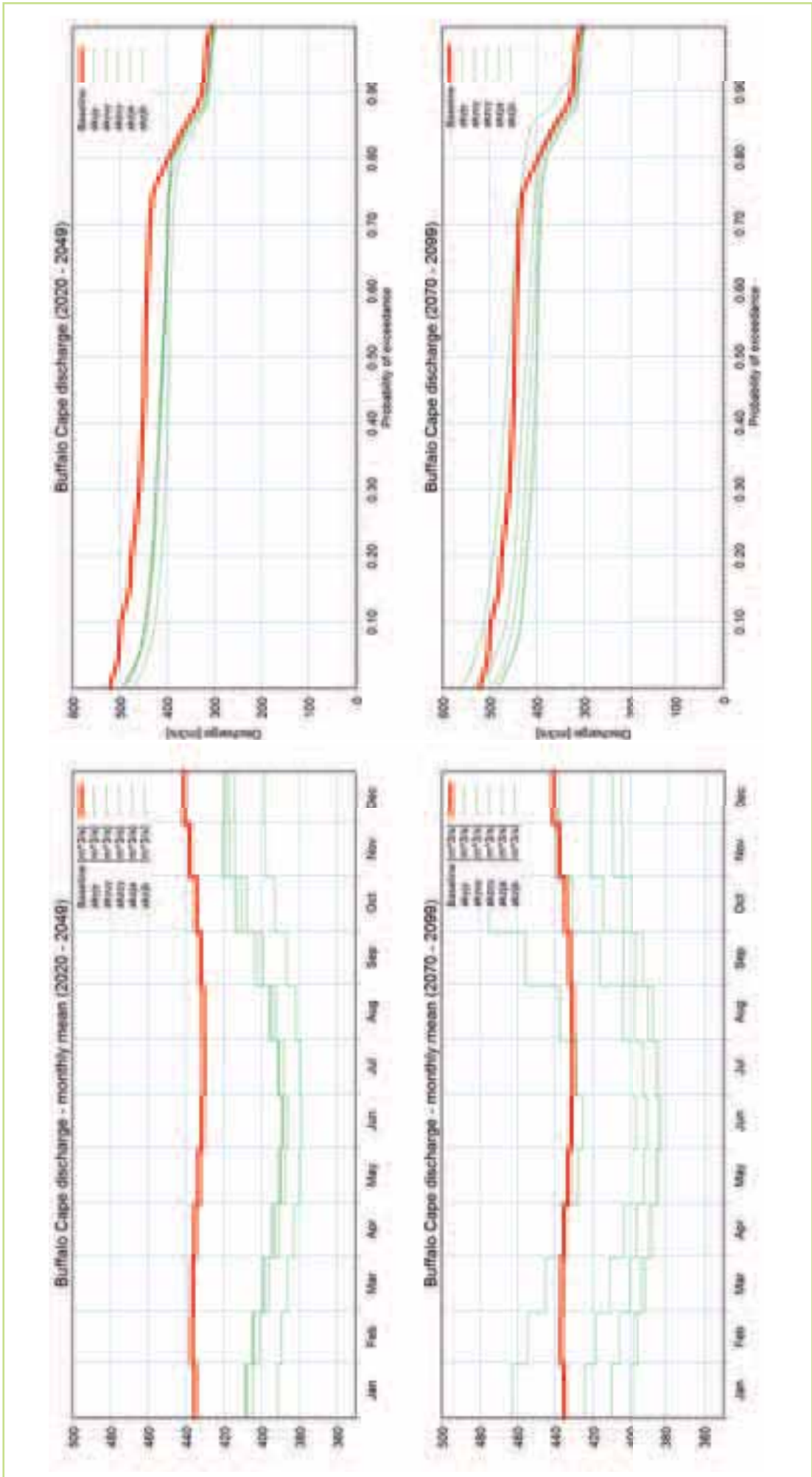
Figure 6.40 Projected changes in the average monthly flows (left) & flow duration curves (right) for the Buffalo Cape station. Projections are shown for two periods; 2020-2049 (top) & 2070-2099 (bottom). The solid (red) line shows the baseline levels (1961-1990) & the thin green lines the different RCM ensemble members
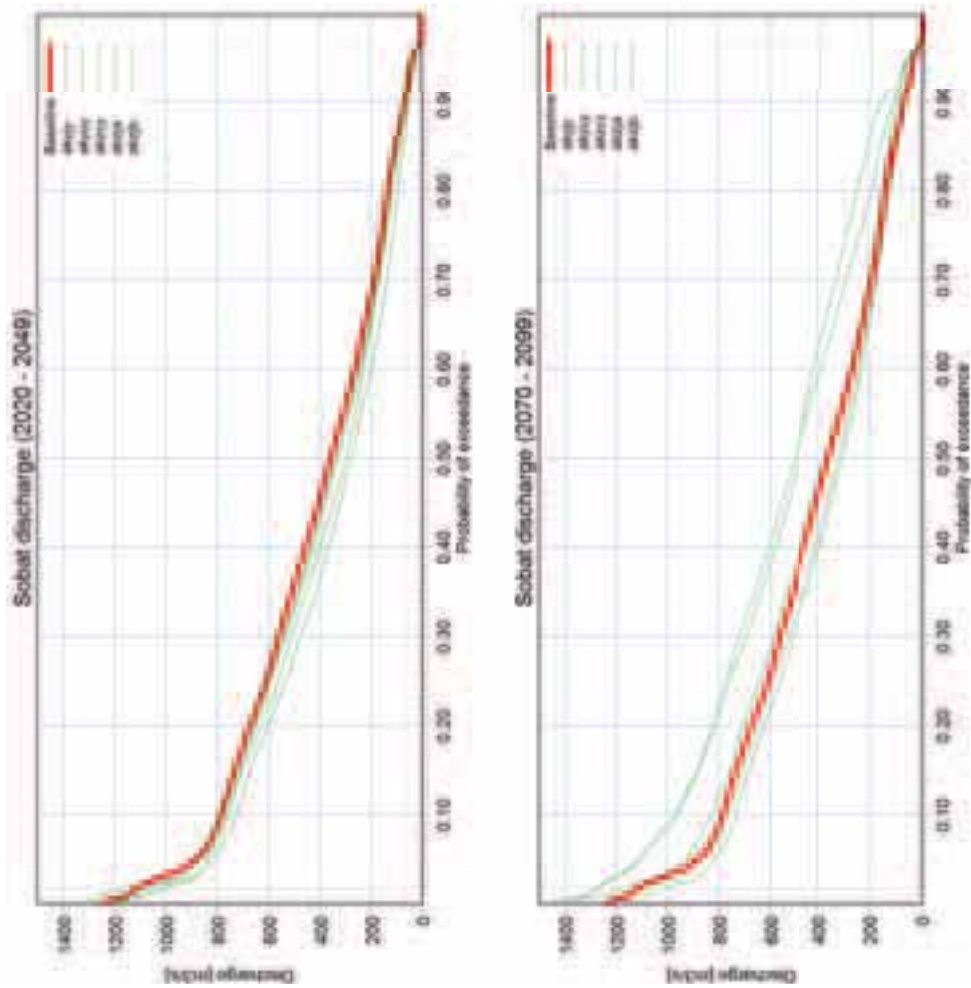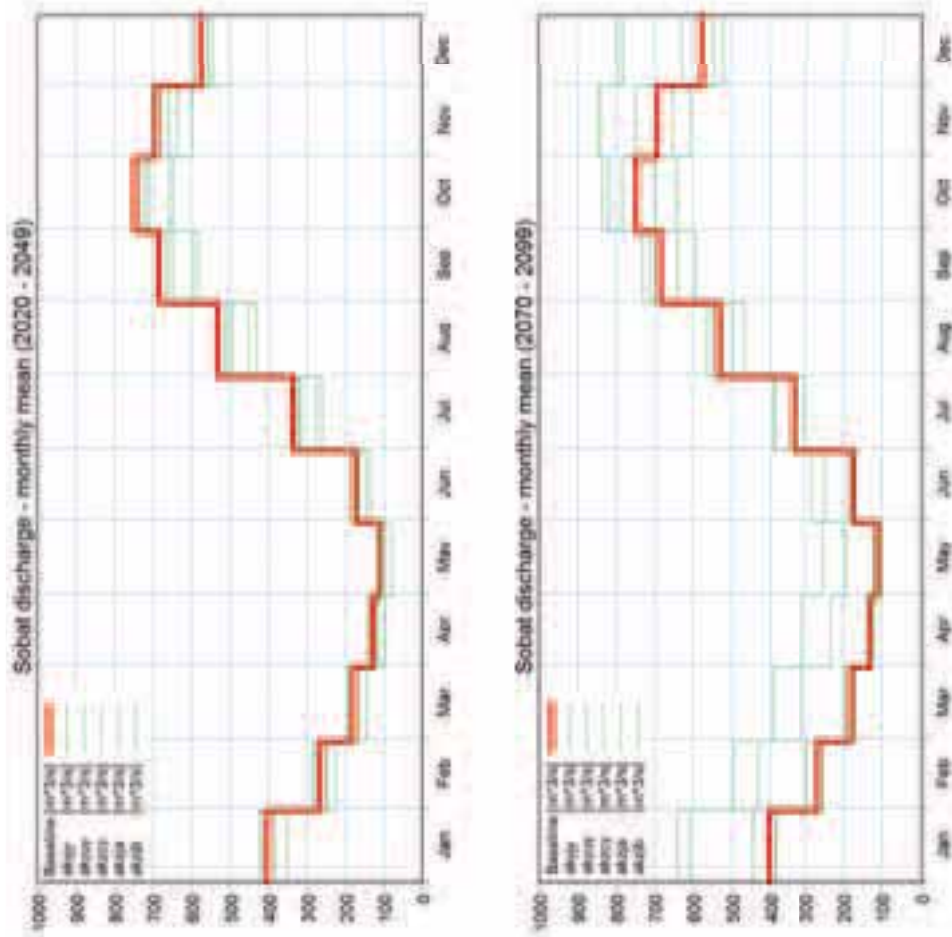
Figure 6.41 Projected changes in the average monthly flows (left) & flow duration curves (right) for the Sobat station. Projections are shown for two periods; 2020-2049 (top) & 2070-2099 (bottom). The solid (red) line shows the baseline levels (1961-1990) & the thin green lines the different RCM ensemble members
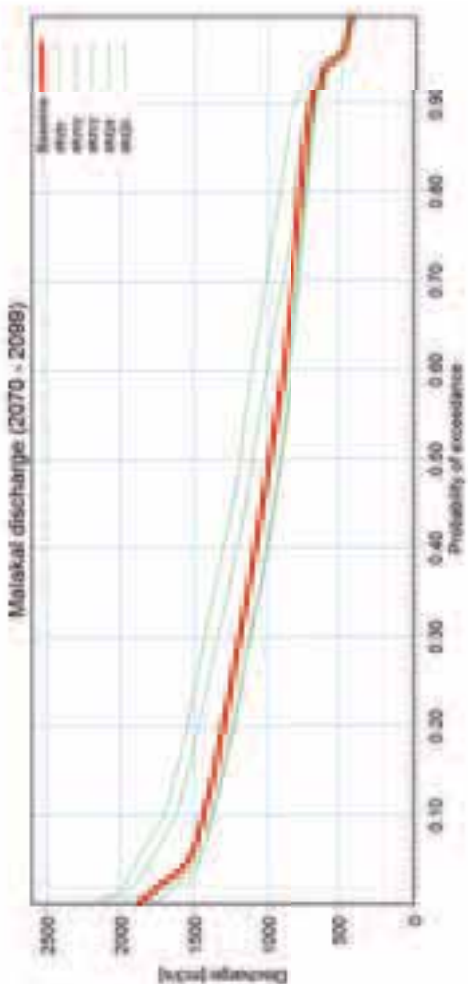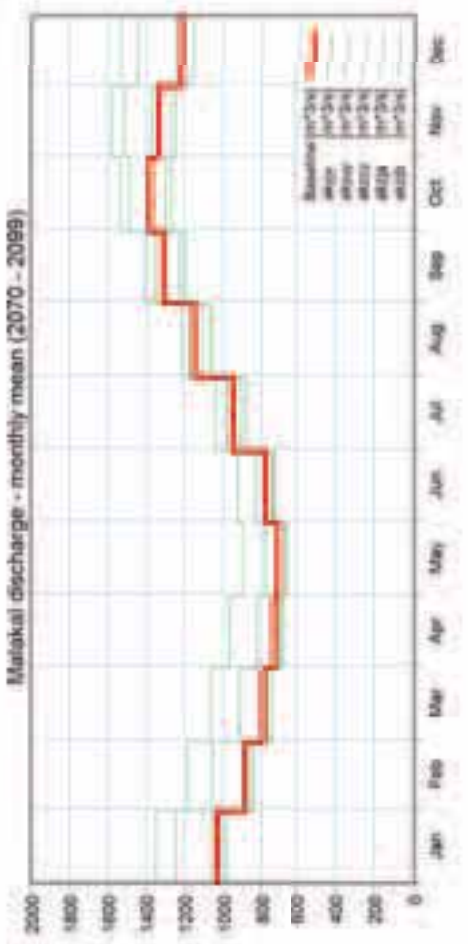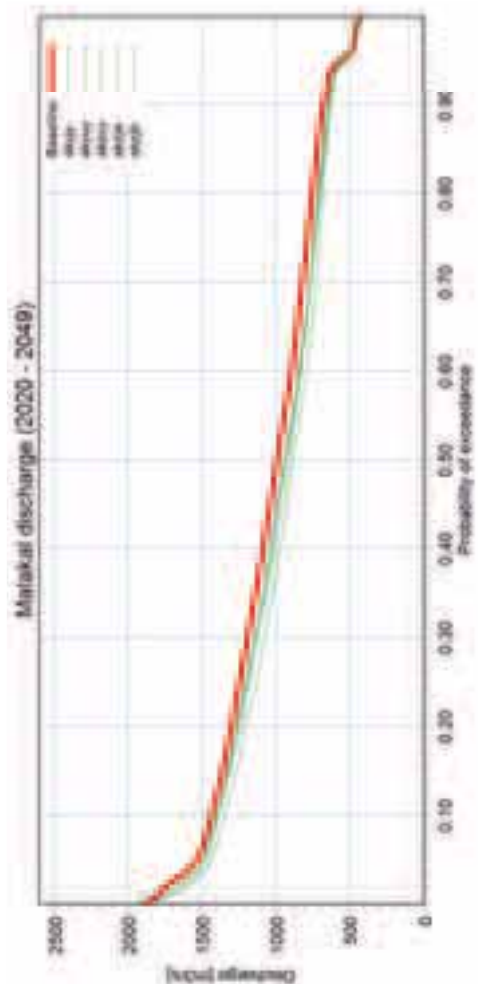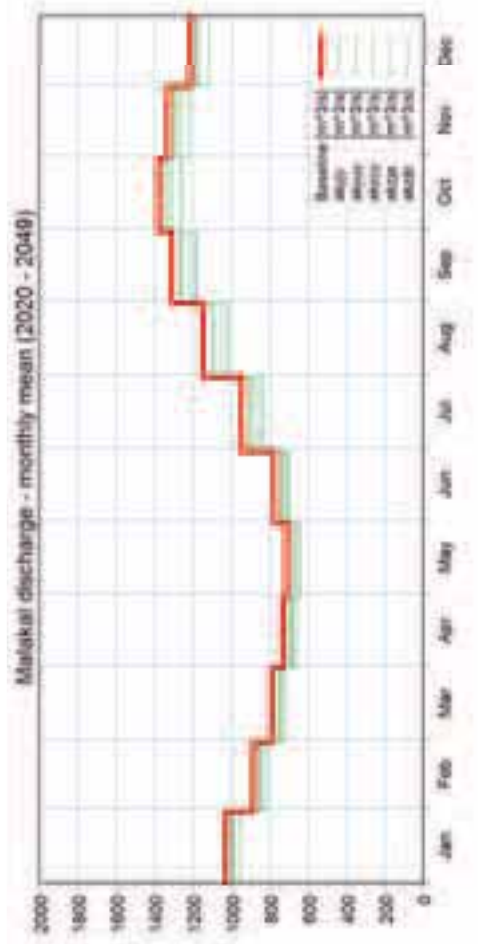
Figure 6.42 Projected changes in the average monthly flows (left) & flow duration curves (right) for the Malakal station. Projections are shown for two periods; 2020-2049 (top) & 2070-2099 (bottom). The solid (red) line shows the baseline levels (1961-1990) & the thin green lines the different RCM ensemble members
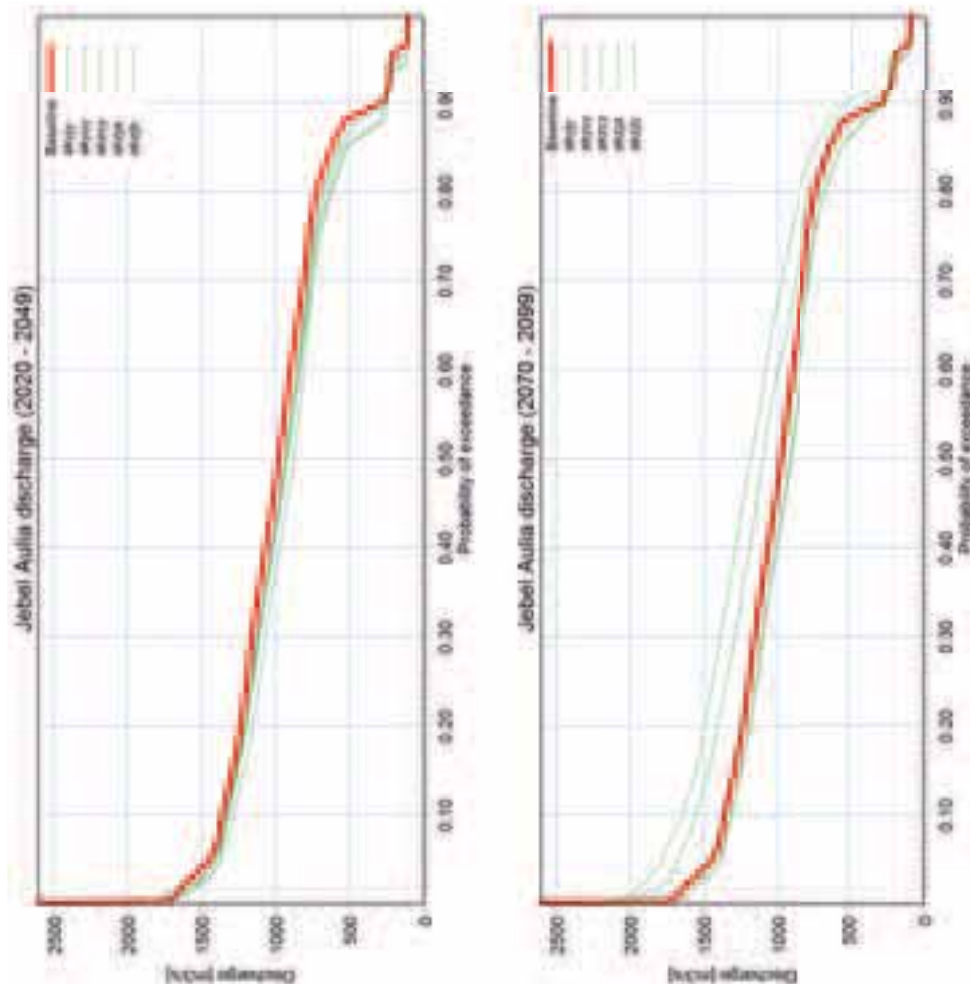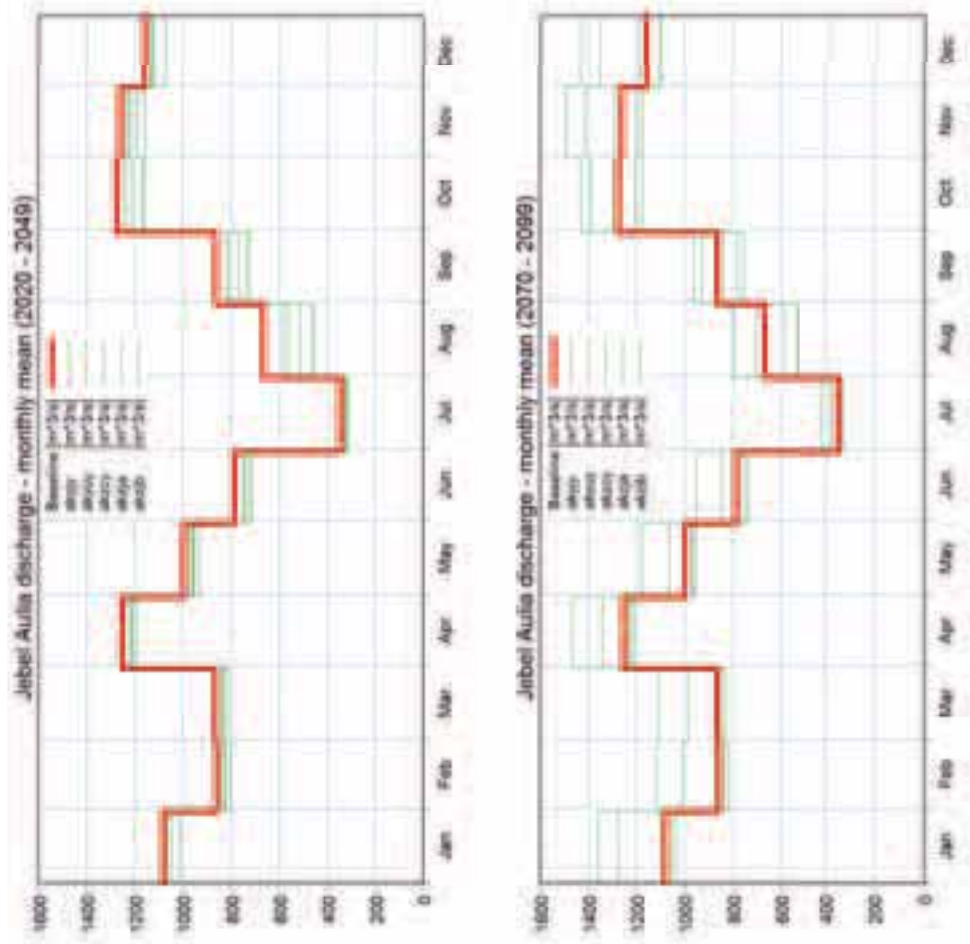
Figure 6.43 Projected changes in the average monthly flows (left) & flow duration curves (right) for the Malakal station. Projections are shown for two periods; 2020-2049 (top) and 2070-2099

6.6.2 Blue Nile & Atbara stations

The Blue Nile and Atbara contribute as much as 75% to the main Nile flows, Figure 1.5. The Abay station (Figure 6.44) represents the behaviour at the upper part of the Blue Nile which is located in Ethiopia, while Khartoum (Figure 6.46) represents the whole Blue Nile (just before the outlet at Khartoum). The 2050 projections for Abay show a general tendency towards increasing flows during the flood season from July to November. There is not however complete consensus among the RCM ensemble members with some small reductions indicated in July and August.

This tendency appears to be strengthened in the 2100 flow projections with a greater range of increases indicated and no reductions with the exception of August for a single ensemble member. This is clearly expressed in the corresponding flow duration curves with increase in the peak flows.

Similar observations can be made for the Khartoum site. There is a general tendency towards increased flows in the period August to November. However there is no complete consensus in the 2050 projections, with reductions indicated for a single ensemble member in July-September. The 2100 projections show a clear shift towards substantially higher mean monthly flows throughout the flood season and a corresponding upward shift in the flow duration curves for flows with an exceedance probability of greater than 0.5 or approx. 1000m³/s.

The Atbara is the northern most tributary to the Nile and lies mainly within the arid to semi-arid climate zone. The runoff is mainly generated in the Ethiopian highlands during a very short rainfall season from June to September. The Atbara can contribute up to around 10% of the peak flows to the Aswan (Figure 1.5). The 2050 flow projections show a slightly different response with consistent decreases in flow in July, but with both increases and decreases in August and September. The consistent decreases in July remain in the 2100 projections however consistent and often very large increases in flow are seen in August and September and consistent but much smaller increases from October to December, too. The Atbara basin response appears to be very sensitive to climate change. The flow duration curves seem to suggest the most significant changes are related to the medium to high flow regime.

6.6.3 Main Nile stations

The Dongala station represents the outlet of the whole of the Nile River; White Nile, Blue Nile and Atbara before it flows into Lake Nasser. As might be expected the response to climate change is dominated by the contributions from the Blue Nile and Atbara and the changes are similar to those observed at Khartoum.

The 2100 projections show a clear shift towards substantially higher mean monthly flows throughout the flood season and a corresponding upward shift in the flow duration curves for flows for the medium to high flow regime, Figure 6.47. The climate signal is more uncertain for the 2050 projections with both increases and decreases in the monthly flows from July to September followed by consistent increases in October and November.

Further downstream and below the Aswan dam at the Gaafra site, the flow regime is quite clearly controlled and the strong seasonality of the Blue Nile and Atbara flows is smoothed out. The 2050 show a consistency tendency towards increasing flows for the period September to January. The 2100 projections however show consistent increases in flows, with the largest increases during the period with largest flows, for some ensemble members by as much as 50%.
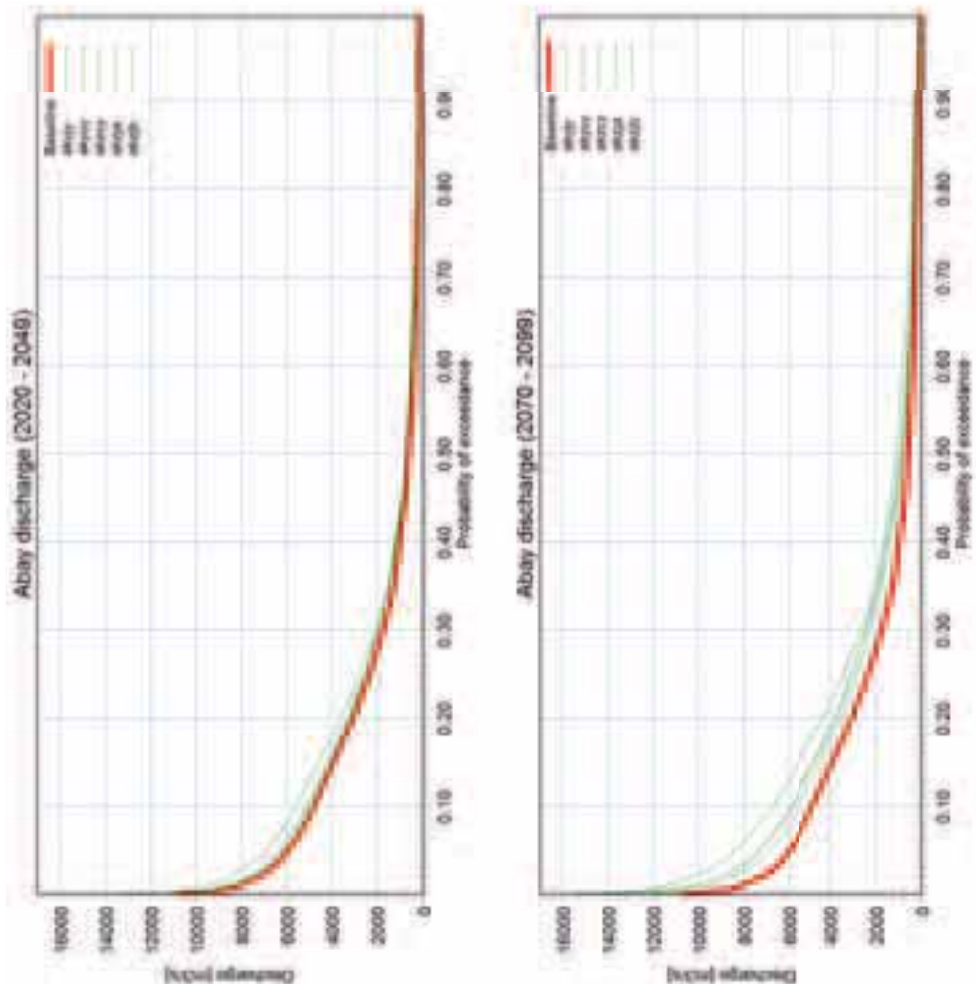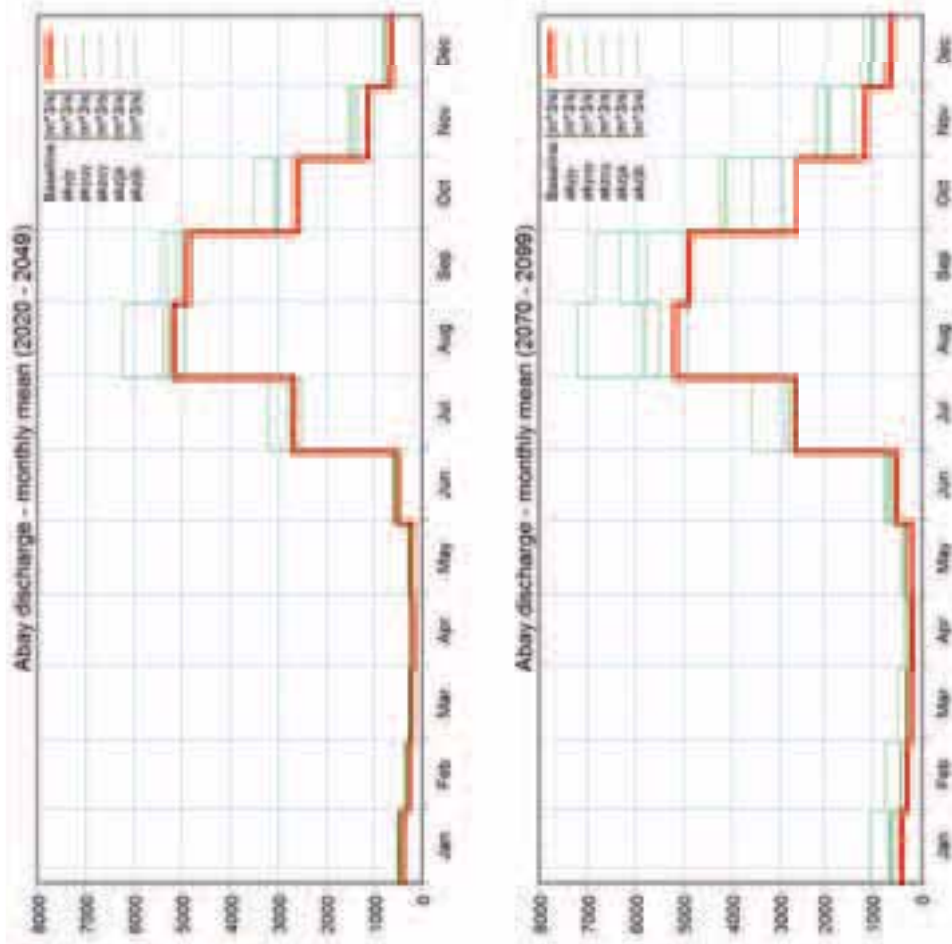
Figure 6.44 Projected changes in the average monthly flows (left) & flow duration curves (right) for the Abay station. Projections are shown for two periods.; 2020-2049 (top) & 2070-2099 (bottom). The solid (red) line shows the baseline levels (1961-1990) & the thin green lines the different RCM ensemble members
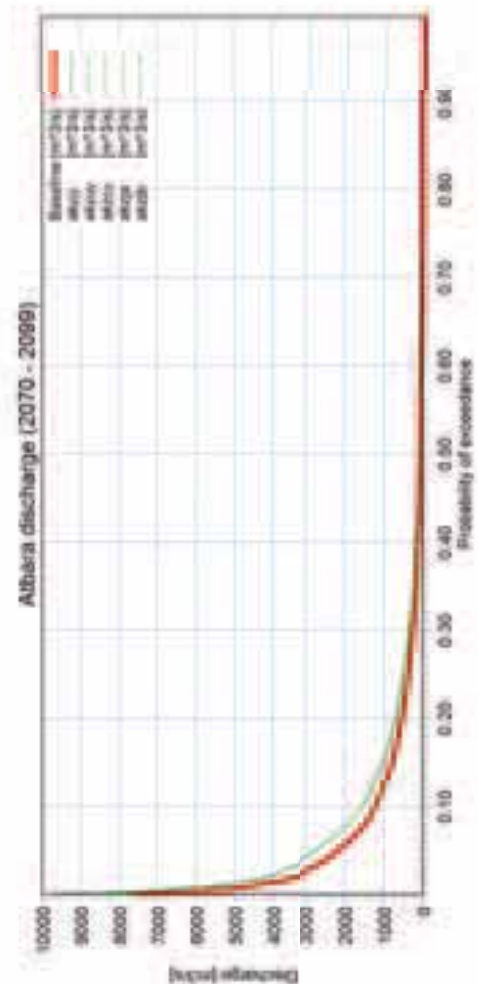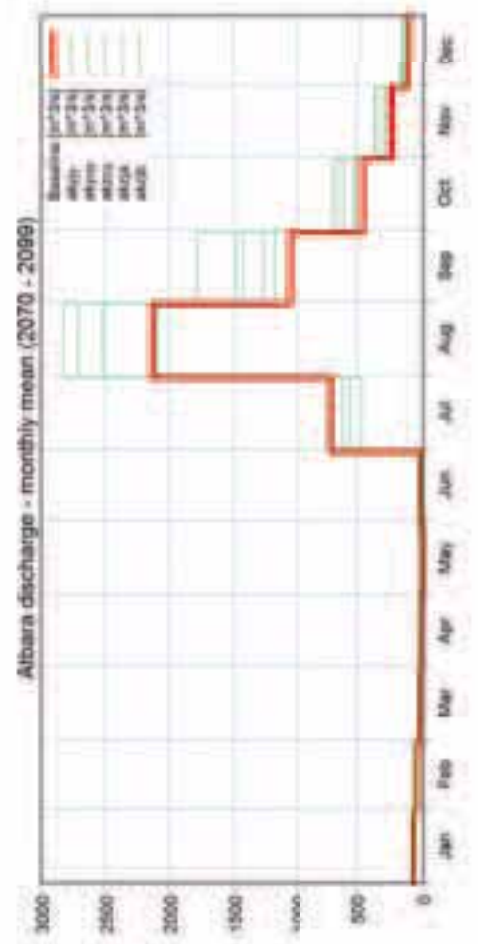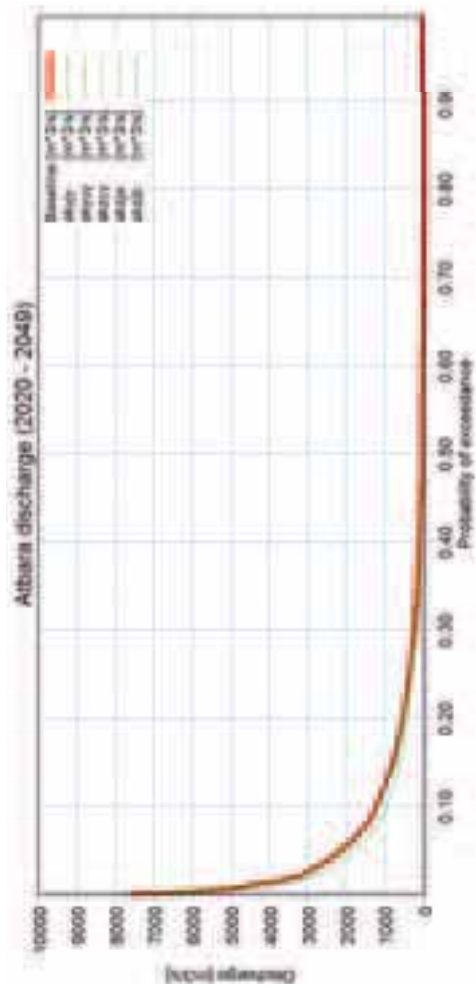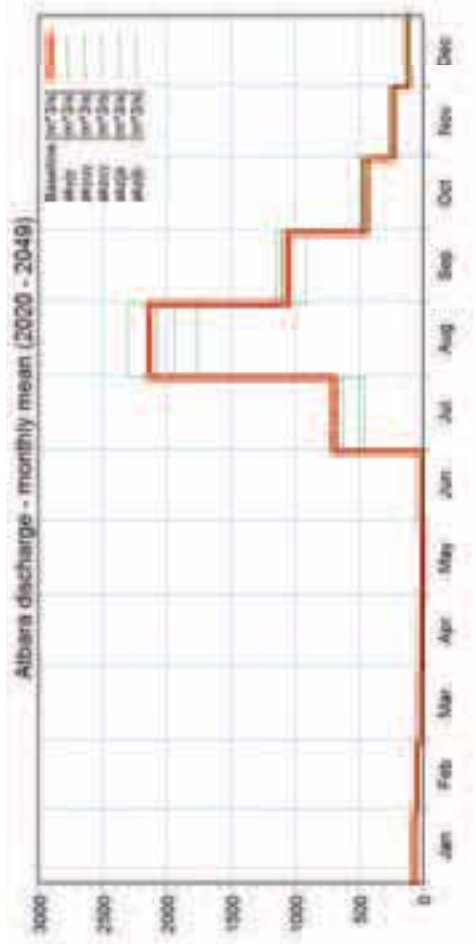
Figure 6 45 Projected changes in the average monthly flows (left) & flow duration curves (right) for the Atbara station. Projections are shown for two periods; 2021-2049 (top) & 2070+-2099
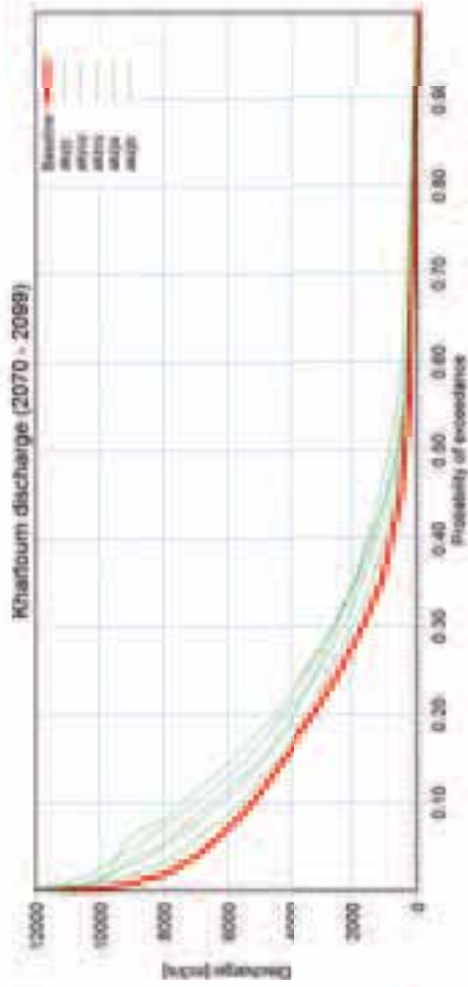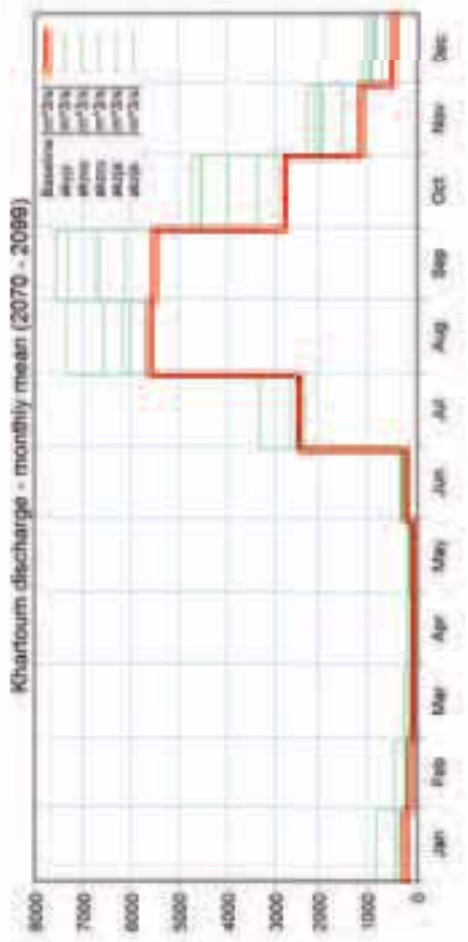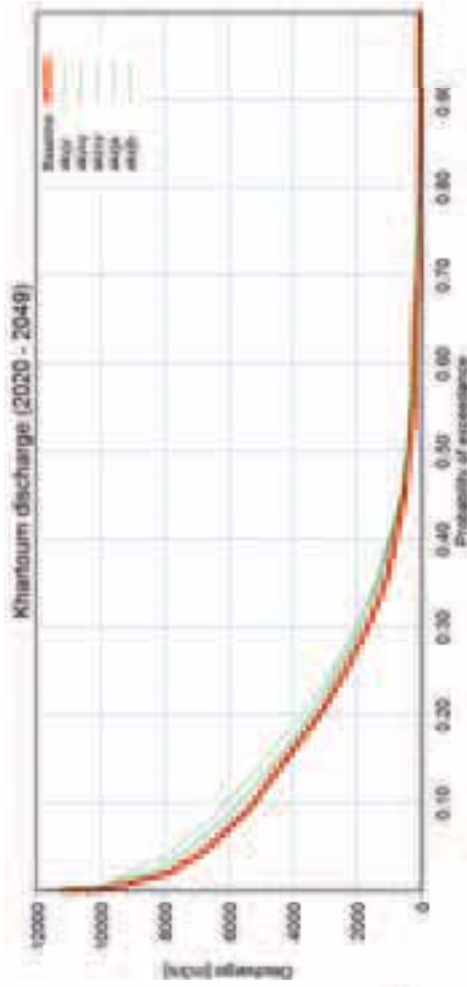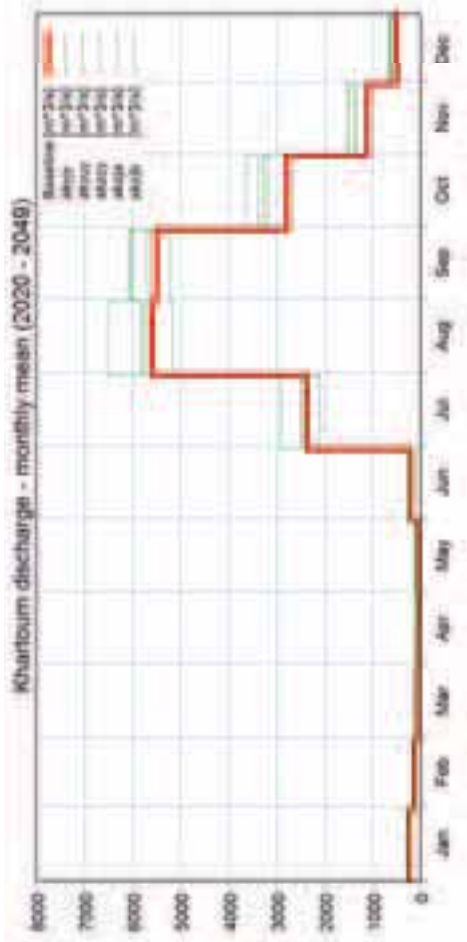
Figure 6.46 Projected changes in the average monthly flows (left) & flow duration curves (right) for the Khartoum station. Projections are shown for two periods; 2020-2049 (top) & 2070-2099 (bottom). The solid (red) line shows the baseline levels (1961-1990) V the thin green lines the different RCM ensemble members.

225
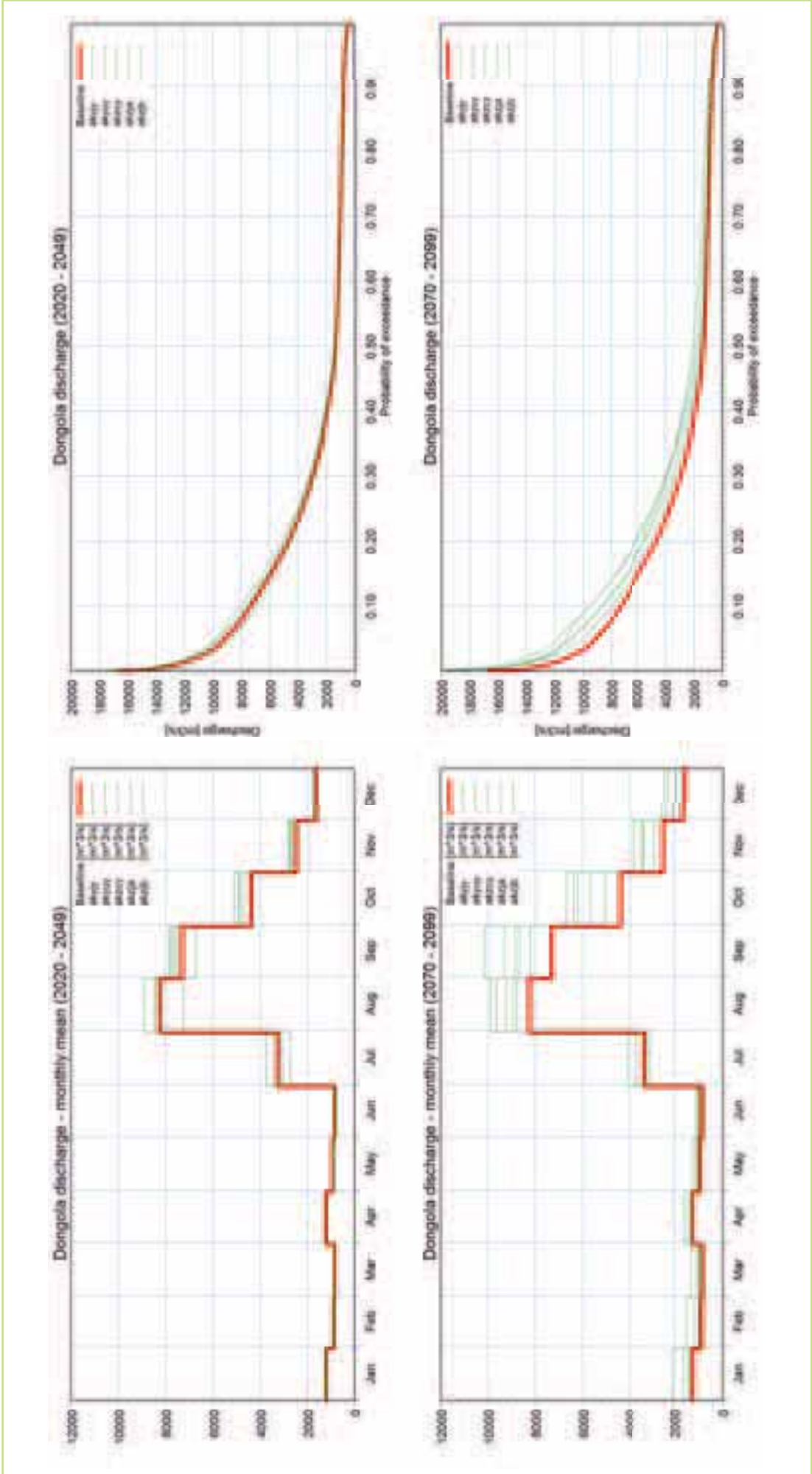
Figure 6.47 Projected changes in the average monthly flows (left) & flow duration curves (right) for the Dongola station. Projections are shown for two periods.; 2020-2049 (top) & 2070-2099 (bottom). The solid (red) line shows the baseline levels (1961-1990) & the thin green lines the different RCM ensemble members
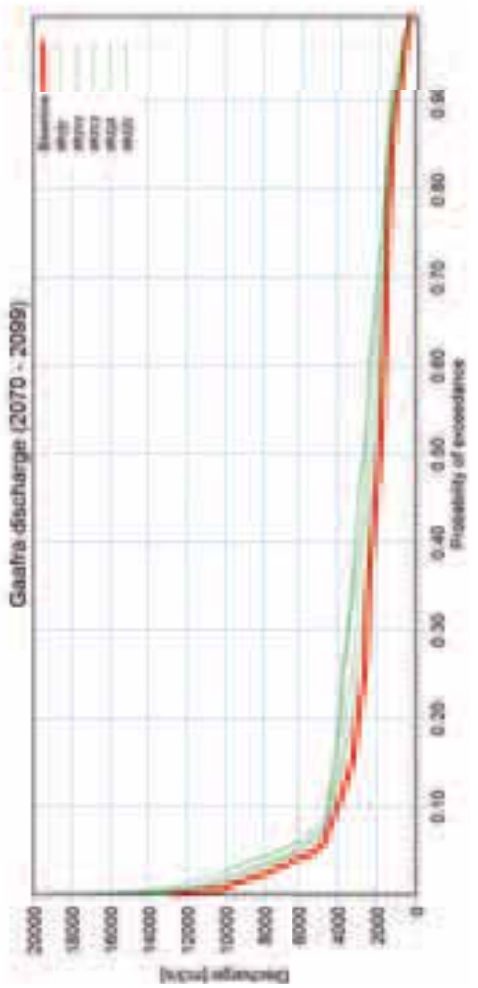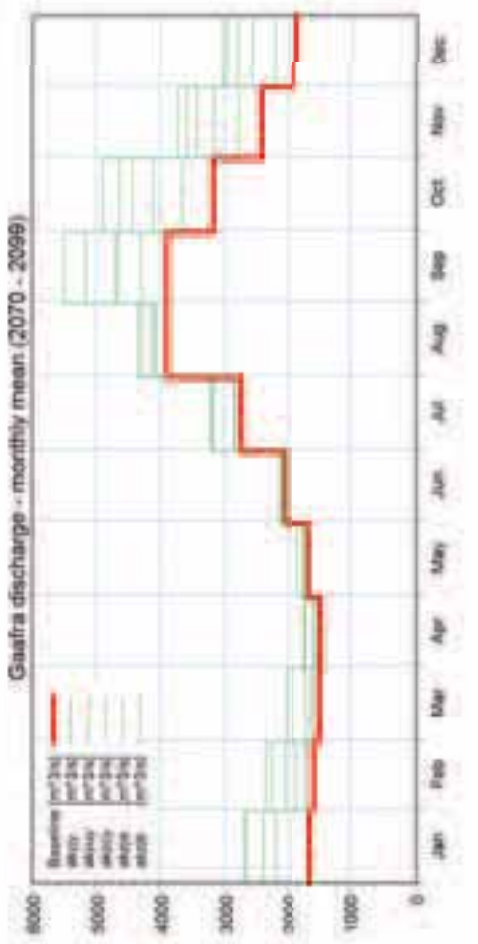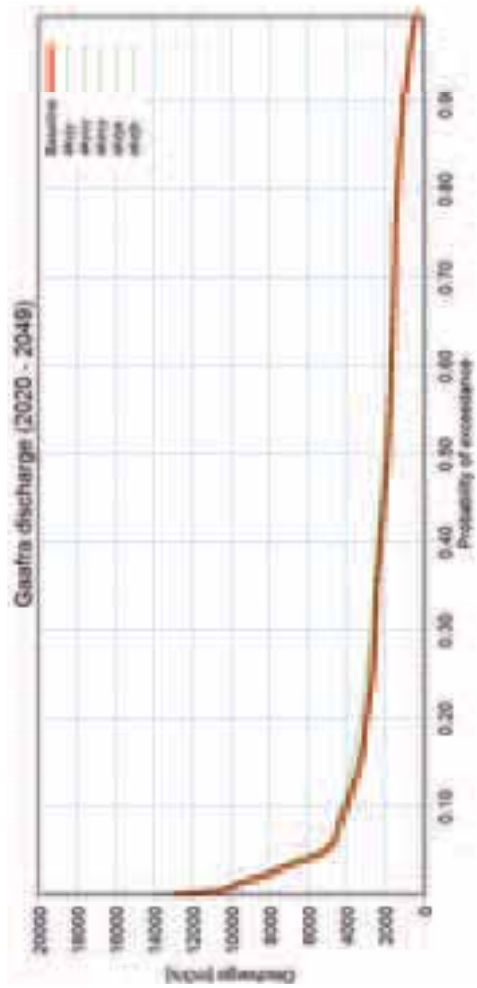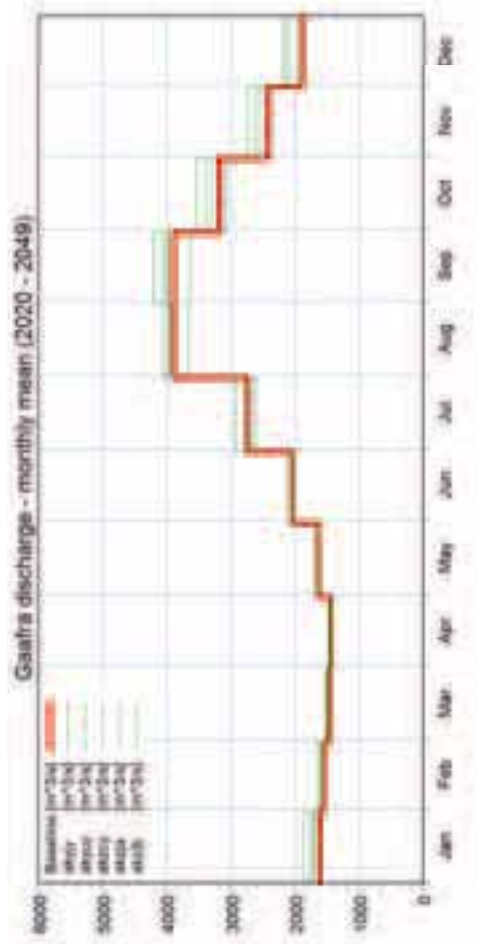
Figure 6.48 Projected changes in the average monthly flows (left) & flow duration curves (right) for the Gaafra (El-Ga'Afra) station. Projections are shown for two periods; 2020-2049 (top) & 2070-2099 (bottom). The solid (red) line shows the baseline levels (1961-1990) & the thin green lines the different RCM ensemble members

6.6.4 Summary of the change in flow volume at key locations

The change in the mean monthly flow and the changes in the flow duration curve based on the 2050 and the 2100 predictions, respectively, provide a good assessment of the possible changes in the flow due to climate change in the near as well as far future. However, to quantify the change in volume at the selected locations and thereby get an idea of the relative impact on the overall change in the Nile flow and not least the flow in the main Nile, the mean annual flow for the reference period (1961-90) and the predicted changes in flow for 2020-2049 and 2070-2099 are provided in Table 6.2.

This table highlights the main patterns of flow change derived from the model projections- For the White Nile reductions in flows are projected for the near future 2020-2049. It should be noted that the RCM seems to over-estimate the rainfall directly over Lake Victoria during the "short" rainy season. A clear trend in flows is not found for the White Nile for the 2070-2099 projections.

This contrasts with the results for the Blue Nile, Atbara and the main Nile where consistent increases in precipitation and therefore flows are found for the 2070-2099 projections. The trend in these flows for the 2020-2049 projections is however less clear. There are generally increases with the exception of Atbara. Within the Blue Nile, the mean flow upstream at Abay is slightly larger than downstream at Khartoum. This pattern is maintained in the projected flows but the changes increase towards the border as a result changes in rainfall over the Rahad and Dindar catchments (see above) downstream of Abay and upstream of Khartoum. This pattern is reversed for 2070-2099 but the differences are +/- 1% and reflect the fact that the water balance in the Blue Nile is highly sensitive to changes in both the precipitation and potential evapotranspiration.

Table 6.2 Summary of the mean flow (flow calculated by the model) for the reference period (1961-1980) as well as the predicted changes in the mean annual flow for 2020-2049 & 2070-99, respectively. The changes are calculated based on the median of the five ensembles

	Location	Mean flow		Projected mean flows & changes		
		1961-1980 m^3/s	2020-2049 (m^3/s)	2070-2099 (m^3/s)	2020-2049 (%)	2070-2099 (%)
1 Semliki		178	161	225 -9.5		26.1
2 Jinja		1260	1187	1267 -5.8		0.5
3 K	amdini	1320	1232	1312 -6.7		-0.6
4 Mongalla		1524	1417	1633 -7.0		7.2
5 Buffalo	Cape	434	401	403 -7.6		-7.1
6 Sobat		403	385	426 -4.5		5.7
7 Malakal		1022	969	1013 -5.2		-0.9
8	Jebel Aulia Dam	951	901	943	-5.3	-0.8
9 Abay		1588	1712	1883	7.8	18.6
10 Khartoum		1562	1702	1830	9.0	17.2
11 Atbara		409	396	512	-3.2	25.2
12 Dongala		2778	2852	3014	2.7	8.5
13 Gaafra		2319	2385	2526	2.8	8.9

7.0 Regional impact of water demand (development) scenarios

In this section we examine the impact of changes in water demand on the flows in the Nile at a regional (basin) level. Direct comparison is made between the impacts of the future water demands and the future impacts of climate change.

7.1 Simulations of the baseline & scenarios

The estimated withdrawals for irrigation, industrial and domestic water supply, by country, are summarised in Table 7.1. The development of the water demand scenarios presented in section 4 show quite clearly the water demand for irrigation accounts for by far the greatest part of the overall water demand in the Nile. Irrigation accounts for 89% of the total estimated water demand for the baseline within the Nile River Basin (Table 7.2). The industrial and municipal water supply demands account for approximately 3.5% and 7.5% respectively.

The estimated spatial distribution of these demands is depicted in Figure 7.1. The spatial distribution of irrigation is derived from FAO estimates (FAO 2011a) of irrigated areas (section 4). The distributions of industrial and domestic water demand are based on the population distribution (Section 4.2) and therefore reflect the large population centres, although the municipal demand appears to be slightly more widespread. The irrigation demand also appears to be strongly correlated to the population centres reflecting the local demand for food supply.

Note that the irrigation demands in Table 7.2 differ slightly from those in Table 7.1 as they are spatially distributed as described in Section 4.3.

Note also that while the projected periods are for 2020-2049 and 2070-2099 as described in Section 2, a conservative approach has been taken to estimating the water demands for these two periods. This is done by estimating the value at the end of each period, i.e. 2050 and 2100 respectively. Thus, for development scenarios the year 2050 represents the period 2020-2049, and 2100 represents the period 2070-2099.

Examining the change in demand towards 2050 (Table 7.2), the annual irrigation demand increases by 16% (approximately 16km^3) and accounts for 84% of the total demand, compared to 89% in the baseline. Together the annual industrial and municipal demands increase by around 72% (approximately 9km^3).

For the model scenarios to be explored under these water demand changes we chose to focus on the impacts of the changes in irrigation, industrial and domestic water demand in Egypt and Sudan. There are several reasons for this. Firstly, one of the "focus" areas identified for this work is the area covering Egypt and Sudan where water demands for irrigation are important and together Egypt and Sudan account for more than 97% of the total irrigation demand in the

Table 7.1 Estimated withdrawals for the baseline period for irrigation, industrial & municipal water supply, for country portions within Nile basin

Country	Irrigation water withdrawals (km³/year)	Industrial water withdrawals (km³/year)	Municipal water withdrawals (km³/year)	Percentage of basin withdrawals by country
Source	FAO 2011a	Calculated (Section 4.2)	Calculated (Section 4.2)	
Burundi 0.048		0.01	0.03	0.1%
Egypt 68.80		3.72	6.67	70.8%
Eritrea 0.127		0.001	0.01	0.1%
Ethiopia 0.483		0.02	0.34	0.8%
Kenya 1.076		0.04	0.18	1.2%
Rwanda 0.317		0.02	0.05	0.3%
Sudan 27.51		0.26	0.96	25.7%
Tanzania 0.003		0.01	0.11	0.1%
Uganda 0.829		0.04	0.12	0.9%
Total	99.19	4.12	8.47	100%

2005 — Water withdrawals

Country portion in basin	Population (million)	Irrigation km³/yr	Irrigation % of country withdrawals from sector	Industrial km³/yr	Industrial % of country withdrawals from sector	Municipal km³/yr	Municipal % of country withdrawals from sector	% of basin withdrawals from each country
Burundi	4.61	0.05	56%	0.01	11%	0.03	33%	0.1%
Congo DR	1.89	-	-	0.005		0.01		0.02%
Egypt	71.76	68.91	87%	3.72	5%	6.67	8%	71.0%
Eritrea	1.70	0.13	91%	0.001	0%	0.01	9%	0.1%
Ethiopia	31.05	0.49	58%	0.02	3%	0.34	40%	0.8%
Kenya	13.37	1.08	84%	0.04	3%	0.18	14%	1.2%
Rwanda	7.69	0.32	82%	0.02	4%	0.05	13%	0.3%
Sudan	32.40	27.33	96%	0.26	1%	0.96	3%	25.6%
Tanzania	7.94	0.003	2%	0.01	4%	0.11	93%	0.1%
Uganda	28.41	0.83	84%	0.04	4%	0.12	12%	0.9%
Total	200.82	99.14	89%	4.12	4%	8.47	8%	100%

2050 — Water withdrawals

Country portion in basin	Population (million)	Irrigation km³/yr	Irrigation % of country withdrawals from sector	Industrial km³/yr	Industrial % of country withdrawals from sector	Municipal km³/yr	Municipal % of country withdrawals from sector	% of basin withdrawals from each country
Burundi	7.69	0.13	68%	0.02	8%	0.05	24%	0.1%
Congo DR	5.43	-	-	0.01	-	0.04	-	0.04%
Egypt	114.58	73.64	82%	5.45	6%	10.49	12%	65.6%
Eritrea	3.49	0.25	90%	0.00	0%	0.03	9%	0.2%
Ethiopia	60.75	1.08	61%	0.04	2%	0.66	37%	1.3%
Kenya	38.85	1.89	75%	0.11	4%	0.51	20%	1.8%
Rwanda	20.91	0.45	71%	0.05	7%	0.14	22%	0.5%
Sudan	84.63	34.64	92%	0.66	2%	2.51	7%	27.7%
Tanzania	26.64	0.01	2%	0.02	5%	0.36	94%	0.3%
Uganda	93.05	2.69	84%	0.15	5%	0.38	12%	2.4%
Total	456.03	114.77	84%	6.50	5%	15.18	11%	100%

Table 7.2 Summary table of the development scenario data showing the changes in population & withdrawals for irrigation, industry & municipal water supply from the baseline (2005) to the future (2050)

Figure 7.1 The magnitude & spatial distribution of the irrigation water demand (left) industrial (middle) & municipal water demand (right) estimated for the baseline or reference case

Nile basin. Similarly Egypt and Sudan account for more than 96% of the estimated total water demand (irrigation, industrial, municipal) in the Nile basin. For this reason, the water use demands implemented in the regional hydrological model were limited to irrigation, industrial and municipal water demands in Egypt and Sudan. This gives a clear indication of the magnitude of the impact on river flows compared to climate change and is consistent with the regional scale focus of this study. It should be noted that water demands from irrigation, domestic and industrial use, are likely to have a local impact at numerous locations outside Egypt and Sudan, and should be included in more detailed and local studies.

The main river stations we have focussed on this study are shown in Figure 7.2.

The impact of increasing water demand, corresponding to the estimated demands in the period 2020-2049 (2050) and 2070-2099 (2100), is assessed in terms of the changes in mean monthly flows (Figure 7.3, Figure 7.5, Figure 7.7, Figure 7.9 and Figure 7.11). For comparison the corresponding projected changes in mean monthly flows derived from the RCM ensemble simulations are shown underneath (Figure 7.4, Figure 7.6, Figure 7.8, Figure 7.10 and Figure 7.12).

The mean monthly flows estimated for the reference period (1960-1990) are derived from the regional model simulations. These simulations cover the period 1960-1980 for which we have concurrent observations of rainfall, PET and discharge (the water demands are taken from the FAO 2005 demands). It is assumed that the monthly averages for this period provide a reasonable approximation to the monthly averages over the full thirty year period. The water demands used in these simulations corresponds to the estimated baseline demands for irrigation, municipal and industrial demand for Sudan and Egypt which account for more than 96% of the estimated total water demand in basin. It was assumed that the baseline demands could be approximated by the 2005 demands. Given the uncertainty in these estimated water demands this was considered a reasonable approximation. A possible alternative was to extrapolate the 2005 backwards in time. However this would be a crude approximation since reliable data for the reference period were not available to validate such an extrapolation. The approach adopted here should therefore be considered as a conservative estimate of the changes in flows caused by increasing water demands.

To estimate these changes the

Figure 7.2 Location of the key regional river gauging stations included in this study

regional model simulations were repeated, applying the estimated irrigation demands for 2050 and 2100. In each case the estimated demands for that year (2050 or 2100) were applied to each year of the regional hydrological model simulations. The annual cropping calendar was assumed to be the same as for the baseline, so the seasonal variation was maintained in the projected demands.

7.2 Scenario results

Only results for the 5 most downstream stations are presented here (Figure 7.3 to Figure 7.12). The changes introduced have no impact above the Jebel Aulia Dam station. With the exception of the Atbara gauge, the increases in water demands have a significant impact on the monthly discharges. The effects are most dramatic at the most downstream stations with reductions of as much as 20% of the flows in the dry season.

At Jebel Aulia, the flow is clearly controlled with limited seasonal variation. The changes in flow with increasing water demand are relatively small. The increase in water demand for the 2100 demands corresponds to reductions of less than 10% for the higher flows. By comparison the expected impacts of climate change appear to be substantially larger, with consistent reductions in the projected flows for 2030-2050 (referred here as 2050 period) during August-October for all the ensemble members. For the projected flows in 2070-2099 (referred to here as 2100 period) the situation seems to be reversed with consistently larger flows during January to June. Significant changes are also predicted in the period August to December however there is no clear agreement amongst the RCM ensemble members.

At Khartoum, reductions of approximately 50-200 m^3/s in the average flows are indicated during the peak flow period. This represents a relatively low fraction of the peak flows but is a substantial fraction of the flows during November to January. For the 2050 period climate changes suggest the possibility of both decreases and increases in the peak flows. A much clearer signal appears in the 2100 period with consistent increases in the projected flows during wet season.

At Dongola, consistent reductions are seen throughout the year and reductions of 100-500 m^3/s in the average flows are indicated during the peak flow period. The impact of climate change for the 2050 period is most obvious in the peak flow period; however there does not appear to be a clear signal as to the direction of these changes. For the 2100 period the projected flows are consistently larger

than the baseline and are largest for the largest flows.

The most dramatic changes are, as might be expected, seen in the Main Nile at the Gaafra station. The withdrawals significantly affect the monthly flows from July to February. For the 2050 period reductions of 200-350 m^3/s or more are projected for September to January, corresponding to 5-20% of the flow. These large reductions particularly in the drier part of the year will substantially increase the vulnerability to water stress in the surrounding region.

This is reflected in the flow duration curves for Khartoum and Gaafra, Figure 7.13 and Figure 7.14, respectively. For Khartoum there is a general reduction across the entire range of flows, while for Gaafra there are strong reductions in the low and medium flows as a result of the increasing water demand.

This is a very strong signal and clearly indicates increasing water stress. It should also be noted that changes in the mean flows are presented so the vulnerability to water stress in dry years or a sequence of dry years may be even larger. The degree of impact is strongly dependent on the operation strategies used in the upstream dams and optimisation of their operation can contribute toward mitigating these impacts. For the same reason, caution must be used in interpreting the changes in the flow duration curves, Figure 7.13 and Figure 7.14 since the operation strategies applied in the model do not change from the reference to the future climate.

Examining the impact of climate change at Gaafra for the 2050 period, it appears that from February to September there is no consistent direction in the simulated flow changes from among the ensemble members. Consistent Increases in monthly average flows are predicted for October to January, which may counteract some of the increased demand in this period. However these increases appear to be smaller than the expected changes from increasing water demand and confined to 3-4 months while the withdrawals affect all but 3 months at the onset of the wet season.

Expected changes in the 2030-2050 correspond to the typical planning horizon for infrastructure projects and therefore the most important to address for water resources planners and managers.

Interestingly, for the 2100 period, the flow projections indicate consistent increases in flow in all but these same 3 months at the onset of the wet season. These increases appear to be similar in magnitude or larger than the reductions in flow estimated from increases in water demand.
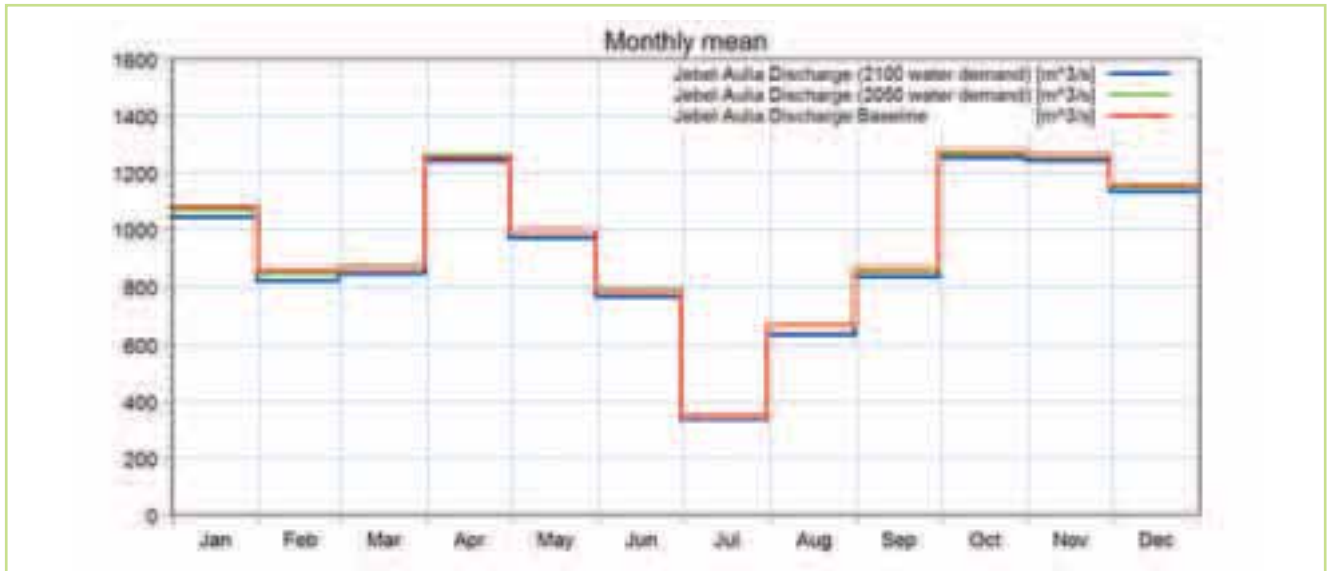
Figure 7.3 Mean monthly discharges for the Jebel Aulia gauge for baseline, 2050 & 2100 water demands
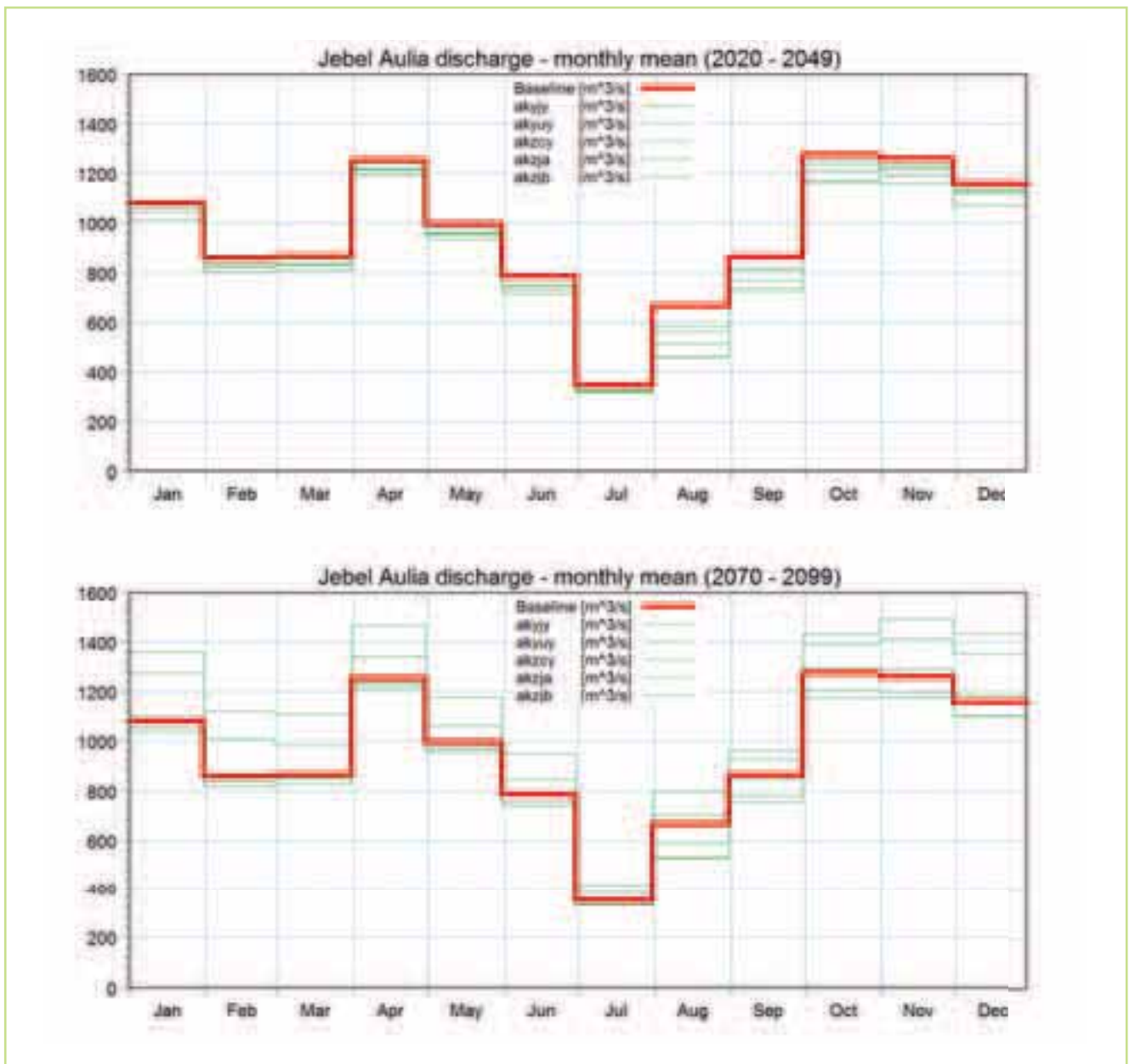
Figure 7.4 Projected changes in the average monthly flows for the Jebel Aulia station for the two periods; 2020-2049 & 2070-2099. The solid (red) line shows the baseline levels (1961-1990) & the thin green lines the different RCM ensemble members
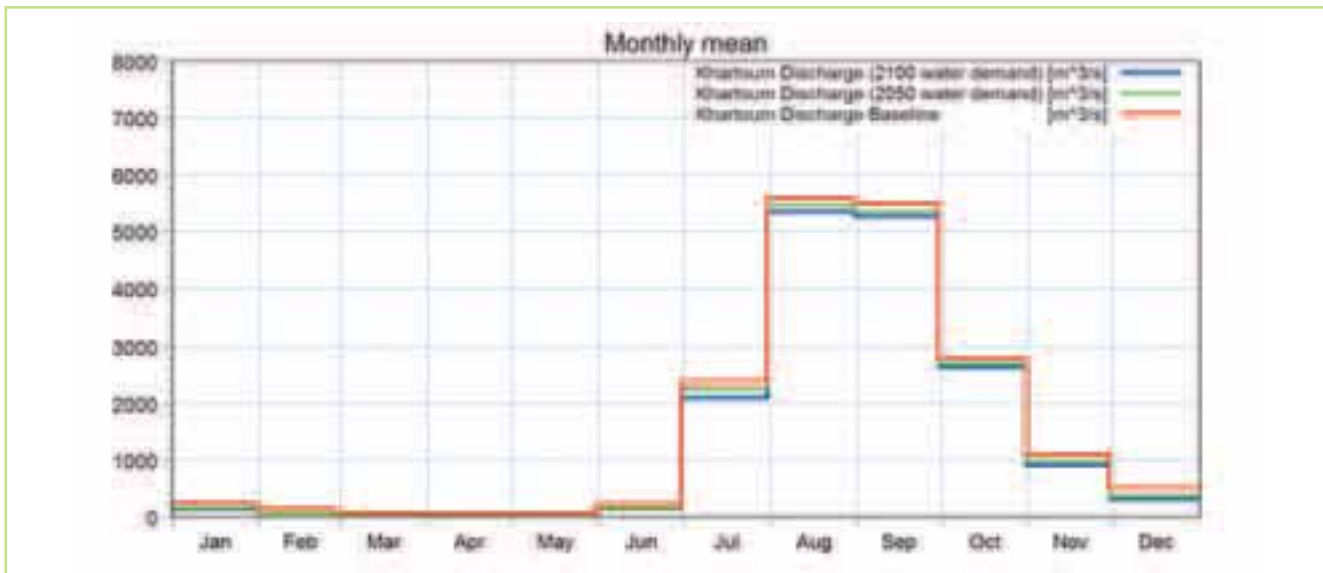
Figure 7.5 Mean monthly discharges for the Khartoum gauge for baseline, 2050 & 2100 water demands
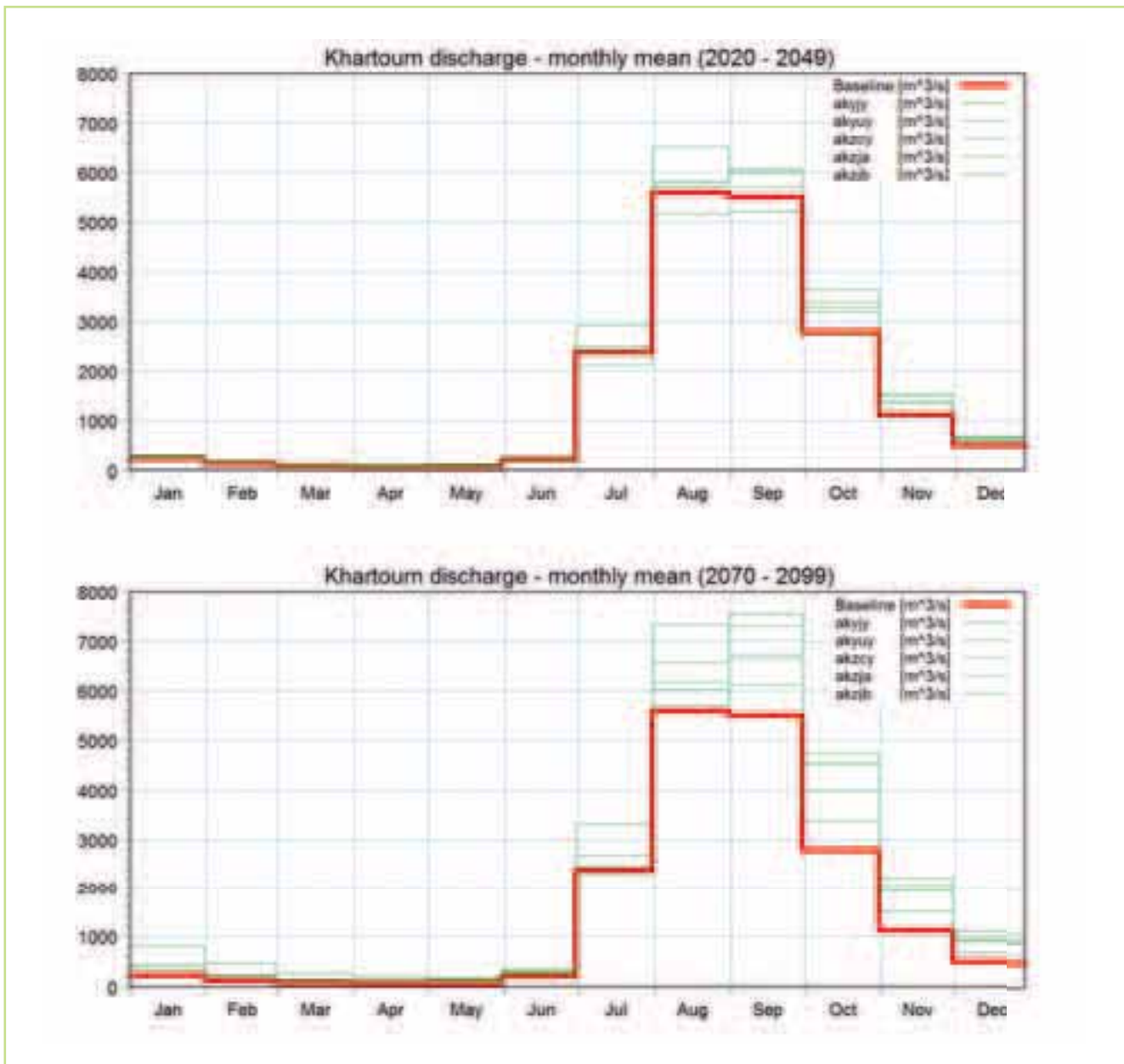
Figure 7.6 Projected changes in the average monthly flows for the Khartoum station for the two periods; 2020-2049 & 2070-2099. The solid (red) line shows the baseline levels (1961-1990) & the thin green lines the different RCM ensemble members
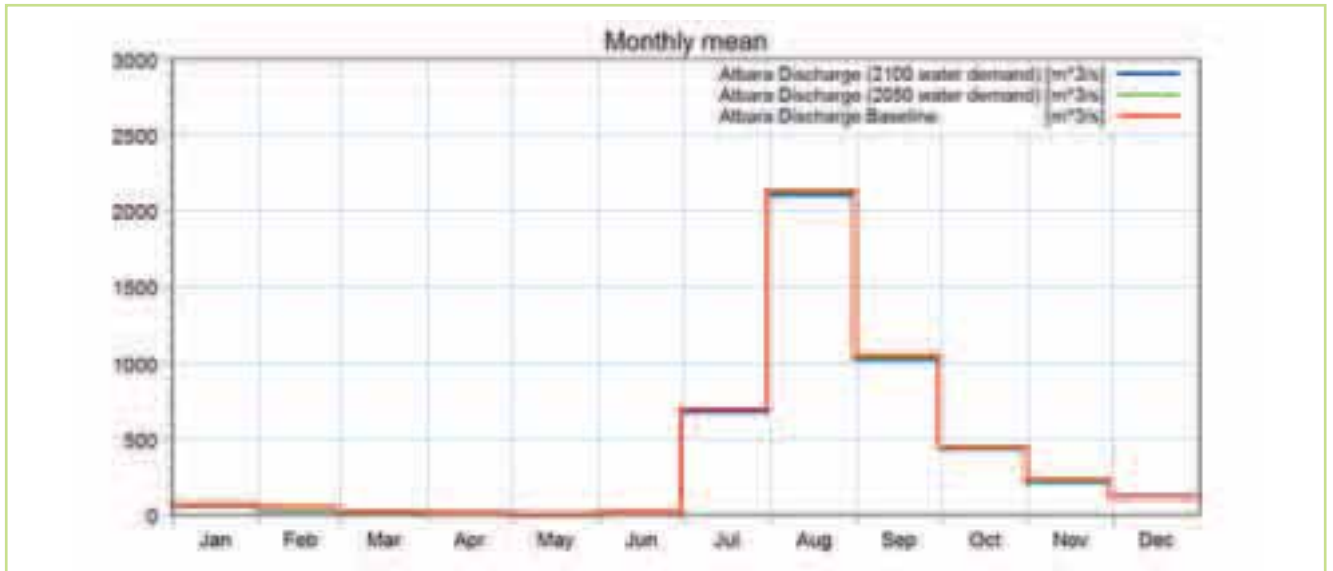
Figure 7.7 Mean monthly discharges for the Atbara gauge for baseline, 2050 & 2100 water demands
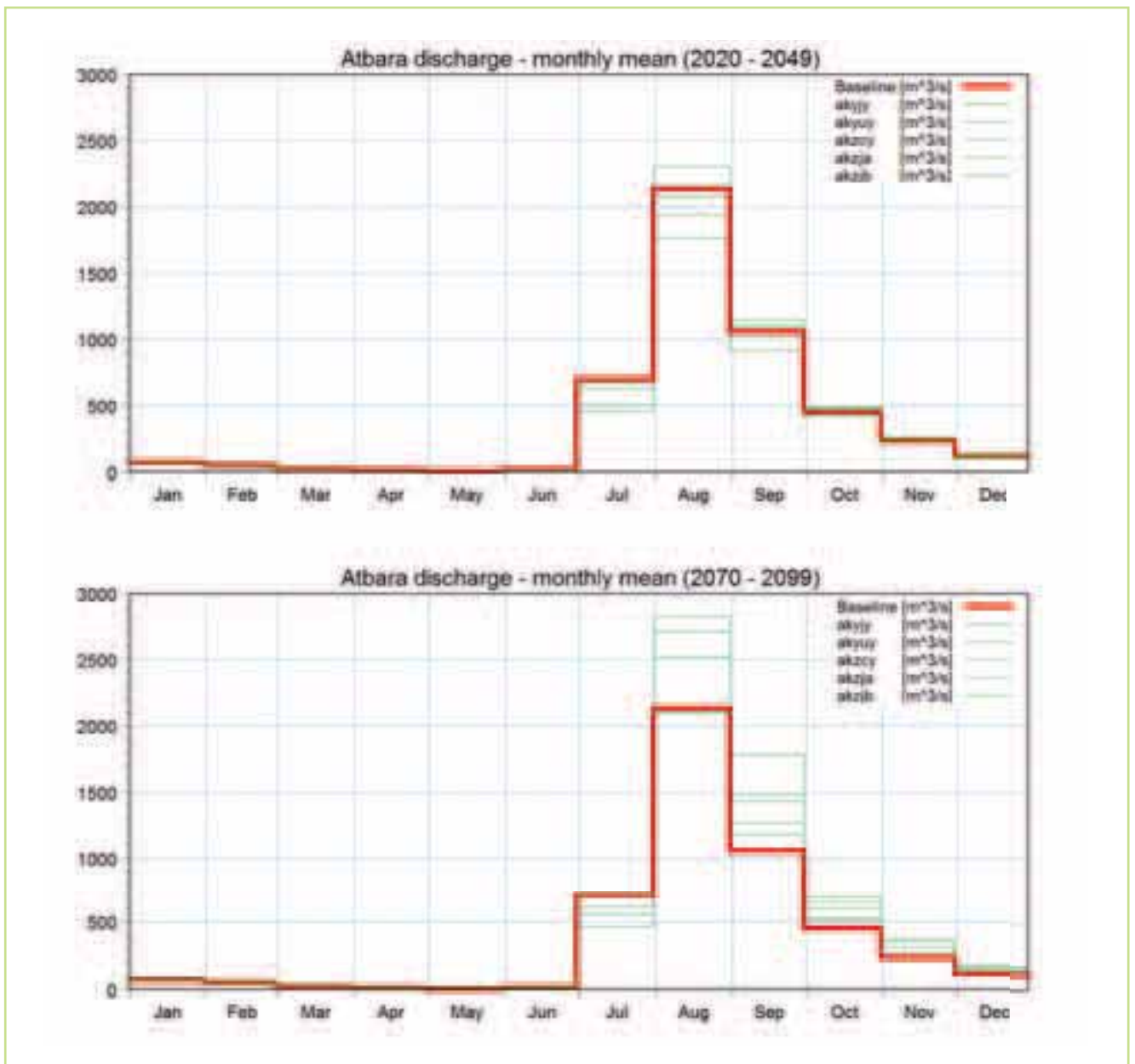
Figure 7.8 Projected changes in the average monthly flows for the Atbara station for the two periods; 2020-2049 & 2070-2099. The solid (red) line shows the baseline levels (1961-1990) & the thin green lines the different RCM ensemble members
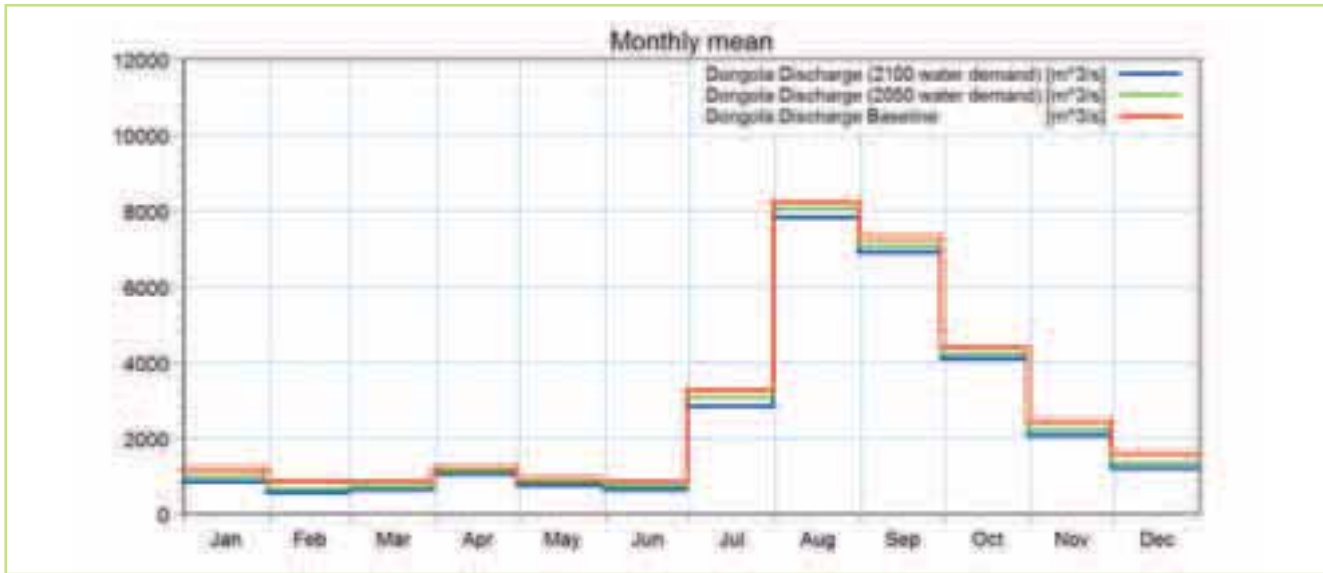
Figure 7.9 Mean monthly discharges for the Dongola gauge for baseline, 2050 & 2100 water demands
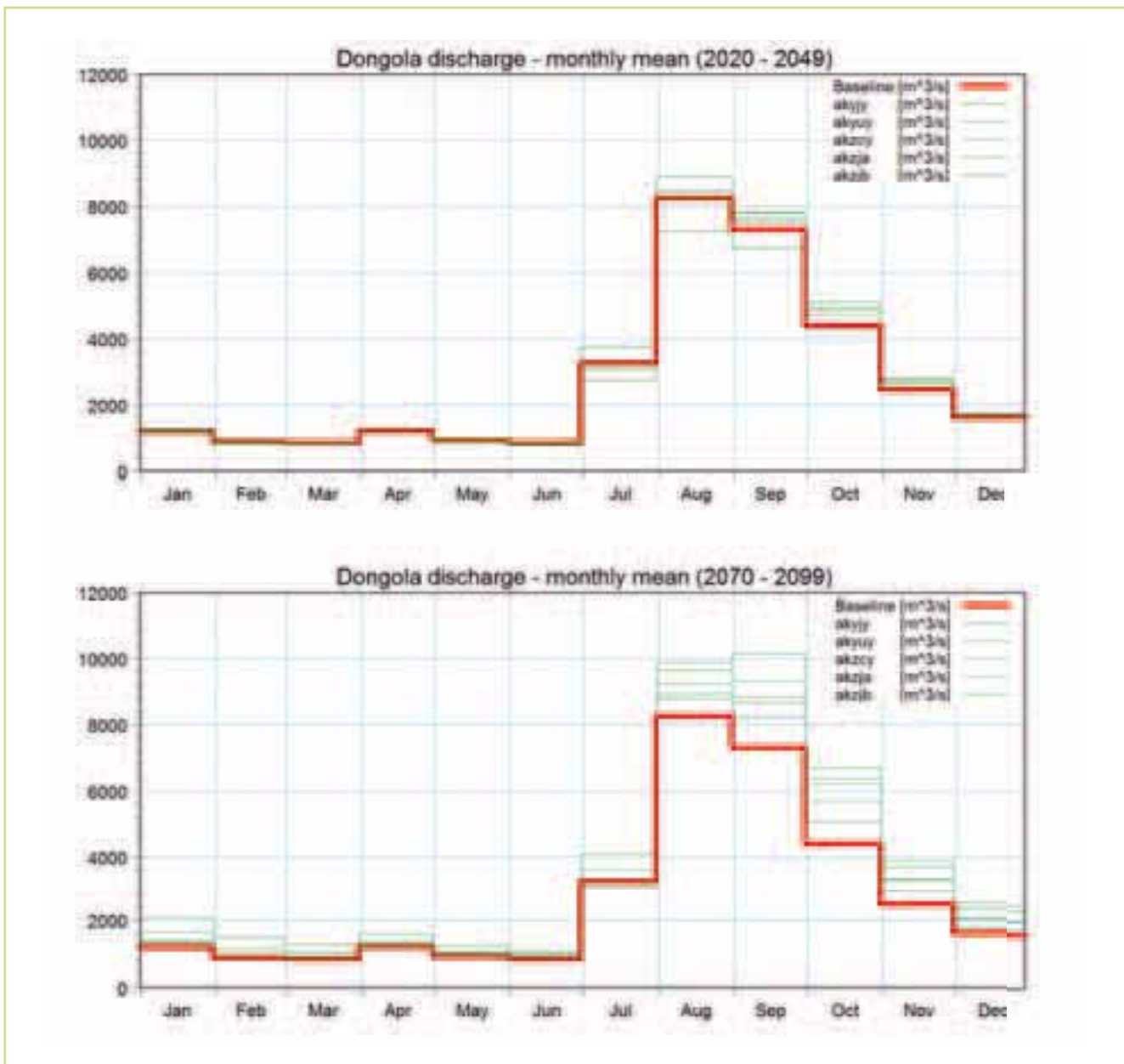
Figure 7.10 Projected changes in the average monthly flows for the Dongola station for the two periods; 2020-2049 & 2070-2099. The solid (red) line shows the baseline levels (1961-1990) & the thin green lines the different RCM ensemble members
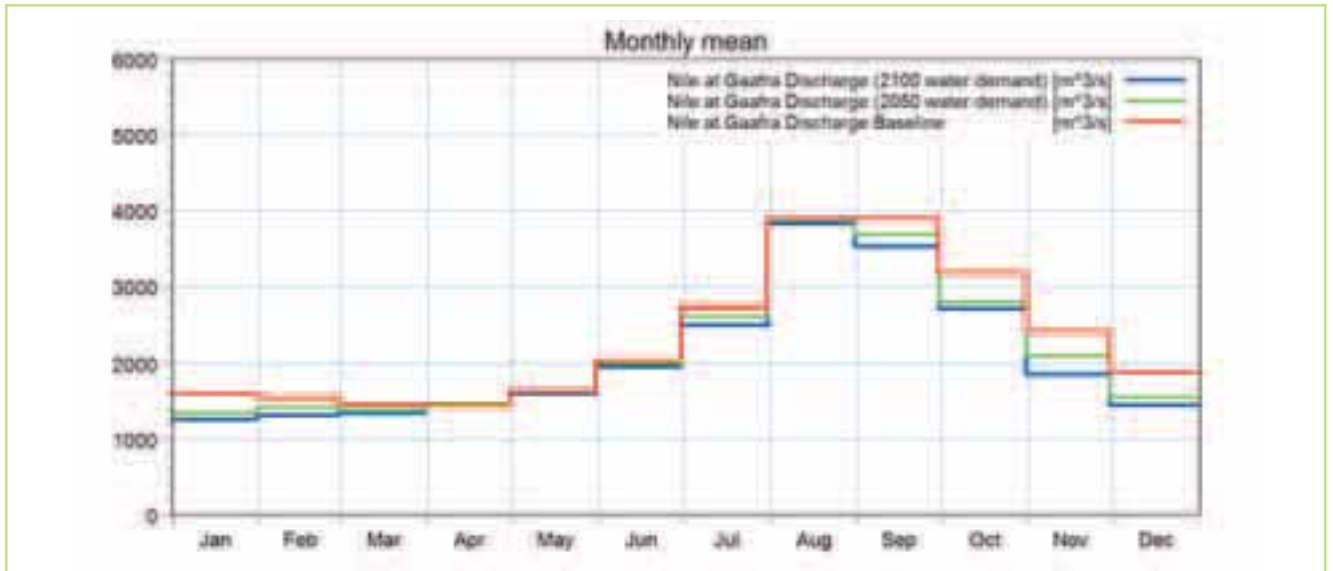
Figure 7.11 Mean monthly discharges for the Gaafra (El-Ga'Afra) gauge for baseline, 2050 & 2100 water demands
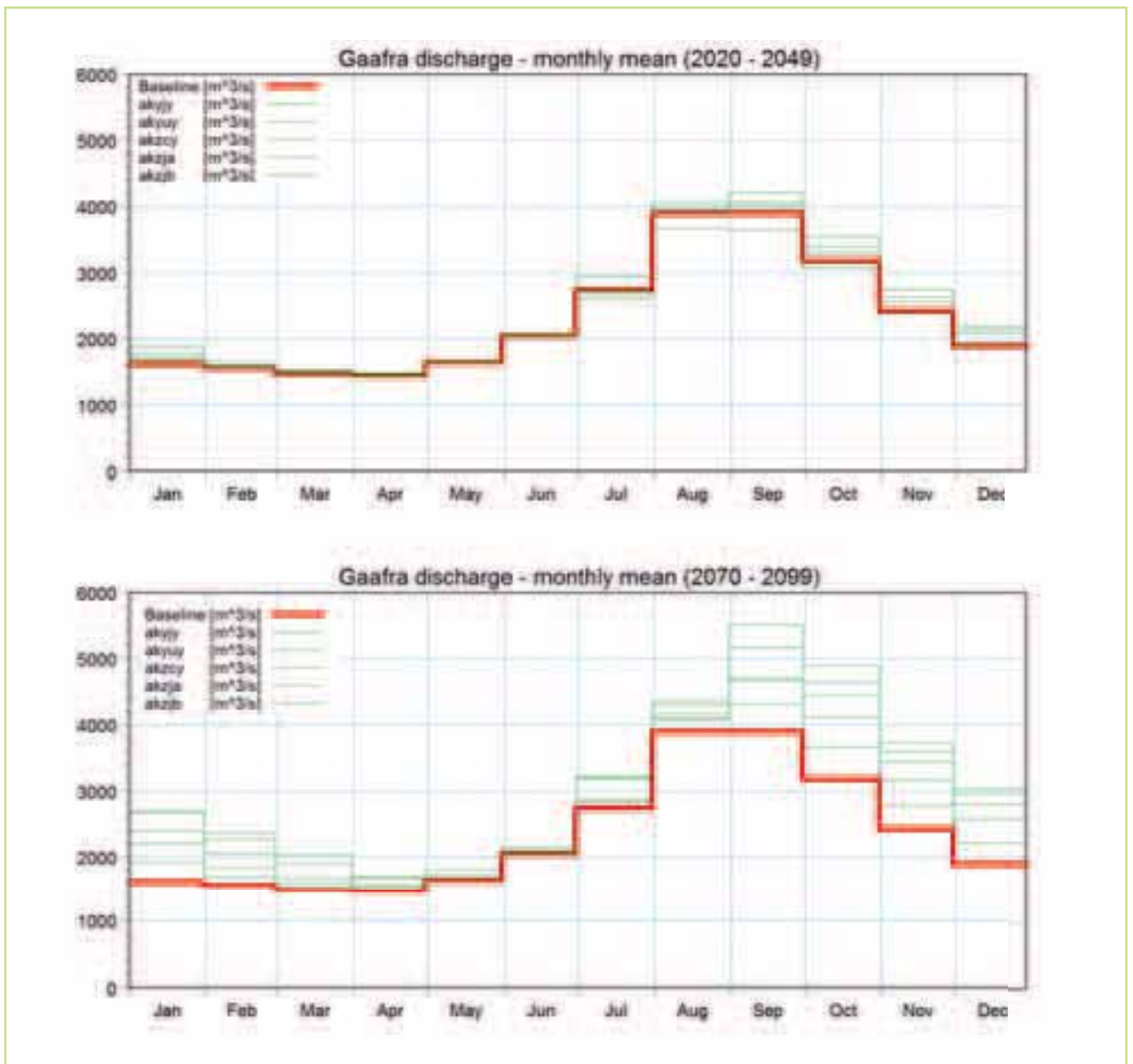
Figure 7.12 Projected changes in the average monthly flows for the Gaafra (El-Ga'Afra) station for the two periods; 2020-2049 & 2070-2099. The solid (red) line shows the baseline levels (1961-1990) & the thin green lines the different RCM ensemble members
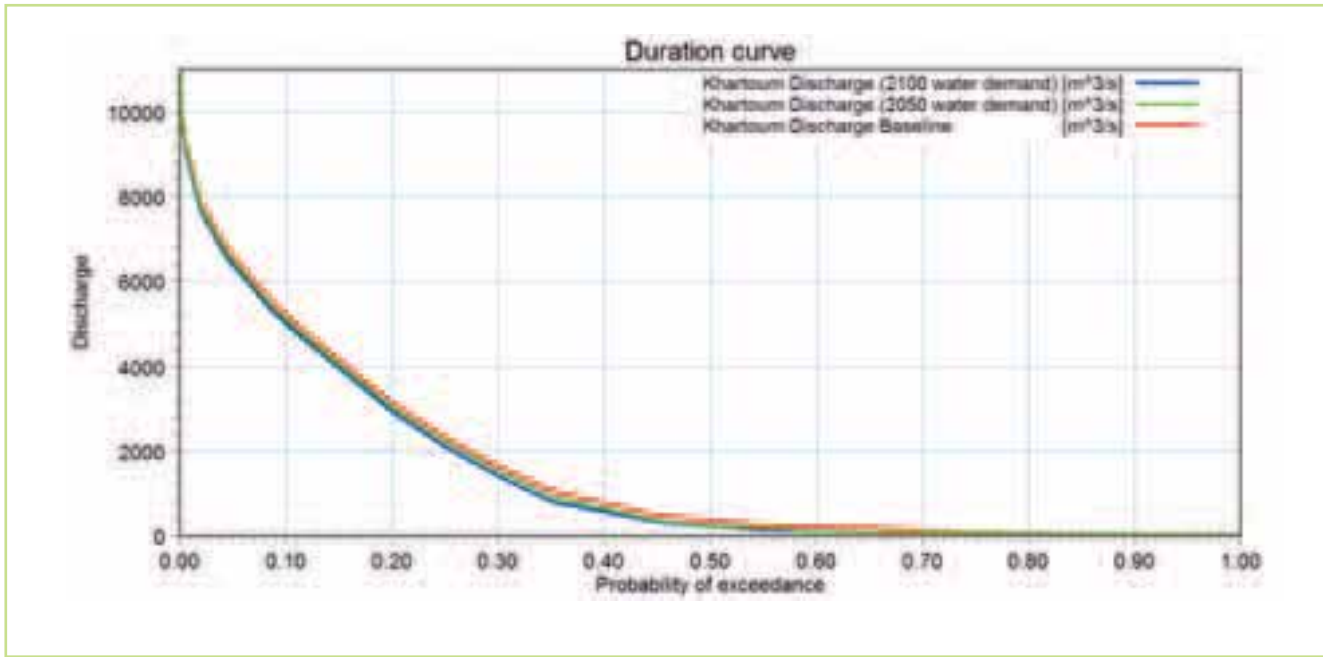
Figure 7.13 Changes in the flow duration curve at Khartoum from baseline (red), 2050 (green) & 2100 (blue)
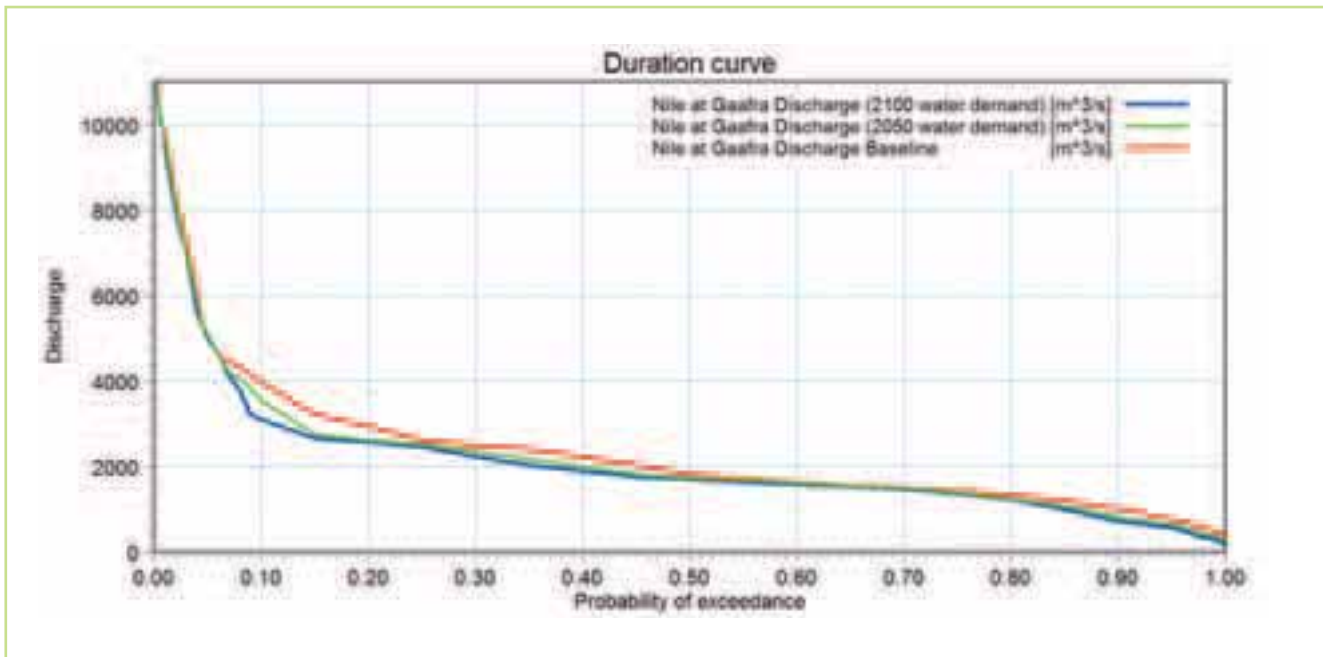
Figure 7.14 Changes in the flow duration curve for the Nile at Gaafra (El-Ga'Afra) from baseline (red), 2050 (green) & 2100 (blue)

8.0 Summary & conclusions

8.1 Background

The Nile River Basin represents one of the most critical and perhaps most important shared water basins in Africa. The countries surrounding the Nile have many different water use requirements including hydropower and crop irrigation. Managing and developing the water resources within the basin must not only address different water uses but also the trade-off between developments upstream and water use downstream between different countries. In addition, the region is facing rising levels of water scarcity, high population growth, watershed degradation and loss of environmental services. Any future changes in the water quantity and quality and their distribution in space and time will have important impacts on the local and basin-wide economies and environment.

To understand the challenge of managing water resources within the Nile, it is necessary to examine the complex geography, climate and hydrology of the basin. While estimates vary, the Nile is some 6850 km in length and drains an area of 3.110 million km2. Many past studies have demonstrated that modelling current and future changes in river runoff presents a number of challenges: the large size of the basin, the complexity of the hydrology (the Nile Basin exhibits one of the most extensive system of lakes and wetlands in the world with little known hydrology), the relative scarcity of data, and its geographical location and the corresponding dramatic variety of climatic conditions. The climate shows significant variability, for example with a strong trend in the annual average rainfall with latitude, and quite different patterns in the distribution through the year. One of most important characteristics of the basin is the contrast between the size of the basin and the relatively small volume of runoff. This is due to most of the rainfall being limited to two relatively small areas, the East African lake region and the Ethiopian highlands (Sutcliffe and Parks 1999), meaning that runoff is generated in less than a third of the basin.

This characteristic means that the flow in the Nile is sensitive to changes in precipitation, showing great variability in runoff from year to year, which in turn means that the Nile is expected to be sensitive to potential effects of climate change. Several studies (e.g. Strzepek et al, 1996; Elshamy 2000; Tidwell 2006) have examined the impacts of climate change on the temperature and precipitation across the region and the subsequent effects on flows within the Nile. For temperature, the current consensus seems to be that warming trends are expected, but projections for precipitation are much more variable. As a result, projections of changes in flows in the Nile due to climate change are associated with a large degree of uncertainty.

The challenge for decision-makers and stakeholders in the water sector is to understand climate change impacts, to determine where and how regions and sectors are vulnerable, and to implement appropriate adaptation measures. This requires information and assessments for decision-makers at the appropriate scale. The challenge for climate scientists and hydrologists is to derive information that can be used and understood by decision-makers given the inherent uncertainty in these projections. The integration of climate adaptation measures in policy making and the coordinated implementation of adaptation measures are relatively new disciplines.

The main focus of this study has been to develop relevant tools and information that can be subsequently used as the basis for climate adaptation to water stress (floods & water scarcity) at a regional scale in the Nile Basin for 1) integration in decision-making and 2) implementation of adaptation measures at the regional scale.

8.2 Outcomes & benefits

This study has contributed to an enhanced understanding of climate vulnerability in the Nile in relation to water stress (high and low flows) and the provision of vulnerability indicators.

Two workshops have been conducted by DHI/UK Met Office for NBI staff to provide in-depth knowledge about:

- Regional scale climate modelling using the PRECIS model (by Met Office Hadley Centre).
- Regional hydrological modelling using the MIKE BASIN/HYDRO model (by DHI).
- Presentation of the methodology, key findings and perspectives for combined climate change and water resources modelling.

More specifically, the project has provided a number of important findings in relation to:

- State-of-the-art regional climate modelling results, including provision of change factors within the

Nile Basin, made available to all NBI countries for application at the regional or national level.

- Improved understanding of the key climatic processes and the predictive ability of regional versus global climate models.
- Regional hydrological modelling results made available to all NBI countries.

As a result of the project the following modelling tools have been established:

- A regional scale hydrological tool suitable for modelling the impact of climate change, water demand scenarios, and the impact of climate adaptation measures at the regional scale in both high and low flow regimes (floods and water scarcity).
- A regional water resource tool that can be used as boundary conditions and starting point for more detailed local modelling of both water resources and climate for investigating national and local adaptation measures for floods and droughts.

This study has used the same hydrological modelling tools (DHI MIKE series), which are currently being used in the region, and for which NBI already has many licenses. It is therefore compatible with other Nile Basin projects, particularly the Decision Support System (DSS) currently being developed by DHI for the basin.

8.3 Innovations in this study

The results of this study have involved a number of key innovations:

- New regional scale climate modelling results using a novel perturbed physics ensemble (PPE) approach. Much of the existing published work has utilised global climate models. One of the key strengths of regional scale climate modelling is the ability to improve the spatial resolution in the climate change assessments.
- This is one of the first applications of the PPE ensemble approach outside Europe. To the authors' knowledge only one other study has used this approach over Nile. This was in the project "Regional Climate Modelling of the Nile Basin: Preparation of climate scenario outputs for assessment of impact on water resources in the Nile Basin" (Butts et al., 2011; Buontempo et al., 2011). The study carried out here includes the following advances to this previous work:
- Larger regional modelling domain compatible with international climate modelling collaborations under CORDEX (Giorgi et al., 2009).

- New methodology for selecting GCM ensemble members to drive the RCM runs, which gives a better representation of uncertainty in the climate modelling
- Upgraded land surface scheme describing the exchange of water between the atmosphere and the land surface
- Alternative treatment of the climate of Lake Victoria based on Sea Surface Temperatures
- The Regional Climate Model runs date from December 1949 to November 2099. This extended time period was one of the key recommendations in Butts et al. 2011.
- Climate change based indicators for climate vulnerability across the entire Nile.
- Uncertainty estimation in the impact on flood and droughts based on a regional climate model ensemble.

8.4 Approach & methodology

The overall approach has been to develop and apply a regional scale framework for assessing climate change effects. This framework consists of combining regional scale climate modelling with a hydrological modelling tool to both assess the impacts of climate change on the water resources and to provide the capability to evaluate adaptation measures at the regional scale. This was motivated by the clear perception that such tools to assess climate adaptation at the regional scale are missing. This is particularly critical for transboundary rivers, where the downstream impacts of national water resources management need to be considered. The implementation of adaptation measures, depending on the type of interventions, may need to treat the basin as a whole and a regional modelling framework is required to evaluate alternatives to avoid regrettable outcomes.

One of the characteristics of the Nile Basin is that the flows within the river constitute the most important component of water resources. To simulate flows and water levels at the regional scale for water resource management, climate change assessment and climate adaptation scenarios, a distributed hydrological modelling approach is required. A regional scale hydrological model for the entire Nile Basin has been developed using the MIKE BASIN/MIKE HYDRO modelling tool. This choice was in part motivated by the implementation of this tool in the Nile Basin DSS. This modelling tool is well-suited to regional scale adaptation as it includes both rainfall-runoff processes as well as facilities for representing reservoirs and their operation, water users, water transfers, and different types of irrigation and other demands.

The regional hydrological model was calibrated using climate observations and discharge measurements primarily from the period 1960-1980. The main goal was to develop a regional model that captured both the flow dynamics (flow regime) and the flow magnitudes to the extent possible given the data available. While limitations in the regional model have been identified, the overall performance of the hydrological model at the regional scale is satisfactory and an appropriate basis for the assessment of changes in the Nile as a result of projected climate change. In particular, the fact that the model can replicate the substantial variation in climate seen in the White Nile in the early 1960's compared to the remainder of this period gives some confidence in the ability of the model to represent future flows under climate change.

The resulting regional model was used to define a baseline or reference simulation. Projections of regional flows have then been derived for future water demand scenarios and climate change, separately, to determine changes in the regional flows compared to this baseline. A pre-requisite for assessing climate change impacts on water resource is the projection of climate change using numerical climate models.

For this study a set of regional climate model (RCM) simulations have been performed for the Nile River Basin using the most recent generation of the UK Met Office GCM-based perturbed physics ensembles (PPE), which supersede previous work. This project presents the first application of this approach for the Nile beyond 2050, showing results for two projection horizons, the near future (2020-2049), and the far future (2070-2099).

The projections for 2020-2049 are particularly relevant for regional water resource planning as this corresponds to typical planning and implementation horizons for major infrastructure projects. The projections for 2070-2099 are more uncertain but indicate whether any trends found in the near future continue into the far future.

While General Circulation Models (GCM's) provide physically-based projections of how climate may change, their spatial resolution is typically a few hundred kilometres. The applied higher resolution RCM modelling in this study is better able to capture the local detail and forcing, which is required for water resource impact assessment at the regional and national levels. The PRECIS RCM model is driven by GCM models at their lateral boundaries (dynamical downscaling). RCM simulations were run using the A1B SRES scenario.

In this study the RCM projections were developed from a subset of five of the most recent Hadley Centre perturbed physics GCM simulation ensembles. This subset was selected using a recently developed systematic methodology (McSweeney et al., 2012) to capture the spread or range of outcomes produced by the full 17 member ensemble, while excluding those unable to represent the African climate realistically. The selection was achieved by evaluating the models against observations of the annual cycles of temperature and precipitation and the spatial patterns of precipitation and 850 hPa winds. Comparisons of these RCM results with observations show that this ensemble appears to correctly capture the annual cycle of temperature, both for Africa as a whole and for the sub-regions. The RCM ensemble appears to slightly over-estimate precipitation, but captures the annual cycle for most of the regions. Most importantly, the RCM ensemble shows a significant improvement over the traditional GCM ensemble in many parts of Africa.

An ensemble-based approach is recommended for two reasons. Firstly, because previous studies, including the IPCC 4th assessment, have shown that projections of precipitation over the Nile are highly variable. Given the sensitivity and vulnerability of the water resources in the Nile basin to climate changes it is therefore important not to limit climate change assessments to one single simulation. Secondly, this is an important step towards quantification of uncertainties, which is fundamental to decision-making, but often overlooked.

This study is a pioneering application of the PPE approach outside of Europe. Although the methodology adopted has been designed to explicitly account for uncertainties in model projections, it is emphasized that it does not account for the full range of uncertainty.

8.5 Key findings

8.5.1 Regional changes in temperature

Although not directly related to the water balance and water resources over the basin, all the RCM projections show consistent increases in temperature for both the near future (2020-2049) and the far future (2070-2099).

The near future scenario shows increases of approximately 1.5°C, though with significant spatial and temporal variation, which is consistent with previous studies (IPCC, 2007b; Butts et al. 2011). It shows maximum increases over Egypt and the northern part of Sudan during the hottest months. This can be expected to increase both the agricultural and domestic water demand in this region.

The far future scenario shows even larger

increases, in the range of 4-6 °C, during the summer months. While these changes are quite large, they are consistent with results from the IPCC 4th assessment, which show increases of 3.5 °C or more during the summer season. Temperature rises may both reduce the productivity of major crops and increase crop water requirements (Eid et al. 2006). The projected large increases in temperature will certainly increase water demand in major population centres both for food production and domestic water supply.

8.5.2 Regional changes in precipitation - GCM's

The projections of precipitation from climate models are generally less reliable and exhibit greater variability than the temperature projections. For example, although global models agree on drying over Africa for the 20th century, there is no robust agreement in their predictions of 21st rainfall (Giannini et al. 2008). Within the Nile Basin several previous studies indicate that there are large uncertainties in both the direction and magnitude of changes in precipitation (e.g. IPCC 2007; Boko et al 2007; Elshamy et al. 2008; Beyene et al., 2010).

Nevertheless the ability of climate models to represent key features of the current climate provides some degree of confidence in the ability of the models to represent future climate. At first glance, the QUMP GCM simulations of precipitation used here as boundary conditions for the regional simulations do not compare well for some sub-regions. It is recognised in the climate modelling community that modelling the climate in Africa is challenging and the IPCC 4th assessment shows systematic errors in and around Africa for many of the GCM's. To keep this in perspective it is worth noting that 90% of these GCM's over-estimate the rainfall (positive bias), by an average of 20%, for southern Africa (Buontempo et al. 2013a). Several have no representation of the West African monsoon (Meehl et al. 2007b) and the Inter-Tropical Convergence Zone (ITCZ) is displaced towards the equator in many cases. By comparison the HadCM3 used here does reasonably well but there are still systematic differences between the GCM simulations and observations. There is still much more work to be done in the climate research community towards improving climate simulations in the region.

These limitations were addressed firstly in the selection process, by eliminating those GCM's that exhibit the largest positive and negative biases across all the sub-regions and seasons. Secondly, downscaling using an RCM, with the addition of regional detail such as higher resolution orography, not only makes the RCM more applicable to local scale impacts but also appears to improve the simulation of

current climate. Finally, monthly change factors were used to develop bias-corrected climate projections. The underlying argument is that although there are biases in the GCM's, it is nevertheless appropriate to use the climate models to predict magnitude of *changes* in relation to the current climate, as opposed to absolute values directly from the climate model.

The RCM projections derived by dynamical downscaling from the QUMP GCM's also reflect the large uncertainties inherent in climate projections of precipitation. The projections for both 2020-2049 and 2070-2099 show large areas for many months where there is no consensus among the 5 RCM ensemble members as to the direction of change. In assessing the impact on water resources, especially the high and the low flows, we should however focus on changes in the two source regions: Equatorial Lakes and the Ethiopian Highlands - see below.

8.5.3 Regional changes in climate & water resources – Introduction

A number of indicators were investigated to assess the impacts of climate change on water resources. The most useful indicators were found to be the "consensus" maps for precipitation (Section 6.5) and the changes in regional flows (Section 6.6).

Maps of the indicators Climate Moisture Index (CMI) and its coefficient of variation (CV CMI) were examined as they represent potential water availability imposed solely by climate and the inter-annual variation of this water availability, respectively. These indicators are particularly useful in identifying vulnerable transition areas (semi-arid or sub-humid), but the spatial extent of changes derived from our climate projections is strongly constrained by the localised regional rainfall and the large arid region in the north of the Nile basin. They therefore provided only limited information of the climate change impacts.

The climate "consensus" maps were found to be a useful means to address the uncertainty in climate projections. Even though the different RCM projections show significant differences in both the direction and magnitude of changes in precipitation, these "consensus" maps highlight regions within the Nile Basin where the regional climate models provide consistent (at least 4 out of 5 agree on the direction) projections and conversely identify areas where the regional models don't agree on the direction of change.

This will better support judgements on the impact of regional climate model uncertainty on floods and droughts. A consensus among the RCM projections for the direction of change provides useful information for decision-makers even if the magnitude of the change

is uncertain. More robust approaches to climate change adaptation are needed in areas where the direction and magnitude of climate change are highly uncertain.

The regional changes in flow provide the most directly relevant impact information, primarily because the flows represent the major part of the water resource for much of the Nile basin. In addition though, the flows integrate the effect of changes in both precipitation and potential evapotranspiration over larger areas. So even if these climate signals are 'noisy' and uncertain, the changes in flows may show a much clearer signal.

8.5.4 Regional changes in climate & water resources – White Nile

The projected changes over the Equatorial Lakes are very important for the projected conditions in the White Nile area.

The near future RCM projections show a significant decrease in precipitation over Lake Victoria from April-November. It should be noted that the RCM in the "short" rainy season (October, November and December) seems to over-estimate the projections, exhibiting a strong positive bias over the lake (Buontempo et al. 2013a). It is emphasised this is a localised effect restricted to the lake area, but nevertheless important as the rainfall directly over the lake constitutes a large fraction of the total inflow to the lake. The exact cause of this bias is not yet fully understood. It is worth noting however that previous work using a different description of processes for Lake Victoria also showed a significant drying during the northern hemisphere summer (June, July, August, September) (Butts et al. 2011). No clear consensus is found regarding the changes over Lake Victoria during the "short" rainy season, but increases are projected north of the Lake from December-January.

The spatial precipitation patterns show an increase in precipitation over the northern part of the White Nile during August-September and November December for both horizons.

The far future projections also show reductions in rainfall over Lake Victoria from April- November, but these are not as large when compared to the near future projections. The changes in precipitation are directly reflected in the projected flows at Jinja in Uganda and Malakal in South Sudan (Figure 8.1).The Jinja station represents the outflows from Lake Victoria which are controlled by the large storage capacity of the Lake and the releases (following the "Agreed Curve") through the Owens Fall dam. The reductions in rainfall lead to a consistent reduction in the flows at Jinja for the 2020-2049 period ranging from almost zero to 15% of the monthly average flows.

For the same period (2020-2049) the flows at Malakal also exhibit a consistent reduction for all 5 RCM projections. Malakal integrates the contributions from all parts of the White Nile, which includes the Equatorial Lakes basin to the south, the Sobat to the east and the Bahr-Jebel basin including the Sudd. Peak flows are shifted as a result of the travel time and the seasonal impact of the upper sub-basins of the Sobat in Ethiopia. The contributions from the Bahr El-Ghazal basin to the west are neglected in the model as previous work has shown that the contributions to the main Nile are negligible, (Shahin 1985). Consistent reductions are found, though the magnitude varies strongly amongst the RCM ensemble members.

The Sudd is an important area of hydrological interest but the hydrology is less well known and therefore difficult to represent accurately in a hydrological model. The presence of swamps and wetland areas lead to large losses but the multiple flow paths make measurements of the flows challenging. However, our results for the Buffalo Cape station, not shown here, suggest that there will be consistent reductions in the flows in the Sudd for the 2020-2049 period that match the reductions seen throughout the White Nile. This trend appears to continue for the 2070-2099 projections, although a single ensemble member simulates an increase in flow.

It is interesting to note that there does not appear to be any clear consensus on the direction and magnitude of the change in flows at these two sites for the far future (2070-2099). Whether this is because there is no long term trend or merely an expression of the large uncertainty is difficult to ascertain.

As mentioned earlier, the 2020-2049 near future period corresponds to the typical planning horizon for many infrastructure projects. The results shown here clearly indicate that any planned adaptation measures must address potential reductions in flow (and water levels) in the White Nile area.

A large uncertainty in both the sign and magnitude of the change in flow has important implications for adaptation strategies to be selected. In general any adaptation measures must be robust to take into account the degree of uncertainty in the flow projections. The reduction in rainfall may have important impacts for rain-fed agriculture within the White Nile, but these may only be critical in the areas where agriculture is already marginal. The impacts of the far future projections are more difficult to adapt to as the uncertainty in projected flow pattern is significant. Here, a robust adaptation strategy that accounts for a wide range of possible future conditions is required.
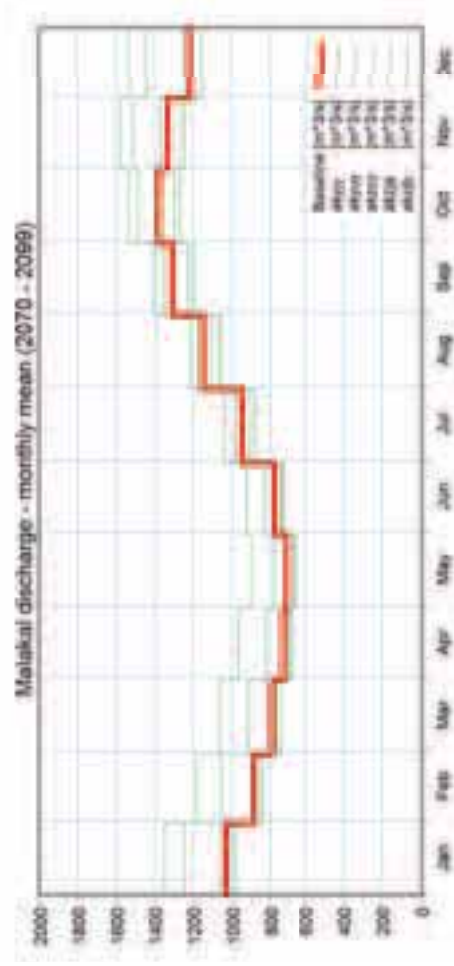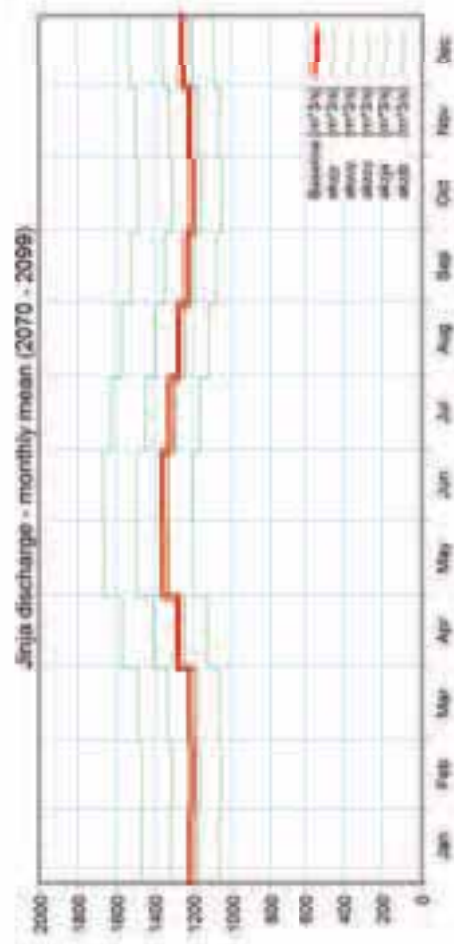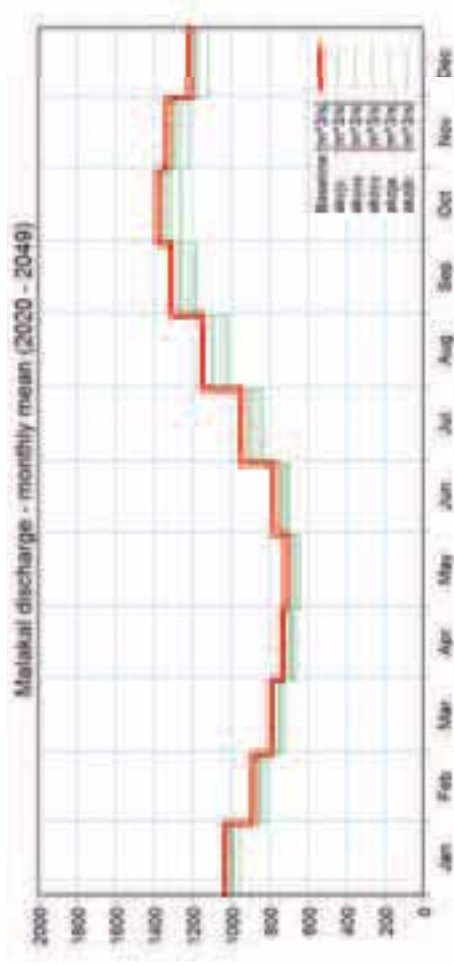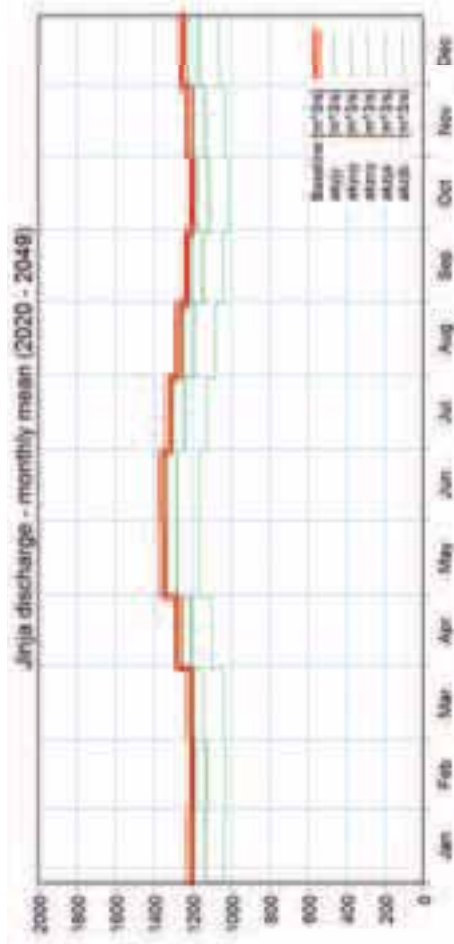
Figure 8.1 Projected changes in the average monthly flows for Jinja (left) & Malakal (right). Projections are shown for two periods; 2020-2049 (top) & 2070-2099 (bottom). The solid (red) line shows the baseline levels (1961-1990) & the thin green lines the different RCM ensemble members

8.5.5 Regional changes in climate & water resources – Blue Nile & Atbara

Together the Blue Nile and Atbara represent a significant part of the water resource in the Nile, and because they account for more than 70% of the main Nile peak flows, are critical to the water resources downstream.

The RCM projections for 2020-2049 show both increases and decreases in rainfall in the region during the wet season, June to September. The decreases appear in the western-most parts of these two catchments, while the increases appear in the south and east and suggest a general increase at the end of the wet season. No clear patterns emerge for the other seasons. By contrast, the 2070-2099 projections show a consistent increase in the eastern-most parts of the Blue Nile and Atbara catchments for most of the year, including the rainy season.

These projections of rainfall changes are also clearly reflected in the resulting river flows in both Atbara and the Blue Nile at Khartoum (Figure 8.2). For the near future (2020-2049), the flows in the Atbara catchment appear to decrease in July and August, though with a large range in the magnitude of these reductions between the ensemble members. For the far future (2070-2099), similar reductions are seen during July but increases are seen in August-December. There is a large range in the magnitude of these increases.

For the Blue Nile at Khartoum, there is general tendency toward increased flows in October-November for the 2020-2049 projections, but both increases and decreases are simulated in July-September. For 2070-2099, the flow projections are consistently higher and for some ensemble members very large but there is a very wide range of flows. This is consistent with previous studies (e.g. Elshamy et al., 2009) that indicate that the Blue Nile is extremely sensitive to small changes in rainfall and PET. These results are also consistent with previous RCM projections (Butts et al., 2011). This study also finds a general increase for the 2020-2049 period but find a less clear signal as some ensemble members project (albeit small) decreases in the flow. This suggests that small changes in either rainfall or PET are amplified in the flows. Furthermore, since the hydrological models developed for these two catchments are based on a limited amount of data, with low spatial and temporal resolution, these projections should be viewed as uncertain and applied with caution. In general the model tends to over-estimate peak flows, although the consistency of changes for the 2070-2099 period relative to the baseline indicate a clear tendency toward increased flows.

Climate adaptation measures to address water availability in this region will have to consider both increases and decreases in the high flow range. Increases in flooding and flood risk can be expected with increasing high flows. The consistent flow reductions seen in July in Atbara are not seen in the Blue Nile and may affect water stress locally in the basin.

8.5.6 Regional changes in climate & water resources – Main Nile

Generally the rainfall in this portion of the Nile is very low but the RCM projections indicate small reductions in the slightly less arid Delta area. The main influences on the water resources in this part of the Nile are expected to be the changes in climate upstream and the extraction of water for irrigation, industrial and domestic uses. The Ethiopian highlands alone contribute about 86% of the annual flow to the High Aswan Dam in Egypt. Any changes in the high flows will be the direct result of changes in the Blue Nile and to a lesser extent from Atbara. The lows flows, outside the peak flow season, are expected to be influenced by changes in the White Nile flows.

The Dongola station represents the flows of the whole Nile before it enters Lake Nasser. The impacts of projected future water demand show significant reductions to the flows for the 2020-2049 period, corresponding to 3% of the peak flows and 8% of the medium range flows (Figure 8.3). The low flows are reduced by as much as 20% in the early part of the year. As expected, the 2070-2099 demand scenario leads to further reductions during both the low flow and peak flow periods. The reductions in flow during a large part of the peak flow period are twice as large in far future period.

It should be noted that the water demand scenarios estimated here are highly uncertain. Firstly, the changes are based on a 2005 baseline estimate, seen to be the most reliable estimate available. Withdrawals for the baseline are likely to be larger than the 1960-1990 climatic baseline period, though improvements in irrigation efficiency balance this effect to some extent. Increases in temperature are likely to further increase water demand but are not quantified here. Finally, while the data, especially for the irrigation demands (FAO, 2011a), are taken from some of the most recent and comprehensive assessments, these remain highly uncertain.

The Gaafra station represents flows downstream between the Aswan Dam and the coast. The simulations using the 2020-2049 water demand projections show significant reductions over the entire
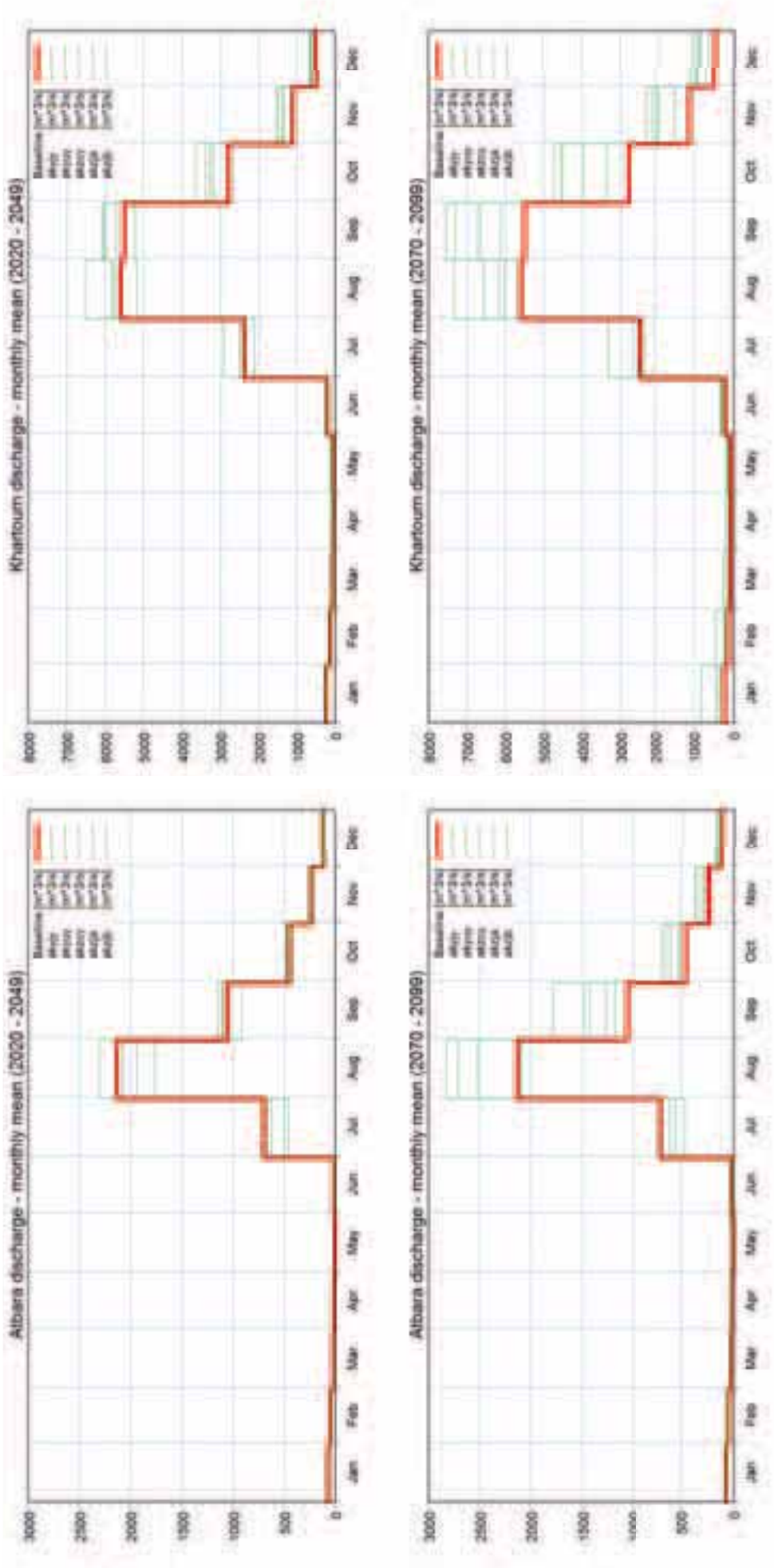
Figure 8.2 Projected changes in the average monthly flows for Atbara (left) & Khartoum (right). Projections are shown for two periods; 2020-2049 (top) & 2070-2099
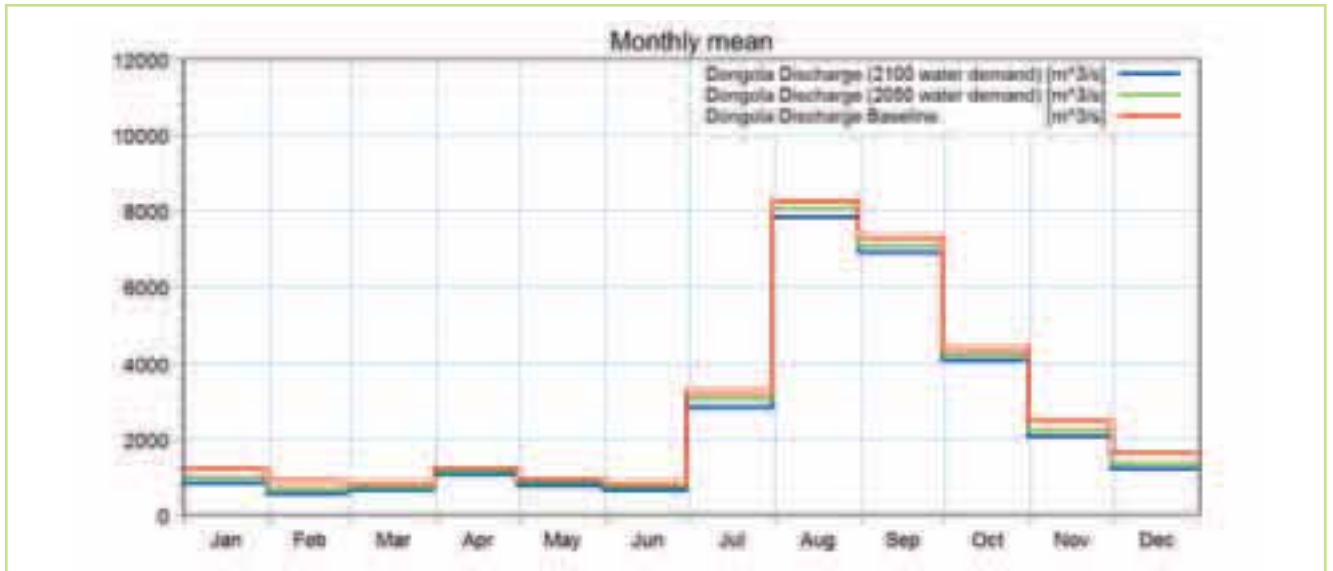
Figure 8.3 Mean monthly discharges for the Dongola gauge for baseline, 2050 & 2100 water demands
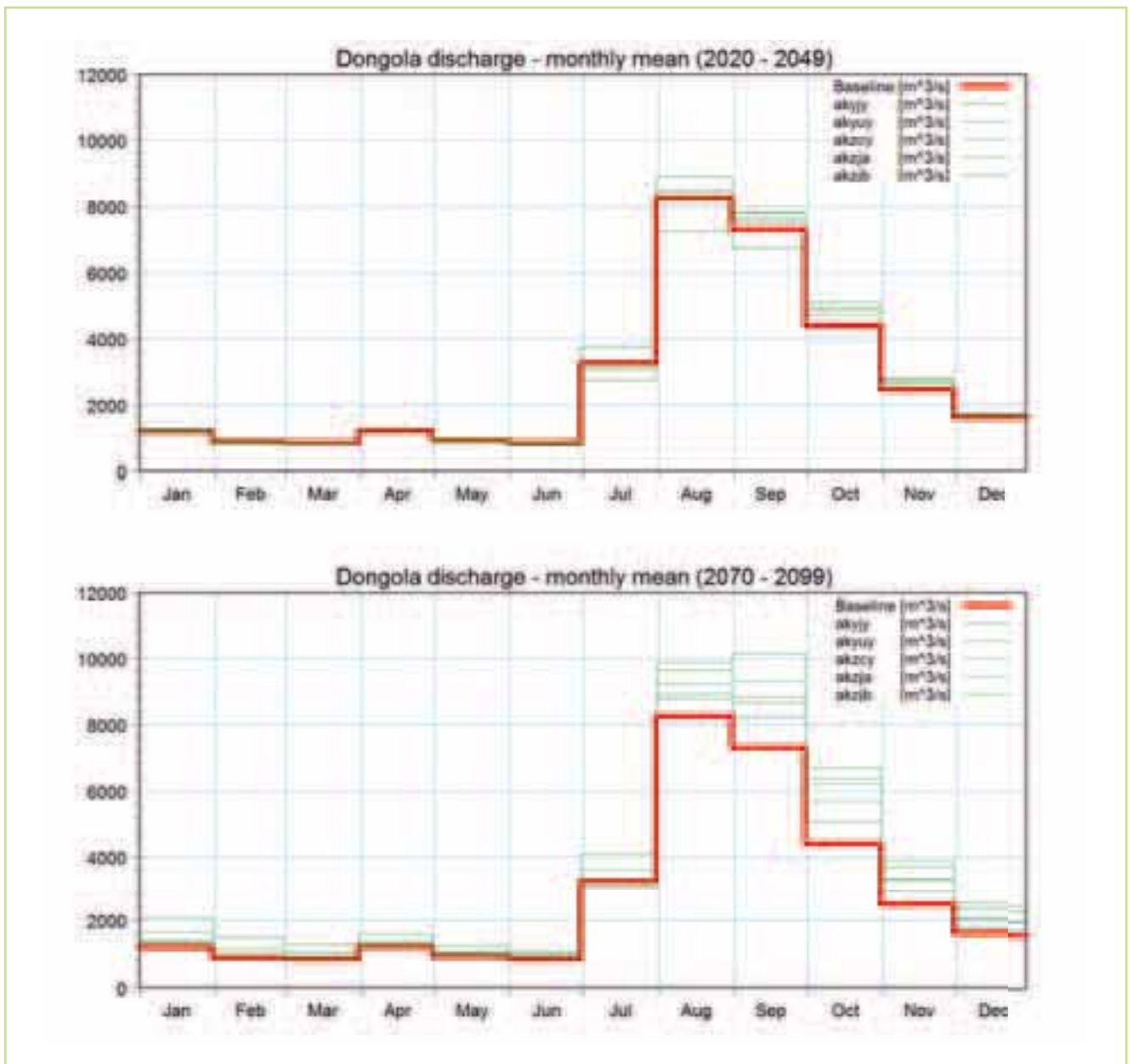
Figure 8.4 Projected changes in the average monthly flows for the Dongola station for the two periods; 2020-2049 & 2070-2099. The solid (red) line shows the baseline levels (1961-1990) & the thin green lines the different RCM ensemble members
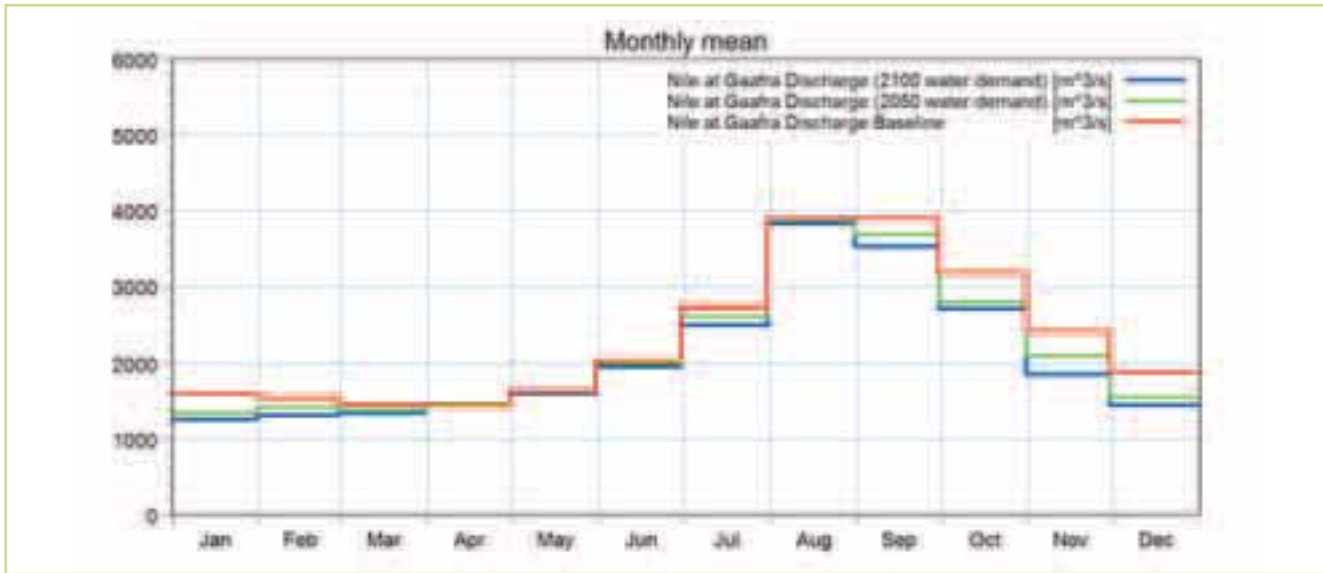
Figure 8.5 Mean monthly discharges for the Gaafra (El-Ga'Afra) gauge for baseline, 2050 & 2100 water demands
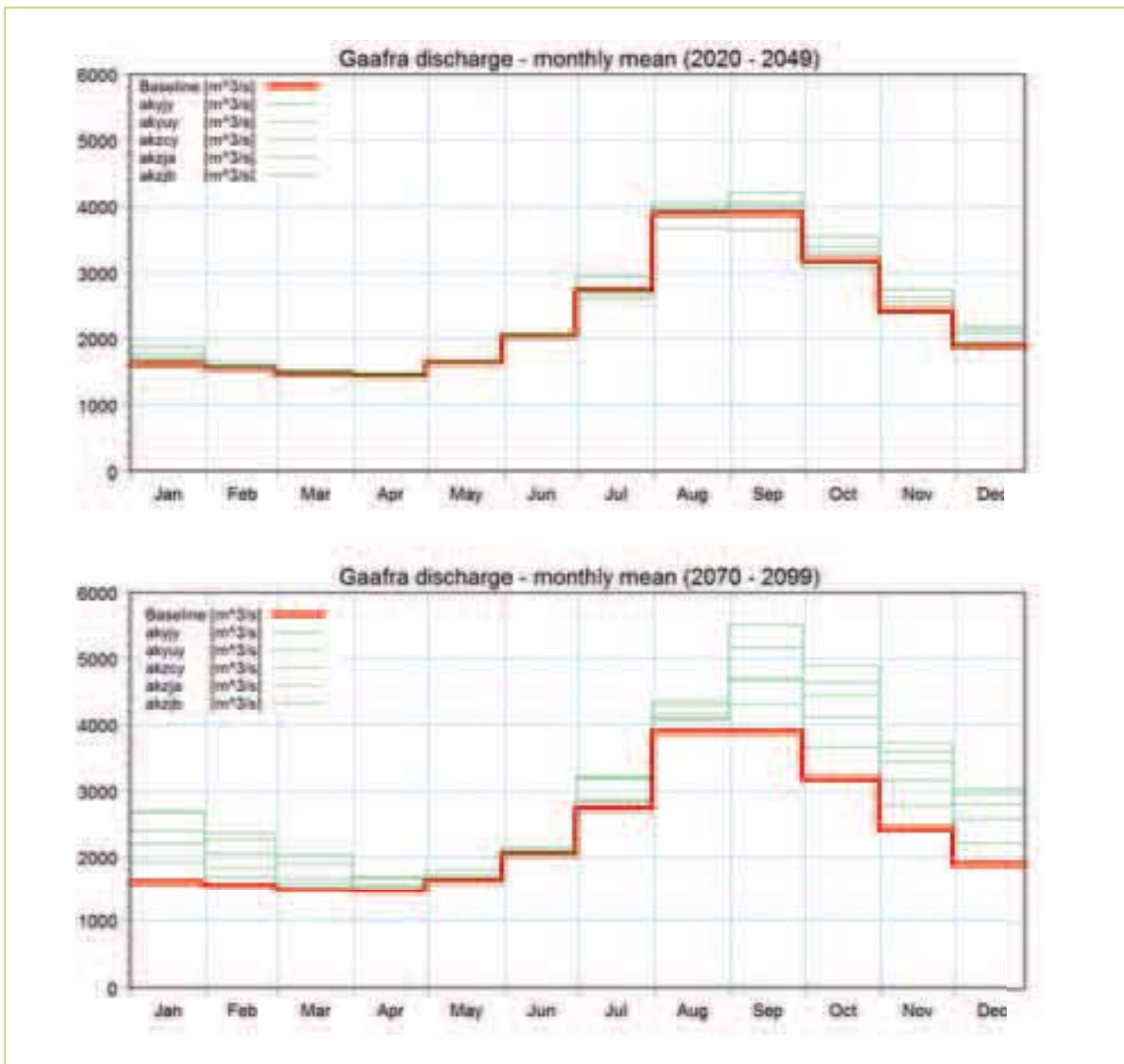
Figure 8.6 Projected changes in the average monthly flows for the Gaafra (El-Ga'Afra) station for the two periods; 2020-2049 & 2070-2099. The solid (red) line shows the baseline levels (1961-1990) & the thin green lines the different RCM ensemble members.

flow range with the exception of April-June (Figure 8.5). These reductions are amplified in the 2070-2099 period. Reductions in the peak flows (August-September) range from 6-16 %. Reductions in the low flows (January-February) range from 7-15%.

Comparison with the range of flow simulations from the RCM climate projections (Figure 8.5 & Figure 8.6) show that the flow changes for the 2020-2049 period are likely to be dominated by the increase in water demands. Even for the RCM projections with the largest increases in flow, the magnitude of the water demands will still exceed these increases in some months. The changes in flow due to climate change at this site during should be viewed with some caution as the reference period includes flows during the construction of the High Aswan Dam and some two years where the actual operation of the dam appears to be different from the operation in the hydrological model. It should be noted that while the climate projections show a range with both increasing and decreasing flows, the demands will only continue to increase. Furthermore, these figures represent changes in the mean flow. Vulnerability to water stress in dry years or a sequence of dry years will be even larger.

A cursory examination of the climate projections for 2070-2099 might suggest that climate change will reduce water stress. However, while general increases in flow are projected, there is a large range of variation in the magnitude of increases among the projections and a larger degree of uncertainty in the ability of the model to represent the reservoir-controlled flows. Increases in the peak flows are consistent with the increases in projected increase in flows in the Blue Nile and Atbara, but as mentioned earlier the hydrological models exhibits a bias towards higher peak flow in these catchments. Therefore is not possible to make any clear-cut conclusions as to the relative impact of increasing water demands compared to the potential increases in flows under climate change on water stress in the basin.

Estimates of projected population for Egypt for 2050 range from 115 to 179 million which indicate how uncertain the future water demands may be, with consequences on water stress in all sectors, including food production. Agriculture consumes about 85% of the water resource and contributes 20% of GDP in Egypt making it highly vulnerable to changes in Nile flows.

8.6 Key recommendations

This study provides a large amount of information related to the projections of future climate over the Nile and future flows in the Nile which will have implications for a large number of sectors. The focus has been to address changes at the regional scale. It has therefore not been possible to investigate all the possible implications of the climate and hydrological projections for all sectors and certainly not at local and national scales. It is anticipated that the results presented here can provide a sound starting point for future analyses.

The basis for analyses of climate change impacts on particular sectors is, of course, a socio-economic evaluation. An important finding in reviewing potential indicators for this study is that there are many relevant indicators that combine climate and hydrological information with socio-economic data. However, the underlying socio-economic data appear to be difficult to obtain and the socio-economic setting varies significantly from country to country. The collection and harmonisation of such data, including the application of consistent development scenarios, would provide a more reliable basis for the assessment of water resource developments, infrastructure projects and climate adaptation measures in general. It could also improve the potential for applying a benefit sharing approach to transboundary water management as opposed to a water allocation approach.

The water demand scenarios developed here, while being sufficient for a regional study, will have to be refined for local studies. Future work should address should address the uncertainties in demand projections, including changes in water use efficiency in each sector (particularly agriculture), population, and overall levels of development, including the spatial distribution of these changes. One of the important areas requiring further investigation is that the projections of irrigation water demands published by FAO do not take into account the effect of climate change on crop water requirements. It should be noted that the MIKE HYDRO hydrological modelling tool includes an irrigation module with the capability to account for changes in crop water demand under climate change.

This study has focussed primarily, on comparing at the regional scale estimates of changes in water demand (agricultural, domestic and industrial) with flow changes arising from climate change. Within the Nile River Basin water demand for irrigation accounts for by far the greatest part (89% of the total estimated water demand for the baseline) of the overall water demand. Traditional rain-fed agriculture however represents a major part of the agricultural production in the Nile for most countries in the region. Therefore future studies should

consider the direct impact of climate change on rain-fed agriculture. A first estimate of the vulnerable areas of rain-fed agriculture could be derived by comparing the indicator maps of CMI and CV CMI developed in the current study with maps of showing the distribution of rain-fed agriculture. The most vulnerable areas are those where changes from semi-humid to semi-arid occur while some benefits may occur where the reverse occurs. The impact on rain-fed agriculture could be quantified in terms of changes in crop yield as a result of water scarcity exploiting the capabilities of the irrigation module and yield model in MIKE HYDRO.

The regional modelling framework developed here could be used in the future to investigate the impacts of alternative water management strategies and adaptation measures at the regional scale. As stated at the outset, some adaptations measures, such as flood protection walls can be implemented locally and will have only local impacts. However, others such as the construction of dams, new irrigation developments, and alternate reservoir operation strategies, may well have important implications across the basin, particularly downstream. The balance between water availability and water demand will be strongly affected by such planned developments. One of the strengths of the regional hydrological model is that it can be incorporated into the Nile Basin Decision Support System (DSS), to allow the NBI countries to evaluate such interventions using the same models and data.

The study carried out here has examined a baseline period of 1960-1980 and the infrastructure development within this period. We also strongly recommend that the impact of both the more recent infrastructure developments and planned developments be examined in future work. These impacts are expected to be significant both for water supply and the regional economy. The regional hydrological model developed within this study can be extended in a straightforward manner to include current and planned water storage dams, diversion structures, and other water infrastructures. To strengthen the link between climate change and the water requirements for key economic sectors like hydropower and irrigation we recommend assessing the regional and local impacts of climate change based on this extended model and indicators such as agricultural or hydropower water supply deficits. In addition to including different infrastructure developments we would propose that such a study could usefully examine the impact of alternative long-term operating rules (for multiple objectives; hydropower, irrigation, etc.) as these can have important economic consequences at the regional scale.

There is a tremendous amount of local information, regarding rainfall, reservoir characteristics, irrigation data and so on which could be incorporated in the regional model or the major sub-basin models as the starting point for local or national water resource or adaption studies. The regional model is a powerful tool for future work in the basin not only because it captures the regional flow regime but also provides an overall framework for more detailed, local studies. We strongly recommend exploiting the regional hydrological model to provide boundary conditions for more detailed local models.

The value of good quality observation data over long periods cannot be overstated. One of the important limitations in the hydrological modelling work carried out here has been the lack of available data to support the formulation and calibration of sub-basin models. In several of the major sub-basins; Sobat, Blue Nile and Atbara the hydrological modelling scale used, for catchments within these major sub-basins, has been dictated by the limited spatial coverage of available hydro-climatic data rather than the underlying variability in hydro-climatic characteristics. The selection of an appropriate modelling scale is a trade-off between data coverage, the hydro-climatic variability and the modelling goals. In practice it is difficult to determine the appropriate modelling scale, a priori. This is a general challenge in catchment modelling and the subject of continuing research. For example, Butts et al., 2012 using a monthly water balance model for the Kagera sub-basin examined the importance of representing the spatial distribution of the hydro-geographic characteristics such as rainfall, soil type, etc., in order to develop a reasonable representation of the water balance. Further work should certainly be focussed on improving the data basis and spatial coverage used for modelling over the Ethiopian Highlands. This is an important source region and highly sensitive to changes in precipitation and evapotranspiration. Therefore improvements in this region will directly improve the quality of the flow projections, particularly for the Sobat, Blue Nile and Atbara sub-basins.

Finally, the reference period used here from 1960-1980 was selected because of the availability of data across the entire basin. If the model were extended with climate time series from more recent years, simulations for these recent years would not only provide a valuable validation of the hydrological model but also a better starting point for flow projections.

9.0 References

Adler, R. F., G.J. Huffman,A. Chang, R. Ferraro, P.-P. Xie, J. Janowiak, B. Rudolf, U. Schneider, S. Curtis, D. Bolvin, A.Gruber, J. Susskind, P. Arkin and E. Nelkin, (2003). The Version-2 Global Precipitation Climatology Project (GPCP) Monthly Precipitation Analysis (1979-Present), J. Hydrometeor, 4, 1147–1167.

Allen, M.R., P.A. Stott, J.F.B. Mitchell, R. Schnur, and T.L. Delworth (2000). Quantifying the uncertainty in forecasts of anthropogenic climate change. Nature 417, 617–620.

Allen, R., L.S. Pereira, D. Raes, and M. Smith (1998). Crop evapotranspiration –Guidelines for computing crop water requirements. FAO Irrigation and Drainage Paper N° 56. Rome, Italy.

Andréasson, J., S. Bergström, B. Carlsson, L.P. Graham, and G. Lindström (2004). Hydro-logical change – climate change impact simulation for Sweden. Ambio 33 (4–5), 228–234.

AQUASTAT (2012). Water use, Water withdrawal by sector, Industrial water withdrawal and Municipal water withdrawal, and associated definitions given therein. (http://www.fao.org/nr/water/aquastat/data/query/index.html ?lang=en last accessed 23/10/2012)

ASCE Task Committee (1993) Criteria for evaluation of watershed models, J. Irrigation and Drainage Engineering, (1993), 429-442.

ATEAM Final project report, (2004), Potsdam Institute for Climate Impact Research (PIK), section 5 & 6 (2001-2004). Available at (http://www.pik-potsdam.de/ateam/)

Bates, B.C., Z.W. Kundzewicz, S. Wu and J.P. Palutikof, Eds. (2008): Climate Change and Water. Technical. Paper of the Intergovernmental Panel on Climate Change, IPCC Secretariat, Geneva, 210.

Benestad R.E., (2004). Tentative probabilistic temperature scenarios for northern Europe. Tellus Series A – Dynamic Meteorology and Oceanography 56, 89–101.

Beyene, T., D.P. Lettenmaier, and P. Krabat (2010). Hydrologic impacts of climate change on the Nile River Basin: Implications of the 2007 IPCC scenarios. Climate Change 100(3-4), 433-461.

Boegh, E., H. Soegaard, and A. Thomsen (2002). Evaluating evapotranspiration rates and surface conditions using Landsat TM to estimate atmospheric resistance and surface resistance. Remote Sensing of Environment 79, 329–343.

Boko, M., I. Niang, A. Nyong, C. Vogel, C., A. Githeko, M. Medany, B. Osman-Elasha, R. Tabo and P. Yanda (2007) Africa. In: Climate Change 2007: Impacts, Adaptation and Vulnerability. Contribution of Working Group II to the Fourth Assessment Report of the Intergovernmental Panel on Climate Change [Parry, M.L., Canziani, O.F., Palutikof, J.P., van der Linden, P.J., Hanson, C.E. (Eds.)]. Cambridge University Press, Cambridge, UK.

Buontempo C., J. K. Lørup, M. Sanderson, M. Butts, E. Palin, R. McCarthy, R. Jones, R. Betts,and M. Antar (2011) The impact of uncertainties in climate impacts assessments: the case of the Nile basin, In : Coping with Global Environmental Change: Climate Change, Soil and Desertification, Water Management, Food and Health, Hexagon Series on Human, Environmental Security and Peace (HESP) (Eds. H-G Brauch, Ú. O. Spring, C. Mesjasz, J. Grin, P. Kameri-M bote, B. Chourou, P. Dunay, J. Birkmann) vol. 5 (Berlin – Heidelberg – New York: Springer-Verlag) 2011. Pages 765-772 ISBN: 978-3-642-17775-0 (Print) ISBN: 978-3-642-17776-7 (Online) DOI 10.1007/978-3-642-17776-7 (http://www.afes-press-books.de/html/hexagon_05.htm).

Buontempo et al (2013a). Regional climate modelling for Africa with PRECIS. (In preparation)

Buontempo et al (2013b). Regional climate model performance in the Lake Victoria Basin (In preparation).

Bürger, G., Y. Chen (2005). Regression-based downscaling of spatial variability for hydrologic applications. Journal of Hydrology 311, 299–317.

Butts, M.B. (2000). Coupling of catchment modelling and meteorological information in flow forecasting (invited paper). Proc. of European Conference on Advances in Flood Research, Potsdam Institute of Climate Research, Vol 2,460-470.

Butts, M. B., J. T. Payne, M. Kristensen, and H. Madsen (2004) An evaluation of the impact of model structure on hydrological modelling uncertainty for streamflow prediction. Journal of Hydrology, 298(1-4), 242-266.

Butts, M.B. A Dubicki, K. Stronska, G. Jørgensen, A. Nalberczynski, A. Lewandowski, and Terry van Kalken (2007). Flood forecasting for the Upper and Middle Odra River Basin. Flood Risk Management in Europe: Innovation in Policy and Practice Series: Advances in Natural and Technological Hazards Research, Vol. 25, Begum, S.; Stive, Marcel J.F.;and Hall, J W. (Eds.) 20067 ISBN: 1-4020-4199-3.

Butts, M., M.T de Sales, T.T. Trung, X. Lei, V. Phipatanasuphorn, and J. Høst-Madsen (2010). Web-based Climate DSS for Decision-Makers and Stakeholders. MIKE by DHI International Conference – Modelling in a World of Change, Copenhagen, Denmark, 6-8 September, 2010.

Butts M., J. K. Lørup, C. Buontempo, M. Elshamy and M. Ahmed (2011). Assessing Regional Climate Change Impacts on the Nile Basin –Technical Report for the project "Regional Climate Modelling of the Nile Basin: Preparation of climate scenario outputs for assessment of impact on water resources in the Nile Basin".

Butts. M., D. Wendi, O. Z. Jessen,, N.D. Riegels (2012) Assessing and managing water scarcity within the Nile River Transboundary Basin, Geophysical Research Abstracts Vol. 14, EGU2012-11232, 2012

Butts, Buontempo et al. (2013). A regional framework for assessing climate change impacts on water resources in the Nile (In preparation)

Christensen JH, T.R. Carter, M. Rummukainen, and G. Amanatidis (2007). Evaluating the performance and utility of regional climate models: the PRUDENCE Project Climatic Change 81 1-6.

Collins, M. and Knight, S.K. (Eds) 2007. Ensembles and probabilities: A new era in the prediction of climate change. Philosophical Transactions of the Royal Society A 365, Number 1857 / August 15, 2007.

Collins, M, B.B.B. Booth,G.R. Harris, J.M. Murphy, D.M.H. Sextonand ,M.J. Webb, (2006). Towards quantifying uncertainty in transient climate change, Clim Dyn, 27:2-3, 127-147.

Conway, D. (2005). From headwater tributaries to international river: Observing and adapting to climate variability and climate change in the Nile Basin. Global Environmental Change 15, 99–11.

Conway, D., C. Hanson, R. Doherty, and R. Persechino, (2007). GCM simulations of the Indian Ocean dipole influence on East African rainfall: present and future. Geophys Res Lett 34: L03705.

DHI, (2009). MIKE BASIN User Manual. Hørsholm, Denmark.

DHI (2012) Water Resources Climate Change Guidelines (http://www.dhigroup.com/Publications/Guidelines.aspx)

Di Baldassarre, G., M. Elshamy, A. van Griensven, E. Soliman, M. Kigobe, P. Ndomba, J. Mutemi, F. Mutua, S. Moges, Y. Xuan, D. Solomatine, and S. Uhlenbrook (2011). Future Hydrology and Climate in the River Nile Basin: A review. Hydrological Sciences Journal 56(2), 199-211.

Dinku, T., S.J. Connor, P.Ceccato, and C. Ropelewski (2008). Comparison of global gridded precipitation products over a mountainous region of Africa. International Journal of Climatology, 1627 - 1638.

Diro, G.T., D.I.F. Grimes and E. Black (2011) Large scale features affecting Ethiopian rainfall. African Climate and Climate Change (Eds. C.J.R. Williams and D.R. Kniveton), Advances in Global Change Reseearch 43 DOI 10.1007/978-90-481-3842-5_2, Springer Science+Business Media B.V. 2011, 13-50.

Diskin, M.H. and E. Simon (1977) A procedure for selection of objective functions for hydrologic simulation models, Journal of Hydrology, 34, 129-149.

Duan, Q., S. Sorooshian, V. Gupta (1992). Effective and efficient global optimization for conceptual rainfall-runoff models.Water Resources Research 28(4), 1015–1031.

Eid, H.M., S.M. El-Marsafawy, S.A. Ouda, (2006). Assessing the Impacts of Climate Change on Agriculture in Egypt: a Ricardian Approach. Centre for Environmental Economics and Policy in Africa (CEEPA) Discussion Paper No. 16, Special Series on Climate Change and Agriculture in Africa, University of Pretoria, Pretoria, 1-33.

Elshamy, M.E.A.M., 2000. Impacts of climate change on Nile flows. Diploma of Imperial College (DIC) thesis, Imperial College London, UK.

Elshamy, M. E., I.A. Seierstad, and A. Sorteberg, (2009). Impacts of climate change on Blue Nile flows using bias-corrected GCM scenarios, Hydrol. Earth Syst. Sci., 13, 551-565, doi:10.5194/hess-13-551-2009.

Essery, R., M. Best, and P. Cox, (2001) Moses 2.2 Technical Documentation, Tech. Rep. 30, Hadley Centre, http: 385 //www.metoffice.gov.uk/media/pdf/9/j/HCTN\30.pdf

EU (2009) Adapting to climate change: Towards a European framework for action, Commission of European Communities White paper, Brussels, 17 pp, April 2009.

FAO (1979) Yield response to water. In: Doorenbos, J., A.H. Kassam, (Eds.), FAO Irrigation and Drainage Paper 33. Rome.

FAO (2000) Review of agricultural water use per country. http://www.fao.org/nr/water/aquastat/water_use_agr/index.stm last accessed 07/11/2012.

FAO (2011a), Projections Report. Agricultural Water Use Projections in the Nile Basin 2030: Comparison with the Food for Thought (F4T) Scenarios. Food and Agriculture Organization of the United Nations (FAO). Rome 2011.

FAO (2011b), Synthesis Report. FAO-Nile Basin Project GCP/INT/945/ITA 2004 to 2009. Food and Agriculture Organization of the United Nations (FAO). Rome 2011.

FAONile 2011, DVD containing a collection of FAO reports, manuals, posters, and the respective GIS data. Population data raster files located at Docs\Poster_Maps\ArcGIS\data\raster_lcc\pop2005 and Docs\Poster_Maps\ArcGIS\data\raster_lcc\pop2020.

FAOStat 2012, Population, Annual time series: Total Population – Both sexes. http://faostat.fao.org/site/550/DesktopDefault.aspx?PageID=550#ancor. Last accessed 24/10/2012. Data derived from UN Population Division.

Fowler H.J., M. Ekström, C.G. Kilsby, P.D. Jones (2005). New estimates of future changes in extreme rainfall across the UK using regional climate model integrations. 1. Assessment of control climate. Journal of Hydrology 300: 212–233.

Fowler H. J., S. Blenkinsop, C. Tebaldi (2007). Review Linking climate change modelling to impact studies: recent advances in downscaling techniques for hydrological modelling, International Journal of Climatology 27 1547-157.

Frei C, R. Schöll, S. Fukutome J. Schmidli, and P.L. Vidale (2006). Future change of precipitation extremes in Europe: an intercomparison of scenarios from regional climate models. Journal of Geophysical Research-Atmospheres 111: D06105, DOI: 10.1029/2005JD005965.

Frei C, J.H. Christensen M. Déqué, D. Jacob, R.G. Jones, and P.L. Vidale (2003) Daily precipitation statistics in regional climate models: evaluation and intercomparison for the European Alps. Journal of Geophysical Research 108(D3): 4124, DOI: 10.1029/2002JD002287.

Giannini A., M. Biasutti, I- Held and A. Sobel (2008) A global perspective on African climate. Climate Change 90(4) 359-383.

Giorgi, F. and R. Francisco (2000). Evaluating uncertainties in the prediction of regional climate change. Geophysical Research Letters 27,1295–1298.

Giorgi, F., C. Jones, and G.R. Asrar (2009) Addressing climate change needs at the regional level: the CORDEX framework, WMO Bulletin, 58 (3), http://euro-cordex.net/uploads/media/Download.pdf.

Green, I.R.A., and D. Stephenson (1986) Criteria for comparison of single event models, Hydro-logical Science Journal, 31(3), 395-411.

Harris, I., P.D. Jones, T.J. Osborn, and D.H. Lister (2012): Updated high-resolution grids of monthly climatic observations - the CRU TS3.10 dataset. Submitted to International Journal of Climatology.

Havnø, K., M.N. Madsen, and J. Dørge (1995). MIKE 11—a generalized river modelling package. In: Singh, V.P., (Ed.), Computer Models of Watershed Hydrology, Water Resources Publications, Colorado, USA, 733–782.

Hewitt, C.D. (2005). The ENSEMBLES Project: Providing ensemble-based predictions of climate changes and their impacts. Published article appears in the EGGS newsletter, 13, 22-25. http://www.the-eggs.org/?issueSel=24

Huth, R., J. Kyselý, and M. Dubrovský (2003). Simulation of surface air temperature by GCMs, statistical downscaling and weather generator: higher order statistical moments. Studia Geophysica et Geodaetica 47, 203–216.

IPCC, 2007a: Climate Change (2007). The Physical Science Basis. Contribution of Working Group I to the Fourth Assessment Report of the Intergovernmental Panel on Climate Change (Eds. Solomon, S., D. Qin, M. Manning, Z. Chen, M. Marquis, K.B. Averyt, M. Tignor and H.L. Miller). Cambridge University Press, Cambridge, United Kingdom and New York, NY, USA, 996.

IPCC, 2007b: Climate Change 2007: Impacts, Adaptation and Vulnerability. Contribution of Working Group II to the Fourth Assessment Report of the Intergovernmental Panel on Climate Change, M.L. Parry, O.F. Canziani, J.P. Palutikof, P.J. van der Linden and C.E. Hanson, Eds., Cambridge University Press, Cambridge, UK, 976pp.

IPCC, 2007c. Climate Change 2007: Mitigation. Contribution of Working Group III to the Fourth Assessment Report of the Intergovernmental Panel on Climate Change [B. Metz, O.R. Davidson, P.R. Bosch, R. Dave, L.A. Meyer (Eds.)], Cambridge University Press, Cambridge, United Kingdom and New York, NY, USA., 852 pp.

IPCC (2008) Climate Change and Water. IPCC Technical Paper Bates, B.C., Z.W. Kundzewicz, S. Wu and J.P. Palutikof, Eds.IPCC Secretariat, Geneva, 210 pp. June 2008

Jones, R. G., J.M. Murphy, M., Noguer. and A.B. Keen (1997), Simulation of climate change over europe using a nested regional-climate model. II: Comparison of driving and regional model responses to a doubling of carbon dioxide. Q.J.R. Meteorol. Soc., 123: 265–292. doi:10.1002/qj.49712353802

Jones, R. G., M. Noguer, D.C. Hassell, D. Hudson, S.S. Wilson, G.J. Jenkins, and J.F.B Mitchell (2004).Generating high resolution climate change scenarios using PRECIS, Met Office Hadley Centre, Exeter, UK, http://www.metoffice.gov.uk/media/pdf/6/5/PRECIS\Handbook.pd%f.

Leung RL, L.O. Mearns F. Giorgi, R.L. Wilby (2003). Regional climate research: Needs and opportunities. Bulletin of the American Meteorological Society 84: 89–95.

Love, T. B., V. Kumar, V., P. Xie, P. and W. Thiaw (2004). A 20-year daily Africa precipitation climatology using satellite and gauge data. In Proceedings of the 84th AMS Annual Meeting, P5.4. Conference on Applied Climatology, Seattle, WA.

Madsen, H., (2000). Automatic calibration of a conceptual rainfall-runoff model using multiple objectives. Journal of Hydrology 235, 276–288.

Madsen, H., G. Wilson, and H.C. Ammentorp (2002).Comparison of different automated strategies for calibration of rainfall-runoff models, Journal of Hydrology, 261(14),. 48-59.

Madsen, H. (2003). Parameter estimation in distributed hydrological catchment modelling using automatic calibration with multiple objectives. Advances in Water Resources 26, 205–216.

Martinec, J. and A. Rango (1989) Merits of statistical criteria for the performance of hydrological models, Water Resources Bulletin, 25(2).

McSweeney, C.F., R.G. Jones, and B.B.B. Booth (2012). Selecting ensemble members to provide regional climate change information, J. Climate, doi:10.1175/JCLI-D-11-00526.1, http://405 dx.doi.org/10.1175/JCLI-D-11-00526.1.

Meehl, G. A., C. Covey, K.E. Taylor, T. Delworth, R.J. Stouffer, M. Latif, B. McAvaney, and J.F.B. Mitchell (2007a) THE WCRP CMIP3 Multimodel Dataset: A New Era in Climate Change Research, Bull. Amer. Meteor. Soc., 88, 1383–1394, doi:10.1175/BAMS-88-9-1383, http://dx.doi.org/10.1175/BAMS-88-9-1383, 410.

Meehl, G. A., T.F. Stocker, W.D. Collins,P. Friedlingstein, A.T. Gaye, J.M. Gregory, A. Kitoh, R. Knutti, J.M. Murphy, A. Noda, S.C.B. Raper, I.G. Watterson, A.J. Weaver, and Z.C. Zhao (2007b). Global climate projections. Climate Change 2007: The Physical Science Basis. Contribution of Working Group I to the Fourth Assessment Report of the Intergovernmental Panel on Climate Change, chap. 10, Cambridge University Press, Cambridge UK, http://www.ipcc.ch/publications\ and\ data/ar4/wg1/en/ch10.ht%ml.

Milly, P.C.D., K.A. Dunne, and A.V. Vecchia, A. V (2005). Global pattern of trends in streamflow and water availability in a changing climate, Nature 438(7066), 625-642.

Mitchell, T. D. and P.D. Jones (2005). An improved method of constructing a database of monthly climate observations and associated high-resolution grids, International Journal of Climatology, 25, 693–712, doi:10.1002/joc.1181, http://dx.doi.org/10.1002/joc.1181.

Mobasher, A.M.A. (2010). Adaptive reservoir operation strategies under changing boundary conditions: The case of the Aswan High Dam reservoir. Thesis submitted to Department of Civil Engineering and Geodesy for the Degree of Doctor of Philosophy, Darmstadt University.

Moss, R.H., J.A. Edmonds, K.A. Hibbard, M.R. Manning, S.K. Rose, D.P.van Vuuren, T.R Carter, S. Emori, M. Kainuma, T. Kram, G.A. Meehl, J.F.B. Mitchell, N. Nakicenovic, K. Riahi, S.J. Smith, R.J. Stouffer, A.M. Thomson, J.P. Weyant, and T.J. Wilbanks (2010). The next generation of scenarios for climate change research and assessment. Nature 463, 747-756 (11 February 2010)

Murphy, J.M., D.M.H. Sexton, D.N. Barnett, G.S. Jones, M.J. Webb, M. Collins, and D.A. Stainforth (2004). Quantification of modelling uncertainties in a large ensemble of climate change simulations. Nature 430, 768–772.

Murphy, JM, D.M.H. Sexton, G.J. Jenkins, B.B.B. Booth, C.C. Brown, R.T. Clark, M. Collins, G.R. Harris, E.J. Kendon, R.A. Betts, S.J. Brown, P. Boorman, T.P. Howard K.A. Humphrey, M.P. McCarthy, R.E. McDonald, A. Stephens, C. Wallace, R. Warren, R. Wilby, and R.A.Wood (2009). UK Climate Projections: Climate change projections. Met Office Hadley Centre, Exeter.

MWRI (2005). National Water Resources Plan 2017: 'Water for the future'. Ministry of Water Resources and Irrigation, Arab Republic of Egypt.

Nakicenovic, N., J. Alcamo, G. Davis, B. de Vries, J. Fenhann, S. Gaffin, K. Gregory, A. Grübler, T.Y. Jung, T. Kram, E.L. La Rovere, L. Michaelis, S. Mori, T. Morita, W. Pepper, H. Pitcher, L. Price, K. Riahi, A. Roehrl, H.-H. Rogner, A. Sankovski, M. Schlesinger, P. Shukla, S. Smith, R. Swart, S. van Rooijen, N. Victor, and Z. Dadi (2000). Special Report on Emissions Scenarios, Tech. rep., IPCC, http: //www.grida.no/publications/other/ipcc\ sr/?src=/climate%/ipcc/emission/.

New, M., D. Lister, M. Hulme, and I. Makin (2002). A high-resolution data set of surface climate over global land areas. Climate Research 21. doi:10.3354/cr021001

Nishida, K., R. Nemani, S. Running, J. Glassy, (2003). An operational remote sensing algorithm of land surface evaporation. Journal of Geophysical Research 108, 4270.

Norman, J., M. Anderson, W. Kustas, A. French, J. Mecikalski, R. Torn, G. Diak, G., T. Schmugge, B. Tanner (2003). Remote sensing of surface energy fluxes at 101-m pixel resolutions. Water Resources Research 39, 1221.

Palmer, T.N. and P.D. Williams (2008). Introduction. Stochastic physics and climate modelling. Philosophical Transactions of the Royal Society. Part A, 366 (1875), 2421-2427. ISSN 1364-503X

Rajaram, H., K.P. Georgakakos, (1989). Recursive parameter estimation of hydrologic models. Water Resources Research 25(2), 281–294.

Refsgaard, J.C., J. Knudsen (1996). Operational validation and intercomparison of different types of hydrological models. Water Resources Research 32(7), 2189–2202.

Ridler, M, I. Sandholt, M. Butts, S. Lerer, E. Mougin, F. Timouk, L. Kergoat, and H. Madsen. (2012) Calibrating a soil–vegetation–atmosphere transfer model with remote sensing estimates of surface temperature and soil surface moisture in a semi-arid environment, J. Hydrol. 436–437, 1-12.

Riegels, N., R. Jensen, L. Bensasson, S. Banou, F. Møller, and P. Bauer-Gottwein (2011) Estimating resource costs of compliance with EU WFD ecological status requirements at the river basin scale, Journal of Hydrology, 396(3–4),197-214.

Rijks, D.A and W.G. Owen (1970): Potential Evaporation in Uganda. Water Development De-partment, Uganda.

Salathé E.P. (2003). Comparison of various precipitation downscaling methods for the simulation of streamflow in a rainshadow river basin. International Journal of Climatology 23, 887–901.

Sandholt, I., H. Andersen (1993). Derivation of actual evapotranspiration in the Senegalese Sahel, using NOAA-AVHRR data during the 1987 growing season. Remote Sensing of Environment 46, 164–172.

SEDAC. (2010). Gridded Population of the World: Future Estimates. Socioeconomic Data and Applications Center (SEDAC); collaboration with CIESIN, UN-FAO, CIAT. Retrieved August 10, 2010, from http://sedac. ciesin.columbia.edu/gpw.

Shahin, M.M.A. (1985) Hydrology of the Nile Basin. Developments in Water Science, 21. Elsevier, Amsterdam.

Shuttleworth, W. (1992). Evaporation. In Handbook of Hydrology. McGraw

Siebert, Stefan, Petra Döll, Sebastian Feick, Jippe Hoogeveen and Karen Frenken (2007) Global Map of Irrigation Areas version 4.0.1. Johann Wolfgang Goethe University, Frankfurt am Main, Germany / Food and Agriculture Organization of the United Nations, Rome, Italy

Stainforth, D.A., T.Aina, C. Christensen, M. Collins, N. Faull, D.J. Frame, J.A. Kettleborough, S. Knight, A. Martin, J.M. Murphy, C. Piani, D. Sexton, L.A. Smith, R.A. Spicer, A.J. Thorpe, M.R. Allen (2005). Uncertainty in predictions of the climate response to rising levels of greenhouse gases. Nature 433, 403–406.

Stott, P.A. and J.A. Kettleborough, (2002). Origins and estimates of uncertainty in predictions of twenty-first century temperature rise. Nature 416, 723–726.

Strzepek, K.M., D.N. Yates, D.E. El Quosy (1996). Vulnerability assessment of water resources in Egypt to climatic change in the Nile Basin Climate Research 6 89-95.

Sutcliffe, J.V. and Y.P. Parks (1999). The Hydrology of the Nile IAHS Special Publication No. 5. IAHS Press.

Tidwell, A.C. (2006). Assessing the impacts of climate change on river basin management: a new method with application to the Nile river. PhD thesis, Georgia Institute of Technology, USA.

UN, (2003): World Water Development Report: Water for Life, Water for People. UNESCO, Paris and Berghahn Books, Barcelona, 36 pp.

UNDESA (2010), World Population Prospects, the 2010 Revision. United Nations, Department of Economic and Social Affairs, Population Division. http://esa.un.org/unpd/wpp/unpp/panel_population.htm

UNEP. (2010). Africa Water Atlas. Division of Early Warning and Assessment (DEWA). United Nations Environment Programme (UNEP). Nairobi, Kenya.

UK Met Office (2009) http://ukclimateprojections.defra.gov.uk/

Uppala, S. M., P.W. Kållberg,, A.J. Simmons, U. Andrae, V. da Costa Bechtold, M. Fiorino, J.K.Gibson, J. Haseler, A. Hernandez, G.A. Kelly, X. Li, K., Onogi, S. Saarinen, N. Sokka, R.P. Allan, E. Andersson, K. Arpe, M.A. Balmaseda, A.C.M. Beljaars, Berg, J. Bidlot, N. Bormann, S. Caires, F. Chevallier, A. Dethof, M. Dragosavac, M. Fisher, M. Fuentes, S. Hagemann, E. Holm, B.J. Hoskins, L. Isaksen,P.A.E.M. Janssen, R. Jenne, A.P. Mcnally, J.F. Mahfouf, J.J. Morcrette, N.A. Rayner, R.W. Saunders, P. Simon, A. Sterl, K.E. Trenberth, A. Untch, D. Vasiljevic, P. Viterbo, and J. Woollen (2005) The ERA-40 re-analysis, Q.J.R. Meteorol. Soc., 131, 2961–3012, doi:10.1256/qj.04.176, http://dx.doi.org/10.1256/qj.04.176.

van Roosmalen, L., J.H. Christensen, M.B. Butts, K.H. Jensen, J.C. Refsgaard (2010). An intercomparison of regional climate model data for hydrological impact studies in Denmark, Journal of Hydrology, Volume 380, Issues 3-4, 30 January 2010, Pages 406-419, ISSN 0022-1694, DOI: 10.1016/j.jhydrol.2009.11.014.

Van Vuuren, D., J. Edmonds, M. Kainuma, K. Riahi, A. Thomson, K. Hibbard, K., G.C. Hurtt, T. Kram, V. Krey, J. Lamarque, T. Masui, M. Meinshausen, N. Nakicenovic, S.J. Smith, S.K. Rose, (2011). The representative concentration pathways: an overview. Climatic Change, 109 pp 5-31.

Vörösmarty, C. J., E.M. Douglas, P.A. Green, and C. Revenga (2005). Geospatial indicators of emerging water stress: an application in Africa. Ambio 34 (3): 230-236.

Willmott, C.J., and J.J. Feddema (1992). A more rational climatic moisture index. Prof. Geographer 44: 84-87.

World Meteorological Organisation (WMO) (1994), Fifth ed., Guide to Hydrological Practices: Data Acquisition, and Processing, Analysis, Forecasting and Other Applications, WMO Publ. No. 168.

Woodhead, T. (1968): Studies of Potential Evaporation in Kenya. East African Agriculture and Forestry Research Organisation, Nairobi, Kenya.

Xie, P. and P.A. Arkin (1997). Global Precipitation: A 17-Year Monthly Analysis Based on Gauge Observations, Satellite Estimates, and Numerical Model Outputs, Bulletin of the American 445 Meteorological Society, 78, 2539–2558.

Xu, C.Y., 1999. From GCMs to river flow: a review of downscaling methods and hydrologic modelling approaches. Progress in Physical Geography 23(2), 229–249

.

For further information:
Ms. Musonda Mumba
Programme Officer
Email: Musonda.Mumba@unep.org
http://www.unep.org/climatechange/adaptation

UNEP